This work was performed for the Jet Propulsion Laboratory, California Institute of Technology, sponsored by the National Aeronautics and Space Administration under Contract NAS7-100.

Surveyor Spacecraft System

SURVEYOR V FLIGHT PERFORMANCE FINAL REPORT

JPL Contract 950056/November 1967

SSD 68189-5

J. D. CLOUD
Manager
System Engineering and Analysis Laboratory

T. B. VAN HORNE
Manager
Analysis Department

W. B. MC INTYRE
Project Engineer
Analysis Department

HUGHES
HUGHES AIRCRAFT COMPANY
SPACE SYSTEMS DIVISION

CONTENTS

			Page
1.0	INTRODUCTION AND SCOPE		1-1
2.0	DESCRIPTION OF SURVEYOR SYSTEM		
	2.1	Surveyor V Mission Objectives	2-1
	2.2	Surveyor V Flight Configuration	2-1
	2.3	References	2-7
3.0	SYSTEM SUMMARY		
	3.1	Summary of Significant Anomalies	3-1
	3.2	System Performance Parameters	3-3
	3.3	Conclusions and Recommendations	3-3
		3.3.1 Conclusions	3-3
		3.3.2 Recommendations	3-3
4.0	SYSTEM PERFORMANCE ANALYSIS		
	4.1	General Mission Summary	4-1
		4.1.1 Spacecraft Transit Phase Command Log	4-1
		4.1.2 Prelaunch Countdown	4-26
		4.1.3 Launch, Injection, and Separation	4-26
		4.1.4 DSIF Acquisition	4-26
		4.1.5 Coast Phase I Including Canopus Acquisition	4-29
		4.1.6 Midcourse Corrections	4-30
		4.1.7 Coast Phase II	4-32
		4.1.8 Terminal Descent Phase	4-35
		4.1.9 Initial Lunar Operation	4-36
	4.2	Reliability Analysis	4-39
		4.2.1 Surveyor V Reliability Estimates	4-39
		4.2.2 Future Reliability Estimates	4-48
	4.3	References and Acknowledgments	4-53
5.0	PERFORMANCE ANALYSIS		
	5.1	THERMAL CONTROL SUBSYSTEM	5.1-1
		5.1.1 Introduction: Surveyor Thermal Control Techniques	5.1-1
		5.1.2 Thermal Anomalies – Failure of Thermal Switches to Open	5.1-2

PRECEDING PAGE BLANK NOT FILMED.

5.1.3	Summary		5.1-2
	5.1.3.1	Transit	5.1-2
	5.1.3.2	Lunar	5.1-3
5.1.4	Thermal Performance in Transit		5.1-4
	5.1.4.1	Prelaunch Phase	5.1-4
	5.1.4.2	Postlaunch Phase	5.1-15
	5.1.4.3	Midcourse and Other Vernier Burns	5.1-15
	5.1.4.4	Coast Phases	5.1-17
	5.1.4.5	Terminal Descent Phase	5.1-21
5.1.5	Thermal Performance – Lunar Day 1		5.1-22
	5.1.5.1	Touchdown Orientation and Configuration	5.1-22
	5.1.5.2	Telecommunication Compartments	5.1-22
	5.1.5.3	Static Firing	5.1-25
	5.1.5.4	Alpha Scattering Operation and Warmup	5.1-25
	5.1.5.5	Oxidizer Tank 1 Leak	5.1-27
	5.1.5.6	Possible Correction of Fuel System Pressure Drop and Collapse of Shock Absorbers 2 and 3	5.1-29
	5.1.5.7	Solar Panel/Planar Array	5.1-29
	5.1.5.8	First Lunar Night	5.1-33
5.1.6	References		5.1-36
5.1.7	Acknowledgment		5.1-37
APPENDICES TO SECTION 5.1			
	A.	Transit Temperature Plots	5.1-A1
	B.	Lunar Day Temperature Plots	5.1-B1
5.2	ELECTRICAL POWER SUBSYSTEM		5.2-1
5.2.1	Introduction		5.2-1
5.2.2	Anomaly Description		5.2-2
5.2.3	Summary and Conclusions		5.2-4
	5.2.3.1	Summary	5.2-4
	5.2.3.2	Conclusion	5.2-4
5.2.4	Analysis		5.2-4
	5.2.4.1	Mission Telemetry Plots	5.2-4
	5.2.4.2	Power Loads and Sources Budget	5.2-4
	5.2.4.3	Comparison of Flight Loads and Flight Acceptance Test Loads	5.2-8
5.2.5	Reference		5.2-10
5.2.6	Acknowledgments		5.2-10

5.3	RF DATA LINK SUBSYSTEM		5.3-1
	5.3.1	Introduction	5.3-1
	5.3.2	Anomaly Discussion	5.3-15
		5.3.2.1 Bias in Receiver B Performance	5.3-15
	5.3.3	Summary and Conclusions	5.3-17
	5.3.4	Subsystem Performance Analysis	5.3-21
		5.3.4.1 General Discussion	5.3-21
		5.3.4.2 Mission Phase One: Prelaunch to Spacecraft Acquisition	5.3-27
		5.3.4.3 Mission Phase Two: Coast	5.3-29
		5.3.4.4 Mission Phase Three: Canopus Acquisition Maneuver	5.3-39
		5.3.4.5 Mission Phase Four: Midcourse Maneuvers	5.3-45
		5.3.4.6 Mission Phase Five: Terminal Maneuver	5.3-46
		5.3.4.7 Mission Phase Six: Descent and Touchdown	5.3-47
		5.3.4.8 Mission Phase Seven: Lunar	5.3-51
		5.3.4.9 Mission Data Plots	5.3-55
	5.3.5	References	5.3-56
	5.3.6	Acknowledgments	5.3-57
5.4	SIGNAL PROCESSING		5.4-1
	5.4.1	Introduction	5.4-1
	5.4.2	Anomalies	5.4-1
	5.4.3	Summary	5.4-1
	5.4.4	Signal Processing Analysis	5.4-2
		5.4.4.1 Unbalance Current Corrections	5.4-2
		5.4.4.2 Potentiometer Reference Voltage Corrections	5.4-2
		5.4.4.3 Current Calibration Signals	5.4-3
		5.4.4.4 Touchdown Strain Gage Data	5.4-5
	5.4.5	Documentation	5.4-5
	5.4.6	Acknowledgments	5.4-10
5.5	FLIGHT CONTROL		
	5.5.1	Introduction	5.5-1
		5.5.1.1 Attitude Control	5.5-1
		5.5.1.2 Angular Maneuvers	5.5-1
		5.5.1.3 Velocity Correction	5.5-1
		5.5.1.4 Soft Landing	5.5-2
		5.5.1.5 Mission Performance	5.5-2
		5.5.1.6 Analysis	5.5-2

5.5.2	Anomaly Description		5.5-10
5.5.3	Summary		5.5-10
5.5.4	Subsystem Performance Analysis		5.5-10
	5.5.4.1	Prelaunch	5.5-10
	5.5.4.2	Launch Through Separation From Centaur	5.5-10
	5.5.4.3	Sun Acquisition	5.5-20
	5.5.4.4	Canopus (Star Acquisition)	5.5-20
	5.5.4.5	Coast Phase	5.5-30
	5.5.4.6	Premidcourse Attitude Maneuvers	5.5-34
	5.5.4.7	Postmidcourse Attitude Maneuvers	5.5-43
	5.5.4.8	Midcourse Velocity Correction	5.5-43
	5.5.4.9	Preretro Maneuvers	5.5-52
	5.5.4.10	Main Retro Phase	5.5-61
	5.5.4.11	Terminal Descent Phase	5.5-66
5.5.5	References		5.5-71
5.5.6	Acknowledgments		5.5-73
5.6	VERNIER PROPULSION		5.6-1
5.6.1	Introduction		5.6-1
	5.6.1.1	Description	5.6-1
	5.6.1.2	Purpose	5.6-1
5.6.2	Anomalies		5.6-3
5.6.3	Summary and Recommendations		5.6-4
	5.6.3.1	Regulator Failure	5.6-4
	5.6.3.2	Pressure Saturation Anomaly	5.6-5
	5.6.3.3	Pressurization Rate Anomaly	5.6-5
5.6.4	Subsystem Performance Analysis		5.6-16
	5.6.4.1	Prelaunch	5.6-16
	5.6.4.2	Launch (L-2 Hours to L+34 Minutes)	5.6-16
	5.6.4.3	Coast Phase (L+34 Minutes to L+17 Hours)	5.6-17
	5.6.4.4	Midcourse (L+17 Hours to L+19 Hours)	5.6-18
	5.6.4.5	Coast II (L+19 Hours to L+63 Hours 30 Minutes)	5.6-20
	5.6.4.6	Terminal Descent (L+63 Hours 30 Minutes to L+65 Hours)	5.6-21
	5.6.4.7	First Lunar Day	5.6-21
5.6.5	References		5.6-27
5.6.6	Acknowledgments		5.6-27

APPENDIX A TO SECTION 5.6. HELIUM REGULATOR FAILURE
Introduction 5.6-A1
Failure Cause 5.6-A1
Discussion 5.6-A3
Corrective Action Summary 5.6-A9
Reference 5.6-A10

5.7 PROPULSION – MAIN RETRO 5.7-1
5.7.1 Introduction 5.7-1
5.7.2 Anomaly Description 5.7-2
5.7.3 Summary and Recommendations 5.7-2
5.7.4 Subsystem Performance Analysis 5.7-3
5.7.4.1 Thrust Versus Time 5.7-3
5.7.4.2 Specific Impulse 5.7-5
5.7.4.3 Retro Disturbance Torques 5.7-5
5.7.4.4 T3500 5.7-5
5.7.5 References 5.7-6
5.7.6 Acknowledgments 5.7-6

5.8 ALTITUDE MARKING RADAR 5.8-1
5.8.1 Introduction 5.8-1
5.8.2 Anomalies 5.8-2
5.8.3 Summary and Recommendations 5.8-3
5.8.3.1 Summary 5.8-3
5.8.3.2 Recommendations 5.8-3
5.8.4 Subsystem Performance Analysis 5.8-4
5.8.4.1 Event Times 5.8-4
5.8.4.2 Load Current Signals 5.8-4
5.8.4.3 Late Gate Signals 5.8-5
5.8.4.4 DB Budget 5.8-5
5.8.4.5 Expected Marking Radar 5.8-7
5.8.4.6 Marking Radar Dispersions 5.8-8
5.8.4.7 AMR Parameter Reconstruction 5.8-10
5.8.4.8 AMR AGC Evaluation 5.8-12
5.8.5 References and Documentation 5.8-12
5.8.6 Acknowledgments 5.8-17

5.9 RADVS PERFORMANCE 5.9-1
5.9.1 Introduction 5.9-1
5.9.2 Anomalies 5.9-4
5.9.3 Summary and Recommendations 5.9-4
5.9.3.1 Summary 5.9-4
5.9.3.2 Recommendations 5.9-7
5.9.4 Subsystem Performance Analysis 5.9-7
5.9.4.1 RADVS Turn-on 5.9-7
5.9.4.2 Velocity Acquisition Conditions 5.9-7
5.9.4.3 Range Acquisition Conditions 5.9-8

	5.9.4.4	Beam Drop-outs	5.9-8
	5.9.4.5	Revised Nominal DB Budget	5.9-13
	5.9.4.6	TM Mode 6 Data Word Summary	5.9-13
	5.9.4.7	Surveyor V Event Times	5.9-16
	5.9.4.8	Descent Reconstruction	5.9-22
	5.9.4.9	Radar Reflecting Analysis	5.9-22
	5.9.4.10	Reflectivity Model	5.9-26
5.9.5	RADVS Documentation		5.9-26
5.9.6	Acknowledgments		5.9-35
	APPENDIX A TO SECTION 5.9. REVISED TERMINAL DESCENT		5.9-A1
5.10	STRUCTURES PERFORMANCE		5.10-1
5.10.1	Introduction		5.10-1
5.10.2	Anomaly Description		5.10-1
5.10.3	Summary		5.10-2
5.10.4	Performance Analysis		5.10-2
	5.10.4.1	Launch Phase	5.10-2
	5.10.4.2	Touchdown	5.10-3
	5.10.4.3	Lunar Operations Phase	5.10-10
5.10.5	Acknowledgments		5.10-17
5.11	MECHANISMS SUBSYSTEM		5.11-1
5.11.1	Introduction		5.11-1
5.11.2	Anomaly Description		5.11-3
5.11.3	Summary and Recommendations		5.11-3
5.11.4	Subsystem Performance Analysis		5.11-3
	5.11.4.1	Landing Gear Deployment	5.11-3
	5.11.4.2	Omnidirectional Antenna Deployment	5.11-3
	5.11.4.3	A/SPP Performance	5.11-3
5.11.5	References		5.11-15
5.11.6	Acknowledgments		5.11-15
5.12	TERMINAL DESCENT TRAJECTORY PERFORMANCE		5.12-1
5.12.1	Introduction		5.12-1
5.12.2	Anomaly Description		5.12-3
5.12.3	Summary and Recommendations		5.12-4
5.12.4	Performance Analysis		5.12-4
	5.12.4.1	Introduction	5.12-4
	5.12.4.2	Postflight Analysis Computer Programs	5.12-9
	5.12.4.3	Velocity Change Due to Thrusting During Retro Phase	5.12-11
	5.12.4.4	Main Retro Thrust Versus Time Curve	5.12-19

		5.12.4.5 Vernier Propellant Consumption	5.12-21
		5.12.4.6 Spacecraft Landing Location	5.12-23
		5.12.4.7 Trajectory Reconstruction	5.12-23
	5.12.5	Acknowledgments	5.12-23
5.13	TELEVISION		5.13-1
	5.13.1	Introduction	5.13-1
	5.13.2	Anomalies	5.13-1
	5.13.3	Summary and Recommendations	5.13-2
		5.13.3.1 Summary	5.13-2
		5.13.3.2 Recommendations	5.13-3
	5.13.4	Subsystem Performance Analysis	5.13-3
		5.13.4.1 Historical Background	5.13-3
		5.13.4.2 Investigation of Anomalies	5.13-3
	5.13.5	References	5.13-6
	5.13.6	Acknowledgments	5.13-7
5.14	ALPHA SCATTERING EXPERIMENT		5.14-1
	5.14.1	Introduction	5.14-1
		5.14.1.1 Purpose	5.14-1
		5.14.1.2 Description	5.14-1
	5.14.2	Anomalies	5.14-4
	5.14.3	Recommendations	5.14-4
	5.14.4	Subsystem Performance Analysis	5.14-4
	5.14.5	Reference	5.14-13
	5.14.6	Acknowledgments	5.14-13

1.0 INTRODUCTION AND SCOPE

On 251:07:57:01.257 GMT (8 September 1967) the fifth Surveyor spacecraft was launched from pad 36B at AFETR at a launch azimuth of 79.517 degrees. The launch into parking orbit was near perfect, with the spacecraft being injected into its translunar trajectory during the second Centaur burn at 251:08:15:25 GMT. Subsequent transit operations (separation, sun acquisition, and star acquisition) were nominal until pressurization of the vernier propulsion system prior to the midcourse correction. At this time, an anomaly in the helium regulator was discovered (a leak of the helium supply). The originally scheduled midcourse and five additional vernier corrections were made prior to a modified and spectacular terminal descent to a soft landing on the moon on 10 September 1967. Over 18,000 high quality television pictures were taken on the first lunar day, and over a thousand additional pictures were taken on the second lunar day. In addition, a total of 93.5 hours was accumulated by the alpha scattering device to give an estimate of the chemical composition of the lunar surface at the Surveyor V site.

The basic purpose of this report is to document the actual performance of this spacecraft throughout the mission, compare its performance with that predicted from spacecraft design, summarize preliminary failure investigations, and recommend any changes or modifications that should be made to the spacecraft design. This report is based on both real-time and postmission data analysis.

PRECEDING PAGE BLANK NOT FILMED.

2.0 DESCRIPTION OF SURVEYOR SYSTEM

The Surveyor spacecraft is designed and built by Hughes Aircraft Company for the National Aeronautics and Space Administration under the direction of the California Institute of Technology Jet Propulsion Laboratory. It has been conceived and designed to effect a transit from earth to the moon, perform a soft landing, and transmit to earth basic scientific and engineering data relative to the moon's environment and characteristics. A brief description of the Surveyor vehicle design is given the Surveyor I final performance report (Reference 1).

2.1 SURVEYOR V MISSION OBJECTIVES

The primary objectives of the Surveyor V spacecraft system were as follows:

1) Accomplish a soft landing on the moon at a site east of the center of the moon

2) Demonstrate spacecraft capability to soft land on the moon with an oblique approach angle not greater than 45 degrees

3) Obtain postlanding television pictures

4) Obtain data on radar reflectivity, thermal characteristics, touchdown dynamics, and other measurements of the lunar surface through use of various payload equipment, including the alpha scattering device.

Surveyor V achieved the foregoing objectives. Soft landing occurred east of the center of the moon at an approach angle of 46.8 degrees. Television pictures were transmitted from the lunar surface, and extensive use was made of the alpha scattering device.

2.2 SURVEYOR V FLIGHT CONFIGURATION

For a summary description of the major Surveyor functions and design mechanization, consult the "Surveyor I Final Performance Report" or the

PRECEDING PAGE BLANK NOT FILMED.

"Surveyor Spacecraft Equipment Specification," Section 2.3 (References 1 and 2). Since Surveyor V was a reconfigured spacecraft (as compared to Surveyor I through 4) only the major Surveyor V design changes are noted (Reference 3) in Table 2-1. To define the spacecraft configuration at launch, a list of Surveyor V control items, separated by subsystem or function, is given in Table 2-2.

TABLE 2-1. MAJOR SURVEYOR V DESIGN CHANGES

Subsystem	Change
RF	Elimination of power dropoff with temperature Elimination of microswitches in transfer and SPDT switches
Signal Processing	Data channel reassignment
Solar Panel	Use of flat cell mounting Lower voltage output
Power	Elimination of auxiliary battery Elimination of OCR in battery charge regulator Higher efficiency and current limiting in boost regulator
Flight Control	Separation latch Increased midcourse timing capability Terminal descent staging Nitrogen tank thermal characteristics
Radars	Improved AMR noise figure RADVS 3-beam crosscoupled sidelobe logic RADVS crosscoupled sidelobe logic at low altitudes RADVS on/off relay
Propulsion	Helium check and relief valve assembly Pressure and temperature transducers on fuel lines
A/SPP	High torque motors Strengthened axes locks Strengthened sector gear Solar axis support tube
Television	Removable mirror assembly – Strengthened drive ring gear and drive shaft Potentiometers – New dry lube and thicker wiper Vidicons – Survival heater and optical front porch Spherical viewing mirrors
Alpha Scattering System	Instrument sensor Deployment mechanism Compartment C – Instrument electronics, instrument auxiliary, and thermal control

TABLE 2-2. SPACECRAFT UNIT CONFIGURATION AT LAUNCH

Subsystem	Part Name, Number, S/N
Electrical Power	Main battery, 237900, S/N 142
	Thermal control and heater A, 283724-1, S/N 11
	Thermal control and heater B, 283724-2, S/N 13
	Boost regulator, 3024240-1, S/N 11
	Battery charge regulator, 3024260-1, S/N 11
	Solar panel, 251167, S/N 3
	Main power switch, 254112, S/N 11
	Engineering mechanisms auxiliary, 263500-9, S/N 14
Flight Control	Flight control sensor group, 3023450-2, S/N 1
	Inertial reference unit, 235100-1, S/N 10
	Roll actuator, 235900-3, S/N 5
	Gas supply, attitude jet, 235600-3, S/N 2
	Attitude jets, 235700-2, S/N 7 and 8
	Attitude jet, 235700-3, S/N 9
	Secondary solar sensor, 235450-1, S/N 8
Radar	Altitude marking radar, 283827-1, S/N 14
	KPSM (RADVS), 232909, S/N 11
	SDC (RADVS), 232908-4, S/N 11
	Altitude velocity sensor antenna (RADVS), 232910, S/N 12
	Velocity sensor antenna (RADVS), 232911-1, S/N 11
	Waveguide assembly (RADVS), 232912-1, S/N 10

Table 2-2 (continued)

Subsystem	Part Name, Number, S/N
Telecommunications	Transmitter A, 3024400-1, S/N 12
	Transmitter B, 3024400-1, S/N 14
	Command receiver A, 231900-3, S/N 19
	Command receiver B, 231900-3, S/N 20
	Omnidirectional antennas A and B, 232400, S/N 31 and 7
	Telemetry buffer amplifiers A and B, 290780-1, S/N 18 and 19
	Planar array antenna, 251167, S/N 3
	Low pass filters A and B, 233466, S/N 22 and 24
	RF switch, SPDT, 284344, S/N 13
	RF transfer switch, 284345, S/N 11
Signal Processing	Signal processing auxiliary, 232540-1, S/N 6
	Central command decoder, 232000-5, S/N 6
	Low data rate auxiliary, 264875-2, S/N 1
	Engineering signal processor, 233350-10, S/N 1
	Auxiliary engineering signal processor, 264900-7, S/N 1
	Central signal processor, 232200-7, S/N 1
	TV auxiliary, 232106-7, S/N 12
Television	Survey camera, 284312-8, S/N 11
	Photo chart, antenna B, 231051, S/N 16
	Photo chart, leg 2, 230992, S/N 16
	Viewing mirror, 3035010, S/N 1
	Viewing mirror, 3035000, S/N 2

Table 2-2 (continued)

Subsystem	Part Name, Number, S/N
Propulsion	Oxidizer tank, 287119, S/N 2
	Oxidizer tank, 287121, S/N 1
	Oxidizer tank, 287120, S/N 2
	Fuel tank, 287117, S/N 11
	Fuel tank, 287118, S/N 1
	Fuel tank, 287117, S/N 2
	Helium tank and valve assembly, 3026042, S/N 2
	Thrust chamber assembly, 285063-4 (Hughes), S/N 560
	Thrust chamber assembly, 285063-7 (Hughes), S/N 553
	Thrust chamber assembly, 285063-5 (Hughes), S/N 565
	Main retro, 238612, S/N A21-28
Mechanisms	Spaceframe, 3025093, S/N 1
	Omnidirectional antenna A mechanism, 3028000-1, S/N 6
	Omnidirectional antenna B mechanism, 273880-1, S/N 1
	Antenna/solar panel positioner, 3035092, S/N 2
	Leg position pots, 988684-1, S/N 334, 346, and 336
	Retro-rocket release mechanisms, 230069-1, S/N 8, 17, and 53
	Separation sensing and arming devices, 293400, S/N 17, 18, and 19
	Shock absorbers, legs 1 through 3, 238927, S/N 8, 10, and 11

Table 2-2 (continued)

Subsystem	Part Name, Number, S/N
Mechanisms (continued)	Landing gear, 261278, S/N 8
	Landing gear, 261279, S/N 7
	Landing gear, 3025100, S/N 1
	Crushable block, 261281, S/N 405
	Crushable block, 3050736, S/N 402
	Crushable block, 3050697, S/N 415
	Accelerometer amplifier, 239011, S/N 6
	Strain gauge amplifier, 238930, S/N 6
Alpha Scattering	Auxiliary, 274350-1, S/N 1
	Electronics, 239305, S/N P4
	Deployment mechanism, 3024801, S/N 3
	Sensor head, 239304, S/N P4
	Standard sample, 239397, S/N 2
	Heater, compartment C, 290900, S/N 1
Thermal Control	Thermal switch A, 3028200-2, S/N 6
	Thermal switch A, 3028200-1, S/N 4, 8, 11, 14, 15, 16, 17, and 19
	Thermal switch B, 3028200-4, S/N 4
	Thermal switch B, 3028200-3, S/N 8, 9, 14, 17, and 24
	Thermal shell, compartment A, 3025262, S/N 2
	Thermal shell, compartment B, 3025288, S/N 2
	Thermal tray, compartment A, 3025094, S/N 2
	Thermal tray, compartment B, 3025096, S/N 1

Table 2-2 (continued)

Subsystem	Part Name, Number, S/N
Harness	Wiring harness compartment B, 3025639, S/N 1
	Wiring harness compartment A, 3025637, S/N 1
	Wiring harness basic bus 1, 3025635, S/N 1
	Wiring harness TV camera, 285833, S/N 1
	Wiring harness basic bus 2, 285828, S/N 2
	Wiring harness TV auxiliary, 3025391, S/N 1
	Wiring harness retro motor, 285832, S/N 3
	Wiring harness battery cell volt, 3025155, S/N 6
	Wiring harness separation squibs, 285831, S/N 1
	Wiring harness A/SPP, 3025420, S/N 5
	Cable, retro igniter, 286927, S/N 2
	Wiring harness ASI, 3025641, S/N 1

2.3 REFERENCES

1. "Surveyor I Flight Performance Final Report," Hughes Aircraft Company, SSD 68189R, October 1966.

2. "Surveyor Spacecraft Equipment Specification," Hughes Aircraft Company 224832, Revision A.

3. "Minutes of SC-5 Consent-To-Ship Meeting," Hughes Aircraft Company, SSD 74081, 13 June 1967.

3.0 SYSTEM SUMMARY

3.1 SUMMARY OF SIGNIFICANT ANOMALIES

The anomalies that occurred during Mission E are summarized in Table 3-1. For this report, an anomaly is defined as an unexpected occurrence that might be indicative of a spacecraft trouble or failure. The anomalies are discussed in greater detail in the sections noted in this table.

Currently, eight spacecraft anomalies have been identified with the Surveyor V mission.

TABLE 3-1. SPACECRAFT ANOMALIES

Number	GMT, day:hr:min:sec	Anomaly	Effect on Mission	TFR Number
1	252:01:42:28	Helium pressure regulator failure allowed gas leakage from helium tank. Attempts to reseat valve with additional vernier burns unsuccessful (see subsection 5.6.2)	Modified mission procedures after first midcourse, especially the terminal descent sequence	18263 (closed)
2	Terminal descent	Pressure saturation on engine 1 and possibly other engines (see subsections 5.6.2 and 5.5.4.11)	No gross effect on low thrust operation	—
3	After 252:01:42:28	Oxidizer tank pressurization rate was slower than that seen on previous spacecraft (see subsection 5.6.2)	None. Throttling rate never approached value sufficient to influence oxidizer regulated pressure	—

PRECEDING PAGE BLANK NOT FILMED.

Table 3-1 (continued)

Number	GMT, day:hr:min:sec	Anomaly	Effect on Mission	TFR Number
4	First lunar day 261:10 to 263:21	Oxidizer leg 3 pressure decreased from 812 psia to 328 psia (see subsection 5.6.2)	At time leakage noted, all mission objectives met. Entire vernier propulsion system exposed to high temperatures during lunar day far in excess of design limits	18265 (closed)
5	Start of first lunar night	Failure of command to lock landing gear. Deflection of 4.4 degrees on leg 2 and 6.9 degrees on leg 3 occurred as spacecraft entered lunar night (see subsection 5.10.2)	None	18266 18267
6	First lunar day	Thermal switches 3028200-3, S/N 9 and 3028200-4, S/N 4 failed to open at their specified operating temperature (see subsection 5.1.2)	None	37014 (closed) 37015 (closed)
7	First lunar day 266	TV camera lens focus, filter wheel, and focal length failed to respond to commands (see subsection 5.13.2)	These three camera functions were recovered on second lunar day. Most likely a temperature related problem.	59592 (closed)
8	Second lunar day 289	Video signals in both normal and emergency mode operation less than 5 percent of normal (see subsection 5.13.2)	Limited television operation. Failure mode duplicated in laboratory and considered random	59593 (closed)

Spacecraft		Actual			
		1	2	3	
Parameters	Units				
					LA
Ignition-liftoff	GMT	0 second is 1966 150:14:41:00.99	0 second is 1966 263:12:31:59.824	0 second is 1967 107:07:05:01.059	0 secon 195:11:
Booster engine cutoff	seconds from liftoff	142.2	142.29	142.5	141.88
Booster jettison		145.6	145.75	145.5	145.38
Insulation panel jettison		176.2	176.06	176.2	176.18
Nose fairing jettison		203.0	202.90	203.5	203.38
Sustainer engine cutoff		239.3	235.17	237.7	237.98
Atlas/Centaur separation		241.8	237.03	239.6	241.58
Centaur main engine cutoff 1		689.3	686.3	569	687.98
Centaur main engine cutoff 2		None	None	2028.8	None
Surveyor:					
Extend landing gear		715.5	710.7	2051.8	715.78
Extend omnidirectional antenna		725.7	720.7	2061.8	725.28
Transmitter to high power		745.4	741.4	2072.5	745.98
Electrical disconnect from Centaur		752.3	742.08	2087.8	751.28
Centaur separation		757.1	752.58	2093.4	756.88
Time to null rates to 0.1 deg/sec	seconds	≤15	<4	<11	<13
Pitch	degrees	≈0	–	–	+0.35
Yaw	degrees	≈2.3	–	–	-2.0
Roll	degrees	≈0	–	–	~0
Centaur retro maneuver time	seconds	L+996.0	L+992.8	L+2355.5	L+996
Solar axis deployment time	seconds	617	360	358	348
Spacecraft separated weight	pounds	~2192.8	2203	2281.3	2294.9
Spacecraft cg location					
X	inch	-0.116	-0.101	+0.058	+0.044
Y	inch	-0.092	+0.010	+0.179	-0.188
Z	inch	~59.185	59.16	58.95	58.88
Spacecraft moment of inertia					
I_{xx}	slug-ft^2	195.4	200	202	204
I_{yy}	slug-ft^2	191.7	196	198	200
I_{zz}	slug-ft^2	213.3	215	223	225
Sun acquisition					
Roll angle	degrees	-87	-71.5	-181	-59.4
Yaw angle	degrees	+99	+15	+38	+42.1
Total time	seconds	372	174.8	438.2	203
Star acquisition					
Proper acquisition and Canopus verification		Manual	Manual	Automatic	Automa
Roll angle from beginning of maneuver to Canopus	degrees	580.6	240	+205	+210.5
Objects identified		Alpha Doradus Phi Eridani Markab Pi Cygni Alderamin Regulus Alpha Hydrae Naos Canopus	Zeta Draconis Beta Draconis Ras Alhague Shaula Theta Scorpii Gamma Arae Alpha Tr. Australis Alpha Arae Zeta C Majoris Canopus	Canopus Moon Jupiter Earth Procyon Altair Adhara	Eta U Delta V Gamma Casio Canopu Moon Earth
Mean roll rate during star map phase	deg/sec	+0.5004	+0.4998	0.5011	0.5003
Effective gain of Canopus sensor	X Canopus	1.5	>1.5	1.03 - 1.22	1.16
Attitude orientation					
Average error from sunline					
Pitch	degree	-0.058	-0.07	0	+0.00
Yaw	degree	-0.053	-0.1	+0.02	+0.08
Roll	degree	-0.055	-0.08	-0.06	~0

FOLDOUT FRAME

3-3A

TABLE 3-2. SUMMARY PERFORMANCE PARAMETERS

4	5	Subsection or Reference	Predicted or Specified for Surveyor V	Reference	Comments
AUNCH TO ACQUISITION SUMMARY					
d is 1967 53:29.215	0 second is 1967 251:07:57:01.257				
	153.4 156.8 198.4 228.6 246.4 248.7 587.0 1103.9	FPAC	153.5 156.6 198.5 228.5 248.2 250.2 579.2 1099.4	Preflight nominal trajectory	
	1124.2 1134.4 1154.7 1160.9		1120.5 1131.0 1146.0 1157.0		
	1165.5		1162.5		
	<20		Within 50 seconds		
88	L+ 1405.5	FPAC	L+ 1167.5		
	298	5.11.4	306		
	2216.8				Spacecraft weight, cg and moments of inertia at separation
	-0.070 +0.779 59.69				
	210 211 211				
COAST SUMMARY					
	-342 +18.0 722	5.5.4.3	18 minutes maximum	224832A (7.3.3.3.4)	Roll maneuver until activation of acquisition sun sensor and then a yaw maneuver until primary sun sensor illumination
tic	Automatic +179	5.5.4.4		224832A (7.3.3.3.5)	
lajoris elorum peiae s	Zeta Ophiuchi (Antares, Tau Scorpii) Gamma Tr. Australis Canopus (Alnitak, Alnilam, Mintaka) Alpha Leporis Earth Bellatrix Polaris				
	0.5007		0.5		
	1.32			Design	Normally the gain setting is 1 x Canopus
	Very small		Within 0.2 degree	224832A (7.3.3.3.6)	Sensor group roll axis shall be held within 0.2 degree of sun-spacecraft line

FOLDOUT FRAME

3.2 SYSTEM PERFORMANCE PARAMETERS

A selected group of performance parameters that could be directly determined through analyses of spacecraft telemetry for the five Surveyor flights are summarized in Table 3-2. Required or predicted values for these parameters for Surveyor V are included in this summary.

3.3 CONCLUSIONS AND RECOMMENDATIONS

3.3.1 Conclusions

Performance of the Surveyor V spacecraft was very good except for a helium regulator problem after the midcourse maneuver. Following a near-perfect injection and coast phase until the midcourse correction, the flight was normal. Subsequent to the midcourse correction, a helium regulator problem emerged which caused reevaluation of the flight. Many nonstandard procedures were used during terminal descent and coast phase II (five additional midcourse corrections in an attempt to reseat the helium regulator valve, to lighten the spacecraft, and to correct the final trajectory back to the original aim point). The value of flexibility in spacecraft operations, subsystem and system analyses, and real-time simulations was evident in the success of the highly nonstandard terminal descent sequence by which Surveyor V soft landed on the moon. Subsections 4.1.7 and 4.1.8 and Sections 5.5 and 5.9 highlight the terminal descent events.

3.3.2 Recommendations

Recommendations from the Surveyor V flight are primarily associated with investigations into the helium regulator anomaly. Recommendations for design corrective action in the vernier propulsion system were as follows:

1) Perform in parallel engineering redesign of relief valve to increase crack pressure

2) Evaluate effects of increased relief valve crack pressure on helium pressurization subsystem

3) Perform tradeoff study to determine suitability of redesign for SC-7

Additional recommendation actions in the area of manufacturing handling and testing are listed in paragraph 5.6.3.1.

Table 3-2 (continued)

Spacecraft		Actual					
		1	2	3	4	5	
Parameters	Units						
COAST SUMMARY (continued)							
Average error from Canopus line of sight							
Pitch	degree	-0.058	-0.07	0	~0	Very small	
Yaw	degree	-0.053	-0.1	+0.02	~0		
Roll	degree	-0.055	-0.08	-0.06	+0.104		
Limit cycle optical mode							
Average amplitude – roll	degrees	0.441	0.441	0.55	0.6	0.46	
Average amplitude – pitch	degrees	0.470	0.45	0.51	0.44	0.37	
Average amplitude – yaw	degrees	0.457	0.37	0.54	0.41	0.50	
Average period	seconds	65	64	68.5	64		
Limit cycle inertial mode							
Average amplitude – roll	degrees	0.415	0.47	0.46	0.48	0.30	
Average amplitude – pitch	degrees	0.443	0.42	0.48	0.46	0.31	
Average amplitude – yaw	degrees	0.417	0.43	0.50	0.53	0.36	
Average period	seconds	50	61	68.5	61		
Gyro drift							
Roll	deg/hr	0.2	-0.78	+1.1	-0.5	+0.85	
Pitch	deg/hr	0	+0.24	+0.6	-1.0	+0.60	
Yaw	deg/hr	0.75	+1.09	-0.8	+0.15	-0.60	
MIDCOURSE SUMMARY							
Time of initiation of vernier burn	GMT	151:06:45:03.801	264:05:00:02	108:05:00:03.433	197:02:30:00	252:01:45±02.3	
						(1) (2) (3) (4) (5) (6)	
Duration of burn(s)	seconds	20.815	NA	4.245	10.48	14.22 10.04 23.04 12.32 33.07 5.40	
Command of first maneuver	GMT	151:06:30:12.888	264:04:44:00	108:04:46:49.8	197:02:15:28.9	252:01:32:57.0	
First maneuver	degrees	86.6 roll	+75.4 roll	+56.7 roll	+72.5 roll	+71.9 roll } Prior to	
Command of second maneuver	GMT	151:06:34:48,861	264:04:48:05	108:04:50:08.2	197:02:21:09.9	252:01:36:27.3 } Midcourse No. 1	
Second maneuver	degrees	58.0 yaw	+110.6 yaw	-39.1 pitch	-64.3 yaw	-35.5 yaw	
Command of third maneuver	GMT	NA	NA	NA	NA	NA	
Third maneuver	degrees	NA	NA	NA	NA	NA	
						(1) (2) (3) (4) (5) (6)	
Midcourse ΔV	m/sec	20.26	NA	4.2	10.13	14.2 9.78 22.54 13.02 32.32 5.28	
Midcourse ΔV error	m/sec	-0.081	NA	0.176	-0.17		
Peak attitude transients at ignition							
Roll	degrees	-0.43	NA	-1.0	–	-0.88 -0.88 -0.84 -0.90 -1.0 -0.82	
Pitch	degrees	0	NA	-0.125	-0.17	-0.24 0 -0.13 -0.05 +0.05 +0.1	
Yaw	degrees	-0.08	NA	+0.30	+0.19	+0.08 +0.25 +0.19 +0.20 +0.22 -0.18	
Peak angular error at shutdown			NA			(1) (2) (3) (4) (5) (6)	
Roll	degrees	–	↓	+0.58	+1.18	+1.2 +1.0 +1.1 -0.44 +0.2 +0.36	
Pitch	degrees	–		+0.96	+1.09	+0.13 +0.16 +0.58 +0.14 +0.71 +1.2	
Yaw	degrees	–		+1.97	+0.10	+0.50 +0.90 +0.48 +1.3 +0.5 -2.2	
Roll actuator position							
Peak at ignition	degrees	+0.9		-0.8	-1.22	– –	
Mean during burn	degrees	+0.65		–	–		
Engine shutoff impulse							
Engine 1	lbs/sec	0.27		-0.31	-0.18	-0.06 -0.10 -0.13 -0.07 -0.53 -0.29	
Engine 2	lbs/sec	-0.37		+0.42	+0.03	+0.05 +0.18 +0.11 +0.1 +0.65 +0.15	
Engine 3	lbs/sec	0.10		-0.11	+0.15	+0.01 +0.08 +0.02 -0.03 -0.12 +0.14	
Shutdown angular rate							
Pitch	deg/sec	–			+0.24	+0.06 +0.06 +0.13 +0.06 +0.46 +0.13	
Yaw	deg/sec	–	↓		-0.01	+0.06 +0.23 +0.12 +0.17 -0.76 ≈0	
TERMINAL DESCENT SUMMARY							
Landing location		2.41°S, 43.35°W	5.5°N, 12.00°S	2.94°S, 23.34°W	0.47°N, 1.44°W	1.50°N, 23.19°E	
Approach flight-path angle	degrees	6.13	NA	23.6	31.5	46.4	
Goldstone visibility							
Pre-touchdown	hours	4		~4.5	NA		
Post-touchdown	hours	5		~10	NA		
Transmitter high power on		153:05:20:18.3		109:23:09:40.7	198:01:09:26.8	253:23:51:41.3	
Telemetry mode	NA	2/3		6	6	6	
Bit rate	bps	1100		1100	1100	1100	
Touchdown strain gages	NA	Yes	↓	Yes	Yes	Yes	

FOLDOUT FRAME

Subsection or Reference	Predicted or Specified for Surveyor V	Reference	Comments
	Within 0.2 degree	224832A (7.3.3.3.6)	Canopus sensor null with respect to sensor group roll pitch plane
5.5.4.6	±0.44 degree	224832A (7.3.3.3.3)	
5.5.4.6	±0.44 degree	224832A (7.3.3.3.3)	
5.5.4.9		224832A (7.3.3.3.3C)	Non g-sensitive
5.5.4.8 and 4.1.6	First burn only		Table 4.6 summarizes vernier burns
5.5.4.8			
5.5.4.8			( ) refers to particular mid-course of Surveyor V
5.5.4.8	Δ Impulse <0.66 lb/sec	224832A (8.3.1.3.2.4.2)	
5.5.4.8			
			SC-2 impacted moon. SC-4 impacted moon. Last signal on terminal descent.

FOLDOUT FRAME

3-5A

Table 3-2 (continued)

Spacecraft		1	2
Parameters	Units		
Command of first maneuver	GMT		NA
First maneuver	degrees	+89.3 roll	
Command of second maneuver	GMT		
Second maneuver	degrees	+60.0 yaw	
Command of third maneuver	GMT		
Third maneuver	degrees	+94.4 roll	
AMR enabled (station time)	GMT	153:06:12:57.684	
AMR mark (station time)	GMT	153:06:14:39.708	
AMR backup mark (station time)	GMT		
Ignition delay time	seconds	7.85	
Retro delay time	seconds	1.1	
Retro action time (T3500)	seconds	38.9	
Maximum retro thrust	pounds	9900	
Thrust to velocity vector	degrees	0.26	
Retro thrust to cg offset	inch	<0.02	
Start RADVS – controlled descent			
Slant range	feet	27820	
Altitude	feet	27800	
V_z	fps	425	
V_x	fps	71.3	
V_y	fps	-4.1	
V-Total	fps	430	
Flight-path angle	degrees		
Peak attitude transient at retro ignition			
Roll	degree	–	
Pitch	degree	-0.41	
Yaw	degree	-1.03	
RODVS acquire condition			
Slant range	feet	55000	
Velocity	fps	3280	
RORA acquire condition			
Slant range	feet	36000	
Velocity	fps	690	
Beam loss of locks			
Retro case	NA	No. 3 once	
Other	NA	None	
Segment acquisition			
Slant range	feet	18000	
Velocity	fps	442	
1000 foot mark conditions			
Time	GMT	153:06:17:10.494	
Velocity	fps	103.1	
Attitude	degree	1.11	
10-fps mark conditions			
Slant range	feet	43	
Time	GMT	153:06:17:28.719	
Attitude	degree	0.7	
Δ Time 1000 foot mark to 10-fps mark	seconds	18.22	
Δ Time 10 fps mark to 14-foot mark	seconds	6.45	
Vernier engine shutoff			
14 foot mark	GMT	153:06:17:34.169	
Altitude (from foot pads)	feet	13	
Vertical velocity	fps	5	
Lateral velocity	fps	≈0	
Angle to local vertical	degree	≈0.3	
Time to touchdown	seconds	1.53	
Touchdown condition trajectory			
Vertical velocity	fps	12.2	
Lateral velocity	fps	≈0.6	
Attitude	degree	≈0	
Touchdown conditions (strain gages)			
Vertical velocity	fps	10	
Lateral velocity	fps	2	
Attitude	degree	1	
Spacecraft attitude after landing			
Roll orientation (+ x-axis to north)	degrees	179 clockwise	
Slope magnitude	degrees		
Slope direction (Negative gradient to north)	degrees		
Vernier fuel used	pounds	139.0	

FOLDOUT FRAME

3-5A

3-5B

Actual			Subsection or Reference	Predicted or Specified for Surveyor V	Reference	Comments
3	4	5				
TERMINAL DESCENT SUMMARY (continued)						
109:23:23:30 -158 yaw 109:23:30:17 -76.8 pitch 109:23:34:35 -64 roll	198:01:24:44.2 +80.8 roll 198:01:29:34.2 +92.7 yaw 198:01:35:04.6 -25.4 roll	254:00:12:15.1 +73.8 roll 254:00:16:20.5 +119.6 yaw None None				
109:23:59:35.252 110:00:01:12.829 110:00:01:13.439	198:02:00:16.99 198:02:01:56.08 198:02:01;56.35	254:00:43:00.9 254:00:44:39.081 254:00:44:46.38				AMR times received at DSS
5.09 1.1 41.02 9550 0.34 0.024	2.73 1.12 ≈42 9250 0.17° –	12.33 1.07 38.56 9950 0.30 -0.048	5.7.3 5.7.3 5.5.3 5.5.3		224832A (7.3.3.3.9)	SC-4 loss of signal at 198:02:02:41.018
36158 32900 462 171 483 26.8	NA 49420 NA NA NA 1092 26.8	6300 4139 +46 -41 +50 79 -35.67	5.12.3	– 4598 – – – 9 -5.05	5.12.3	Burnout data for SC-4 is at signal loss
-0.22 -0.10 ~0	~0 -0.09 -0.35	-0.16 +0.5 -0.5	5.53		224832A (7.3.3.3.10)	
63900 3230	78000 3414					
43700 640	NA NA					
No. 4 once Nos. 3, 4 once	None None	Nos. 4, 3 once None				
22300 495	NA	806 97	5.12.3 5.12.3	1500 117	SSD74131	
110:00:03:53.023 103.27 0.51		254:00:46:19.697 96.03 -7.5	5.12.3 5.12.3	106.46 -8.3		
46 110:00:04:10.623 0.025		46 254:00:46:37.097 -0.53	5.12.3 5.12.3	43 -0.24		
17.6		17.4				
NA		5.6				
NA NA NA NA NA NA		254:00:46:42.697 14.5 5.2 -0.11 1.7	5.12.3 5.12.3 5.12.3	13.0 5.04 -0.10		
6-8 ≈0 ≈0		13.5 0.5 ≈0	5.12.3 5.12.3 5.12.3	13.5 0.5 –		
6 0.5 ≈0		12 to 13 <1 ≈0	5.10.4.2 5.10.4.2			
134.2 clockwise 12 277 clockwise		114.5 clockwise 19.5 7.6 clockwise				
140.1		136.62	5.12.3	136.65	SSD74131	

FOLDOUT FRAME

4.0 SYSTEM PERFORMANCE ANALYSIS

4.1 GENERAL MISSION SUMMARY

Surveyor V was launched from pad 36B at Cape Kennedy on a parking orbit lunar intercept trajectory at a launch azimuth of 79.517 degrees and culminated in a soft landing in a crater in the Sea of Tranquility on the moon. The flight of Surveyor V originated on 8 September (PDT) (GMT 251:07:57:01.257) 1967 and softlanded on the moon 10 September (PDT) (GMT 254:00:46:44) 1967. A total of 18,006 television pictures was received, and 93.5 hours of lunar surface data were accumulated by the alpha-scattering experiment during the first lunar day (GMT day 254 to 266). The spacecraft was successfully revived during the second lunar day, and an additional 1048 television pictures were received, giving a total of 19,054 television pictures for Surveyor V. Performance of the Atlas and Centaur AC-13 launch vehicles appeared excellent throughout the flight period as all mark events occurred very close to the predicted times.

A summary of the mission event history is contained in Table 4-1. Injection of the spacecraft occurred at GMT 251:08:16:26.8 on a trajectory that would have provided with no midcourse correction a total miss of 28.5 miles from the targeted aiming point of +0.83 degree latitude and 24.00 degrees longitude. During transit, sun acquisition, solar panel deployment, DSIF acquisition, initial commanding and interrogations, star acquisition and verification, and the first midcourse maneuvers were all successfully executed. After the first midcourse maneuver, the spacecraft encountered a helium regulator problem, and a series of additional vernier burns were performed to aid in a successful landing on the moon.

The earth track traced by Surveyor V is shown in Figure 4-1. Specific events such as sun and Canopus acquisition, the six midcourse corrections, and touchdown are shown. The predicted view periods for the tracking stations are given in Table 4-2.

4.1.1 Spacecraft Transit Phase Command Log

A detailed list of spacecraft commands sent during the transit flight is presented in Table 4-3. This table includes the time the command was sent, as well as the tracking station originating the command.

TABLE 4-1. SURVEYOR V MISSION MILESTONES

Event	GMT, day:hr:min:sec
Launch	251:07:57:01.257
Separation-electrical disconnect*	251:08:16:21.34
Separation-mechanical (injection)*	251:08:16:26.8
Automatic sun acquisition completed	251:08:27:11
A/SPP solar panel unlocked	251:08:16:27.965
A/SPP solar panel locked in transit position	251:08:22:29
A/SPP roll axis locked in transit position	251:08:25:
Initial DSS acquisition (one-way) confirmed*	251:08:24:25
Initial DSS acquisition (two-way lock) confirmed*	251:08:30:11
First ground command sent to spacecraft	251:08:36:59.8
Canopus verification begins	251:14:10:01
Canopus lockon	251:14:27:52
First premidcourse (nominal) maneuver executed	252:01:32:57.0
First midcourse thrust executed	252:01:45:02.3
Second midcourse thrust (sunline) executed	252:02:12:02.2
Third midcourse thrust (anti-sunline) executed	252:02:39.50.6
Fourth midcourse thrust executed	252:04:18:48.4
Fifth midcourse thrust executed	252:08:24:03.7
Sixth midcourse thrust executed	252:23:30:58.0
Sun reacquired	252:23:39:28
Canopus reacquired	252:23:46:37
Initiation of roll maneuver (terminal descent)	254:00:12:15.1
Initiation of yaw maneuver	254:00:16:20.5

Table 4-1 (continued)

Event	GMT, day:hr:min:sec
Select nominal thrust (150 pounds)	254:00:23:18.5
Enter retro delay (12.325 seconds)	254:00:24:48.8
Retro sequence mode on	254:00:38:57.3
AMR power on	254:00:40:00.4
Flight control thrust phase power on	254:00:41:00.4
AMR enable	254:00:43:00.9
AMR mark*	254:00:44:39.081±0.025
AMR backup mark (from command 0730)*	254:00:44:46.38±0.05
Vernier ignition*	254:00:44:51.426±0.02
Retro ignition*	254:00:44:52.496±0.05
RADVS pyro switch (EP33)*	254:00:44:53.256±0.6
RADVS on (R28)*	254:00:44:53.456±0.6
RODVS*	254:00:45:24.155±0.6
RORA*	254:00:45:20.555±0.6
3.5-g signal*	254:00:45:31.355±0.6
Retro burnout (FC-30)*	254:00:45:31.495±0.05
Emergency retro eject command (0732)	254:00:45:37.9
Retro eject command (plus two-way transmission time)	254:00:45:40.36
Retro eject (FC-31)*	254:00:45:40.395±0.05
Retro ejected (V4)*	254:00:45:40.855±0.6
Vernier engine high thrust command (0725)	254:00:45:38.4
High thrust command (plus two-way transmission time)	254:00:45:40.86
Start maximum thrust (FC-78)*	254:00:45:40.955±0.6
Emergency start programmed thrust command (0733)	254:00:45:39.9
Programmed thrust command (plus two-way transmission time)	254:00:45:42.36

Table 4-1 (continued)

Event	GMT, day:hr:min:sec
Start RADVS-controlled descent (FC-42)*	254:00:45:42.395±0.05
Segment intercept (range = 878 feet, vertical velocity = 97 fps)*	254:00:46:22.33±0.2
1000-foot mark*	254:00:46:19.697±0.05
10-fps mark*	254:00:46:37.097±0.05
14-foot mark*	254:00:46:42.697±0.05
Touchdown (strain gage)*	254:00:46:44.397+0,-0.07

	From	To
Initial TV (18 200-line pictures)	254:02:00:53	254:02:38:42
Alpha scattering power on	254:02:39:00	254:04:02:76
Earth search, part 1	254:02:58:15	254:03:55:30
Sun search and acquisition	254:03:56	254:04:10:23
Earth search and acquisition	254:05:14:36	254:05:20:25
TV	254:05:30(+)	254:09:55
Investigate FC-16 apparent problem	254:09:55:24	
Sun fine positioning	254:10:43:10	254:11:30:32
Earth fine positioning, part 1	254:11:49:38	254:12:09
Deploy alpha scattering	254:12:09	
Earth fine position complete	254:12:18:25	254:12:44:21
BCR to unregulated bus	254:18:24	
Flight control checkout in preparation for static fire	255:11:30:57	255:12:53:08
Static fire preparation	256:04:01:05	
Static firing	256:05:38:08	
Return to normal		256:06:06:28
Spacecraft into "standby" to reduce battery temperature (on and off)	257:10:00	258:00:15

Table 4-1 (continued)

Event	GMT, day:hr:min:sec From	To	
Signal processing experiment (No. 15)	258:11:43	– 258:13:32	
Bit error test (No. 17)	258:16:00	258:18:06 258:21:39	(DSS-42) (DSS-61)
Antenna pattern mapping sequence	259:04:40	– 259:10:36	
Times of A/SPP positioning for shade (259:2400 = 260:0000) lunar noon	258:21:45 259:04:16, 17:36, 20:13 260:23:15 261:08:30		
Best lock frequency determination	261:20:53	– 261:21:02	
Second best lock frequency determination	262:19:43	– 262:20:15	
Special bit error test	263:12:18	– 263:14:33	
TV gain margin (No. 22)	263:15:30	– 263:18:24	
Third best lock frequency	263:20:15	– 263:20:40	
Combined RF and signal processing assessment (No. 15)	264:18:45	– 264:23:36	
Sunset	265:15:30		
Shadow times on parts of spacecraft	to 267:11:30		

*Telemetry time received.

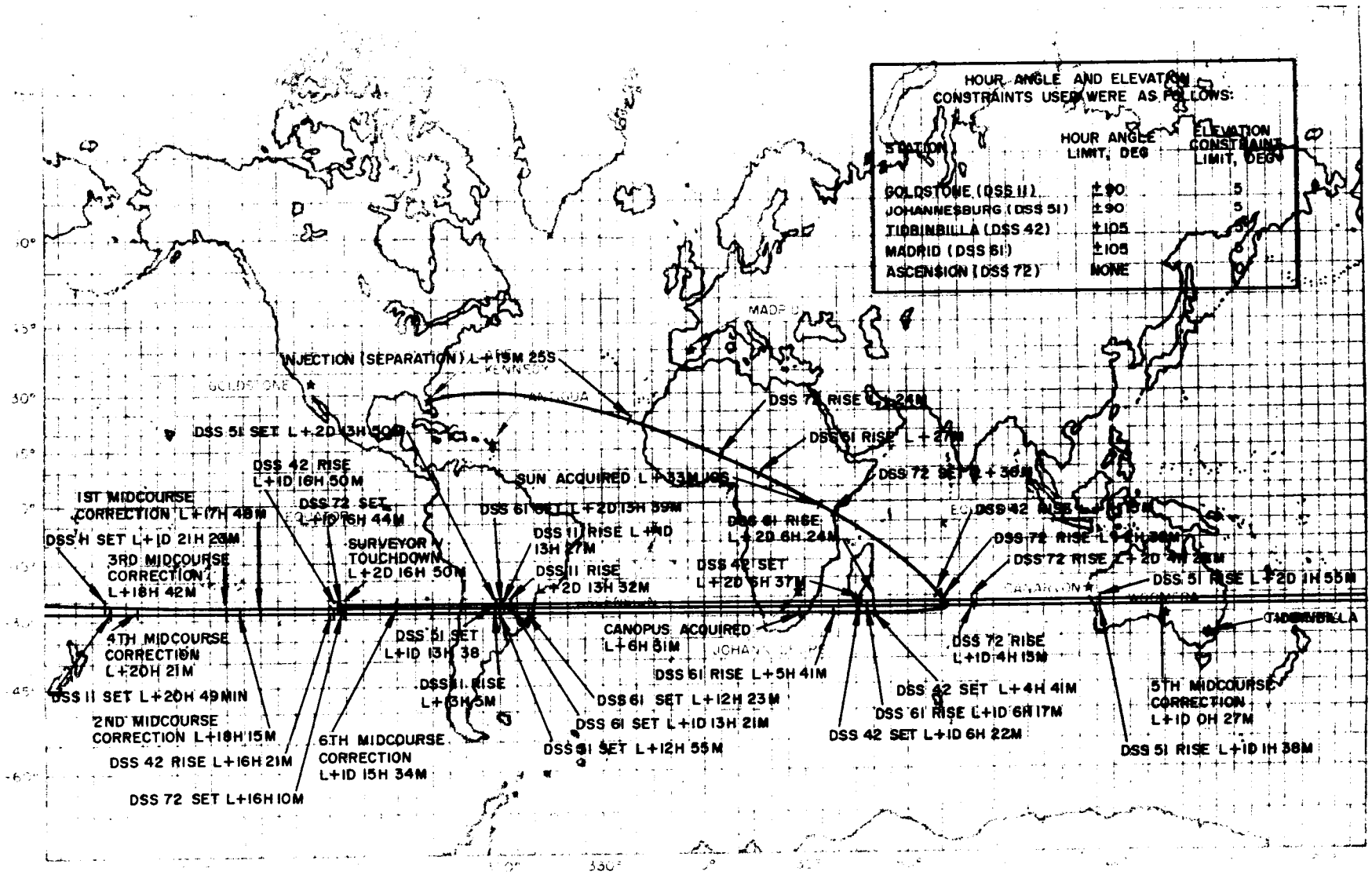

Figure 4-1. Surveyor V Earth Track

TABLE 4-2. PREDICTED VIEW PERIOD SUMMARY

Station	Event	GMT		
		September 1967	Hours	Minutes
DSS 72 Ascension	0 degree elevation rise	8	8	21
DSS 51 Johannesburg	5 degrees elevation rise	8	8	24
DSS 72 Ascension	0 degree elevation set	8	8	33
DSS 42 Tidbinbilla	5 degrees elevation rise	8	9	12
DSS 72 Ascension	0 degree elevation rise	8	10	29
DSS 42 Tidbinbilla	5 degrees elevation set	8	12	38
DSS 61 Madrid	5 degrees elevation rise	8	13	38
DSS 61 Madrid	5 degrees elevation set	8	20	20
DSS 51 Johannesburg	90 degrees hour angle set	8	20	52
DSS 11 Goldstone	5 degrees elevation rise	8	21	2
DSS 72 Ascension	0 degree elevation set	9	0	7
DSS 42 Tidbinbilla	5 degrees elevation rise	9	0	18
DSS 11 Goldstone	5 degrees elevation set	9	4	46
DSS 51 Johannesburg	270 degrees hour angle rise	9	9	35
DSS 72 Ascension	0 degree elevation rise	9	12	10

Table 4-2 (continued)

Station	Event	GMT		
		September 1967	Hours	Minutes
DSS 61 Madrid	5 degrees elevation rise	9	14	14
DSS 42 Tidbinbilla	5 degrees elevation set	9	14	19
DSS 61 Madrid	5 degrees elevation set	9	21	18
DSS 11 Goldstone	5 degrees elevation rise	9	21	24
DSS 51 Johannesburg	90 degrees hour angle set	9	21	35
DSS 72 Ascension	0 degree elevation set	10	0	41
DSS 42 Tidbinbilla	5 degrees elevation rise	10	0	47
DSS 11 Goldstone	5 degrees elevation set	10	5	20
DSS 51 Johannesburg	270 degrees hour angle rise	10	9	52
DSS 72 Ascension	0 degree elevation rise	10	12	25
DSS 61 Madrid	5 degrees elevation rise	10	14	21
DSS 42 Tidbinbilla	5 degrees elevation set	10	14	34
DSS 11 Goldstone	5 degrees elevation rise	10	21	29
DSS 61 Madrid	5 degrees elevation set	10	21	37
DSS 51 Johannesburg	90 degrees hour angle set	10	21	47

TABLE 4-3. SURVEYOR V COMMAND SEQUENCE

Command Number	Description	GMT, hr:min:sec	Telemetry Mode	Bit Rate
	Day 251 — DSS-51			
0107	Xmtr Hi Volt Off	08:36:59.8	5	550
0110	Xmtr Fil Pwr Off	37:06.8		
0130	Xfer Sw B Lo Pwr	37:07.3		
0236	A/D Iso Amp Off	42:20.7		
0316	SP Deploy Logic Off	42:21.2		
0126	Xfer Sw A Lo Pwr	42:21.7		
0402	Step SP Minus (x10)	43:27.7		
0401	Step SP Plus (x5)	43:35.7		
0405	Step Roll Axis Plus (x10)	44:24.9		
0406	Step Roll Axis Minus (x5)	44:25.4		
0510	AESP Off	45:32.7		
0226	Mode 1	45:38.7	1	
0237	Low Mod SCO's Off	46:50.2		
0216	7.35 kc SCO On	46:50.7		
0205	1100 bps	46:51.2		1100
0231	Mode 4	48:19.2	4	
0227	Mode 2	51:00.7	2	
0232	ESP Off	52:49.7		
0507	Mode 6	52:55.7	6	
0506	Mode 5	08:59:59.7	5	
0120	Select Omni A	12:19:01.7		
	Day 251 — DSS-61			
0510	AESP Off	13:47:45.8		
0231	Mode 4	47:54.3	4	
0227	Mode 2	51:16.0	2	
0226	Mode 1	54:12.2	1	
0105	Xmtr B Fil Pwr On	59:17.2		
0306	SP Sw On, Bypass Off	14:02:28.9		
0127	Xfer Sw B Hi Pwr	03:27.9		
0106	Xmtr Hi Volt On	03:28.4		
0121	Select Omni B	04:31.2		
0220	7.35 kc SCO Off	05:39.6		
0217	33 kc SCO On	05:40.1		
0206	4400 bps	05:40.6		4400
0704	Cruise Mode	08:52.1		
0715	Man Delay Mode	08:52.6		
0710	Pos Angle Maneuver	08:53.1		
0714	Sun and Roll	10:01.6		
0703	Sun-Star Acq Mode On	25:35.6		
0704	Cruise Mode	30:10.0		
0232	ESP Off	30:55.1		
0506	Mode 5	31:02.5	5	
0205	1100 bps	14:32:38.5		1100

Table 4-3 (continued)

Command Number	Description	GMT, hr:min:sec	Telemetry Mode	Bit Rate
0220	Hi Data Rate SCO's Off	14:32:39.0	5	1100
0216	7.35 Kc SCO On	32:39.5		
0107	Xmtr Hi Volt Off	33:41.0		
0110	Xmtr Fil Pwr Off	33:48.5		
0130	Xfer Sw B Lo Pwr	33:49.0		
0306	SP Sw On, Bypass Off	15:08:26.1		
	Day 251 — DSS-51			
0700	Inertial Mode	15:45:51.6		
0306	SP Sw On, Bypass Off	55:28.6		
0306	SP Sw On, Bypass Off	16:42:15.3		
0306	SP Sw On, Bypass Off	17:16:17.3		
0510	AESP Off	22:06.2		
0231	Mode 4	22:16.1	4	
0232	ESP Off	26:39.1		
0506	Mode 5	26:50.1	5	
0306	SP Sw On, Bypass Off	44:05.0		
0704	Cruise Mode	18:16:27.9		
0306	SP Sw On, Bypass Off	33:29.4		
0700	Inertial Mode	34:28.3		
0306	SP Sw On, Bypass Off	53:43.8		
0306	SP Sw On, Bypass Off	19:34:24.5		
0306	SP Sw On, Bypass Off	20:07:37.8		
0704	Cruise Mode	16:02.3		
0504	137.5 bps	18:09.8		137.5
0204	Coast Phase Clock Rates	18:20.3		
0220	7.35 Kc SCO Off	18:28.3		
0500	Coast Phase I SCO On	18:35.8		
	Day 251 — DSS-72			
0505	17.2 bps	20:43:01		17.2
0502	Coast Phase SCO's Off	43:12		
0501	Coast Phase II SCO On	43:26		
	Day 251 — DSS-11			
0306	SP Sw On, Bypass Off	21:38:54.6		
0502	Coast Phase SCOs Off	39:59.6		
0216	7.35 Kc SCO On	40:14.1		1100
0205	1100 bps	41:05.6		
0702	Sun Acq Mode On	43:57.6		
0510	AESP Off	47:47.6		
0231	Mode 4	47:56.1	4	
0227	Mode 2	53:24.1	2	
0226	Mode 1	56:43.0	1	
0232	ESP Off	22:00:58.0		
0506	Mode 5	01:05.5	5	
0704	Cruise Mode	23:40:33.1		

Table 4-3 (continued)

Command Number	Description	GMT, hr:min:sec	Telemetry Mode	Bit Rate
0510	AESP Off	23:41:38.0	5	1100
0231	Mode 4	41:45.0	4	
0227	Mode 2	45:46.3	2	
0226	Mode 1	48:46.3	1	
0232	ESP Off	53:48.4		
0506	Mode 5	53:55.4	5	
0220	33, 7.35, 3.9 kc SCOs Off	55:01.9		
0221	Gyro Spd Sig Pro On	55:14.4		
0222	Next Gyro	56:37.9		
0222	Next Gyro	57:26.9		
0222	Next Gyro	58:02.4		
0223	Gyro Spd Sig Pro Off	58:46.9		
0216	7.35 kc SCO On	58:56.9		
	Day 252 – DSS-11			
0510	AESP Off	00:59:38.6		
0231	Mode 4	59:44.6	4	
0227	Mode 2	01:02:42.0	2	
0226	Mode 1	05:55.5	1	
0105	Xmtr B Fil Pwr On	13:26.1		
0127	Xfer Sw B Hi Pwr	15:19.4		
0106	Xmtr Hi Volt On	15:19.9		
0220	37, 7.35, 3.9 Kc SCOs Off	15:55.9		
0217	33 Kc SCO On	15:56.4		
0206	4400 bps	15:56.9		4400
0704	Cruise Mode	25:11.0		
0710	Pos Angle Maneuver	25:11.5		
3617	Interlock	25:12.0		
M 1310	Magnitude (360 BCD) (+71.9 degrees)	25:12.5		
0714	Sun and Roll	32:57.0		
0702	Sun Acq Mode On	36:26.3		
3617	Interlock	36:26.8		
M 0523	Magnitude (179 BCD) (- 35.5 degrees)	36:27.3		
0713	Yaw	38:06.4		
0227	Mode 2	39:44.9	2	
0226	Mode 1	40:45.8	1	
0521	Prop S-Gage Pwr On	41:45.8		
0700	Inertial Mode	41:46.3		
0720	Reset – Set IV Outputs	41:58.3		
0604	AMR Htr Off	42:24.4		
0613	VL2 FT2 Ther Pwr Off	42:24.9		
0616	VL1 OT2 Ther Pwr Off	42:25.4		
0621	VL3 OT3 Ther Pwr Off	42:25.9		
3617	Interlock	01:42:26.4		

Table 4-3 (continued)

Command Number	Description	GMT hr:min:sec	Telemetry Mode	Bit Rate
0605	Unlk Roll Act, Press VPS	01:42:26.9	1	4400
0727	FC T-φ Pwr On	43:16.8		
3617	Interlock	43:30.9		
M 0417	Magnitude (143 BCD)	43:31.4		
3617	Interlock	45:01.8		
0721	Vernier Ignition No. 1	45:02.3		
0735	Emer Vernier Eng Off	45:19.3		
0735	Emer Vernier Eng Off	45:20.8		
0737	FC T-φ Pwr Off	45:34.3		
0737	FC T-φ Pwr Off	45:36.3		
0522	Prop S-Gage Pwr Off	45:55.3		
0516	TD S-Gage Pwr Off	45:55.8		
0232	ESP Off	46:27.8		
0506	Mode 5	46:34.3	5	
0611	VL2 Ther Pwr On	48:05.8		
0614	VL1 Ther Pwr On	48:06.3		
0617	VL3 Ther Pwr On	48:07.3		
0624	AMR Htr On	48:07.8		
0510	AESP Off	49:49.3		
0226	Mode 1	49:55.3	1	
0710	Pos Angle Maneuver	52:50.5		
3617	Interlock	52:51.0		
M 0523	Magnitude (179 BCD) (+35.5 degrees)	52:51.5		
0713	Yaw	53:50.9		
0702	Sun Acq Mode On	02:00:09.2		
3617	Interlock	01:03.2		
M 1310	Magnitude (360 BCD)	01:03.7		
0521	Prop S-Gage Pwr On	04:39.7		
0700	Inertial Mode	04:46.2		
0720	Reset Set IV Outputs	05:01.3		
0727	FC T-φ Pwr On	05:56.6		
3617	Interlock	07:39.2		
M 0305	Magnitude (101 BCD) (10.1 seconds)	07:39.7		
3617	Interlock	12:01.7		
0721	Vernier Ignition No 2	12:02.2		
0735	Emer Vernier Eng Off	12:14.3		
0735	Emer Vernier Eng Off	12:18.8		
0737	FC T-φ Pwr Off	12:39.4		
0522	Prop S-Gage Pwr Off	12:55.9		
0516	TD S-Gage Pwr Off	13:04.3		
0702	Sun Acq Mode On	15:49.1		
0232	ESP Off	17:44.1		
0506	Mode 5	17:48.6	5	
3617	Interlock	02:19:19.6		

Table 4-3 (continued)

Command Number	Description	GMT, hr:min:sec	Telemetry Mode	Bit Rate
M 3405	Magnitude (901 BCD) (-180. 1 degrees)	02:19:20. 1	5	4400
0510	AESP Off	20:18. 1		
0226	Mode 1	20:22. 6	1	
0713	Yaw	24:33. 0		
0521	Prop S-Gage Pwr On	33:29. 0		
0700	Inertial Mode	33:34. 0		
0720	Reset Set IV Outputs	33:40. 0		
0727	FC T-φ Pwr On	34:07. 5		
3617	Interlock	35:25. 6		
M 0707	Magnitude (231 BCD) (23. 1 seconds)	35:26. 1		
3617	Interlock	37:35. 4		
M 0721	Magnitude (sent by error)	37:35. 9		
0735	Emer Vernier Eng Off	38:00. 6		
0735	Emer Vernier Eng Off	38:02. 6		
3617	Interlock	38:39. 0		
M 0707	Magnitude (231 BCD) (23. 1 seconds)	38:39. 5		
3617	Interlock	39:50. 1		
0721	Vernier Ignition No 3	39:50. 6		
0735	Emer Vernier Eng Off	40:15. 5		
0735	Emer Vernier Eng Off	40:17. 0		
0737	FC T-φ Pwr Off	40:35. 0		
0737	FC T-φ Pwr Off	40:37. 0		
0522	Prop S-Gage Pwr Off	41:00. 1		
0516	TD S-Gage Pwr Off	41:04. 6		
3617	Interlock	44:35. 4		
M 3405	Magnitude (901 BCD) (+180. 1 degrees)	44:35. 9		
0713	Yaw	45:21. 9		
0702	Sun Acq Mode On	53:23. 5		
0205	1100 bps	54:55. 9		1100
0220	33, 7. 35, 3. 9 kc SCO Off	55:04. 4		
0216	7. 35 kc SCO On	55:11. 9		
0107	Xmtr Hi Volt Off	55:41. 4		
0110	Xmtr Fil Pwr Off	55:45. 9		
0130	Xfer Sw B Lo Pwr	55:50. 9		
0232	ESP Off	56. 49. 9		
0506	Mode 5	02:56:53. 9	5	
3617	Interlock	03:59:58. 6		
M 1310	Magnitude (360 BCD) (-71. 9 degrees)	59:59. 1		
0714	Sun and Roll	04:00:46. 5		
0704	Cruise Mode	04:18. 5		
0710	Pos Angle Maneuver	04:31. 0		
3617	Interlock	04:04:54. 6		

Table 4-3 (continued)

Command Number	Description	GMT, hr:min:sec	Telemetry Mode	Bit Rate
M 1227	Magnitude (343 BCD) (+68.5 degrees)	04:04:55.1	5	1100
0714	Sun and Roll	05:54.6		
3617	Interlock	08:44.5		
M 2026	Magnitude (534 BCD) (+106.7 degrees)	08:46.0		
0713	Yaw	09:33.0		
0510	AESP Off	13:38.4		
0226	Mode 1	13:43.9	1	
0521	Prop S-Gage Pwr On	14:20.4		
0700	Inertial Mode	14:34.9		
0720	Reset Set IV Outputs	15:03.9		
0715	Man Delay Mode On	15:22.9		
0727	FC T-φ Pwr On	16:14.5		
3617	Interlock	18:47.9		
0721	Vernier Ignition No 4A (12.1 seconds)	18:48.4		
0735	Emer Vernier Eng Off	19:00.5		
3617	Interlock	19:01.0		
0721	Vernier Ignition No 4B (0.5 second)	19:01.5		
0735	Emer Vernier Eng Off	19:02.0		
3617	Interlock	19:02.5		
0721	Vernier Ignition No 4C (0.5 second)	19:03.0		
0735	Emer Vernier Eng Off	19:03.5		
0735	Emer Vernier Eng Off	19:04.0		
0737	FC T-φ Pwr Off	19:22.5		
0737	FC T-φ Pwr Off	19:24.0		
0522	Prop S-Gage Pwr Off	19:49.5		
0516	TD S-Gage Pwr Off	04:19:53.5		
	Day 252 – DSS-42			
0700	Inertial Mode	04:56:37.5		
3617	Interlock	57:32.0		
M 2026	Magnitude (534 BCD) (-106.7 degrees)	57:32.5		
0713	Yaw	58:13.0		
0702	Sun Acq Mode On	05:03:00.5		
3617	Interlock	03:29.5		
M 1227	Magnitude (343 BCD) (-68.5 degrees)	03:30.0		
0714	Sun and Roll	04:10.5		
0704	Cruise Mode	07:51.1		
0227	Mode 2	26:43.7	2	
0231	Mode 4	05:32:52.3	4	

Table 4-3 (continued)

Command Number	Description	GMT, hr:min:sec	Telemetry Mode	Bit Rate
0232	ESP Off	05:43:56.4	4	1100
0506	Mode 5	44:02.4	5	
0136	Comp C Temp Cont On	46:47.7		
0604	AMR Htr Off	48:45.2		
1136	Sur Camera ETC On	50:45.2		
0510	AESP Off	06:05:45.7		
0231	Mode 4	05:53.2	4	
0226	Mode 1	15:27.3	1	
0231	Mode 4	29:11.8	4	
0232	ESP Off	38:15.8		
0506	Mode 5	38:23.8	5	
0135	Comp C Temp Cont Off	38:57.3		
1137	Sur Camera ETC Off	39:20.3		
0624	AMR Htr On	06:39:39.8		
0105	Xmtr B Fil Pwr On	07:47:18.7		
0127	Xfer Sw B Hi Pwr	49:24.6		
0106	Xmtr Hi Volt On	49:35.1		
0206	4400 bps	50:29.4		4400
0220	33, 7.35, 3.9 kc SCOs Off	51:14.6		
0217	33 kc SCO On	51:25.1		
0510	AESP Off	52:04.1		
0226	Mode 1	52:11.1	1	
0704	Cruise Mode	:53:04.6		
0710	Pos Angle Maneuver	53:30.1		
3617	Interlock	53:51.6		
M 1203	Magnitude (323 BCD) (+64.5 degrees)	53:52.1		
0714	Sun and Roll	54:30.1		
3617	Interlock	57:54.6		
M 2615	Magnitude (717 BCD) (+143.3 degrees)	57:55.1		
0713	Yaw	58:31.1		
0521	Prop S-Gage Pwr On	08:18:38.2		
0700	Inertial Mode	18:47.0		
0720	Reset Set IV Outputs	18:56.0		
0604	AMR Htr Off	19:45.0		
0613	VL2 FT2 Ther Pwr Off	19:56.0		
0616	VL1 OT2 Ther Pwr Off	20:04.2		
0621	VL3 OT3 Ther Pwr Off	20:12.2		
3617	Interlock	20:24.2		
0605	Unlk Roll Act, Press VPS	20:24.7		
0727	FC T-φ Pwr On	21:10.9		
3617	Interlock	22:34.2		
M 1213	Magnitude (331 BCD) (33.1 seconds)	22:34.7		
3617	Interlock	24:03.2		
0721	Vernier Ignition No 5	08:24:03.7		

Table 4-3 (continued)

Command Number	Description	GMT, hr:min:sec	Telemetry Mode	Bit Rate
0735	Emer Vernier Eng Off	08:24:38.2	1	4400
0737	FC T-φ Pwr Off	25:00.9		
0737	FC T-φ Pwr Off	25:01.9		
0522	Prop S-Gage Pwr Off	25:18.9		
0516	TD S-Gage Pwr Off	25:23.9		
0232	ESP Off	25:59.0		
0506	Mode 5	26:09.7	5	
0611	VL2 Ther Pwr On	28:42.7		
0614	VL1 Ther Pwr On	28:52.2		
0617	VL3 Ther Pwr On	29:04.2		
0624	AMR Htr On	29:11.2		
0510	AESP Off	29:58.2		
0226	Mode 1	30:04.2	1	
0700	Inertial Mode	32:15.7		
3617	Interlock	33:20.7		
M 2615	Magnitude (717 BCD) (-143.3 degrees)	33:21.2		
0713	Yaw	33:51.2		
0702	Sun Acq Mode On	39:26.7		
3617	Interlock	39:53.7		
M 1203	Magnitude (323 BCD) (-64.5 degrees)	39:54.2		
0714	Sun and Roll	40:35.2		
0704	Cruise Mode	44:26.7		
0205	1100 bps	45:23.7	1	1100
0220	33, 7.35, 3.9 KC SCOs Off	45:32.7		
0216	7.35 KC SCO On	45:42.7		
0107	Xmtr Hi Volt Off	46:51.2		
0110	Xmtr Fil Pwr Off	46:58.7		
0130	Xfer Sw B Lo Pwr	47:01.2		
0136	Comp C Temp Cont On	49:13.2		
0700	Inertial Mode	09:08:32.4		
0231	Mode 4	21:03.0	4	
0503	550 bps	22:00.4		550
0204	Coast φ Clk Rates	22:15.4		
0220	33, 7.35, 3.9 KC SCOs Off	22:23.4		
0215	3.9 KC SCO On	22:30.9		
0226	Mode 1	55:12.0	1	
0704	Cruise Mode	56:50.5		
0227	Mode 2	10:02:03.5	2	
0232	ESP Off	05:40.5		
0506	Mode 5	05:47.5	5	
0510	AESP Off	11:10.0		
0231	Mode 4	11:17.0	4	
0105	Xmtr B Fil Pwr On	31:21.6		
0127	Xfer Sw B Hi Pwr	33:18.6		
0106	Xmtr Hi Volt On	10:33:26.6		

Table 4-3 (continued)

Command Number	Description	GMT, hr:min:sec	Telemetry Mode	Bit Rate
0220	33, 7.35, 3.9 SCOs Off	10:34:43.6	4	550
0200	Low Mod SCO On	34:53.6		
0207	Pre Sum Amp On	35:03.1		
3501	Alpha Scat Pwr On	36:47.6		
3515	Alpha Det 1 and 2 Off	51:18.6		
3516	Proton Det 1 and 2 Off	51:28.6		
3512	Proton Det 3 and 4 Off	51:36.1		
3510	Calibration On	55:17.6		
3507	Alpha Det 1 On	59:19.2		
3515	Alpha Det 1 and 2 Off	11:02:18.4		
3517	Proton Det 1 On	02:33.2		
3523	Alpha Det 2 On	05:23.2		
3516	Proton Det 1 and 2 Off	05:33.2		
3513	Proton Det 2 On	05:42.7		
3507	Alpha Det 1 On	08:25.7		
3516	Proton Det 1 and 2 Off	08:34.4		
3522	Proton Det 3 On	08:44.5		
3512	Proton Det 3 and 4 Off	12:21.2		
3511	Proton Det 4 On	12:30.7		
3520	Calibration Off	15:31.7		
3517	Proton Det 1 On	15:40.7		
3513	Proton Det 2 On	15:50.4		
3522	Proton Det 3 On	15:58.7		
3502	Alpha Scat Pwr Off	27:43.2		
0237	Low Mod SCO Off	29:22.7		
0215	3.9 kc SCO On	29:30.8		
0107	Xmtr Hi Volt Off	30:20.4		
0110	Xmtr Fil Pwr Off	30:27.8		
0130	Xfer Sw B Lo Pwr	30:33.8		
0135	Comp C Temp Cont Off	31:50.4		
0226	Mode 1	32:50.8	1	
0700	Inertial Mode	39:31.3		
0232	ESP Off	44:17.8		
0506	Mode 5	44:25.3	5	
0510	AESP Off	47:09.8		
0226	Mode 1	11:47:16.8	1	
	Day 252 — DSS-51			
0232	ESP Off	12:54:44.6		
0506	Mode 5	54:53.7	5	
0510	AESP Off	59:46.2		
0226	Mode 1	59:54.2	1	
0704	Cruise Mode	13:15:28.6		
0702	Sun Acq Mode On	17:56.6		
0231	Mode 4	53:27.5	4	
0232	ESP Off	13:56:45.9		

Table 4-3 (continued)

Command Number	Description	GMT, hr:min:sec	Telemetry Mode	Bit Rate
0506	Mode 5	13:56:53.4	5	550
0510	AESP Off	14:01:06.4		
0227	Mode 2	01:16.9	2	
0226	Mode 1	04:17.7	1	
0232	ESP Off	15:02:25.6		
0506	Mode 5	02:33.6	5	
0704	Cruise Mode	08:09.0		
0700	Inertial Mode	10:41.0		
0510	AESP Off	11:28.0		
0226	Mode 1	11:36.5	1	
0231	Mode 4	16:04:27.2	4	
0232	ESP Off	17:00.2		
0506	Mode 5	17:07.7	5	
0510	AESP Off	24:23.6		
0226	Mode 1	16:24:32.1	1	
	Day 252 – DSS-61			
0232	ESP Off	17:12:20.2		
0506	Mode 5	12:26.2	5	
0510	AESP Off	15:23.1		
0226	Mode 1	15:28.6	1	
0704	Cruise Mode	18:08.1		
0700	Inertial Mode	59:58.5		
0232	ESP Off	18:00:32.4		
0506	Mode 5	00:36.4	5	
0510	AESP Off	11:12.7		
0231	Mode 4	11:17.2	4	
0226	Mode 1	16:03.2	1	
0227	Mode 2	19:09:56.3	2	
0232	ESP Off	12:46.9		
0506	Mode 5	12:51.4	5	
0510	AESP Off	16:17.8		
0226	Mode 1	16:21.8	1	
0231	Mode 4	20:00:59.0	4	
0232	ESP Off	05:25.7		
0506	Mode 5	05:30.2	5	
0510	AESP Off	09:48.9		
0226	Mode 1	09:54.4	1	
0704	Cruise Mode	10:23.4		
	Day 252 – DSS-51			
0700	Inertial Mode	59:04.8		
0232	ESP Off	59:44.4		
0506	Mode 5	20:59:50.4	5	

Table 4-3 (continued)

Command Number	Description	GMT, hr:min:sec	Telemetry Mode	Bit Rate
	Day 252 — DSS-11			
0704	Cruise Mode	21:48:51.5	5	550
0510	AESP Off	22:34:10.0		
0231	Mode 4	34:17.2	4	
0227	Mode 2	35:58.2	2	
0226	Mode 1	38:03.7	1	
0105	Xmtr B Fil Pwr On	23:04:17.6		
0127	Xfer SW B Hi Pwr	06:29.5		
0106	Xmtr Hi Volt On	06:30.0		
0220	33, 7.35, 3.9 kc SCOs Off	07:15.5		
0217	33 kc SCO On	07:16.0		
0206	4400 bps	07:16.5		4400
0704	Cruise Mode	12:17.5		
3617	Interlock	12:29.0		
M 1334	Magnitude (380 BCD) (-75.9 degrees)	12:29.5		
0714	Sun and Roll	13:51.0		
3617	Interlock	18:18.0		
M 1727	Magnitude (503 BCD) (-100.5 degrees)	18:19.0		
0713	Yaw	19:36.4		
0227	Mode 2	23:50.0	2	
0226	Mode 1	24:48.9	1	
0521	Prop S-Gage Pwr On	25:12.0		
0700	Inertial Mode	25:19.9		
0720	Reset Set IV Outputs	25:20.4		
1134	Sur Camera VTC Off	25:44.1		
0604	AMR Htr Off	25:44.6		
0613	VL2 FT2 Ther Pwr Off	25:45.1		
0616	VL1 OT2 Ther Pwr Off	25:45.6		
0621	VL3 OT3 Ther Pwr Off	25:46.1		
3617	Interlock	25:46.6		
0605	Unlk Roll Act, Press VPS	25:47.1		
0727	FC T-φ Pwr On	26:06.5		
3617	Interlock	27:37.3		
M 0315	Magnitude	27:37.8		
3617	Interlock	29:22.5		
M 0127	Magnitude (55 BCD) (5.5 seconds)	29:23.0		
3617	Interlock	30:57.5		
0721	Vernier Ignition No 6	30:58.0		
0735	Emer Vernier Eng Off	31:06.0		
0735	Emer Vernier Eng Off	31:07.0		
0522	Prop S-Gage Pwr Off	31:23.0		
0737	FC T-φ Pwr Off	31:29.0		
0737	FC T-φ Pwr Off	23:31:30.5		

Table 4-3 (continued)

Command Number	Description	GMT, hr:min:sec	Telemetry Mode	Bit Rate
0232	ESP Off	23:32:16.5	1	4400
0506	Mode 5	32:23.9	5	
0611	VL2 Ther Pwr On	33:19.0		
0614	VL1 Ther Pwr On	33:29.9		
0617	VL2 Ther Pwr On	33:40.3		
0624	AMR Htr On	33:48.9		
0710	Pos Angle Maneuver	35:01.3		
3617	Interlock	35:10.4		
M 1727	Magnitude (503 BCD) (+100.5 degrees)	35:10.9		
0713	Yaw	36:07.0		
0516	TD S-Gage Pwr Off	41:01.6		
0702	Sun Acq Mode On	42:11.5		
0710	Pos Angle Maneuver	43:02.8		
3617	Interlock	43:10.9		
M 1334	Magnitude (380 BCD) (+75.9 degrees)	43:11.4		
0714	Sun and Roll	44:04.9		
0704	Cruise Mode	49:06.7		
0510	AESP Off	49:41.8		
0227	Mode 2	49:52.8	2	
0503	550 bps	50:46.7		550
0204	Coast φ Clk Rates	50:47.2		
0220	33, 7.35, 3.9 kc SCOs Off	50:48.2		
0215	3.9 kc SCO On	50:48.7		
0107	Xmtr Hi Volt Off	51:34.8		
0110	Xmtr Fil Pwr Off	51:41.3		
0130	Xfer Sw B Lo Pwr	51:41.8		
0231	Mode 4	54:06.3	4	
0232	ESP Off	56:46.8		
0506	Mode 5	56:54.3	5	
	Day 253 — DSS-11			
0510	AESP Off	00:07:48.3		
0226	Mode 1	07:54.8	1	
0232	ESP Off	01:16:00.6		
0506	Mode 5	16:06.6	5	
0510	AESP Off	21:59.6		
0231	Mode 4	22:04.6	4	
0227	Mode 2	27:36.3	2	
0226	Mode 1	34:17.2	1	
0700	Inertial Mode	35:18.7		
0232	ESP Off	58:24.1		
0506	Mode 5	58:32.6	5	
0510	AESP Off	02:02:27.1		
0231	Mode 4	02:02:36.1	4	

Table 4-3 (continued)

Command Number	Description	GMT, hr:min:sec	Telemetry Mode	Bit Rate
0226	Mode 1	02:06:51.5	1	550
0232	ESP Off	46:24.9		
0506	Mode 5	46:33.8	5	
	Day 253 – DSS-42			
0510	AESP Off	03:16:12.2		550
0231	Mode 4	16:20.2	4	
0227	Mode 2	23:36.2	2	
0226	Mode 1	30:14.7	1	
0704	Cruise Mode	04:33:03.4		
0232	ESP Off	34:11.4		
0506	Mode 5	34:20.4	5	
0510	AESP Off	42:40.4		
0231	Mode 4	42:49.4	4	
0227	Mode 2	51:52.0	2	
0226	Mode 1	58:35.5	1	
0232	ESP Off	06:05:35.7		
0506	Mode 5	05:46.2	5	
0510	AESP Off	13:11.7		
0231	Mode 4	13:21.7	4	
0615	OT2 Ther Pwr On	20:07.8		
0227	Mode 2	20:57.9	2	
0226	Mode 1	24:36.7	1	
0232	ESP Off	07:08:14.9		
0506	Mode 5	08:23.9	5	
0510	AESP Off	14:22.4		
0231	Mode 4	14:32.9	4	
0227	Mode 2	17:41.4	2	
0226	Mode 1	20:30.1	1	
0232	ESP Off	08:14:37.6		
0232	ESP Off	16:08.6		
0506	Mode 5	16:18.1	5	
0510	AESP Off	22:35.1		
0231	Mode 4	22:45.1	4	
0227	Mode 2	28:26.1	2	
0226	Mode 1	30:16.6	1	
0232	ESP Off	09:17:35.8		
0506	Mode 5	17:43.8	5	
0510	AESP Off	23:00.8		
0231	Mode 4	23:12.3	4	
0504	137.5 bps	25:11.8		137.5
0503	550 bps	27:56.3		550
0227	Mode 2	30:29.3	2	
0226	Mode 1	32:46.3	1	
0232	ESP Off	10:16:42.0		

Table 4-3 (continued)

Command Number	Description	GMT, hr:min:sec	Telemetry Mode	Bit Rate
0506	Mode 5	10:16:51.4	5	550
0510	AESP Off	28:36.5		
0231	Mode 4	28:46.5	4	
0227	Mode 2	30:34.0	2	
0226	Mode 1	32:16.6	1	
0232	ESP Off	11:38:13.2		
0506	Mode 5	38:22.2	5	
0510	AESP Off	41:07.2		
0231	Mode 4	41:16.7	4	
0227	Mode 2	42:51.7	2	
0226	Mode 1	44:25.2	1	
	Day 253 – DSS-51			
0232	ESP Off	12:52:29.0		
0506	Mode 5	52:35.9	5	
0510	AESP Off	56:55.2		
0231	Mode 4	57:01.7	4	
0227	Mode 2	59:37.4	2	
0226	Mode 1	13:04:23.3	1	
0702	Sun Acq Mode On	05:03.3		
0411	Comp A Htr Pwr On	31:01.8		
0232	ESP Off	14:05:44.0		
0506	Mode 5	05:51.5	5	
0510	AESP Off	11:25.0		
0231	Mode 4	11:32.5	4	
0227	Mode 2	15:06.0	2	
0226	Mode 1	18:53.0	1	
0232	ESP Off	15:09:54.7		
0506	Mode 5	10:00.7	5	
0510	AESP Off	14:18.5		
0231	Mode 4	14:33.7	4	
0227	Mode 2	20:16.7	2	
0226	Mode 1	22:33.7	1	
0704	Cruise Mode	24:13.2		
0700	Inertial Mode	27:08.1		
0232	ESP Off	16:17:24.4		
0506	Mode 5	17:32.9	5	
0510	AESP Off	23:23.7		
0231	Mode 4	23:33.4	4	
0227	Mode 2	26:25.9	2	
0226	Mode 1	30:13.8	1	
0232	ESP Off	17:24:58.8		
0506	Mode 5	25:05.3	5	
0510	AESP Off	29:21.5		
0231	Mode 4	29:28.0	4	
0227	Mode 2	17:34:32.5	2	

Table 4-3 (continued)

Command Number	Description	GMT, hr:min:sec	Telemetry Mode	Bit Rate
0226	Mode 1	17:37:33.0	1	550
0136	Comp C Temp Cont On	43:57.0		
0704	Cruise Mode	59:42.4		
0710	Pos Angle Maneuver	18:10:36.8		
3617	Interlock	11:18.8		
M 3404	Magnitude (900 BCD) (+180 degrees)	11:19.3		
0713	Yaw	12:15.8		
3617	Interlock	22:09.8		
M 3405	Magnitude (901 BCD) (+180 degrees)	22:10.3		
0713	Yaw	22:51.6		
0704	Cruise Mode	30:13.5		
0232	ESP Off	32:02.7		
0506	Mode 5	32:09.2	5	
0510	AESP Off	37:00.2		
0231	Mode 4	37:07.2	4	
0227	Mode 2	56:26.6	2	
0226	Mode 1	19:01:01.1	1	
0232	ESP Off	31:28.5		
0506	Mode 5	31:37.4	5	
0510	AESP Off	35:03.4		
0231	Mode 4	35:11.4	4	
1136	Sur Camera ETC On	37:25.4		
0227	Mode 2	41:51.4	2	
0226	Mode 1	49:00.8	1	
0231	Mode 4	20:12:33.7	4	
3503	Alpha Scat Htr Pwr On	29:52.1		
0226	Mode 1	39:57.8	1	
0232	ESP Off	21:15:50.5		
0506	Mode 5	15:58.5	5	
	Day 253 – DSS-11			
0510	AESP Off	51:06.9		
0231	Mode 4	51:14.4	4	
0227	Mode 2	56:06.3	2	
0226	Mode 1	59:07.8	1	
0232	ESP Off	22:01:30.9		
0506	Mode 5	01:39.3	5	
0510	AESP Off	32:48.7		
0231	Mode 4	32:56.1	4	
0227	Mode 2	34:20.9	2	
0226	Mode 1	36:20.6	1	
0232	ESP Off	38:32.1		
0506	Mode 5	38:39.6	5	
0220	33, 7.35, 3.9 kc SCOs Off	22:45:19.6		

Table 4-3 (continued)

Command Number	Description	GMT, hr:min:sec	Telemetry Mode	Bit Rate
0221	Gyro Spd Sig Pro On	22:45:29.6	5	550
0222	Next Gyro	46:29.6		
0222	Next Gyro	49:28.5		
0222	Next Gyro	50:13.5		
0223	Gyro Spd Sig Pro Off	50:44.0		
0215	3.9 kc SCO On	50:54.5		
0124	Xpdr Pwr Off	53:47.4		
0123	Xpdr B Pwr On	55:32.5		
0413	Comp A Htr Pwr Off	23:40:34.3		
1133	Sur Camera VTC On	41:26.8		
0507	Mode 6	42:21.7	6	
0510	AESP Off	44:32.9		
0231	Mode 4	44:40.2	4	
0105	Xmtr B Fil Pwr On	49:57.7		
0127	Xfer Sw B Hi Pwr	51:40.8		
0106	Xmtr Hi Volt On	51:41.3		
0220	33, 7.35, 3.9 kc SCOs Off	52:17.7		
0216	7.35 kc SCO On	52:18.2		
0205	1100 bps	52:18.7		1100
0214	Sum Amps Off	54:39.7		
0211	Phase Sum Amp B On	54:40.2		
0227	Mode 2	55:23.7	2	
0226	Mode 1	57:05.2	1	
0232	ESP Off	59:06.2		
0506	Mode 5	23:59:13.2	5	
	Day 254 – DSS-11			
0521	Prop S-Gage Pwr On	00:00:31.4		
0515	TD S-Gage Pwr On	03:07.6		
0517	TD S-Gage D-Ch On	03:08.1		
0124	Xpdr Pwr Off	04:21.1		
0704	Cruise	08:57.9		
0710	Pos Angle Maneuver	08:58.4		
3617	Interlock	08:58.9		
M 1322	Magnitude (370 BCD) (+73.8 degrees)	08:59.4		
0714	Sun and Roll	12:15.1		
3617	Interlock	15:24.6		
M 2226	Magnitude (598 BCD) (+119.6 degrees)	15:25.1		
0713	Yaw	16:20.5		
0207	Pre Sum Amp On	21:38.0		
0722	Select Nom Thr Bias	23:18.5		
3617	Interlock	24:48.3		
M 0727	Retro Seq Delay (247 BCD) (12.3 seconds)	00:24:48.8		

Table 4-3 (continued)

Command Number	Description	GMT, hr:min:sec	Telemetry Mode	Bit Rate
0507	Mode 6	00:30:07.5	6	1100
0720	Reset Set IV Outputs	31:54.5		
3617	Interlock	38:56.4		
0724	Retro Seq Mode On	38:56.9		
0613	VL2 FT2 Ther Pwr Off	39:11.4		
0616	VL1 OT2 Ther Pwr Off	39:12.4		
0621	VL3 OT3 Ther Pwr Off	39:12.9		
1134	Sur Camera VTC Off	39:13.4		
1137	Sur Camera ETC Off	39:13.9		
0604	AMR Htr Off	39:14.4		
0135	Comp C Temp Cont Off	39:15.4		
3504	Alpha Scat Htr Off	39:15.9		
0625	AMR Pwr On	40:00.4		
0727	FC T-φ Pwr On	41:00.4		
0626	Enable AMR	43:00.9		
0730	Emer AMR Signal	44:43.9		
0732	Emer Retro Eject	45:37.9		
0725	Vernier Eng Hi Thrust	45:38.4		
0733	Emer Start Pgrmd Thrust	45:39.9		
0737	FC T-φ Pwr Off	47:39.4		
0737	FC T-φ Pwr Off	47:40.9		
3617	Interlock	48:24.3		
0630	RADVS Pwr Off	48:24.8		
3617	Interlock	48:25.3		
0630	RADVS Pwr Off	48:25.8		
3617	Interlock	48:26.3		
0311	All FC Pwr Off	48:27.3		
3617	Interlock	48:27.8		
0311	All FC Pwr Off	00:48:28.3		

4.1.2 Prelaunch Countdown

Until the T-5M hold on GMT day 251, there was just one suspected anomaly, which was reported. At T-35M, it was noted that the receiver A signal level was varying $\approx$ 100 BCD while receiver B signal level was steady. This problem was resolved when AFETR personnel were able to show that the signal became steady when the ground antenna (through which the launch team was communicating with the spacecraft) was moved. The countdown proceeded normally until T-5M, when the built-in 10-minute hold was extended for 18 minutes because of an unstable condition in the Atlas propellant utilization system, resulting in a liftoff from pad 36-B on 251:07:57:01.257 GMT at a launch azimuth of 79.517 degrees.

Performance values for transit flight are summarized in Table 3-2.

4.1.3 Launch, Injection, and Separation

The parking orbit boost phase was normal, with the Atlas roll and pitch programs and the normal opening and closing of the spacecraft inertia switch being confirmed by spacecraft telemetry. Figure 4-2 shows the major events of the trajectory through separation as seen in profile. Table 4-4 contains Atlas/Centaur mark events as well as spacecraft telemetry verification of Centaur-initiated commands. Subsequent to injection and just prior to its separation from the spacecraft, the Centaur issued the preprogrammed commands "extend landing gears," "extend omni antennas," and "transmitter high power on," all of which are verified by spacecraft telemetry. Separation of Centaur and Surveyor occurred immediately thereafter.

Following separation, solar panel stepping was initiated, the cold gas jets were enabled, and the roll-yaw sequence to acquire the sun was initiated. The poor quality of data prevented effective monitoring of the solar panel stepping and the spacecraft maneuvers to acquire the sun. Verification of solar-panel-axis stepping to the transit position, A/SPP roll-axis stepping to the transit position, and achievement of sun lock on were finally accomplished.

4.1.4 DSIF Acquisition

At 251:08:24:25 GMT, the spacecraft became visible to DSS 51 (Johannesburg), which achieved one-way lock at this time. At 251:08:30:11 GMT, the acquisition was completed when two-way lock was established between DSS 51 and the spacecraft.

The first ground-controlled sequence (initial spacecraft operations) was initiated at L+39M59S by commanding off the transmitter high voltage and filament power. In addition, commands were sent to the spacecraft to turn off other equipment required only for the launch-to-DSIF-acquisition phase (e.g., solar panel deployment logic off and A/D isolation amplifier off), to seat the solar panel and roll axis locking pins securely (i.e., by rocking the axes back and forth), to switch from the 550 bps-low-modulation-index mode to the 1100 bps-normal-modulation-index mode, and to interrogate

68189-5-106(U)

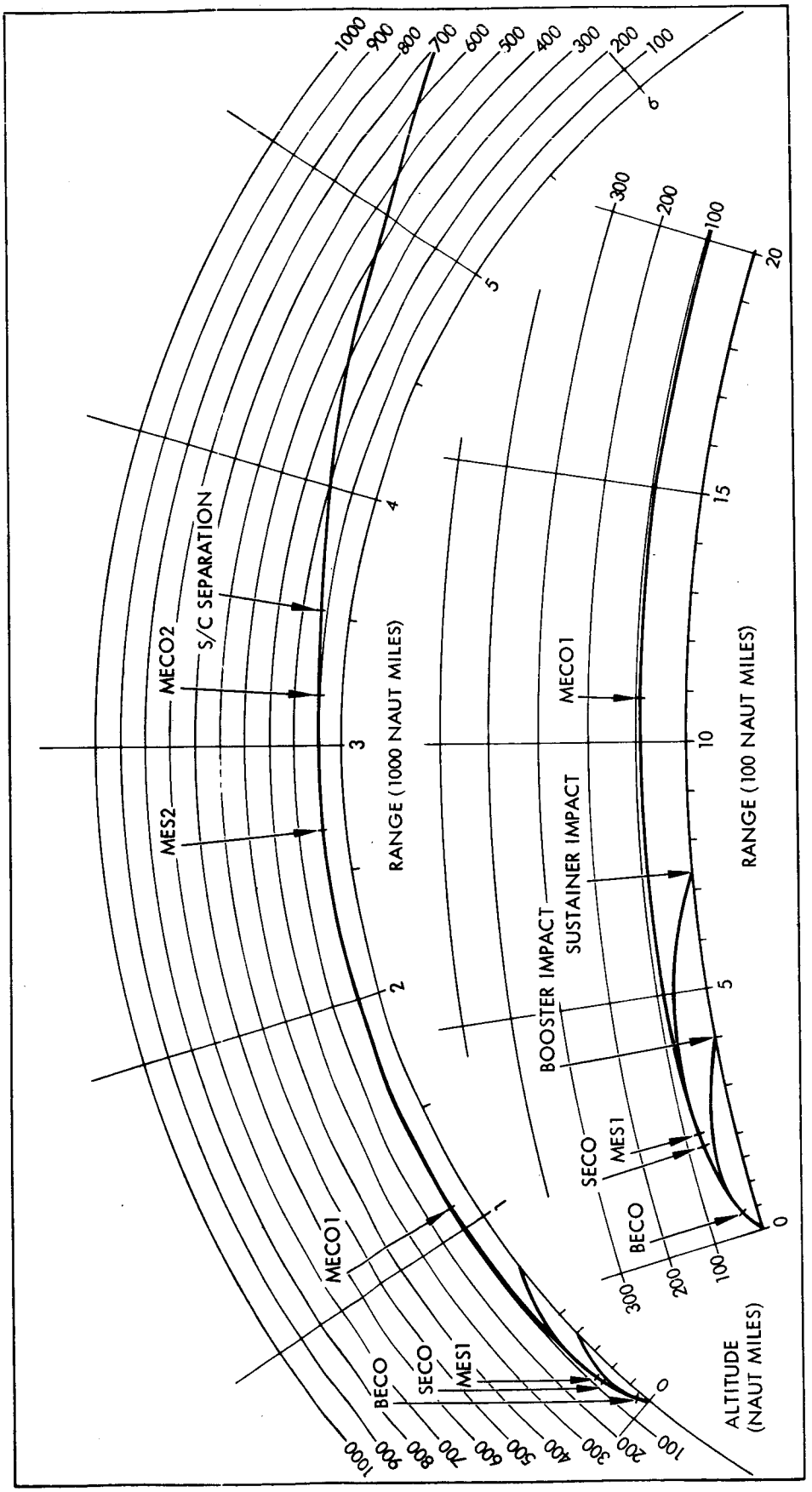

Figure 4-2. AC-13 Launch Phase Trajectory Profile

TABLE 4-4. LIFTOFF AND BOOST EVENTS

Launch Vehicle Mark Number	Event	Actual Time, GMT, hr:min:sec	Actual Time From Launch, seconds	Nominal Time From Launch, seconds	Nominal Time From Separation, seconds
	Liftoff (2-inch motion)	07:57:01.257	0.0	0.0	
1	Atlas boost engine cutoff (BECO)	07:59:34.65	153.4	153.5	
2	Atlas boost engine jettison	07:59:38.05	156.8	156.6	
3	Centaur insulation panel jettison	08:00:19.65	198.4	198.5	
4	Centaur nose fairing jettison	08:00:49.9	228.6	228.5	
5	Atlas SECO and VECO	08:01:07.7	246.4	248.2	
6	Atlas/Centaur separation	08:01:10	248.7	250.2	
7	Centaur main engine start (1)	08:01:20.3	259.0	259.7	
8	Centaur main engine cutoff (1)	08:06:48.3	587.0	579.2	
–	Centaur burn duration (1)	–	(328.0)	(319.5)	
9	100-pound thrust on	08:06:51.3	590.0	579.2	
10	100-pound thrust off	08:08:15.2	673.9	655.6	
11	6-pound thrust on	08:08:06	664.7	655.6	
12	100-pound thrust on	NA	NA	946.5	-216.0
13, 14	Centaur main engine start (2)	08:13:32.2	990.9	986.5	-176.0
15	Centaur main engine cutoff (2)	08:15:25.2	1103.9	1099.4	-63.1
–	Centaur burn duration (2)	–	(113.0)	(112.9)	
16	Extend landing gear command	08:15:45.5	1124.2	1120.5	-42.0
–	Legs down (telemetry)	08:15:47.8±1.2	1126.5		
17	Unlock omnidirectional antenna command	08:15:55.7	1134.4	1131.0	-31.5
–	Omnis extended (telemetry)	08:15:56.8±0.2	1135.5		
18	Surveyor high power transmitter on	08:16:16.0	1154.7	1146.0	-11.0
–	High power on (telemetry)	08:16:16.0±1.2	1154.7		
19	Centaur/Surveyor electrical disconnect	08:16:22.2	1160.9	1157.0	-5.5
–	Vehicle electrical separation (telemetry)	08:16:21.34±0.03	1160.0		
20	Spacecraft separation	08:16:26.8	1165.5	1162.5	0.0
21	Begin Centaur turn around maneuver	08:17:29.8	1228.5	1167.5	5.0
22	Start Centaur lateral thrust	NA	NA	1207.5	45.0
23	End Centaur lateral thrust	NA	NA	1227.5	65.0
24	Start Centaur tank blowdown	08:20:26.8	1405.5	1402.5	240.0
25	End Centaur tank blowdown	08:24:37.2	1655.9	1652.5	490.0
26	Power changeover switch	08:26:16.5	1755.2	1752.5	590.0

telemetry commutator modes so that the overall condition of the spacecraft could be assessed. All spacecraft responses to commands were normal.

During the period when the initial spacecraft operations sequences were being executed, two particles passed through the field of view of the Canopus sensor. Therefore, it was decided that the cruise mode on command should be delayed. Also, it was determined that there would be no need to implement the "if-required" sequence for turning on transponder A for permitting receiver A to lock on to the ground transmitter signal since the receiver was already tracking the signal in the AFC mode.

4.1.5 Coast Phase I Including Canopus Acquisition

The spacecraft continued to coast normally with its pitch-yaw attitude controlled to track the sun and with its roll axis held inertially fixed. Tracking and telemetry data were being obtained by the use of transmitter B operating in low power in the transponder mode.

At L+4H3M, both DSS 51 and DSS 42 reported poor data quality and a relatively low signal level ($\approx$ -138 dbm). This was attributed to the spacecraft roll orientation being such that the earth/spacecraft vector was in a null region of omnidirectional antenna B (since the spacecraft was not yet locked on to Canopus). At this point, two alternatives were possible: 1) switching spacecraft transmission to omnidirectional antenna A or 2) commanding a lower spacecraft data transmission rate. At L+4H22M01S, the command was sent to switch spacecraft transmission to omnidirectional antenna A. The signal strength rose to -125 dbm, and the quality of the data improved.

The pre-star verification engineering interrogation was initiated at L+5H50M54S. During the interrogation of mode 4, the solar panel switch tripped off since the battery voltage had built up to over 27 volts. It was recommended that time (approximately 15 minutes) be allowed to permit the battery to discharge until the battery voltage decreased below the solar panel switch trip level. Interrogation of modes 2 and 1 was normal, and transmitter B filament power was turned on at L+6H2M16S. At L+6H5M28S, the solar panel switch was commanded back on. Transmitter B high voltage and switching to omnidirectional antenna B were commanded at L+6H6M27S and 6H7M30S. Switching to omnidirectional antenna B resulted in a decrease in signal level of approximately 20 db, verifying that the earth/spacecraft vector was still in a deep null of omnidirectional antenna B.

The spacecraft roll sequence for obtaining the star map and for locking on to Canopus was initiated at L+6H13M01S. During the star map revolution, star intensity signals from 10 stars (Table 4-5) in addition to Canopus, and a strong earth signal were identified. Canopus was recognized after 179 degrees of roll. Automatic Canopus acquisition was accomplished at 251:14:27:52 GMT after some 539.4 degrees of roll. The vehicle returned to coasting with its roll attitude being controlled so that its star sensor remained locked to Canopus.

Coast mode data were transmitted continuously at 1100 bps via transmitter B operating in the transponder mode until L+9H25M3S when a special mode 4 interrogation was initiated to obtain alpha scattering sensor head and electronic temperatures (which are only available in mode 4). During this interval, the solar panel switch tripped five more times and had to be commanded back on. The spacecraft was commanded to switch back to its transmission of coast mode data at L+9H29M37S. It was necessary to reduce the spacecraft data rate initially from 1100 to 137.5 bps and then to 17.2 bps to permit DSS 72 (which was the only station having visibility of the spacecraft) to obtain satisfactory data. The data rate was later increased to 1100 bps when DSS 11 acquired the spacecraft.

In the period from the return to coast mode data until midcourse, the solar panel switch tripped six more times, requiring the switch to be commanded back on repeatedly. Coast mode data were transmitted at all times during this interval except for engineering interrogations of modes 4, 2, and 1 (the latter two being the premidcourse interrogations) and the premidcourse gyro speed check (at L+15H58M12S). Two three-axis gyro drift checks and one roll-only drift check were also made during this phase.

4.1.6 Midcourse Corrections

A number of midcourse corrections were executed during the transit phase of Surveyor V to 1) correct lunar impact conditions, 2) attempt to reseat the leaky helium valve, 3) burn off propellant to reduce the main retro burnout velocity, and 4) increase gas volume in the propellant tanks so that maximum propellant could be expelled in the terminal phase. Six corrections were made, with only the first and last corrections based upon orbit determination. A description of each maneuver and rationale follows:

1) The first correction was computed to correct the transit phase trajectory provided by the Atlas/Centaur boost vehicle to allow touchdown at the desired mission aim point. The maneuver was based upon 16 hours of tracking and consisted of a 14.25-second engine burn.

2) The second correction was executed 22 minutes later as an emergency attempt to reseat the leaky helium valve observed following the first correction. As time was critical, the engines were ignited while the spacecraft was locked upon the sun. The engine burn of 10.05 seconds moved the spacecraft impact point from the desired site to the east 1600 km. The new impact location would have been 2.89°N, 77.52°E, with an unbraked impact angle of 81.5 degrees.

TABLE 4-5. DESCRIPTION OF SURVEYOR V STAR MAP

Roll Angle From Start of Maneuver, degrees	Object in Star Sensor Field of View	Angle From Canopus, degrees	
		Actual	Preflight Prediction
0	(Start of roll)	-179.8	
65.7	Zeta Ophiuchi	-114.1	-113.9
82.2	Antares/ Tau Scorpii	- 97.6	- 97.81 - 96.3
88.9	Object 1	- 91.0	—
91.9	Object 2	- 87.9	—
125.6	Gamma Tr Australis	- 54.3	- 54.1
179.8	Canopus		
215.8	Alpha Leporis	35.9	36.4
233.8	Alnitak/ Alnilam/ Mintaka	53.9	52.01 52.91 53.9
240.4	Bellatrix	60.5	60.7
267.1	Earth	87.3	88
323.8	Polaris	144.0	144.2
425.8	Zeta Ophiuchi	246.0	246.1
442.2	Antares/ Tau Scorpii	262.4	262.21 263.7
448.5	Object 1	268.7	—
485.2	Gamma Tr Australis	305.4	305.9
539.4	Canopus		

3) The third correction was made 27 minutes later as an additional attempt to reseat the helium valve. To prevent compounding the landing site error, the spacecraft was yawed -180 degrees and the engines were then ignited for 23.05 seconds. This resulting delta velocity, directly away from the sun, moved the spacecraft impact point 2685 km to the west, past the original target point and into lunar night. The impact point was then 0.86°N, 347.99°E, with an unbraked impact angle of 20.7 degrees.

4) The fourth midcourse correction was executed 1 hour, 39 minutes later as an attempt to a) reseat the leaky helium valve, b) burn off propellant to reduce retro burnout velocity, and c) return to the original target point. A new trajectory was calculated that included flight path changes due to the first midcourse, the sunline midcourse, and the anti-sunline midcourse. The new trajectory was then used to determine a critical plane velocity, to null miss, of 8.30 m/sec which was combined with a +11.0 m/sec noncritical velocity component to increase time of flight and reduce burnout velocity. The total correction was determined to be 13.81 m/sec (14.09 seconds of burn). The actual correction, modified in an attempt to reseat the helium valve, was conducted as a 12.0-second burn followed by two 0.5-second burns at 1-second intervals.

5) The fifth correction was executed 4 hours, 6 minutes later to further reduce the retro burnout velocity and maximize usable propellant in the terminal phase by increasing gas volume in the propellant tanks. The spacecraft was reoriented to allow the delta velocity to be directed toward the positive noncritical direction so as to not significantly change the lunar impact point but reduce the impact and retro burnout velocities. The engines were burned for 33.0 seconds following a roll-yaw rotation sequence.

6) The sixth and final midcourse correction was conducted 15 hours, 7 minutes later and was based on 13 hours of tracking. This correction was used to a) adjust spacecraft weight and burnout velocity and further increase gas volume to optimal values, and b) correct a 267-km residual miss from mountainous terrain to the original target point. The critical plane velocity required to correct the miss was determined to be 3.87 m/sec, and the noncritical component (used to adjust terminal parameters) was calculated to be +3.6 m/sec. The total delta velocity added to the spacecraft was then 5.32 m/sec (an engine burn of 5.45 seconds). This maneuver resulted in a soft touchdown at 1.50°N, 23.19°E, approximately 30 km from the original target point.

Figure 4-3 shows the various impact points on the lunar surface following earth injection and each maneuver. Table 4-6 gives maneuver times, rotations, burn times, resulting impact points, and unbraked impact angles.

4.1.7 Coast Phase II

In addition to the normal spacecraft operations in the second coast phase, the alpha scattering instrument was operated successfully for calibration purposes. Some twelve gyro drift checks were performed during transit to provide accurate gyro rates for terminal operations planning. The gyro drift rates were: roll (+0.85 deg/hr), pitch (+0.60 deg/hr), and yaw (-0.60 deg/hr).

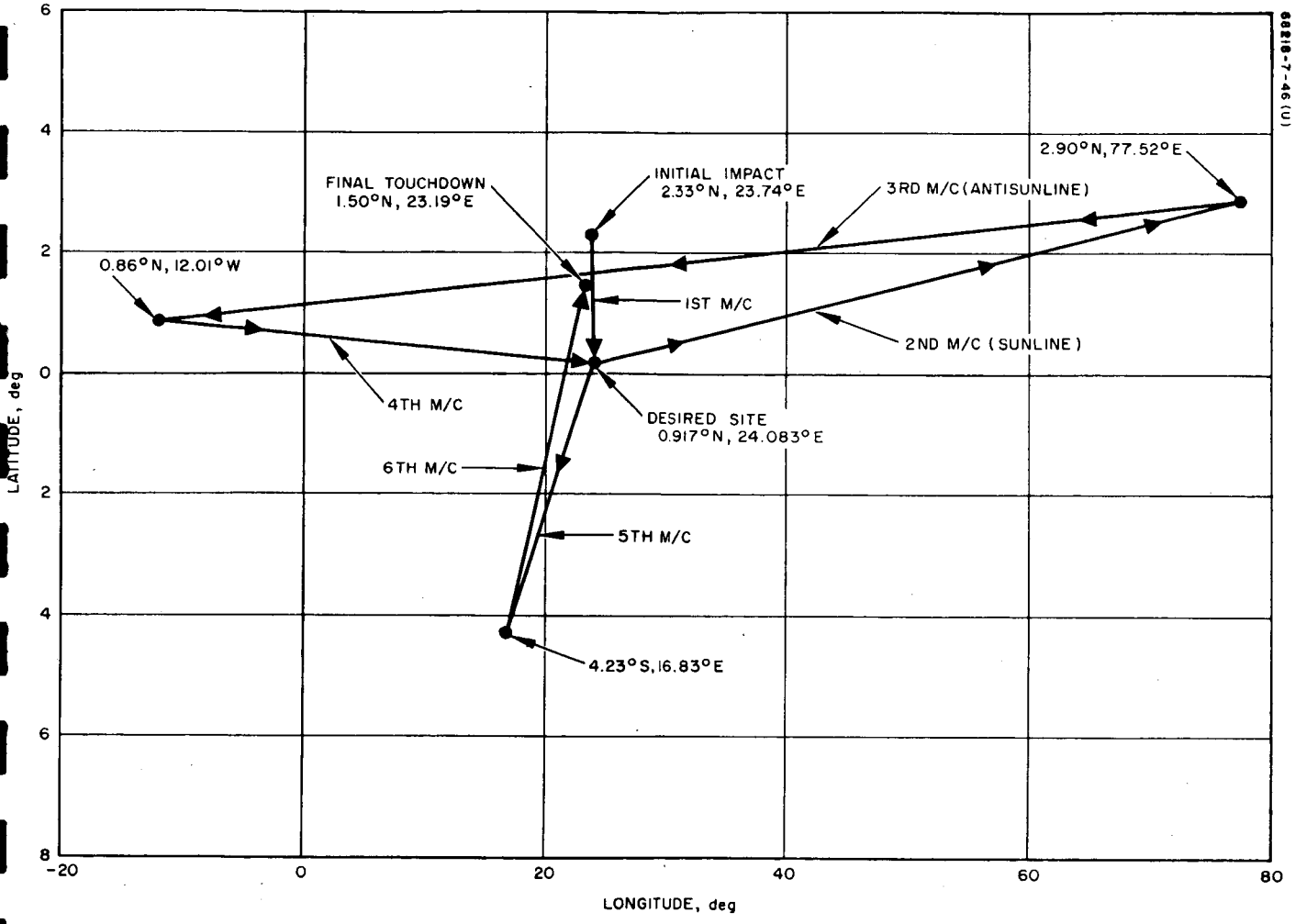

Figure 4-3. Impact Points on Lunar Surface Following Earth Injection and Six Midcourse Corrections

TABLE 4-6. MIDCOURSE MANEUVER DATA

Maneuver	GMT (9 Sept. 1967)	Attitude Rotations	Burn Time (sec)	Prior Impact Point	Resultant Touchdown Point	Impact Angle, Γ
Nominal Midcourse	$01^h\ 45^m\ 02^s$	Roll +71.8° Yaw -35.6°	14.25	2.33°N 23.74°E	0.917°N 24.083°E *	46.4°
Sunline Maneuver	$02^h\ 12^m\ 02^s$	None	10.05	0.917°N 24.083°E	2.89°N 77.52°E	81.5°
Anti-Sunline Maneuver	$02^h\ 39^m\ 50^s$	Yaw -180°	23.05	2.89°N 77.52°E	0.86°N 347.99°E	20.7°
Fourth Midcourse	$04^h\ 18^m\ 48^s$	Roll +68.5° Yaw +106.8°	13.0	0.86°N 347.99°E	0.917°N 24.083°E	46.6°
Fifth Midcourse	$08^h\ 24^m\ 02^s$	Roll +64.6° Yaw +143.2°	33.0	0.917°N 24.083°E	4.23°S 16.83°E	46.7°
Sixth Midcourse	$23^h\ 31^m\ 00^s$	Roll -76.0° Yaw -100.6°	5.45	4.23°S 16.83°E	1.50°N 23.19°E	46.8°

*Desired Touchdown Point.

The predicted retro engine temperature at retro ignition was also computed, and the resulting engine burn time of 39.04 seconds (from ignition to the 3500-pound thrust level at engine tailoff) was provided. It was also recommended that no correction be made for the measured error of 0.005 deg/sec in the yaw attitude maneuver rate since this error was within the measurement accuracy.

The final timing desired in the terminal descent sequence for use in preparing the final terminal message was: 1) emergency AMR mark to be sent 7 seconds after the predicted time of AMR mark, 2) emergency retro eject to be sent 59 seconds after emergency AMR mark, 3) delay high thrust to be sent 0.5 second after emergency retro eject, and 4) emergency start RADVS control to be sent 1.5 seconds after the delay high thrust. Although this sequence initiated the doppler steering phase approximately 4 seconds earlier than normal, it did not begin this phase while the retro engine was still burning (reflecting the results of tests which indicated that it would not be feasible to attempt to initiate the doppler steering phase before retro engine burnout due to saturation of the acceleration loop). Three other points of interest regarding this sequence are: 1) the sequence was based on the normal automatic initiation of the vernier engine ignition, retro engine ignition, and RADVS turn on by the altitude marking radar trigger generated at a start range of 60 miles from the surface; 2) the commanded delay time between the generation of AMR mark and vernier engine ignition was increased to adjust the retro engine ignition altitude (and range) to the desired lower values; and 3) the time at which the emergency AMR mark command was sent to the spacecraft was significantly delayed from its normal time to ensure that the probability of sending it too soon was negligible.

4.1.8 Terminal Descent Phase

Terminal descent preparations were initiated at L+63H45M42S with the performance of the last engineering interrogation. The initiation of the first terminal descent maneuver (a positive roll of 73.9 degrees) was delayed until a Canopus error null was observed. Similarly, initiation of the second maneuver (a positive yaw of 119.5 degrees) was delayed until the sun sensor yaw error was crossing its null position. These maneuvers aligned the retro engine thrust axis to the desired direction. Since the spacecraft roll orientation which resulted from these maneuvers was satisfactory from a RADVS and telecommunication standpoint, there was no need to execute a third attitude maneuver.

The two attitude maneuvers, as well as other preretro ignition spacecraft operations (e.g., loading the proper altitude-mark-to-vernier-ignition delay quantity – 12.325 seconds, establishing retro sequence mode for ensuring that the desired automatic flight control sequences would occur in response to the altitude radar mark, establishing the proper vernier engine thrust level – 150 pounds total – for the retro burning phase, turning on flight control thrust phase power, etc.) were executed on schedule without any difficulty. In addition, the altitude marking radar was turned on at L+64H42M59S and enabled at L+64H46M0S.

The automatic descent sequence for vernier ignition, retro ignition, and RADVS on was initiated by the altitude marking radar mark, confirmed on the ground at 254:00:44:40 GMT. Vernier ignition, retro ignition, and RADVS turnon occurred at the proper time (Table 4-1). The engines were turned off automatically by the 14-foot mark, and a soft landing was verified from the retention of the communication link and continued nominal spacecraft performance, and later by the touchdown strain gage data. The helium, oxidizer, and fuel tank pressures were approximately 560 psia at touchdown, with evidence that vernier engine No. 1 and perhaps 2 may have gone into pressure saturation during the acquisition of the final descent segment.

Strain gage data indicated that touchdown occurred at approximately 00:46:44 GMT, with leg 1 touching the surface first, followed by the touchdown of legs 2 and 3 at practically the same time. The peak loads experienced by legs 1, 2, and 3 were approximately 1265, 1635, and 1640 pounds, respectively. These levels are indicative of a landing velocity of approximately 12 - 13 fps on a surface with a 4-psi bearing pressure and with a slope of approximately 17 degrees.

4.1.9 Initial Lunar Operation

4.1.9.1 Initial Postlanding Sun-Earth Acquisition

In an effort to minimize the time required for planar array earth acquisition, sun acquisition was bypassed initially. The planar array mainlobe was swept (for earth acquisition) through an area which would have allowed for spacecraft roll and tilt uncertainties of about 10 to 15 degrees; however, the highest signal strength observed was more than 20 db below the anticipated peak value. Larger sweeps of the mainlobe were precluded because of a mechanical interference problem between the solar panel and the television camera hood. This problem occurred because of the decision to keep the solar axis pinned until after sun fine positioning had been performed in order to increase the accuracy of the subsequent attitude determination.

It was then decided that a coarse sun acquisition should be performed to reduce the earth location uncertainty. Knowing the sun location in spacecraft coordinates reduces the earth uncertainty area to a segment of arc about the spacecraft-sunline. The length of the arc is determined by the assumed amount of spacecraft tilt about this line. Upon stepping the mainlobe to the nearest end of an arc corresponding to a 20-degree slope, a signal strength was detected which was adequate for 600-line television.

During the subsequent sun fine positioning for attitude determination, the solar panel was first moved out of the area of television interference. Then, after sun fine positioning, the solar axis was unpinned and the solar angle was stepped negative to remove the solar panel from the interference region during earth fine positioning.

No anomalies were observed in the performance of the redesigned Surveyor V mechanical drives during the initial acquisitions. Increased tolerances in angular position, however, were responsible for the decision not to unlock the solar and elevation axes until the initial attitude determination was completed. This may have caused some time loss in the initial earth acquisition.

Table 4-7 shows the times involved in the Mission E sun/earth acquisition. The initial sun-earth fine positionings for attitude determination were performed between 254:10:43 GMT and 254:12:44 GMT.

TABLE 4-7. SURVEYOR V SUN-EARTH ACQUISITION TIMES

Action	GMT, day:hr:min:sec
Spacecraft touchdown	254:00:44:48
Initiate earth search	254:02:58:15
Abandon earth search and initiate sun search	254:03:55:30
Complete sun acquisition	254:04:10:23
Resume earth search	254:05:14:36
Complete earth acquisition	254:05:20:25

4.1.9.2 Spacecraft Attitude Determination from A/SPP Data

The primary method of Surveyor V attitude determination on the lunar surface was based on sun and earth position data obtained via the ASPP. Since the selenographic coordinates of the sun and earth were known as a function of time, it was possible to calculate a selenographic-to-spacecraft transformation matrix once the corresponding spacecraft coordinates of the two bodies were established. The Surveyor postlanding attitude program (PLAS) was used to perform these calculations. Sun position was established by stepping the ASPP to a position that maximized output of the solar panel secondary sun sensor center cell; earth position was established by stepping the ASPP to a position that maximized DSN received signal strength from the planar array.

For the Surveyor V mission, an error analysis for establishing gimbal positions was performed from ASPP command step-count data. The step-count method is based on the assumption that each command to the polar axis produces 0.0685 degree of motion and each command to the other

three axes produces 0.1385 degree of motion. Attitude determination errors are a function of uncertainties in the positions of the ASPP gimbals when sun and earth sightings are obtained. Because the true angle between the sun and earth vector is a known quantity, a partial correction of ASPP gimbal errors can be performed. The weighting of correction factors is determined from the analysis of ASPP error sources. Using this same error analysis, it is also possible to perform a Monte Carlo evaluation to establish the correspondence between spacecraft X and Y tilt tolerances and position errors in the four ASPP gimbal drive mechanisms. If an ASPP axis can be left pinned during a sun-earth sighting, accuracy of that sighting is increased.

Two attitude determinations were performed for Surveyor V from ASPP step-count data. The first attitude determination was performed with both the solar and elevation axes pinned. The attitude parameters and their associated 3σ tolerances are given below. This attitude was evaluated prior to vernier engine static firing.

Pre-Static Firing Spacecraft Attitude

X_{slope} = -2.69 degrees $3\sigma_x$ = 0.795 degree

Y_{slope} = -19.34 degrees $3\sigma_y$ = 0.61 degree

Magnitude of slope= 19.50 degrees, direction = 262.37

Roll orientation {X axis CW from sel. east}

θ = 24.51 $3\sigma_\theta$ = 2.19 degrees

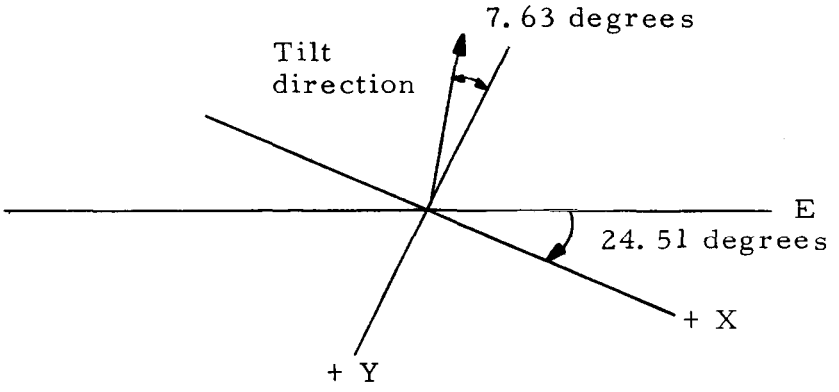

After vernier engine static firing, it was decided that another ASPP attitude determination should be performed in an attempt to ascertain spacecraft motion. This attitude determination was performed with only the elevation axis pinned. The solar panel axis was previously unlocked for sun tracking. The attitude parameters and their associated error tolerances are given below.

Post-Static Firing Spacecraft Attitude

X_{slope} = -3.51 degrees $3\sigma_x$ = 1.50 degrees

Y_{slope} = -19.45 degrees $3\sigma_y$ = 1.62 degrees

Magnitude of slope = 19.71 degrees, direction = 260.15 degrees

Roll orientation {+ X axis CW from sel. east}

θ = 25.24 $3\sigma_\theta$ = 3.09 degrees

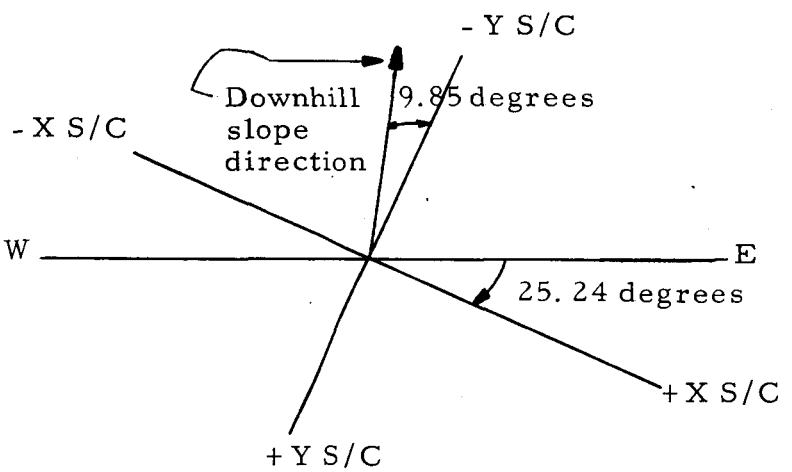

4.2 RELIABILITY ANALYSIS

4.2.1 Surveyor V Reliability Estimates

4.2.1.1 System and Subsystem Reliability

The final reliability point estimate for Surveyor V is 0.72. This estimate is based upon Surveyor V flight and systems test data and applicable Surveyor I, 2, III, and 4 system test and flight experience.

Final reliability point estimates for each subsystem are given in Table 4-8.

TABLE 4-8. SUBSYSTEM FINAL RELIABILITY POINT ESTIMATES

Subsystem		Reliability Estimates
Telecommunications		0.987
Vehicle and mechanisms		0.853
Propulsion		0.934
Electrical power		0.985
Flight control		0.945
Spacecraft	0.733	
Systems interaction reliability factor	0.986	
Spacecraft reliability (0.733)(0.986) = 0.72		

4.2.1.2 Summary of Data Base for Surveyor V Reliability Estimates

The primary source of data for reliability estimates is the operating time and cycles experienced by Surveyor V units during systems tests and flight and the accumulated reliability relevant failure data provided by TFRs. Data from Surveyors I, 2, III, and 4 test and flight experience are included where there are no significant design differences between the units. A failure is considered relevant if it affects equipment reliability and could occur during a mission. Relevance of failures is based upon a joint reliability-systems engineering decision. In addition, relevant failures are weighted as follows:

1.0 Critical – Would normally cause a safety hazard, mission abort, or failure of mission objective

0.6 Major – Would significantly degrade system performance but not cause mission abort or failure

0.1 Minor – Would not significantly affect ability of system to function as designed

A data base for Surveyor V reliability estimates is summarized in Table 4-9.

4.2.1.3 Time/Cycle/Reliability History for All Surveyor I, 2, III, and 4 Units

Table 4-10 presents a history of time/cycle/reliability data for each major control item for Surveyors I, 2, III, and 4.

Table 5.1-1 (continued)

Flight Sensor Location by Subsystem		Transit Steady-State Temperature °F						Temperature Limits, °F	
		Mission A Actual	Mission B Actual	Mission C Actual	Mission D Actual	Mission E			
						Predicted	Actual	Operational	Survival
Television, SM/SS, and alpha scattering device									
TV 3 mirror assembly	TV-17	-120	-120	-120	-125	-120	-126	180/-50	185/-220
TV 3 ECU	TV-16	-134	-128**	-128	-130	-125	-136	165/-20	165/-250
Auxiliary electronics	SS-12	*	*	-35	-35	*	*	158/-4	185/-67
SM/SS substructure	SS-13	*	*	*	-104	*	*	0 minimum	–
Compartment C electronics†	AS-4	*	*	*	*	-28	-20	131/-4	185/-67
Sensor head electronics†	AS-3	*	*	*	*	25	35	122/-40	167/-300

*Not on spacecraft.

**Steady state not obtained.

†Corrected for bit rate errors.

††Launch temperature/touchdown temperature for Missions A, C, D, and E; launch temperature/midcourse temperature for Mission B.

TABLE 5.1-2. MISSION THERMAL EVENT LOG

Day	GMT hr:min	Mission Time hr:min	Event
251	07:57	0	Launch and enter earth shadow
	08:07	00:10	MECO 1 leave earth shadow
	08:16	00:19	Separation
	08:17	00:20	Transmitter B high power on
	08:30	00:33	Sun acquisition
	08:37	00:40	Transmitter B high power off
	09:50	01:53	Line 2 heater cycling
	14:03	06:06	Transmitter B high power on
	14:12	06:15	Line 3 heater cycling
	14:27	06:30	Star acquisition
	14:33	06:36	Transmitter B high power off
	15:36	07:39	Solar panel switch off
	15:46	07:49	Start gyro drift check (three-axes)
	15:55	07:58	Solar panel switch on
	16:23	08:26	Solar panel switch off
	16:42	08:45	Solar panel switch on
	17:13	09:16	Solar panel switch off
	17:16	09:19	Solar panel switch on
	17:34	09:37	Solar panel switch off
	17:44	09:47	Solar panel switch on
	18:16	10:19	Terminate gyro drift check (all axes)
	18:28	10:31	Solar panel switch off
	18:33	10:36	Solar panel switch on
	18:34	10:37	Initiate gyro drift check (all axes)
	18:50	10:53	Solar panel switch off
	18:53	10:56	Solar panel switch on
	19:30	11:33	Solar panel switch off
	19:34	11:37	Solar panel switch on
	20:02	12:05	Solar panel switch off
	20:07	12:10	Solar panel switch on

Table 5.1-2 (continued)

Day	GMT hr:min	Mission Time hr:min	Event
251	20:15	12:18	Terminate gyro drift check
	20:59	13:02	Solar panel switch off
	21:35	13:38	Solar panel switch on
	21:43	13:46	Gyro drift check (roll only)
	23:40	15:43	End roll drift check
252	01:15	17:18	Transmitter B high power on
	01:32	17:35	Start roll maneuver
	01:35	17:38	End roll (71.5 degrees)
	01:38	17:41	Start yaw maneuver
	01:39	17:42	Complete yaw (-35.5 degrees)
	01:42	17:45	Heaters off; AMR and lines 1, 2, and 3
	01:43	17:46	Thrust phase power on
	01:44	17:47	First midcourse (14 second burn)
	01:45	17:48	Thrust phase power off
	01:48	17:51	Line heaters on and AMR heaters on
	01:53	17:56	Yaw maneuver (35.5 degrees)
	02:12	18:15	Second engine burn (10.05 seconds)
	02:12	18:15	Thrust phase power off
	02:24	18:27	Begin yaw
	02:30	18:33	End yaw (+180 degrees)
	02:39	18:42	Thrust phase power on
	02:40	18:43	Third engine burn (22.5 seconds)
	02:40	18:43	Thrust phase power off
	02:45	18:48	Begin yaw
	02:51	18:54	End yaw (-180 degrees)
	02:55	18:58	High power off
	04:00	20:03	Sun and roll (-71.9 degrees)
	04:05	20:08	Sun and roll (68.5 degrees)
	04:09	20:12	Yaw (+106.7 degrees)

Table 5.1-2 (continued)

Day	GMT hr:min	Mission Time hr:min	Event
252	04:16	20:19	Thrust phase power on
	04:18	20:21	Fourth engine burning sequence: 12 seconds on, 1 off, 1/2 on, 1 off, 1/2 on
	04:19	20:22	Thrust phase power off
	04:58	21:01	Yaw maneuver start
	05:01	21:04	End of yaw (-106.7 degrees)
	05:04	21:07	Start roll maneuver
	05:06	21:09	End roll maneuver (-68.5 degrees) in nominal transit position
	05:31	21:34	TV electronics heater on
	05:47	21:50	Compartment C heater on
	05:49	21:52	AMR heater off
	06:39	22:42	TV electronics heater off, AMR heater on and compartment C heater off
	07:49	23:52	Transmitter B high power on
	07:54	23:57	Sun and roll start 64.6 degrees
	07:58	24:01	Start yaw (143.2 degrees)
	08:20	24:23	Line heaters and AMR heater off
	08:24	24:27	Fifth engine firing: 8 seconds on, 6 seconds off, 9 1/2 seconds on, 8 seconds off and 12 seconds on
	08:29	24:32	Line heaters and AMR heater on
	08:33	24:36	Yaw maneuver (-143.2 degrees)
	08:40	24:43	Roll maneuver (-64.6 degrees)
	08:46	24:49	High power off
	08:49	24:52	Compartment C heater on
	10:33	26:36	Transmitter B high power on
	10:37	26:40	Alpha scattering instrument power on
	11:25	27:28	Alpha scattering instrument power off
	11:30	27:33	Transmitter B high power off
	11:32	27:35	Compartment C heater off

Table 5.1-2 (continued)

Day	GMT hr:min	Mission Time hr:min	Event
252	11:39	27:42	Initiate three-axes drift check
	13:16	29:19	End three-axes drift check
	13:17	29:20	Initiate roll axis drift check
	15:08	31:11	Terminate roll axis drift check
	15:10	31:13	Initiate three-axes drift check
	17:18	32:21	Terminate gyro drift check
	18:00	34:03	Initiate gyro drift check (all axes)
	20:10	36:13	Terminate gyro drift check
	20:59	37:02	Initiate three-axes gyro drift check
	21:48	37:51	Terminate gyro drift check
	23:06	39:09	Transmitter B high power on
	23:14	39:17	Initiate negative roll
	23:16	39:19	End roll (-75.9 degrees)
	23:20	39:23	Start yaw positive roll
	23:23	39:26	End yaw (-101 degrees)
	23:25	39:28	Heaters off
	23:25	39:28	Thrust phase power on
	23:30	39:34	Sixth engine firing (5.45 seconds)
	23:31	39:33	Thrust phase power off
	23:33	39:36	Heaters on
	23:36	39:39	Start of yaw (+101 degrees)
	23:39	39:42	End of yaw
	23:44	39:47	Start of roll (+75.9 degrees)
	23:50	39:53	Transmitter B high power off
253	01:35	41:38	Start gyro drift check (three-axes)
	04:33	44:36	Terminate three-axes drift check
	06:20	46:23	Enabled oxidizer tank 2 heaters
	13:05	53:08	Initiate roll gyro drift check
	13:31	53:34	Compartment A heater on

Table 5.1-2 (continued)

Day	GMT hr:min	Mission Time hr:min	Event
253	15:24	55:27	Terminate roll gyro drift check
	15:27	55:20	Initiate three-axes gyro drift check
	17:43	57:46	Compartment C heater control on
	17:59	58:02	Terminate gyro drift check
	18:12	58:15	Positive yaw 179.9 degrees
	18:22	58:25	Positive yaw 180.1 degrees
	19:37	59:40	TV electronics heater on
	20:29	60:32	Alpha scattering heater on
	23:40	63:43	Compartment A heater off
	23:41	63:44	TV vidicon thermal control on
	23:51	63:54	Transmitter B high power on
254	00:00	64:03	Prop strain gage power on
	00:02	64:05	TD strain gage power on
	00:12	64:15	Begin positive roll (73.9 degrees)
	00:15	64:18	End roll
	00:16	64:18	Begin positive yaw (119 degrees)
	00:20	64:23	End yaw
	00:30	64:33	Mode 6 on
	00:39	64:42	Cyclic heaters off
	00:40	64:43	AMR power on
	00:41	64:44	Thrust phase power on
	00:43	64:46	AMR enabled
	00:44	64:47	Retro ignition
	00:46:44	64:49:43	Touchdown
	00:48	64:51	RADVS off
	00:54	64:57	Compartment C and alpha scat heaters on
	00:55	64:58	TV electronic and vid heater on
	00:56	64:59	Line heaters on and oxidizer tank 2 heater on
	01:09	65:12	Transmitter B high power off
	01:19	65:22	Transmitter A high power on

Prelaunch air conditioning was provided as required. Conditioned air was maintained at approximately 70° F until 2 hours and 18 minutes prior to launch, whereupon the air temperature control was raised to 85° F. During the last hour prior to launch, the payload adapter temperature was maintained at about 86° F.

5.1.4.2 Postlaunch Phase

The spacecraft was injected into a parking orbit for approximately 9 minutes and was in the earth's shadow for approximately 11.5 minutes. This time interval was small enough that most components were not subjected to any large temperature variations. The solar panel was an exception: its temperature decreased to 30° F while it was shaded.

5.1.4.3 Midcourse and Other Vernier Burns

A total of six series of engine firings was completed prior to terminal descent. A summary of these burns, along with the thermal response of the engines, is presented in Table 5.1-3. The preignition upper operational limits of engines 1 and 3 (P-7 and P-11) were violated for burns 2 and 3. The upper operational limit for engine 2 was violated only on burn 3. Also, the 1-hour constraint between engine firings was violated. These constraint violations were due to the urgency of nonstandard operation necessitated because of the failure of the helium regulator to seat properly. The maximum engine temperature of 464° F was observed on engine 3 as a result of burn 3. This burn produced higher engine temperatures than any of the other transit burns. Although burn 5 was longer than burn 3, peak engine temperatures were slightly lower on burn 5 because preignition temperatures for this burn were considerably lower than for burn 3.

For burn 4, the spacecraft was in an off-sun attitude for about 57 minutes without having allowed a 2-hour on-sun attitude recovery time after the previous off-sun period. However, all spacecraft systems were maintained within their proper temperature limits during off-sun attitude periods.

All cyclic heater loads (except the gyro heaters) were commanded off for approximately 6 minutes, 9 minutes, and 7 minutes for burns 1, 5, and 6, respectively. The heaters were commanded off to remove cyclic loads so that critical electrical loads could be observed during vernier burns without ambiguity. The heaters were not commanded off for burns 2, 3, and 4 due to the urgency and desired simplicity of the nonstandard operations initiated after the first vernier burn.

Propellant temperature stratification was observed on this flight as in all previous flights (see Figures 5.1-28, 5.1-29, 5.1-36, 5.1-37, 5.1-38, and 5.1-39 in Appendix A to Section 5.1). However, temperature gradients within the propellants were greatly negated due to the propellant motion induced during thrusting. Thus, the amount of temperature change observed on the propellant tank temperature sensors after thrusting decreased with each subsequent firing.

TABLE 5.1-3. SURVEYOR V VERNIER BURNS

Burn Number	Start Time, GMT (day 252), hr:min:sec	Burn Duration, seconds	Engine 1 (P-7)		Engine 2 (P-10)		Engine 3 (P-11)		Comments
			Preignition, °F	Peak, °F	Preignition, °F	Peak, °F	Preignition, °F	Peak, °F	
1	01:45:02	14.25	60	303	62	299	71	338	To target site (roll 71.5 degrees, yaw 35.5 degrees)
2	02:12:03	10.1	143	315	117	286	156	398	Along sunline
3	02:39:50	23.05	166	377	135	373	174	464	180 degrees opposite sunline (yaw 180 degrees)
4	04:18:48	13.0	106	332	109	307	113	395	To target site (opposite burn 1) (roll 70 degrees, yaw 106 degrees)
5	08:24:02	33.0	88	368*	93	357*	95	448*	$\dot{U}_3$ direction (roll 64.6 degrees, yaw 143.2 degrees)
6	23:31:00	5.45	68	236	51	214	67	208	To target site (roll 76 degrees, yaw 101 degrees)

Note: The preignition transit upper operational temperature limits for the SC-5 thrust chamber assemblies (P-7, P-10, and P-11) are 120°, 130°, and 120° F, respectively.

*Highest temperature observed on available data.

5.1.4.4 Coast Phases

Heater Performance

Vernier line 2 was the first heater-controlled component on the spacecraft to cycle, other than the gyros, after launch. It started cycling 1 hour and 53 minutes after launch and stayed in its cycling range of 18 to 26 degrees throughout the mission, with the exception of the maneuvers when it went as high as 40 degrees. (See Table 5.1-4 for the heater duty cycles.)

The AMR started to cycle about L+6 hours into the mission. It remained in its cycling range while it was enabled. It was commanded off for 50 minutes at 21:52 mission hours, the time when an earth orbit was being considered as an alternative to a soft landing. At 06:15 mission hours, the vernier line 3 heater began cycling and remained in its cycling range except during maneuvers. Table 5.1-5 lists the times the heaters were enabled during transit.

TABLE 5.1-4. HEATER AND GYRO DUTY CYCLES

Mission Time hr:min	Vernier Line 2, percent	Vernier Line 3, percent	AMR, percent
Heater Duty Cycles			
19.08	26.9	10.8	63.5
49.44	36.9	31.5	67.5

Mission Time hr:min	Yaw gyro, percent	Pitch gyro, percent	Roll gyro, percent
Gyro Duty Cycle			
07:03	31.6	42.5	16.5
48:00	27.5	40.2	17.6

Propellant Tank

Oxidizer tank 2 temperature normally decreases throughout the transit phase from launch until the thermostatically-controlled heater is activated late in the mission. Based on solar thermal vacuum test experience, the heater on oxidizer tank 2 normally cycles when the flight temperature sensor P-16 indicates 17° F. The tank temperature reached 17° F at 52 hours mission time and continued to cool to 14° F at retro

TABLE 5.1-5. ENABLED TIMES OF HEATERS*

Mission Time, hr:min	Lines			Tanks			AMR	Compartment C	TV Electronics	TV Video	Alpha Scattering Head	Compartment A
	1	2	3	Oxidizer 2	Fuel 2	Oxidizer 3						
Prelaunch	ON	ON	ON	OFF	OFF	OFF	ON	OFF	OFF	OFF	OFF	OFF
17:45	OFF	OFF	OFF				OFF					
17:51	ON	ON	ON				ON					
21:34									ON			
21:50								ON				
21:52							OFF					
22:42							ON	OFF	OFF			
24:23	OFF	OFF	OFF				OFF					
24:32	ON	ON	ON				ON					
23:25	OFF	OFF	OFF				OFF					
23:33	ON	ON	ON				ON					
46:23				ON								
53:34												ON
57:46								ON				
59:40									ON			
60:32											ON	
63:43												OFF
63:44										ON		
64:39	OFF	OFF	OFF	OFF			OFF	OFF	OFF	OFF	OFF	
64:57								ON			ON	
64:58									ON	ON		
64:59	ON	ON	ON	ON								

* ON Enabled, OFF Disabled.

ignition without cycling. A special test was performed during the first lunar night to verify heater operation. The heater was enabled momentarily during the lunar night at a tank temperature (P-16) of -20° F, and operation was verified by an increase in the nonessential current.

Gyro Drift Checks

There were 12 drift checks during the transit phase. The average measured values of the drift were +0.85 deg/hr for roll, +0.60 deg/hr for pitch, and -0.66 deg/hr for yaw. During all axes drift checks, a drop in temperature of as much as 24° F was noted on engine 2. Also, the compartment radiators were slightly affected. For example, V-25 dropped 15 degrees during one drift check. All other components registered negligible temperature variation due to gyro drift.

Earth Orbit Considerations

A sequence was designed and thermally initiated to place the spacecraft in an earth orbit at 05:50 GMT on day 252 (21:52 mission hours). This included turning on the compartment C heater for the alpha scattering device, and turning the TV electronics heater on. The AMR electronics heater was then turned off as a power consideration. These steps were reversed at 07:43 GMT when it was decided a soft landing could still be achieved, and the spacecraft was returned to the normal transit condition.

Temperature Variations with Solar Panel Switching

The solar panel and associated electrical circuitry was redesigned for Surveyor V and subsequent spacecraft. This new system has a capability of turning off the electrical flow from the solar panel through the use of a solar panel switch. When the bus voltage exceeds a preset value, the solar panel switch trips to the off position and must be reset by command. When the switch is in the off condition, 100 percent of the absorbed solar energy is converted to heat in the solar panel, resulting in an increase in solar panel temperature.

The solar panel switch tripped off many times during transit due to small fluctuations in bus voltage which was very near the switch trip setting. Whenever the switch tripped off, the solar panel temperature would increase. The solar panel equilibrium temperature (EP-12) with the switch on was 126° F. However, with the switch in the off condition, the panel temperature would increase at approximately 7° F/hr to a new equilibrium temperature of approximately 142° F (see Figure 5.1-11 in Appendix A). The solar panel remained within operational limits throughout transit.

Alpha Scattering Subsystem

The thermal performance of the alpha scattering units, which were flown for the first time in Mission E, is summarized in Table 5.1-1 and Figures 5.1-6 and 5.1-7 in Appendix A. It can be observed that flight temperatures were close to predicted values. All temperatures were corrected for bit rate errors of 2° F at 550 bits/sec, 6° F at 1100 bits/sec, and 14° F at 4400 bits/sec.

The subsystem comprises electronics housed in compartment C and the deployable instrument with its electronics. Compartment C is thermally isolated on five sides. All electronics are mounted to an upward-facing white radiator which provides the primary thermal control. A 10-watt, thermostatically controlled heater with an on-set point of approximately 20° F is used to warm the electronics from the transit equilibrium temperature to a temperature above the lower operational limit of -4° F. The instrument head contains electronics in an isolated compartment and an upward-facing radiator plate which employs a Vycor glass mirror (second surface radiator) to maintain thermal control. The package also contains a 5-watt, thermostatically-controlled heater with a 50° F set point. This heater is used in transit to warm up the unit from its steady-state temperature to approximately 50° F prior to touchdown. The normal sequence is to first warm up compartment C to -4° F prior to turning on the instrument heater.

It is known that deadbands of 7° F amplitude occur with the high accuracy sensors AS-3 and AS-4 at temperatures corresponding to certain binary number combinations. One deadband occurs at nominally 32° F, which is near the steady-state temperature of the alpha instrument head (AS-3). The occurrence of this temperature deadband cannot be observed in the data with absolute certainty. The constant temperatures (see Figure 5.1-6 in Appendix A) of 25° F between 05:32 and 06:38 GMT on day 252 are probably on a deadband, since the alpha head should be in a transient warmup at this time. The instrument head temperature had cooled down during the maneuver in the fourth vernier engine thrusting sequence at 252:04:24 GMT, and the temperature would be expected to be increasing to the steady-state temperature in the subsequent time interval and not stay constant.

Due to the helium system leak problem and the uncertainty of performing a safe landing, SSAC decided to operate the alpha scattering system during the transit phase to obtain a background count and calibration data. Normally, the system is not operated until after touchdown.

The required warmup from the transit nonoperating steady-state temperature of -20° to -4°F prior to activation of the electronics was initiated at 252:08:49 GMT (L + 24 hours 32 minutes) with turn-on of the compartment C heater. SSAC decided not to wait for completion of the warmup cycle. Alpha scattering power on was therefore commanded at 252:10:37 GMT, at which time the compartment C electronics temperature was -11° F (7° F below its lower operational limit). This experiment was useful for making predictions of the times at which the compartment C and alpha instrument heaters should be turned on prior to touchdown.

The preterminal descent warmup of compartment C was initiated at R-7 hours. After a 2.6-hour warmup of the compartment to -4° F, the alpha head heater was commanded on. The head temperature warmed up to the required 50° F in 1.0 hour. This compares to preflight predicted warmup times of 1.2 and 0.6 hours for the compartment and the instrument, respectively. Operational temperatures were achieved 3 hours prior to touchdown.

Telecommunication Compartments. Compartment A steady-state temperatures in transit were 7° F cooler than predicted as shown in Table 5.1-1 and Figures 5.1-7, 5.1-8, 5.1-10, 5.1-13, 5.1-53 and 5.1-54 of Appendix A. Temperatures in compartment A were significantly cooler than in previous flights due to a reduction in power dissipation in the redesigned battery charge regulator.

The peak transmitter B temperature was 126° F and occurred with the transmitter in high power at initial RF acquisition. No thermal problems were encountered as a result.

It was necessary to warm up the main battery in compartment A from the transit phase steady-state temperature of 58° to 90° F at the time of retro ignition, as shown in Figure 5.1-10 in Appendix A, as it was desired to have at this time the main battery at 90° F to ensure sufficiently high battery terminal voltage during RADVS operation. The warmup was accomplished by turning on the compartment A thermal control and heater assembly between R-11 hours 10 minutes, and R-01 hours 06 minutes. Additional warmup occurred from the high power operation in the terminal phase. A temperature of 90° F was obtained 2 minutes prior to RADVS activation.

Compartment B steady-state temperatures in transit were 7° F higher than predicted as can be seen in Table 5.1-1 and Figures 5.1-58 and 5.1-59 of Appendix A.

5.1.4.5 Terminal Descent Phase

The thermal response during the modified terminal descent was nominal. The maximum temperatures recorded on the vernier engines were 411°, 309°, and 426° F on engines 1, 2, and 3, respectively. The KPSM temperature increased from 33° to 119° F during RADVS operation. At retro ignition, the retro bulk temperature was 53° F.

The spacecraft was in an off-sun attitude for approximately 31 minutes prior to touchdown. All temperatures remained within proper temperature limits during this period.

Transmitter B high power operation was initiated at TD-56 minutes and terminated at TD+22 minutes (approximately 78 minutes of high power). During this period, the maximum temperature reached by transmitter B was 116° F. The battery temperature increased from 90° F at RADVS turn-on to 97° F at termination of transmitter B high power operation.

5.1.5 THERMAL PERFORMANCE – LUNAR DAY 1

A summary of maximum lunar day temperatures and minimum temperatures during an eclipse is shown in Table 5.1-6. Plots of thermal parameters during the lunar day are presented in Appendix B to this section.

5.1.5.1 Touchdown Orientation and Configuration

The spacecraft was located at 1.45° N and 22.25° E, approximately 18 miles northwest of its original landing spot. Leg 1 was located +172 degrees from north or +18 degrees from the -Y axis. The spacecraft was sitting on an approximately 20-degree slope in a small crater, approximately 30 feet across, and leg 1 was pointing uphill. At touchdown all heaters were off (254:00:47 GMT), but the compartment C heater, alpha scattering, television electronics, and vidicon were all commanded on at 254:00:55. However, the temperatures were increasing and they did not cycle at this time.

5.1.5.2 Telecommunication Compartments

Spacecraft lunar operations on Surveyor V were more restricted by the compartment temperature levels than on either Surveyor I or Surveyor III. The reduced thermal performance is primarily due to the small crater with walls sloping at approximately 20 degrees in which the spacecraft is cradled. The heat rejection capability of compartments A and B is reduced by 10 and 7 watts, respectively, because of the radiant interchange between the lunar surface and the compartment radiators. Another factor, though probably secondary, is an increase in the effective solar absorptance of the radiators due to the presence of lunar dirt particles. These particles, as shown by television pictures, resulted directly from the static firing on day 256.

For a period of 4 earth days (257:10:00 to 261:14:35 GMT), a combination of shading compartment A with the solar panel, placing the spacecraft in a standby electronic configuration, and limiting the battery charge rate, were used to maintain battery temperature at or below 115° F. During standby periods when no spacecraft data were being received, earth lock was broken to rotate the A/SPP in the orientation which yielded maximum solar panel shadowing on compartment A. Up to 60 percent of the radiator surface could be shadowed during this period. During standby, compartment A electronics heat dissipation was reduced from 20 watts in low power operation to either 11 or 7 watts, depending on whether the battery was being charged or the solar switch was off and the battery was in a discharge mode. In general, the battery was not charged in excess of a 0.75-ampere rate during this period.

On day 260, an RF experiment was performed. High power was commanded on three times on transmitter A until the upper limit of 185° F was reached. The on times were 30, 25, and 20 minutes, respectively. The decrease in operational time is due to increase in heat sink temperature from the high power operation.

TABLE 5. 1-6. MAXIMUM QUASI-STEADY-STATE TEMPERATURES AND MINIMUM TEMPERATURES ON LUNAR SURFACE

Sensor and Location		Maximum Temperature, °F			Eclipse Minimum Temperature, °F	
		Surveyor I	Surveyor III	Surveyor V	Surveyor III	Surveyor V
AS-3	Alpha scattering sensor head	–	–	143/146	–	14
AS-4	Compartment C electronics	–	–	132/138	–	23
D-13	Transmitter A	185	118	120/112	47	64
D-14	Transmitter B	106	110	109/111	43	64
EP-8	Main battery	118	116	114/118	74	101
EP-12	Solar panel	237	220	248/250	-185	-166
EP-13	Boost regulator	132	132	124/127	32	66
EP-26	Auxiliary heater	155	166	–	140	–
EP-34	Battery charge regulator	142	125	124/125	72	99
FC-44	Flight control electronics	192	202	180/184	53	25
FC-45	Flight control electronics	200	201	185/190	-3	31
FC-46	Roll gyro	167	198	157/290*	11	116
FC-47	Canopus	130	194	170/177	-20	6
FC-48	Nitrogen tank	173	165	195/187	–	16
FC-54	Pitch gyro	188	–	157/289*	–	112
FC-55	Yaw gyro	170	–	157/291*	–	114
FC-70	Attitude jet 2	205	210	219/226	-52	-66
FC-71	Roll actuator	224	239	230/238	-16	28
M-8	Planar array	228	230	296/296	-140	-133
M-10	Solar motor	218	230	242/245	-43	-52
M-12	Elevation motor	190	201	210/208	14	-3
P-4	Oxidizer line 2	203	203	210/207	76	81
P-5	Fuel tank 2	164	197	206/201	165	136
P-6	Oxidizer tank 3	154	179	173/181	105	136
P-7	Vernier engine 1	244	256	250/250	-12	40
P-8	Oxidizer line 1	221	202	220/226	8	52
P-9	Oxidizer line 3	184	200	182/186	62	-1
P-10	Vernier engine 2	229	256	272/252	36	-12
P-11	Vernier engine 3	227	232	210/219	22	12
P-13	Fuel tank 1	190	208	209/204	23	174
P-14	Fuel tank 3	171	186	166/160	137	124
P-15	Oxidizer tank 1	173	183	192/187	96	149
P-16	Oxidizer tank 2	166	185	182/183	153	129
P-17	Helium tank	145	178	197/213	21	-19
P-23	Fuel line 1	–	–	213/210	–	142
P-24	Fuel line 2	–	–	219/208	–	84
P-25	Fuel line 3	–	–	210/210	–	33
R-8	Klystron power supply modulator	225	214	222/227	23	43
R-9	Signal data converter	149	168	174/180	8	42

Table 5. 1-6 (continued)

Sensor and Location		Maximum Temperature, °F			Eclipse Minimum Temperature, °F	
		Surveyor I	Surveyor III	Surveyor V	Surveyor III	Surveyor V
R-10	Doppler preamplifier	235	260	260/260	-33	31
R-13	Altitude preamplifier	214	232	243/226	2	-31
SS-12	Surface sampler electronics	–	144	–	-18	–
TV-16	TV electronics	127	140	150/157	-10	0
TV-17	TV hood	124	148	152/155	-12	-1
V-15	A tray top	110	109	109/117	41	64
V-16	A tray bottom	118	117	119/124	68	89
V-17	Compartment A shell, retainer	–	120	–	69	–
V-18	Compartment A shell, cannister	–	108	100/110	-170	-160
V-19	Compartment A switch 5, base	–	112	108/115	45	62
V-20	Compartment A switch 5, radiator	78	101	100/104	18	24
V-21	B tray top	118	117	117/122	21	59
V-22	B tray bottom	124	122	124/127	29	70
V-23	Compartment B shell, canister	111	152	105/114	-154	-153
V-24	Compartment B switch 4, radiator	99	100	100/106	-16	11
V-25	Compartment A switch 8, radiator	88	100	100/110	13	8
V-26	Compartment B switch 4, base	–	114	114/118	21	52
V-27	Upper spaceframe	138	156	160/168	-75	-70
V-28	Lower spaceframe	190	186	196/201	-32	-8
V-29	Thermal tunnel	–	115	130/134	47	73
V-30	Shock absorber 1	193	190	178/187	-51	-65
V-31	Leg 2 upper web	148	158	–	–	–
V-32	Shock absorber 2	171	183	195/201	-57	-67
V-33	Shock absorber 3	175	186	189/195	-35	-55
V-34	Antenna/solar panel positioner mast	130	142	–	-102	–
V-35	Upper spaceframe	125	154	168/172	-70	-81
V-36	Lower spaceframe	166	179	187/188	-45	-46
V-37	Retro bolt 1	222	202	219/222	-2	14
V-38	Retro bolt 2	175	227	222/206	32	-29
V-39	Retro bolt 3	185	200	185/188	-11	-7
V-44	Crushable block 3 heat shield	189	193	210/211	-29	-15
V-45	Compartment B switch 1, radiator	104	105	108/112	-95	25
V-46	Compartment B switch 5, radiator	96	100	100/105	-5	-30
V-47	Compartment A switch 2, radiator	–	104	105/110	18	9
V-49	Compartment A switch 3, radiator	–	–	105/110	–	18

*IRU radiator damaged during lunar night.

5.1.5.3 Static Firing

At 255:09:30 GMT, a practice static firing was initiated to check the flight control sensor group (FCSG) and to gain operational experience with the static firing sequence. The warmup of the FCSG to operational temperatures was monitored.

The transient thermal capability was in excess of that documented in the lunar hopper kit, as shown in Figure 5.1-1. The actual warmup rate of the gyros and electronics was lower than the predictions. The FCSG was operated for 3 hours 19 minutes without overheating. The actual operating time for the FCSG during a static firing was known to be less because the actual sequence was on tape. The experimental data obtained in the practice were used to determine the turnon time of the FCSG for the actual firing.

The temperature limit of the engines prior to start of static firing is 220° F. Based on Surveyor I and III lunar day experience, the temperature of the warmest vernier engine was anticipated to be 210° F subsequent to touchdown (after the cooldown from the terminal descent ignition temperatures). However, the engine 2 temperature rose from 178° F at 15 minutes after touchdown to 220° F 5.25 hours after touchdown (see Figure 5.1-33). The temperature of engine 2 eventually rose to 273° F 2 days and 4 hours subsequent to touchdown (256:04:30 GMT).

The elevated temperature of the engine and the approximate 20-degree tilt of the spacecraft were of concern in attempting a static firing. On day 256, it became apparent that the temperature of engine 2 would not decrease significantly in the next 3 earth days while, at the same time, the temperature of engine 1 was rising. Based on predicted shadowing (Reference 1) Thermal Control predicted the engine 1 temperature would reach 220°F within the next 12 hours. Consequently, it was decided to risk the static firing without further delay.

The vernier engine static firing occurred at 256:05:38:05 GMT. Thrust chamber assemblies (TCA) 1, 2, and 3 exhibited temperatures of 120°, 267°, and 136°F, respectively, at the initiation of the vernier burn. The TCAs burned for 0.5 second at minimum thrust as commanded. Vernier engines 1, 2, and 3 developed 22, 17, and 26 pounds of thrust, respectively, during the burn. TCA solenoid valves performed normally despite the higher temperatures. Maximum engine temperatures observed after the burn were 131°, 293°, and 143°F on TCAs 1, 2, and 3, respectively.

5.1.5.4 Alpha Scattering Operation and Warmup

At touchdown, the alpha scattering head temperature was 50°F and increasing at the rate of 1°F/hr. The heater which had been enabled after touchdown never cycled and was later commanded off. At approximately 12 hours after touchdown, the alpha scattering head was deployed to the background position and, at TD+15 hours, it was deployed to the surface. Its temperature was still increasing at about 1°F/hr at this time and continued

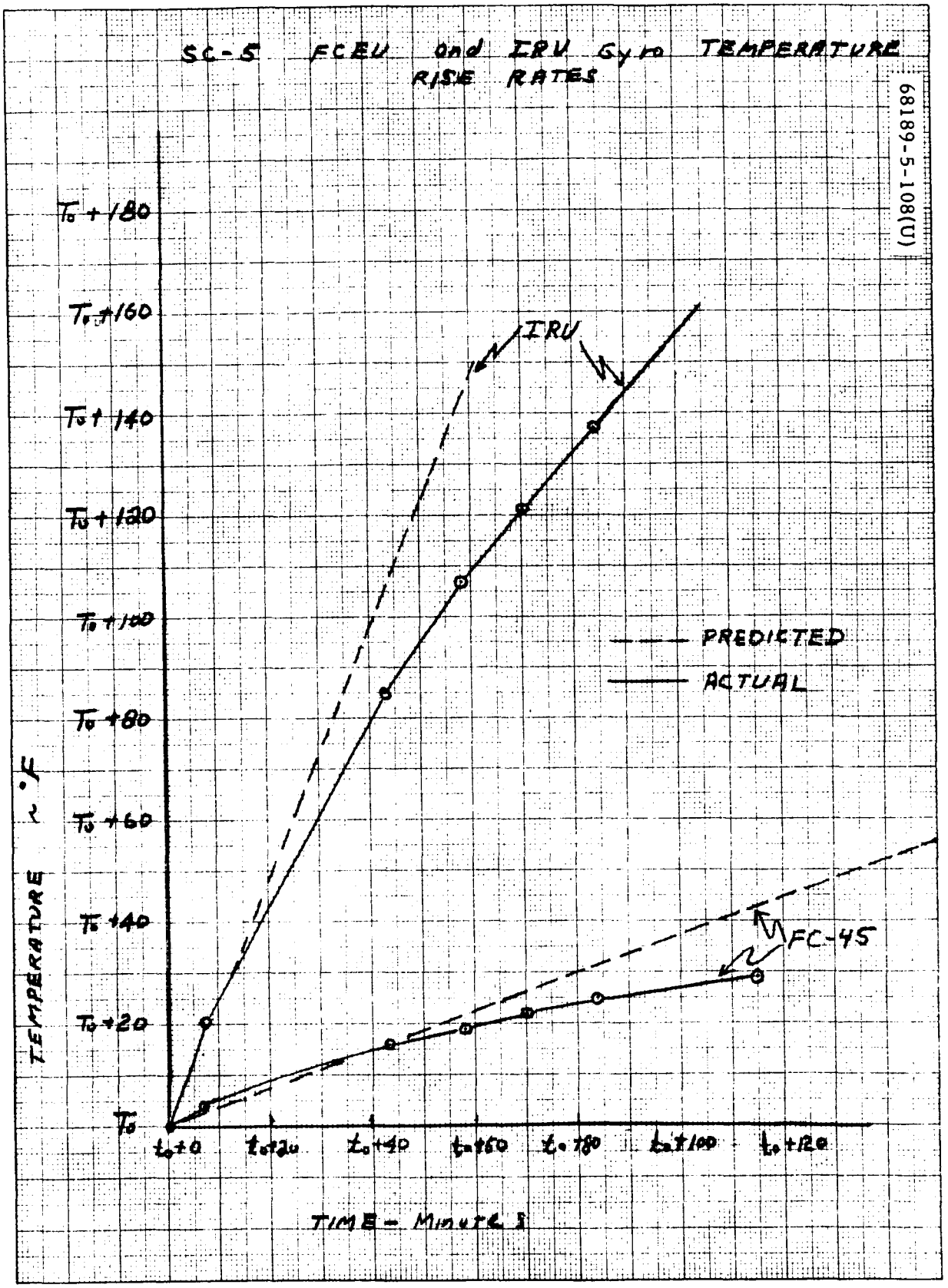

Figure 5.1-1. Selected Temperatures During Static Firing

to do so until it reached 140°F at 259:10:00. At this time, the solar panel was stepped in order to shade the television camera, and it also shaded the alpha scattering head. This caused the head temperature to drop approximately 5°F/hr until it became necessary to enable the heater to keep it from violating its lower operational limit. On day 265, the alpha head was allowed to go below its operational limit of -40°F and operated without encountering any difficulty. The head had also been allowed (with SSAE approval) to exceed its upper operational limit of 122°F earlier in the mission (day 256) without any ill effects to its operation. This operation had the approval of Space Science and may result in a revision of the printed limits for Surveyor 6 and SC-7. The bit rate corrections and the dead bands in the temperature sensors, as mentioned in subsection 5.1.4.4, were still present throughout the lunar phase.

5.1.5.5 Oxidizer Tank 1 Leak

Review (Reference 2) of the thermal data on day 261 between 08:00 and 13:00 GMT indicates that many items on the spacecraft experienced rather large temperature variations during this period. The majority of the items were located in the leg 2 region. The temperature responses of these items can be time correlated to repositioning of the solar panel/planar array assembly. Items that cannot be time correlated with the repositioning periods are 1) retro attach point 1, 2) oxidizer line 1, and 3) oxidizer tank 1. The temperature profiles for these items are presented in Figure 5.1-2.

Since the spacecraft axis is tilted approximately 20 degrees in the northerly direction with leg 1 facing south, it is not possible to shade the leg 1 region with either the solar panel or planar array. Thus, the temperature responses shown in Figure 5.1-2 must be the result of shading by other components or localized cooling resulting from expansion of either a liquid or a gas. Localized shading can be eliminated for the following reasons:

1) No temperature variations were observed on either leg 1 fuel tank or fuel line. Because of the proximity and symmetry of the fuel and oxidizer systems, local component shading would have resulted in fuel side temperature variations.

2) As evidenced by other lunar day data, total shading is not sufficient to produce a propellant tank temperature decrease of 100 degrees during a 5-hour period. In fact, based on the retro bolt 1 temperature data (Figure 5.1-2), the period of temperature change can be reduced to the interval between 10:43 and 12:08 GMT, or 1 hour and 25 minutes.

3) After the onset of lunar night, oxidizer tank 1 decreased at only 7°F/hr.

From this discussion it must be concluded that the observed oxidizer tank 1 temperature drop was the result of a sudden loss of fluid from the tank. The possibility of a helium leak can be eliminated since the latent heat of vaporization associated with the oxidizer is necessary to result in the magnitude of

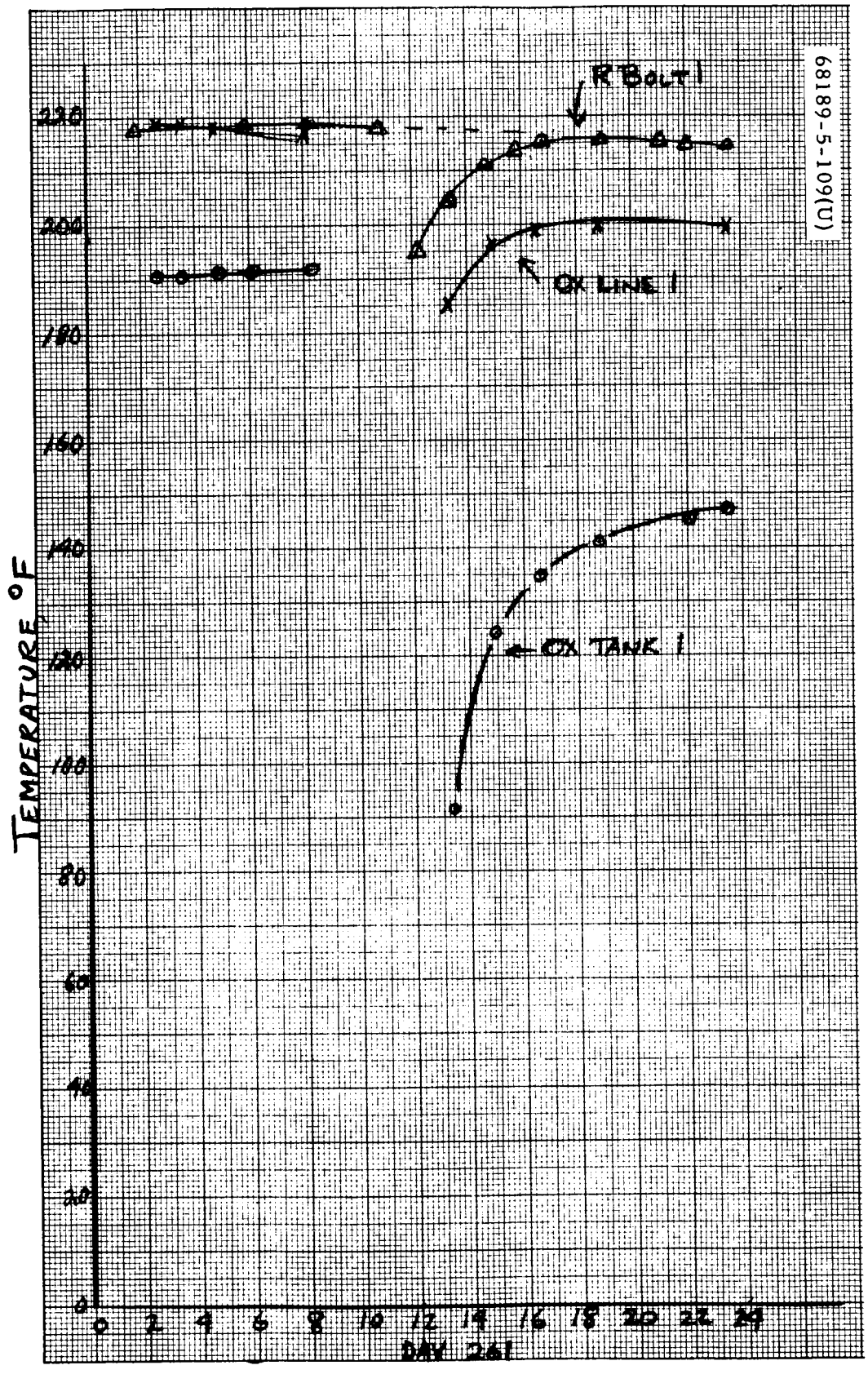

Figure 5.1-2. Temperatures Associated With Oxidizer Tank 1 Leak

cooling observed. The time of the leak can be established to be between 10:43 and 12:08 GMT on day 261.

5.1.5.6 Possible Correlation of Fuel System Pressure Drop and Collapse of Shock Absorbers 2 and 3

An attempt was made to correlate thermal date with the fuel system pressure drop on day 265 and the collapse of two of the shock absorbers on days 266 and 267.

Figures 5.1-3, 5.1-4, and 5.1-5 present the temperature histories of those items exhibiting an apparent change in cooldown rate during this time interval.

The units in the leg 1 region (Figure 5.1-3) show a discontinuity at approximately 06:00 GMT on day 266. This time does not correspond with either the decrease in fuel pressure or collapsing of the shock absorbers (first observed after 22:00 GMT on day 266). It is probable that the response is due to changes in local unit shadowing and/or solar reflections brought about by the relatively low solar elevation angle. (The shadow of the solar panel/planar array assembly is well away from the vehicle.) There is no thermal evidence to suggest a fuel leak during this time.

The units in the leg 2 (Figure 5.1-4) region exhibit discontinuities during the latter part of day 266. Again the data cannot be correlated to either the fuel pressure decay or the collapsing of the shock absorbers. It is felt that the response is the result of the sun passing through the spacecraft and illuminating units such as the shock absorber and gas jet which had previously been in a region of local spacecraft shadow.

Oxidizer line 3 (Figure 5.1-5) exhibits a slight discontinuity in cooldown during day 266. The change is gradual, however, and would appear to be the result of local solar illumination variations. There is no evidence of variations in the response of the helium tank.

In conclusion, review of the Surveyor V lunar day thermal data reveals that only the oxidizer tank 1, retro attach point 1, and oxidizer line 1 temperature data from day 261 cannot be explained by either normal sun elevation progression or movement of the solar panel/planar array assembly. The data show no correlation with either the fuel pressure decay or the collapse of the shock absorbers.

5.1.5.7 Solar Panel/Planar Array

During lunar day, both the solar panel and the planar array antenna reached temperatures higher than those experienced on previous spacecraft. The planar array exceeded its upper temperature limit of 280° F by 16 degrees on day 260. On the basis of type approval tests, it was decided that the planar array could operate at temperatures as high as 375° F. It was recommended that the allowable limit be changed for future operation and future spacecraft.

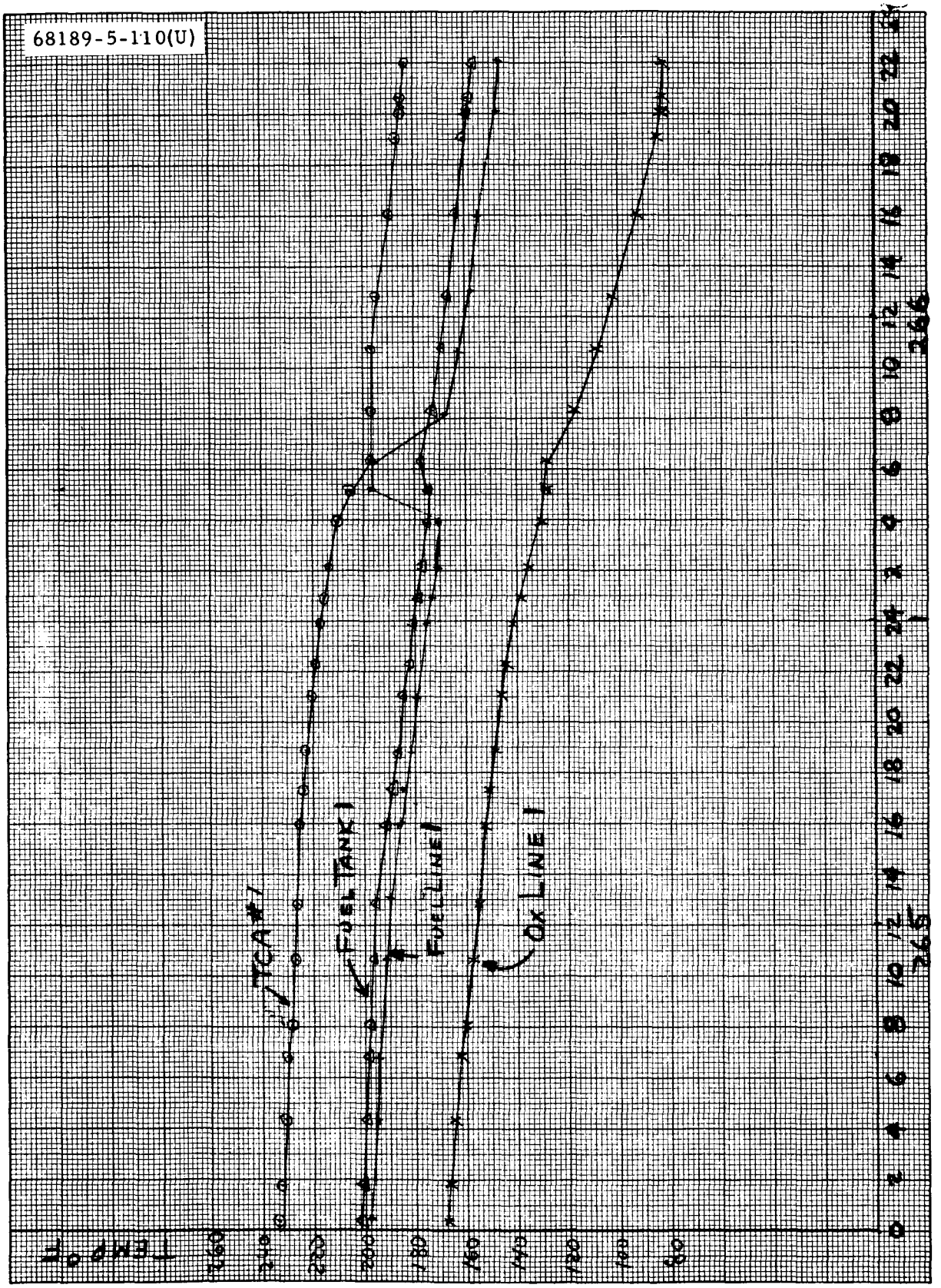

Figure 5.1-3. Temperatures in Leg 1 Region

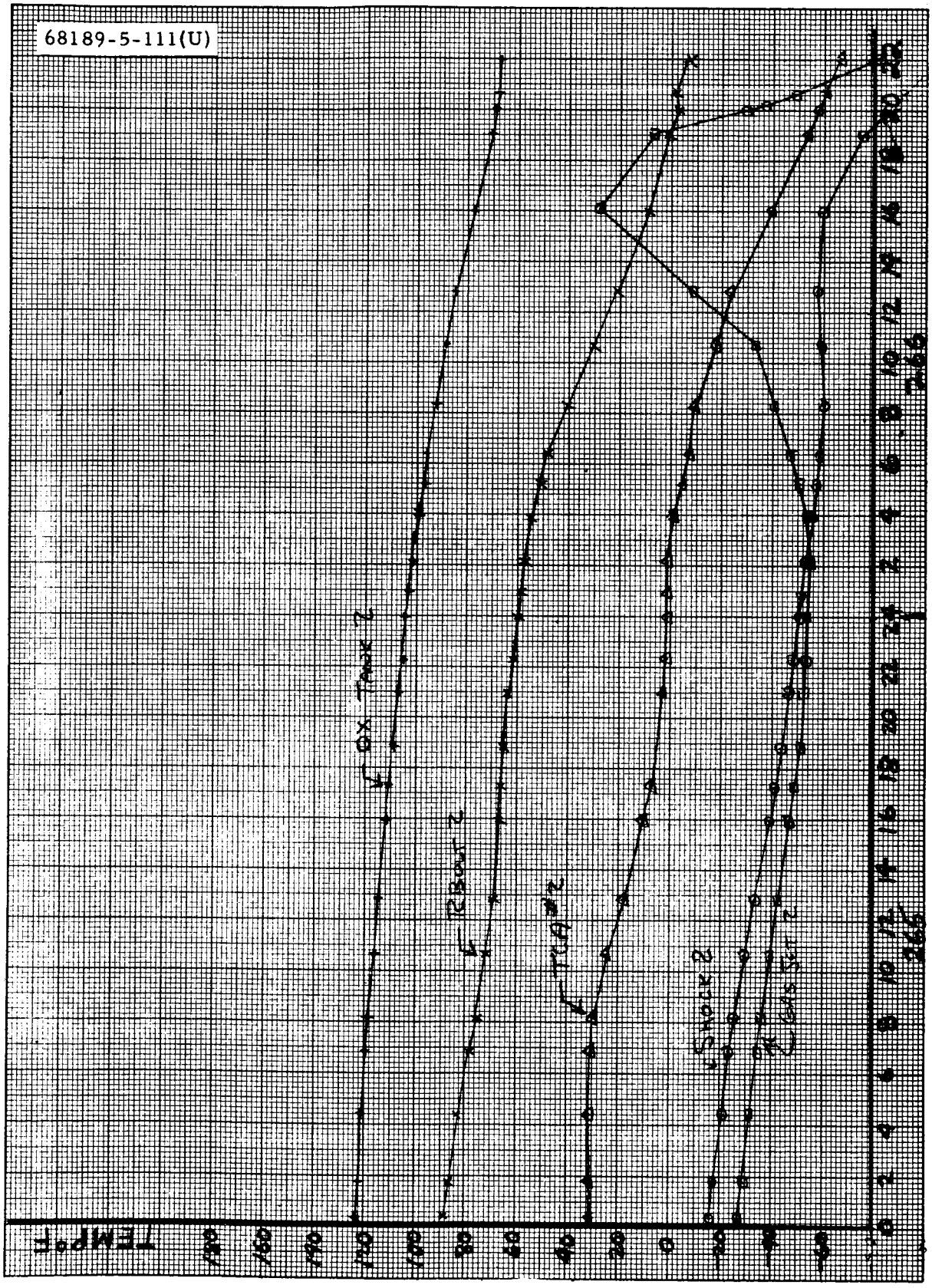

Figure 5.1-4. Temperatures in Leg 2 Region

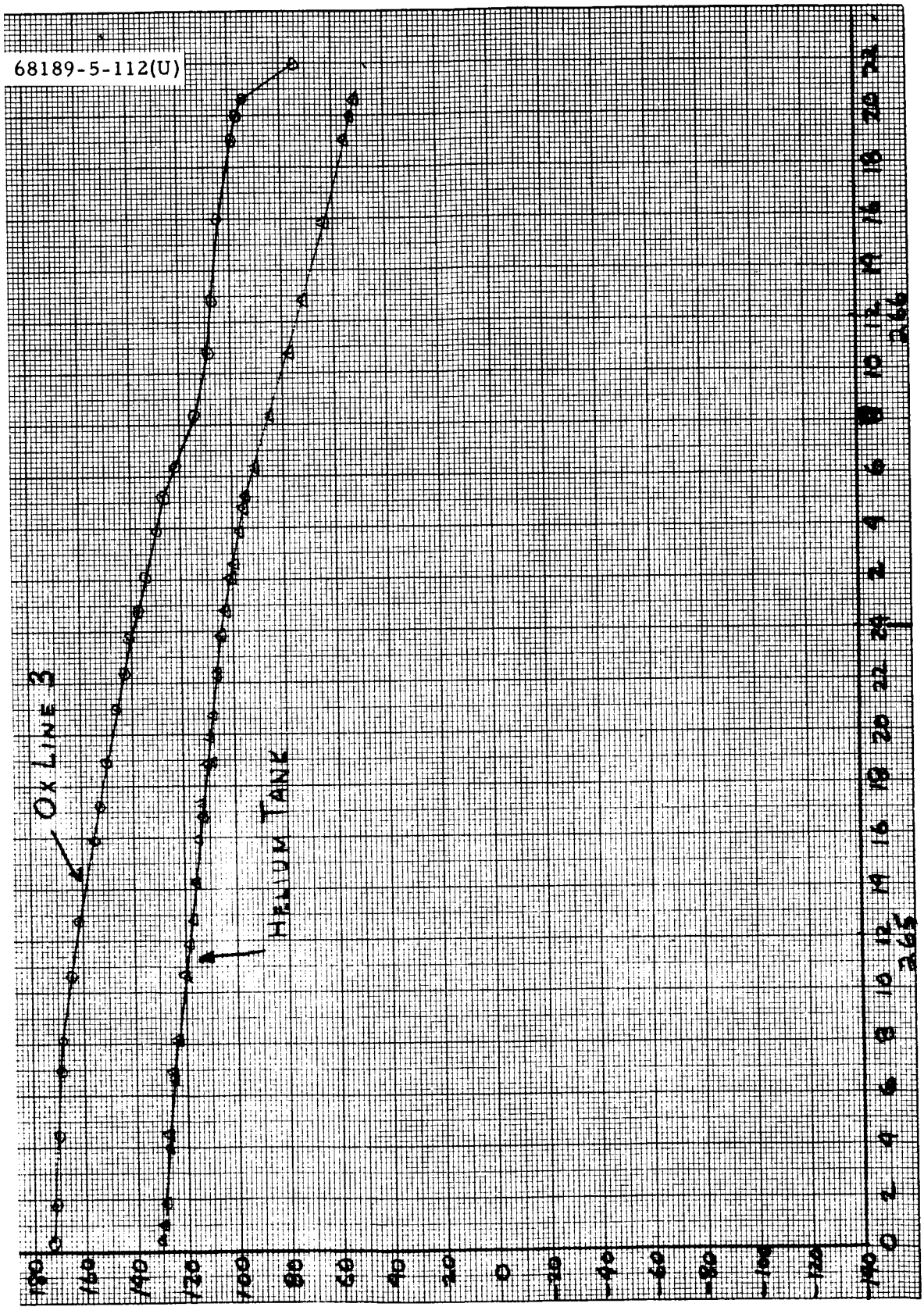

Figure 5.1-5. Oxidizer Line 3 Temperature (GMT-255-256)

The solar panel exceeded its upper temperature limit of 235°F beginning on day 257. On day 260, the temperature increased to 272°F and it became necessary to step the panel down to lower its temperature.

The excessive solar panel temperature was partially due to the solar panel switch turning off during television operations as a result of transients causing increased energy dissipation in the panel. This will be avoided in the future by either operating in bypass mode or with battery logic off during television operation and at other times when solar panel switch trip is likely.

Operation of the solar panel at elevated temperatures for short periods of time will not do significant harm to the panel (Reference 3). However, it was recommended not to change the allowable temperature limit to avoid casual operation at elevated temperatures.

5.1.5.8 First Lunar Night

The first lunar night survival program consisted of two plans. The first plan, suggested by SPAC and lasting the first 59 hours of lunar night, was to maintain the compartment B upper tray (V-21) between 20° and -16°F, which would automatically keep the main battery in compartment A above 20°F due to the interrogations and TC & HA use in compartment B. The second plan, suggested to simplify operations and conserve power, called for dissipating just enough heat in the compartment A and B electronics to hold their temperatures steady.

The first survival plan consisted of: 1) determining the lunar night heat losses from the compartment system, and 2) determining a plan of action to control the main battery above 20°F and compartment B above its lower specified operational limit. The compartment B lower specified operational limit for the upper tray (V-21) was 0°F; however, SPAC obtained permission to operate the upper tray to -20°F.

The initial period of the first plan consisted of determining compartment heat losses and thermal switch openings. All of the four monitored thermal switches on compartment A opened within their specified temperature range. Only one (V-46) of the three monitored thermal switches on compartment B opened within specifications. One thermal switch (V-24) on compartment B opened out of specification when the upper tray temperature (V-21) was -4°F, and the last monitored thermal switch (V-45) never opened even though the upper tray was dropped to -22°F several times. It was determined through analysis that, at the beginning of the lunar night compartment deep freeze, all the thermal switches in compartment A were open, and all but one thermal switch in compartment B were open.

The initial plan of action was to control the compartment temperatures using the following general philosophy: 1) keep compartment B upper tray (V-21) above -20°F by turning the compartment B TC & HA on at the beginning of each interrogation and off at the end of it, 2) go into standby mode between interrogations to conserve power consumption, and 3) the main battery in compartment A should not drop in temperature due to the heat supplied by the interrogations.

Compartment B

$$q\ (avg.) = (0.137)(16.9) + (0.863)(9.9)$$

$$= 10.86 \text{ watts}$$

Therefore, it can be concluded that the heat losses from the Surveyor V compartment A and B were:

	Heat Loss, watts		
	Total Compartment Loss	Less Stuck Switch Loss	Compartment System Loss
Compartment A at 20 F	9.23	—	9.23
Compartment B at -15 F	10.86	3.4 (T_{rad} = -42°F)	7.46

The actual lunar night temperature of compartments A and B up to the point of shutdown are presented in Figures 5.1-121 to 5.1-131.

5.1.6 REFERENCES

1) E.R. Shelton, "Nominal Mission E Shadow Plots," Hughes IDC 2292/375, 26 August 1967.

2) R.R. Garipay, "Preliminary Review of SC-5 Lunar Day Temperature Data," Hughes IDC 2221.19/229, 10 October 1967.

3) J.C. Jensen, "Revising S/P Maximum Temperature Limit," Hughes IDC 2255.1/3093, 3 November 1967.

4) T.A. Harvey, Jr., "SC-5 Lunar Night Report and Analysis," Hughes IDC 2221.19/230, 12 October 1967.

5) L.L. Gamer, "SC-5 Spacecraft Shadow Plots for First Lunar Day Using Actual A/SPP Stepping History," Hughes IDC 2292/409, 13 October 1967.

6) Material for the transit discussion was, in general, abstracted from: "Surveyor Mission E Space Flight Operations Report," Hughes Aircraft Company, SSD 78160, October 1967.

5.1.7 ACKNOWLEDGMENT

This section was coordinated by Jon B. Goodblatt of the Surveyor Thermal Control Section.

APPENDIX A
TO SECTION 5.1
TRANSIT TEMPERATURE PLOTS

Appendix A contains Figures 5.1-6 to 5.1-78 which are transit thermal plots.

PRECEDING PAGE BLANK NOT FILMED.

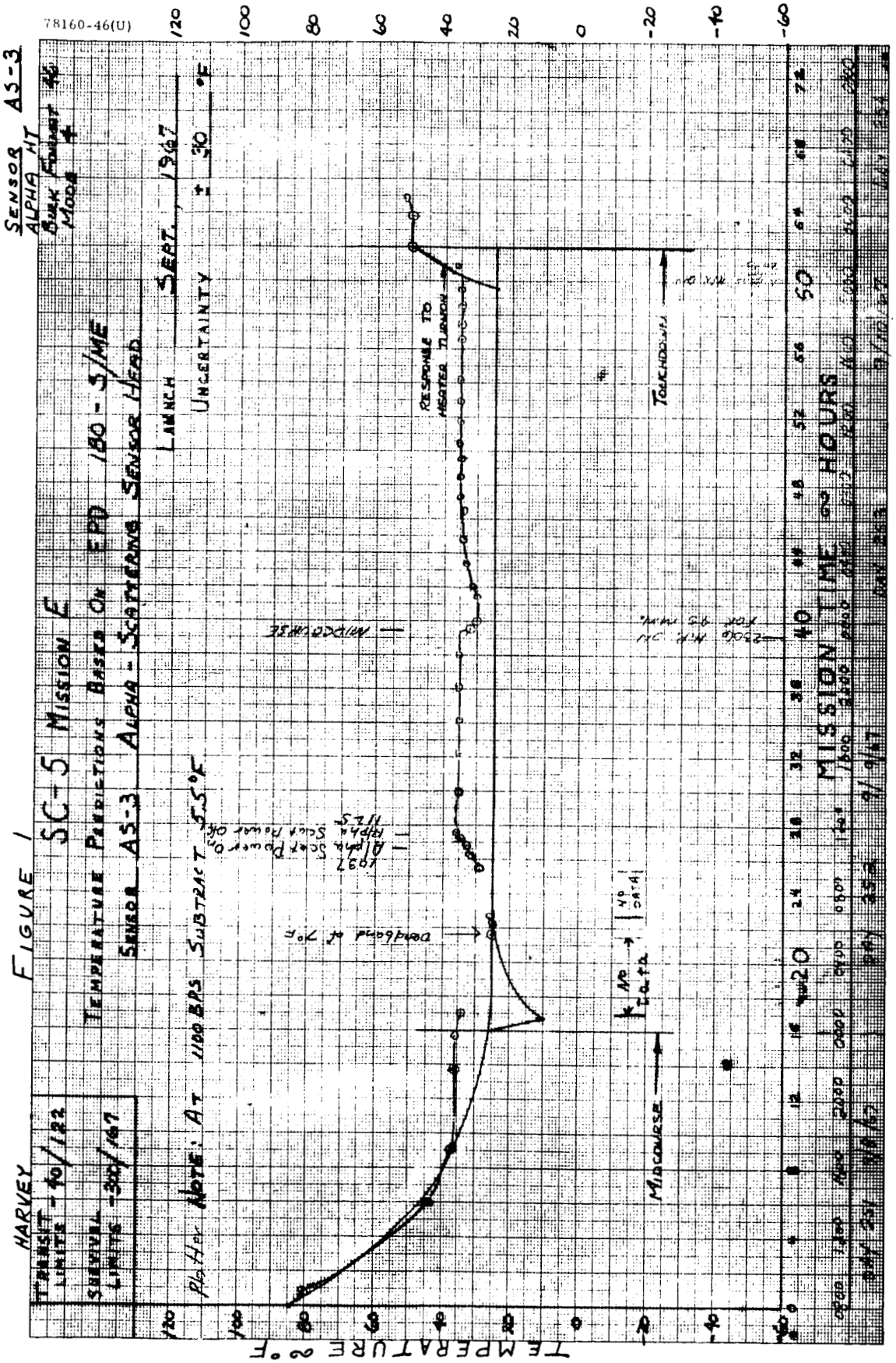

Figure 5.1-6. Sensor AS-3: Alpha Scattering Sensor Head

PRECEDING PAGE BLANK NOT FILMED.

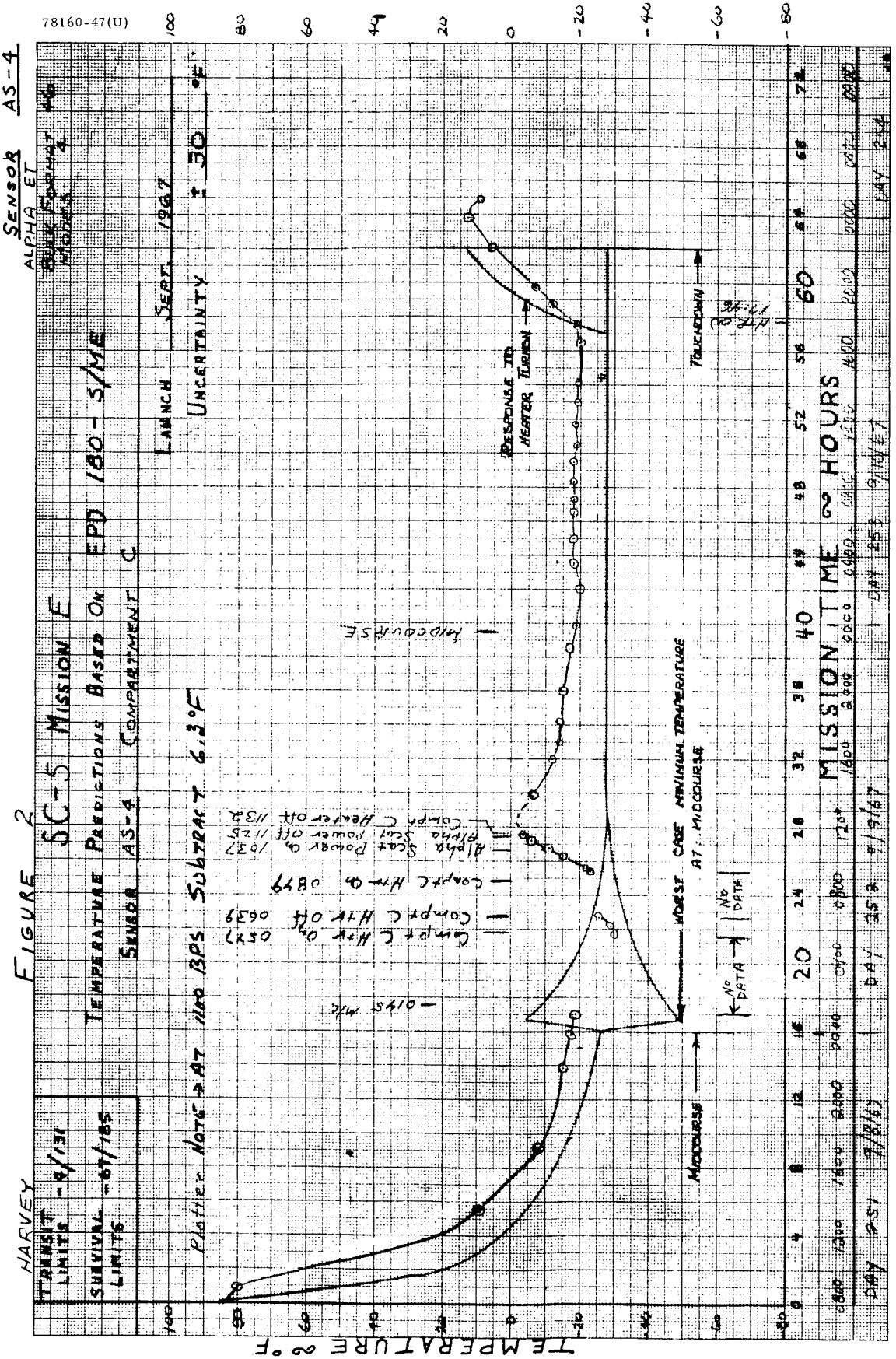
78160-47(U)
FIGURE 2
SC-5 Mission E
Temperature Predictions Based On EPD 180-5/ME
Sensor AS-4 Compartment C
Launch Sept. 1967
Uncertainty ± 30 °F
Sensor AS-4
ALPHA ET
Bulk Foam 4
Models
HARVEY
Transit -4/136
Survival -67/185
Limits
Plotted Nov 67 at 1100 BPS Subject 6.2°F
Midcourse
Response to Heater Turn On
Touchdown
Worst Case Minimum Temperature
At Midcourse
No Data
Mission Time 60 Hours
Temperature °F
Day 351 12/17/67
Day 352 12/18/67
Day 353 12/19/67
Day 354 12/20/67
Day 355 12/21/67
Day 356 12/22/67
Day 357 12/23/67
Day 358 12/24/67
Day 359 12/25/67
Day 360 12/26/67
Day 361 12/27/67
Day 362 12/28/67
Day 363 12/29/67
Day 364 12/30/67
Day 365 12/31/67
Day 1 1/1/68
Day 2 1/2/68
Day 3 1/3/68
Day 4 1/4/68
Day 5 1/5/68
Day 6 1/6/68
Day 7 1/7/68
Day 8 1/8/68
Day 9 1/9/68
Day 10 1/10/68
Day 11 1/11/68
Day 12 1/12/68
Day 13 1/13/68
Day 14 1/14/68
Day 15 1/15/68
Day 16 1/16/68
Day 17 1/17/68
Day 18 1/18/68
Day 19 1/19/68
Day 20 1/20/68
Day 21 1/21/68
Day 22 1/22/68
Day 23 1/23/68
Day 24 1/24/68
Day 25 1/25/68
Day 26 1/26/68
Day 27 1/27/68
Day 28 1/28/68
Day 29 1/29/68
Day 30 1/30/68
Day 31 1/31/68
Day 32 2/1/68
Day 33 2/2/68
Day 34 2/3/68
Day 35 2/4/68
Day 36 2/5/68
Day 37 2/6/68
Day 38 2/7/68
Day 39 2/8/68
Day 40 2/9/68
Day 41 2/10/68
Day 42 2/11/68
Day 43 2/12/68
Day 44 2/13/68
Day 45 2/14/68
Day 46 2/15/68
Day 47 2/16/68
Day 48 2/17/68
Day 49 2/18/68
Day 50 2/19/68
Day 51 2/20/68
Day 52 2/21/68
Day 53 2/22/68
Day 54 2/23/68
Day 55 2/24/68
Day 56 2/25/68
Day 57 2/26/68
Day 58 2/27/68
Day 59 2/28/68
Day 60 2/29/68
Day 61 3/1/68
Day 62 3/2/68
Day 63 3/3/68
Day 64 3/4/68
Day 65 3/5/68
Day 66 3/6/68
Day 67 3/7/68
Day 68 3/8/68
Day 69 3/9/68
Day 70 3/10/68
Day 71 3/11/68
Day 72 3/12/68
Day 73 3/13/68
Day 74 3/14/68
Day 75 3/15/68
Day 76 3/16/68
Day 77 3/17/68
Day 78 3/18/68
Day 79 3/19/68
Day 80 3/20/68
Day 81 3/21/68
Day 82 3/22/68
Day 83 3/23/68
Day 84 3/24/68
Day 85 3/25/68
Day 86 3/26/68
Day 87 3/27/68
Day 88 3/28/68
Day 89 3/29/68
Day 90 3/30/68
Day 91 3/31/68
Day 92 4/1/68
Day 93 4/2/68
Day 94 4/3/68
Day 95 4/4/68
Day 96 4/5/68
Day 97 4/6/68
Day 98 4/7/68
Day 99 4/8/68
Day 100 4/9/68
Day 101 4/10/68
Day 102 4/11/68
Day 103 4/12/68
Day 104 4/13/68
Day 105 4/14/68
Day 106 4/15/68
Day 107 4/16/68
Day 108 4/17/68
Day 109 4/18/68
Day 110 4/19/68
Day 111 4/20/68
Day 112 4/21/68
Day 113 4/22/68
Day 114 4/23/68
Day 115 4/24/68
Day 116 4/25/68
Day 117 4/26/68
Day 118 4/27/68
Day 119 4/28/68
Day 120 4/29/68
Day 121 4/30/68
Day 122 5/1/68
Day 123 5/2/68
Day 124 5/3/68
Day 125 5/4/68
Day 126 5/5/68
Day 127 5/6/68
Day 128 5/7/68
Day 129 5/8/68
Day 130 5/9/68
Day 131 5/10/68
Day 132 5/11/68
Day 133 5/12/68
Day 134 5/13/68
Day 135 5/14/68
Day 136 5/15/68
Day 137 5/16/68
Day 138 5/17/68
Day 139 5/18/68
Day 140 5/19/68
Day 141 5/20/68
Day 142 5/21/68
Day 143 5/22/68
Day 144 5/23/68
Day 145 5/24/68
Day 146 5/25/68
Day 147 5/26/68
Day 148 5/27/68
Day 149 5/28/68
Day 150 5/29/68
Day 151 5/30/68
Day 152 5/31/68
Day 153 6/1/68
Day 154 6/2/68
Day 155 6/3/68
Day 156 6/4/68
Day 157 6/5/68
Day 158 6/6/68
Day 159 6/7/68
Day 160 6/8/68
Day 161 6/9/68
Day 162 6/10/68
Day 163 6/11/68
Day 164 6/12/68
Day 165 6/13/68
Day 166 6/14/68
Day 167 6/15/68
Day 168 6/16/68
Day 169 6/17/68
Day 170 6/18/68
Day 171 6/19/68
Day 172 6/20/68
Day 173 6/21/68
Day 174 6/22/68
Day 175 6/23/68
Day 176 6/24/68
Day 177 6/25/68
Day 178 6/26/68
Day 179 6/27/68
Day 180 6/28/68
Day 181 6/29/68
Day 182 6/30/68
Day 183 7/1/68
Day 184 7/2/68
Day 185 7/3/68
Day 186 7/4/68
Day 187 7/5/68
Day 188 7/6/68
Day 189 7/7/68
Day 190 7/8/68
Day 191 7/9/68
Day 192 7/10/68
Day 193 7/11/68
Day 194 7/12/68
Day 195 7/13/68
Day 196 7/14/68
Day 197 7/15/68
Day 198 7/16/68
Day 199 7/17/68
Day 200 7/18/68
Day 201 7/19/68
Day 202 7/20/68
Day 203 7/21/68
Day 204 7/22/68
Day 205 7/23/68
Day 206 7/24/68
Day 207 7/25/68
Day 208 7/26/68
Day 209 7/27/68
Day 210 7/28/68
Day 211 7/29/68
Day 212 7/30/68
Day 213 7/31/68
Day 214 8/1/68
Day 215 8/2/68
Day 216 8/3/68
Day 217 8/4/68
Day 218 8/5/68
Day 219 8/6/68
Day 220 8/7/68
Day 221 8/8/68
Day 222 8/9/68
Day 223 8/10/68
Day 224 8/11/68
Day 225 8/12/68
Day 226 8/13/68
Day 227 8/14/68
Day 228 8/15/68
Day 229 8/16/68
Day 230 8/17/68
Day 231 8/18/68
Day 232 8/19/68
Day 233 8/20/68
Day 234 8/21/68
Day 235 8/22/68
Day 236 8/23/68
Day 237 8/24/68
Day 238 8/25/68
Day 239 8/26/68
Day 240 8/27/68
Day 241 8/28/68
Day 242 8/29/68
Day 243 8/30/68
Day 244 8/31/68
Day 245 9/1/68
Day 246 9/2/68
Day 247 9/3/68
Day 248 9/4/68
Day 249 9/5/68
Day 250 9/6/68
Day 251 9/7/68
Day 252 9/8/68
Day 253 9/9/68
Day 254 9/10/68
Day 255 9/11/68
Day 256 9/12/68
Day 257 9/13/68
Day 258 9/14/68
Day 259 9/15/68
Day 260 9/16/68
Day 261 9/17/68
Day 262 9/18/68
Day 263 9/19/68
Day 264 9/20/68
Day 265 9/21/68
Day 266 9/22/68
Day 267 9/23/68
Day 268 9/24/68
Day 269 9/25/68
Day 270 9/26/68
Day 271 9/27/68
Day 272 9/28/68
Day 273 9/29/68
Day 274 9/30/68
Day 275 10/1/68
Day 276 10/2/68
Day 277 10/3/68
Day 278 10/4/68
Day 279 10/5/68
Day 280 10/6/68
Day 281 10/7/68
Day 282 10/8/68
Day 283 10/9/68
Day 284 10/10/68
Day 285 10/11/68
Day 286 10/12/68
Day 287 10/13/68
Day 288 10/14/68
Day 289 10/15/68
Day 290 10/16/68
Day 291 10/17/68
Day 292 10/18/68
Day 293 10/19/68
Day 294 10/20/68
Day 295 10/21/68
Day 296 10/22/68
Day 297 10/23/68
Day 298 10/24/68
Day 299 10/25/68
Day 300 10/26/68
Day 301 10/27/68
Day 302 10/28/68
Day 303 10/29/68
Day 304 10/30/68
Day 305 10/31/68
Day 306 11/1/68
Day 307 11/2/68
Day 308 11/3/68
Day 309 11/4/68
Day 310 11/5/68
Day 311 11/6/68
Day 312 11/7/68
Day 313 11/8/68
Day 314 11/9/68
Day 315 11/10/68
Day 316 11/11/68
Day 317 11/12/68
Day 318 11/13/68
Day 319 11/14/68
Day 320 11/15/68
Day 321 11/16/68
Day 322 11/17/68
Day 323 11/18/68
Day 324 11/19/68
Day 325 11/20/68
Day 326 11/21/68
Day 327 11/22/68
Day 328 11/23/68
Day 329 11/24/68
Day 330 11/25/68
Day 331 11/26/68
Day 332 11/27/68
Day 333 11/28/68
Day 334 11/29/68
Day 335 11/30/68
Day 336 12/1/68
Day 337 12/2/68
Day 338 12/3/68
Day 339 12/4/68
Day 340 12/5/68
Day 341 12/6/68
Day 342 12/7/68
Day 343 12/8/68
Day 344 12/9/68
Day 345 12/10/68
Day 346 12/11/68
Day 347 12/12/68
Day 348 12/13/68
Day 349 12/14/68
Day 350 12/15/68
Day 351 12/16/68
Day 352 12/17/68
Day 353 12/18/68
Day 354 12/19/68
Day 355 12/20/68
Day 356 12/21/68
Day 357 12/22/68
Day 358 12/23/68
Day 359 12/24/68
Day 360 12/25/68
Day 361 12/26/68
Day 362 12/27/68
Day 363 12/28/68
Day 364 12/29/68
Day 365 12/30/68
Day 366 12/31/68
Day 367 1/1/69
Day 368 1/2/69
Day 369 1/3/69
Day 370 1/4/69
Day 371 1/5/69
Day 372 1/6/69
Day 373 1/7/69
Day 374 1/8/69
Day 375 1/9/69
Day 376 1/10/69
Day 377 1/11/69
Day 378 1/12/69
Day 379 1/13/69
Day 380 1/14/69
Day 381 1/15/69
Day 382 1/16/69
Day 383 1/17/69
Day 384 1/18/69
Day 385 1/19/69
Day 386 1/20/69
Day 387 1/21/69
Day 388 1/22/69
Day 389 1/23/69
Day 390 1/24/69
Day 391 1/25/69
Day 392 1/26/69
Day 393 1/27/69
Day 394 1/28/69
Day 395 1/29/69
Day 396 1/30/69
Day 397 1/31/69
Day 398 2/1/69
Day 399 2/2/69
Day 400 2/3/69
Day 401 2/4/69
Day 402 2/5/69
Day 403 2/6/69
Day 404 2/7/69
Day 405 2/8/69
Day 406 2/9/69
Day 407 2/10/69
Day 408 2/11/69
Day 409 2/12/69
Day 410 2/13/69
Day 411 2/14/69
Day 412 2/15/69
Day 413 2/16/69
Day 414 2/17/69
Day 415 2/18/69
Day 416 2/19/69
Day 417 2/20/69
Day 418 2/21/69
Day 419 2/22/69
Day 420 2/23/69
Day 421 2/24/69
Day 422 2/25/69
Day 423 2/26/69
Day 424 2/27/69
Day 425 2/28/69
Day 426 3/1/69
Day 427 3/2/69
Day 428 3/3/69
Day 429 3/4/69
Day 430 3/5/69
Day 431 3/6/69
Day 432 3/7/69
Day 433 3/8/69
Day 434 3/9/69
Day 435 3/10/69
Day 436 3/11/69
Day 437 3/12/69
Day 438 3/13/69
Day 439 3/14/69
Day 440 3/15/69
Day 441 3/16/69
Day 442 3/17/69
Day 443 3/18/69
Day 444 3/19/69
Day 445 3/20/69
Day 446 3/21/69
Day 447 3/22/69
Day 448 3/23/69
Day 449 3/24/69
Day 450 3/25/69
Day 451 3/26/69
Day 452 3/27/69
Day 453 3/28/69
Day 454 3/29/69
Day 455 3/30/69
Day 456 3/31/69
Day 457 4/1/69
Day 458 4/2/69
Day 459 4/3/69
Day 460 4/4/69
Day 461 4/5/69
Day 462 4/6/69
Day 463 4/7/69
Day 464 4/8/69
Day 465 4/9/69
Day 466 4/10/69
Day 467 4/11/69
Day 468 4/12/69
Day 469 4/13/69
Day 470 4/14/69
Day 471 4/15/69
Day 472 4/16/69
Day 473 4/17/69
Day 474 4/18/69
Day 475 4/19/69
Day 476 4/20/69
Day 477 4/21/69
Day 478 4/22/69
Day 479 4/23/69
Day 480 4/24/69
Day 481 4/25/69
Day 482 4/26/69
Day 483 4/27/69
Day 484 4/28/69
Day 485 4/29/69
Day 486 4/30/69
Day 487 5/1/69
Day 488 5/2/69
Day 489 5/3/69
Day 490 5/4/69
Day 491 5/5/69
Day 492 5/6/69
Day 493 5/7/69
Day 494 5/8/69
Day 495 5/9/69
Day 496 5/10/69
Day 497 5/11/69
Day 498 5/12/69
Day 499 5/13/69
Day 500 5/14/69
Day 501 5/15/69
Day 502 5/16/69
Day 503 5/17/69
Day 504 5/18/69
Day 505 5/19/69
Day 506 5/20/69
Day 507 5/21/69
Day 508 5/22/69
Day 509 5/23/69
Day 510 5/24/69
Day 511 5/25/69
Day 512 5/26/69
Day 513 5/27/69
Day 514 5/28/69
Day 515 5/29/69
Day 516 5/30/69
Day 517 5/31/69
Day 518 6/1/69
Day 519 6/2/69
Day 520 6/3/69
Day 521 6/4/69
Day 522 6/5/69
Day 523 6/6/69
Day 524 6/7/69
Day 525 6/8/69
Day 526 6/9/69
Day 527 6/10/69
Day 528 6/11/69
Day 529 6/12/69
Day 530 6/13/69
Day 531 6/14/69
Day 532 6/15/69
Day 533 6/16/69
Day 534 6/17/69
Day 535 6/18/69
Day 536 6/19/69
Day 537 6/20/69
Day 538 6/21/69
Day 539 6/22/69
Day 540 6/23/69
Day 541 6/24/69
Day 542 6/25/69
Day 543 6/26/69
Day 544 6/27/69
Day 545 6/28/69
Day 546 6/29/69
Day 547 6/30/69
Day 548 7/1/69
Day 549 7/2/69
Day 550 7/3/69
Day 551 7/4/69
Day 552 7/5/69
Day 553 7/6/69
Day 554 7/7/69
Day 555 7/8/69
Day 556 7/9/69
Day 557 7/10/69
Day 558 7/11/69
Day 559 7/12/69
Day 560 7/13/69
Day 561 7/14/69
Day 562 7/15/69
Day 563 7/16/69
Day 564 7/17/69
Day 565 7/18/69
Day 566 7/19/69
Day 567 7/20/69
Day 568 7/21/69
Day 569 7/22/69
Day 570 7/23/69
Day 571 7/24/69
Day 572 7/25/69
Day 573 7/26/69
Day 574 7/27/69
Day 575 7/28/69
Day 576 7/29/69
Day 577 7/30/69
Day 578 7/31/69
Day 579 8/1/69
Day 580 8/2/69
Day 581 8/3/69
Day 582 8/4/69
Day 583 8/5/69
Day 584 8/6/69
Day 585 8/7/69
Day 586 8/8/69
Day 587 8/9/69
Day 588 8/10/69
Day 589 8/11/69
Day 590 8/12/69
Day 591 8/13/69
Day 592 8/14/69
Day 593 8/15/69
Day 594 8/16/69
Day 595 8/17/69
Day 596 8/18/69
Day 597 8/19/69
Day 598 8/20/69
Day 599 8/21/69
Day 600 8/22/69
Day 601 8/23/69
Day 602 8/24/69
Day 603 8/25/69
Day 604 8/26/69
Day 605 8/27/69
Day 606 8/28/69
Day 607 8/29/69
Day 608 8/30/69
Day 609 8/31/69
Day 610 9/1/69
Day 611 9/2/69
Day 612 9/3/69
Day 613 9/4/69
Day 614 9/5/69
Day 615 9/6/69
Day 616 9/7/69
Day 617 9/8/69
Day 618 9/9/69
Day 619 9/10/69
Day 620 9/11/69
Day 621 9/12/69
Day 622 9/13/69
Day 623 9/14/69
Day 624 9/15/69
Day 625 9/16/69
Day 626 9/17/69
Day 627 9/18/69
Day 628 9/19/69
Day 629 9/20/69
Day 630 9/21/69
Day 631 9/22/69
Day 632 9/23/69
Day 633 9/24/69
Day 634 9/25/69
Day 635 9/26/69
Day 636 9/27/69
Day 637 9/28/69
Day 638 9/29/69
Day 639 9/30/69
Day 640 10/1/69
Day 641 10/2/69
Day 642 10/3/69
Day 643 10/4/69
Day 644 10/5/69
Day 645 10/6/69
Day 646 10/7/69
Day 647 10/8/69
Day 648 10/9/69
Day 649 10/10/69
Day 650 10/11/69
Day 651 10/12/69
Day 652 10/13/69
Day 653 10/14/69
Day 654 10/15/69
Day 655 10/16/69
Day 656 10/17/69
Day 657 10/18/69
Day 658 10/19/69
Day 659 10/20/69
Day 660 10/21/69
Day 661 10/22/69
Day 662 10/23/69
Day 663 10/24/69
Day 664 10/25/69
Day 665 10/26/69
Day 666 10/27/69
Day 667 10/28/69
Day 668 10/29/69
Day 669 10/30/69
Day 670 10/31/69
Day 671 11/1/69
Day 672 11/2/69
Day 673 11/3/69
Day 674 11/4/69
Day 675 11/5/69
Day 676 11/6/69
Day 677 11/7/69
Day 678 11/8/69
Day 679 11/9/69
Day 680 11/10/69
Day 681 11/11/69
Day 682 11/12/69
Day 683 11/13/69
Day 684 11/14/69
Day 685 11/15/69
Day 686 11/16/69
Day 687 11/17/69
Day 688 11/18/69
Day 689 11/19/69
Day 690 11/20/69
Day 691 11/21/69
Day 692 11/22/69
Day 693 11/23/69
Day 694 11/24/69
Day 695 11/25/69
Day 696 11/26/69
Day 697 11/27/69
Day 698 11/28/69
Day 699 11/29/69
Day 700 11/30/69
Day 701 12/1/69
Day 702 12/2/69
Day 703 12/3/69
Day 704 12/4/69
Day 705 12/5/69
Day 706 12/6/69
Day 707 12/7/69
Day 708 12/8/69
Day 709 12/9/69
Day 710 12/10/69
Day 711 12/11/69
Day 712 12/12/69
Day 713 12/13/69
Day 714 12/14/69
Day 715 12/15/69
Day 716 12/16/69
Day 717 12/17/69
Day 718 12/18/69
Day 719 12/19/69
Day 720 12/20/69
Day 721 12/21/69
Day 722 12/22/69
Day 723 12/23/69
Day 724 12/24/69
Day 725 12/25/69
Day 726 12/26/69
Day 727 12/27/69
Day 728 12/28/69
Day 729 12/29/69
Day 730 12/30/69
Day 731 12/31/69
Day 732 1/1/70
Day 733 1/2/70
Day 734 1/3/70
Day 735 1/4/70
Day 736 1/5/70
Day 737 1/6/70
Day 738 1/7/70
Day 739 1/8/70
Day 740 1/9/70
Day 741 1/10/70
Day 742 1/11/70
Day 743 1/12/70
Day 744 1/13/70
Day 745 1/14/70
Day 746 1/15/70
Day 747 1/16/70
Day 748 1/17/70
Day 749 1/18/70
Day 750 1/19/70
Day 751 1/20/70
Day 752 1/21/70
Day 753 1/22/70
Day 754 1/23/70
Day 755 1/24/70
Day 756 1/25/70
Day 757 1/26/70
Day 758 1/27/70
Day 759 1/28/70
Day 760 1/29/70
Day 761 1/30/70
Day 762 1/31/70
Day 763 2/1/70
Day 764 2/2/70
Day 765 2/3/70
Day 766 2/4/70
Day 767 2/5/70
Day 768 2/6/70
Day 769 2/7/70
Day 770 2/8/70
Day 771 2/9/70
Day 772 2/10/70
Day 773 2/11/70
Day 774 2/12/70
Day 775 2/13/70
Day 776 2/14/70
Day 777 2/15/70
Day 778 2/16/70
Day 779 2/17/70
Day 780 2/18/70
Day 781 2/19/70
Day 782 2/20/70
Day 783 2/21/70
Day 784 2/22/70
Day 785 2/23/70
Day 786 2/24/70
Day 787 2/25/70
Day 788 2/26/70
Day 789 2/27/70
Day 790 2/28/70
Day 791 3/1/70
Day 792 3/2/70
Day 793 3/3/70
Day 794 3/4/70
Day 795 3/5/70
Day 796 3/6/70
Day 797 3/7/70
Day 798 3/8/70
Day 799 3/9/70
Day 800 3/10/70
Day 801 3/11/70
Day 802 3/12/70
Day 803 3/13/70
Day 804 3/14/70
Day 805 3/15/70
Day 806 3/16/70
Day 807 3/17/70
Day 808 3/18/70
Day 809 3/19/70
Day 810 3/20/70
Day 811 3/21/70
Day 812 3/22/70
Day 813 3/23/70
Day 814 3/24/70
Day 815 3/25/70
Day 816 3/26/70
Day 817 3/27/70
Day 818 3/28/70
Day 819 3/29/70
Day 820 3/30/70
Day 821 3/31/70
Day 822 4/1/70
Day 823 4/2/70
Day 824 4/3/70
Day 825 4/4/70
Day 826 4/5/70
Day 827 4/6/70
Day 828 4/7/70
Day 829 4/8/70
Day 830 4/9/70
Day 831 4/10/70
Day 832 4/11/70
Day 833 4/12/70
Day 834 4/13/70
Day 835 4/14/70
Day 836 4/15/70
Day 837 4/16/70
Day 838 4/17/70
Day 839 4/18/70
Day 840 4/19/70
Day 841 4/20/70
Day 842 4/21/70
Day 843 4/22/70
Day 844 4/23/70
Day 845 4/24/70
Day 846 4/25/70
Day 847 4/26/70
Day 848 4/27/70
Day 849 4/28/70
Day 850 4/29/70
Day 851 4/30/70
Day 852 5/1/70
Day 853 5/2/70
Day 854 5/3/70
Day 855 5/4/70
Day 856 5/5/70
Day 857 5/6/70
Day 858 5/7/70
Day 859 5/8/70
Day 860 5/9/70
Day 861 5/10/70
Day 862 5/11/70
Day 863 5/12/70
Day 864 5/13/70
Day 865 5/14/70
Day 866 5/15/70
Day 867 5/16/70
Day 868 5/17/70
Day 869 5/18/70
Day 870 5/19/70
Day 871 5/20/70
Day 872 5/21/70
Day 873 5/22/70
Day 874 5/23/70
Day 875 5/24/70
Day 876 5/25/70
Day 877 5/26/70
Day 878 5/27/70
Day 879 5/28/70
Day 880 5/29/70
Day 881 5/30/70
Day 882 5/31/70
Day 883 6/1/70
Day 884 6/2/70
Day 885 6/3/70
Day 886 6/4/70
Day 887 6/5/70
Day 888 6/6/70
Day 889 6/7/70
Day 890 6/8/70
Day 891 6/9/70
Day 892 6/10/70
Day 893 6/11/70
Day 894 6/12/70
Day 895 6/13/70
Day 896 6/14/70
Day 897 6/15/70
Day 898 6/16/70
Day 899 6/17/70
Day 900 6/18/70
Day 901 6/19/70
Day 902 6/20/70
Day 903 6/21/70
Day 904 6/22/70
Day 905 6/23/70
Day 906 6/24/70
Day 907 6/25/70
Day 908 6/26/70
Day 909 6/27/70
Day 910 6/28/70
Day 911 6/29/70
Day 912 6/30/70
Day 913 7/1/70
Day 914 7/2/70
Day 915 7/3/70
Day 916 7/4/70
Day 917 7/5/70
Day 918 7/6/70
Day 919 7/7/70
Day 920 7/8/70
Day 921 7/9/70
Day 922 7/10/70
Day 923 7/11/70
Day 924 7/12/70
Day 925 7/13/70
Day 926 7/14/70
Day 927 7/15/70
Day 928 7/16/70
Day 929 7/17/70
Day 930 7/18/70
Day 931 7/19/70
Day 932 7/20/70
Day 933 7/21/70
Day 934 7/22/70
Day 935 7/23/70
Day 936 7/24/70
Day 937 7/25/70
Day 938 7/26/70
Day 939 7/27/70
Day 940 7/28/70
Day 941 7/29/70
Day 942 7/30/70
Day 943 7/31/70
Day 944 8/1/70
Day 945 8/2/70
Day 946 8/3/70
Day 947 8/4/70
Day 948 8/5/70
Day 949 8/6/70
Day 950 8/7/70
Day 951 8/8/70
Day 952 8/9/70
Day 953 8/10/70
Day 954 8/11/70
Day 955 8/12/70
Day 956 8/13/70
Day 957 8/14/70
Day 958 8/15/70
Day 959 8/16/70
Day 960 8/17/70
Day 961 8/18/70
Day 962 8/19/70
Day 963 8/20/70
Day 964 8/21/70
Day 965 8/22/70
Day 966 8/23/70
Day 967 8/24/70
Day 968 8/25/70
Day 969 8/26/70
Day 970 8/27/70
Day 971 8/28/70
Day 972 8/29/70
Day 973 8/30/70
Day 974 8/31/70
Day 975 9/1/70
Day 976 9/2/70
Day 977 9/3/70
Day 978 9/4/70
Day 979 9/5/70
Day 980 9/6/70
Day 981 9/7/70
Day 982 9/8/70
Day 983 9/9/70
Day 984 9/10/70
Day 985 9/11/70
Day 986 9/12/70
Day 987 9/13/70
Day 988 9/14/70
Day 989 9/15/70
Day 990 9/16/70
Day 991 9/17/70
Day 992 9/18/70
Day 993 9/19/70
Day 994 9/20/70
Day 995 9/21/70
Day 996 9/22/70
Day 997 9/23/70
Day 998 9/24/70
Day 999 9/25/70
Day 1000 9/26/70
Day 1001 9/27/70
Day 1002 9/28/70
Day 1003 9/29/70
Day 1004 9/30/70
Day 1005 10/1/70
Day 1006 10/2/70
Day 1007 10/3/70
Day 1008 10/4/70
Day 1009 10/5/70
Day 1010 10/6/70
Day 1011 10/7/70
Day 1012 10/8/70
Day 1013 10/9/70
Day 1014 10/10/70
Day 1015 10/11/70
Day 1016 10/12/70
Day 1017 10/13/70
Day 1018 10/14/70
Day 1019 10/15/70
Day 1020 10/16/70
Day 1021 10/17/70
Day 1022 10/18/70
Day 1023 10/19/70
Day 1024 10/20/70
Day 1025 10/21/70
Day 1026 10/22/70
Day 1027 10/23/70
Day 1028 10/24/70
Day 1029 10/25/70
Day 1030 10/26/70
Day 1031 10/27/70
Day 1032 10/28/70
Day 1033 10/29/70
Day 1034 10/30/70
Day 1035 10/31/70
Day 1036 11/1/70
Day 1037 11/2/70
Day 1038 11/3/70
Day 1039 11/4/70
Day 1040 11/5/70
Day 1041 11/6/70
Day 1042 11/7/70
Day 1043 11/8/70
Day 1044 11/9/70
Day 1045 11/10/70
Day 1046 11/11/70
Day 1047 11/12/70
Day 1048 11/13/70
Day 1049 11/14/70
Day 1050 11/15/70
Day 1051 11/16/70
Day 1052 11/17/70
Day 1053 11/18/70
Day 1054 11/19/70
Day 1055 11/20/70
Day 1056 11/21/70
Day 1057 11/22/70
Day 1058 11/23/70
Day 1059 11/24/70
Day 1060 11/25/70
Day 1061 11/26/70
Day 1062 11/27/70
Day 1063 11/28/70
Day 1064 11/29/70
Day 1065 11/30/70
Day 1066 12/1/70
Day 1067 12/2/70
Day 1068 12/3/70
Day 1069 12/4/70
Day 1070 12/5/70
Day 1071 12/6/70
Day 1072 12/7/70
Day 1073 12/8/70
Day 1074 12/9/70
Day 1075 12/10/70
Day 1076 12/11/70
Day 1077 12/12/70
Day 1078 12/13/70
Day 1079 12/14/70
Day 1080 12/15/70
Day 1081 12/16/70
Day 1082 12/17/70
Day 1083 12/18/70
Day 1084 12/19/70
Day 1085 12/20/70
Day 1086 12/21/70
Day 1087 12/22/70
Day 1088 12/23/70
Day 1089 12/24/70
Day 1090 12/25/70
Day 1091 12/26/70
Day 1092 12/27/70
Day 1093 12/28/70
Day 1094 12/29/70
Day 1095 12/30/70
Day 1096 12/31/70
Day 1097 1/1/71
Day 1098 1/2/71
Day 1099 1/3/71
Day 1100 1/4/71
Day 1101 1/5/71
Day 1102 1/6/71
Day 1103 1/7/71
Day 1104 1/8/71
Day 1105 1/9/71
Day 1106 1/10/71
Day 1107 1/11/71
Day 1108 1/12/71
Day 1109 1/13/71
Day 1110 1/14/71
Day 1111 1/15/71
Day 1112 1/16/71
Day 1113 1/17/71
Day 1114 1/18/71
Day 1115 1/19/71
Day 1116 1/20/71
Day 1117 1/21/71
Day 1118 1/22/71
Day 1119 1/23/71
Day 1120 1/24/71
Day 1121 1/25/71
Day 1122 1/26/71
Day 1123 1/27/71
Day 1124 1/28/71
Day 1125 1/29/71
Day 1126 1/30/71
Day 1127 1/31/71
Day 1128 2/1/71
Day 1129 2/2/71
Day 1130 2/3/71
Day 1131 2/4/71
Day 1132 2/5/71
Day 1133 2/6/71
Day 1134 2/7/71
Day 1135 2/8/71
Day 1136 2/9/71
Day 1137 2/10/71
Day 1138 2/11/71
Day 1139 2/12/71
Day 1140 2/13/71
Day 1141 2/14/71
Day 1142 2/15/71
Day 1143 2/16/71
Day 1144 2/17/71
Day 1145 2/18/71
Day 1146 2/19/71
Day 1147 2/20/71
Day 1148 2/21/71
Day 1149 2/22/71
Day 1150 2/23/71
Day 1151 2/24/71
Day 1152 2/25/71
Day 1153 2/26/71
Day 1154 2/27/71
Day 1155 2/28/71
Day 1156 3/1/71
Day 1157 3/2/71
Day 1158 3/3/71
Day 1159 3/4/71
Day 1160 3/5/71
Day 1161 3/6/71
Day 1162 3/7/71
Day 1163 3/8/71
Day 1164 3/9/71
Day 1165 3/10/71
Day 1166 3/11/71
Day 1167 3/12/71
Day 1168 3/13/71
Day 1169 3/14/71
Day 1170 3/15/71
Day 1171 3/16/71
Day 1172 3/17/71
Day 1173 3/18/71
Day 1174 3/19/71
Day 1175 3/20/71
Day 1176 3/21/71
Day 1177 3/22/71
Day 1178 3/23/71
Day 1179 3/24/71
Day 1180 3/25/71
Day 1181 3/26/71
Day 1182 3/27/71
Day 1183 3/28/71
Day 1184 3/29/71
Day 1185 3/30/71
Day 1186 3/31/71
Day 1187 4/1/71
Day 1188 4/2/71
Day 1189 4/3/71
Day 1190 4/4/71
Day 1191 4/5/71
Day 1192 4/6/71
Day 1193 4/7/71
Day 1194 4/8/71
Day 1195 4/9/71
Day 1196 4/10/71
Day 1197 4/11/71
Day 1198 4/12/71
Day 1199 4/13/71
Day 1200 4/14/71
Day 1201 4/15/71
Day 1202 4/16/71
Day 1203 4/17/71
Day 1204 4/18/71
Day 1205 4/19/71
Day 1206 4/20/71
Day 1207 4/21/71
Day 1208 4/22/71
Day 1209 4/23/71
Day 1210 4/24/71
Day 1211 4/25/71
Day 1212 4/26/71
Day 1213 4/27/71
Day 1214 4/28/71
Day 1215 4/29/71
Day 1216 4/30/71
Day 1217 5/1/71
Day 1218 5/2/71
Day 1219 5/3/71
Day 1220 5/4/71
Day 1221 5/5/71
Day 1222 5/6/71
Day 1223 5/7/71
Day 1224 5/8/71
Day 1225 5/9/71
Day 1226 5/10/71
Day 1227 5/11/71
Day 1228 5/12/71
Day 1229 5/13/71
Day 1230 5/14/71
Day 1231 5/15/71
Day 1232 5/16/71
Day 1233 5/17/71
Day 1234 5/18/71
Day 1235 5/19/71
Day 1236 5/20/71
Day 1237 5/21/71
Day 1238 5/22/71
Day 1239 5/23/71
Day 1240 5/24/71
Day 1241 5/25/71
Day 1242 5/26/71
Day 1243 5/27/71
Day 1244 5/28/71
Day 1245 5/29/71
Day 1246 5/30/71
Day 1247 5/31/71
Day 1248 6/1/71
Day 1249 6/2/71
Day 1250 6/3/71
Day 1251 6/4/71
Day 1252 6/5/71
Day 1253 6/6/71
Day 1254 6/7/71
Day 1255 6/8/71
Day 1256 6/9/71
Day 1257 6/10/71
Day 1258 6/11/71
Day 1259 6/12/71
Day 1260 6/13/71
Day 1261 6/14/71
Day 1262 6/15/71
Day 1263 6/16/71
Day 1264 6/17/71
Day 1265 6/18/71
Day 1266 6/19/71
Day 1267 6/20/71
Day 1268 6/21/71
Day 1269 6/22/71
Day 1270 6/23/71
Day 1271 6/24/71
Day 1272 6/25/71
Day 1273 6/26/71
Day 1274 6/27/71
Day 1275 6/28/71
Day 1276 6/29/71
Day 1277 6/30/71
Day 1278 7/1/71
Day 1279 7/2/71
Day 1280 7/3/71
Day 1281 7/4/71
Day 1282 7/5/71
Day 1283 7/6/71
Day 1284 7/7/71
Day 1285 7/8/71
Day 1286 7/9/71
Day 1287 7/10/71
Day 1288 7/11/71
Day 1289 7/12/71
Day 1290 7/13/71
Day 1291 7/14/71
Day 1292 7/15/71
Day 1293 7/16/71
Day 1294 7/17/71
Day 1295 7/18/71
Day 1296 7/19/71
Day 1297 7/20/71
Day 1298 7/21/71
Day 1299 7/22/71
Day 1300 7/23/71
Day 1301 7/24/71
Day 1302 7/25/71
Day 1303 7/26/71
Day 1304 7/27/71
Day 1305 7/28/71
Day 1306 7/29/71
Day 1307 7/30/71
Day 1308 7/31/71
Day 1309 8/1/71
Day 1310 8/2/71
Day 1311 8/3/71
Day 1312 8/4/71
Day 1313 8/5/71
Day 1314 8/6/71
Day 1315 8/7/71
Day 1316 8/8/71
Day 1317 8/9/71
Day 1318 8/10/71
Day 1319 8/11/71
Day 1320 8/12/71
Day 1321 8/13/71
Day 1322 8/14/71
Day 1323 8/15/71
Day 1324 8/16/71
Day 1325 8/17/71
Day 1326 8/18/71
Day 1327 8/19/71
Day 1328 8/20/71
Day 1329 8/21/71
Day 1330 8/22/71
Day 1331 8/23/71
Day 1332 8/24/71
Day 1333 8/25/71
Day 1334 8/26/71
Day 1335 8/27/71
Day 1336 8/28/71
Day 1337 8/29/71
Day 1338 8/30/71
Day 1339 8/31/71
Day 1340 9/1/71
Day 1341 9/2/71
Day 1342 9/3/71
Day 1343 9/4/71
Day 1344 9/5/71
Day 1345 9/6/71
Day 1346 9/7/71
Day 1347 9/8/71
Day 1348 9/9/71
Day 1349 9/10/71
Day 1350 9/11/71
Day 1351 9/12/71
Day 1352 9/13/71
Day 1353 9/14/71
Day 1354 9/15/71
Day 1355 9/16/71
Day 1356 9/17/71
Day 1357 9/18/71
Day 1358 9/19/71
Day 1359 9/20/71
Day 1360 9/21/71
Day 1361 9/22/71
Day 1362 9/23/71
Day 1363 9/24/71
Day 1364 9/25/71
Day 1365 9/26/71
Day 1366 9/27/71
Day 1367 9/28/71
Day 1368 9/29/71
Day 1369 9/30/71
Day 1370 10/1/71
Day 1371 10/2/71
Day 1372 10/3/71
Day 1373 10/4/71
Day 1374 10/5/71
Day 1375 10/6/71
Day 1376 10/7/71
Day 1377 10/8/71
Day 1378 10/9/71
Day 1

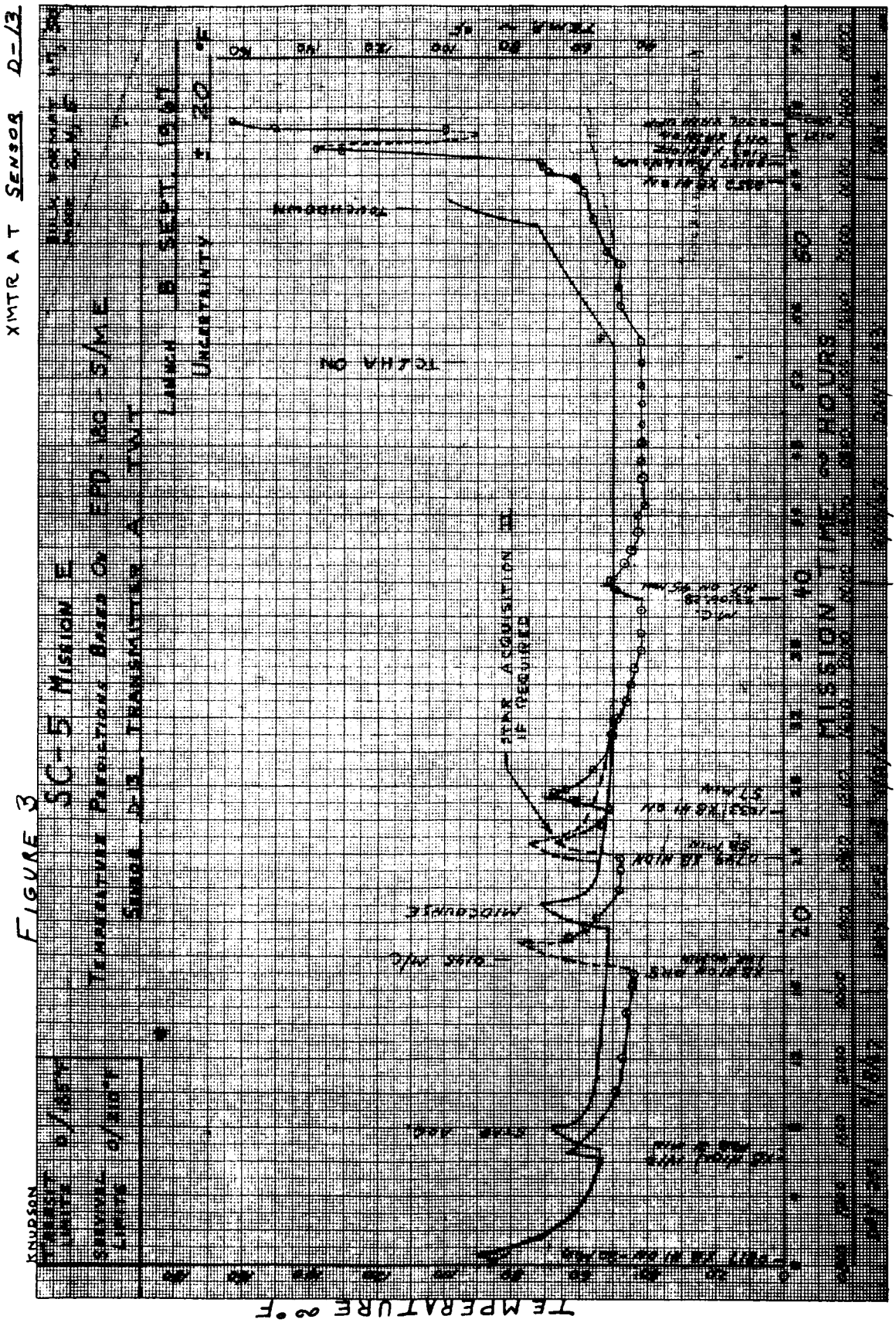

Figure 5.1-8. Sensor D-13: Transmitter A TWT

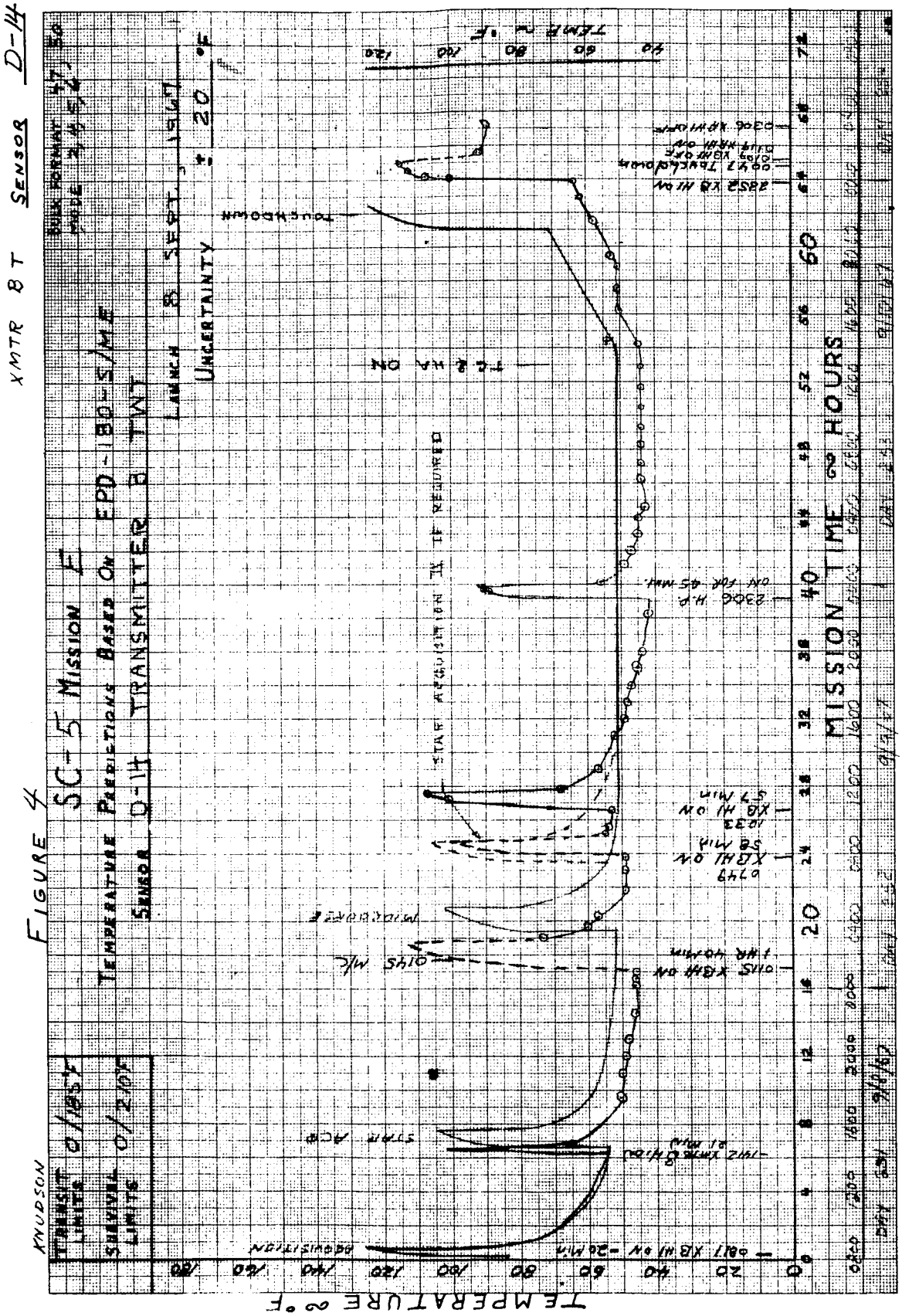

Figure 5.1-9. Sensor D-14: Transmitter B TWT

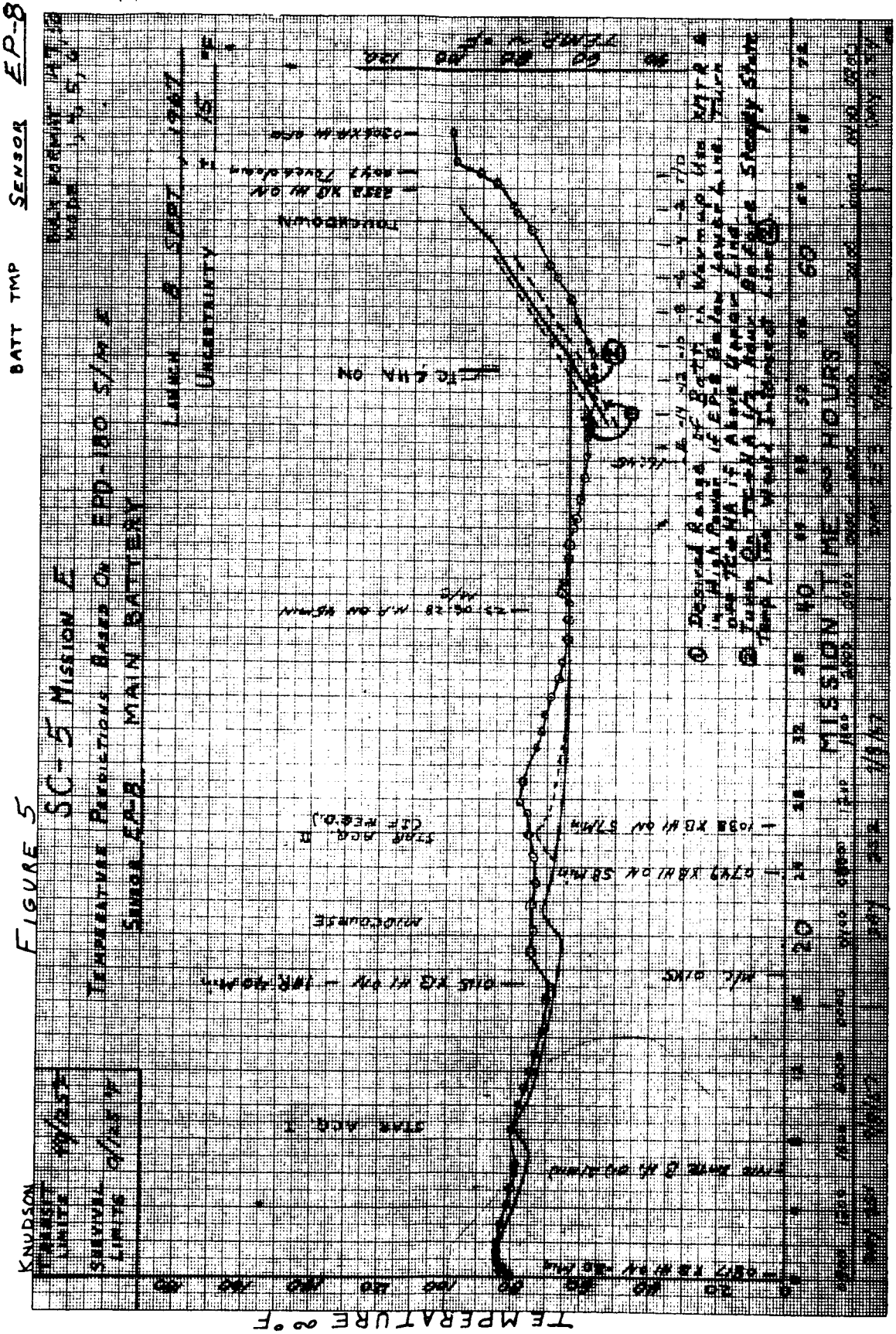

Figure 5.1-10. Sensor EP-8: Main Battery

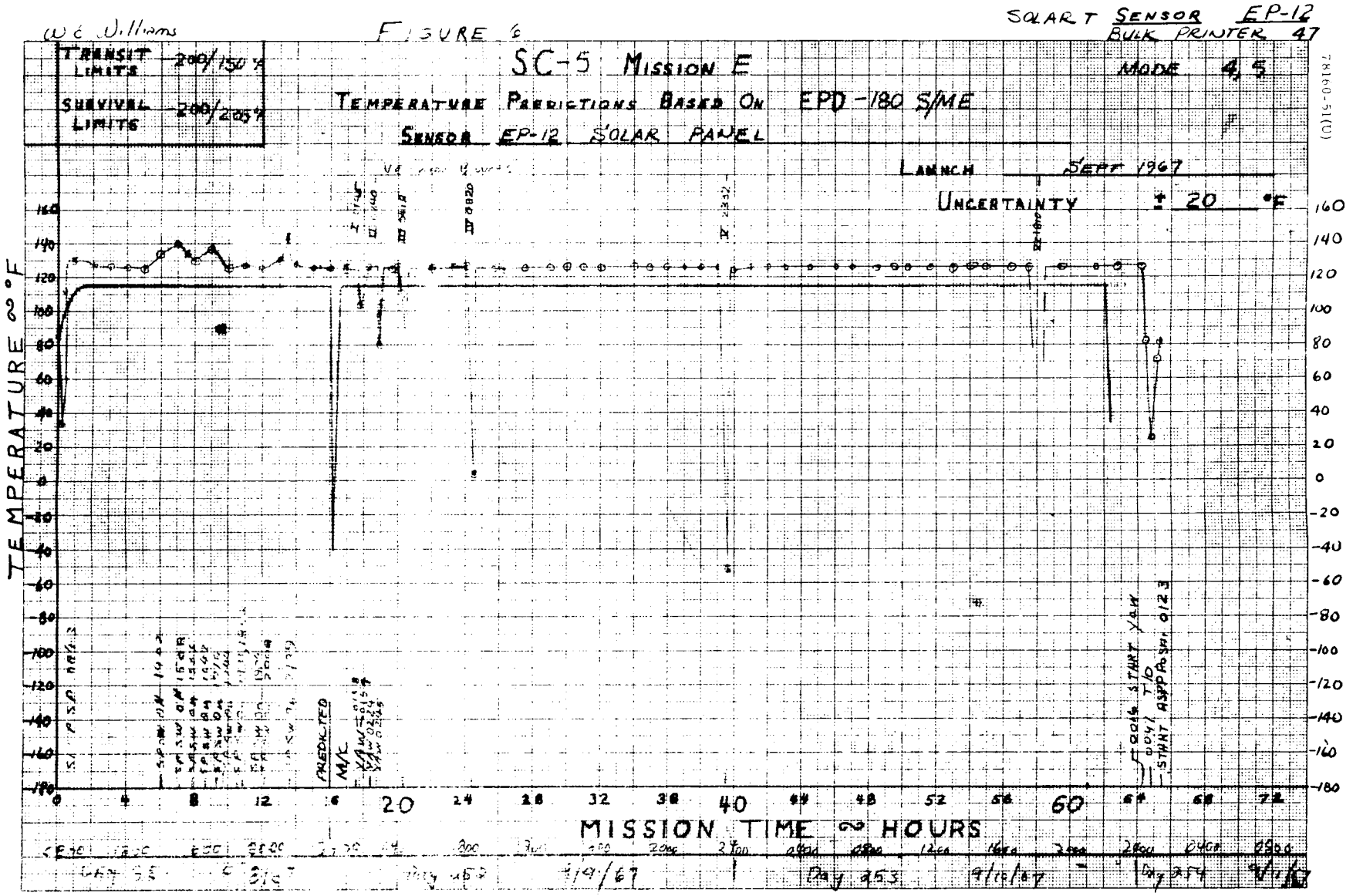

Figure 5.1-A8. Sensor EP-12: Solar Panel

78160-52(U)

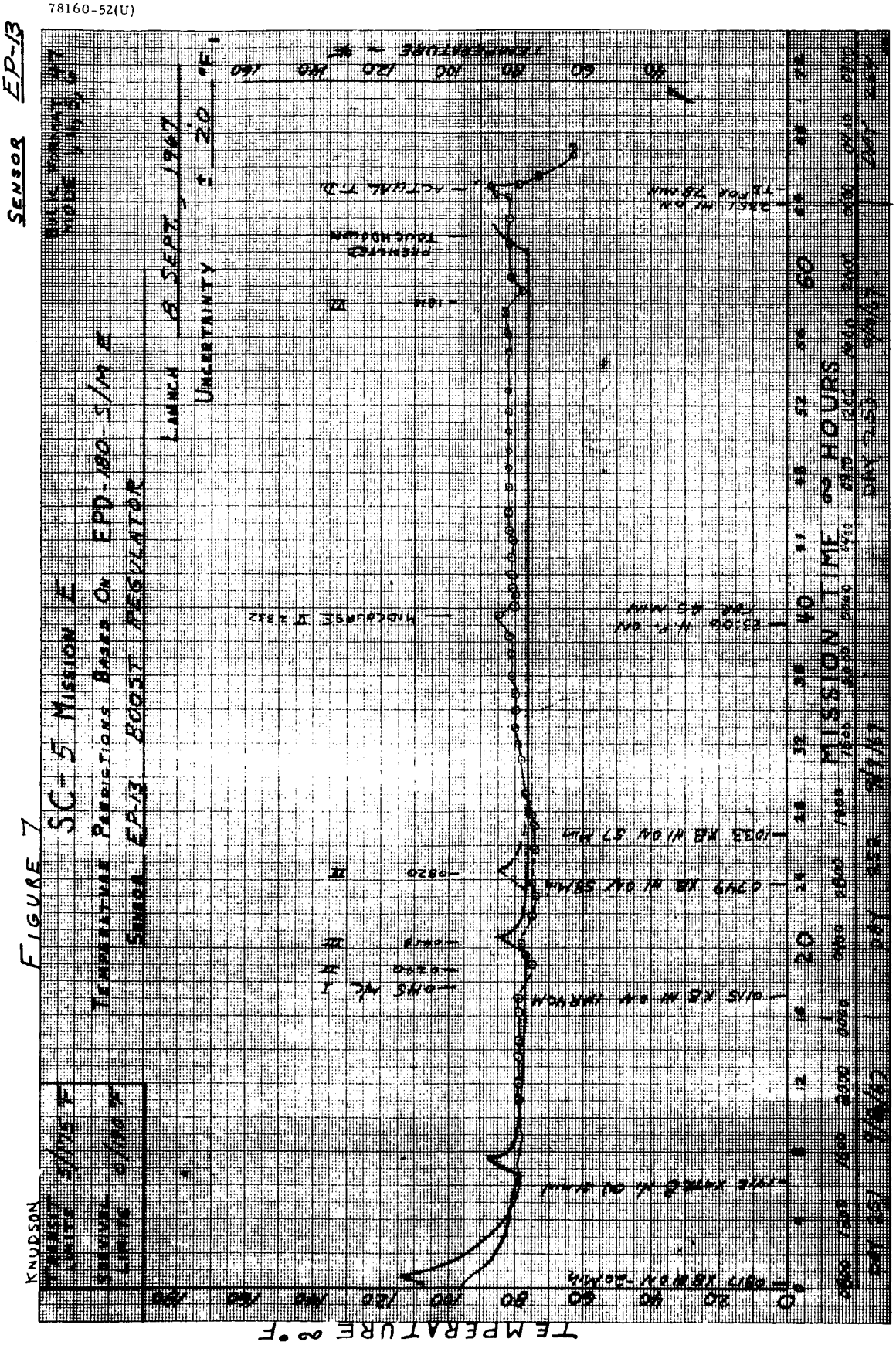

Figure 5.1-12. Sensor EP-13: Boost Regulator

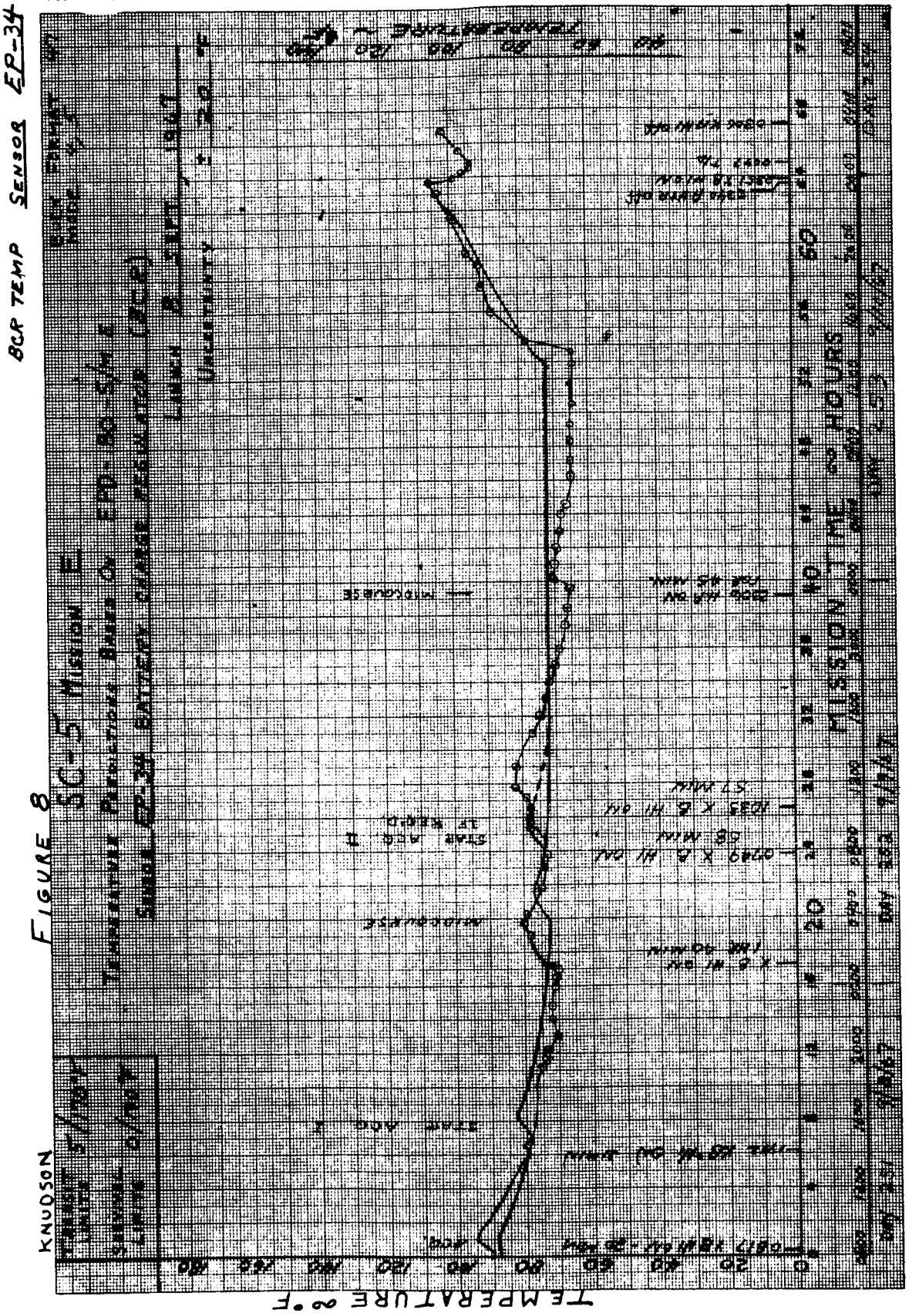

Figure 5.1-13. Sensor EP-34: Battery Charge Regulator

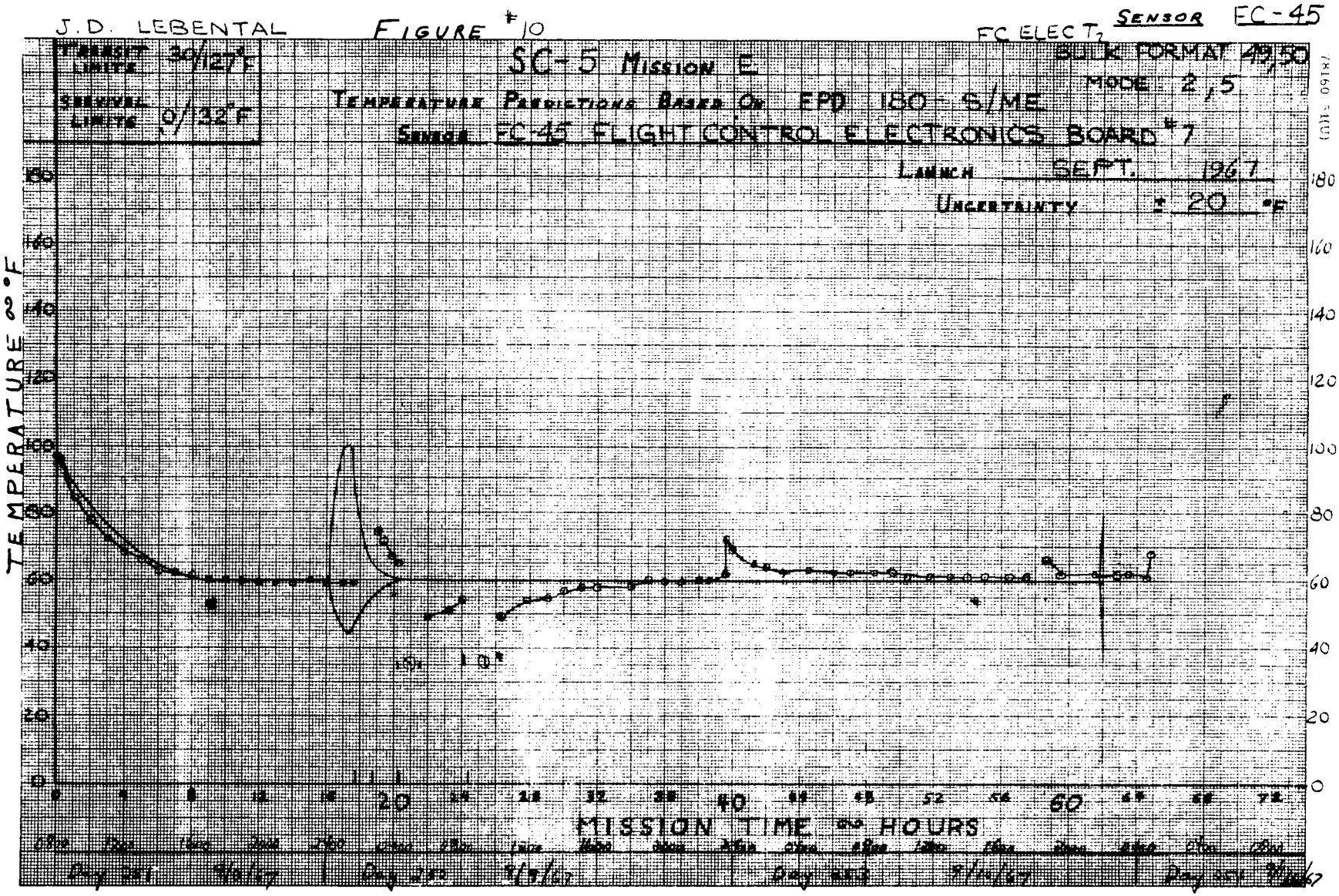

Figure 5.1-14. Sensor FC-45: Flight Control Electronics Board 7

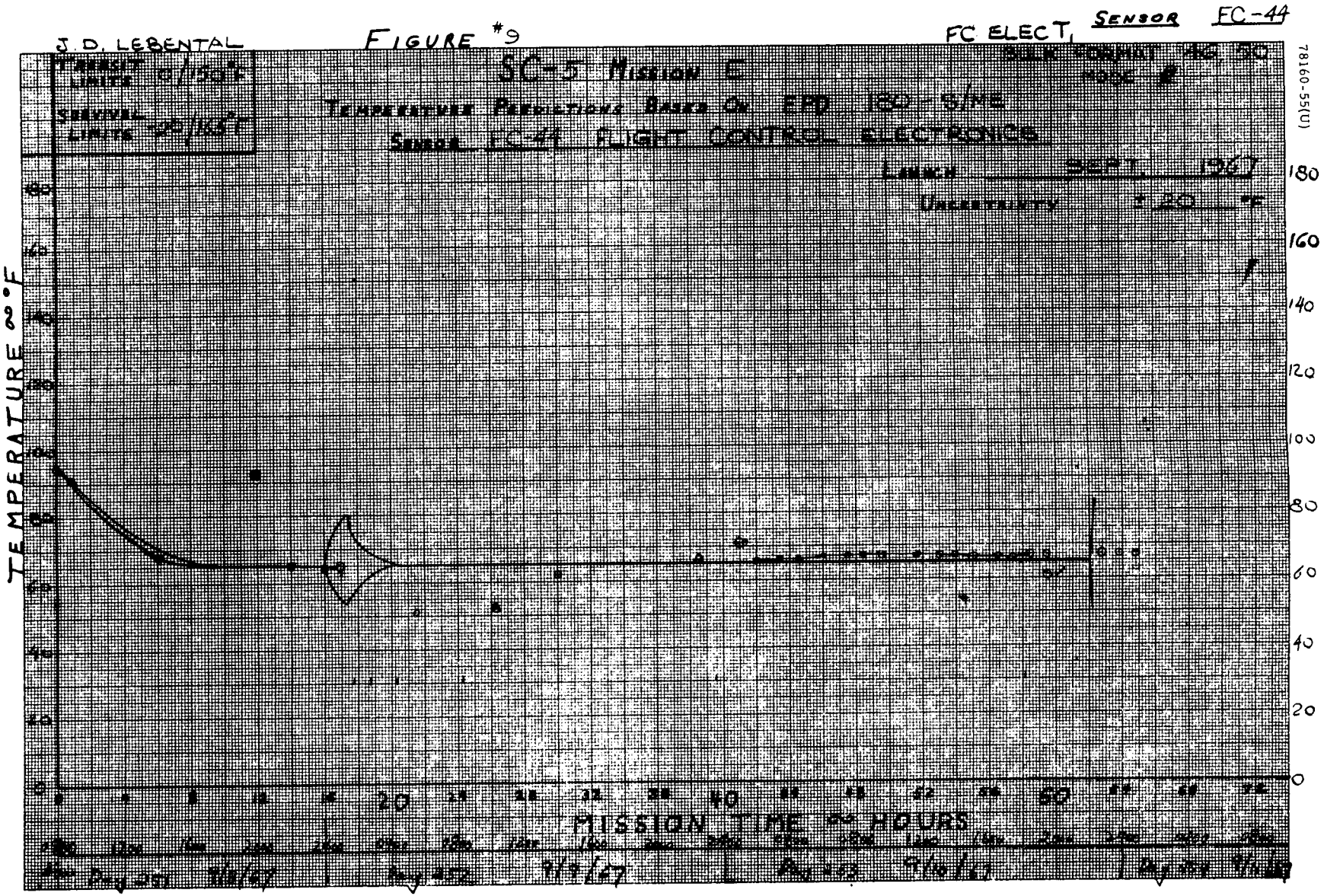

Figure 5.1-15. Sensor FC-44: Flight Control Electronics

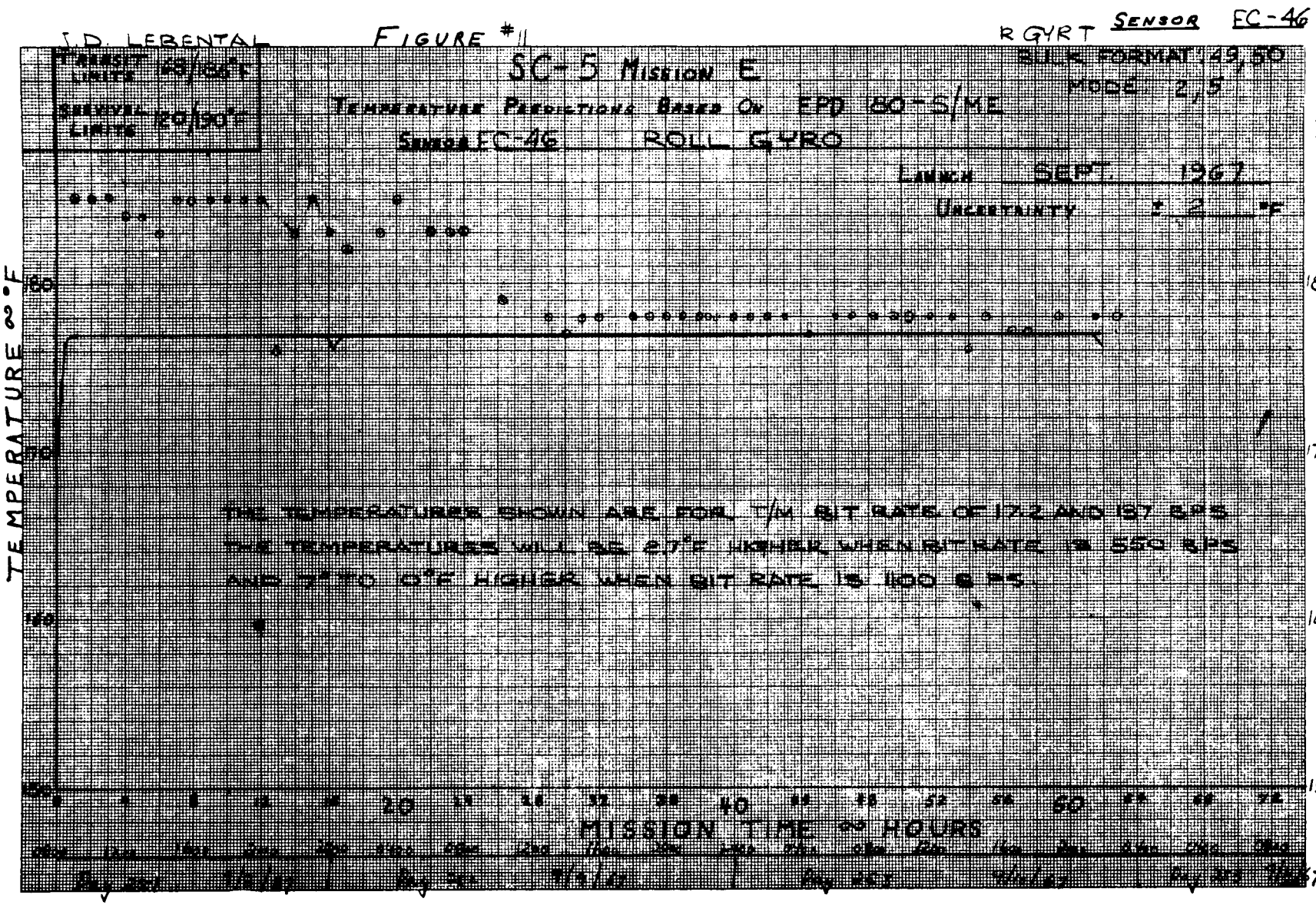

Figure 5.1-16. Sensor FC-46: Roll Gyro

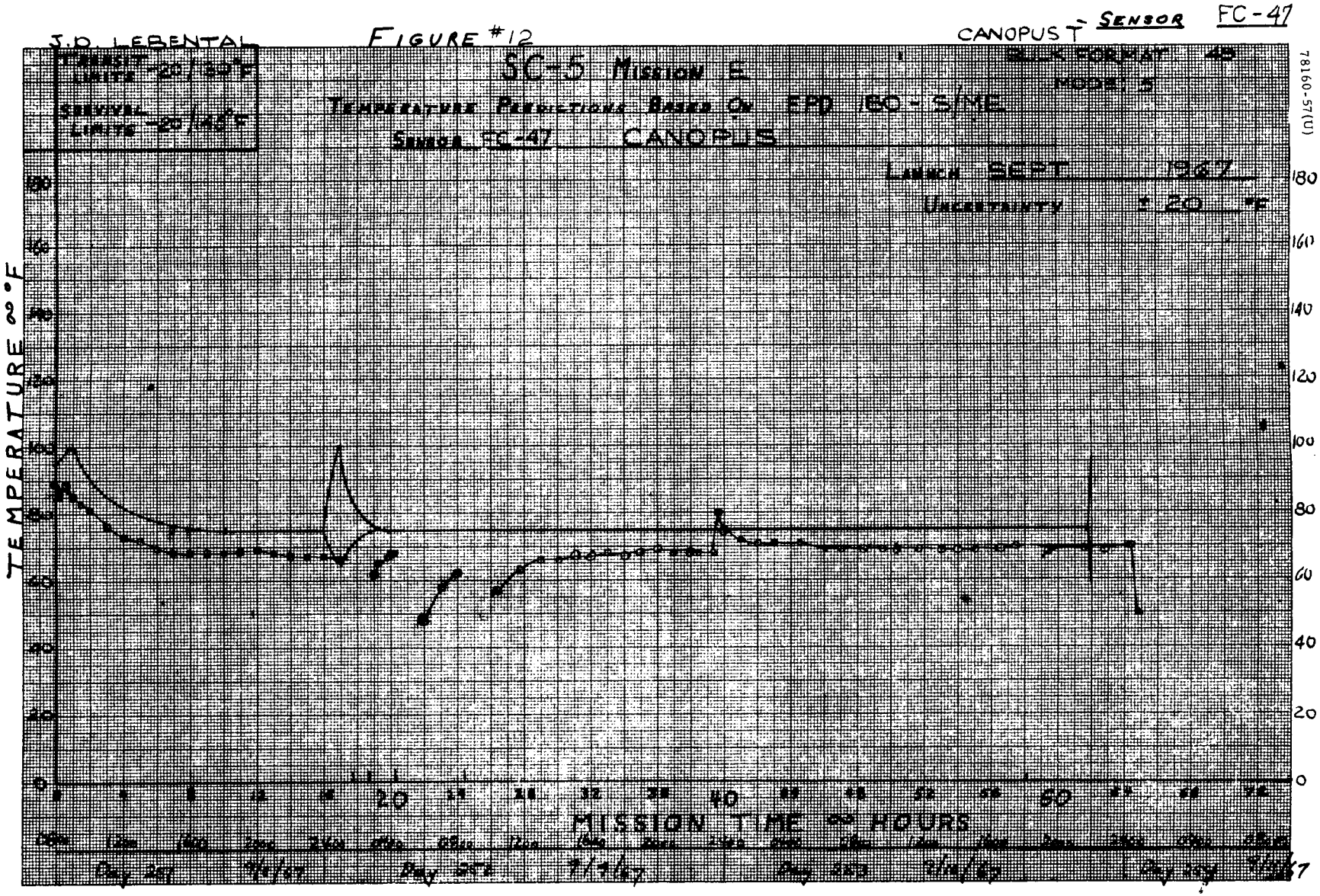

Figure 5.1-17. Sensor FC-47: Canopus

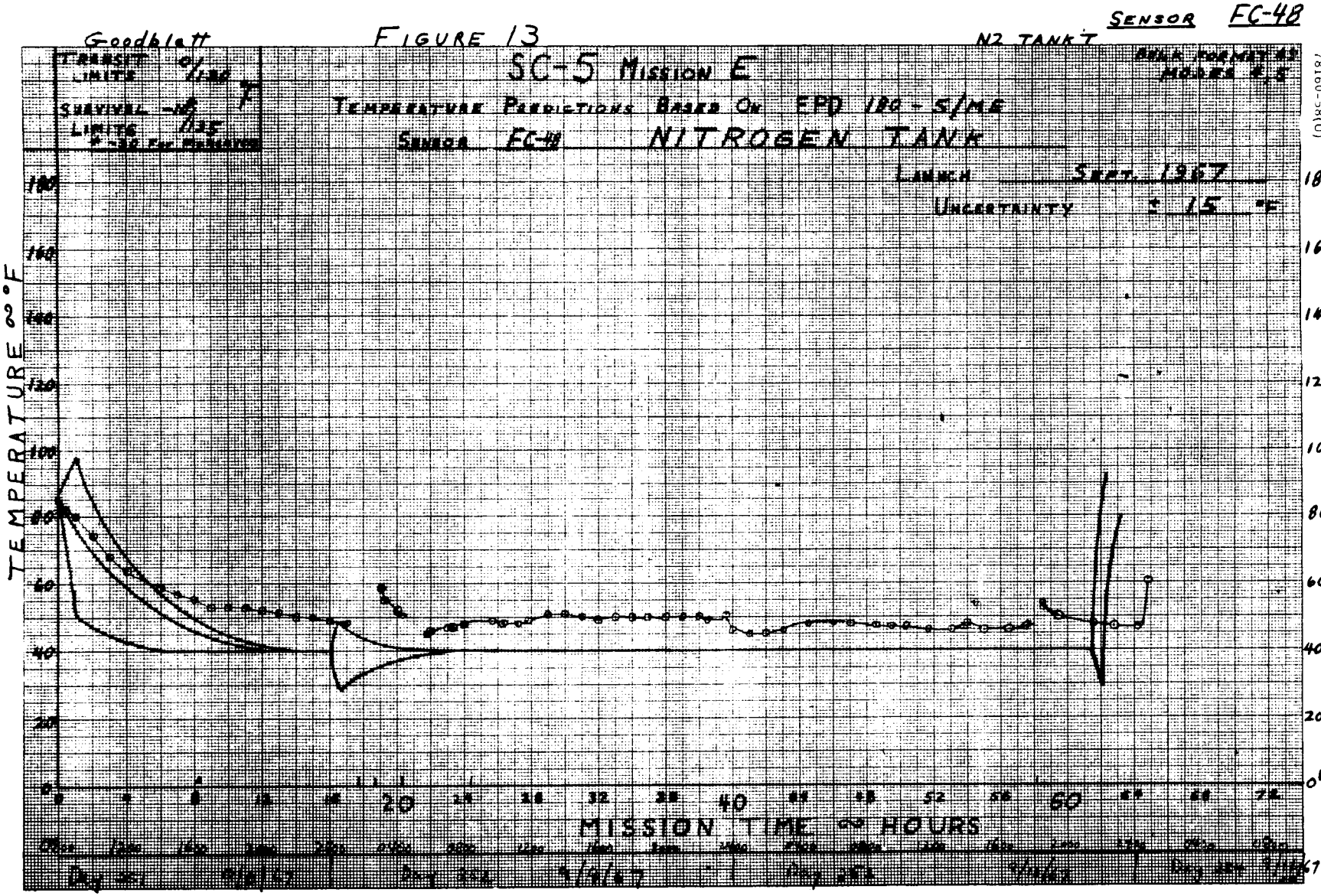

Figure 5.1-18. Sensor FC-48: Nitrogen Tank

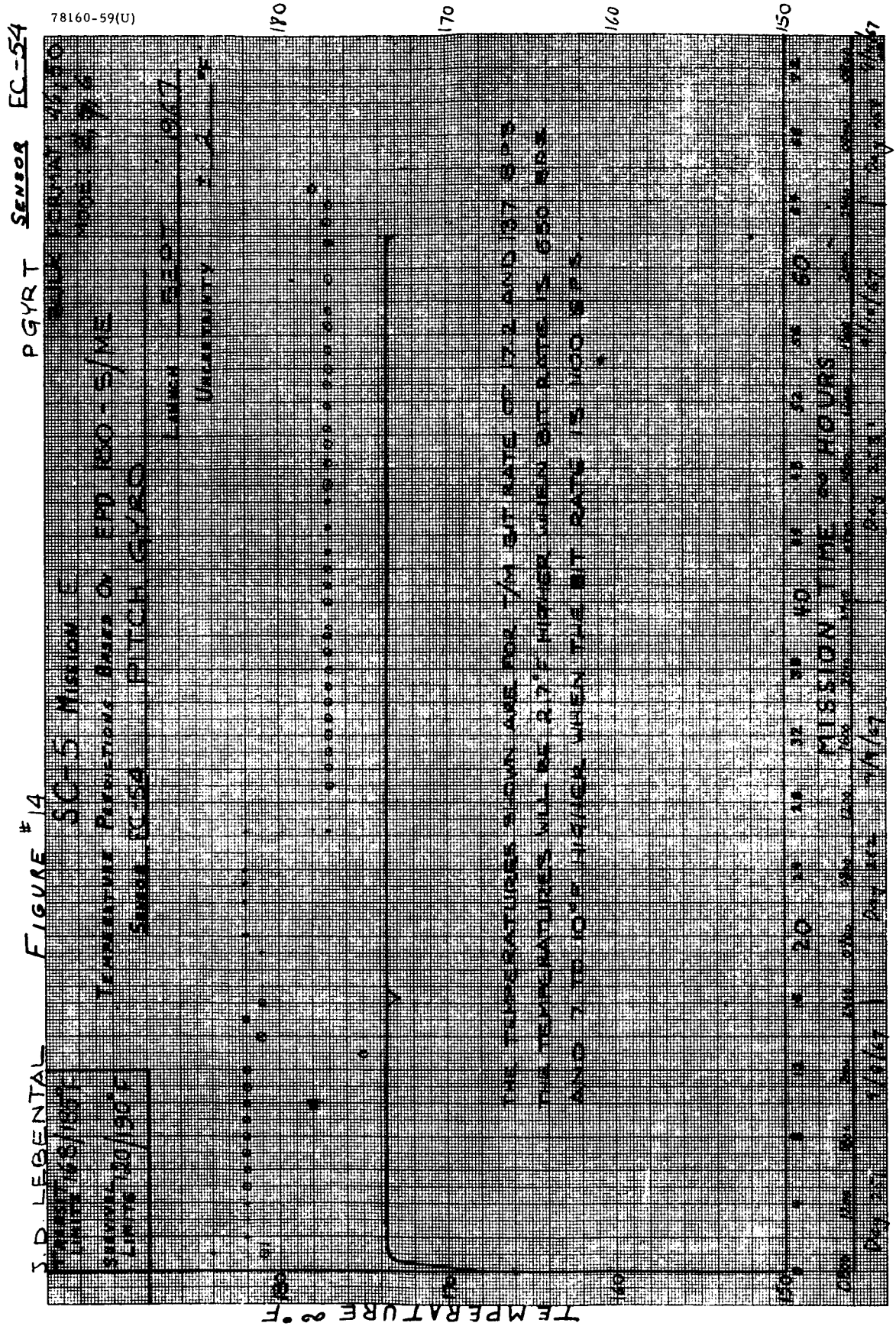

Figure 5.1-19. Sensor FC-54: Pitch Gyro

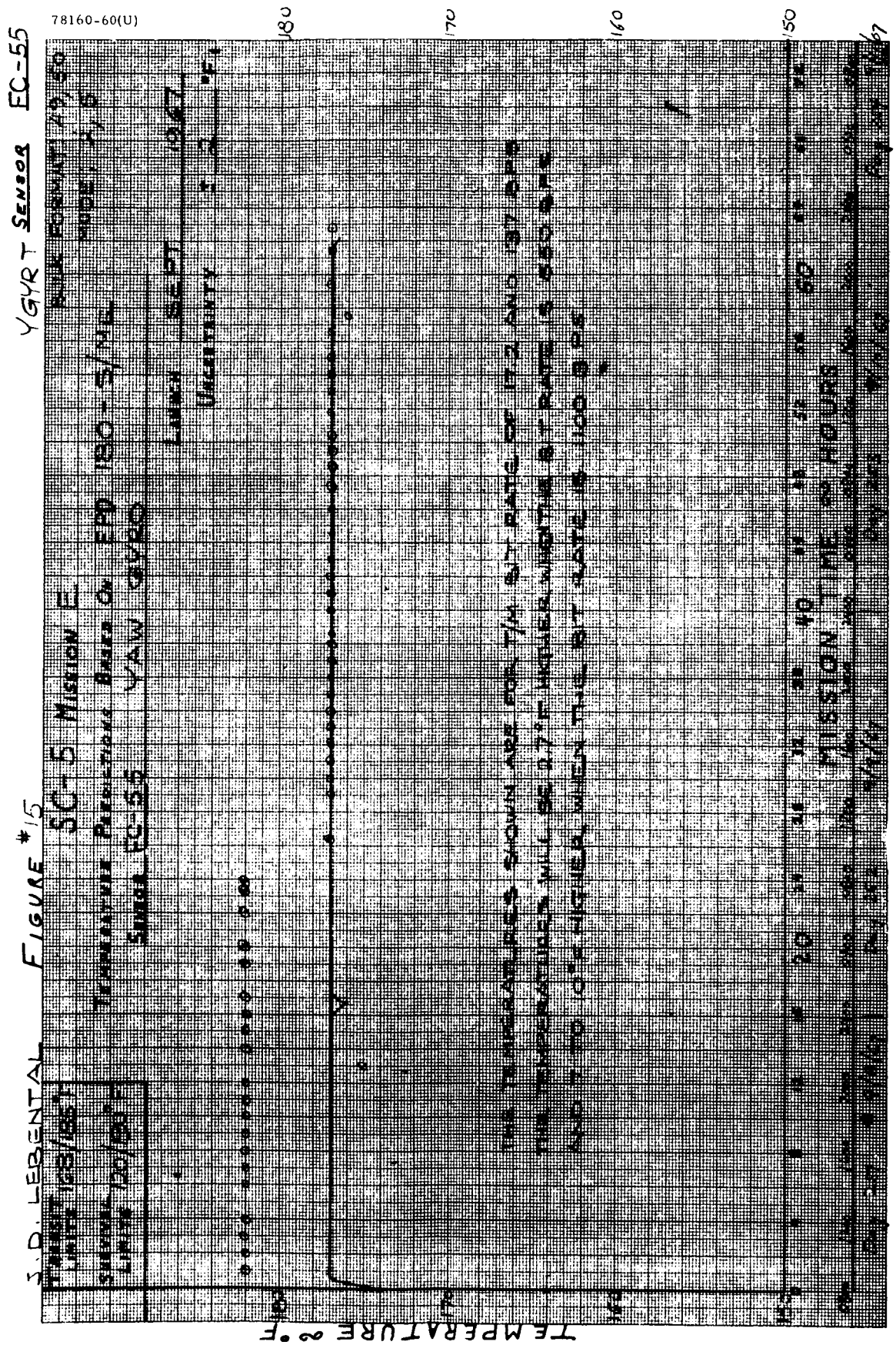

Figure 5.1-20. Sensor FC-55: Yaw Gyro

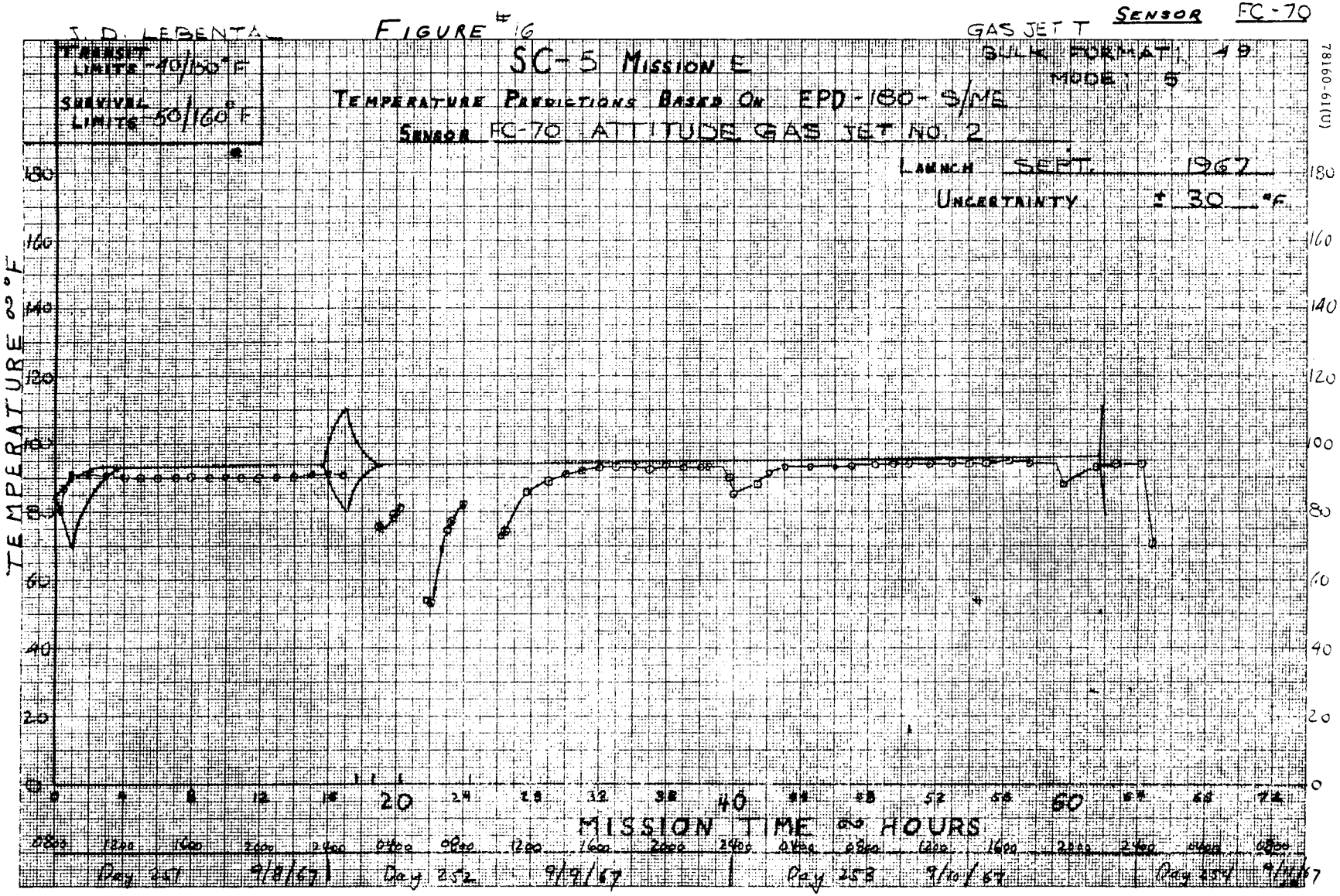

Figure 5.1-21. Sensor FC-70: Attitude Gas Jet 2

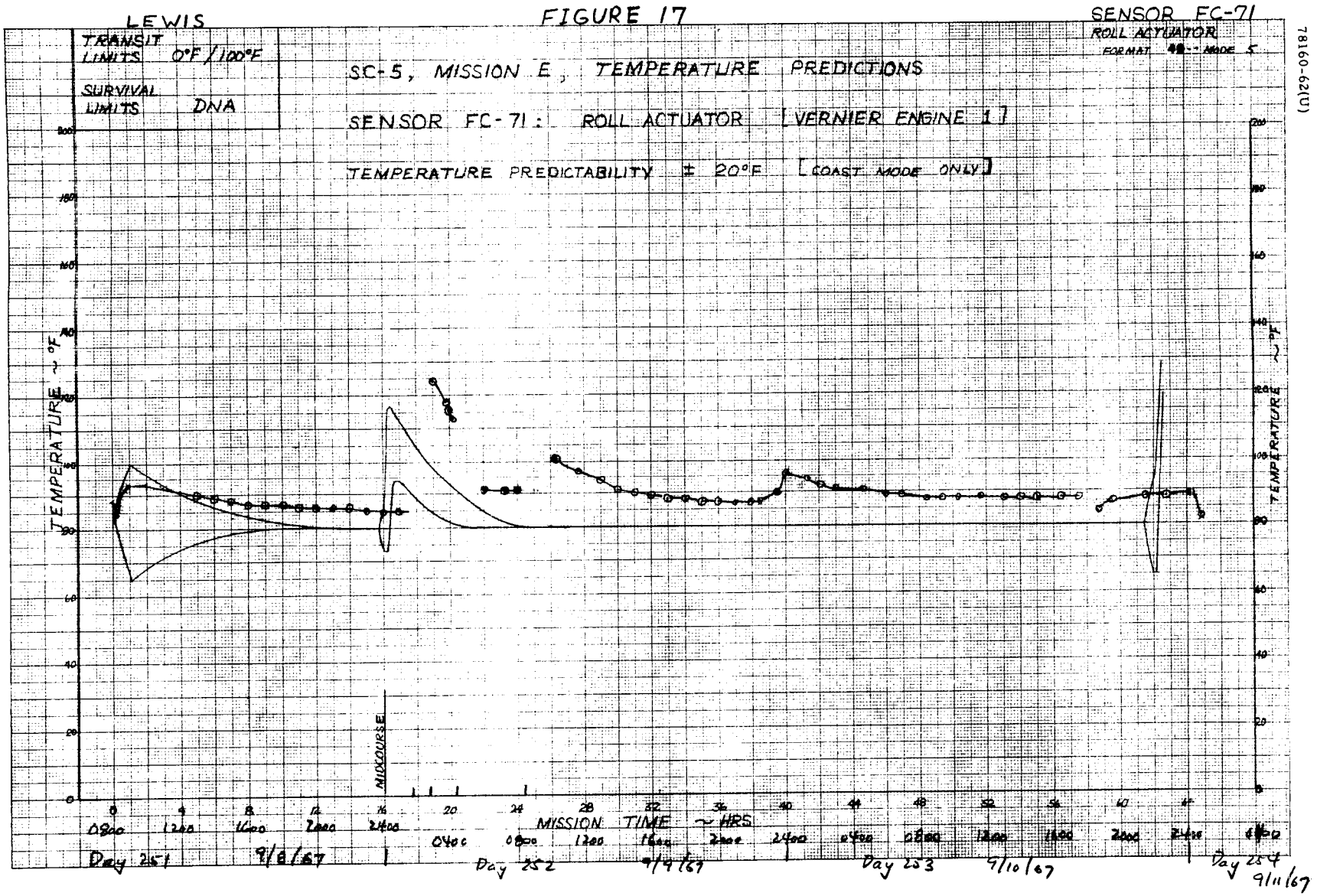

Figure 5.1-22. Sensor FC-71: Roll Actuator – Vernier Engine 1

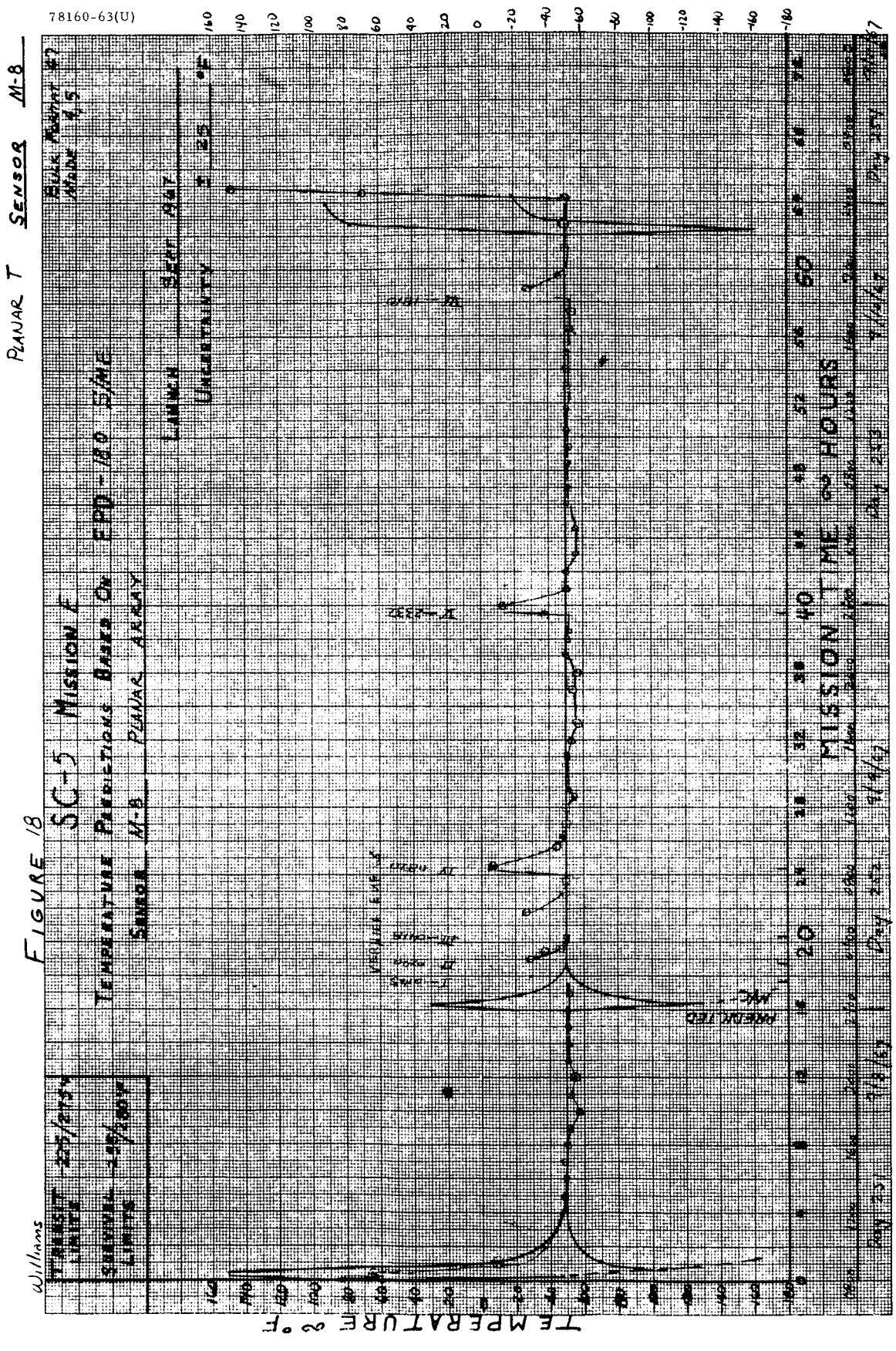

Figure 5.1-23. Sensor M-8: Planar Array

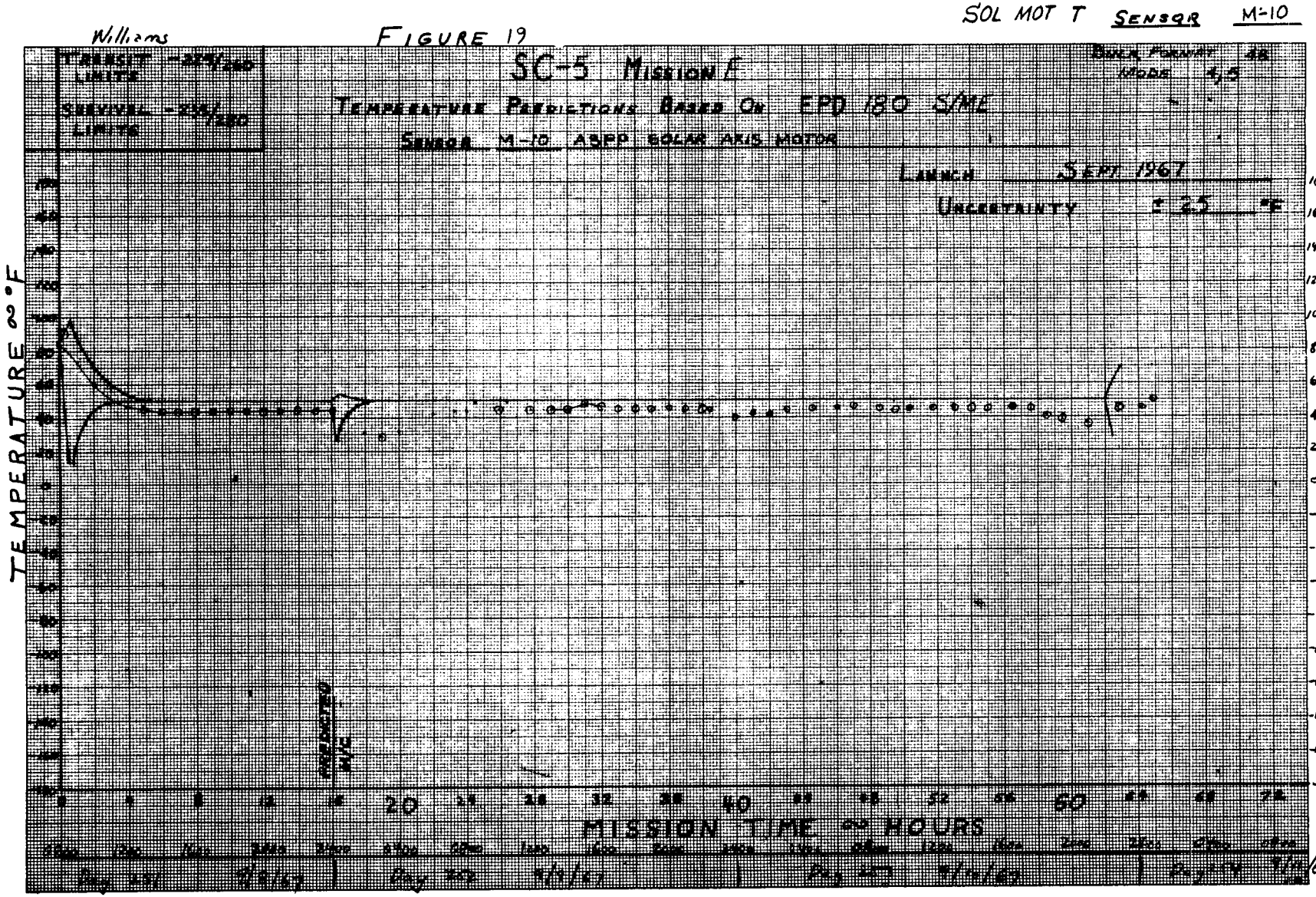

Figure 5.1-24. Sensor M-10: A/SPP Solar Axis Motor

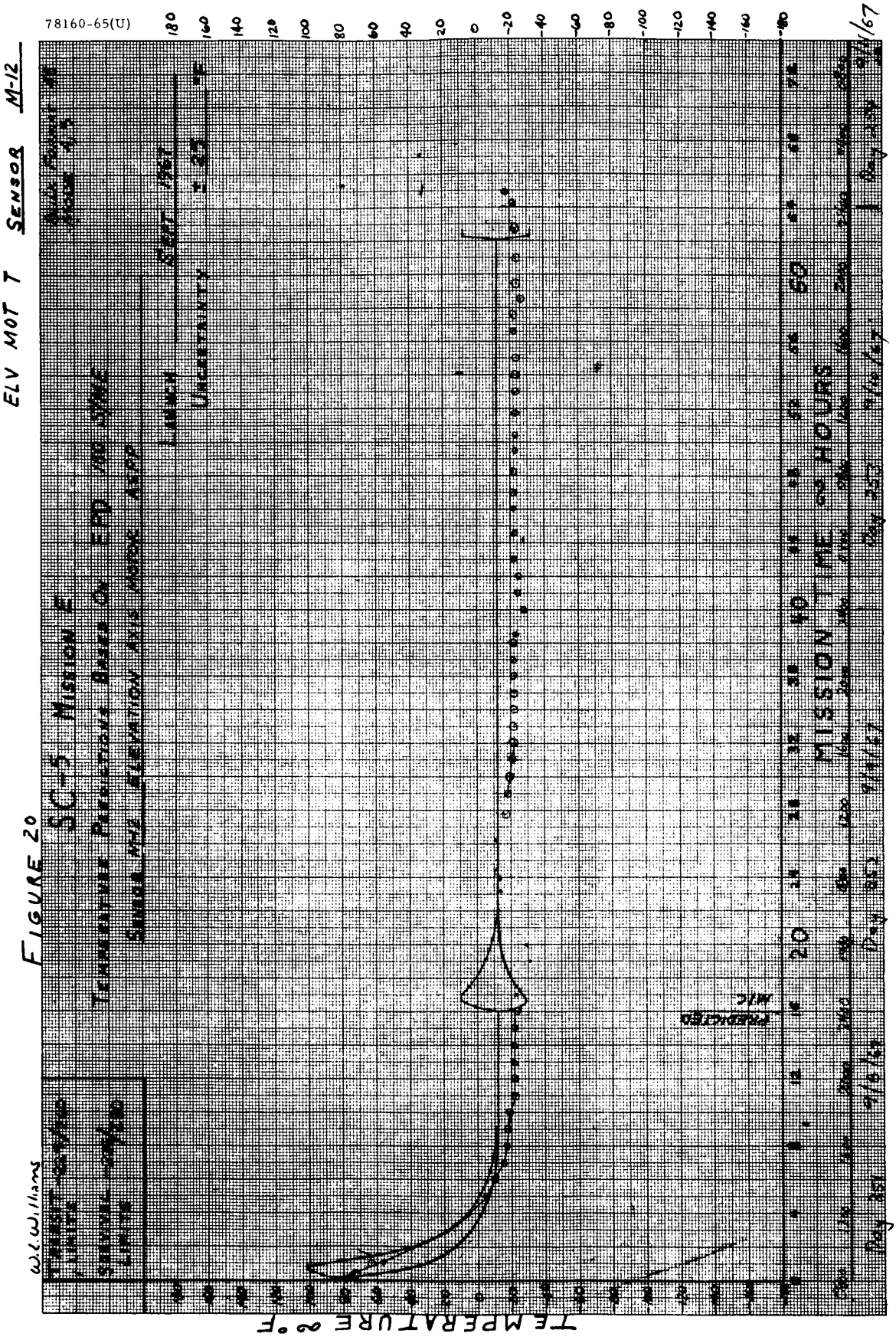

Figure 5.1-25. Sensor M-12: A/SPP Elevation Axis Motor

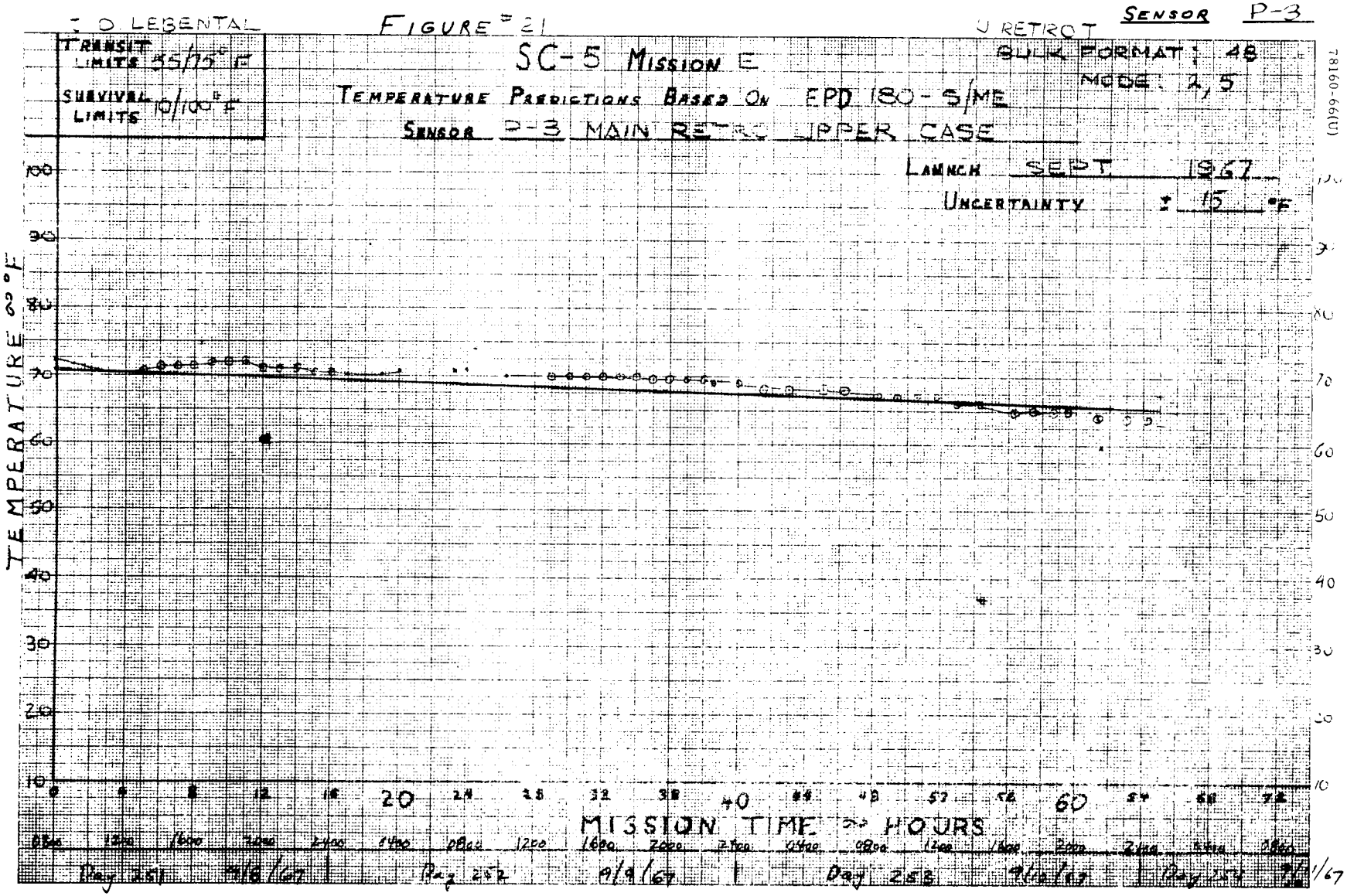

Figure 5.1-26. Sensor P-3: Main Retro Upper Case

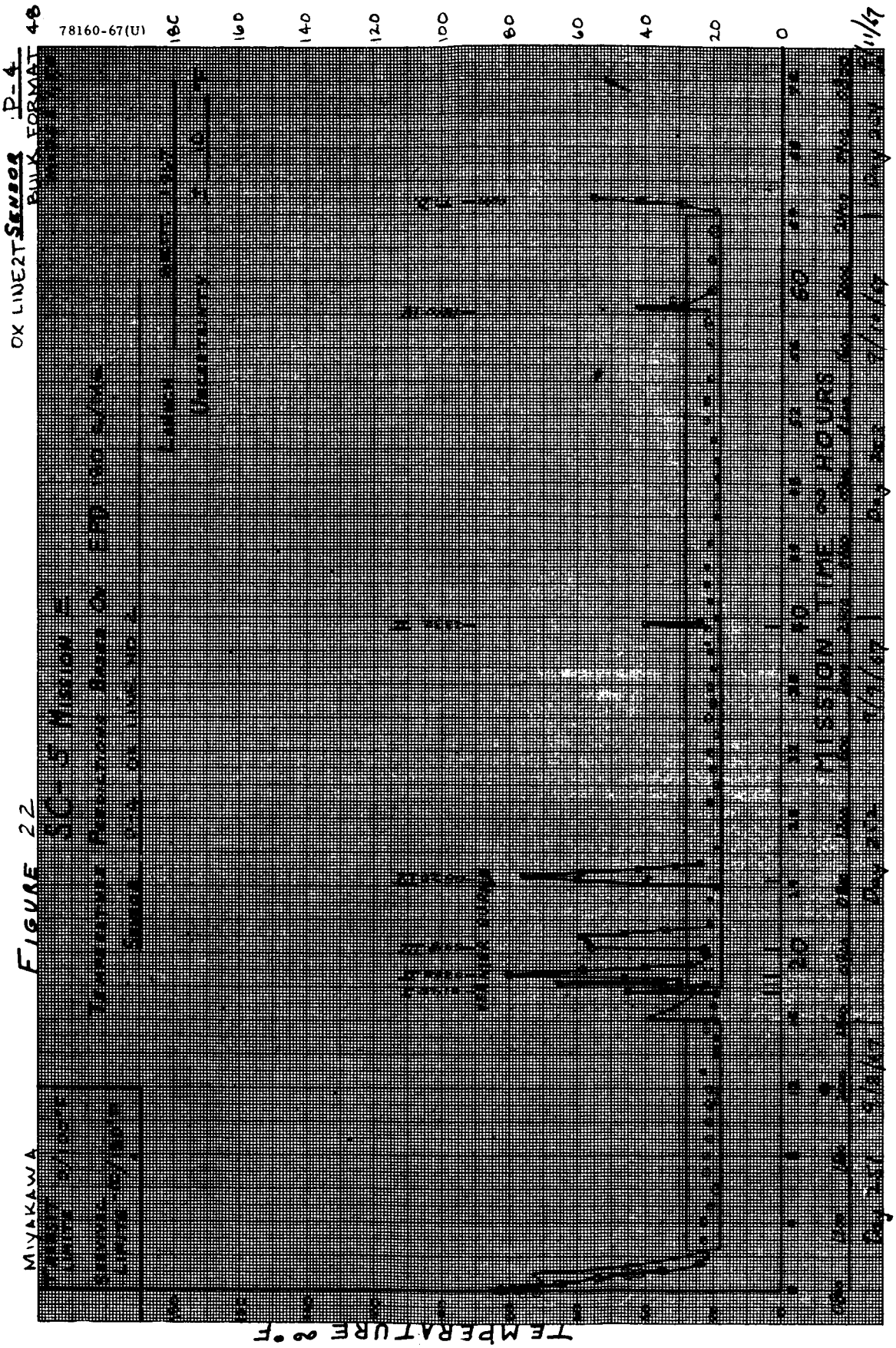

Figure 5.1-27. Sensor P-4: Oxidizer Line 2

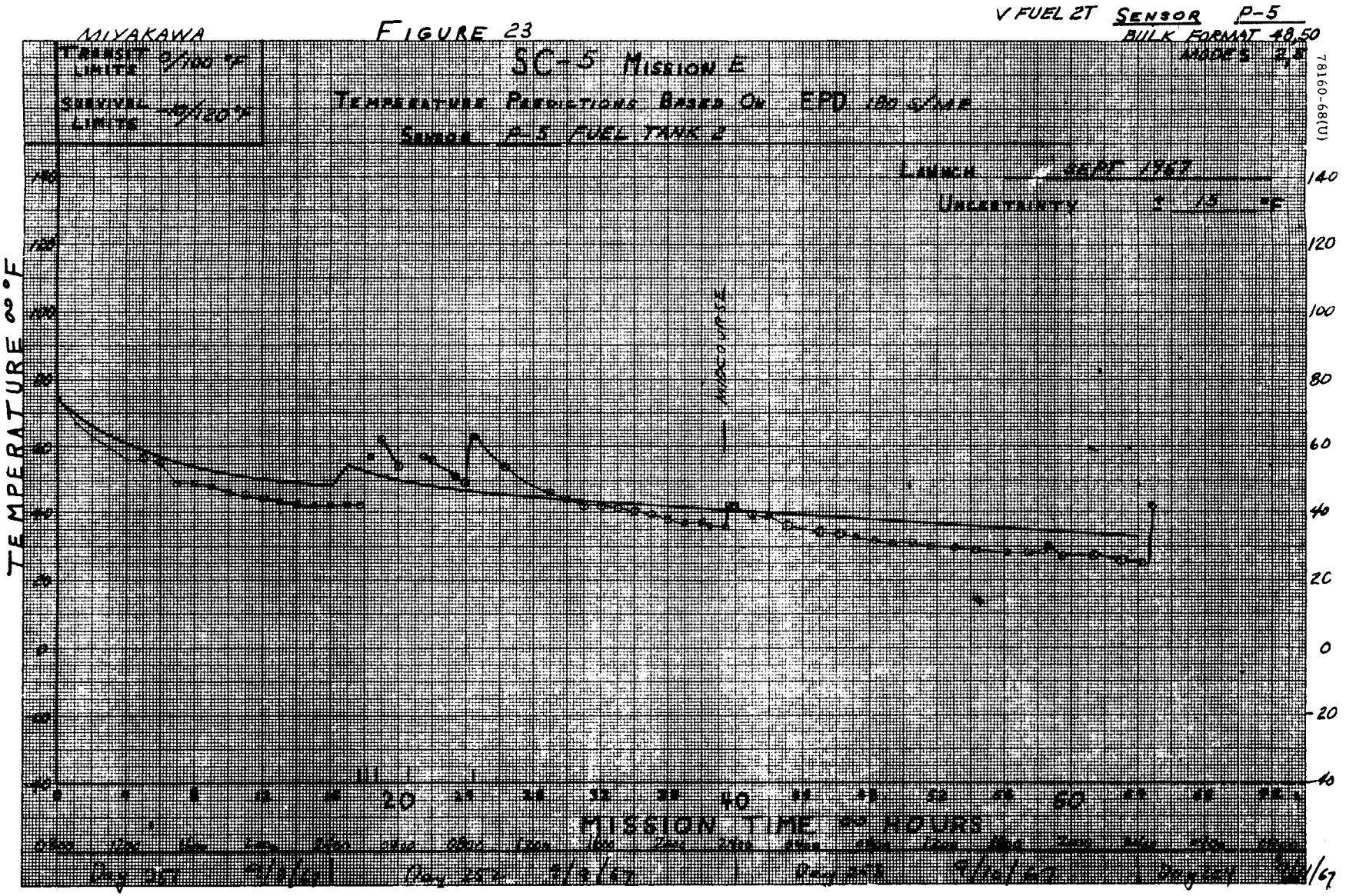

Figure 5.1-28. Sensor P-5: Fuel Tank 2

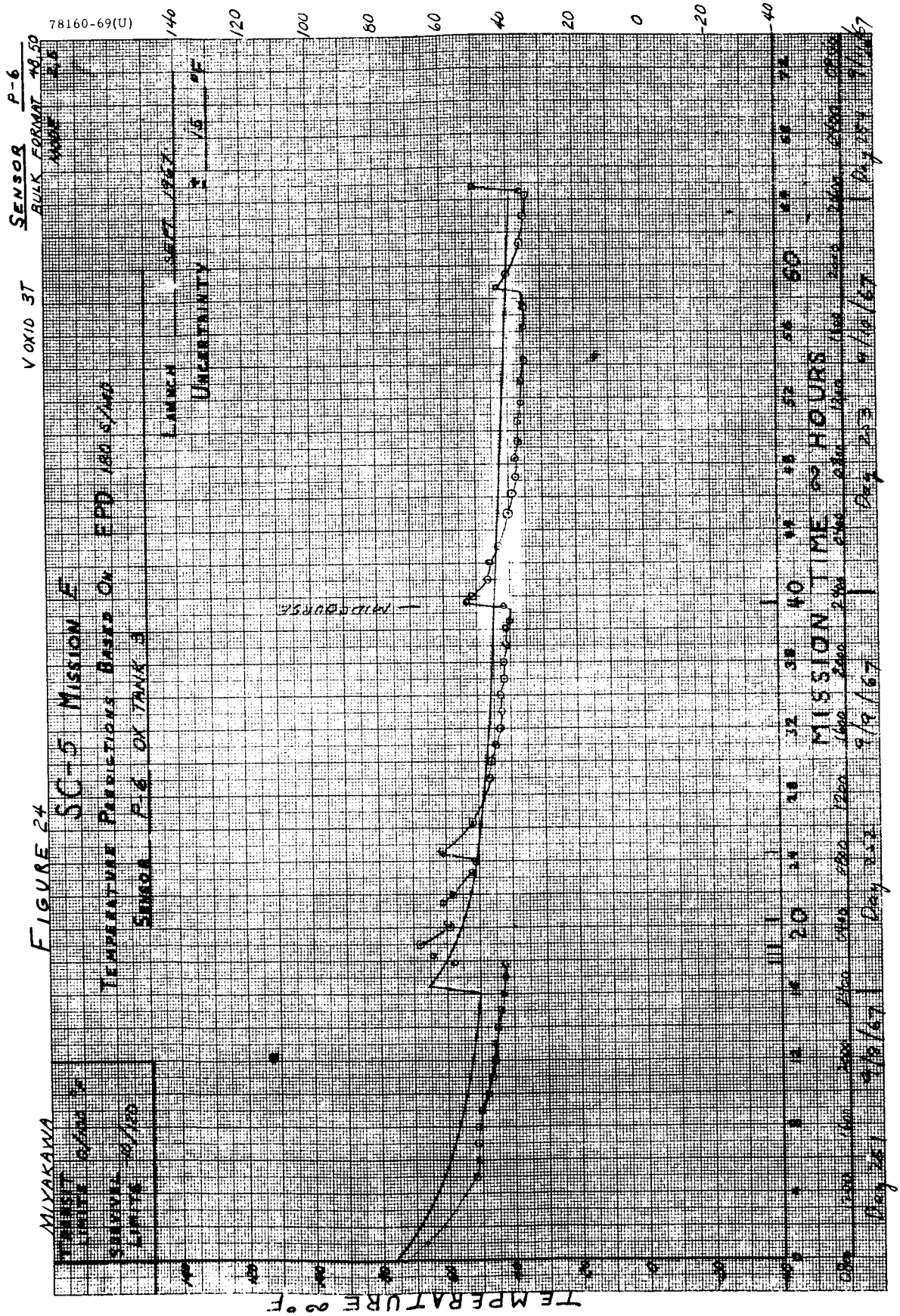

Figure 5.1-29. Sensor P-6: Oxidizer Tank 3

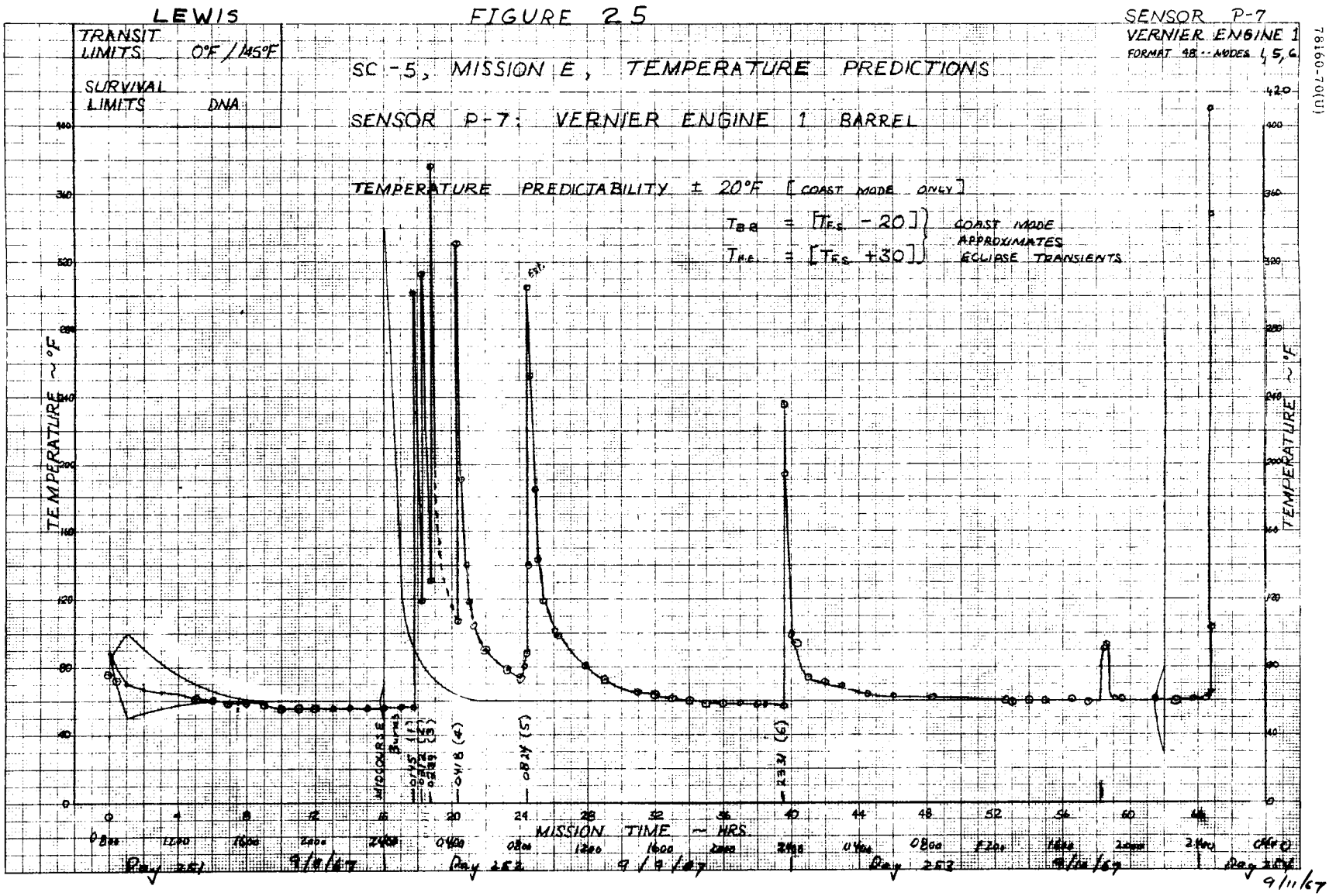

Figure 5.1-30. Sensor P-7: Vernier Engine 1 Barrel

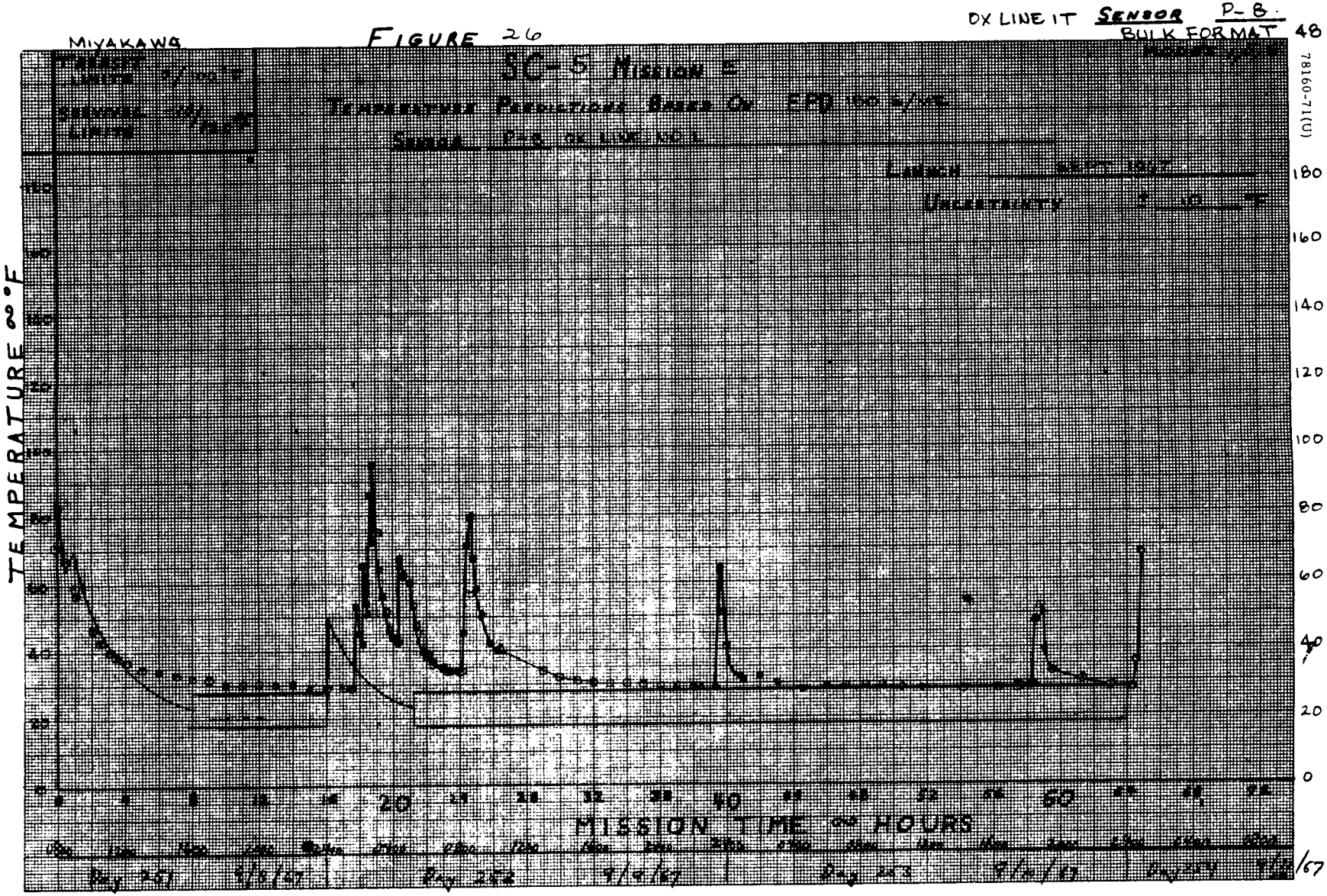

Figure 5.1-31. Sensor P-8: Oxidizer Line 1

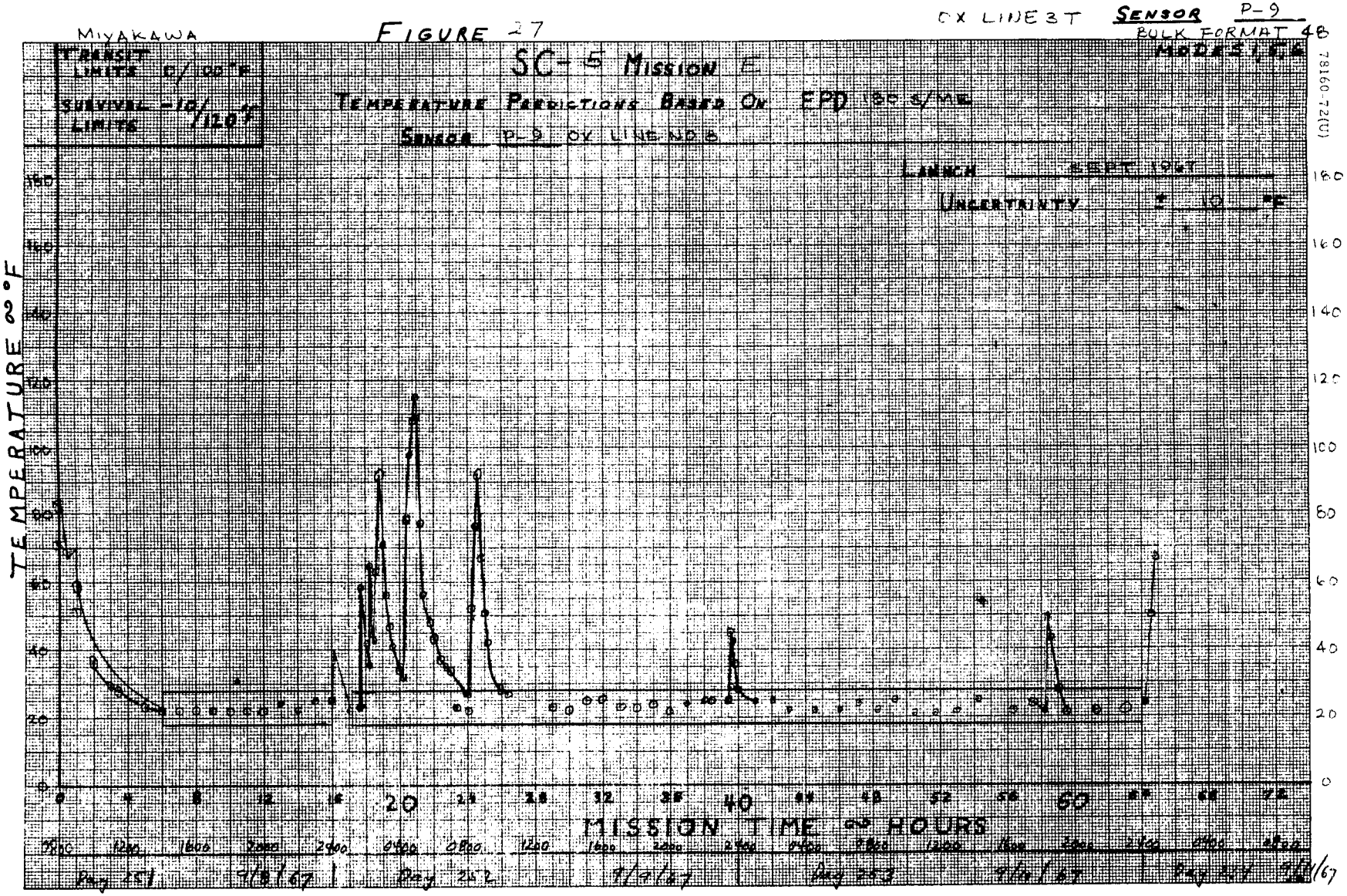

Figure 5.1-32. Sensor P-9: Oxidizer Line 3

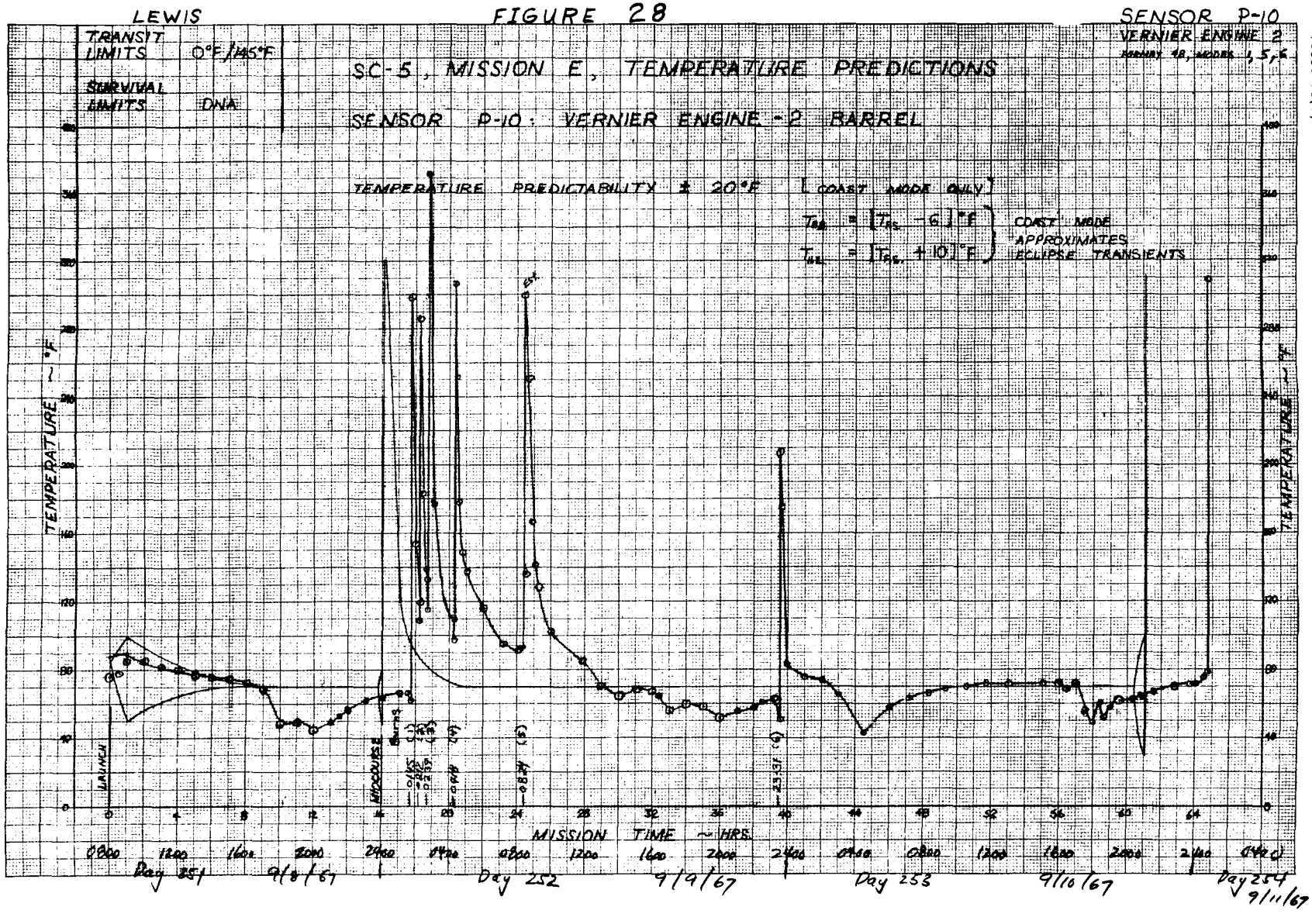

78160-73(U)

Figure 5.1-33. Sensor P-10: Vernier Engine 2 Barrel

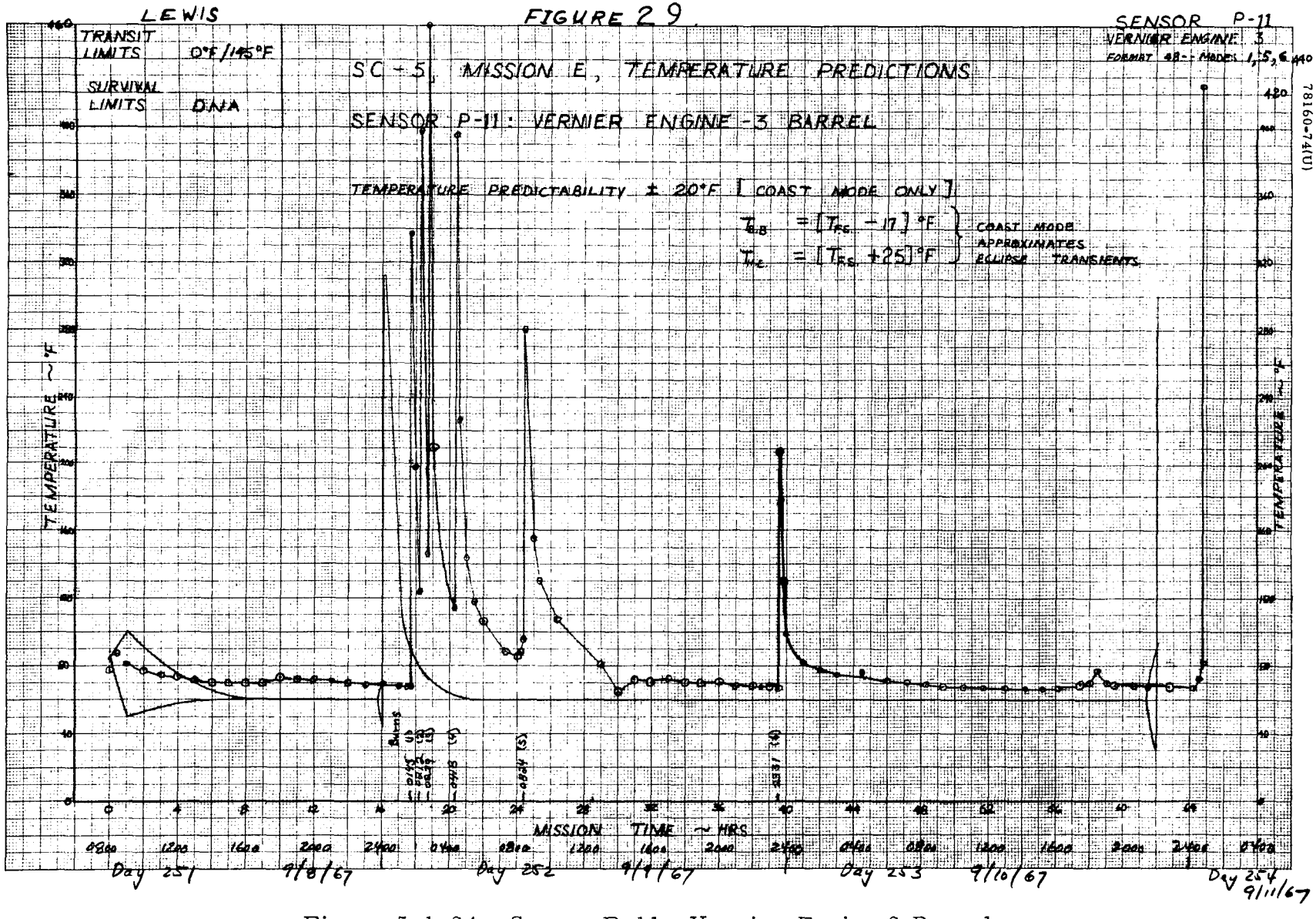

Figure 5.1-34. Sensor P-11: Vernier Engine 3 Barrel

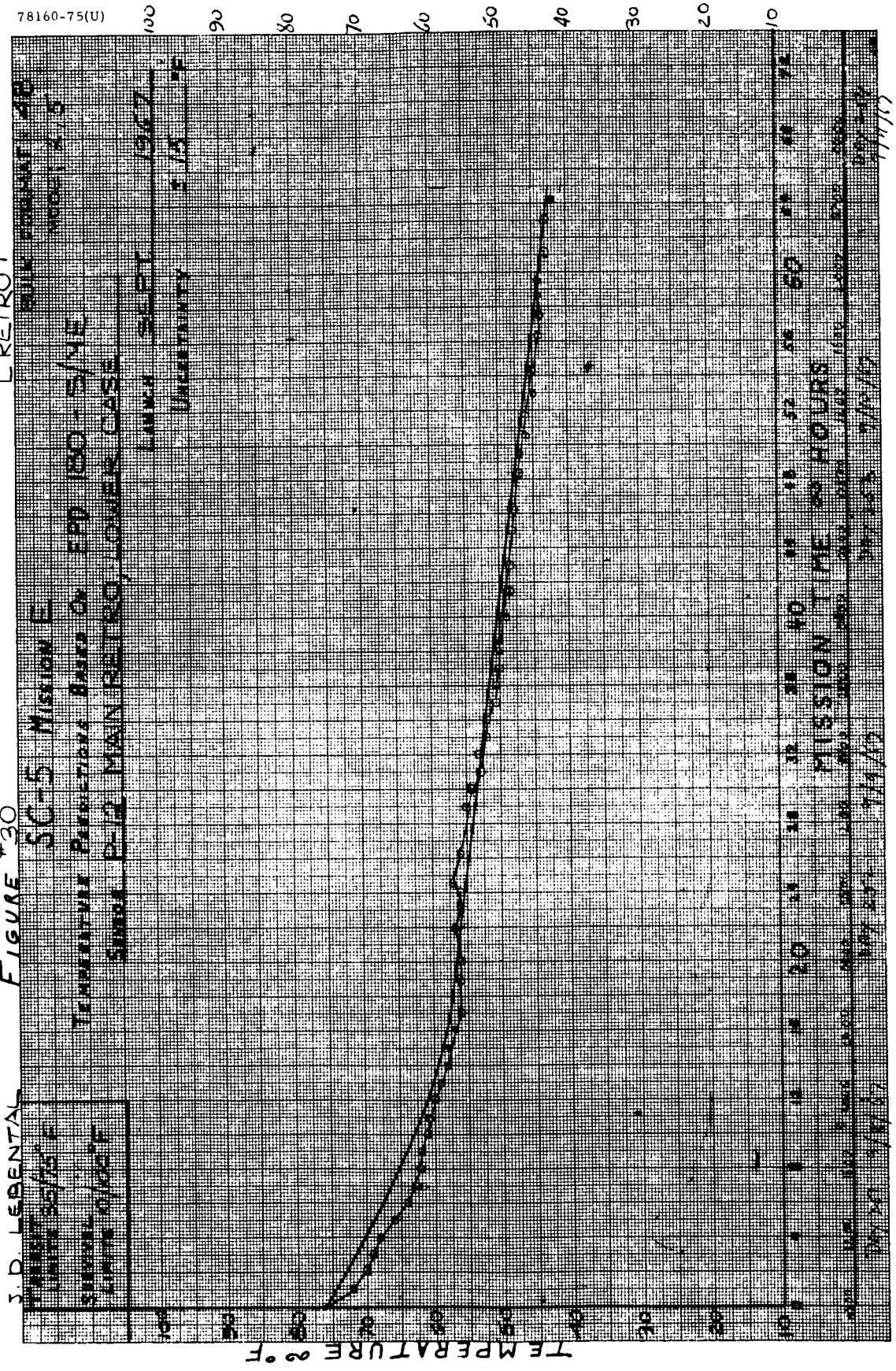

Figure 5.1-35. Sensor P-12: Main Retro, Lower Case

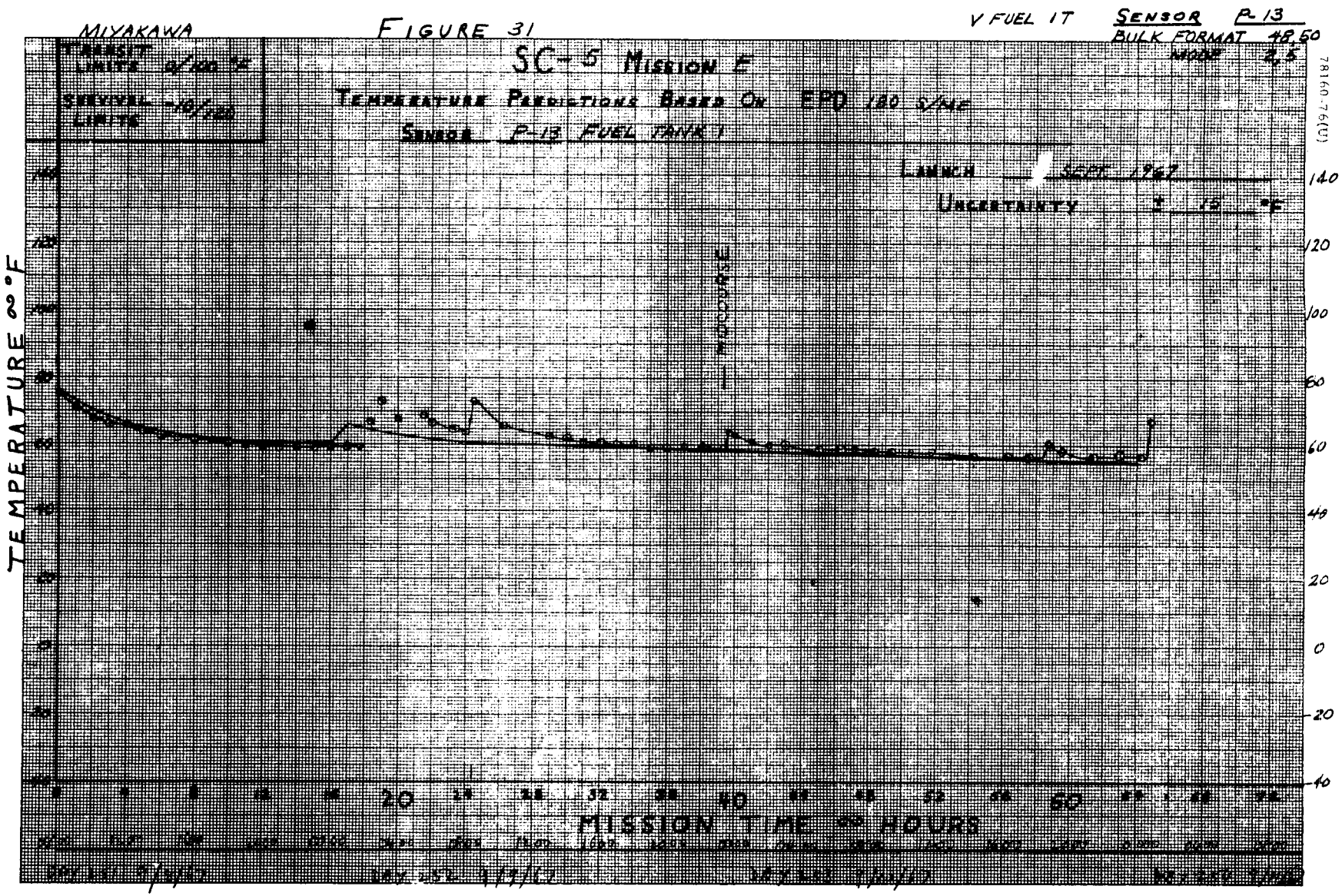

Figure 5.1-36. Sensor P-13: Fuel Tank 1

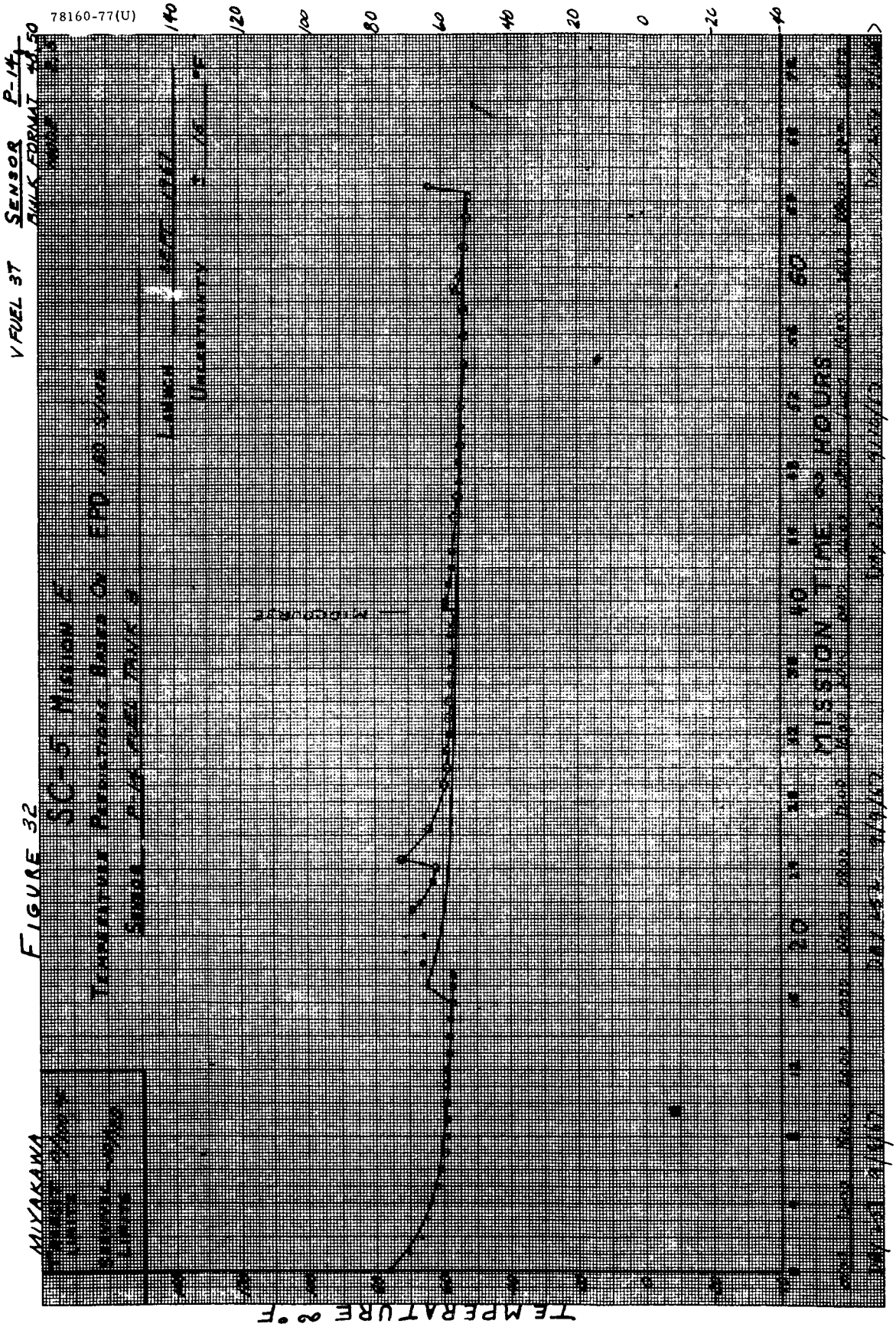

Figure 5.1-37. Sensor P-14: Fuel Tank 3

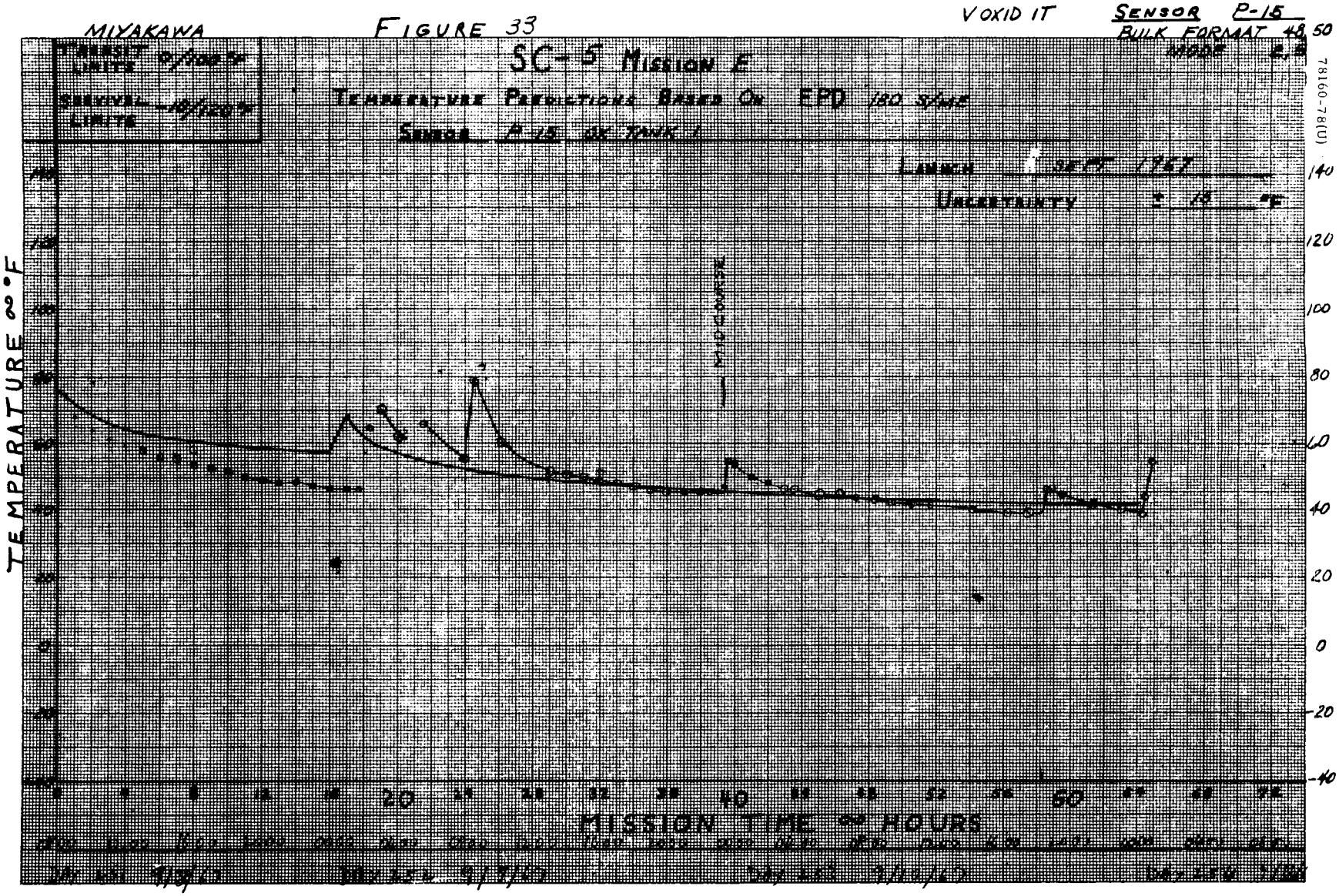

Figure 5.1-38. Sensor P-15: Oxidizer Tank 1

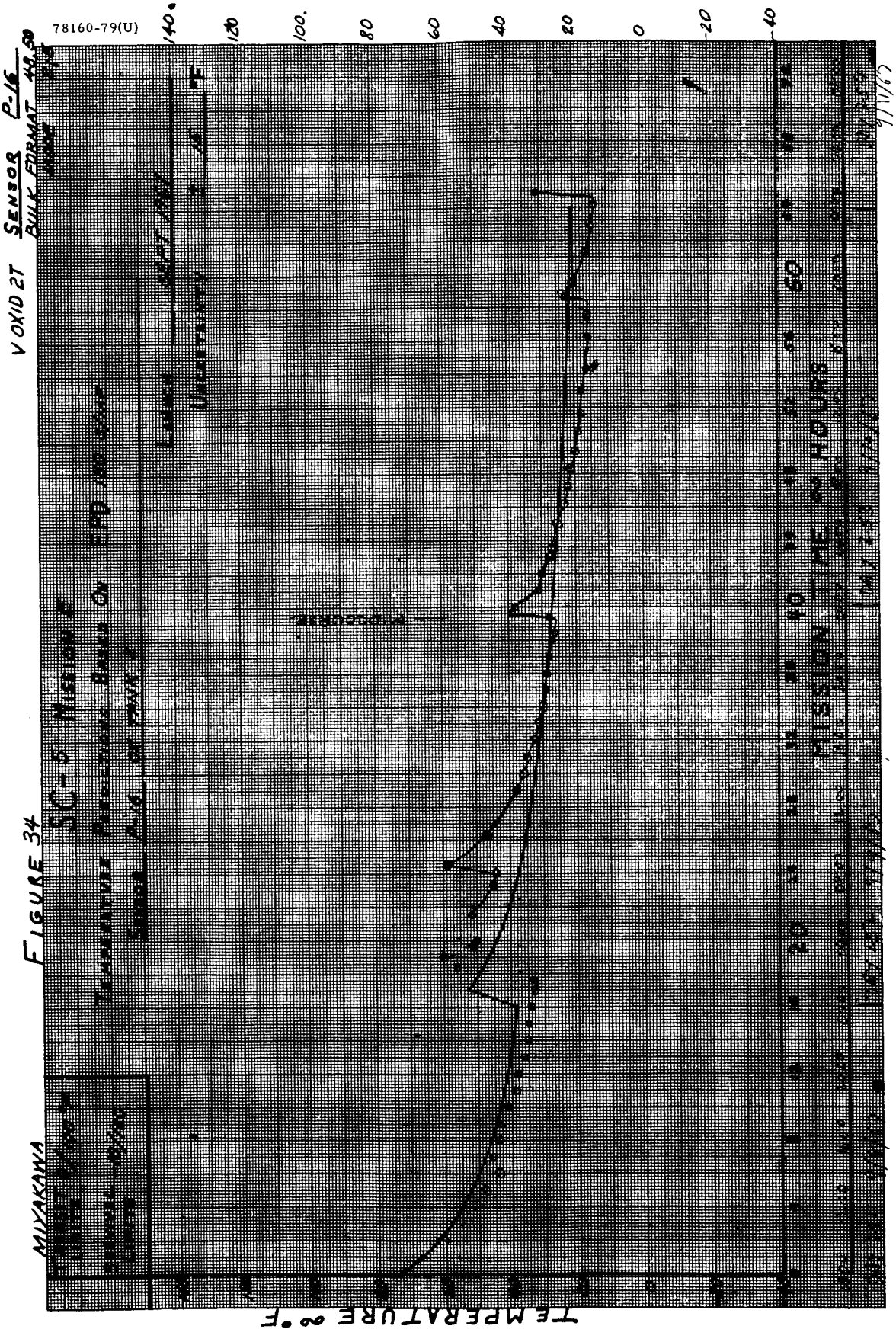

Figure 5.1-39. Sensor P-16: Oxidizer Tank 2

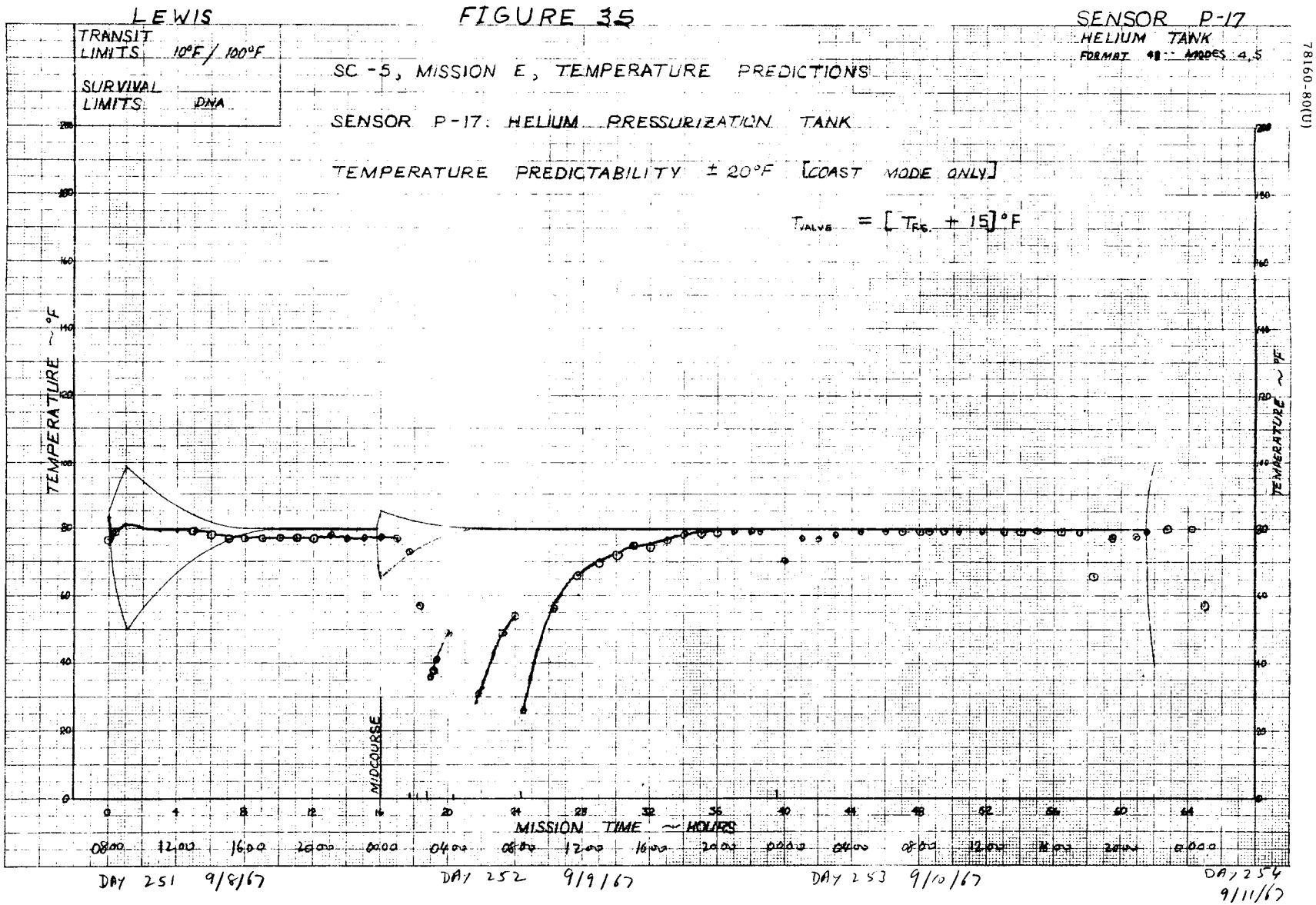

Figure 5.1-40. Sensor P-17: Helium Pressurization Tank

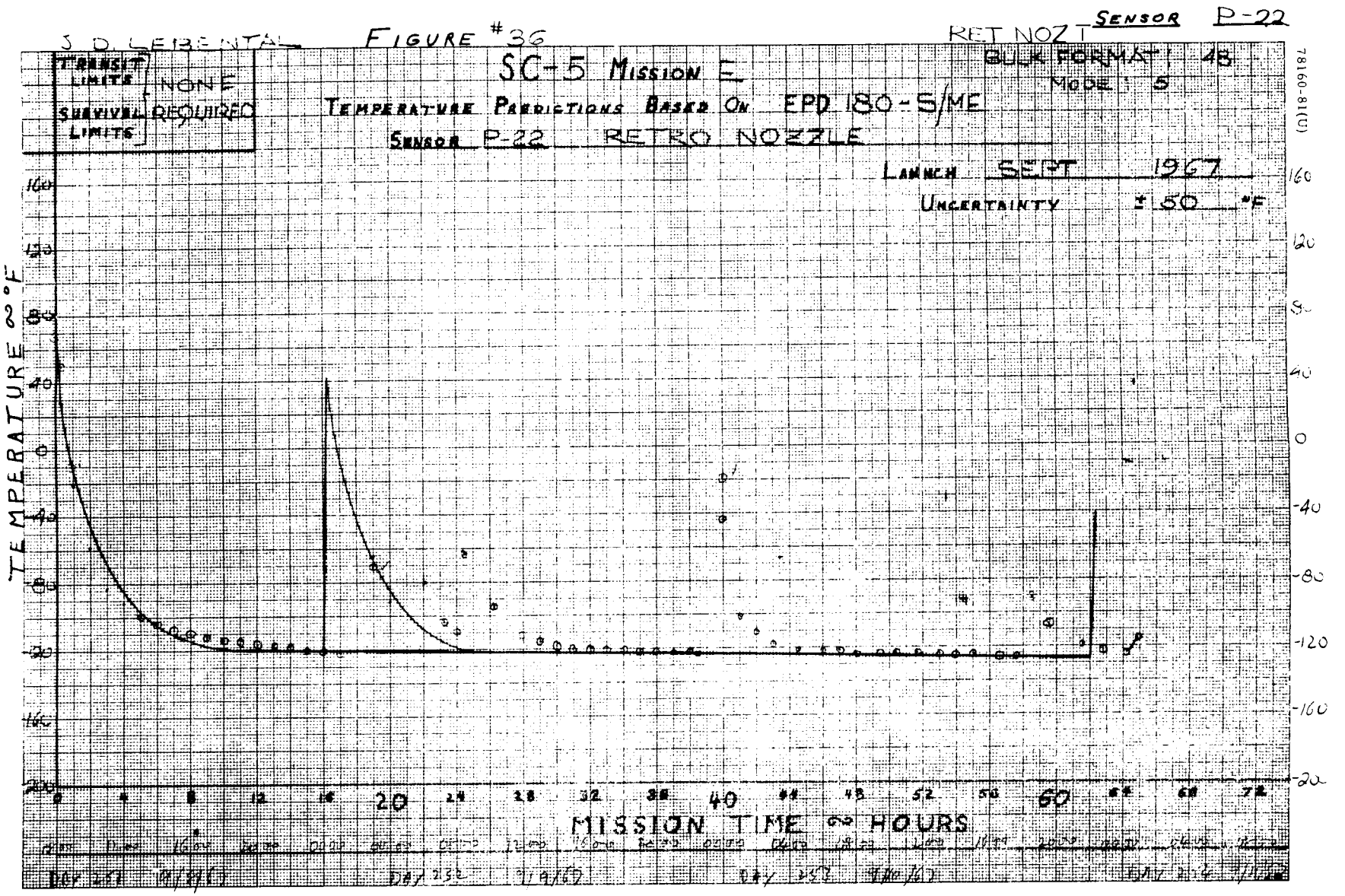

Figure 5.1-41. Sensor P-22: Retro Nozzle

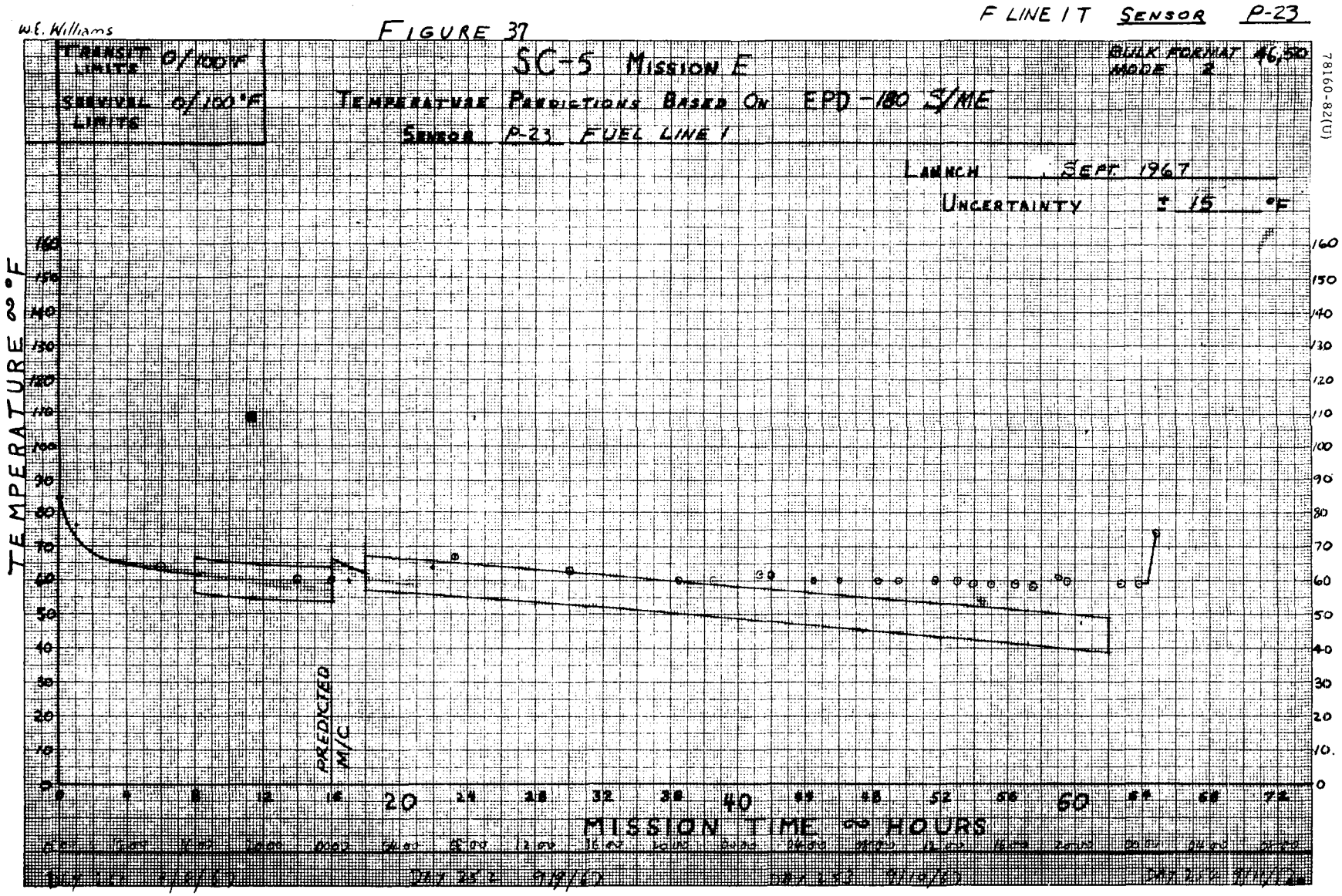

Figure 5.1-42. Sensor P-23: Fuel Line 1

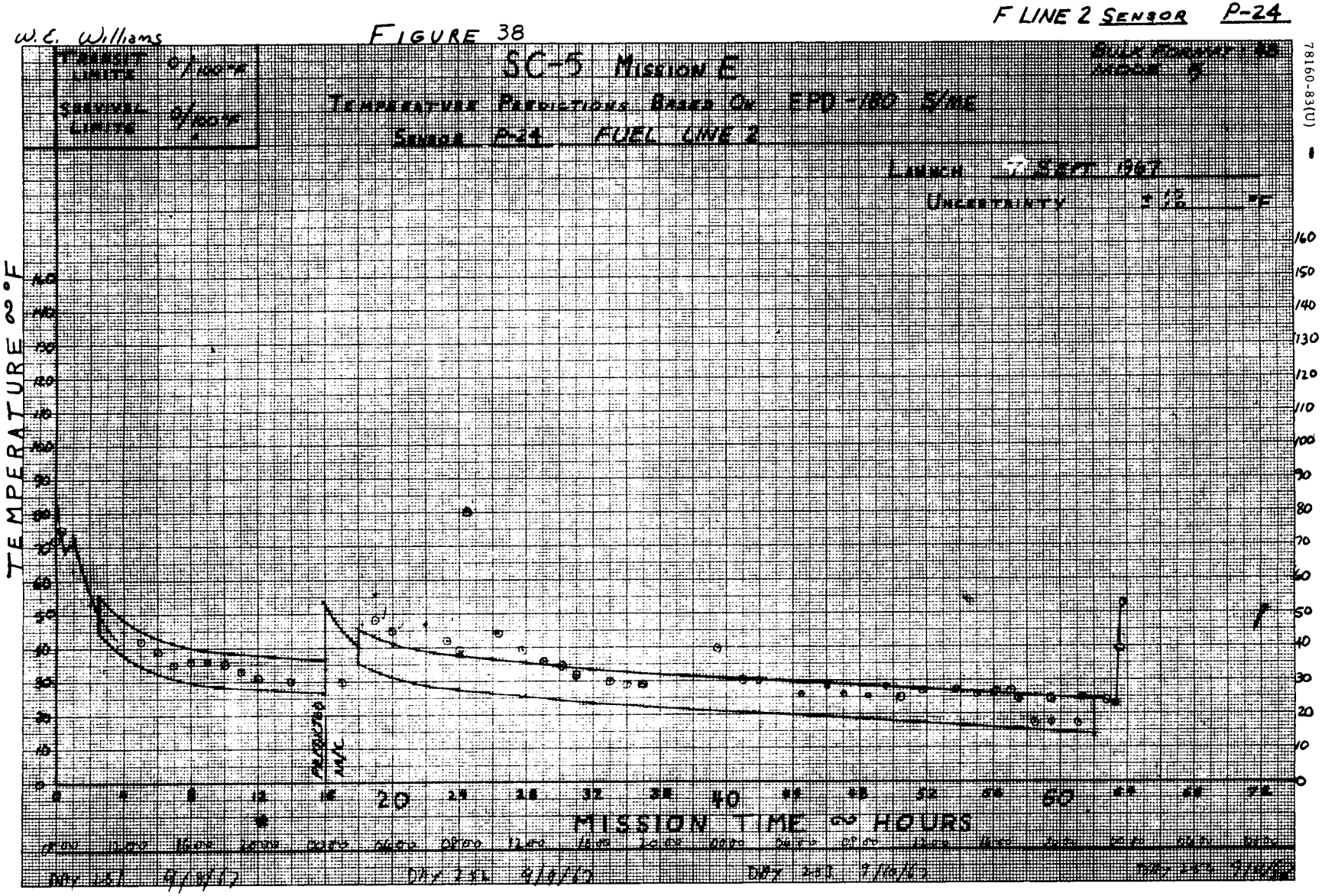

Figure 5.1-43. Sensor P-24: Fuel Line 2

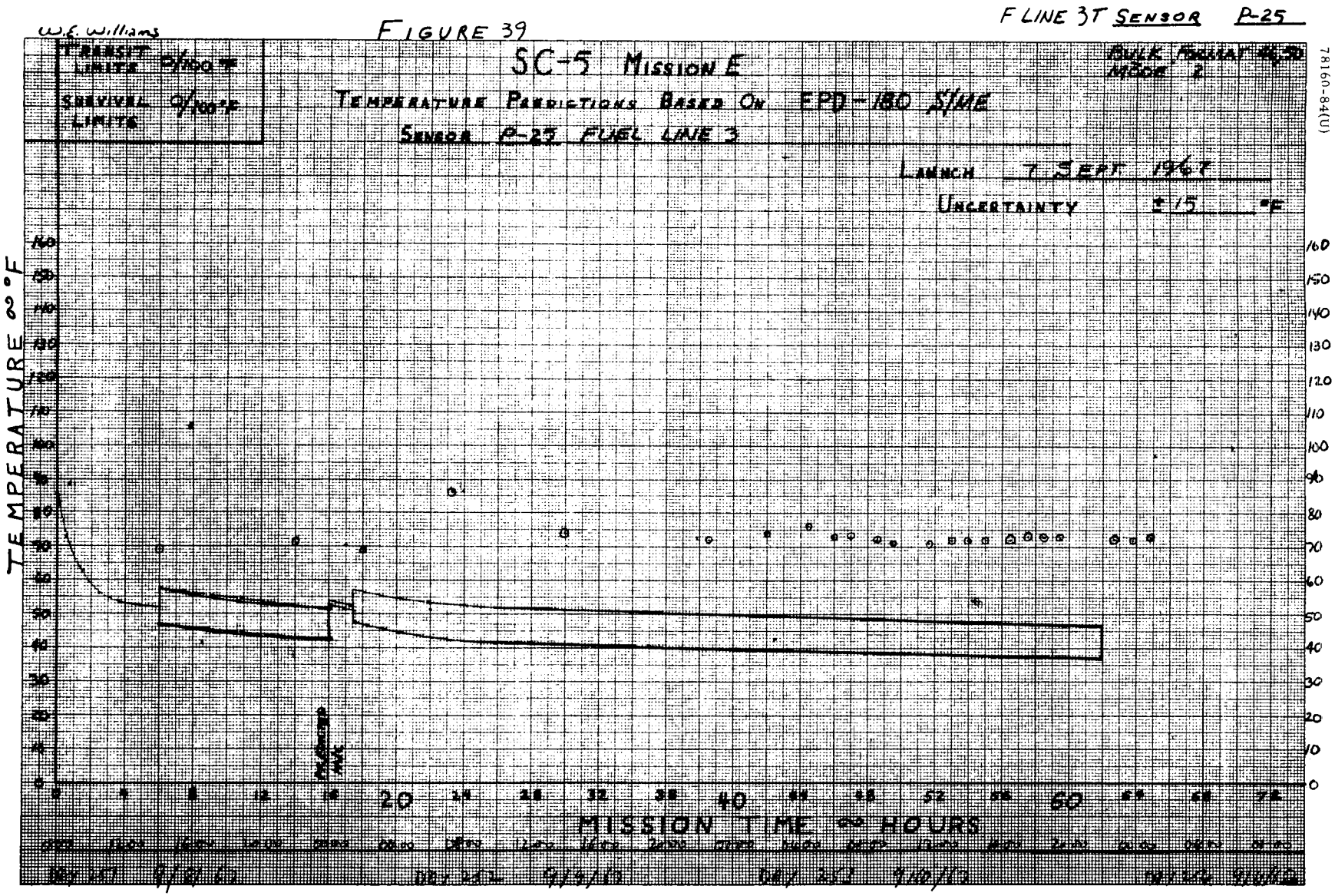

Figure 5.1-44. Sensor P-25: Fuel Line 3

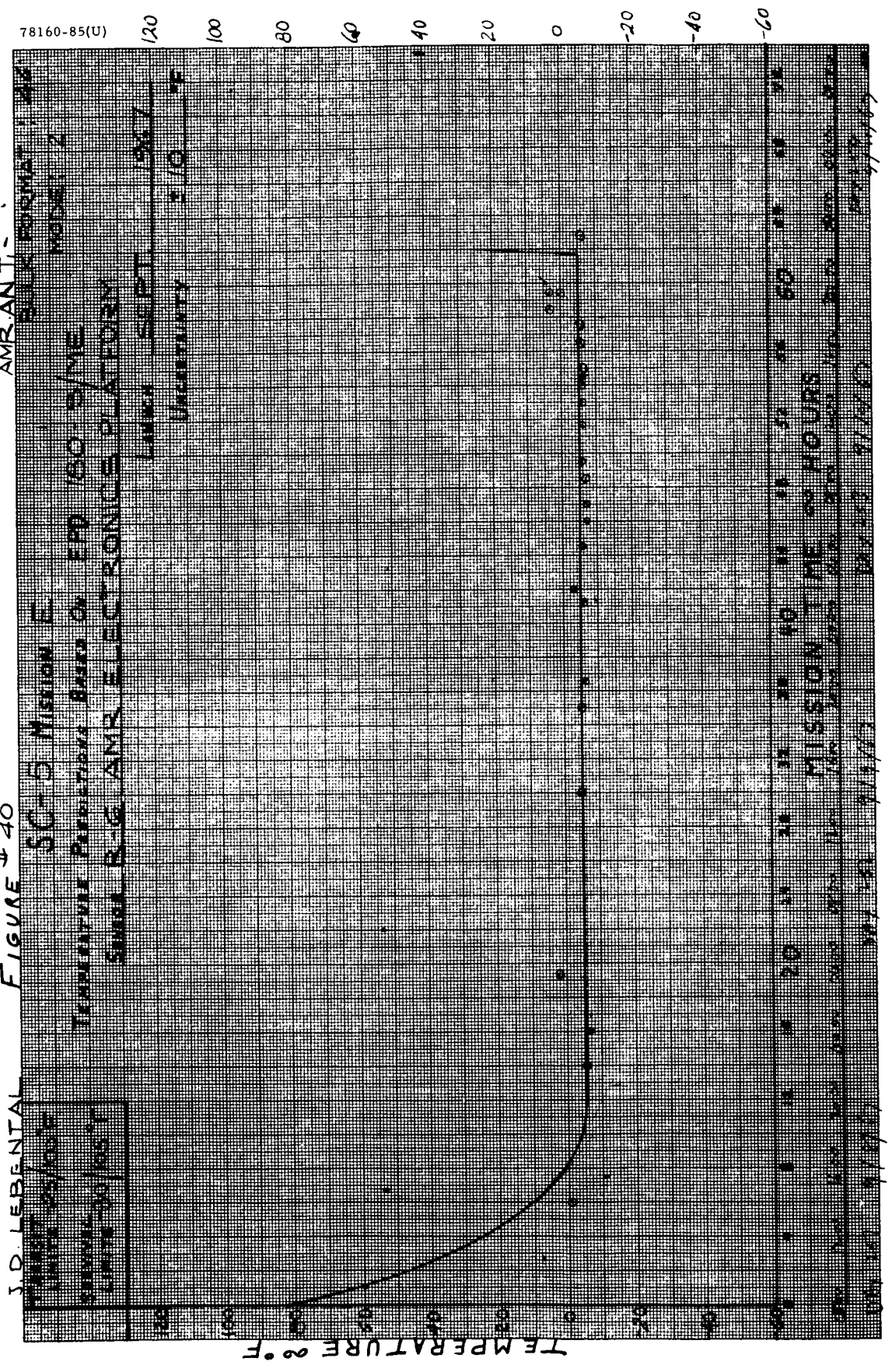

Figure 5.1-45. Sensor R-6: AMR Electronics Platform

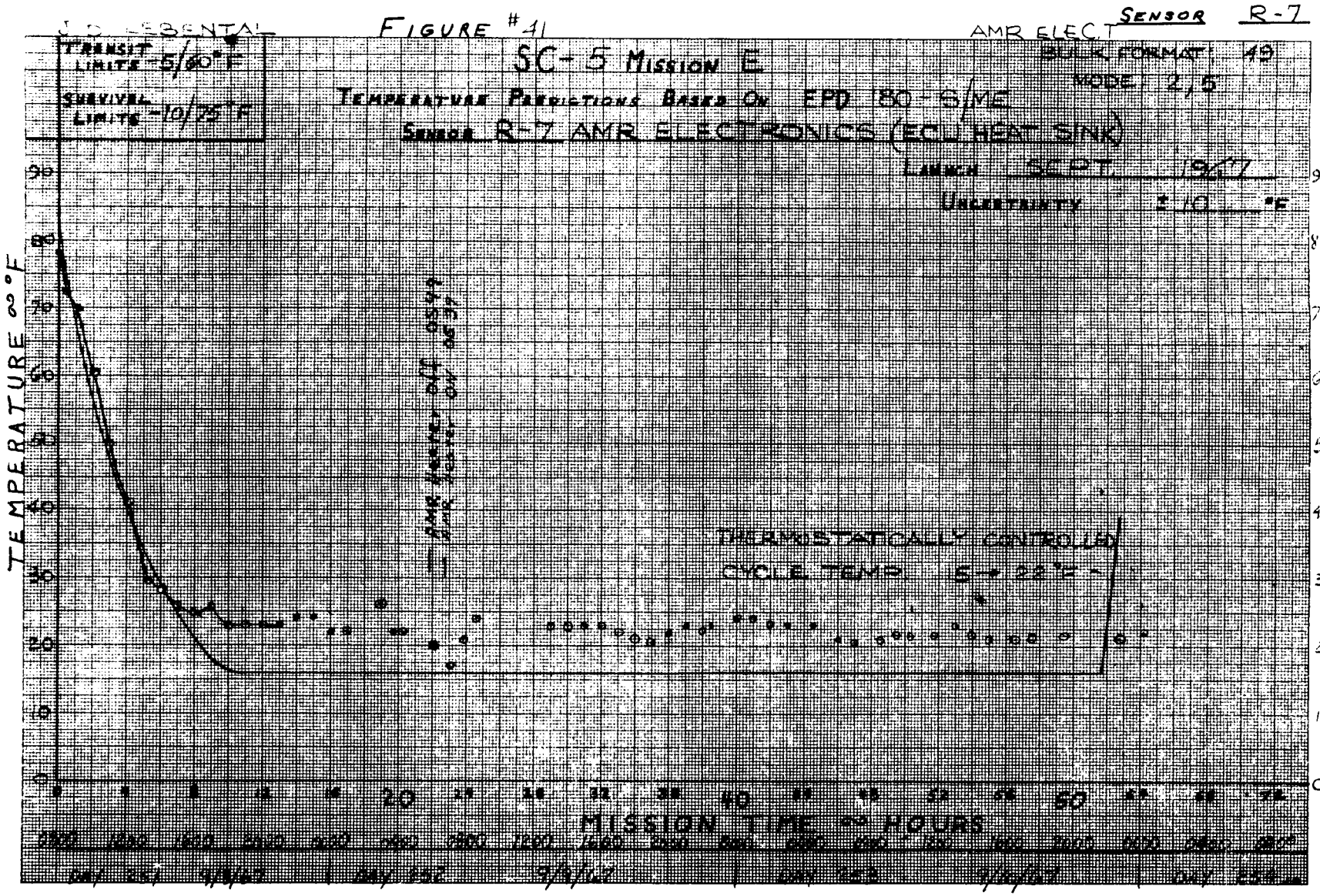

Figure 5.1-46. Sensor R-7: AMR Electronics – ECU Heat Sink

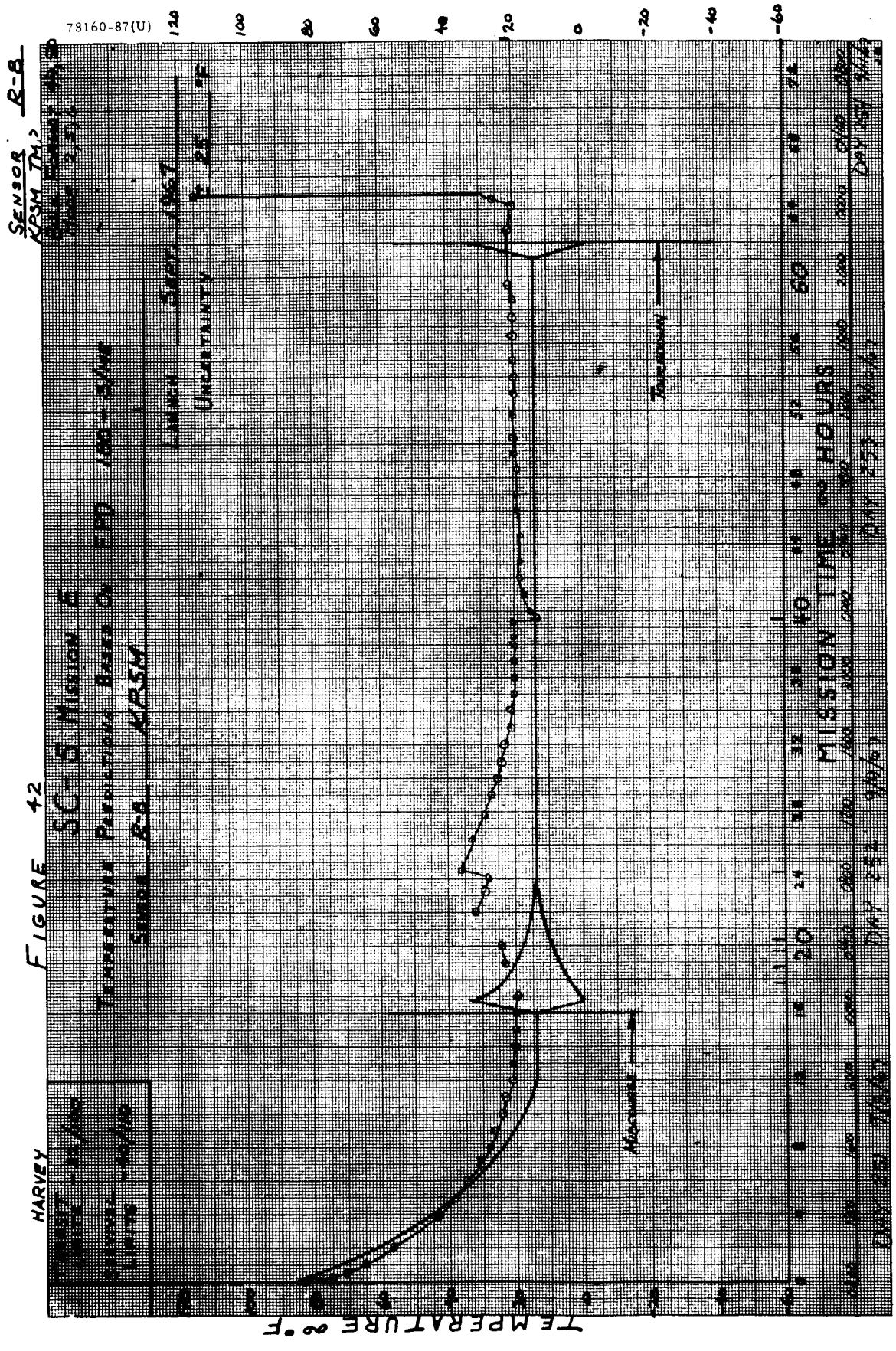

Figure 5.1-47. Sensor R-8: Klystron Power Supply Modulator

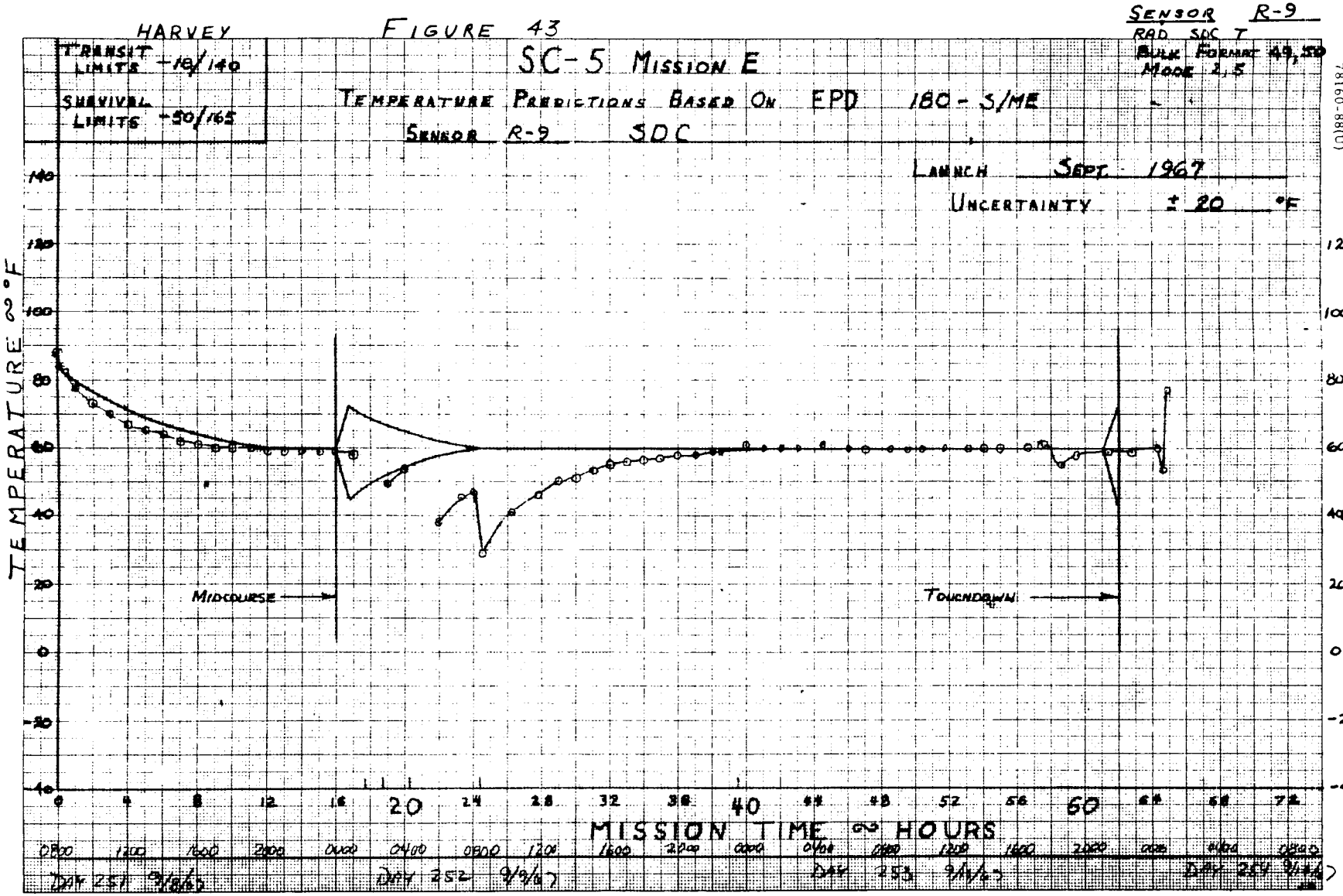

Figure 5.1-48. Sensor R-9: Signal Data Converter

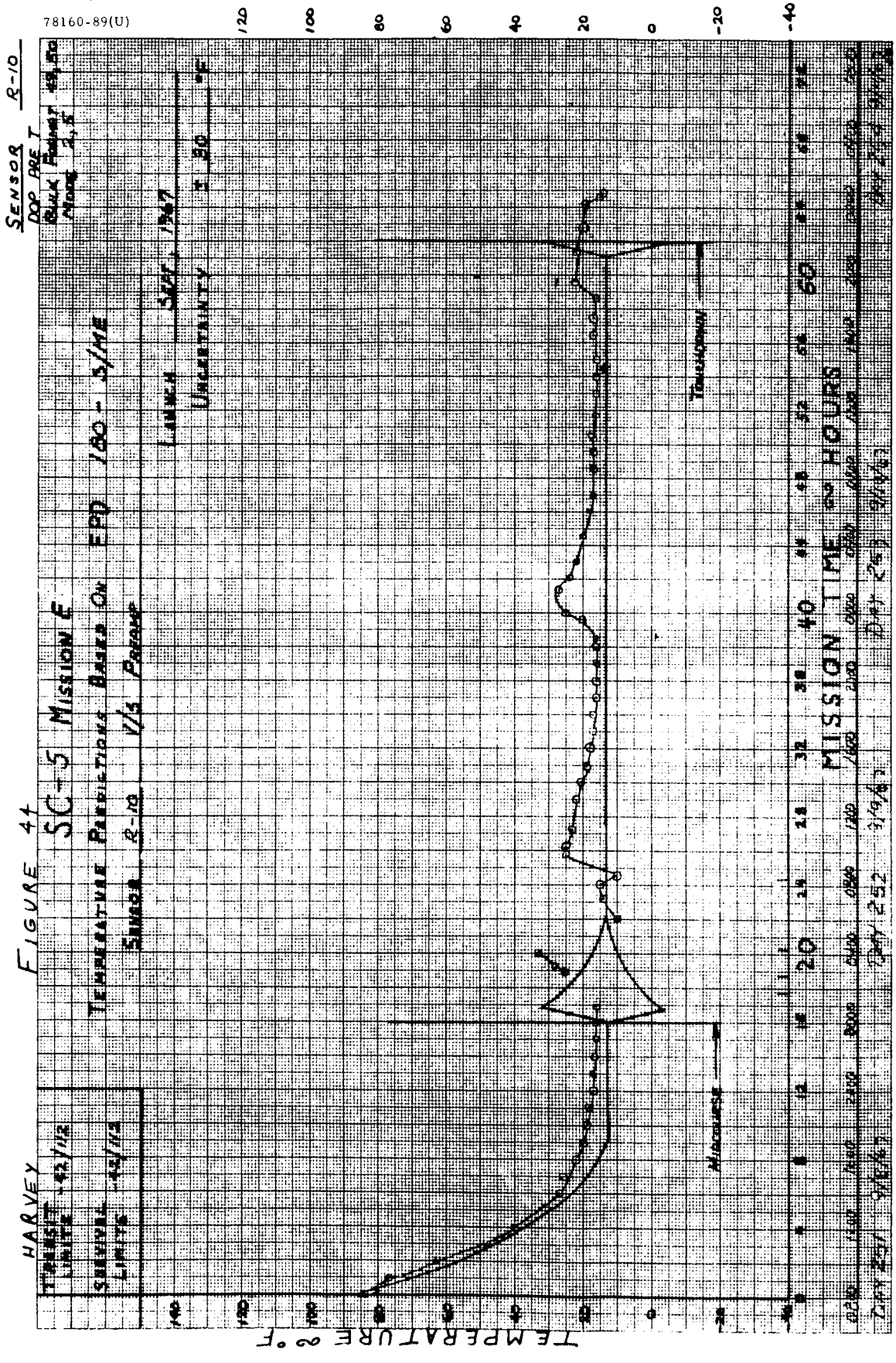

Figure 5.1-49. Sensor R-10: V/S Preamplifier

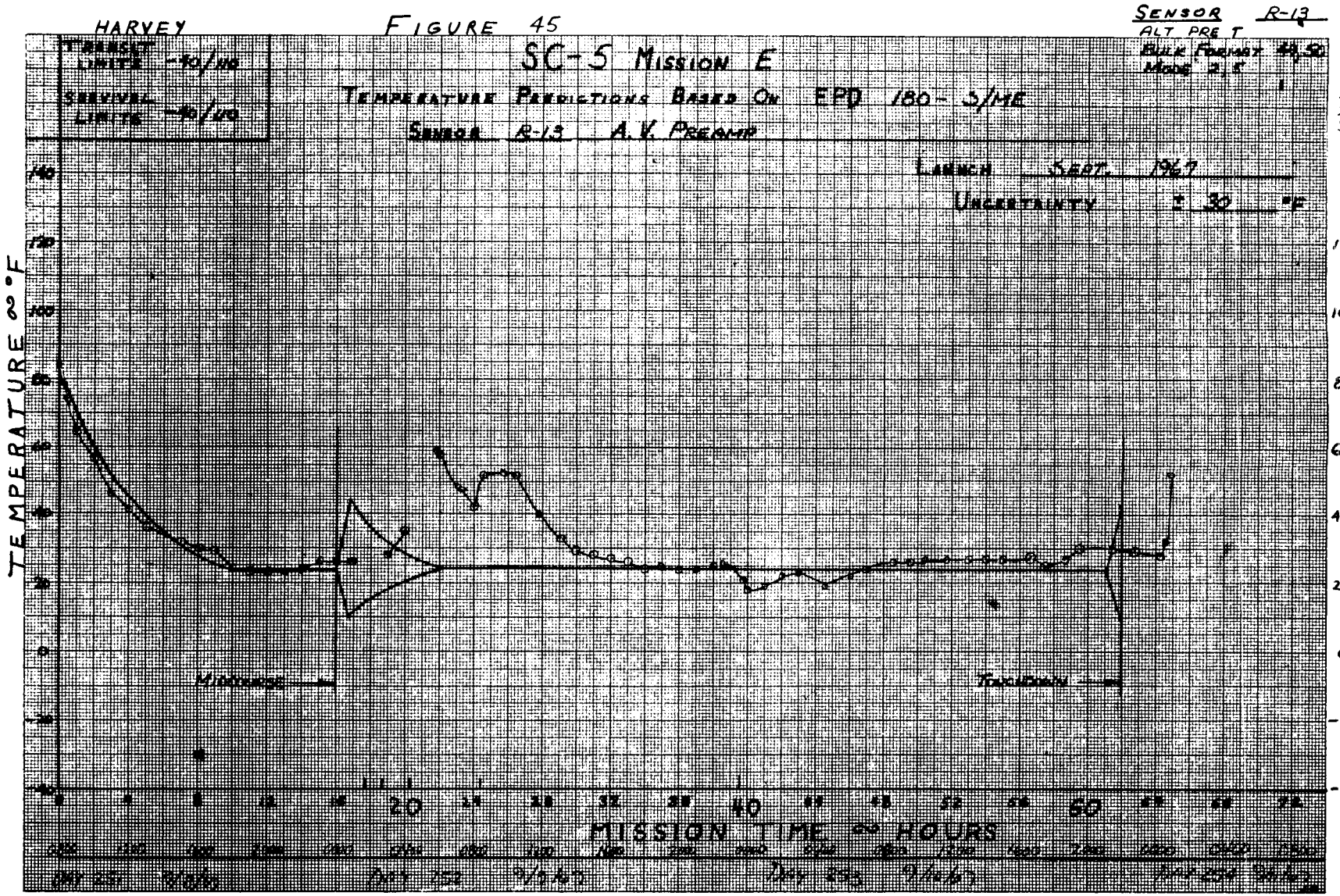

Figure 5.1-50. Sensor R-13: AV Preamplifier

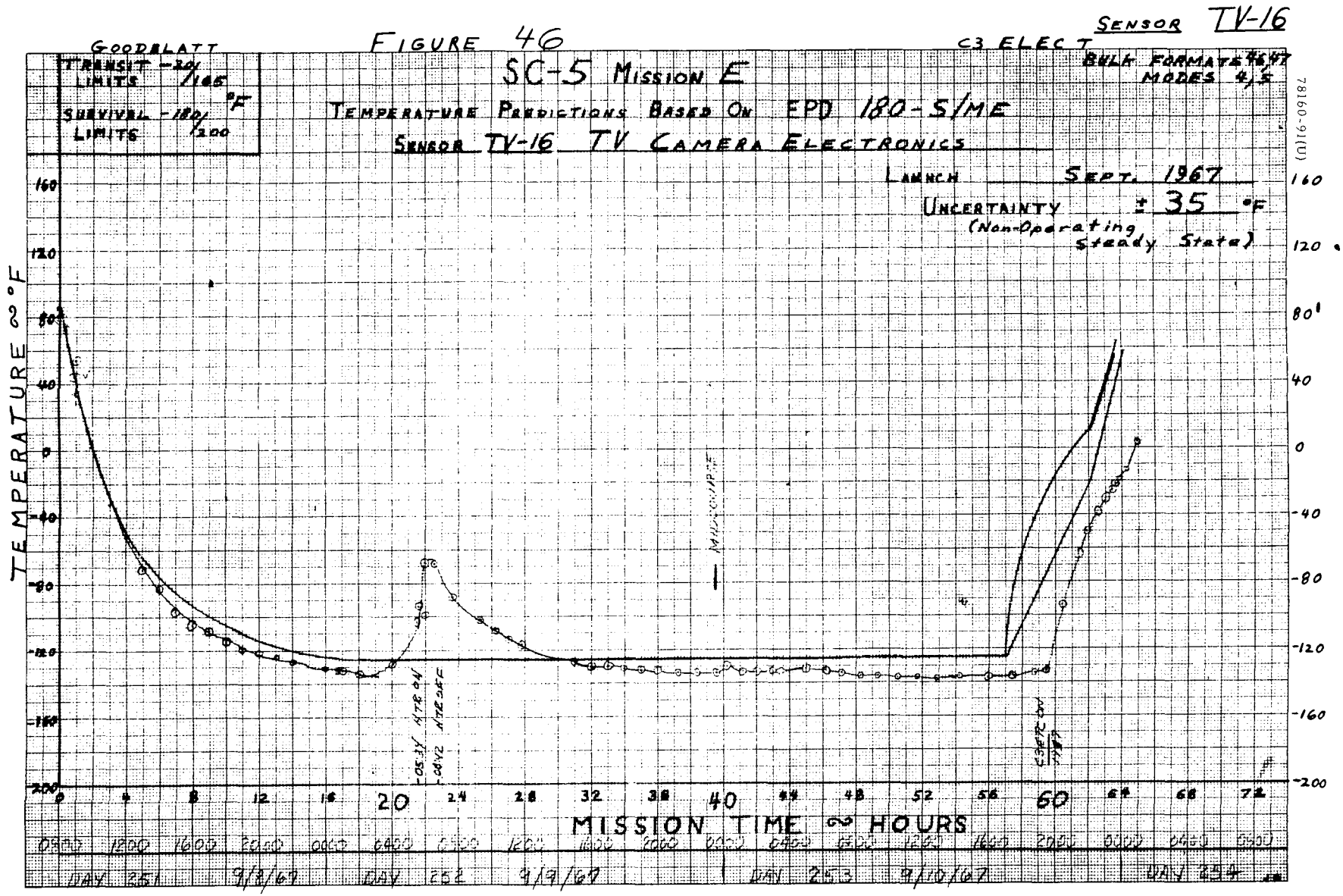

Figure 5.1-51. Sensor TV-16: TV Camera Electronics

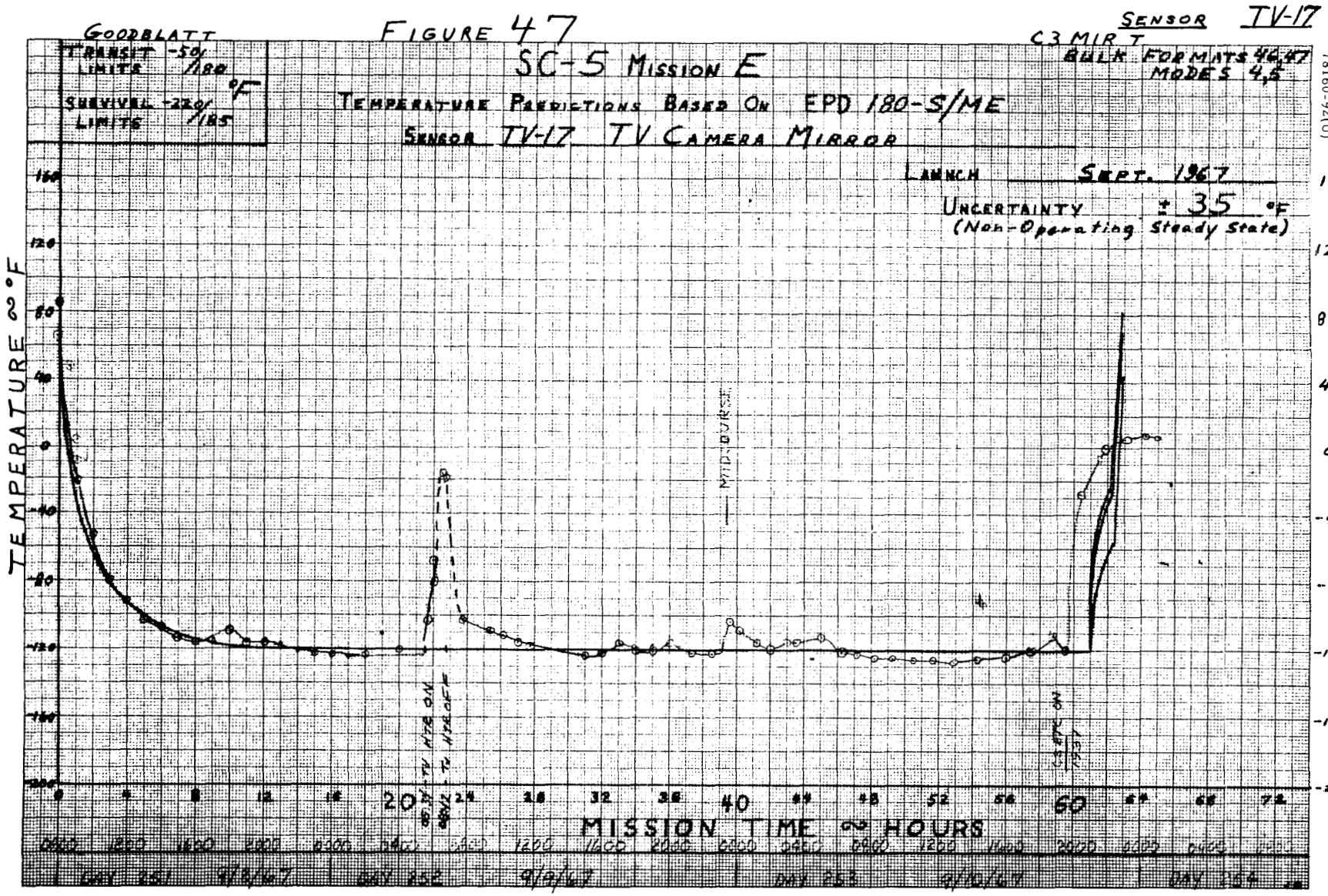

Figure 5.1-52. Sensor TV-17: TV Camera Mirror

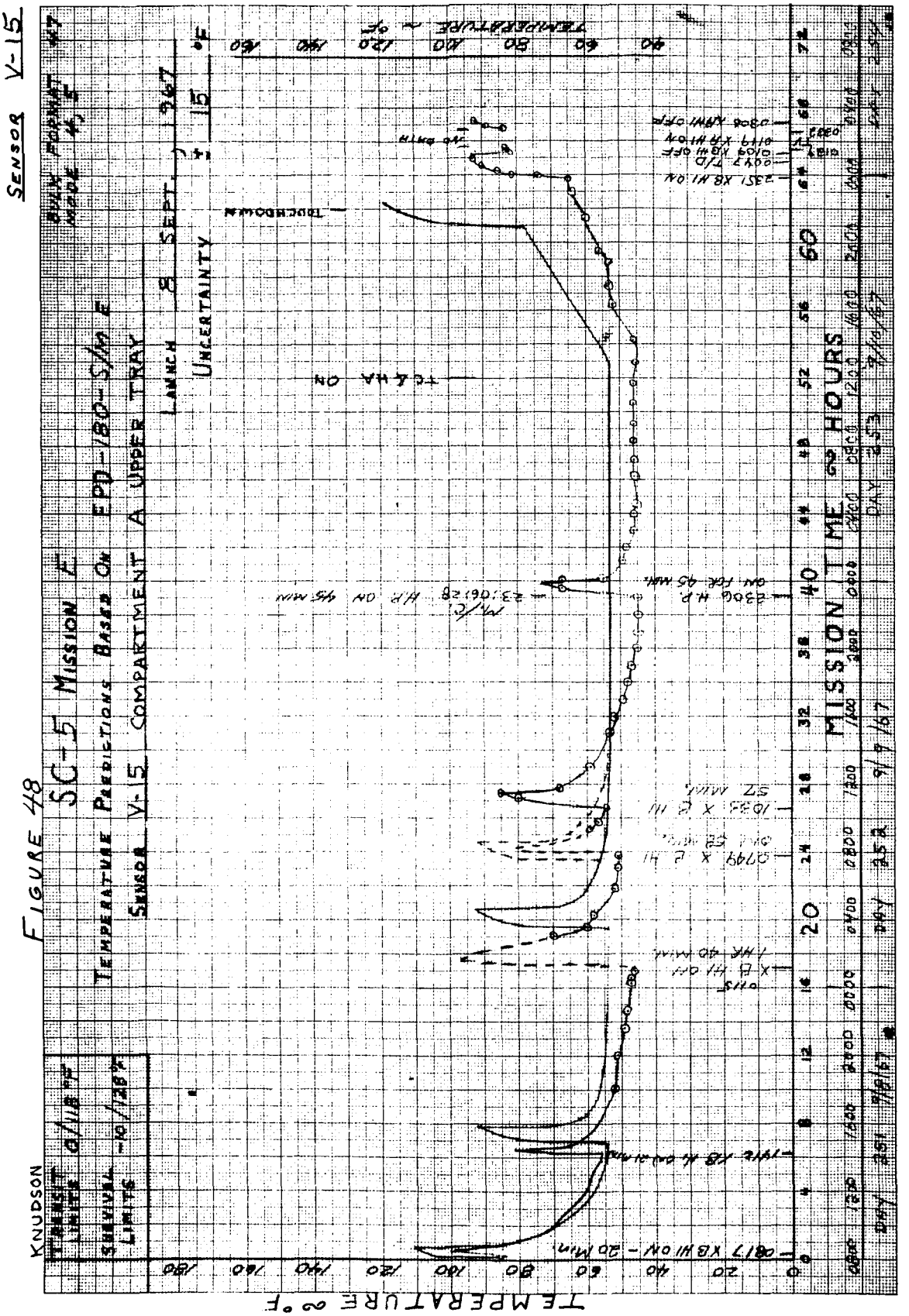

Figure 5.1-53. Sensor V-15: Compartment A Upper Tray

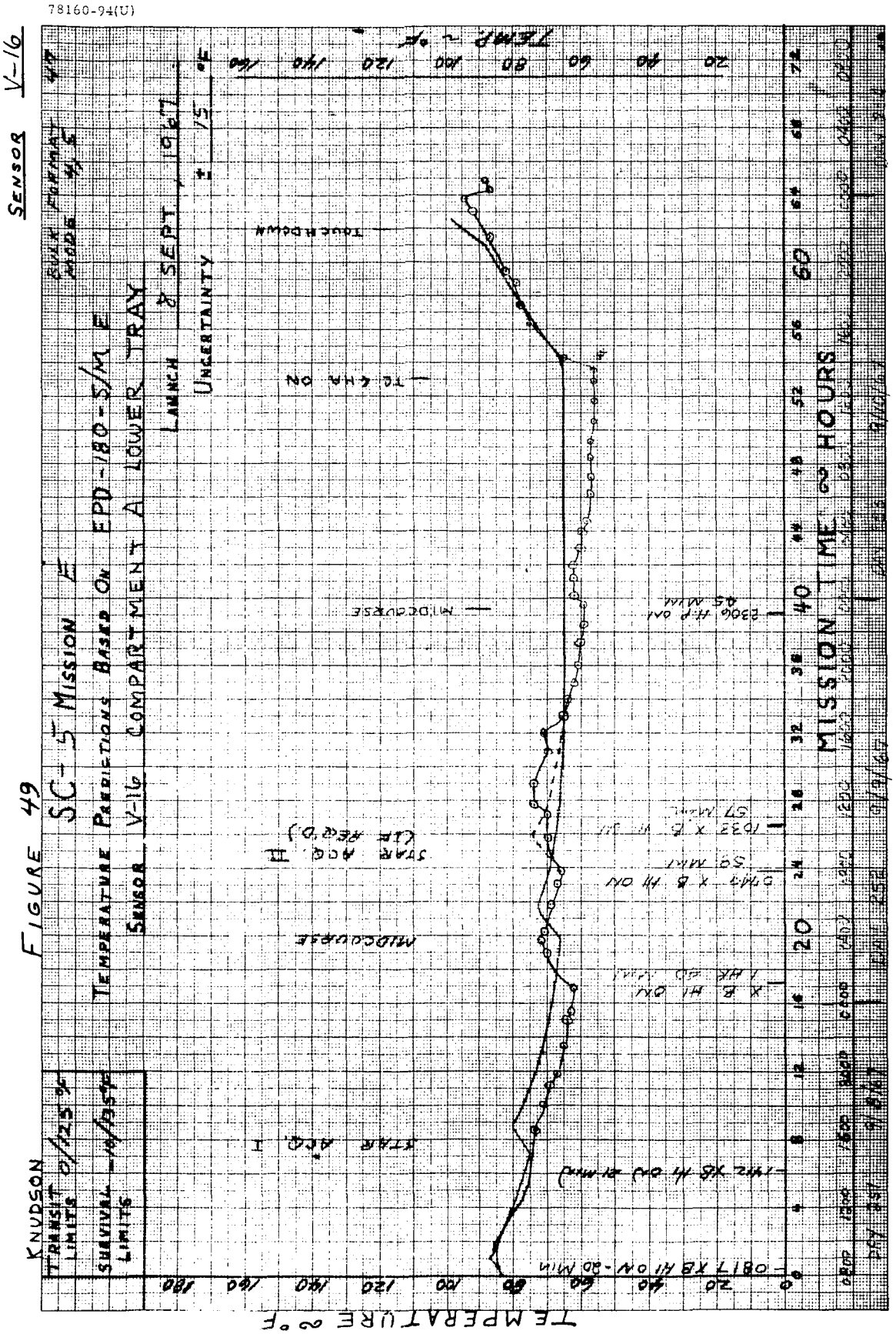

Figure 5.1-54. Sensor V-16: Compartment A Lower Tray

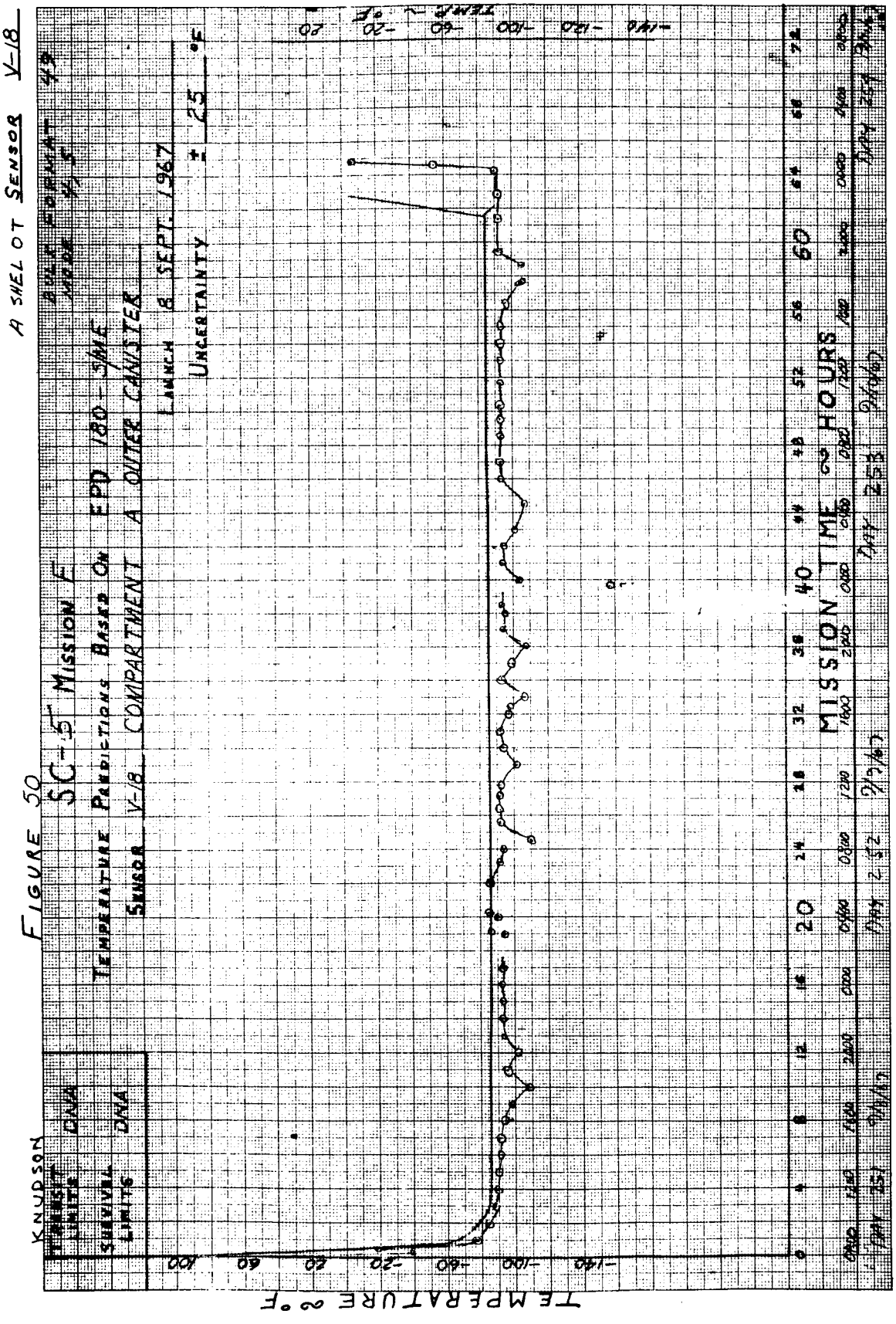

Figure 5.1-55. Sensor V-18: Compartment A Outer Canister

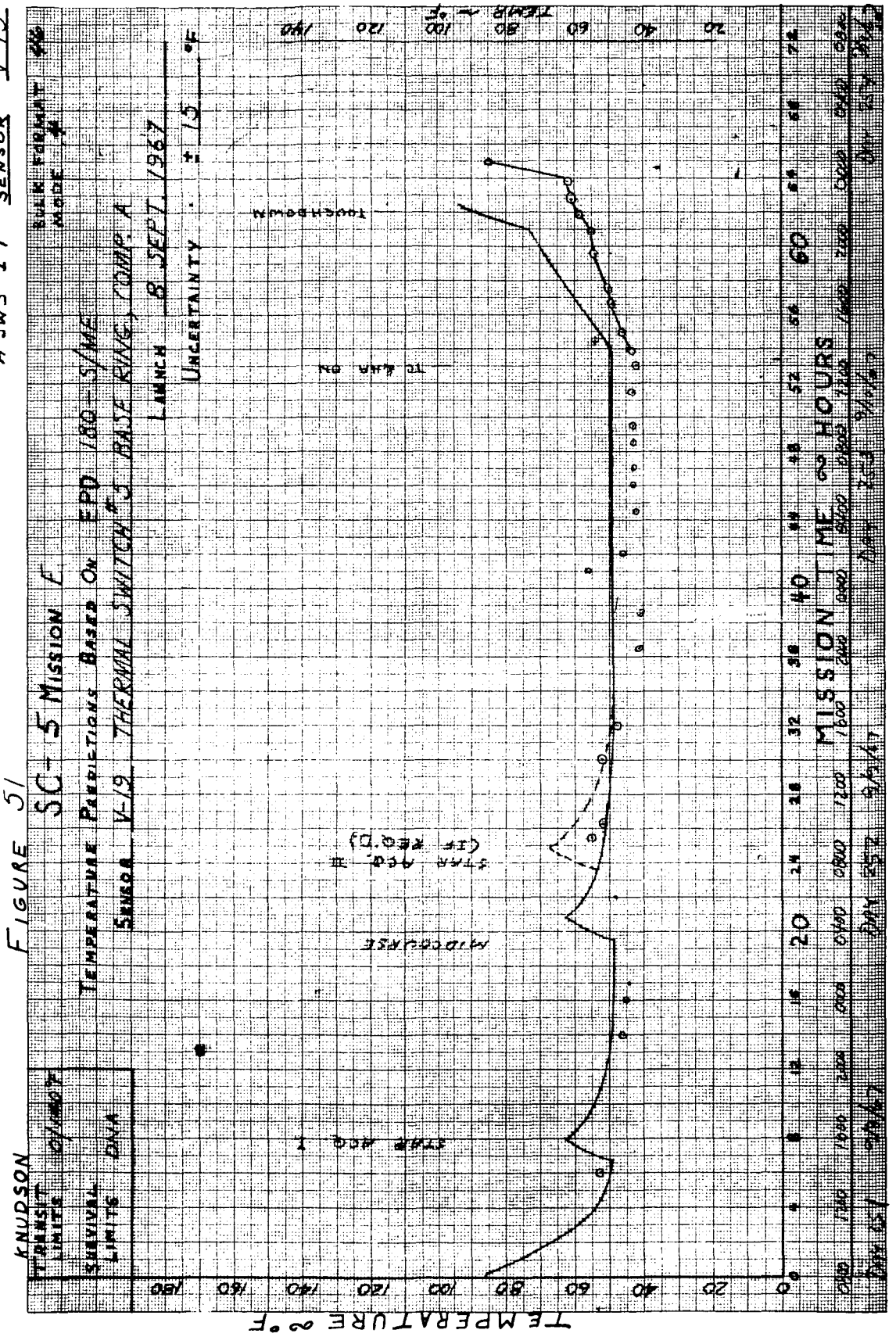

Figure 5.1-56. Sensor V-19: Thermal Switch 5 Base Ring, Compartment A

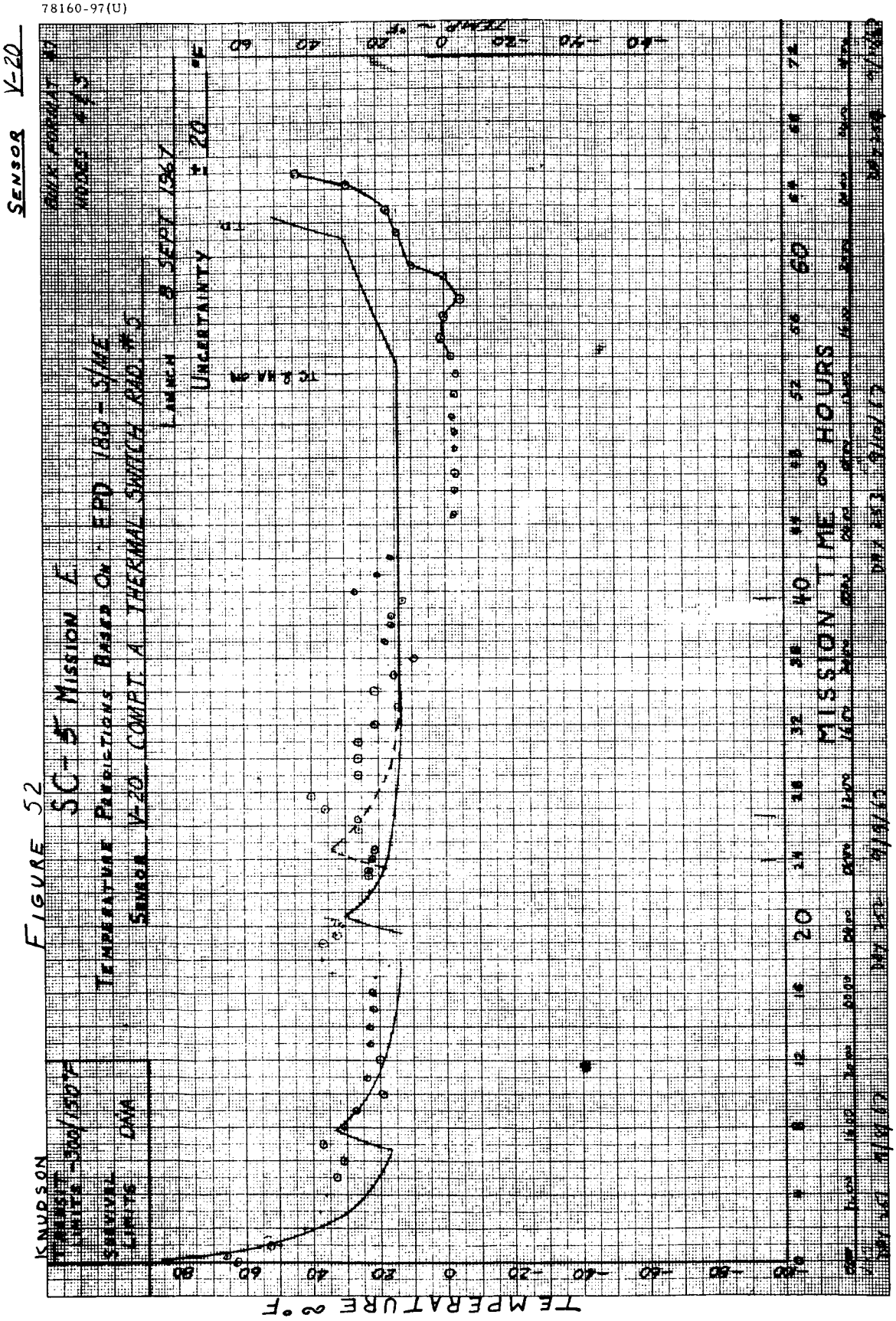

Figure 5.1-57. Sensor V-20: Compartment A Thermal Switch Radiator 5

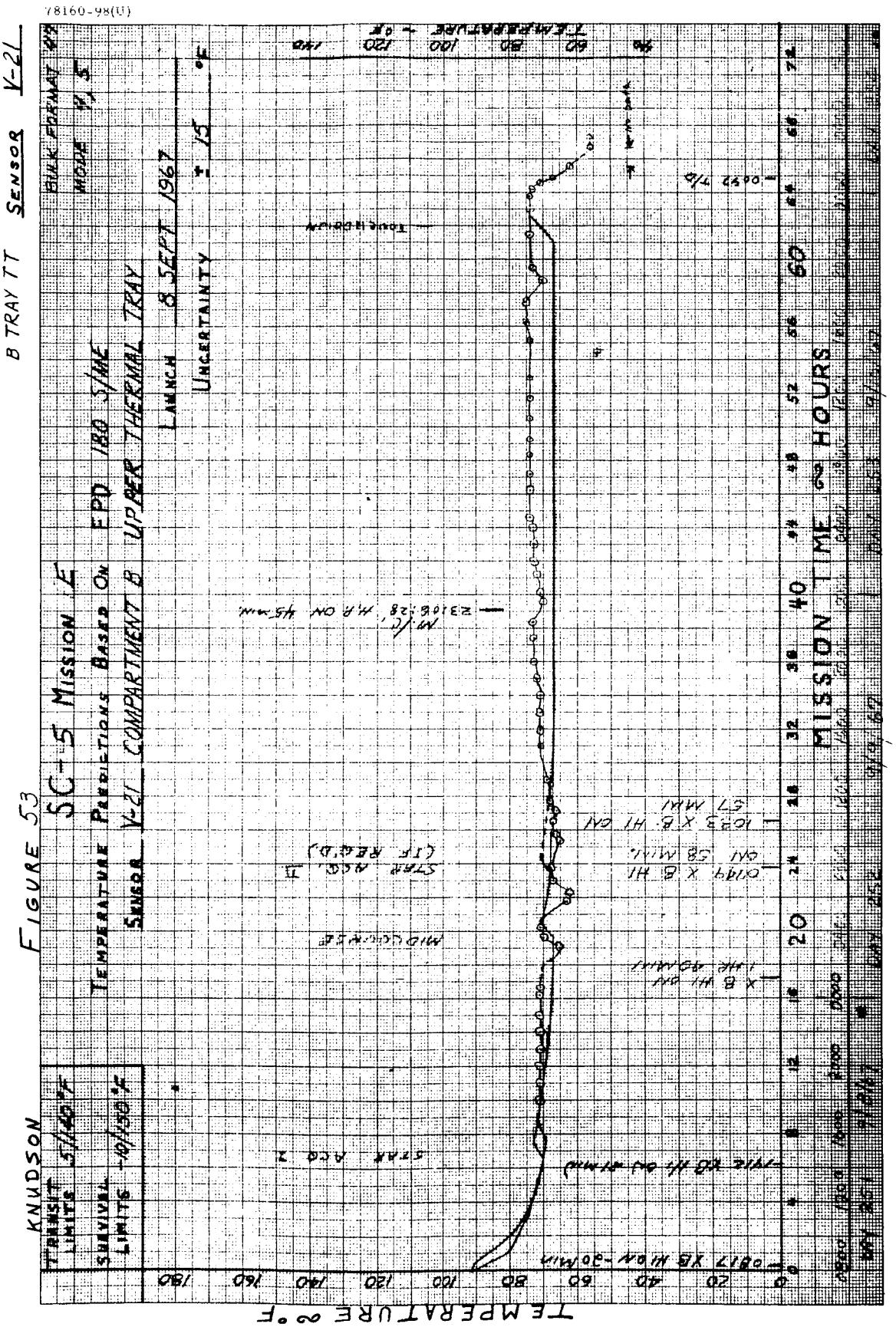

Figure 5.1-58. Sensor V-21: Compartment B Upper Thermal Tray

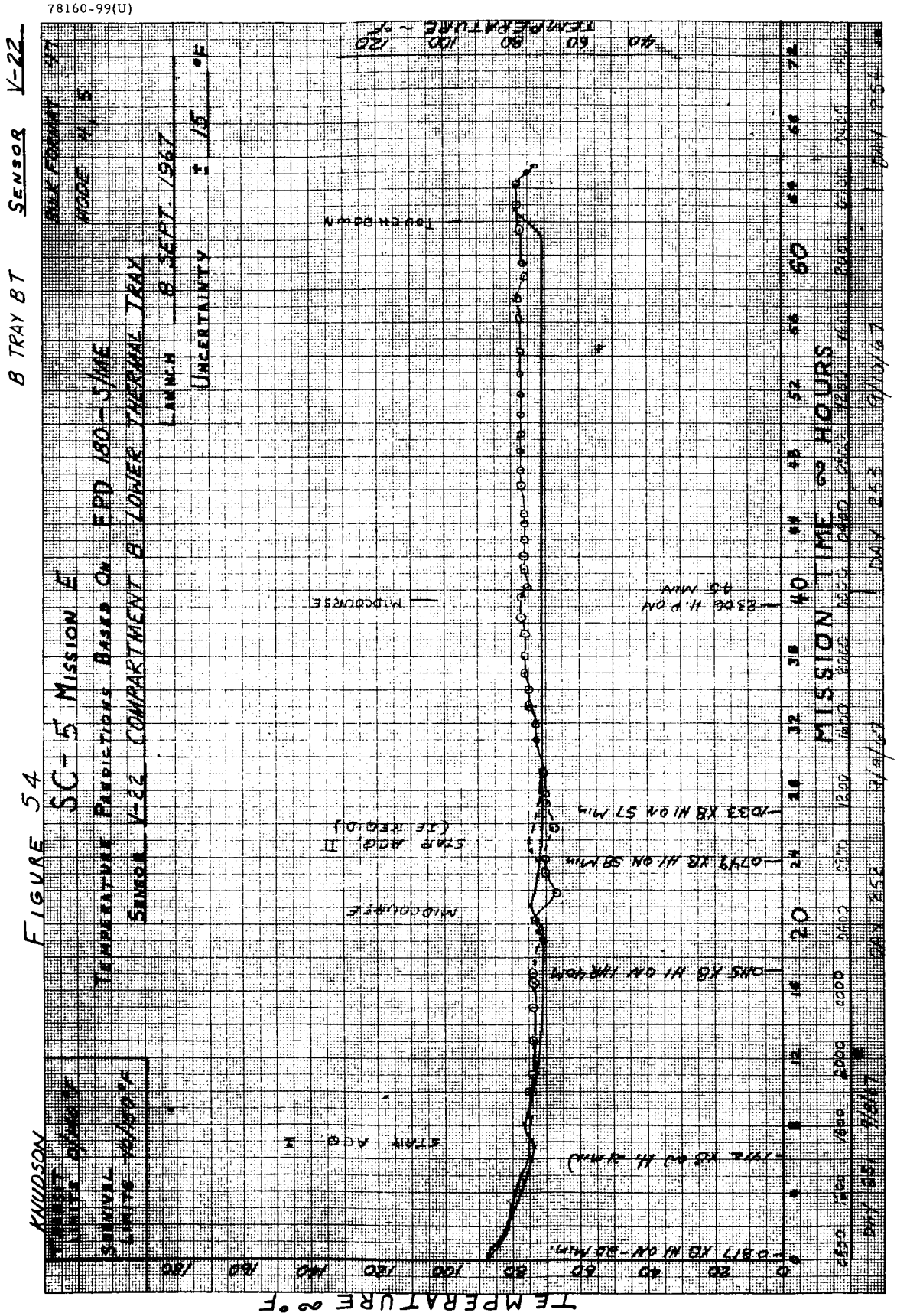

Figure 5.1-59. Sensor V-22: Compartment B Lower Thermal Tray

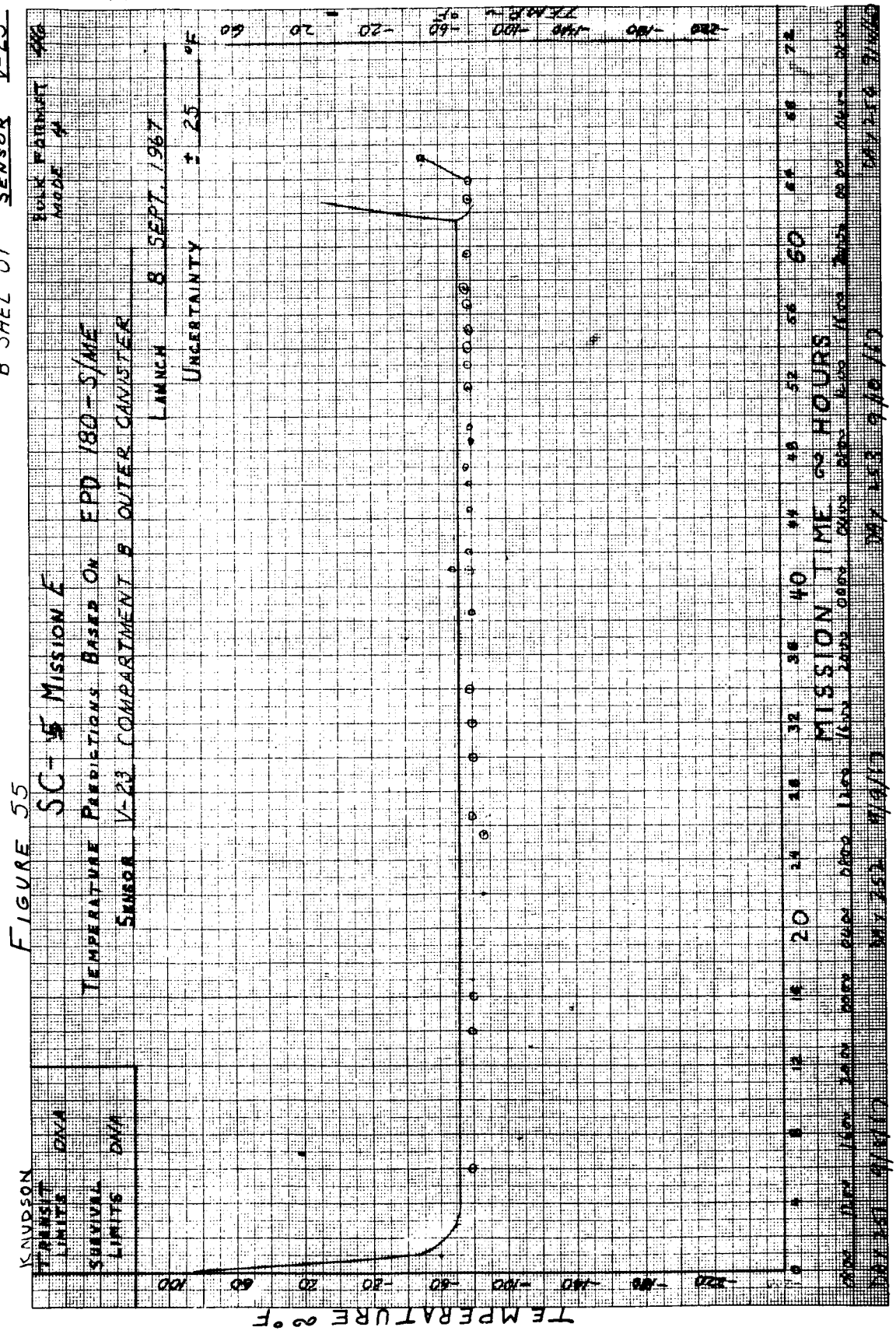

Figure 5.1-60. Sensor V-23: Compartment B Outer Canister

78160-101(U)

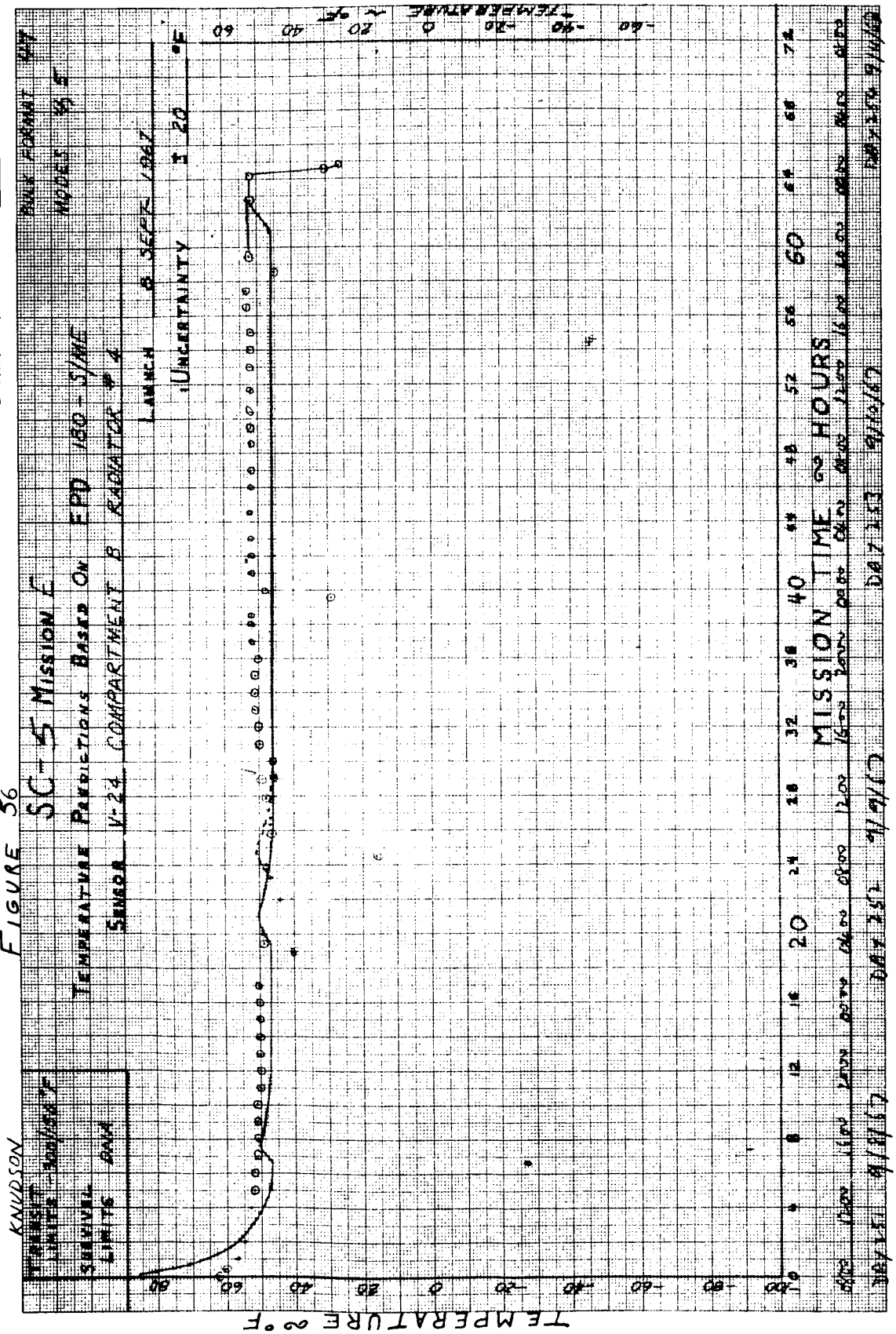

Figure 5.1-61. Sensor V-24: Compartment B Radiator 4

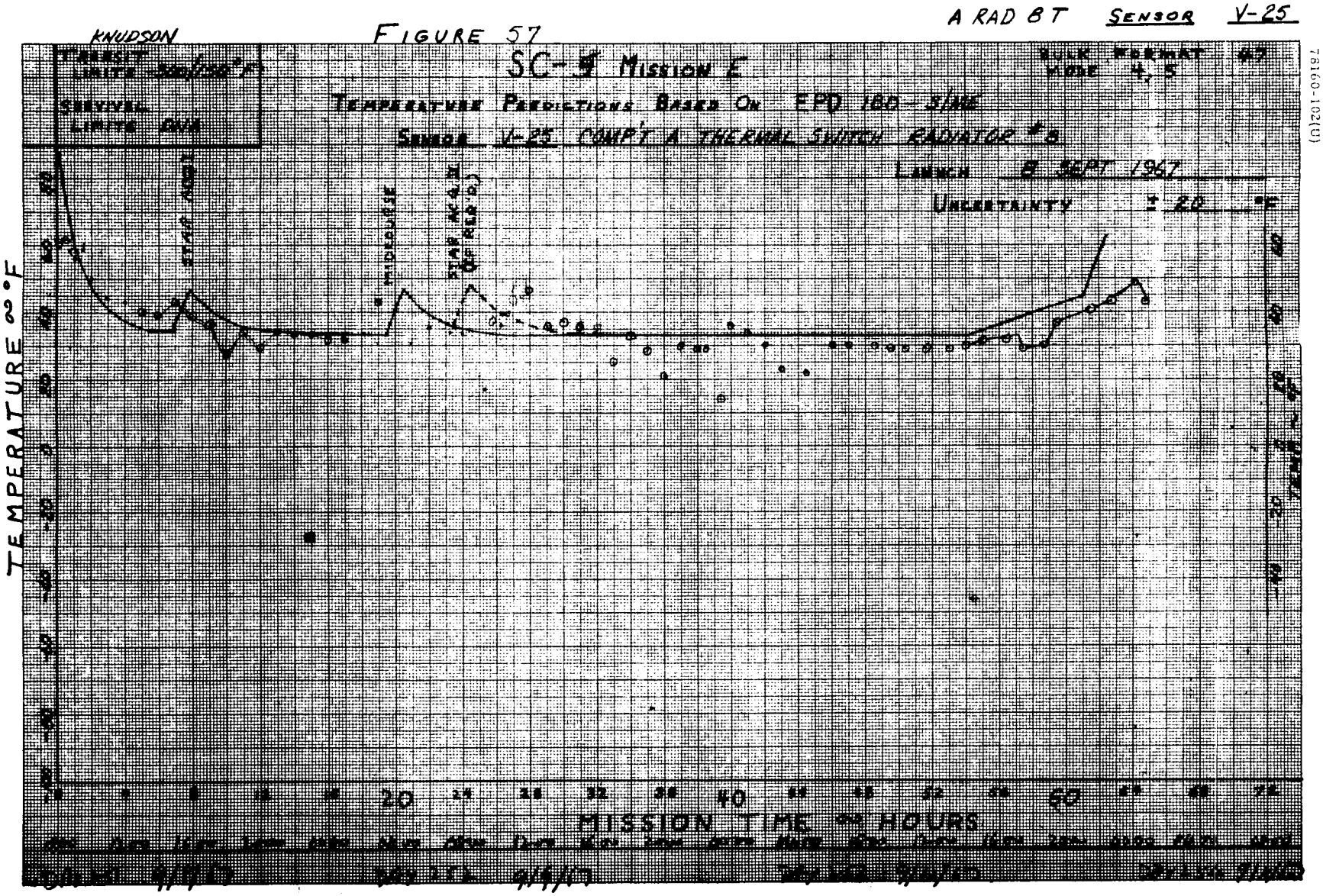

Figure 5.1-62. Sensor V-25: Compartment A Thermal Switch Radiator 8

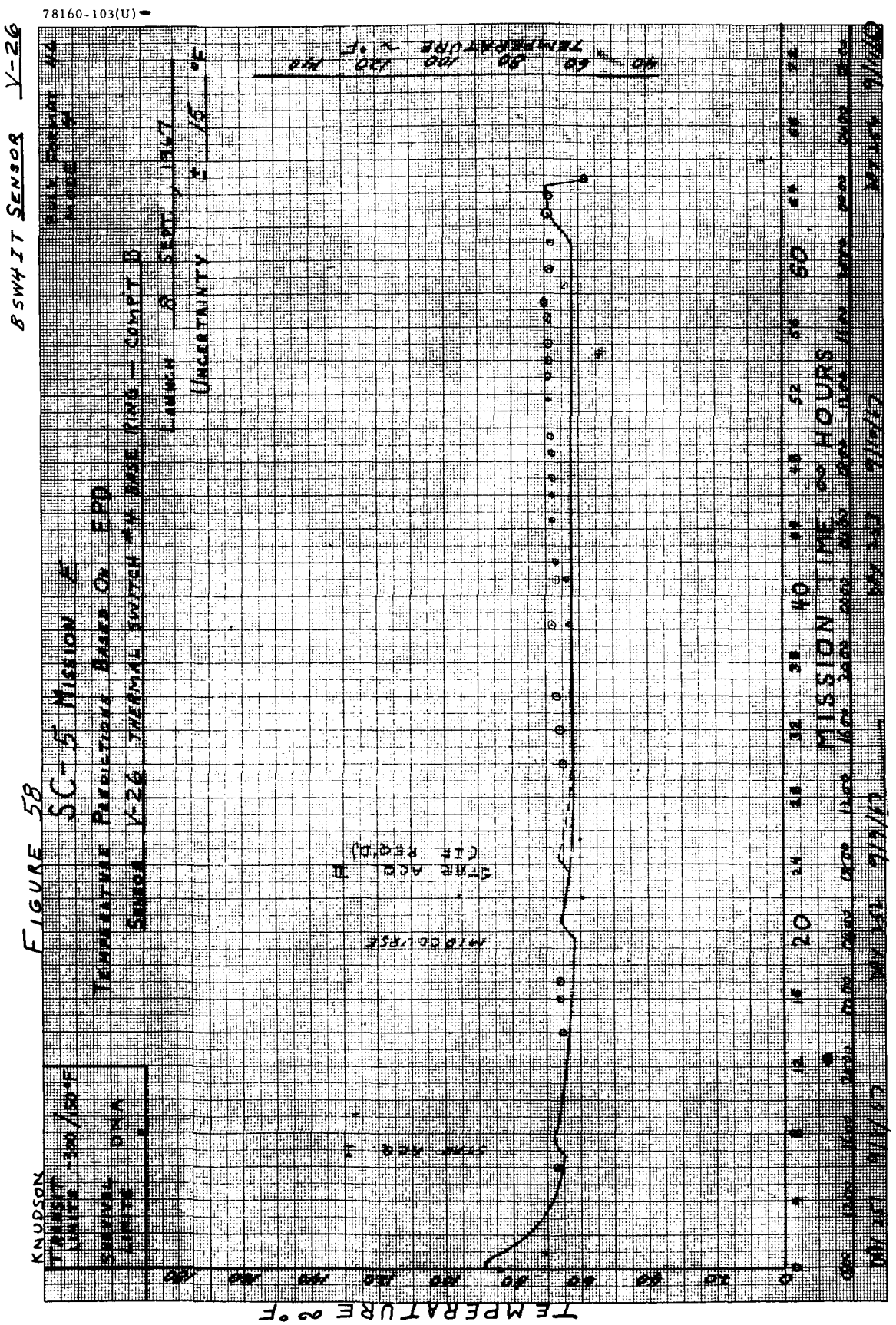

Figure 5.1-63. Sensor V-26: Thermal Switch 4 Base Ring Compartment B

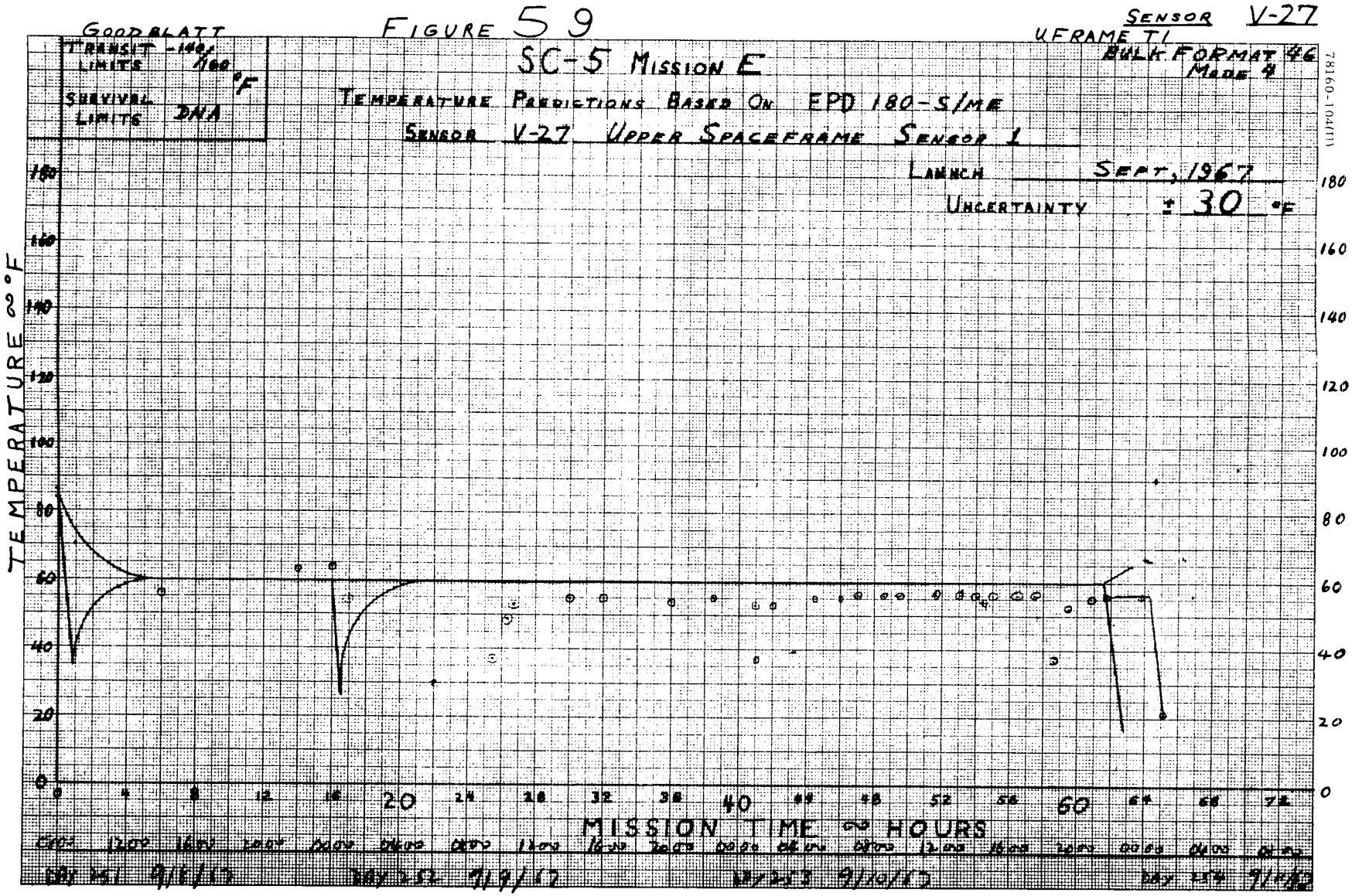

Figure 5.1-64. Sensor V-27: Upper Spaceframe, Sensor 1

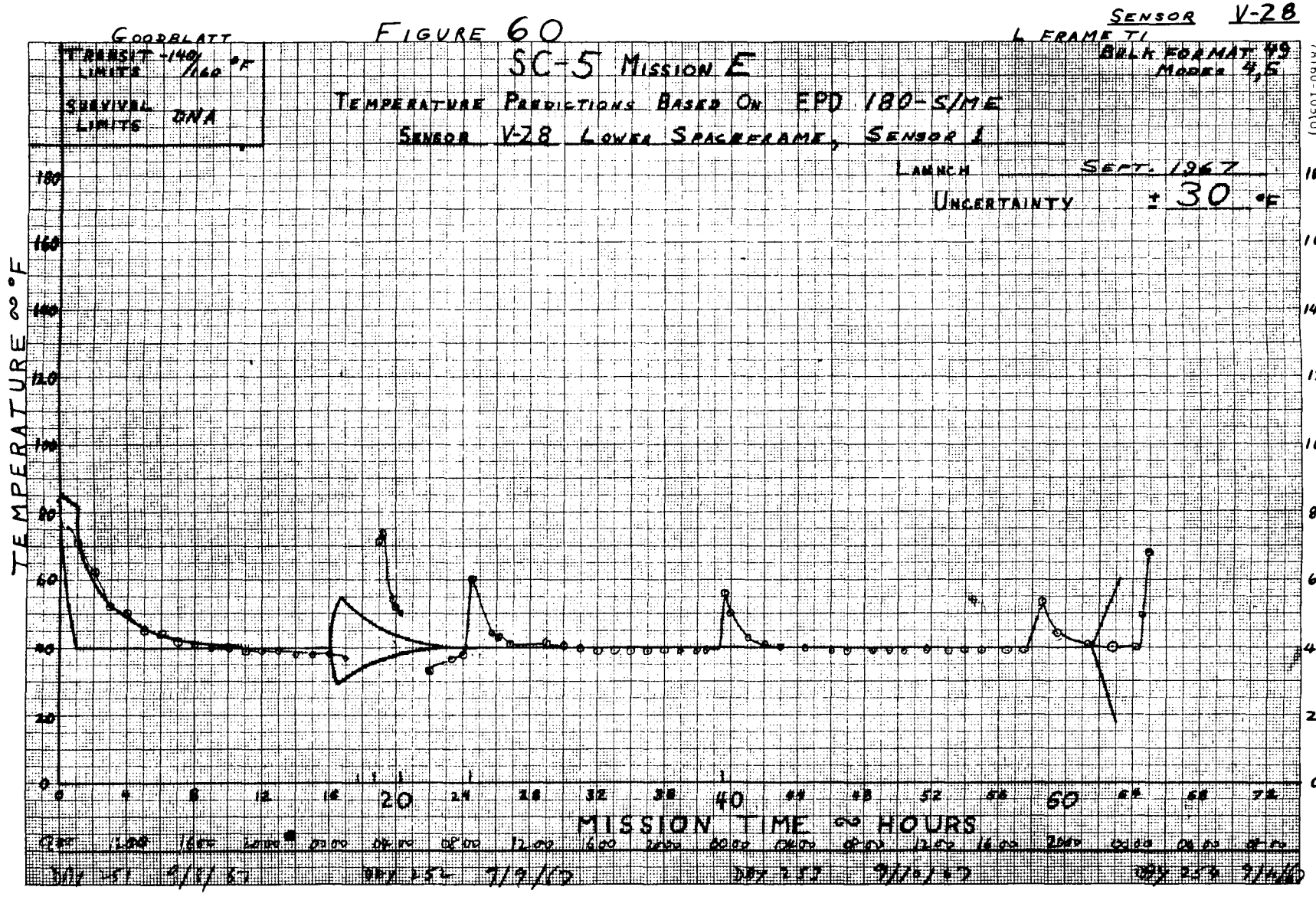

Figure 5.1-65. Sensor V-28: Lower Spaceframe, Sensor 1

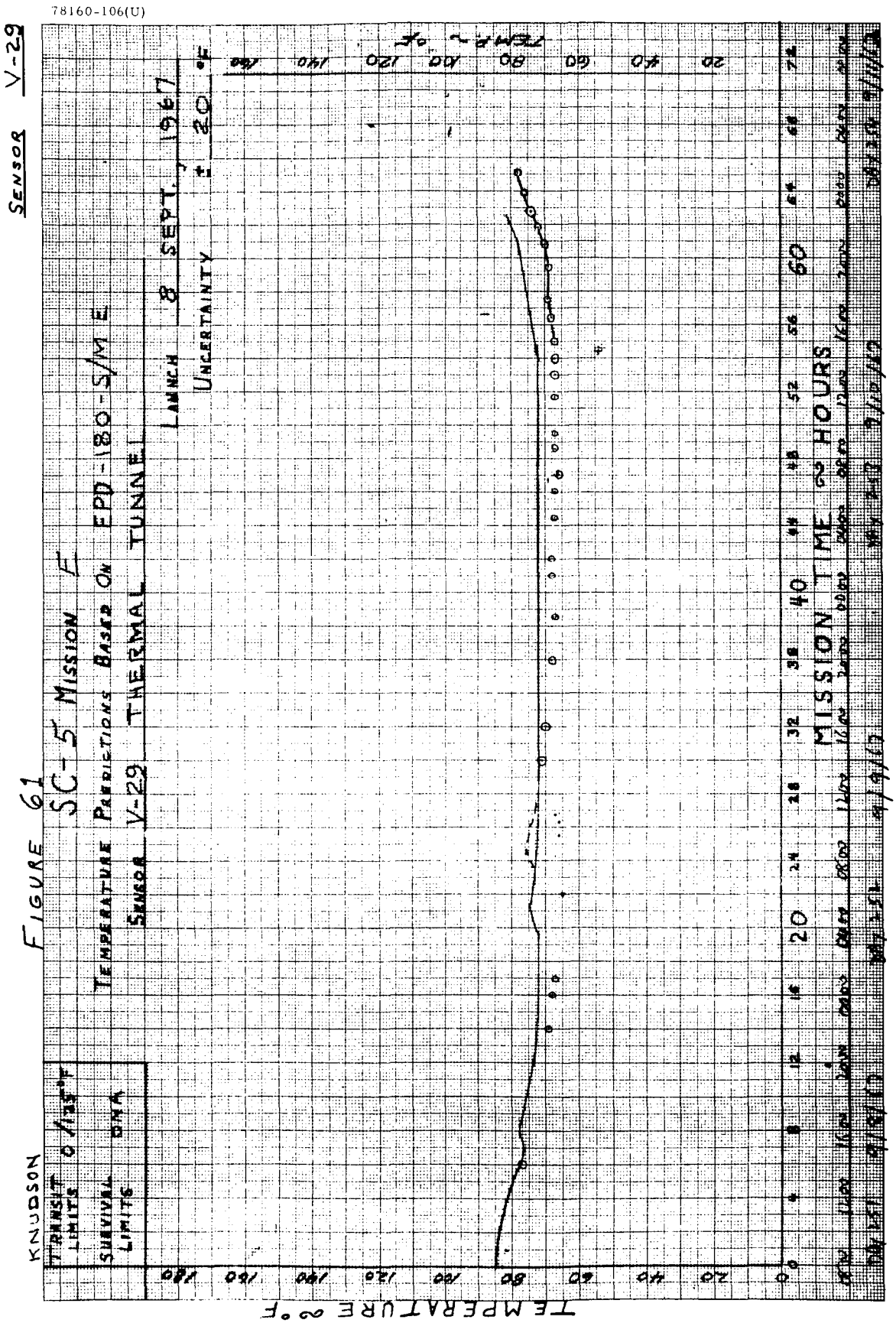

Figure 5.1-66. Sensor V-29: Thermal Tunnel

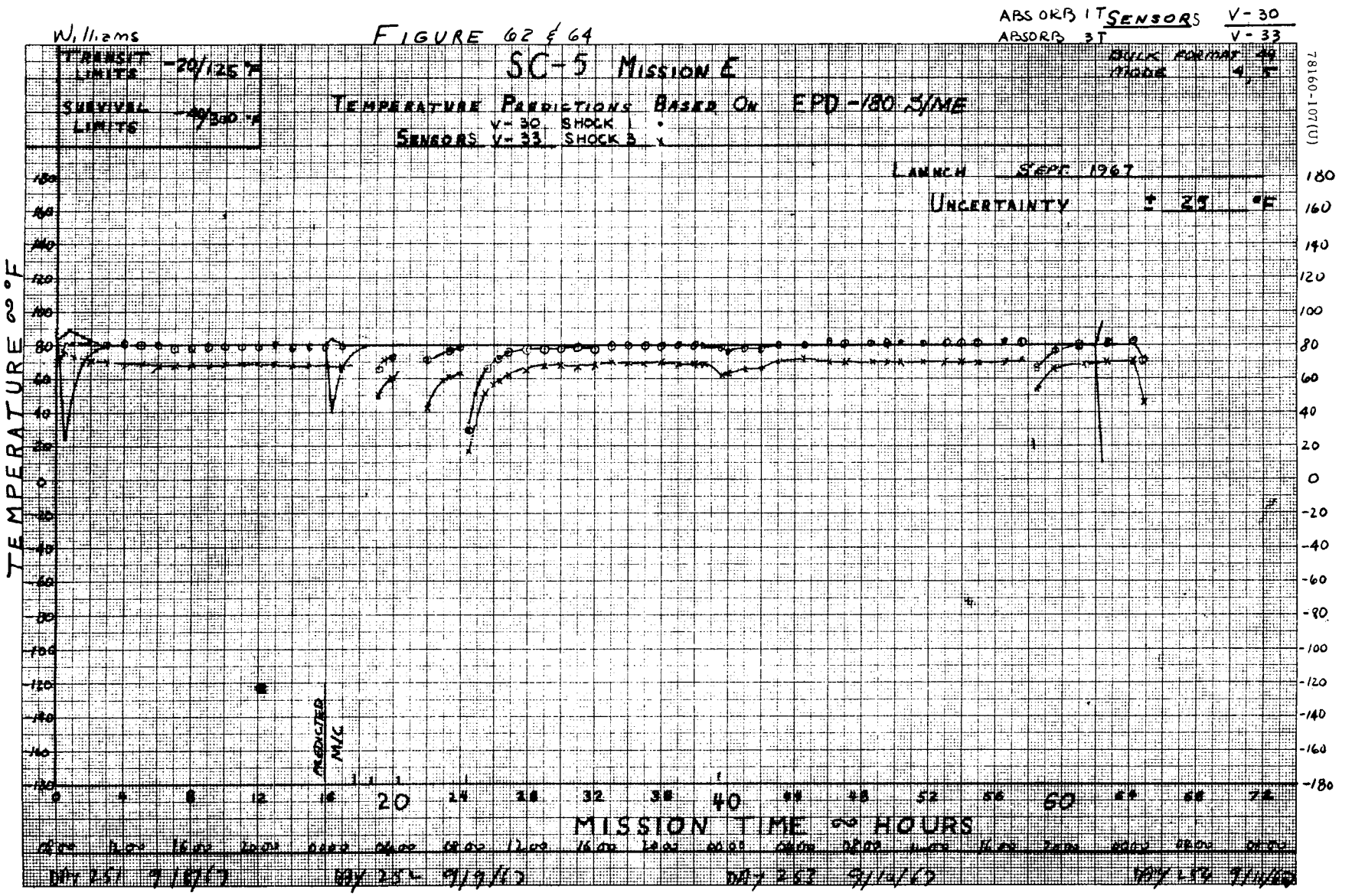

Figure 5.1-67. Sensor V-30: Shock 1; V-33: Shock 3

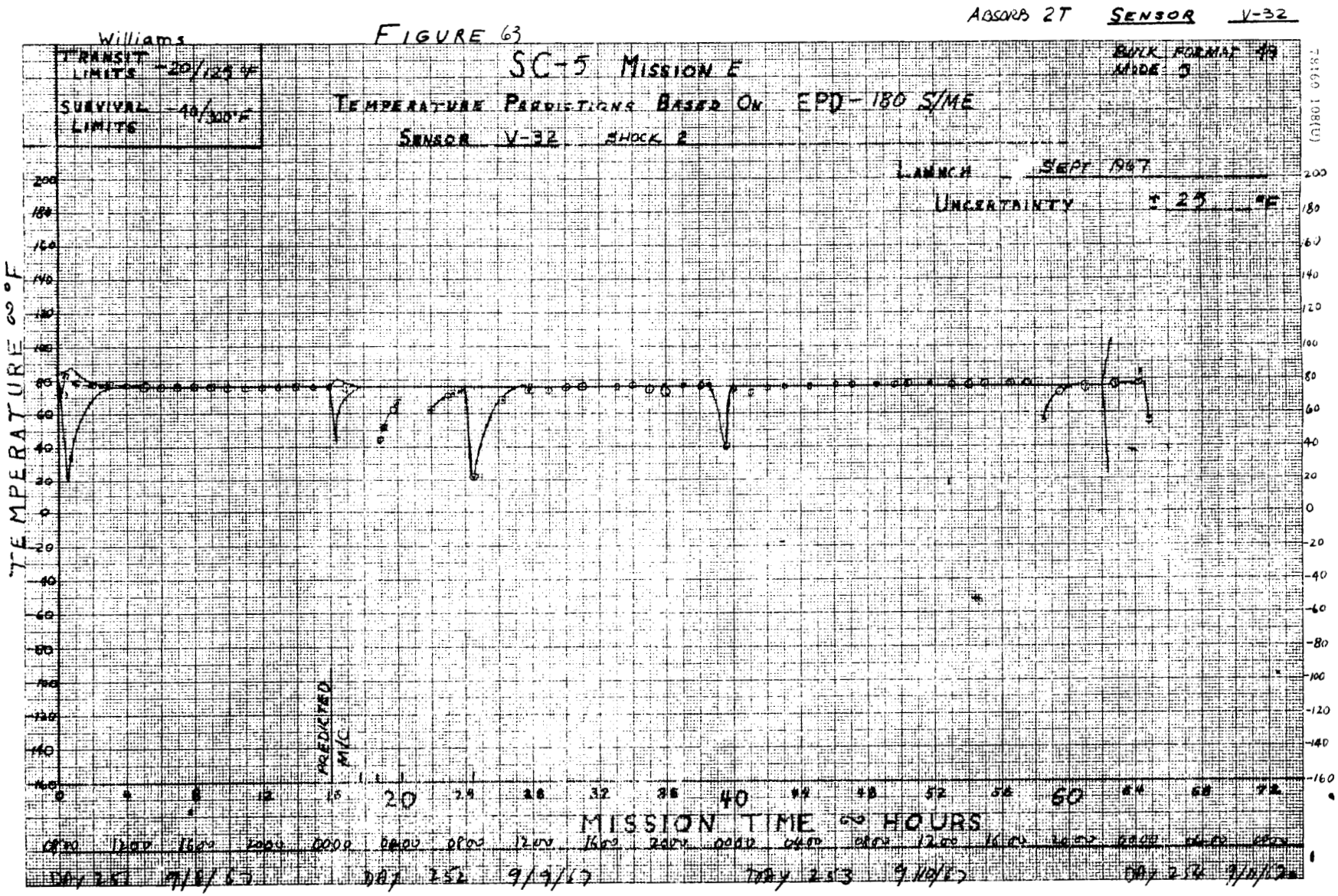

Figure 5.1-68. Sensor V-32: Shock 2

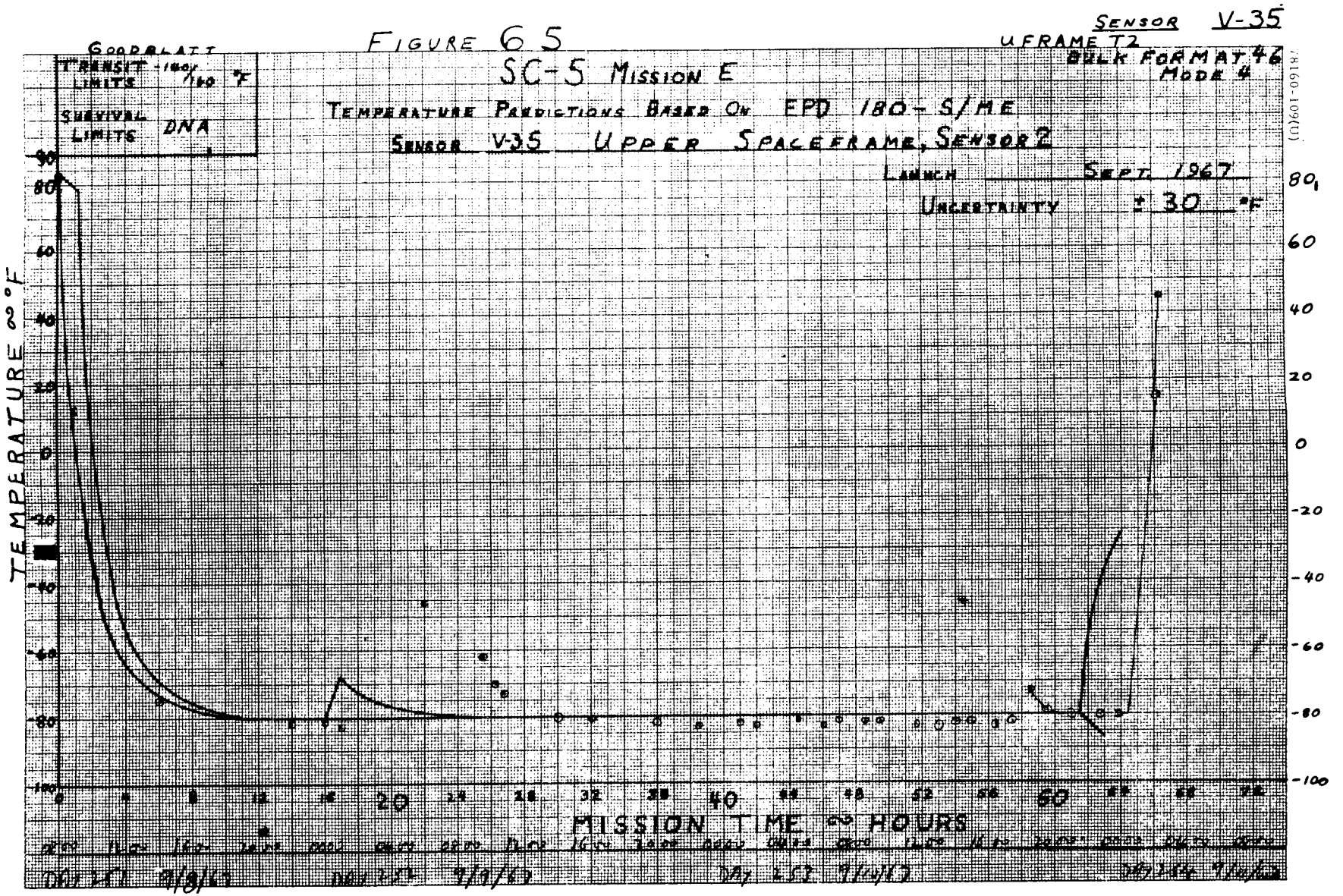

Figure 5.1-69. Sensor V-35: Upper Spaceframe, Sensor 2

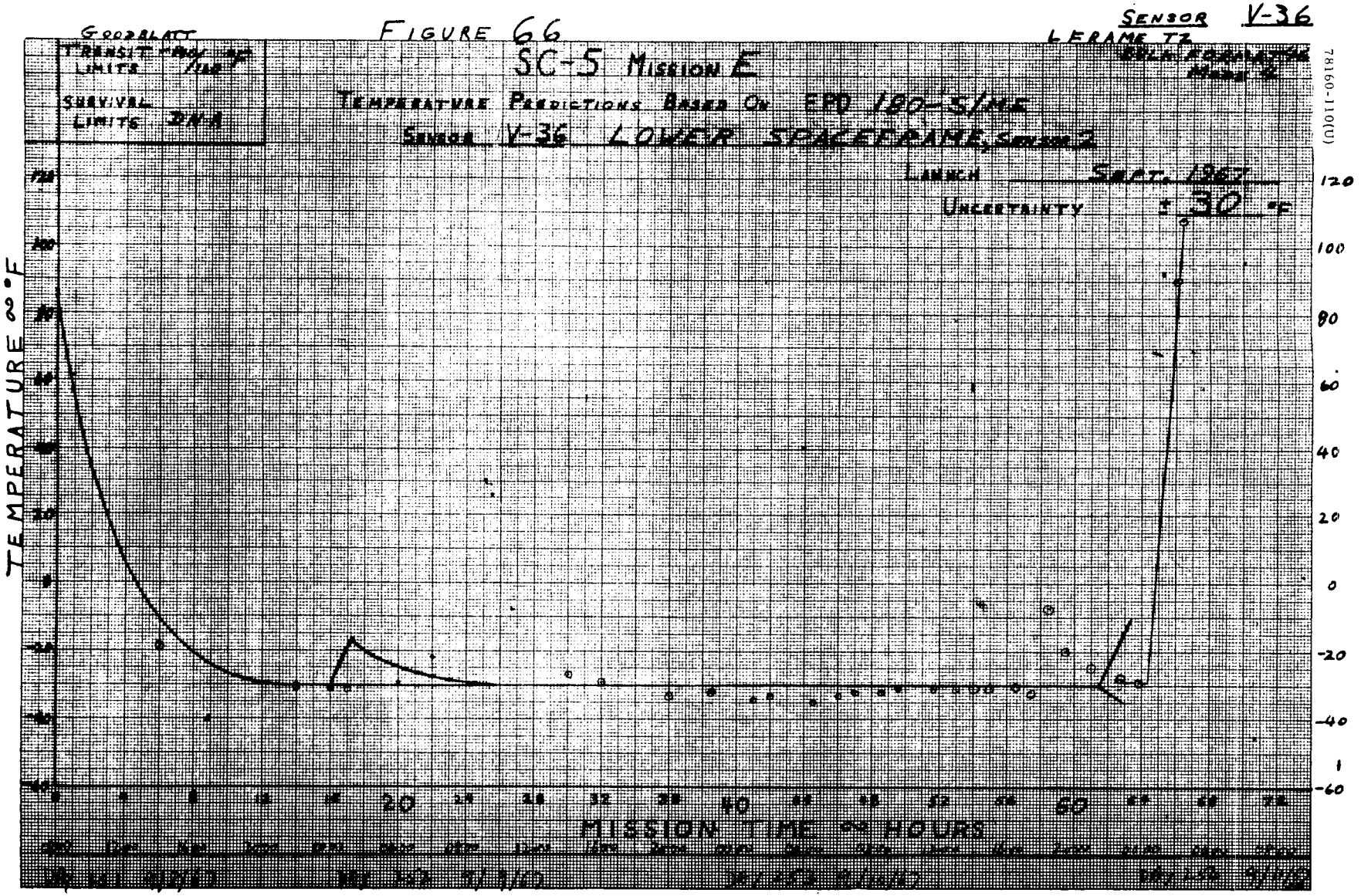

Figure 5.1-70. Sensor V-36: Lower Spaceframe, Sensor 2

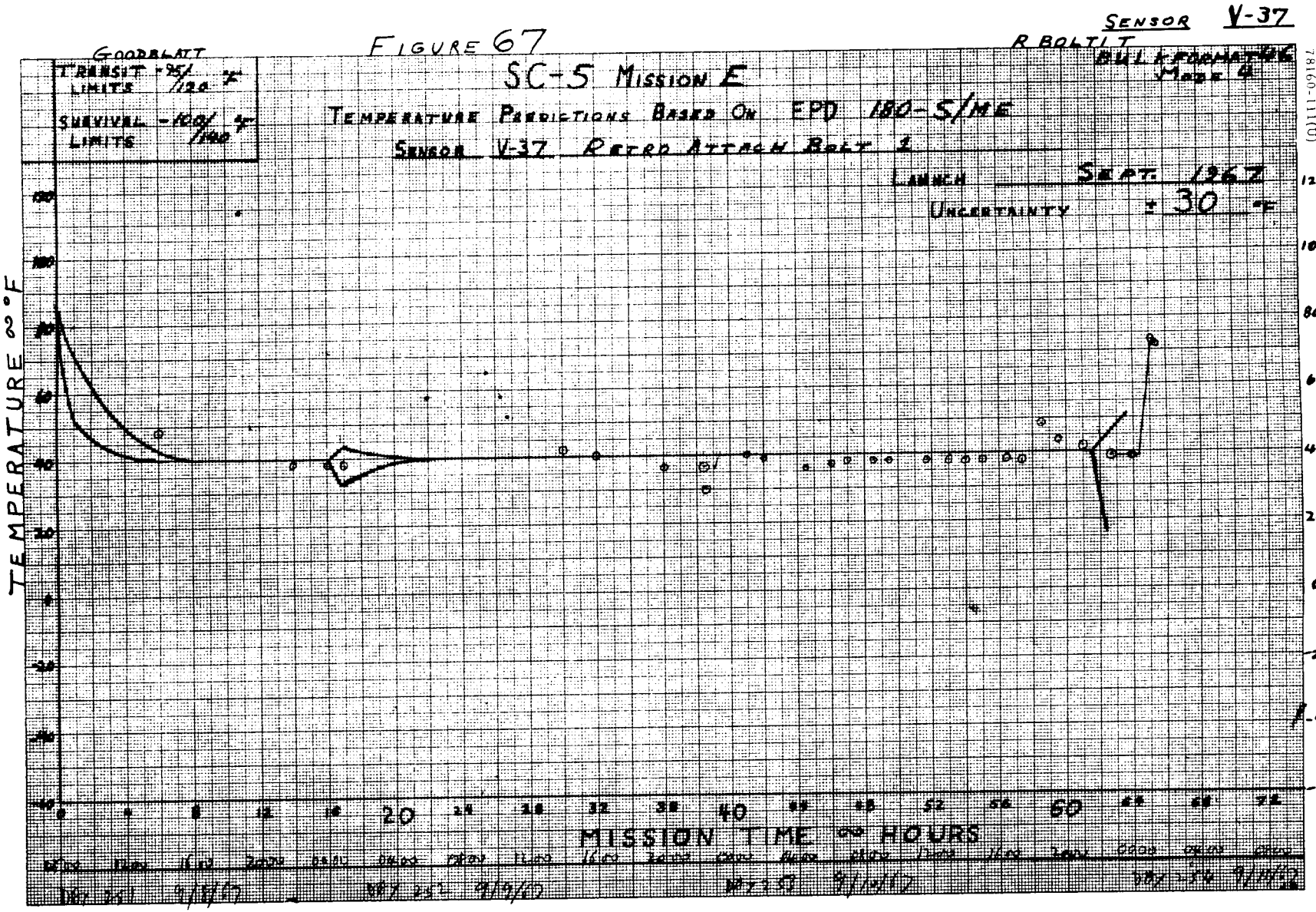

Figure 5.1-71. Sensor V-37: Retro Attach Bolt 1

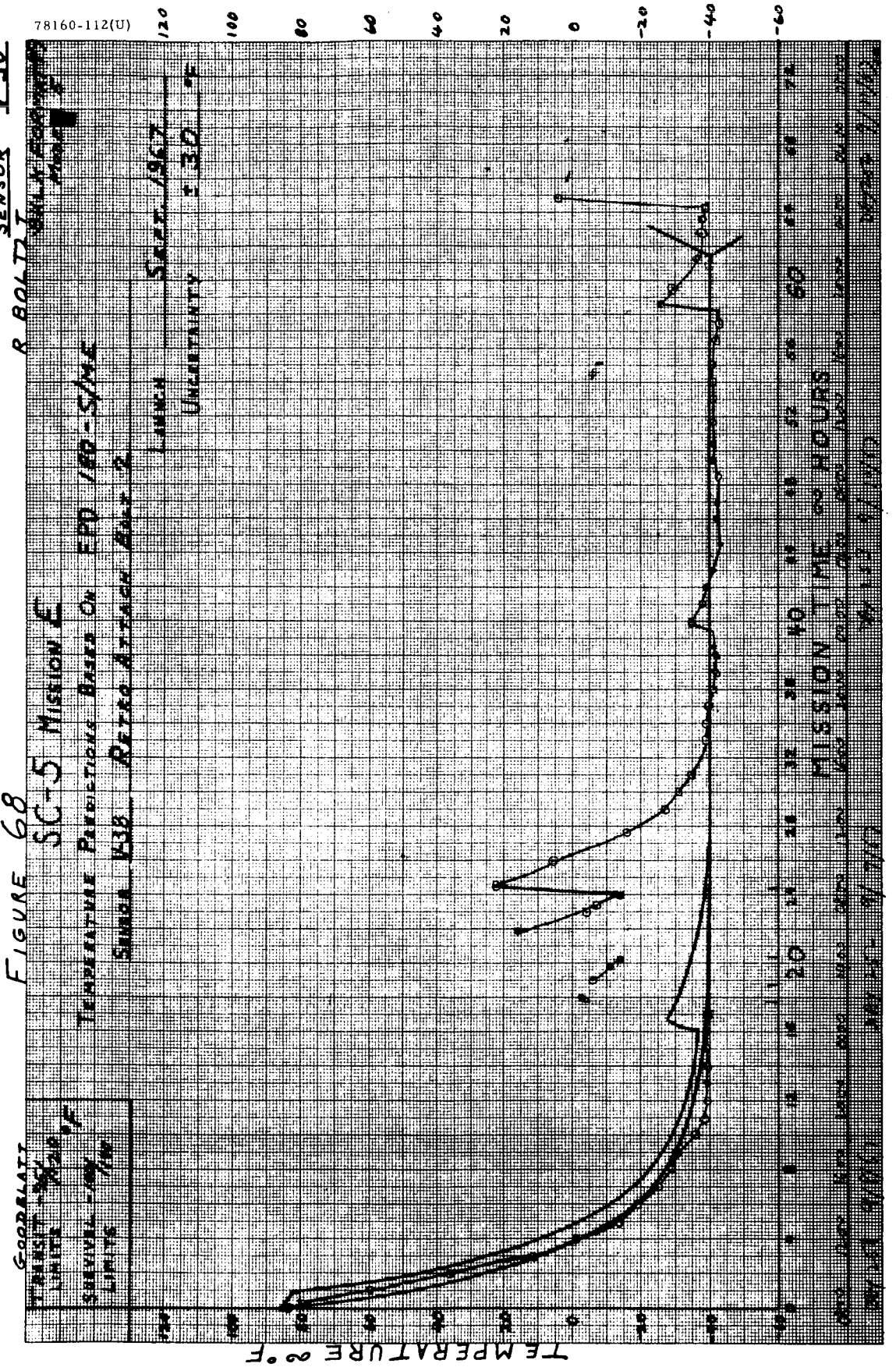

Figure 5.1-72. Sensor V-38: Retro Attach Bolt 2

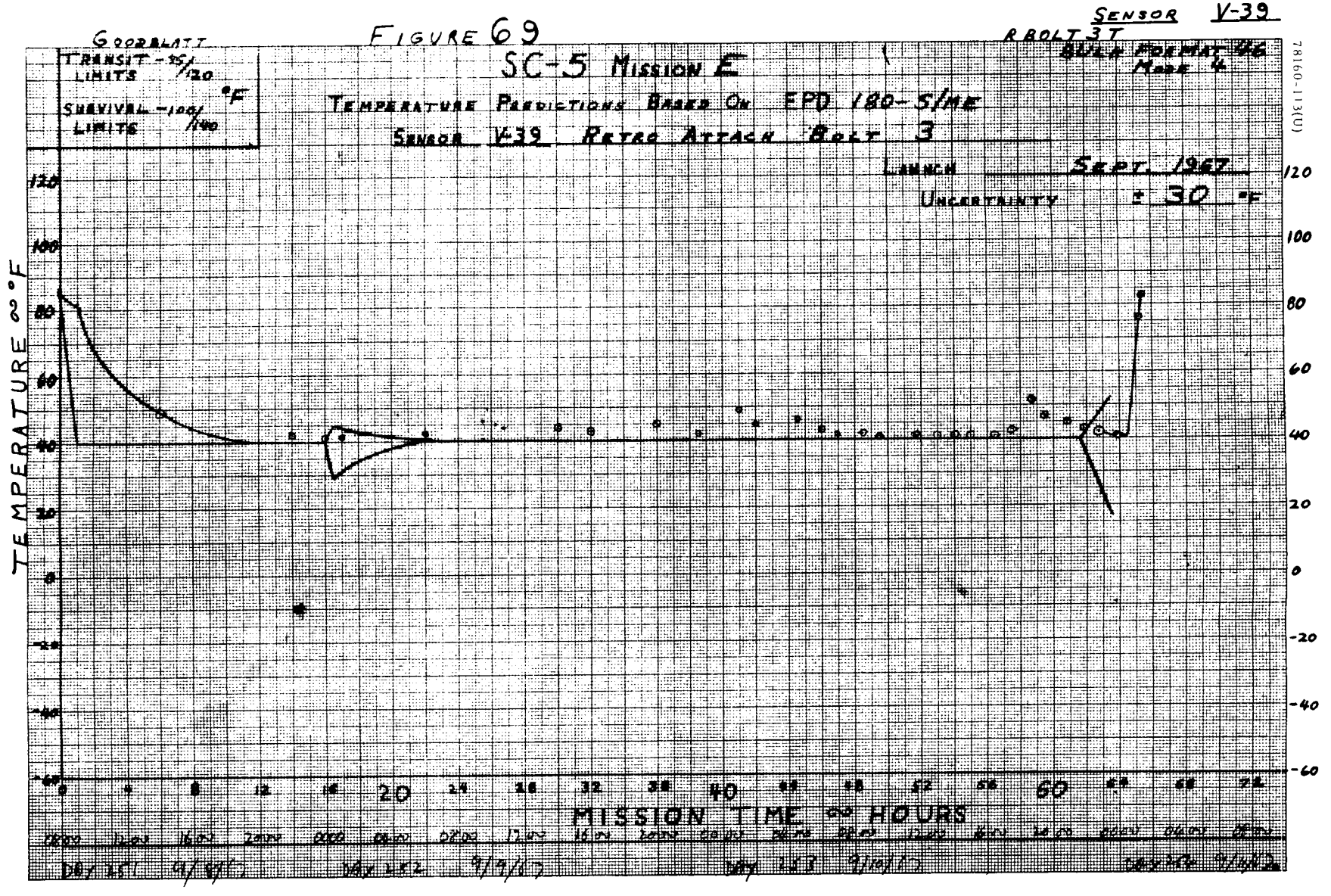

Figure 5.1-73. Sensor V-39: Retro Attach Bolt 3

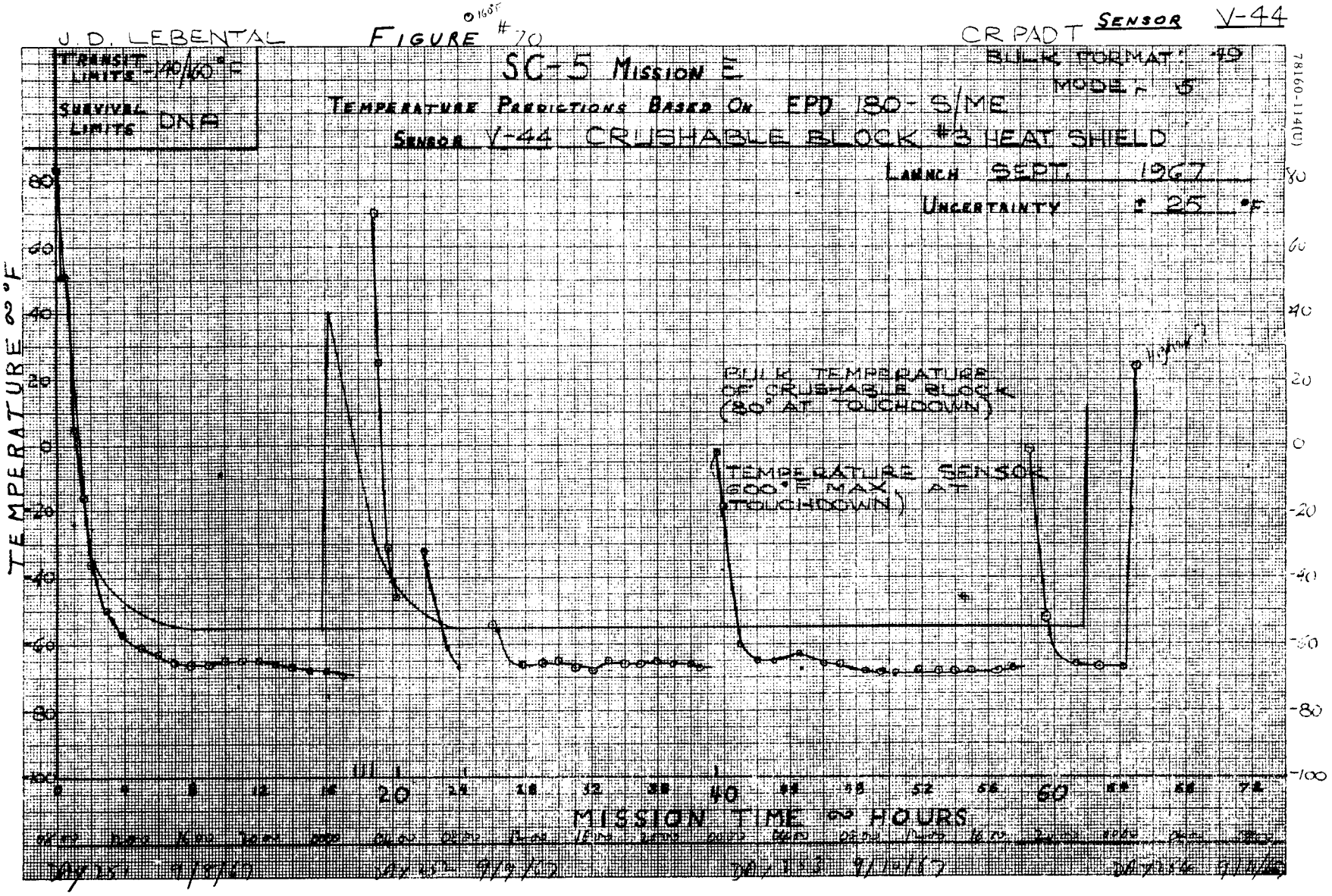

Figure 5.1-74. Sensor V-44: Crushable Block 3 Heat Shield

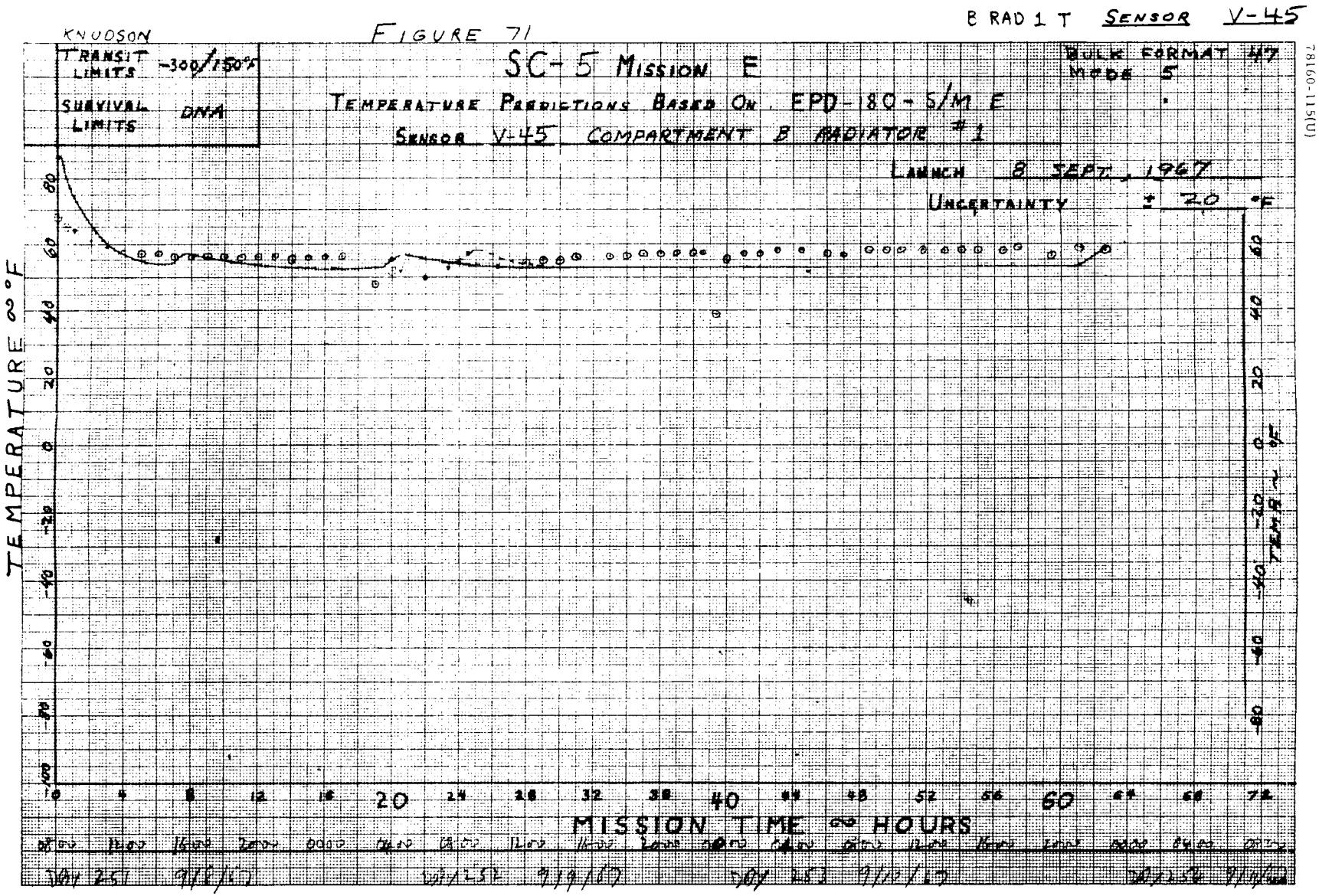

Figure 5.1-75. Sensor V-45: Compartment B Radiator 1

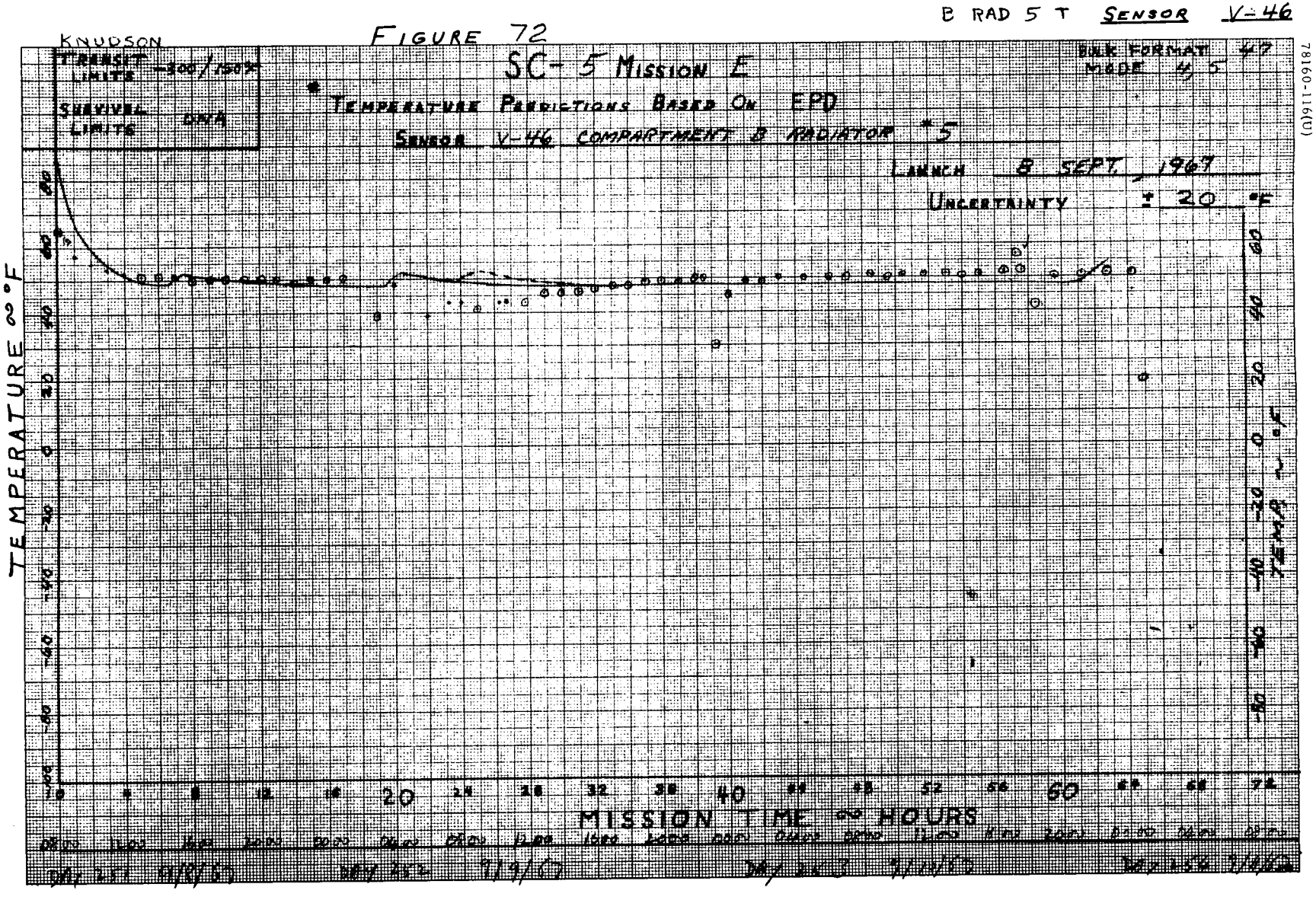

Figure 5.1-76. Sensor V-46: Compartment B Radiator 5

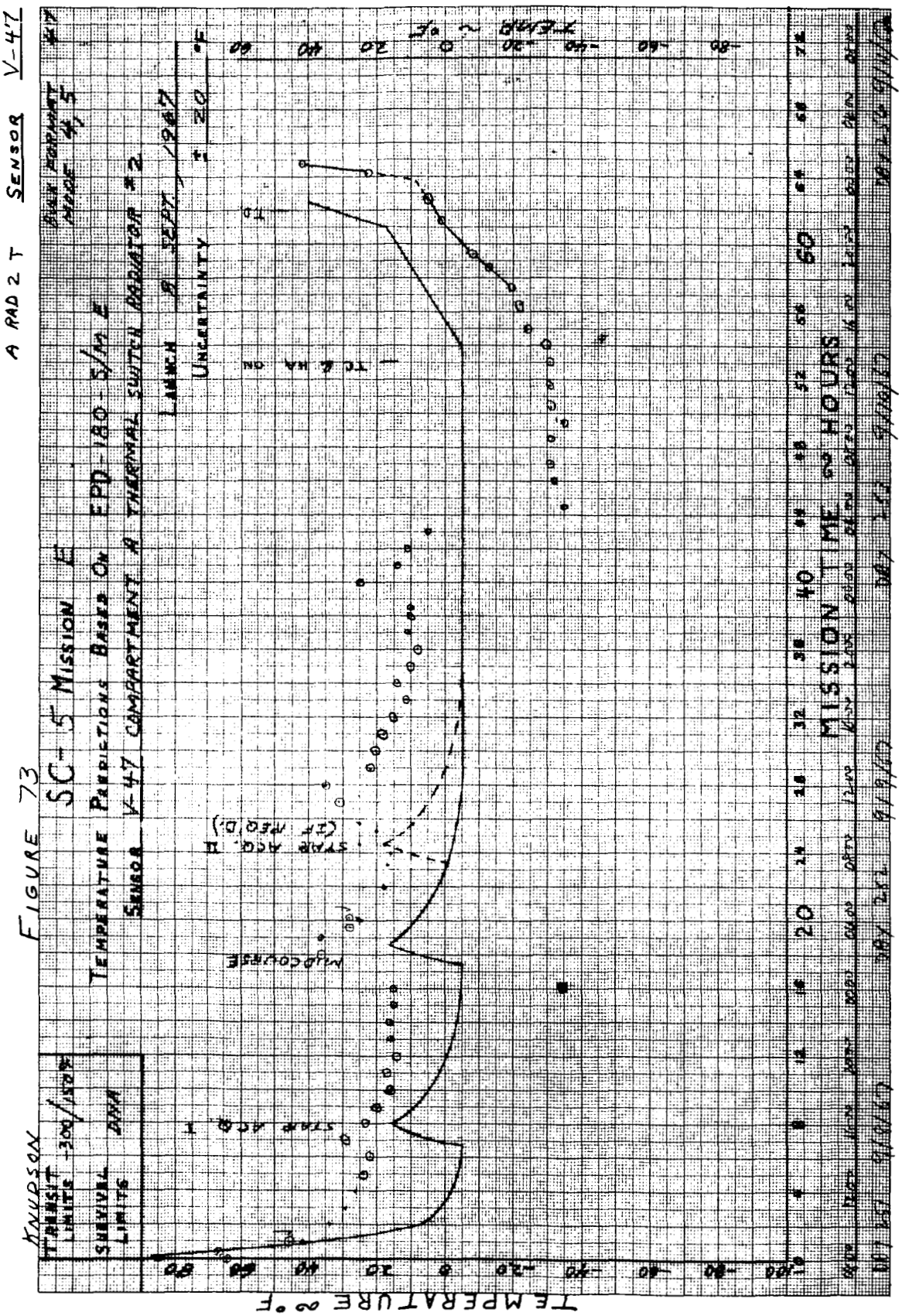

Figure 5.1-77. Sensor V-47: Compartment A Thermal Switch Radiator 2

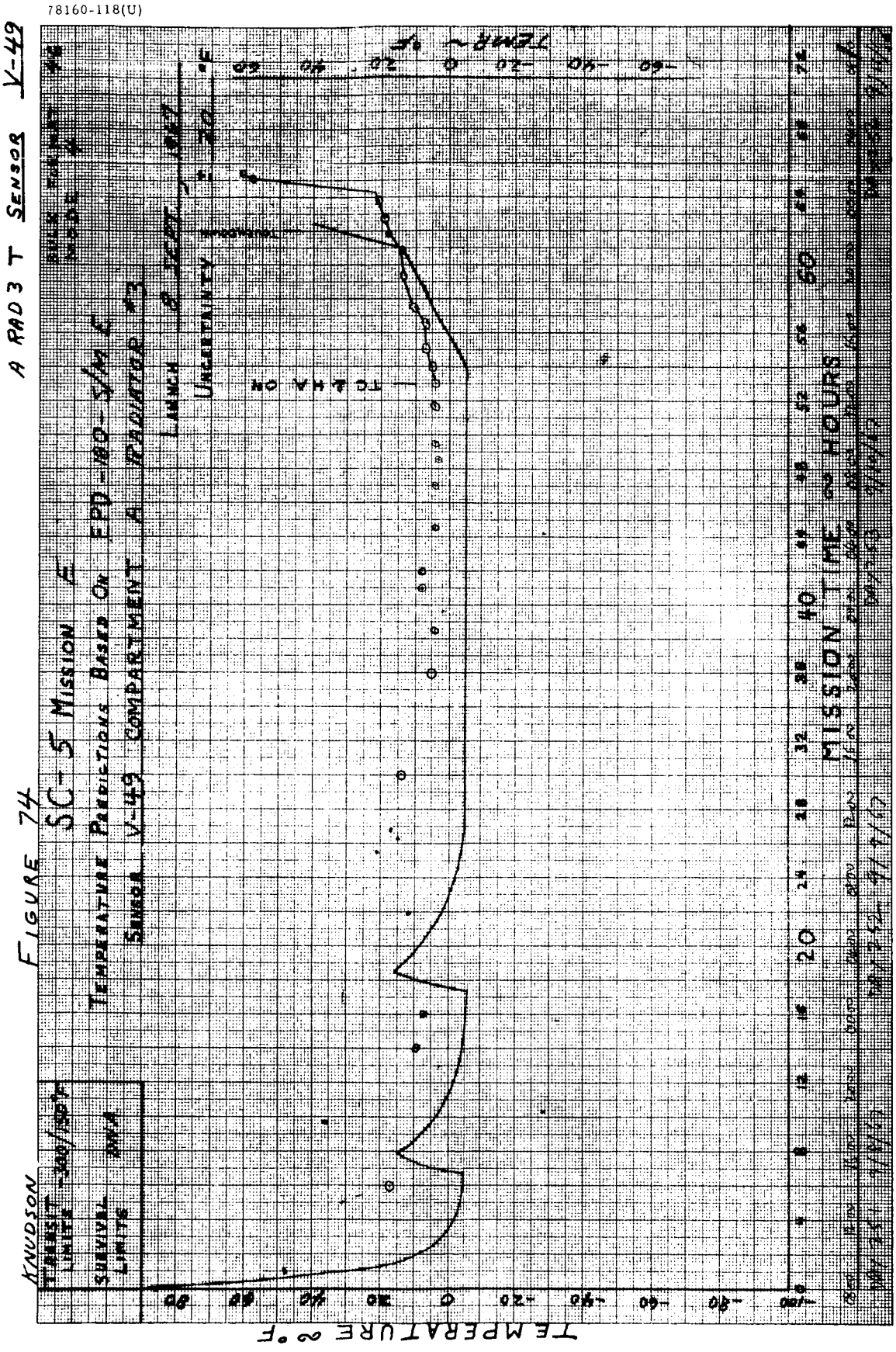

Figure 5.1-78. Sensor V-49: Compartment A Radiator 3

APPENDIX B
TO SECTION 5.1
LUNAR DAY TEMPERATURE PLOTS

Appendix B contains Figures 5.1-79 to 5.1-147 which are the first lunar day temperature plots. The sun incidence angle noted on these plots was derived from information available in Reference 5. Table 5.1-B1 lists times of high power operation during Lunar Day One.

PRECEDING PAGE BLANK NOT FILMED.

TABLE 5. 1-B1. HIGH POWER – LUNAR DAY ONE

Day:Hr:Min	Event
254:01:09	High power off – transmitter B
01:19	High power on – transmitter A
03:06	Low power on – transmitter A
03:51	High power on – transmitter A
04:44	Low power on – transmitter A
12:15	Alpha scattering device to background position
15:36	Alpha scattering device deployed to lunar surface
256:00:09	High power on – transmitter A
01:50	High voltage off – transmitter A
05:14	High power on – transmitter A
05:32	Static firing
05:43	Low power – transmitter A
258:02:34	High power on – transmitter A
04:44	High power off – transmitter A
259:03:35	Alpha scattering heater on (cycling from 50° to 60°F)
260:01:47	Lunar noon
04:15	Alpha scattering heater off
04:40	High power on – transmitter A
05:10	High power off – transmitter A
07:37	High power on – transmitter A
08:02	High power off – transmitter A
10:16	High power on – transmitter A
10:36	High power off – transmitter A
23:31	Spacecraft shutdown
261:01:46	Spacecraft on
04:50	High power on – transmitter A
05:52	High power off – transmitter A
263:16:45	High power on – transmitter A
17:25	High power off – transmitter A
17:41	High power on – transmitter A
18:05	High power off – transmitter A
264:03:51	High power on – transmitter A
03:56	High power off – transmitter A

Surveyor V revised for second lunar day on 288:08:10.

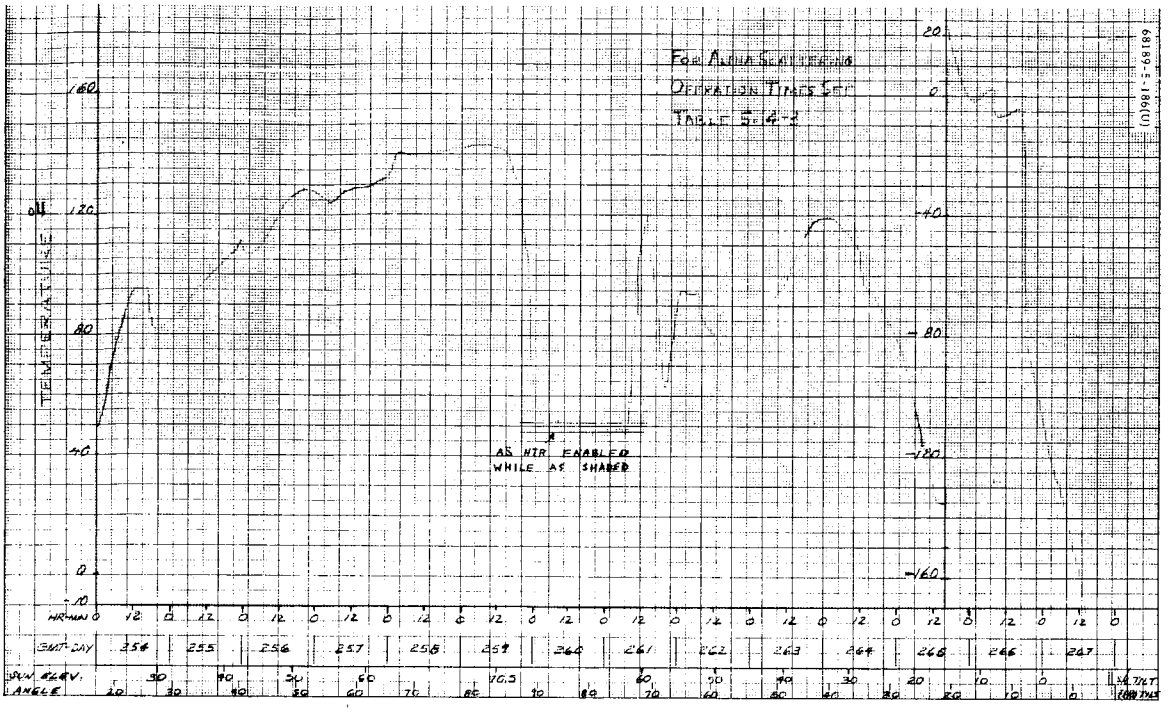

Figure 5.1-79. Sensor AS-3: Sensor Head Temperature

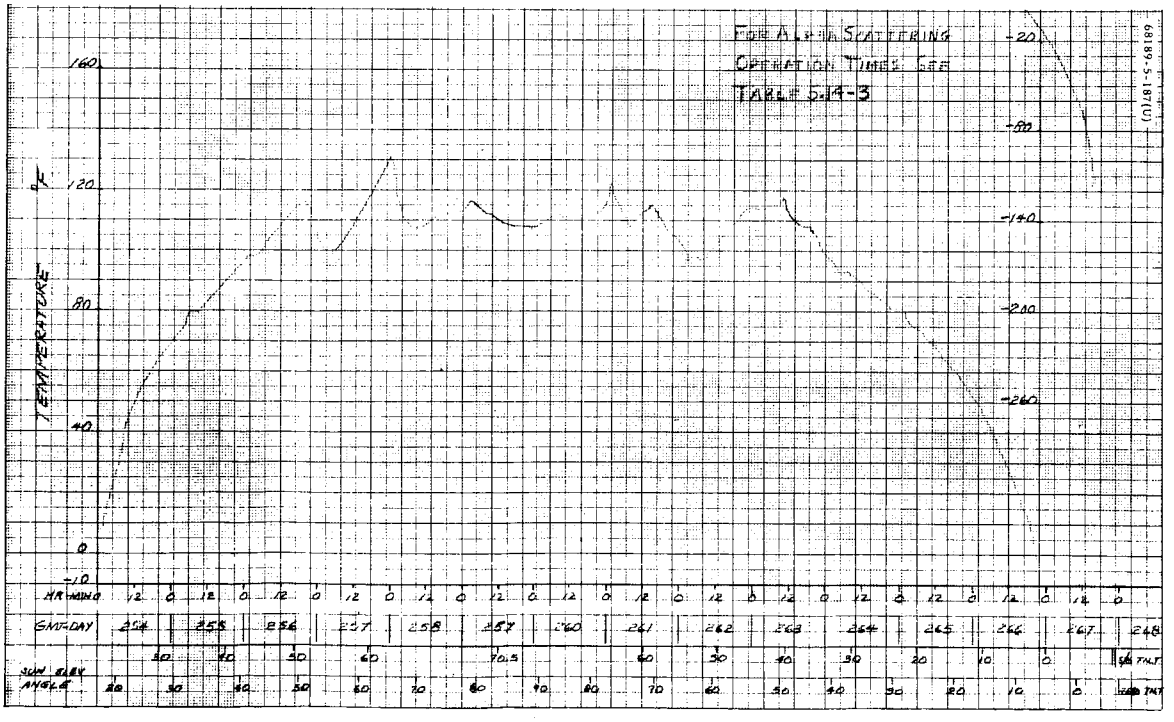

Figure 5.1-80. Sensor AS-4: Electronic Temperature

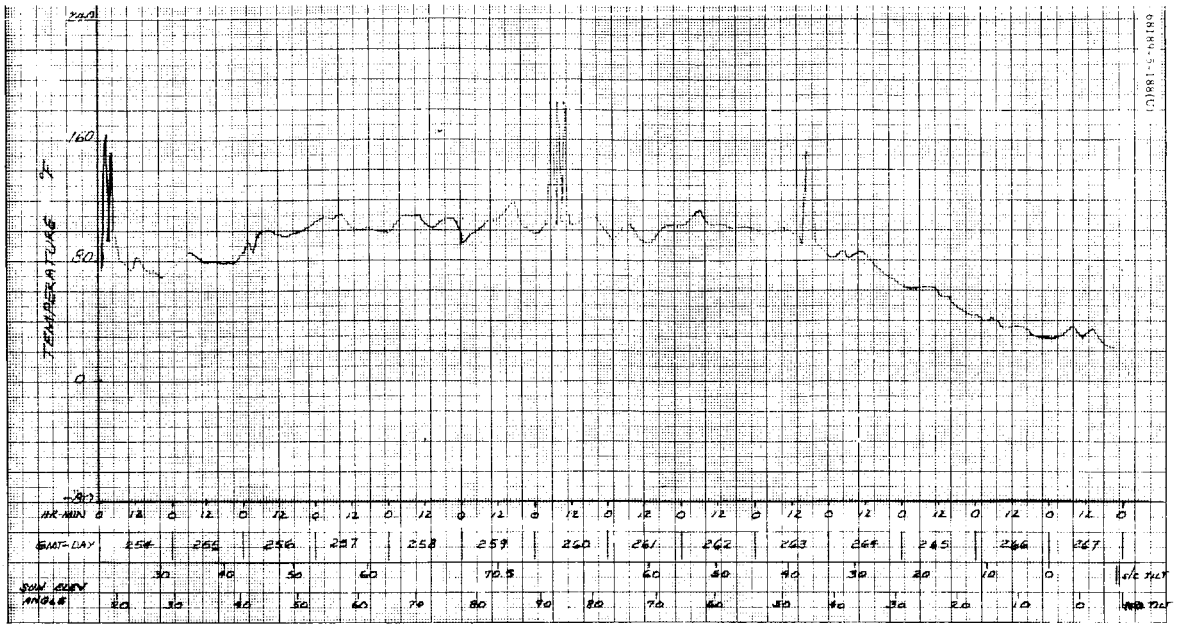

Figure 5.1-81. Sensor D-13: Transmitter A Temperature

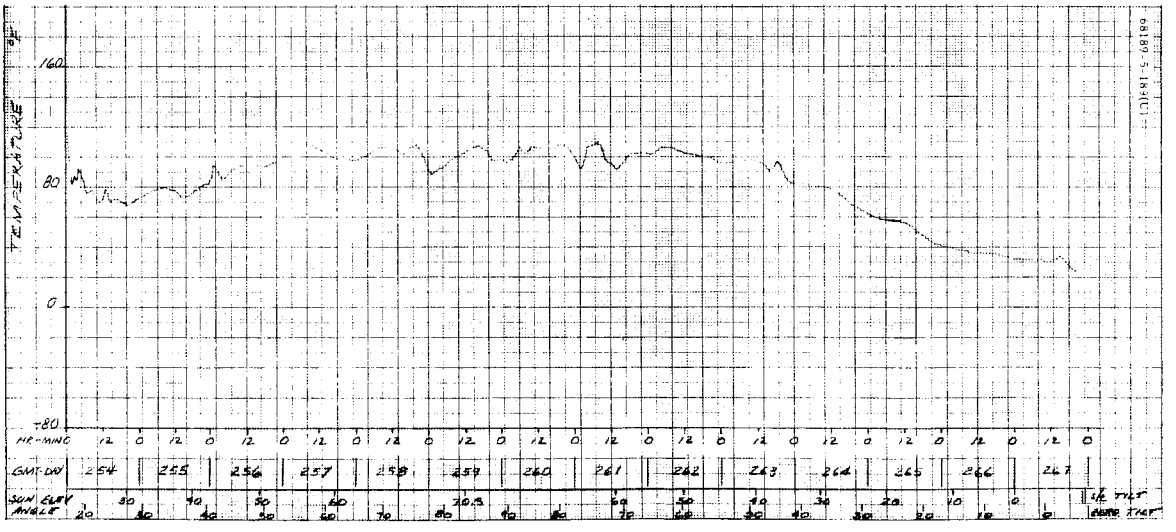

Figure 5.1-82. Sensor D-14: Transmitter B Temperature

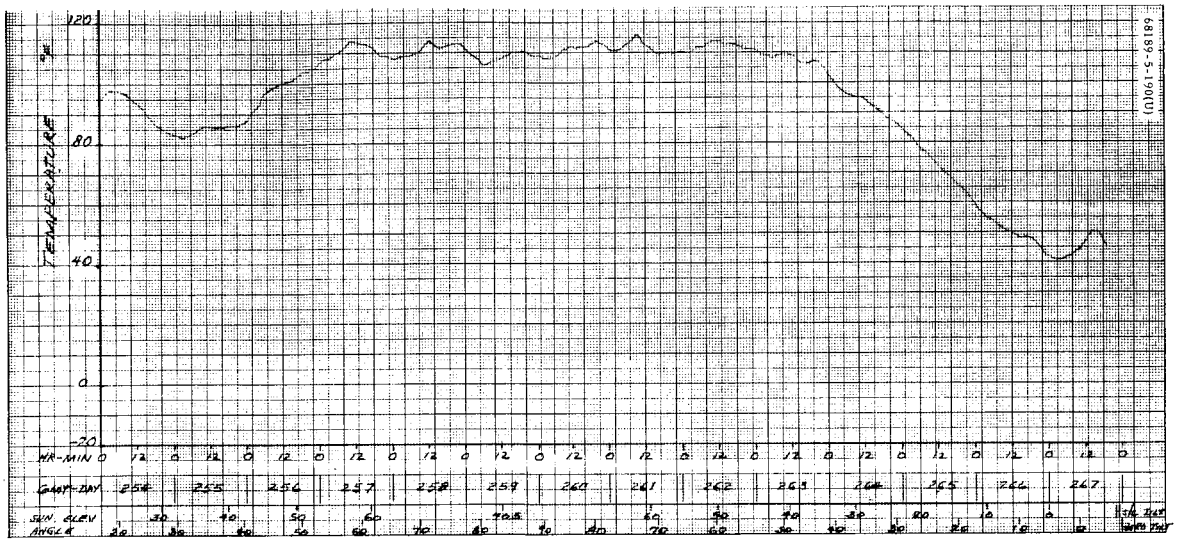

Figure 5.1-83. Sensor EP-8: Main Battery Temperature

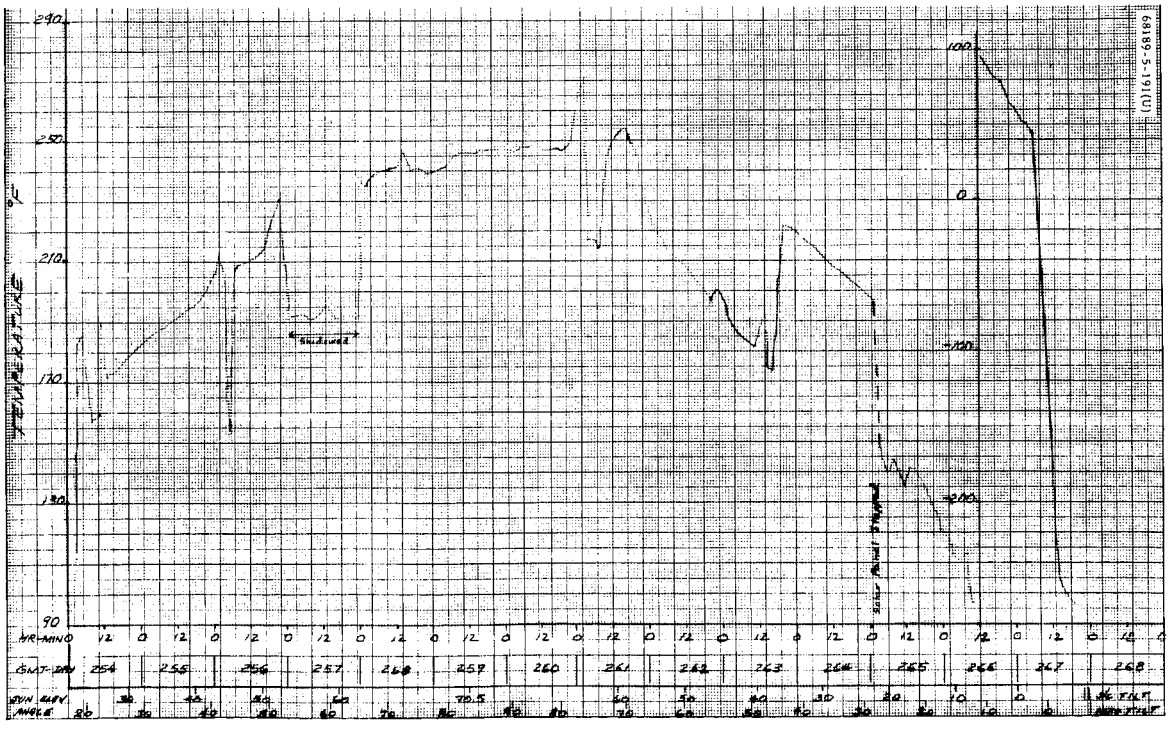

Figure 5.1-84. Sensor EP-12: Solar All Array Temperature

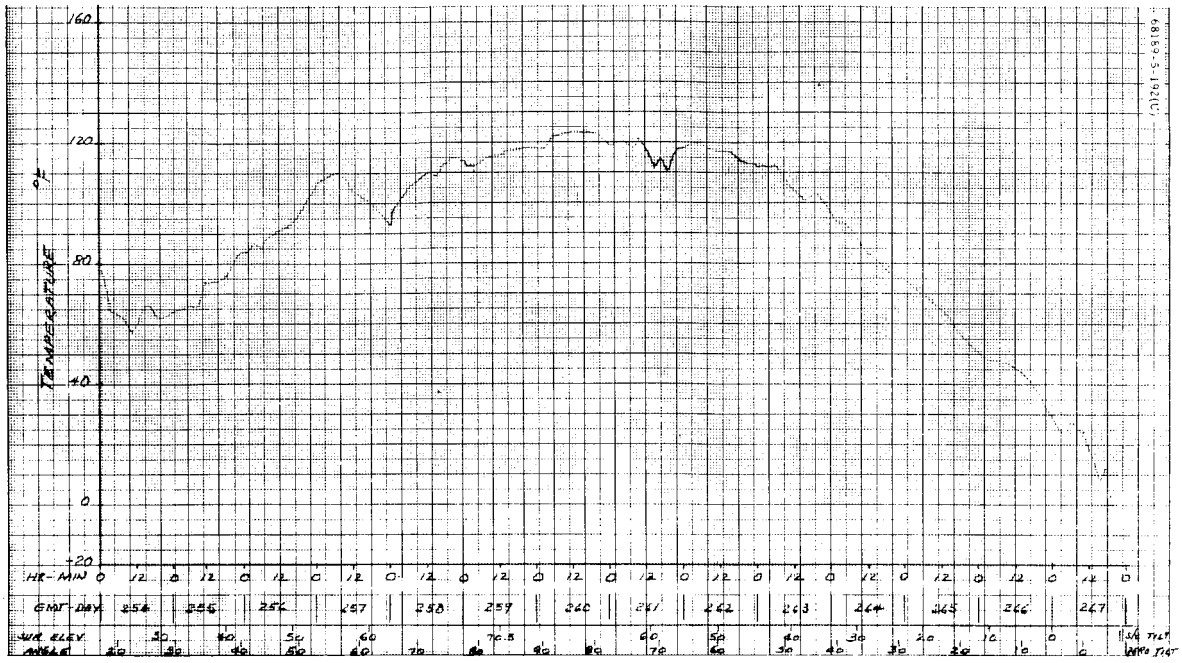

Figure 5.1-85. Sensor EP-13: Boost Regulator Temperature

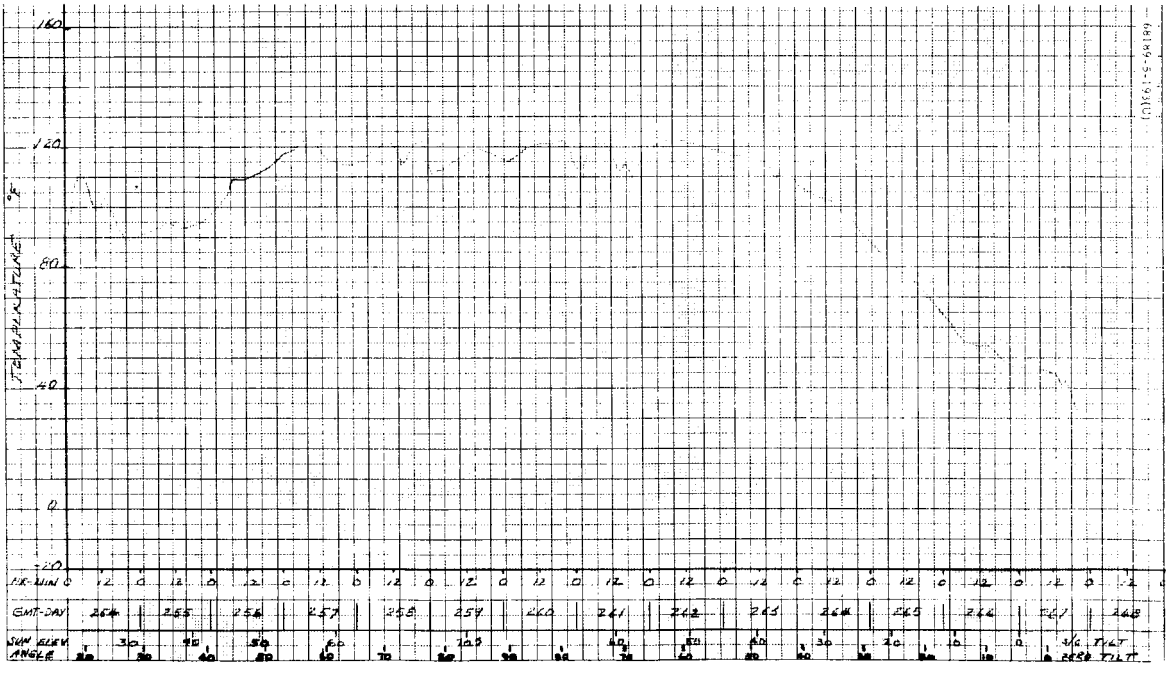

Figure 5.1-86. Sensor EP-34: Battery Charge Regulator Temperature

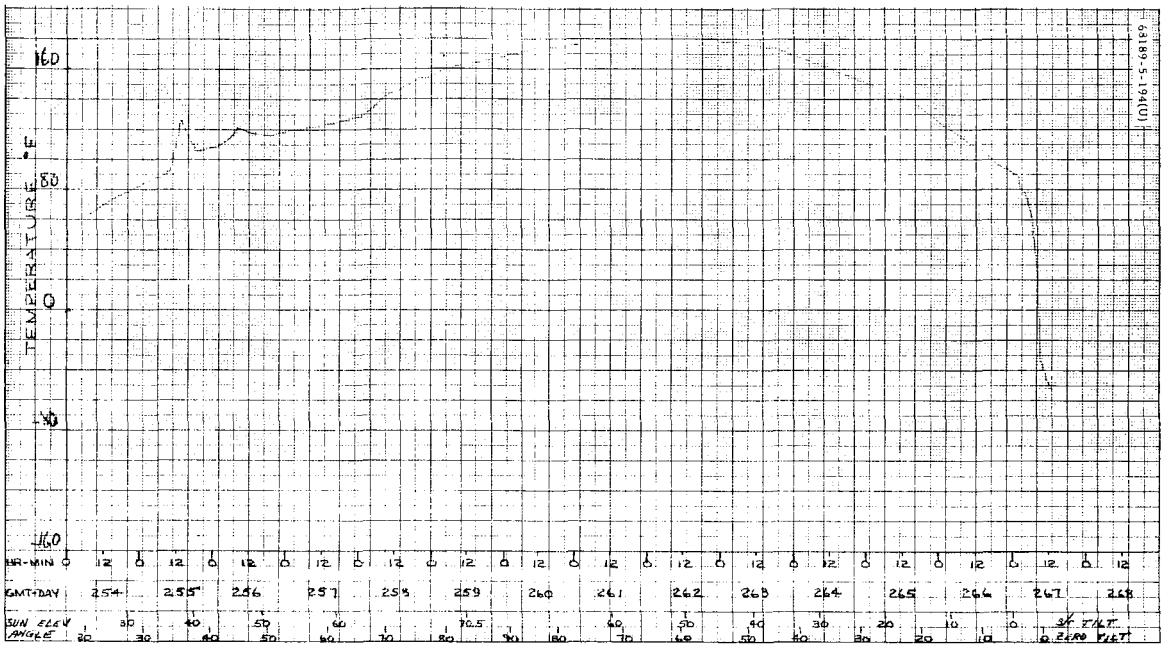

Figure 5.1-87. Sensor FC-44: Flight Control Electronics Temperature 1

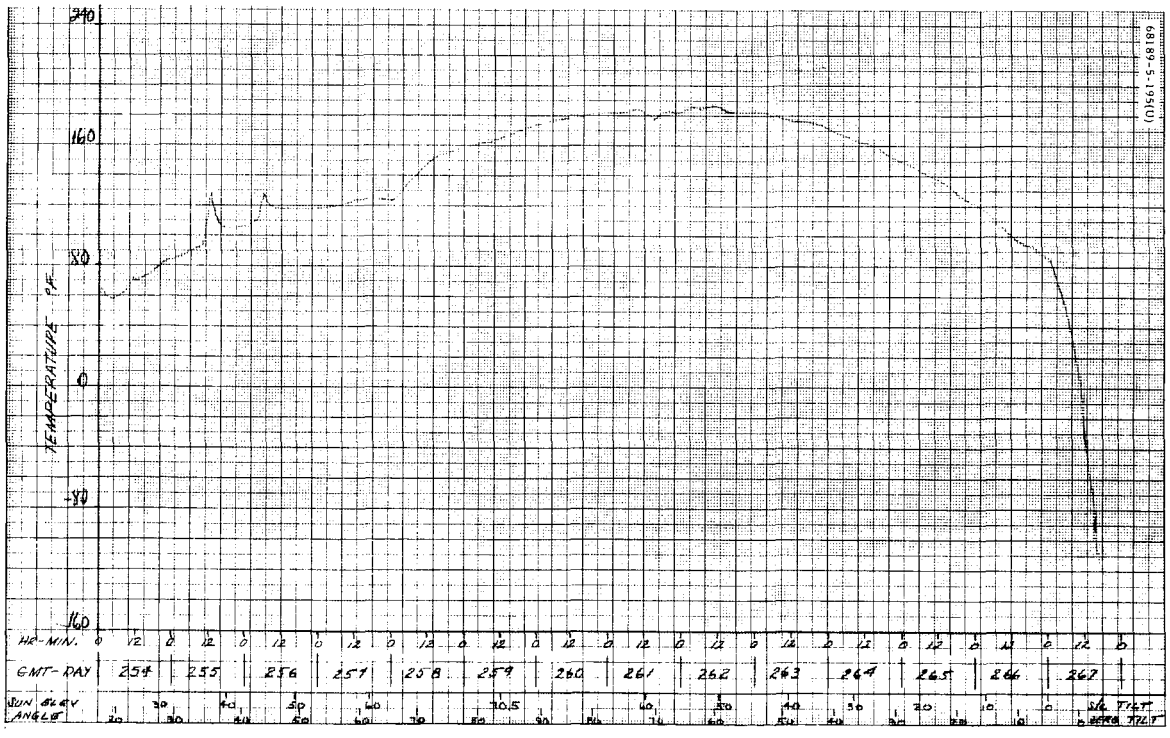

Figure 5.1-88. Sensor FC-45: Flight Control Electronics Temperature 2

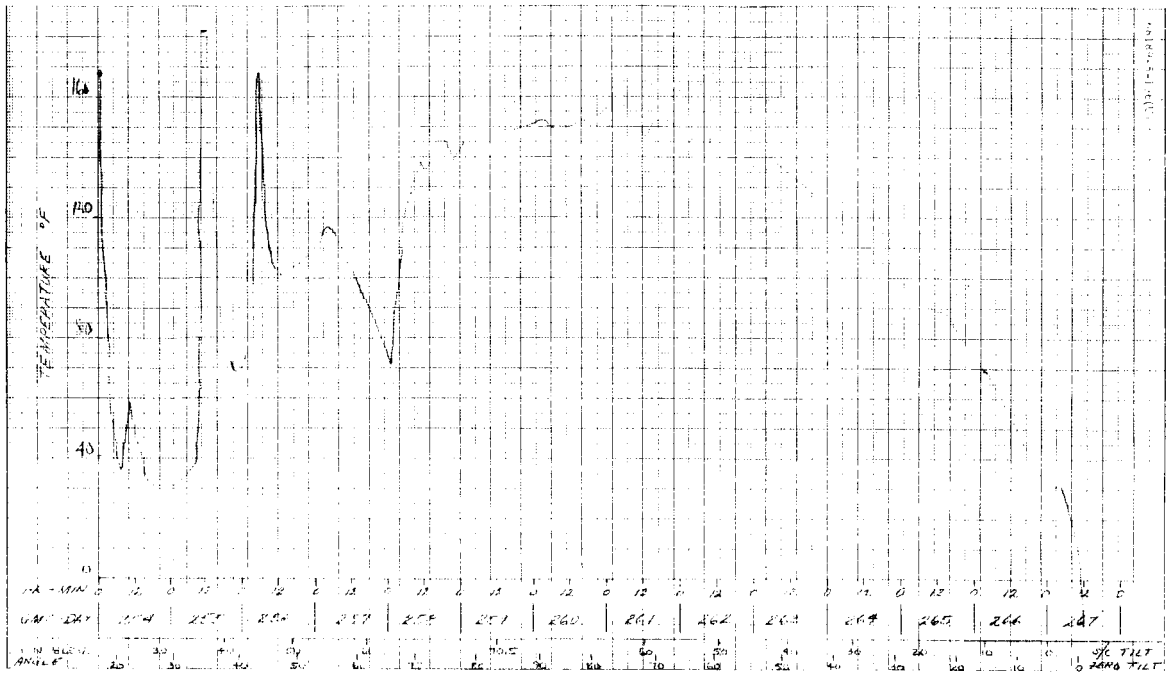

Figure 5.1-89. Sensor FC-46: Roll Gyro Temperature

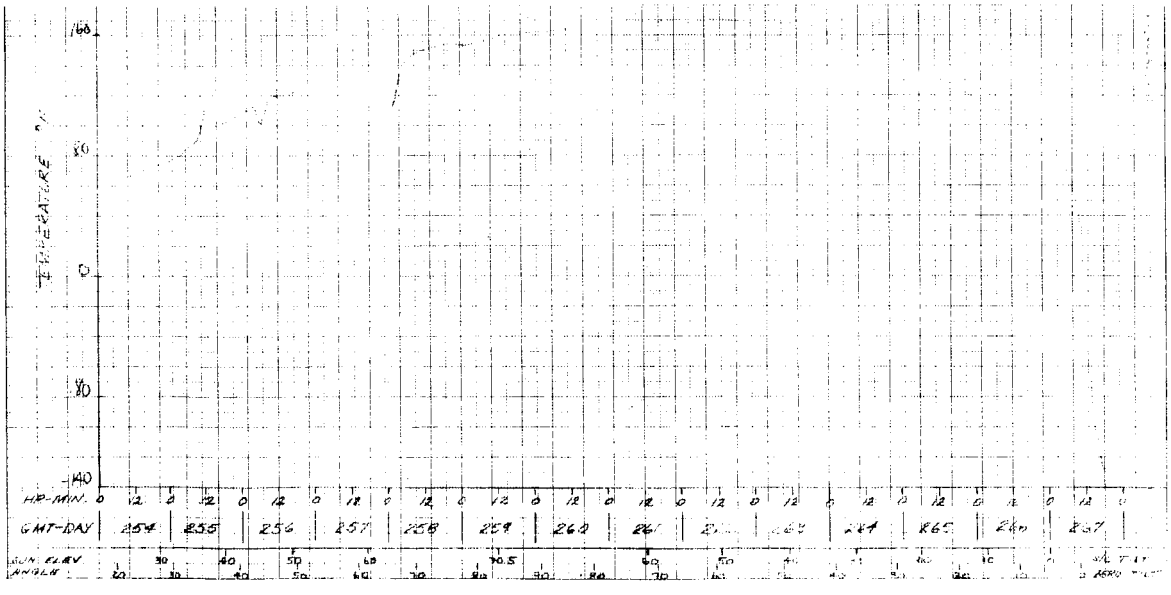

Figure 5.1-90. Sensor FC-47: Canopus Sensor Temperature

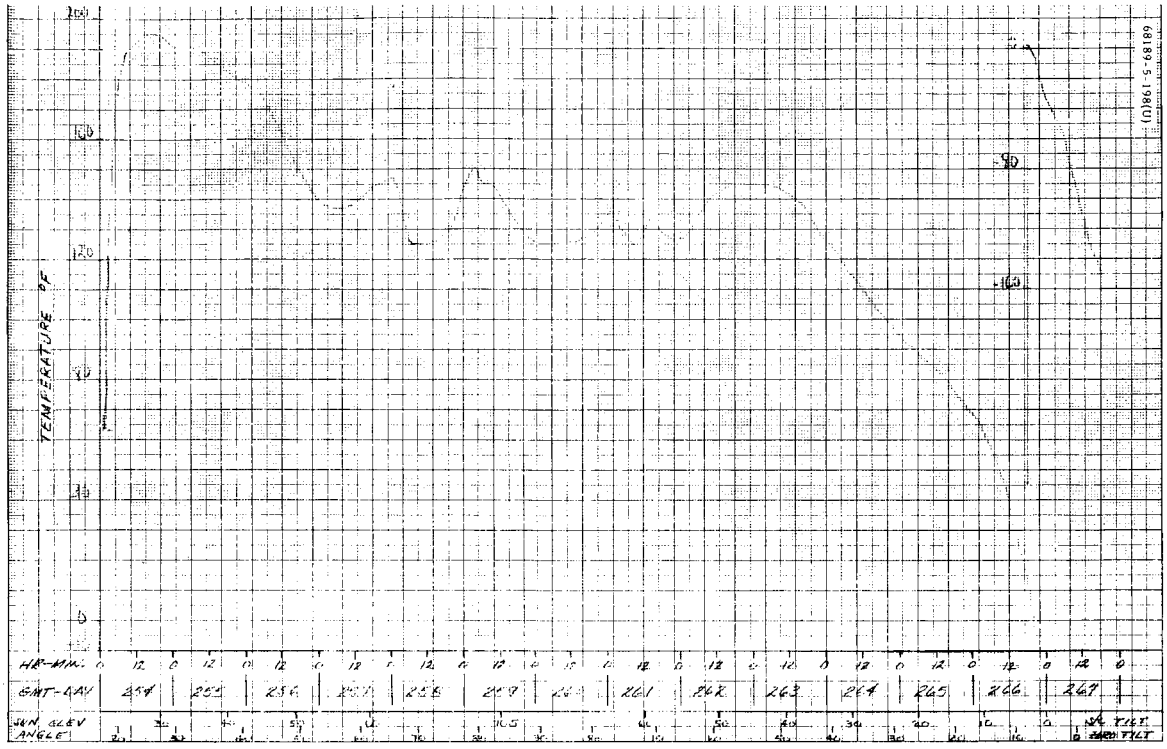

Figure 5.1-91. Sensor FC-48: Nitrogen Gas Tank Temperature

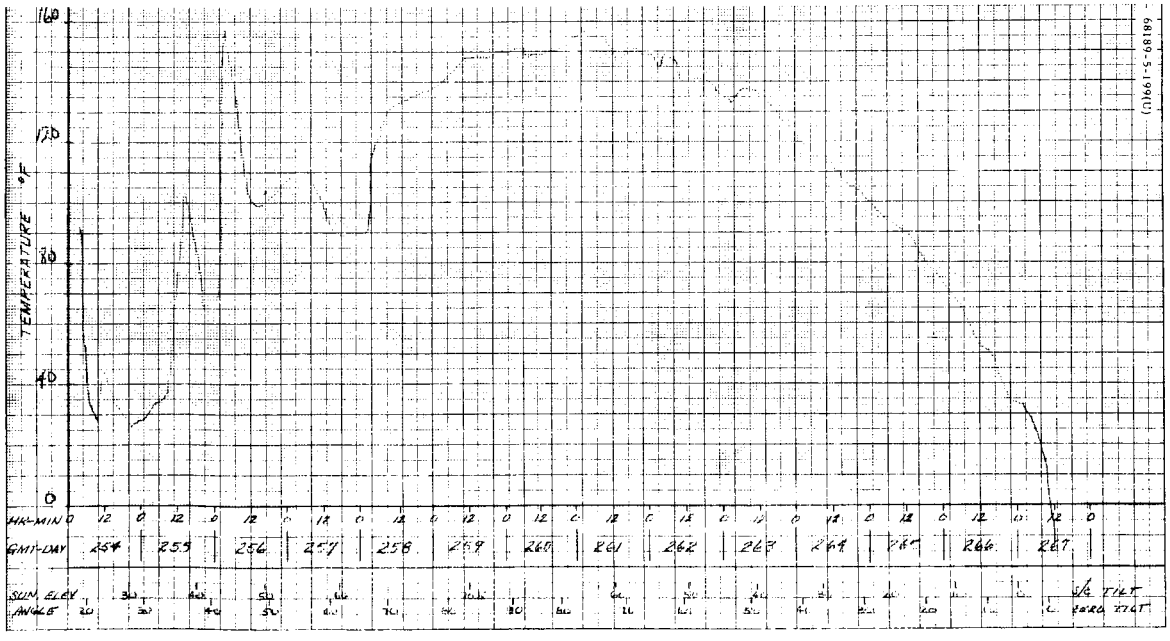

Figure 5.1-92. Sensor FC-54: Pitch Gryo Temperature

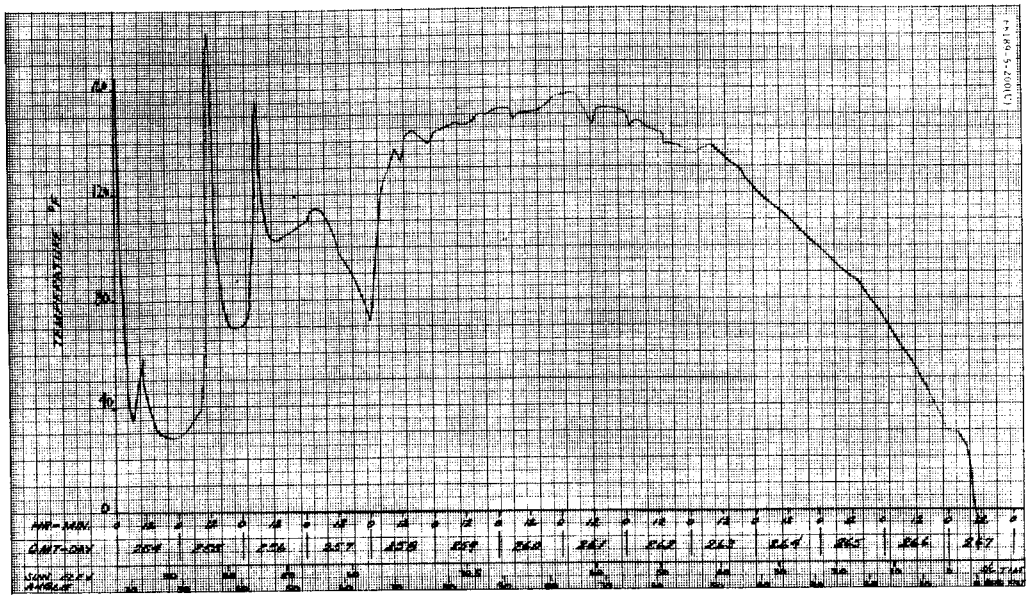

Figure 5.1-93. Sensor FC-55: Yaw Gyro Temperature

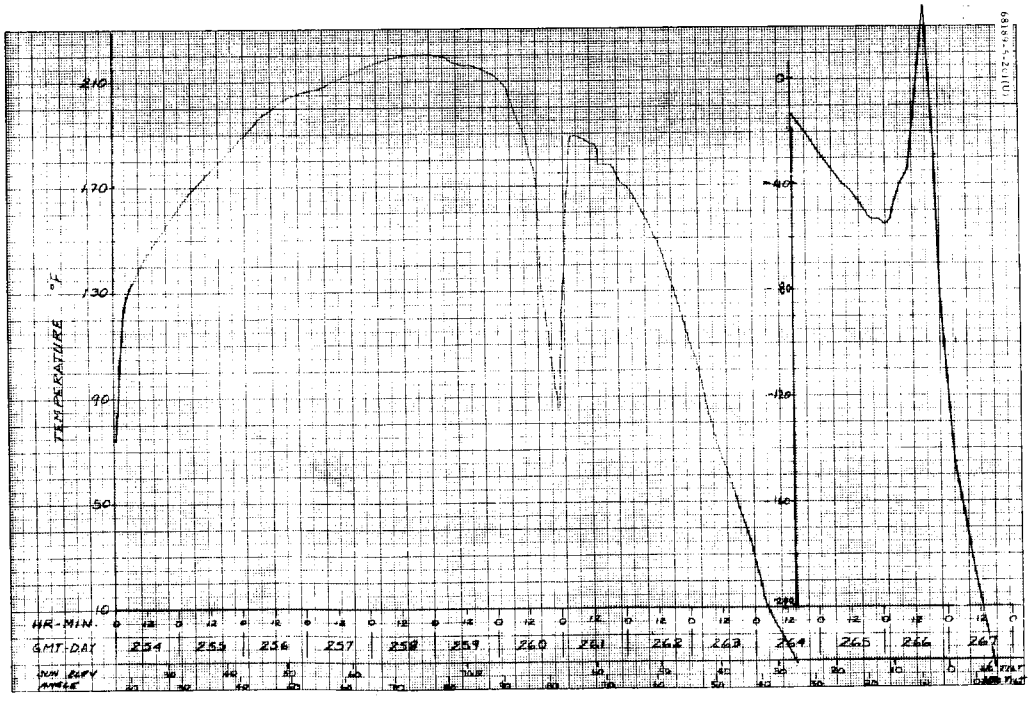

Figure 5.1-94. Sensor FC-70: Attitude Gas Jet 2 Temperature

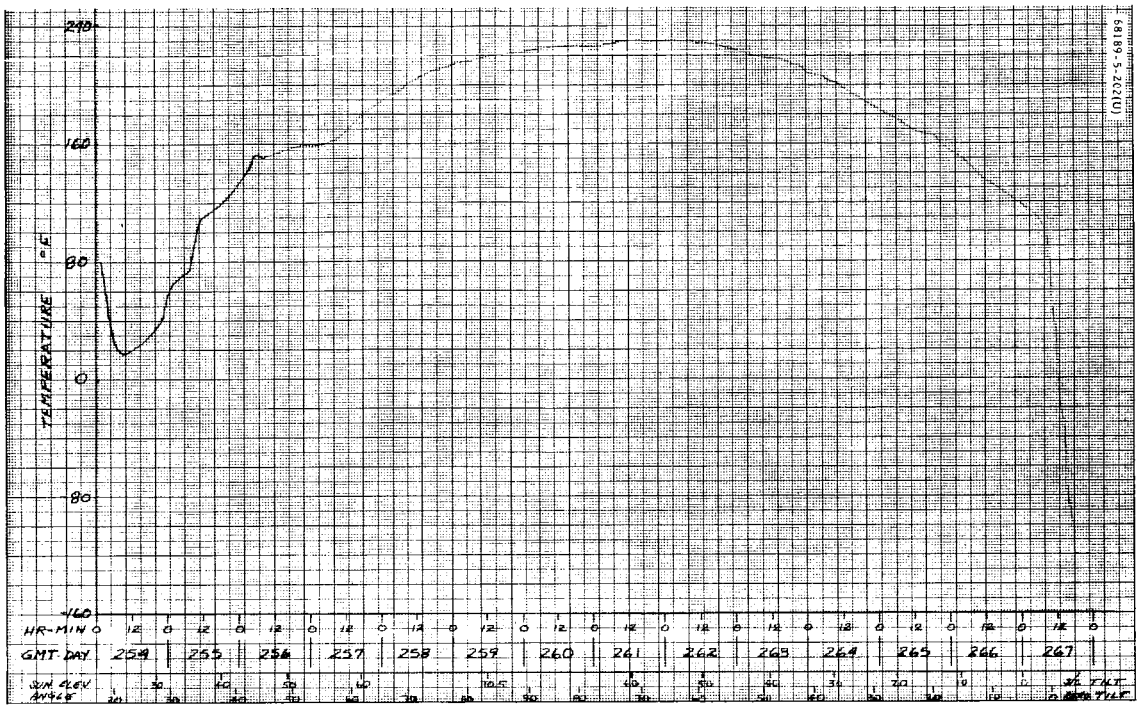

Figure 5.1-95. Sensor FC-71: Roll Actuator Temperature

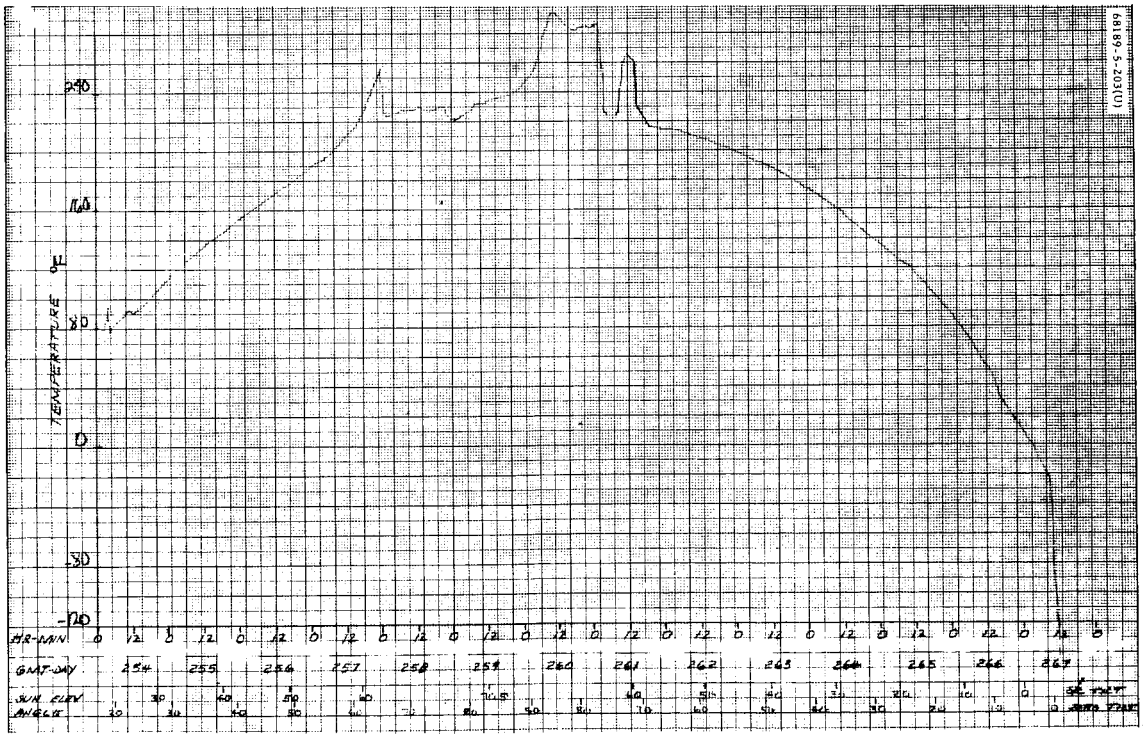

Figure 5.1-96. Sensor M-8: Planar Array Temperature

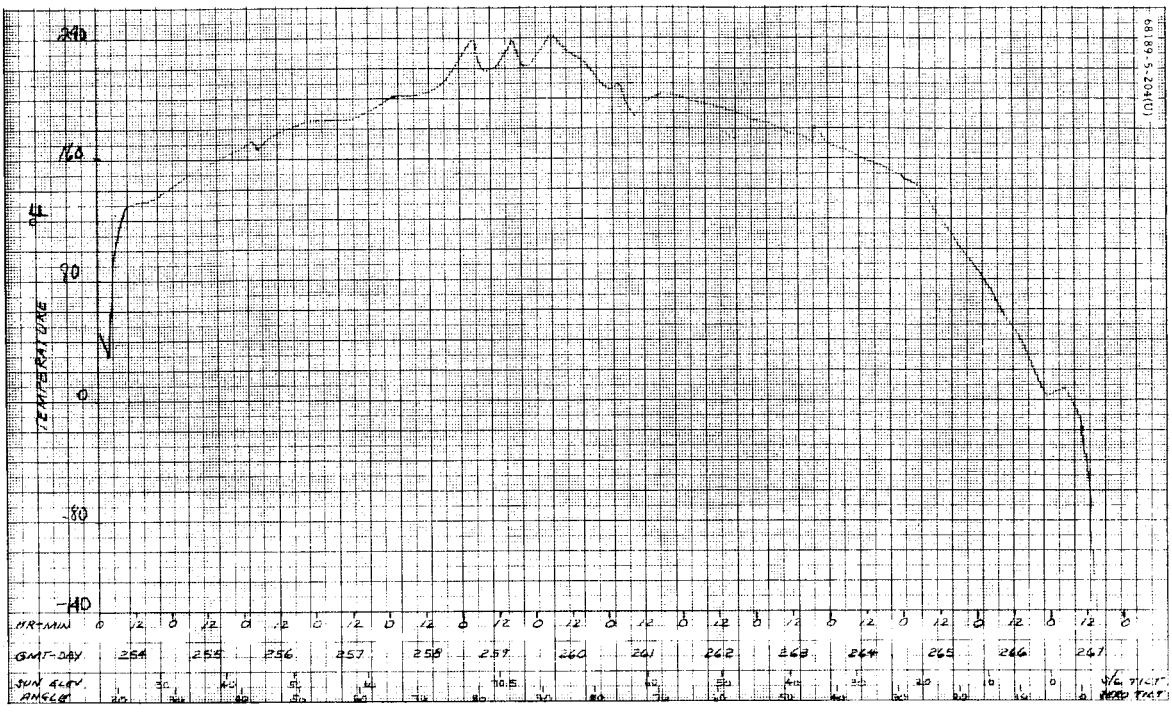

Figure 5.1-97. Sensor M-10: Solar Panel Stepping Motor Temperature

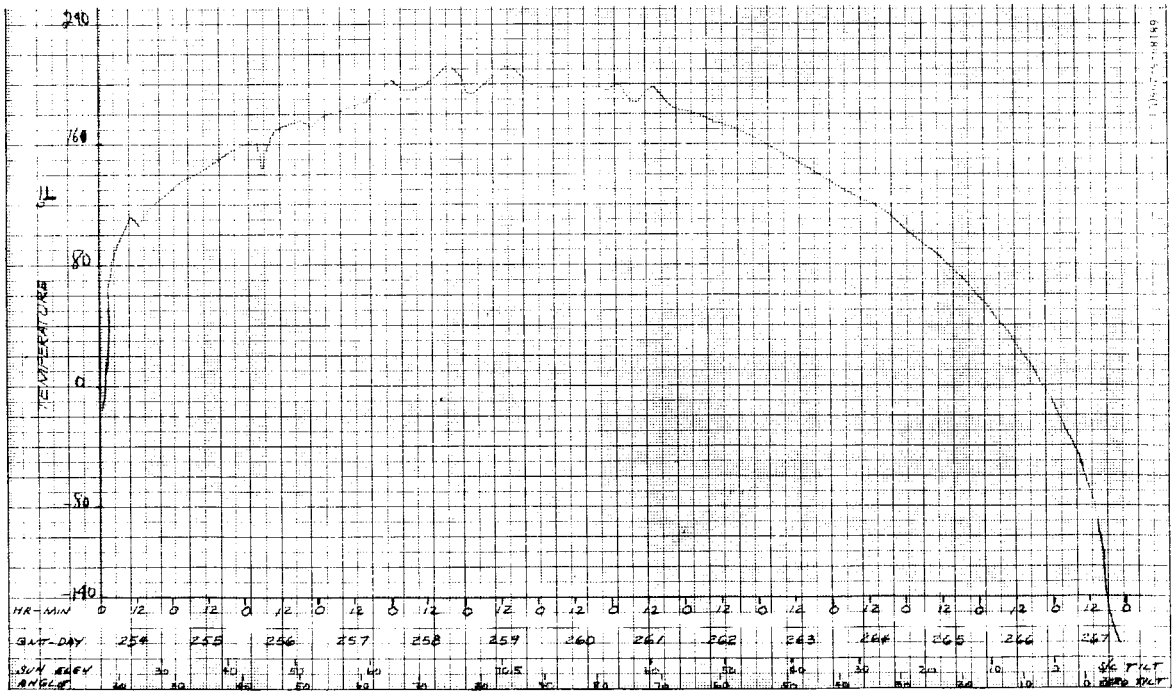

Figure 5.1-98. Sensor M-12: Elevation Axis Stepping Motor Temperature

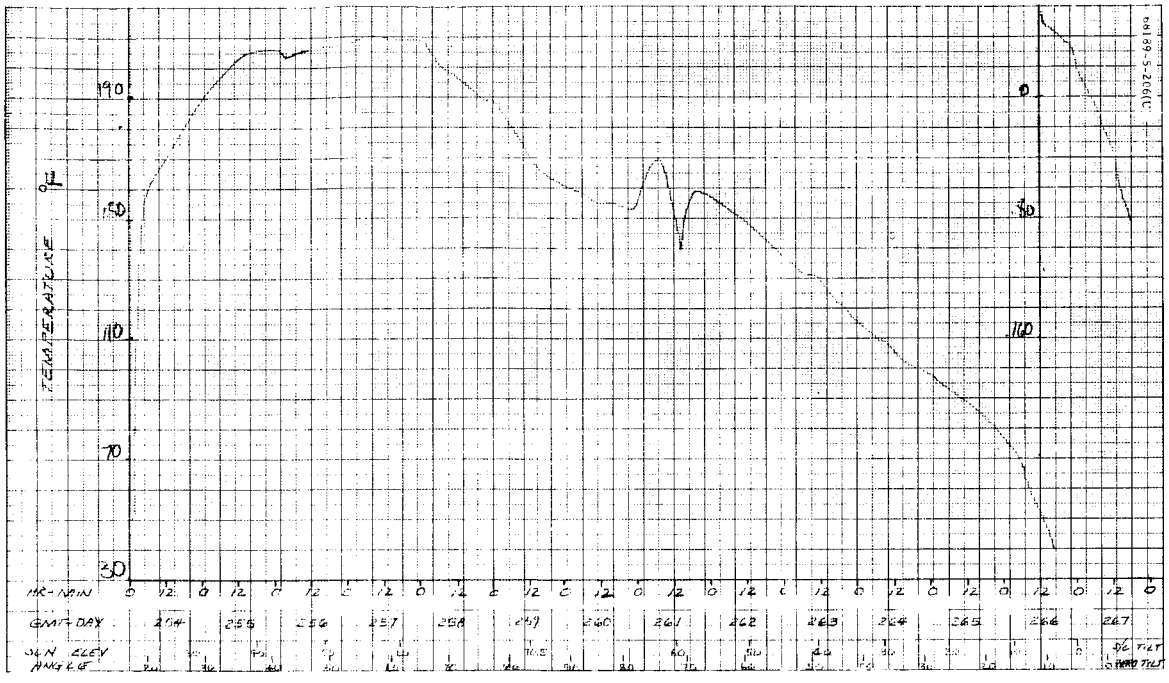

Figure 5.1-99. Sensor P-4: Vernier Lines 2 Temperature

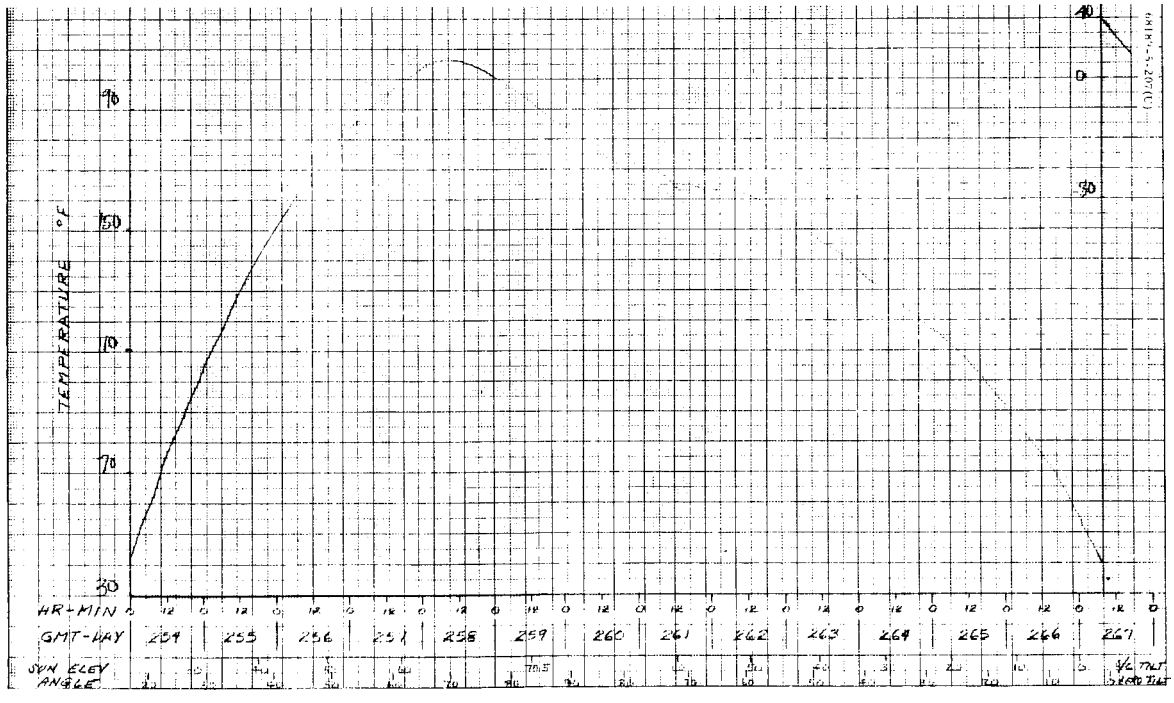

Figure 5.1-100. Sensor P-5: Vernier Fuel Tank 2 Temperature

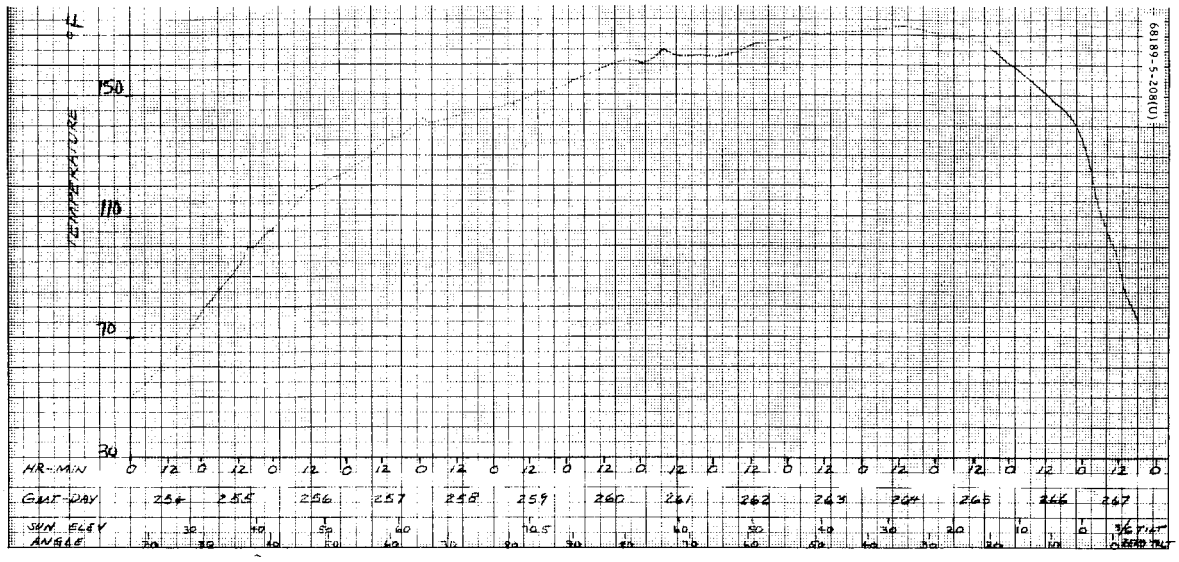

Figure 5.1-101. Sensor P-6: Vernier Oxidizer Tank 3 Temperature

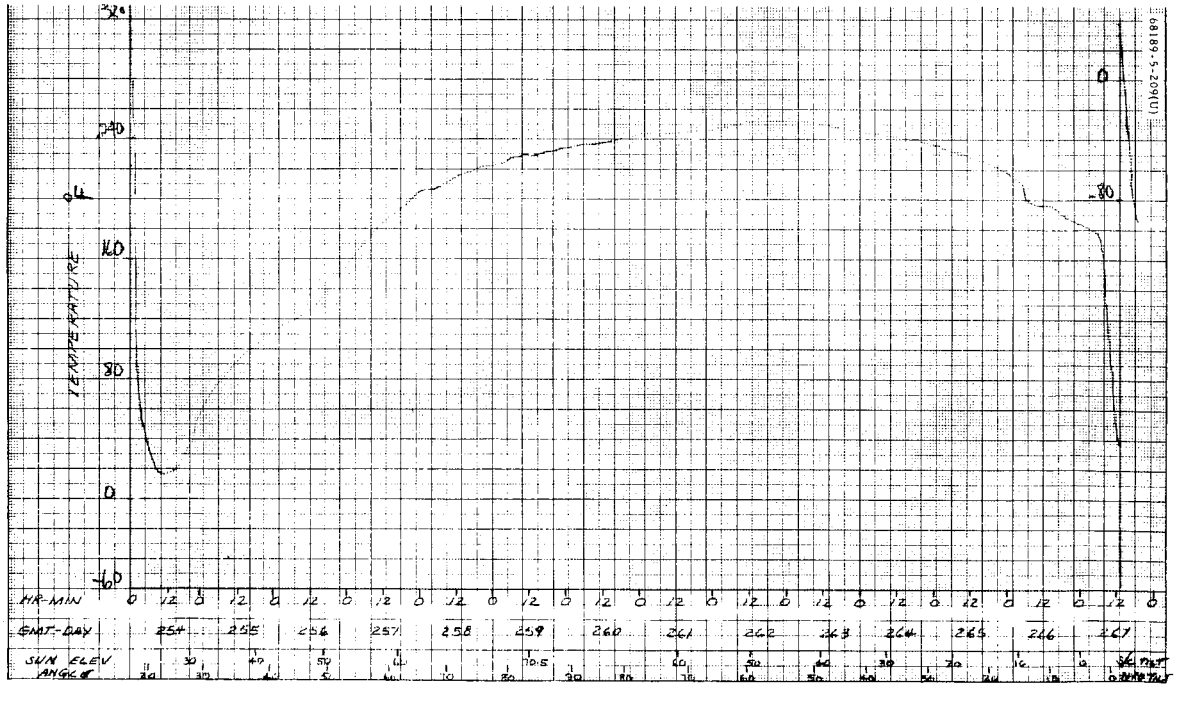

Figure 5.1-102. Sensor P-7: Vernier Engine 1 Temperature

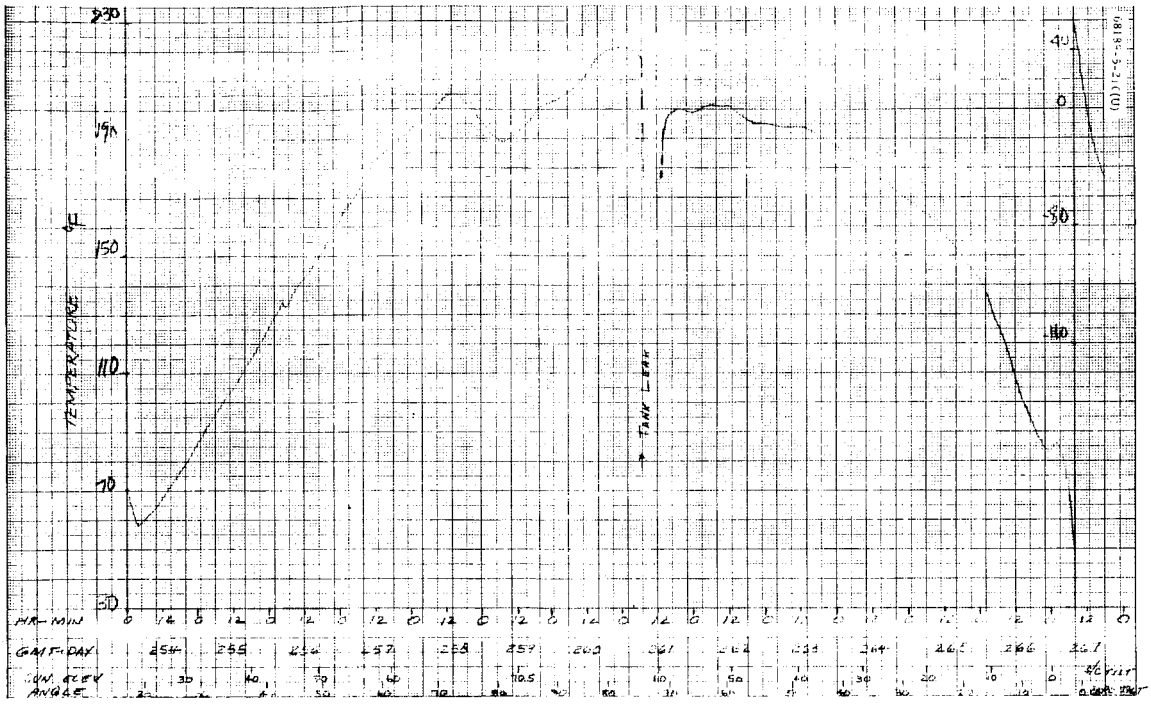

Figure 5.1-103. Sensor P-8: Vernier Lines 1 Temperature

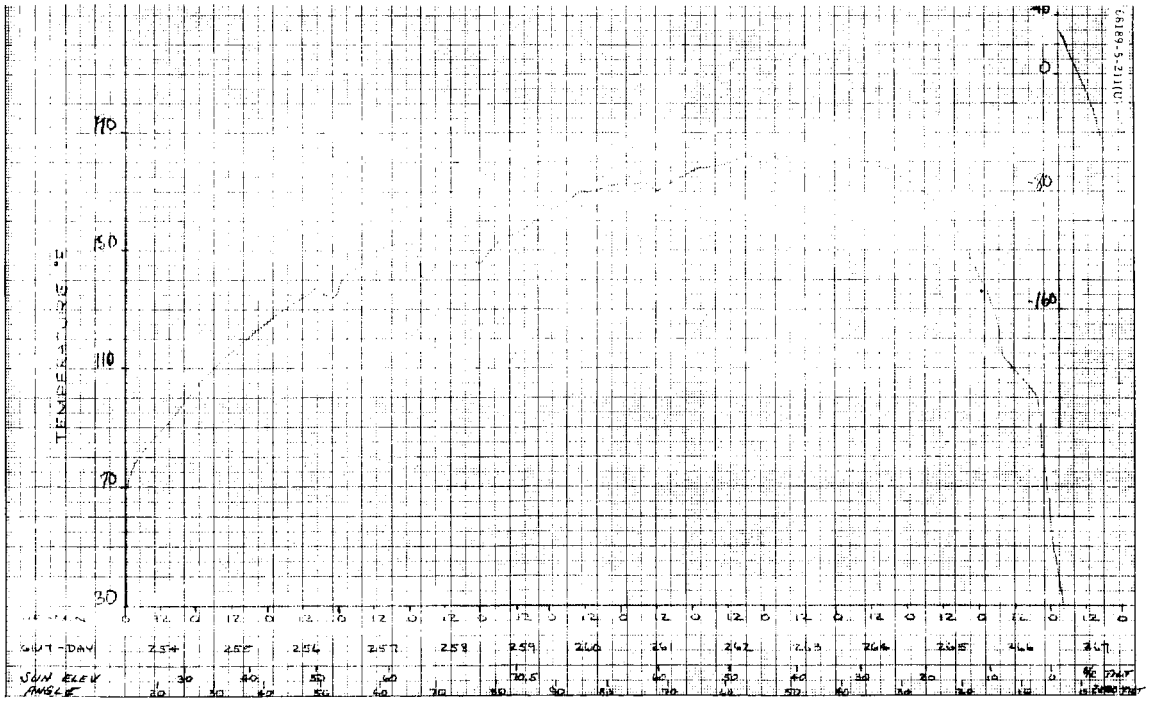

Figure 5.1-104. Sensor P-9: Vernier Lines 3 Temperature

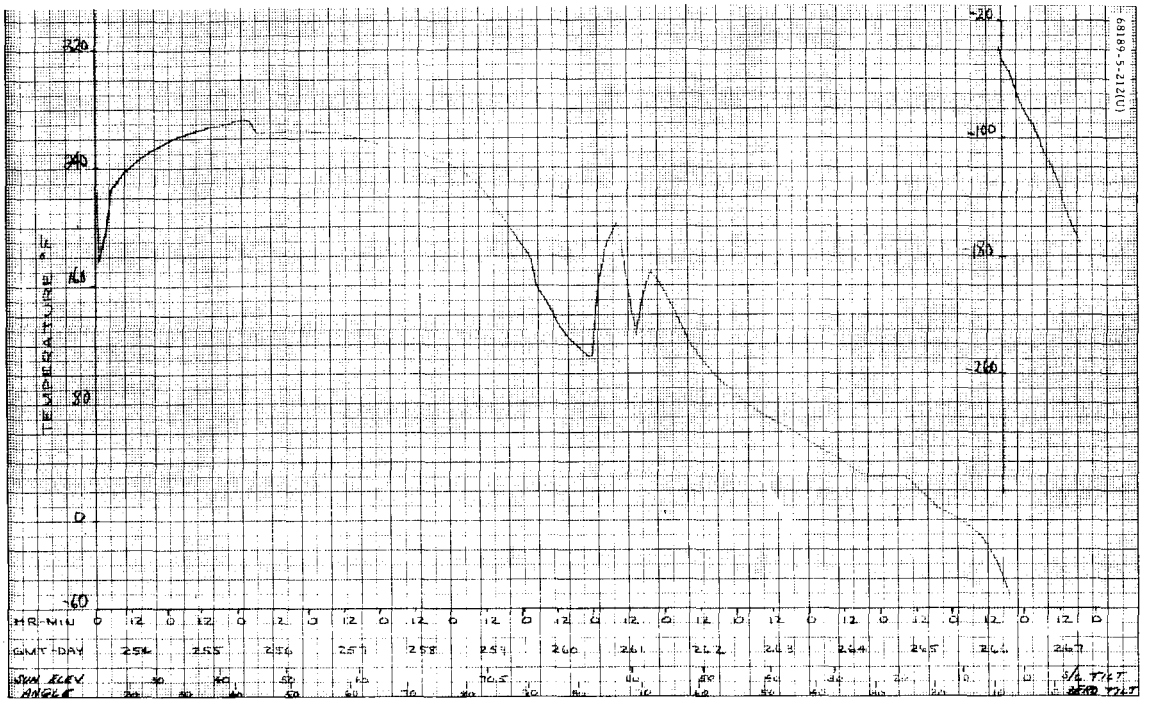

Figure 5.1-105. Sensor P-10: Vernier Engine 2 Temperature

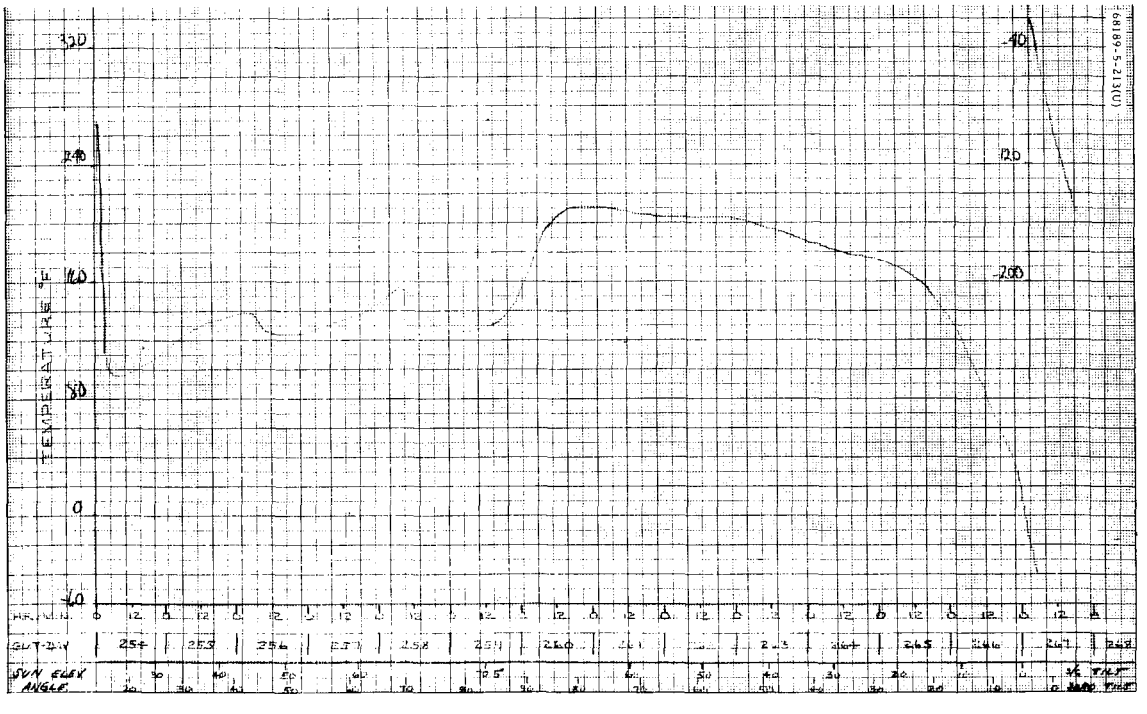

Figure 5.1-106. Sensor P-11: Vernier Engine 3 Temperature

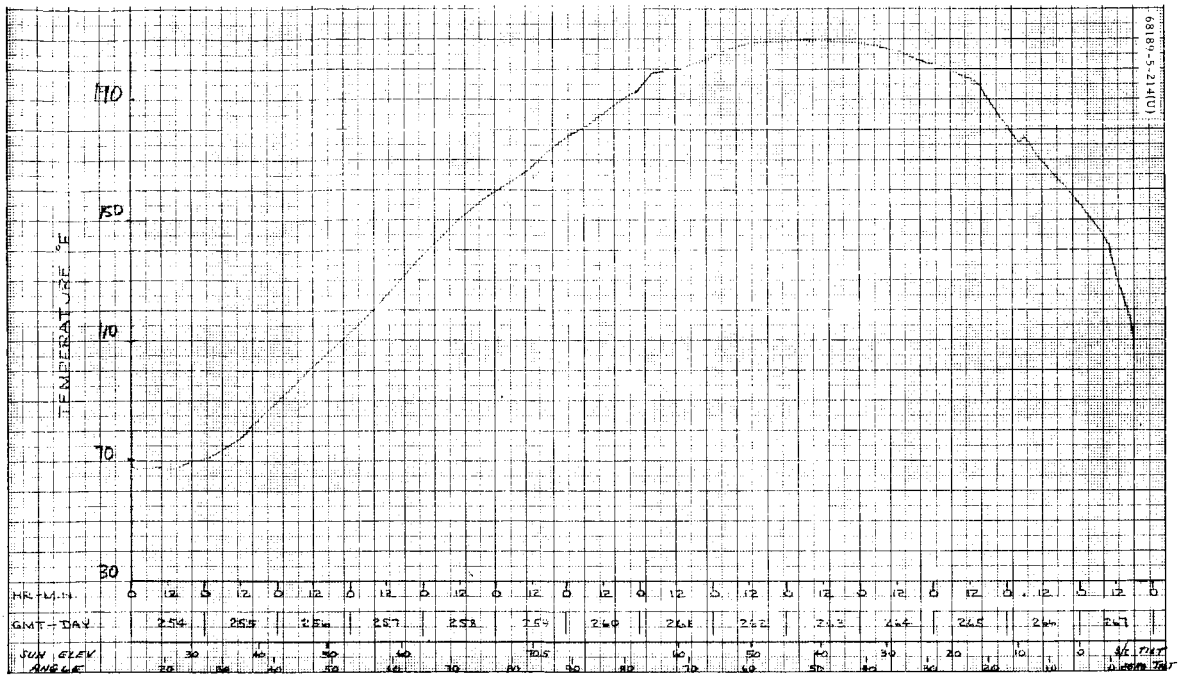

Figure 5.1-107. Sensor P-13: Vernier Fuel Tank 1 Temperature

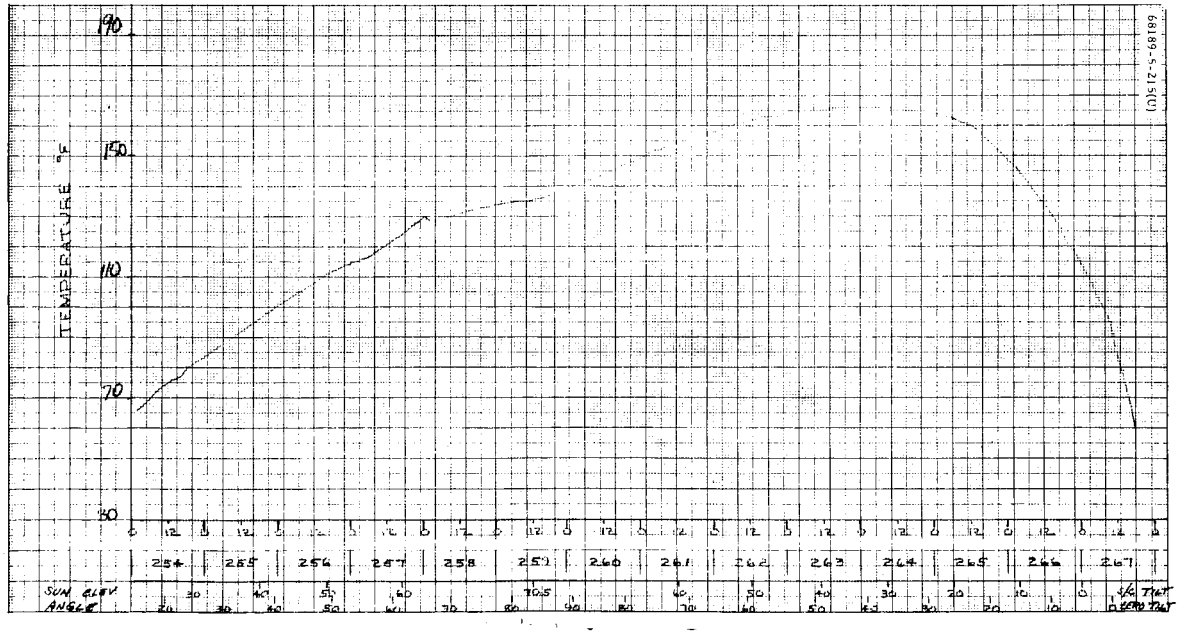

Figure 5.1-108. Sensor P-14: Vernier Fuel Tank 3 Temperature

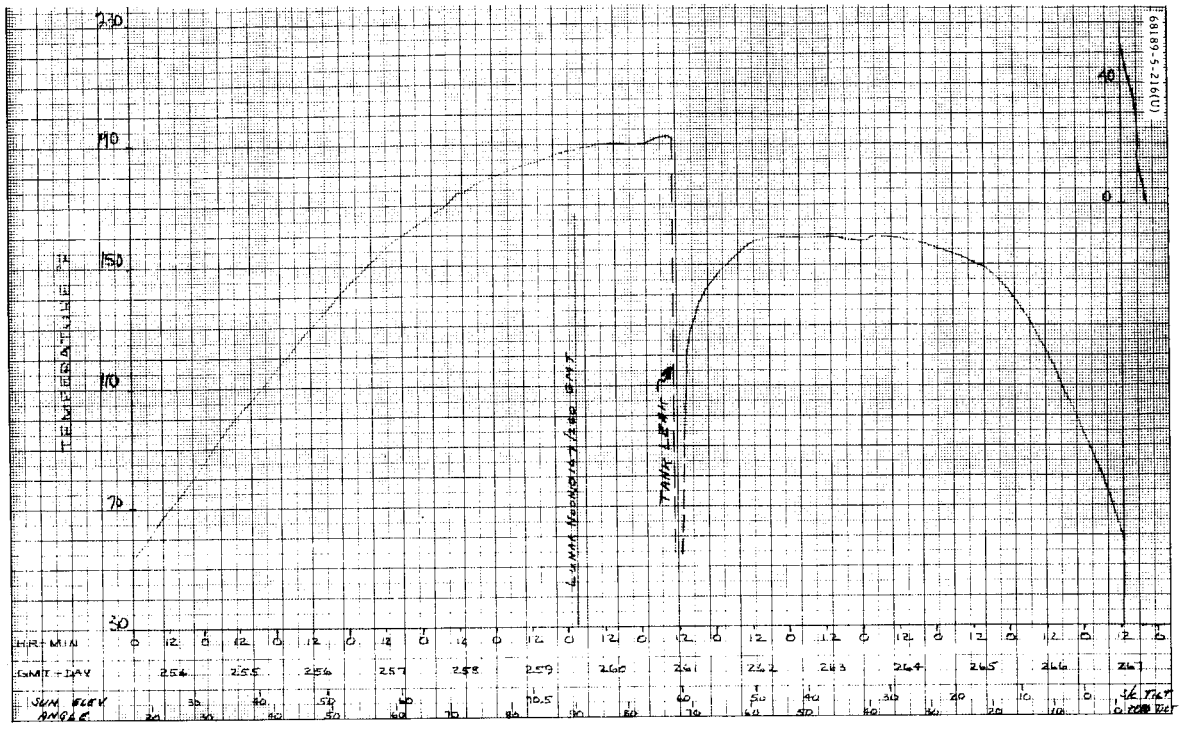

Figure 5.1-109. Sensor P-15: Vernier Oxidizer Tank 1 Temperature

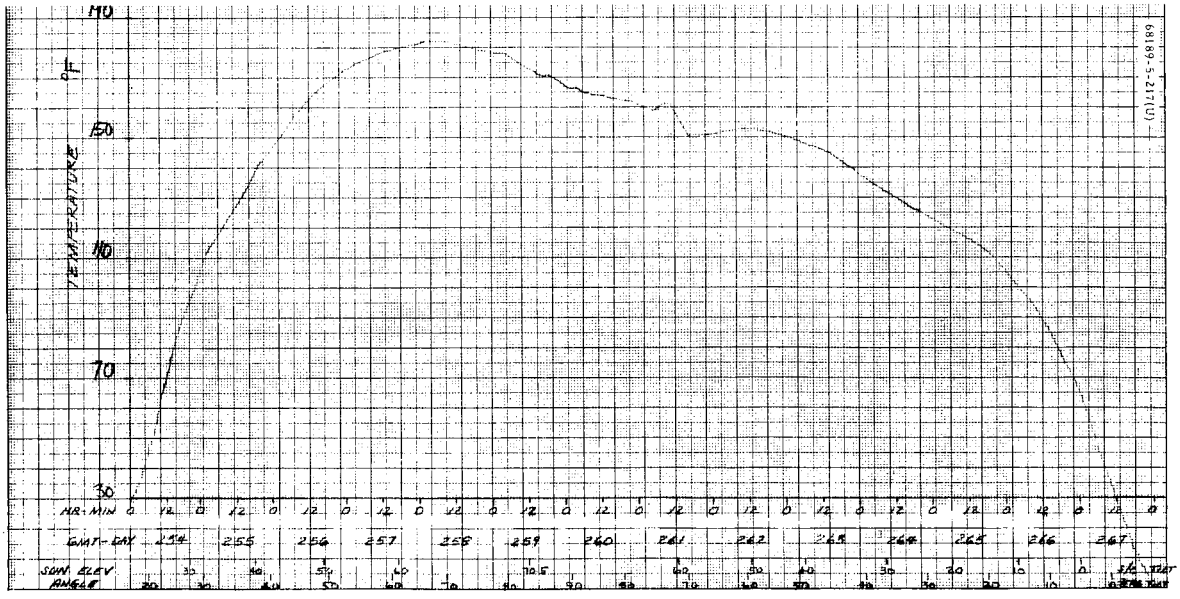

Figure 5.1-110. Sensor P-16: Vernier Oxidizer Tank 2 Temperature

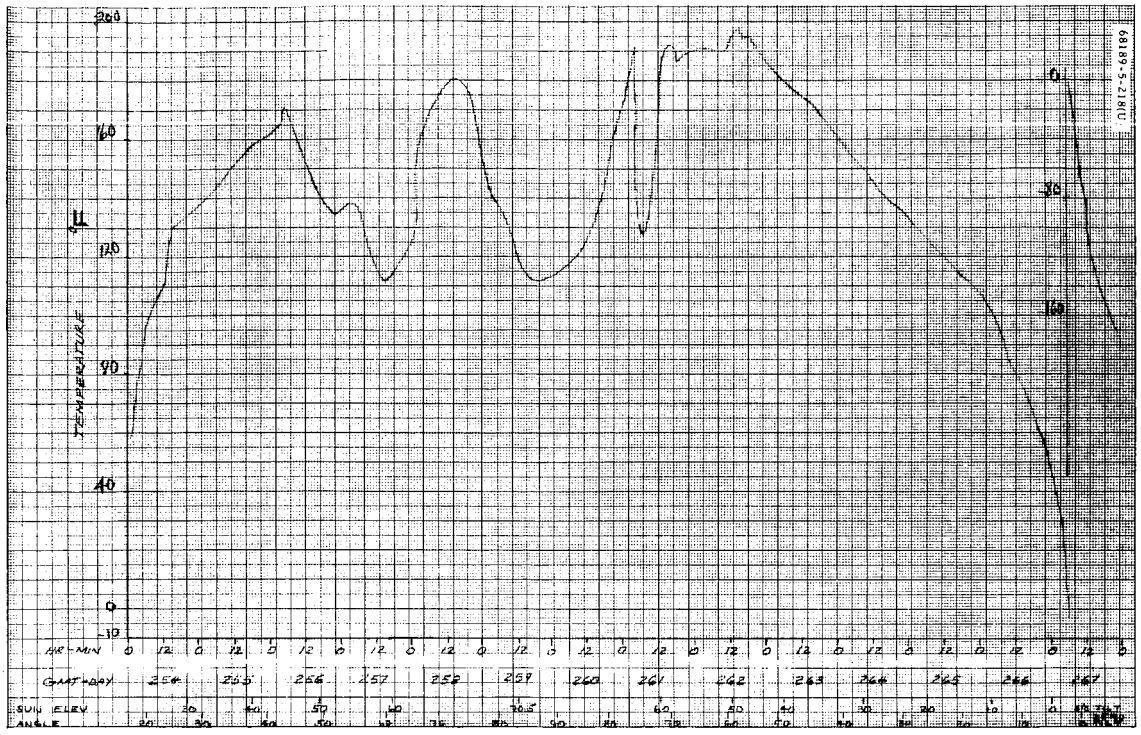

Figure 5.1-111. Sensor P-17: Helium Tank Temperature

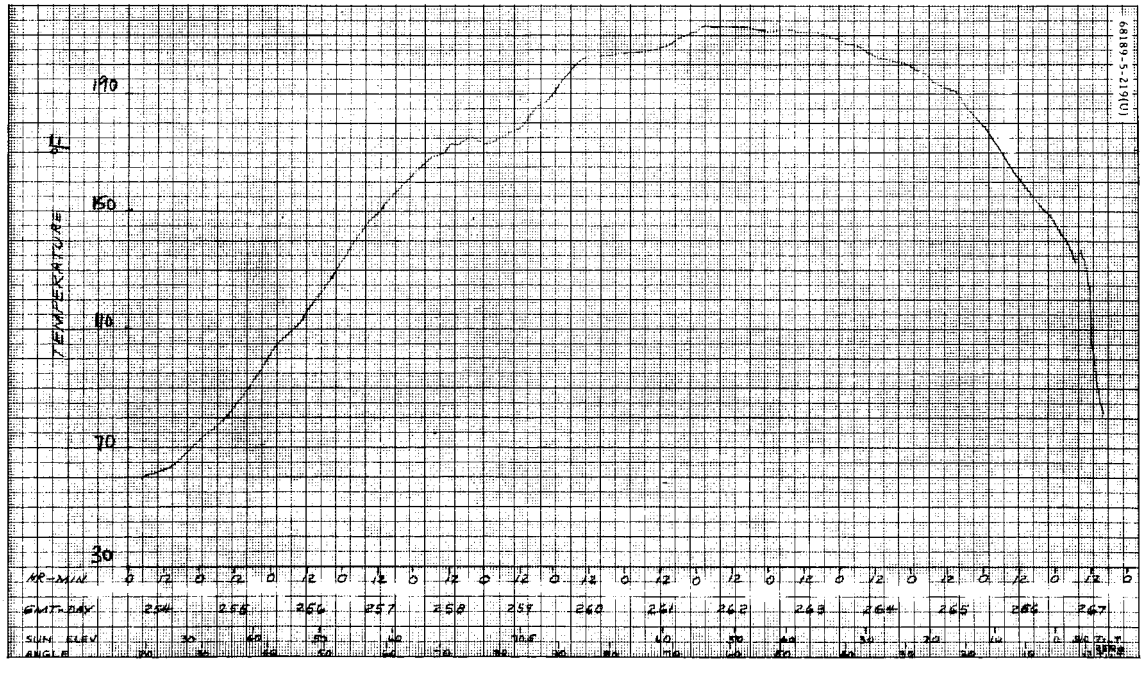

Figure 5.1-112. Sensor P-23: Vernier Fuel Line 1 Temperature

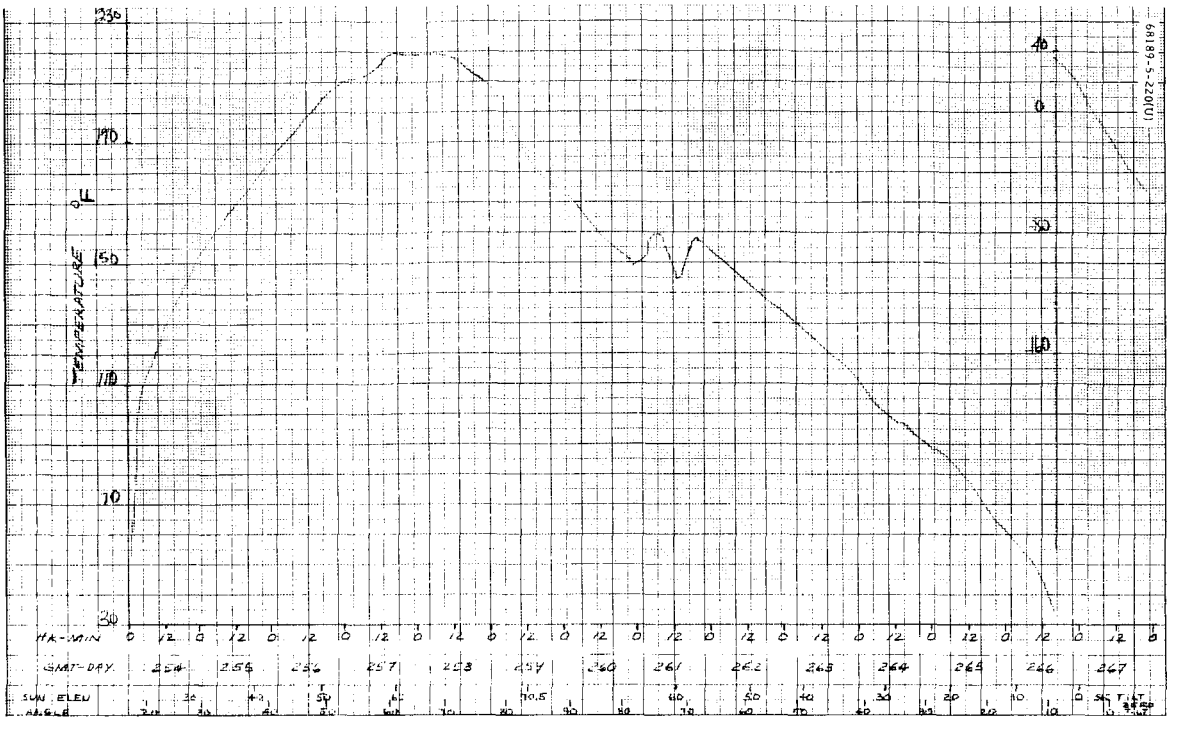

Figure 5.1-113. Sensor P-24: Vernier Fuel Line 2 Temperature

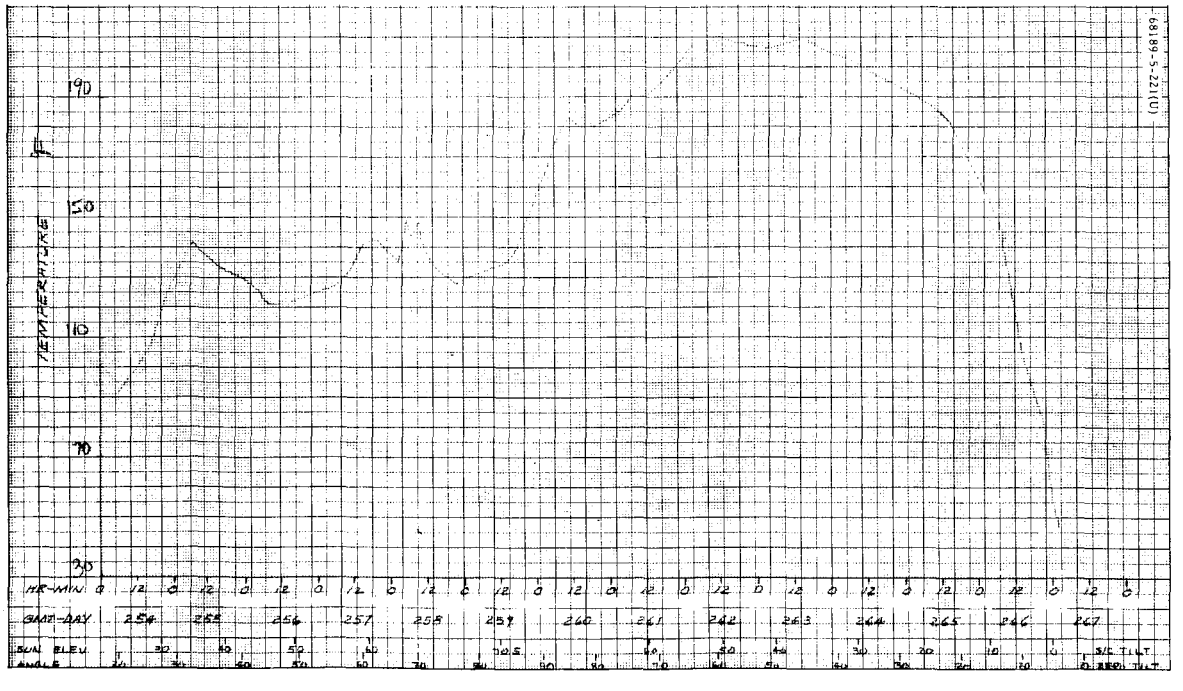

Figure 5.1-114. Sensor P-25: Vernier Fuel Line 3 Temperature

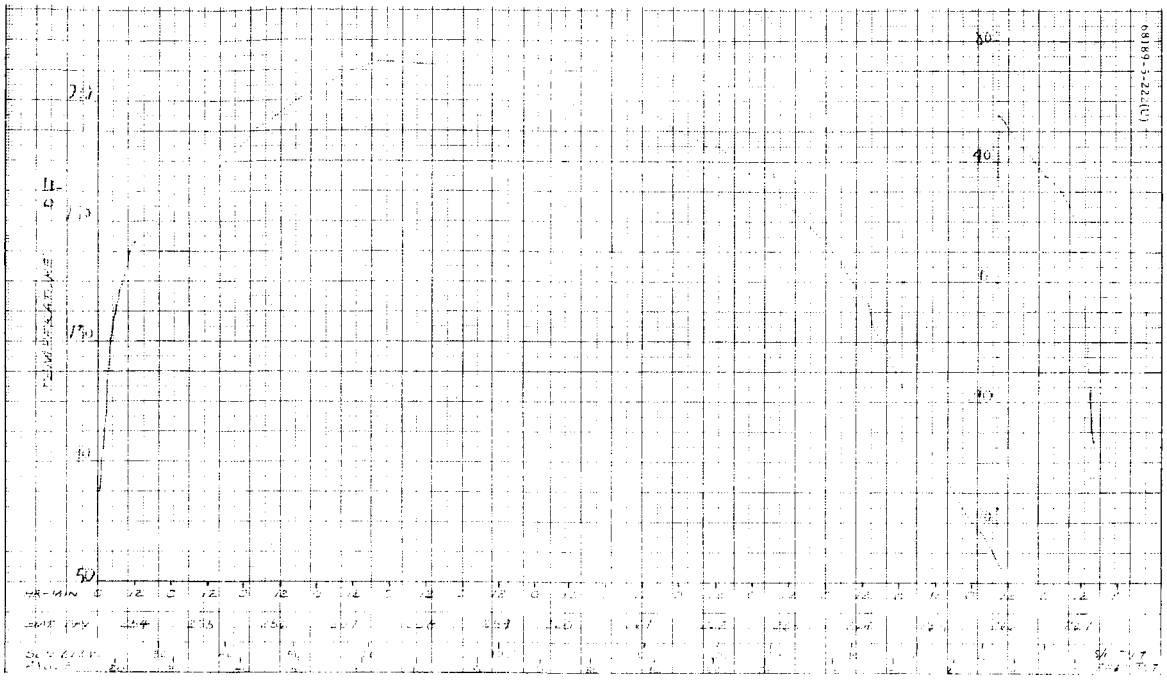

Figure 5.1-115. Sensor R-8: RADVS (KLY) Unit Temperature

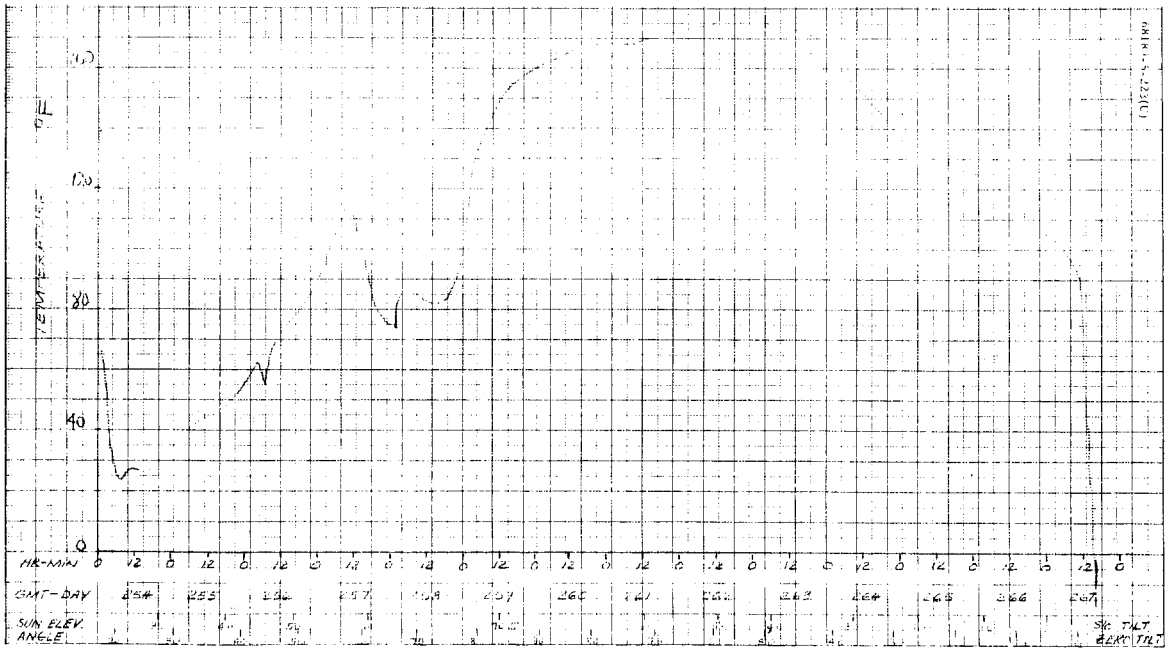

Figure 5.1-116. Sensor R-9: RADVS Signal Data Converter Temperature

Figure 5.1-117. Sensor R-10: Doppler Radar Sensor Temperature

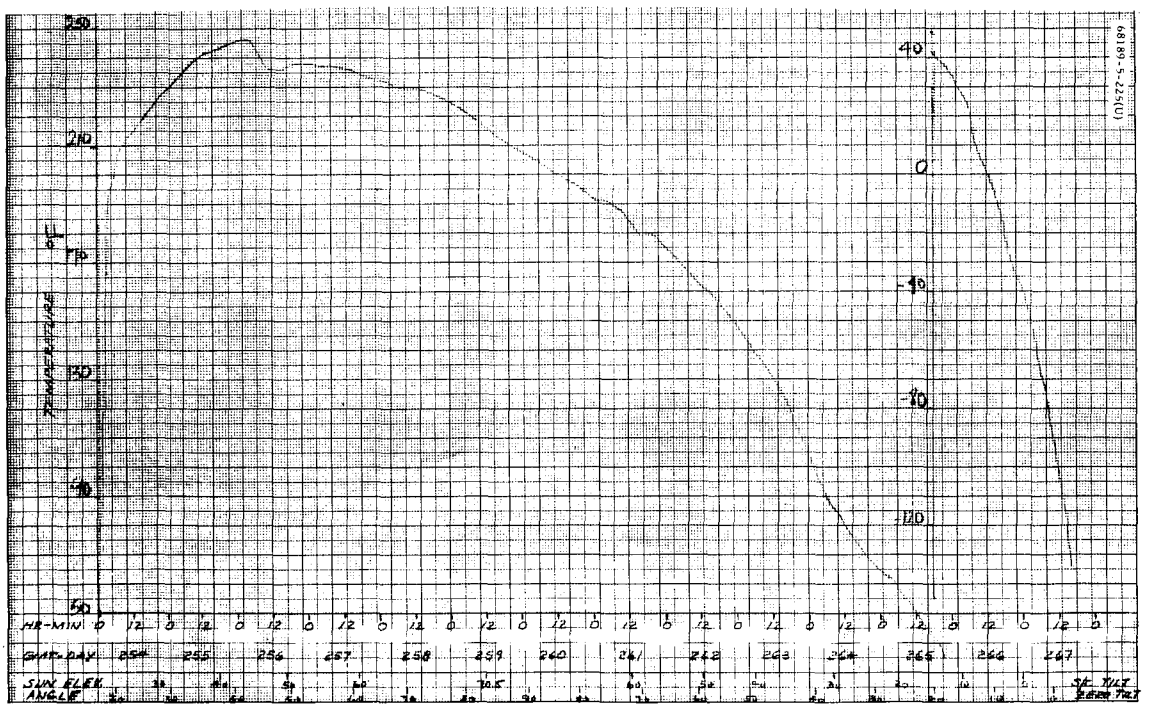

Figure 5.1-118. Sensor R-13: Altimeter Radar Sensor Temperature

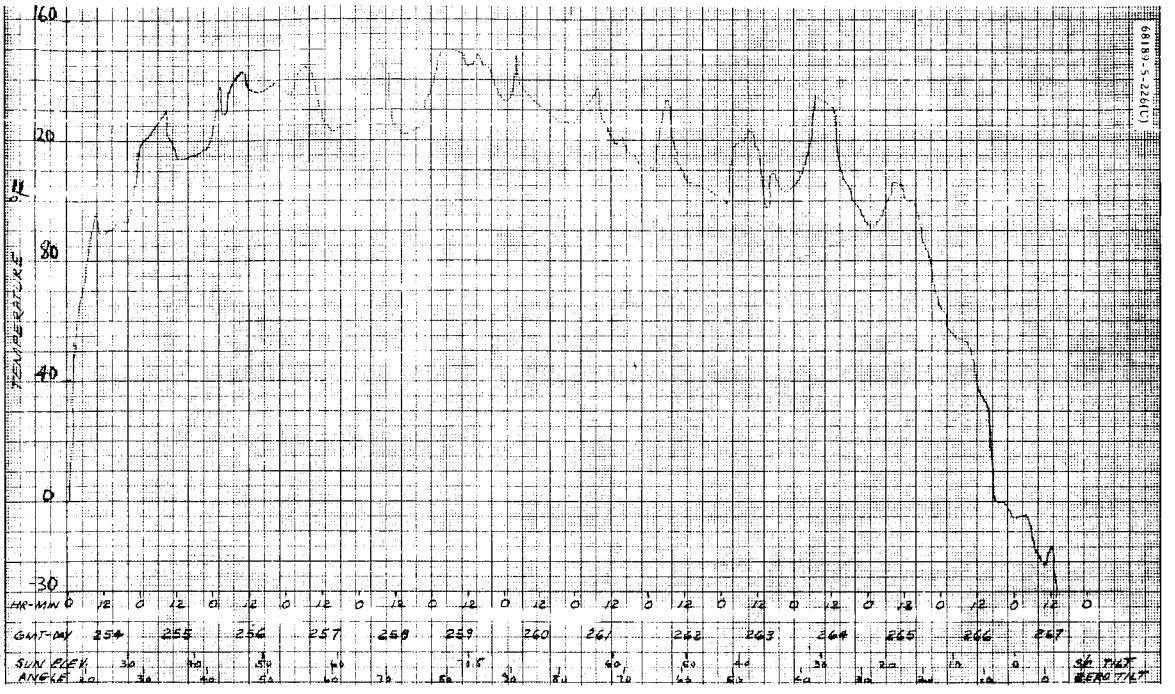

Figure 5.1-119. Sensor TV-16: Surveyor Camera Electronics Temperature

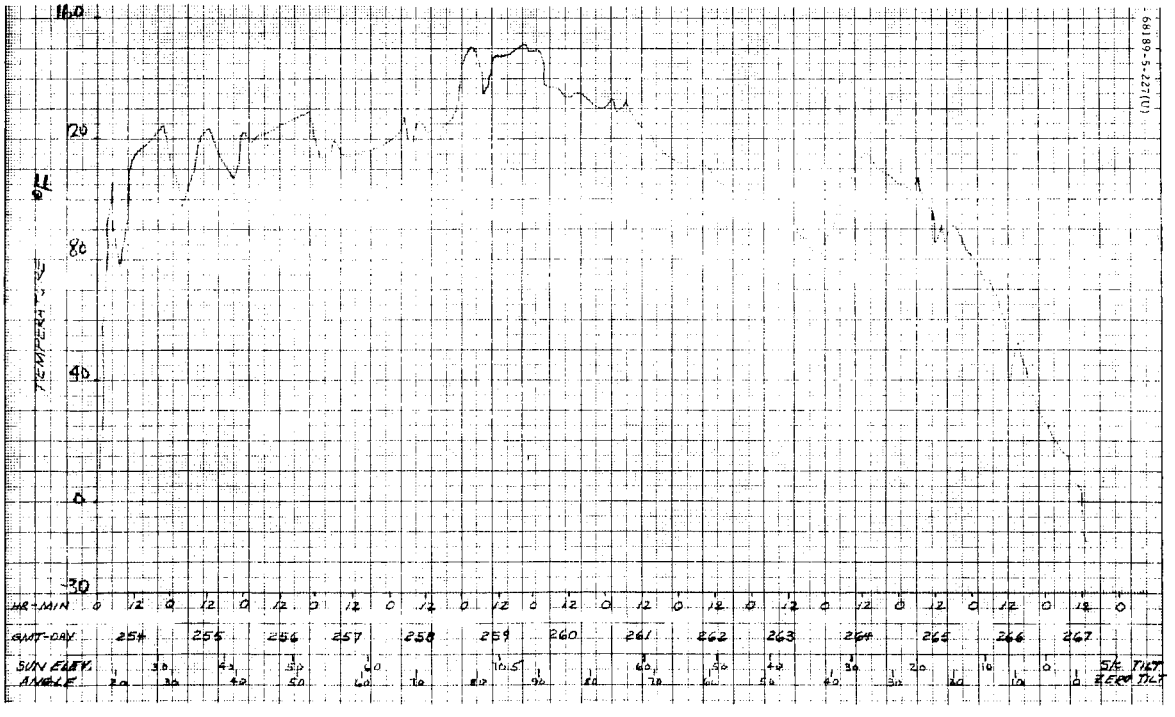

Figure 5.1-120. Sensor TV-17: Surveyor Camera Mirror Assembly

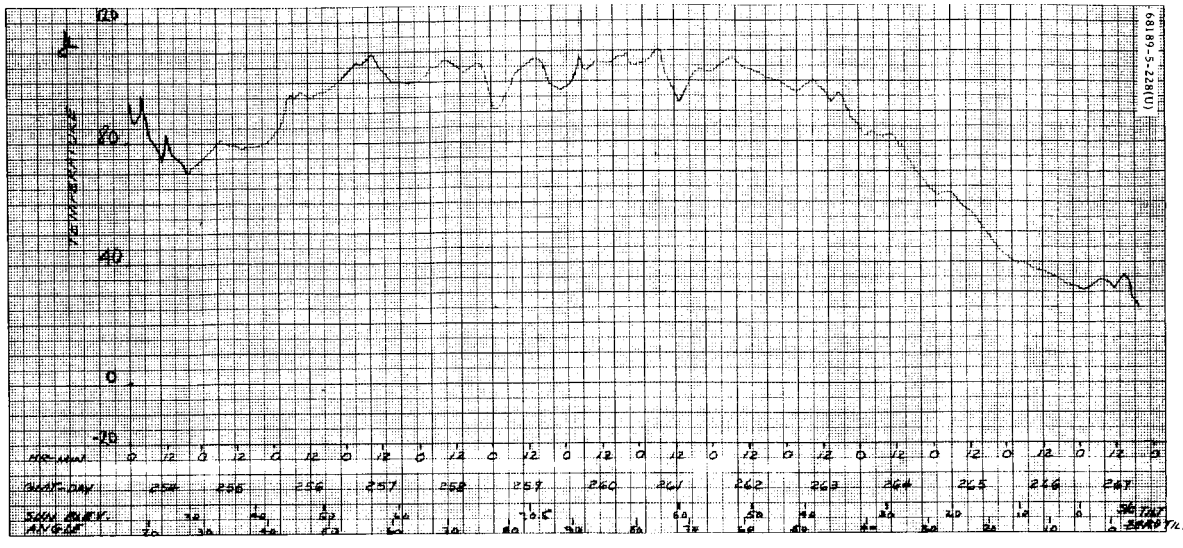

Figure 5.1-121. Sensor V-15: Compartment A Thermal Tray Temperature

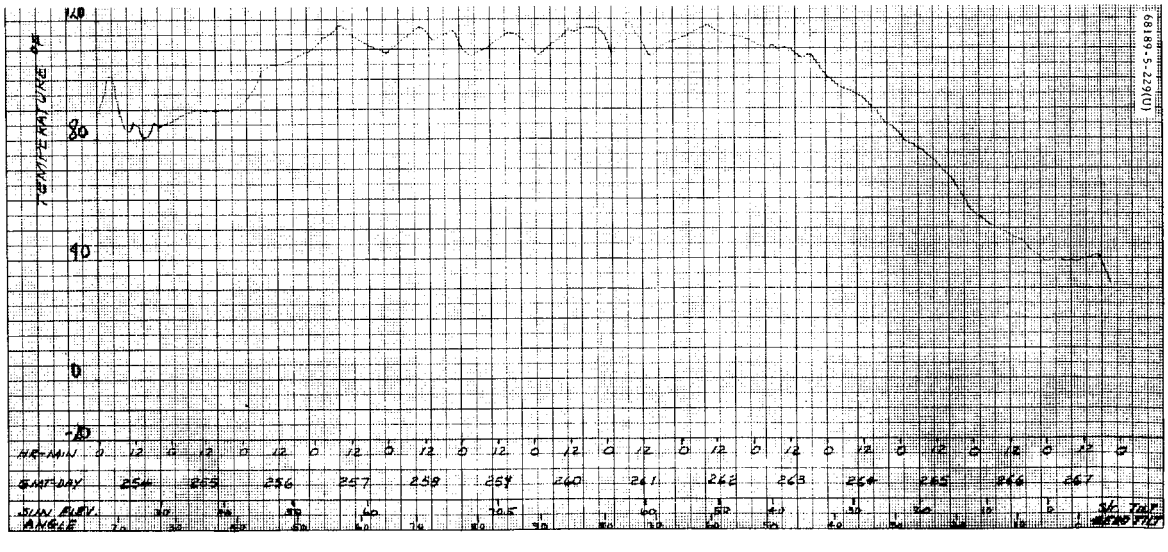

Figure 5.1-122. Sensor V-16: Compartment A Lower Support Temperature

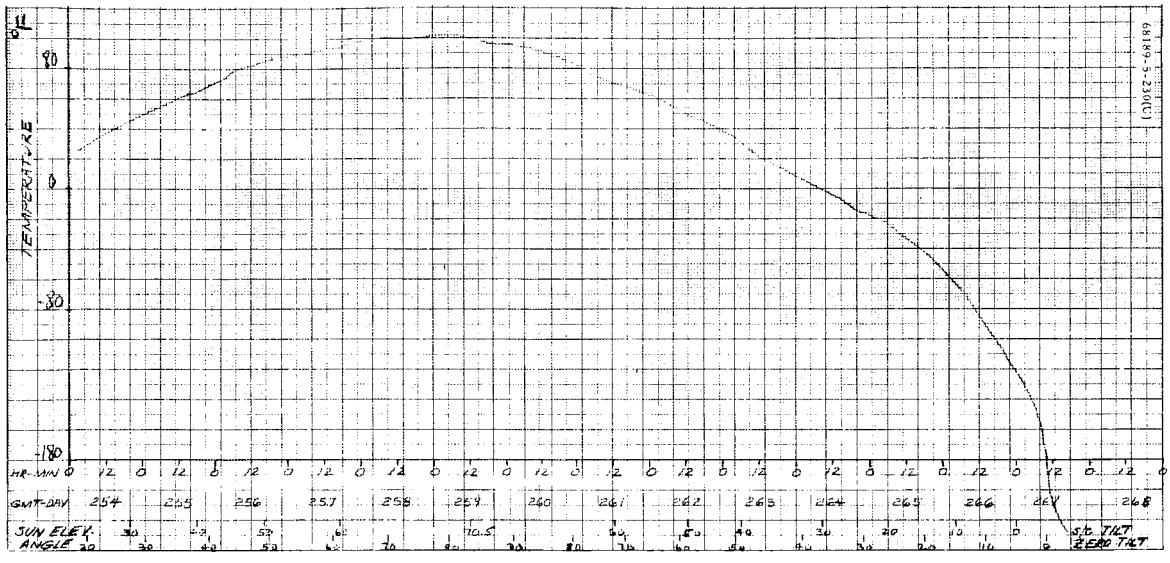

Figure 5.1-123. Sensor V-18: Compartment A Canister Temperature

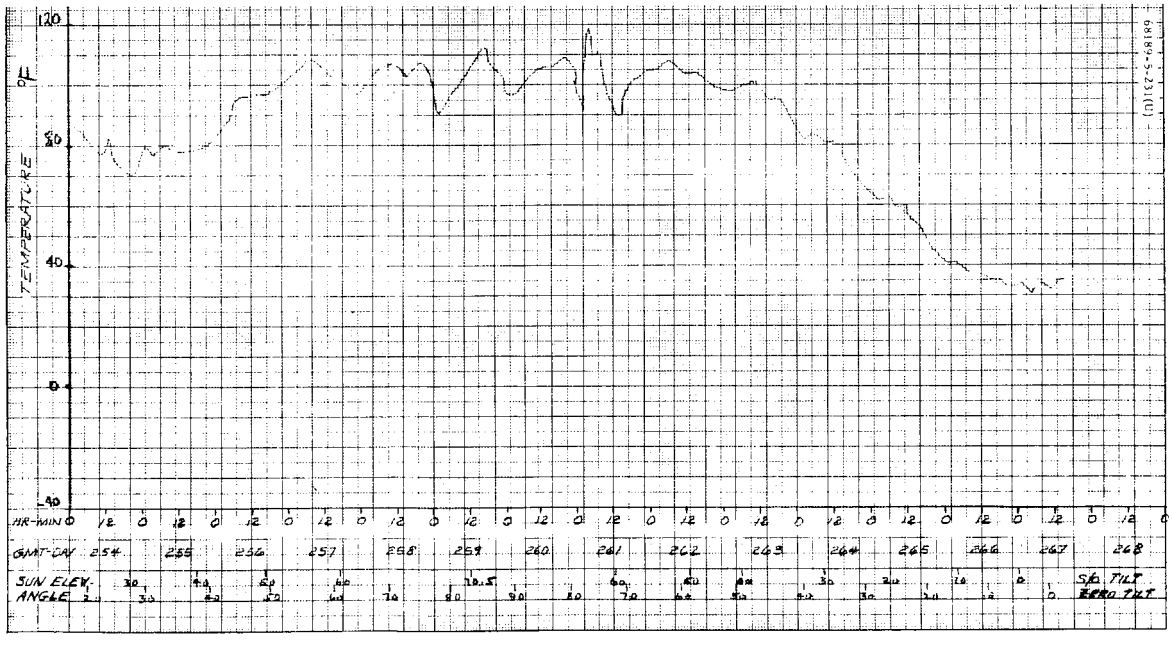

Figure 5.1-124. Sensor V-19: Compartment A Switch 5 Base Temperature

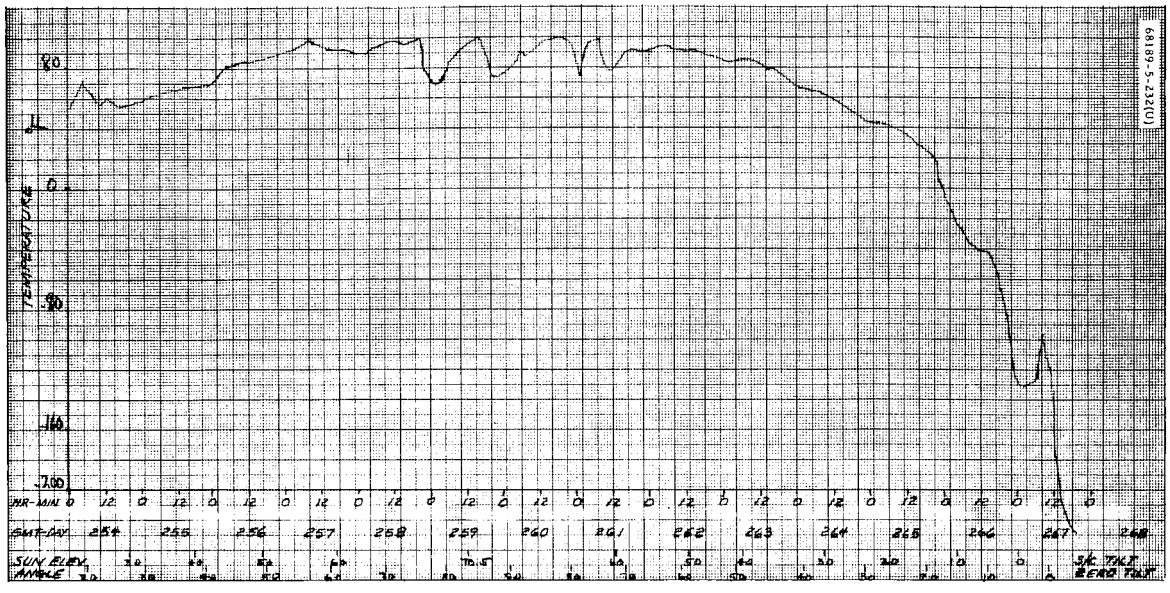

Figure 5.1-125. Sensor V-20: Compartment A Switch 5 in Face Radiator Temperature

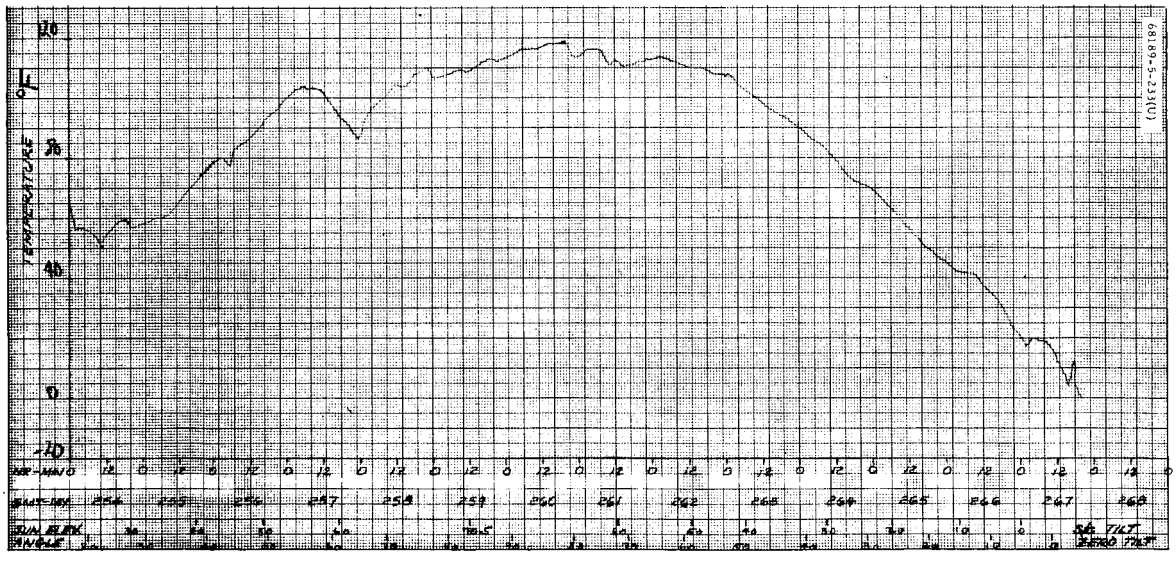

Figure 5.1-126. Sensor V-21: Compartment B Tray Top Center Temperature

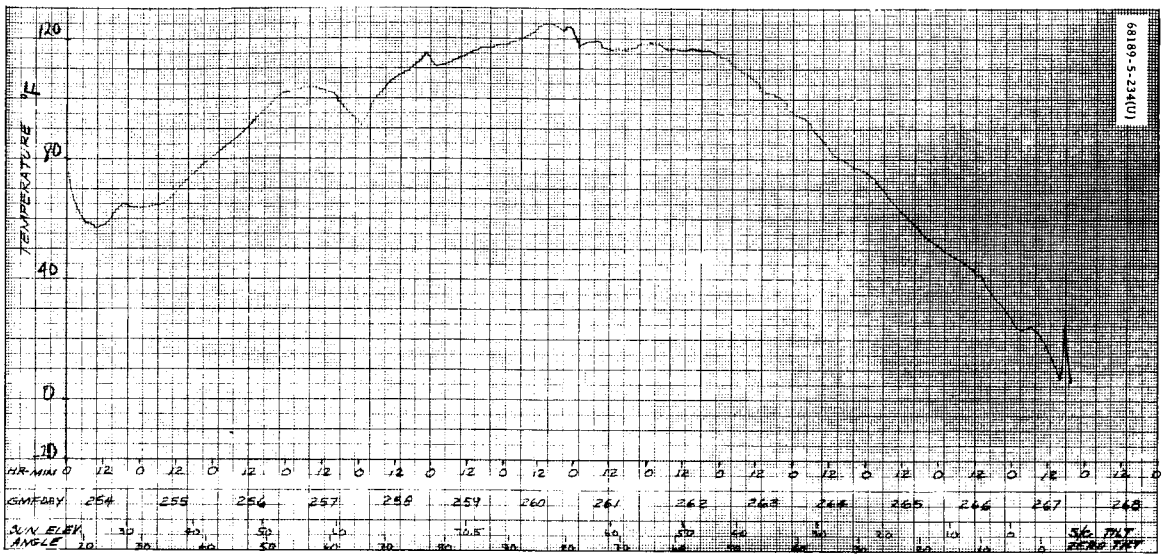

Figure 5.1-127 Sensor V-22: Compartment B Lower Support Temperature

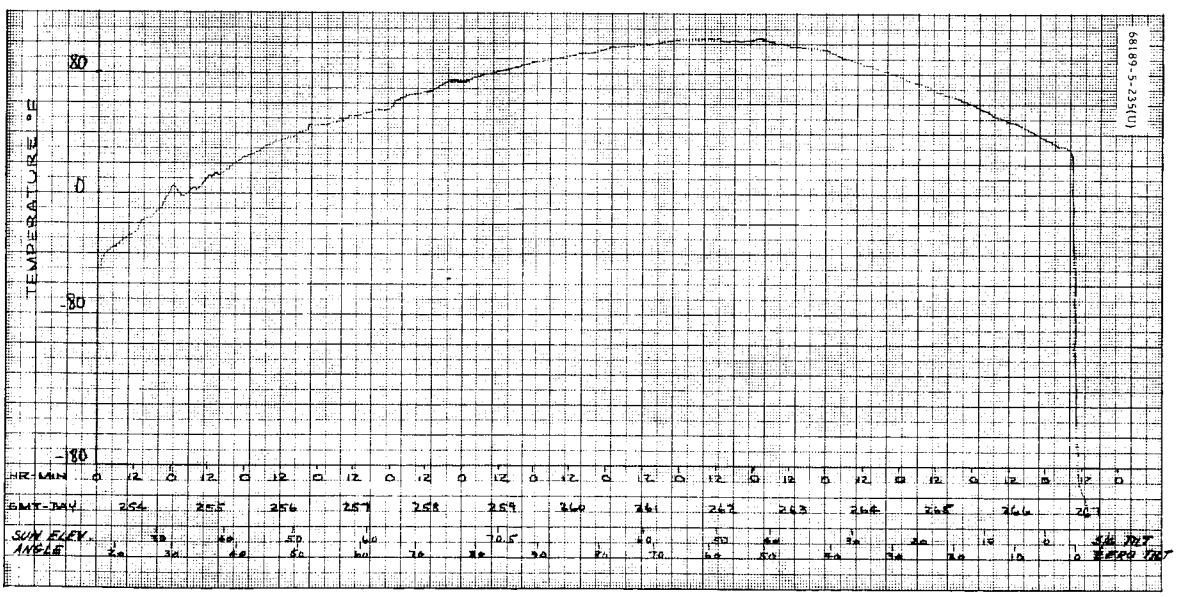

Figure 5.1-128. Sensor V-23: Compartment B Canister Temperature

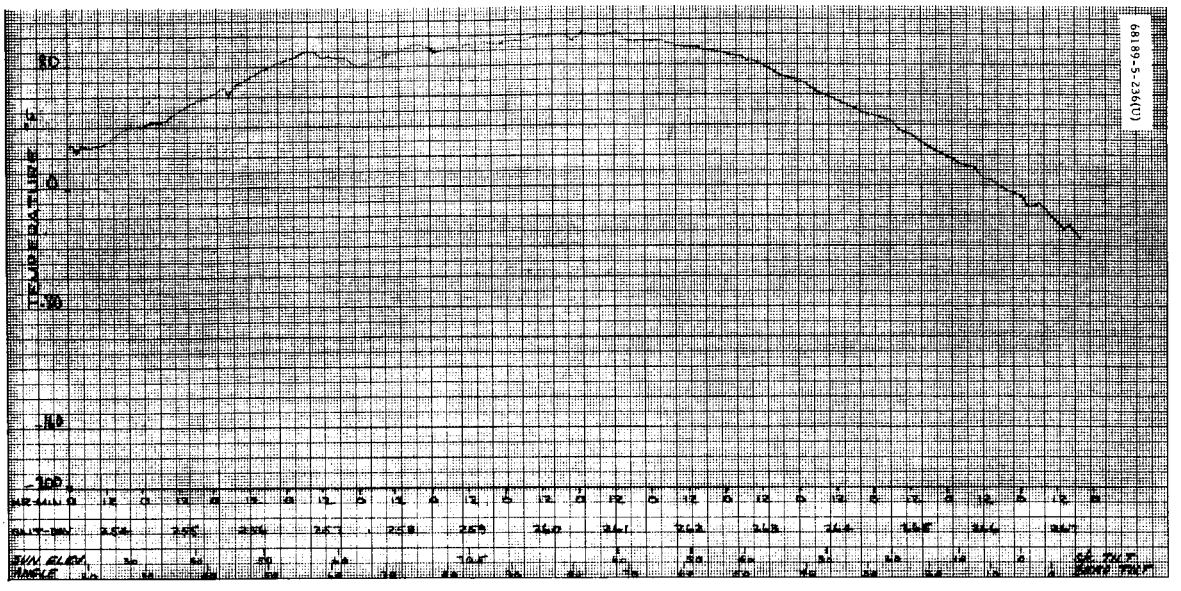

Figure 5.1-129. Sensor V-24: Compartment B Switch 4 in Face Radiator Temperature

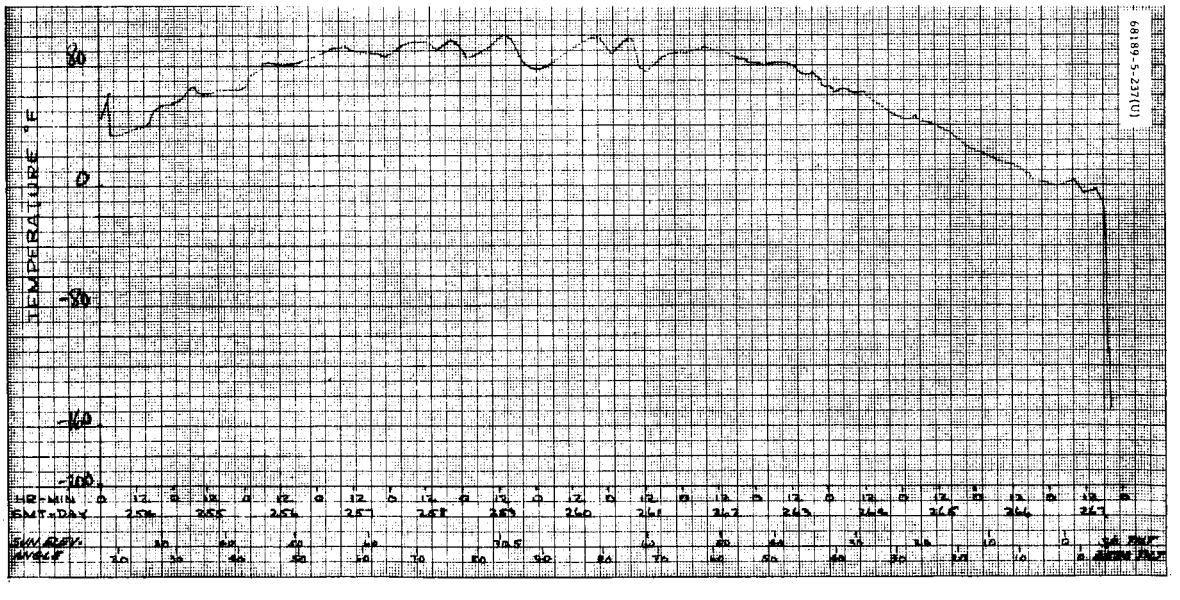

Figure 5.1-130. Sensor V-25: Compartment A Switch 8 in Face Radiator Temperature

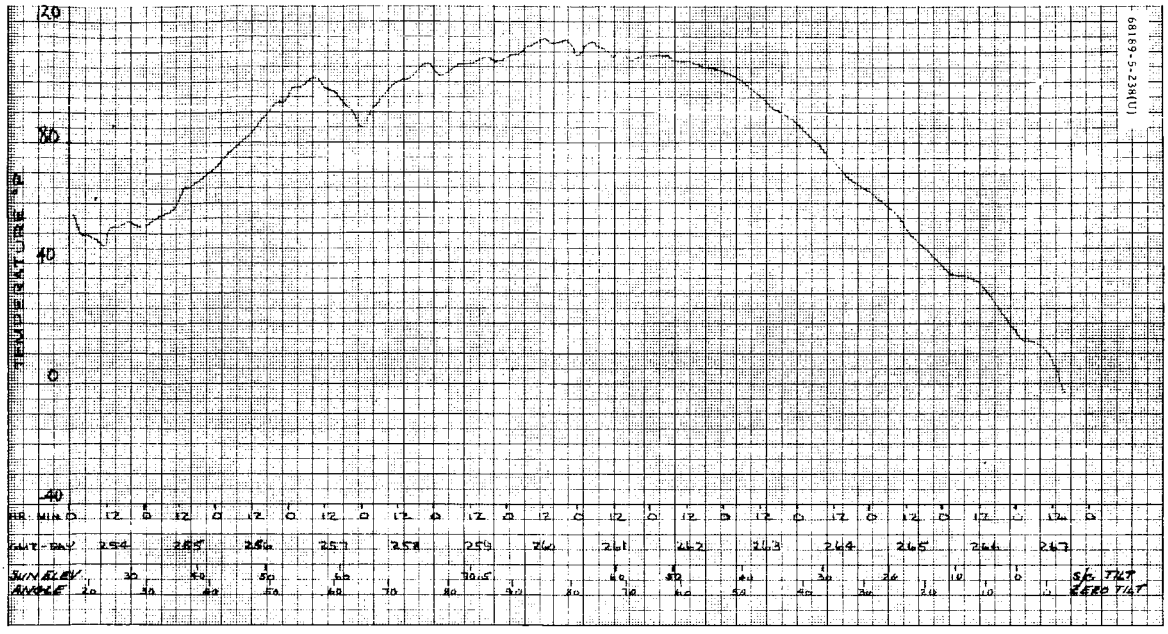

Figure 5.1-131. Sensor V-26: Compartment B Switch 4 Base Temperature

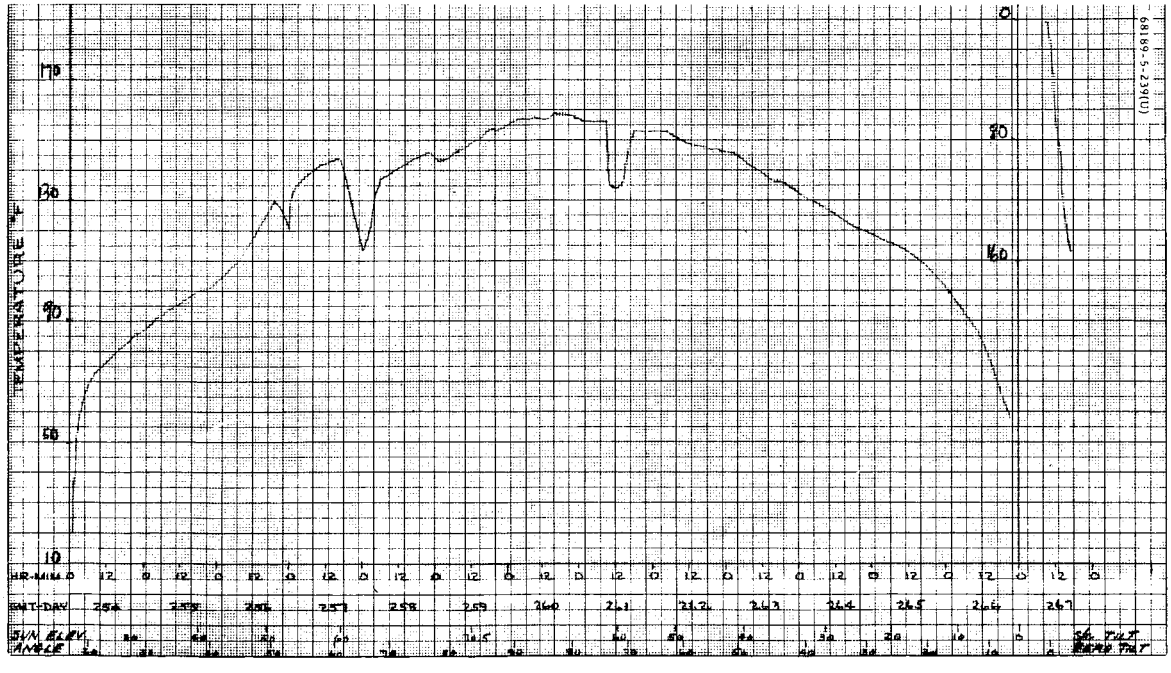

Figure 5.1-132. Sensor V-27: Upper Spaceframe 1 Temperature

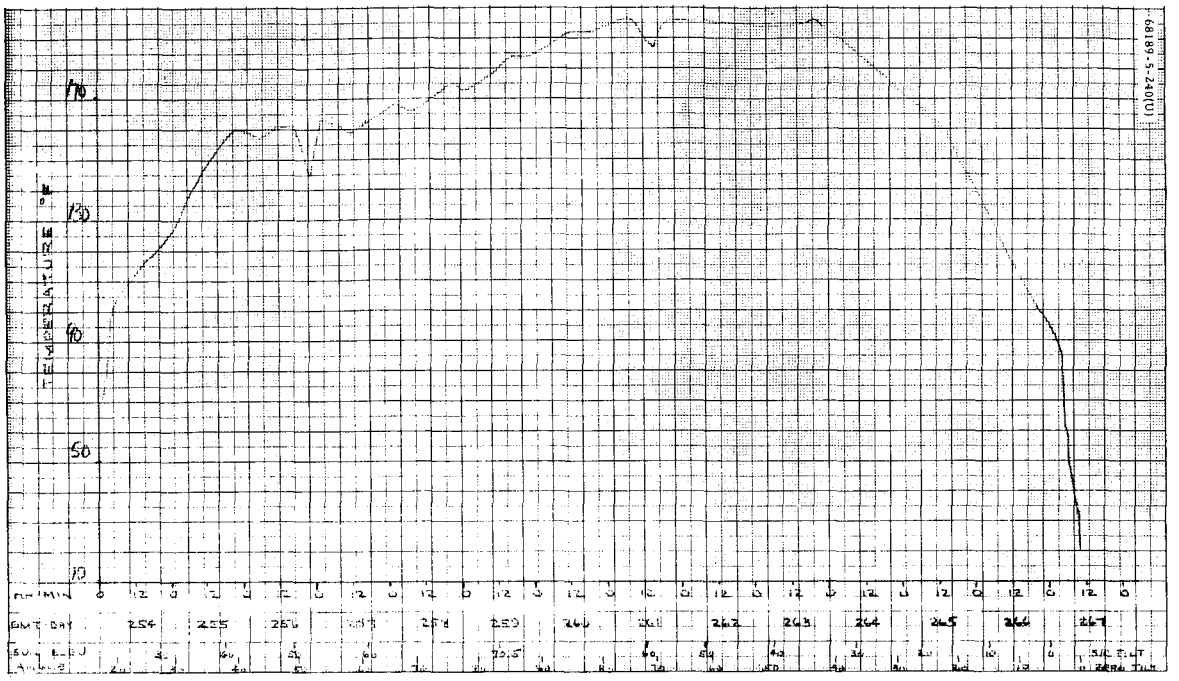

Figure 5.1-133. Sensor V-28: Spaceframe Temperature Under Compartment A

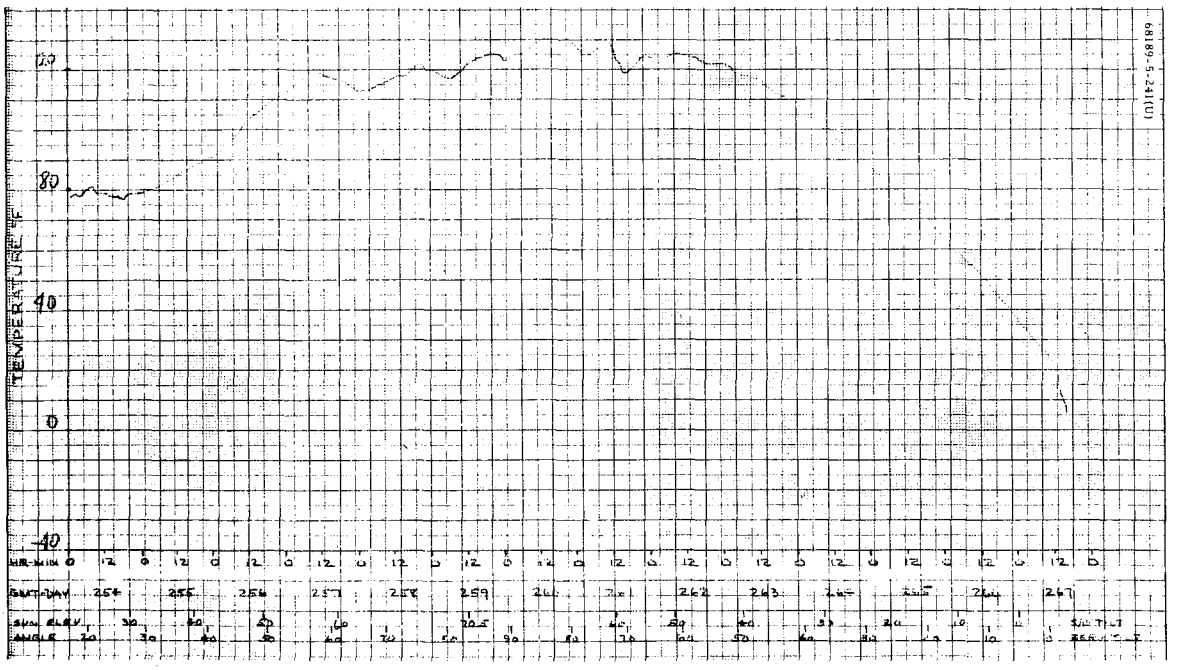

Figure 5.1-134. Sensor V-29: Wire Harness Temperature Thermal Tunnel

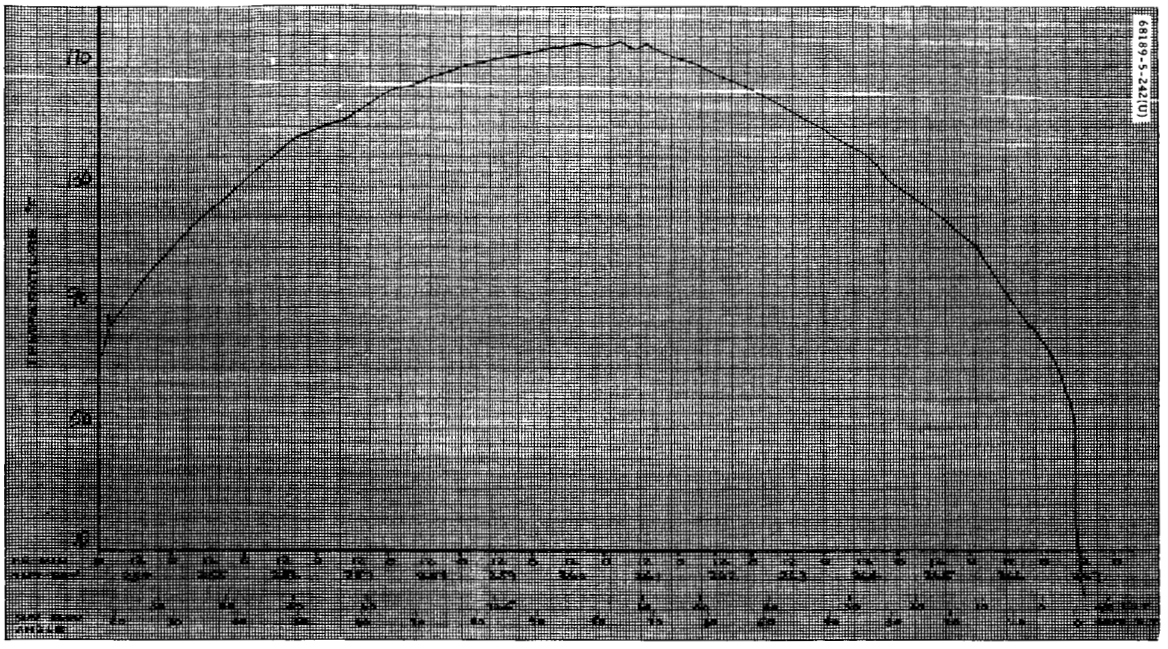

Figure 5.1-135. Sensor V-30: Shock Absorber 1 Temperature

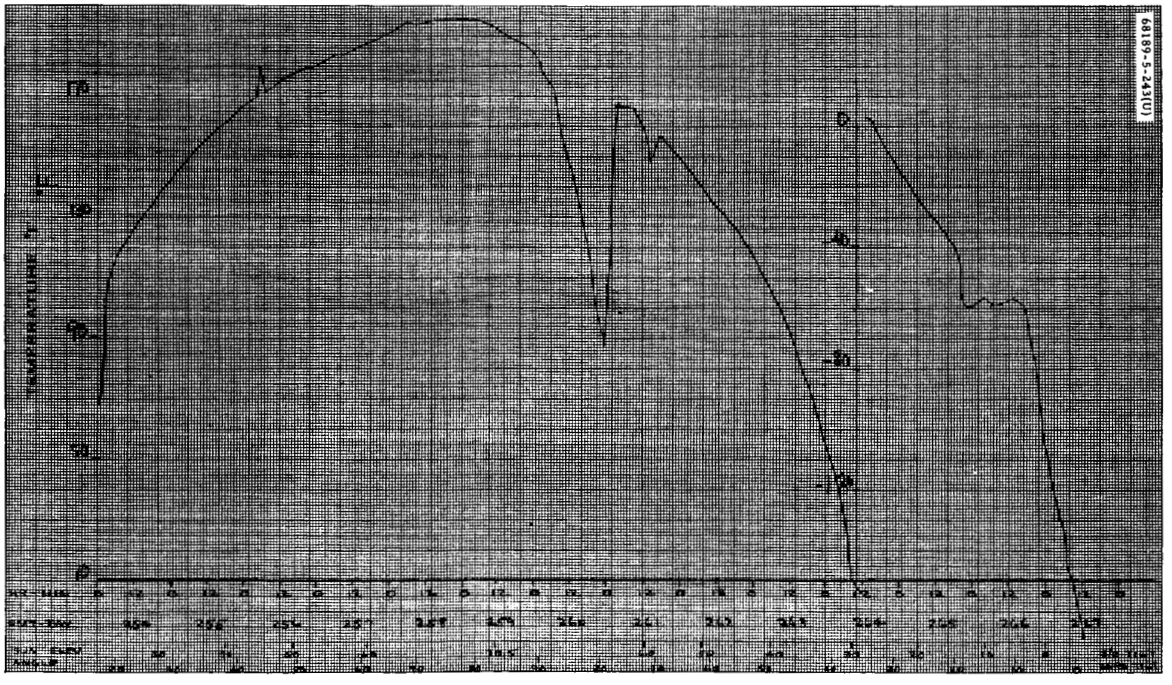

Figure 5.1-136. Sensor V-32: Shock Absorber 2 Temperature

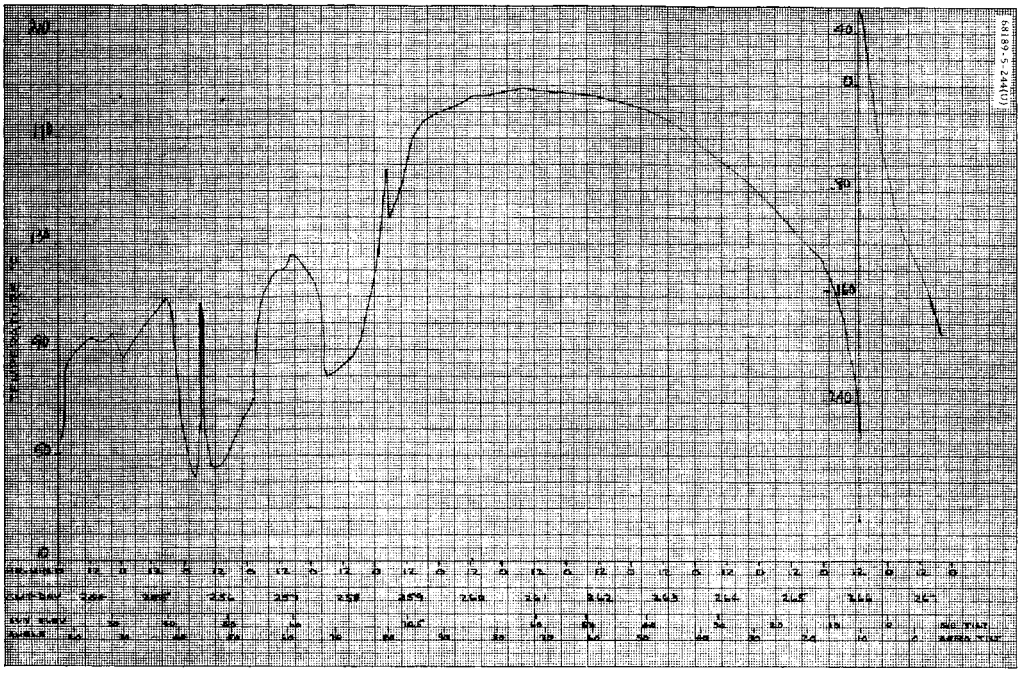

Figure 5.1-137. Sensor V-33: Shock Absorber 3 Temperature

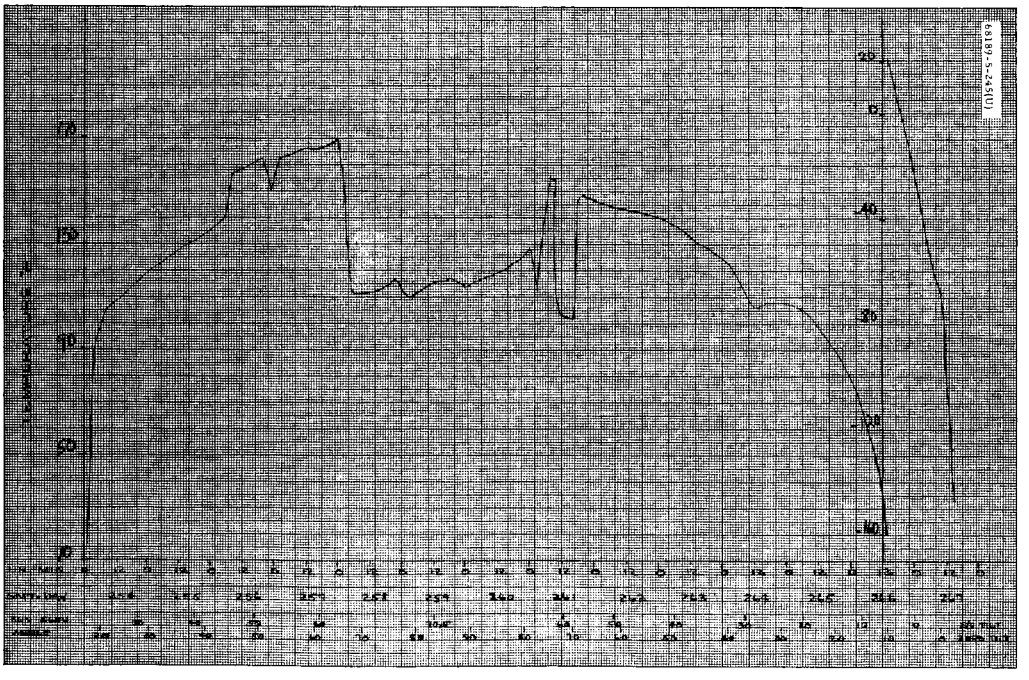

Figure 5.1-138. Sensor V-35: Upper Spaceframe 2 Temperature

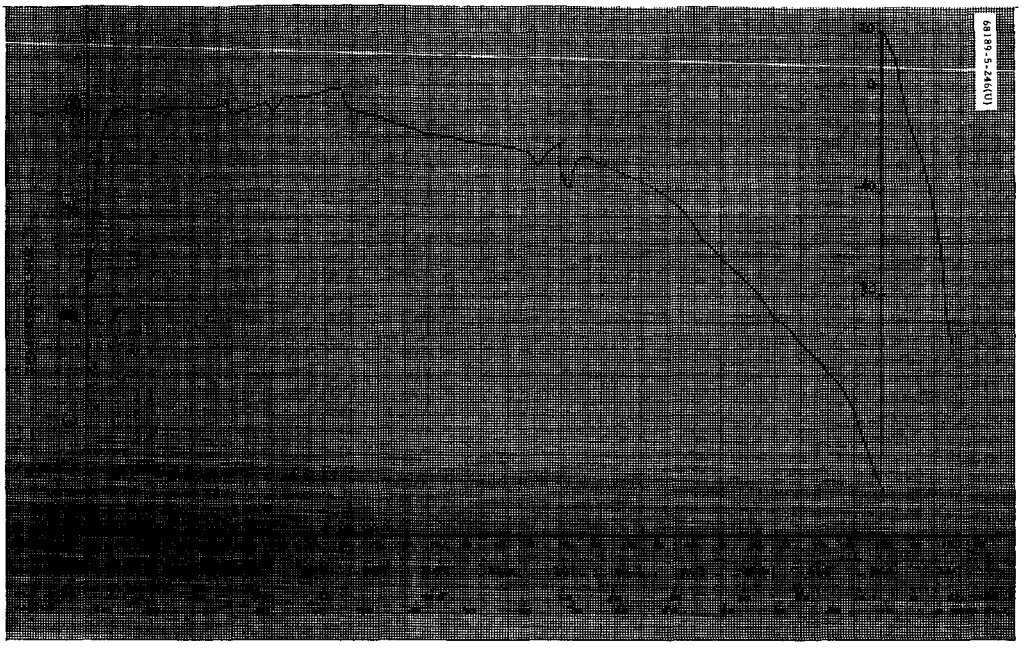

Figure 5.1-139. Sensor V-36: Spaceframe Temperature Under Compartment 3

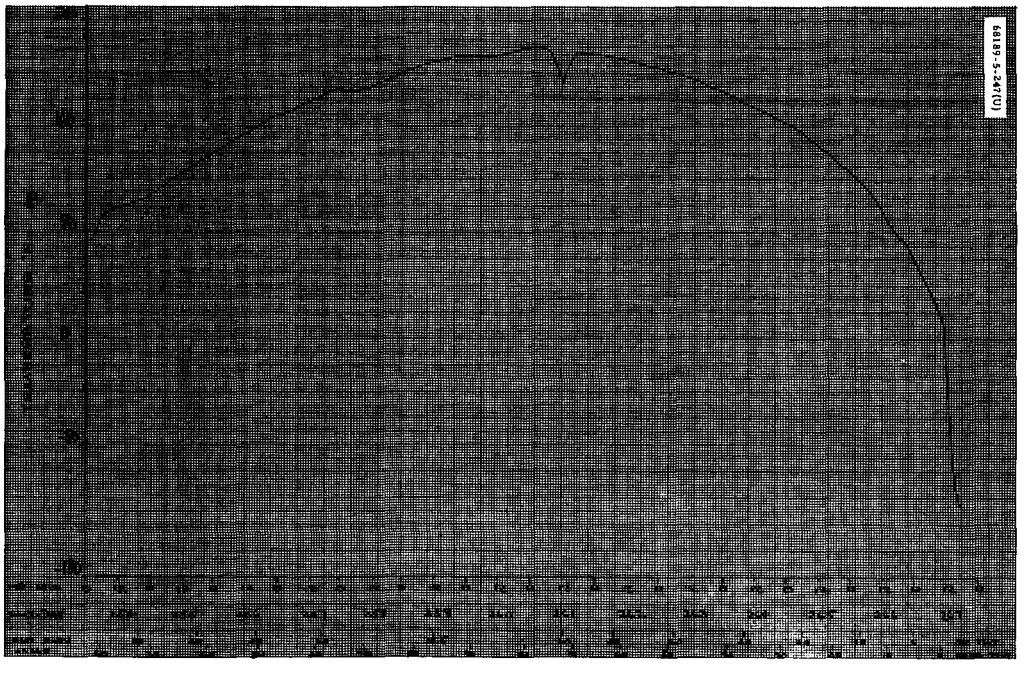

Figure 5.1-140. Sensor V-37: Retro Attach Point 1 Temperature

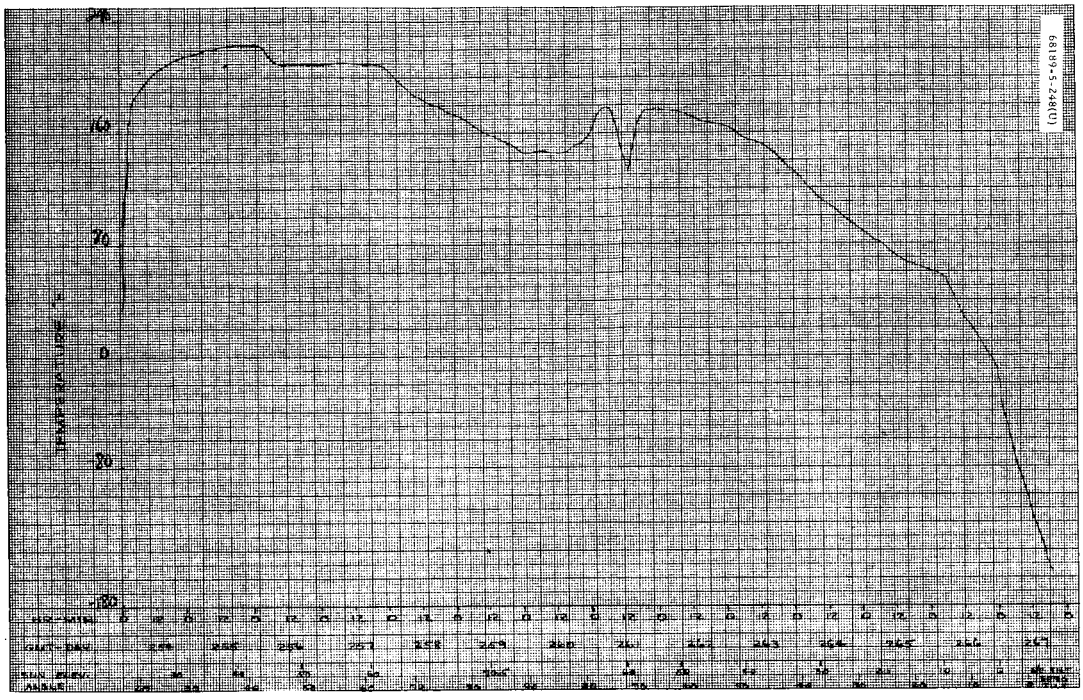

Figure 5.1-141. Sensor V-38: Retro Attach Point 2 Temperature

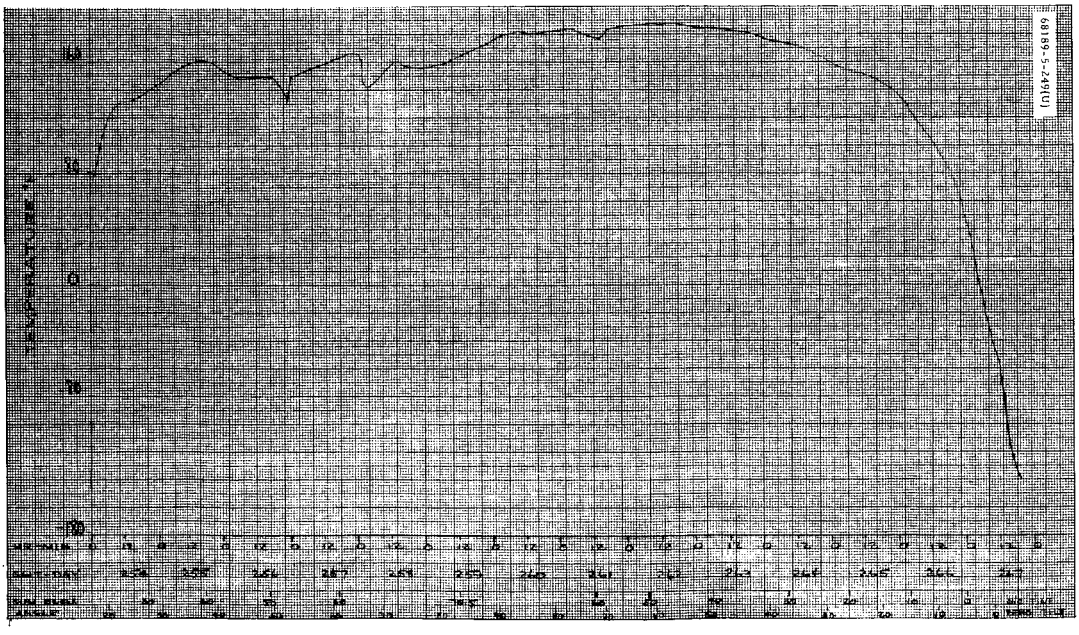

Figure 5.1-142. Sensor V-39: Retro Attach Point 3 Temperature

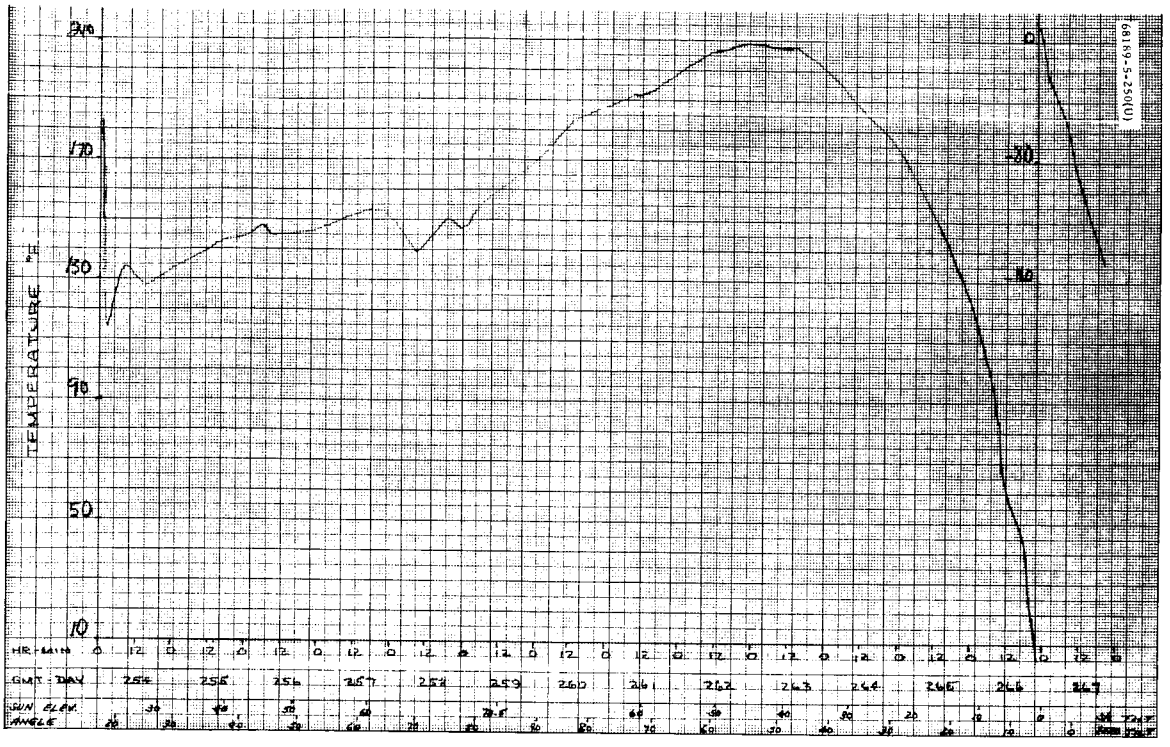

Figure 5.1-143. Sensor V-44: Crushable Block Temperature

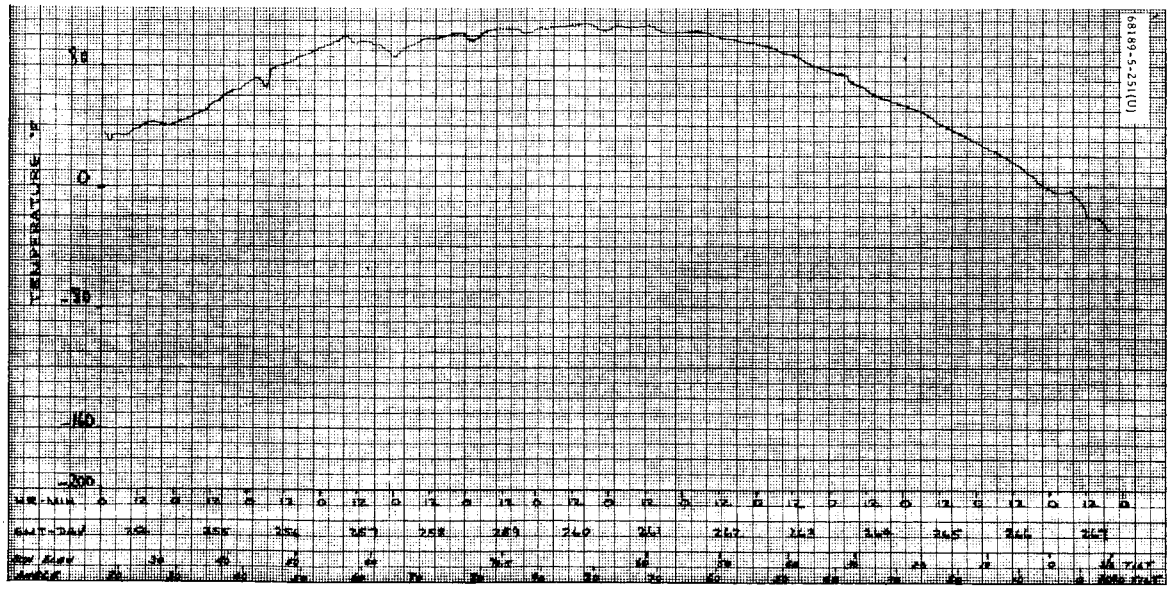

Figure 5.1-144. Sensor V-45: Compartment B Temperature Switch 1 in Face Radiator

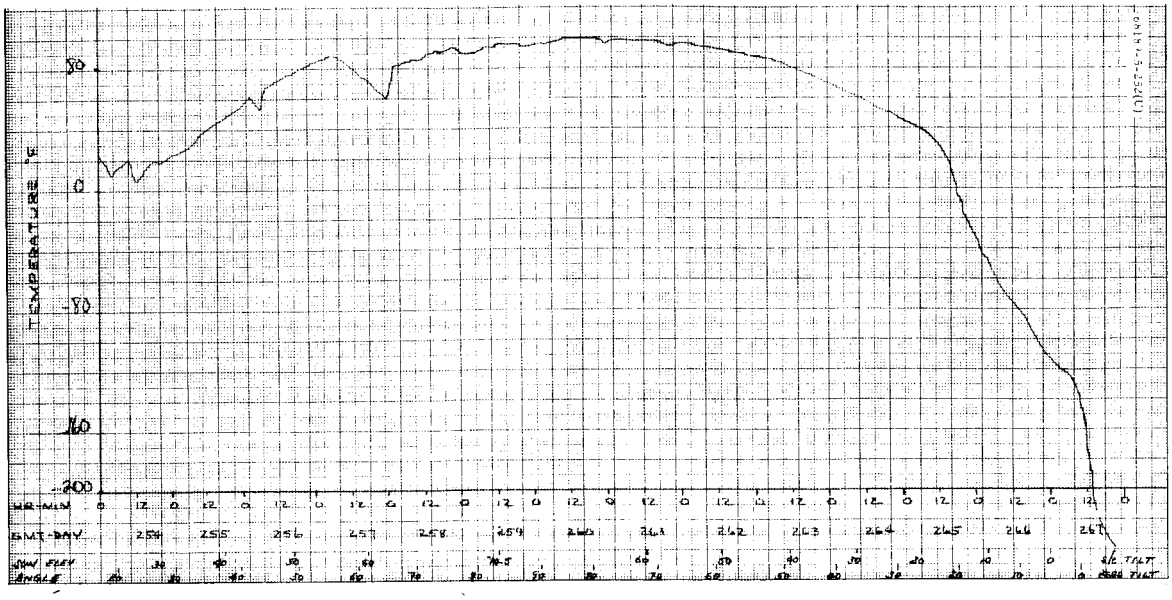

Figure 5.1-145. Sensor V-46: Compartment B Temperature Switch 5 in Face Radiator

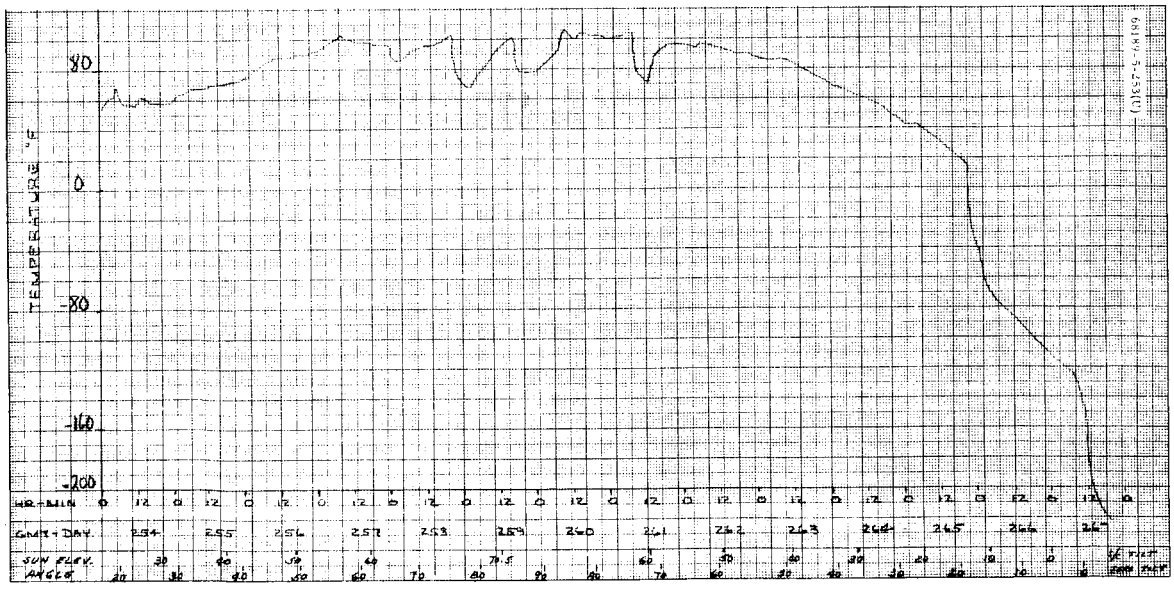

Figure 5.1-146. Sensor V-47: Compartment A Temperature Switch 2 in Face Radiator

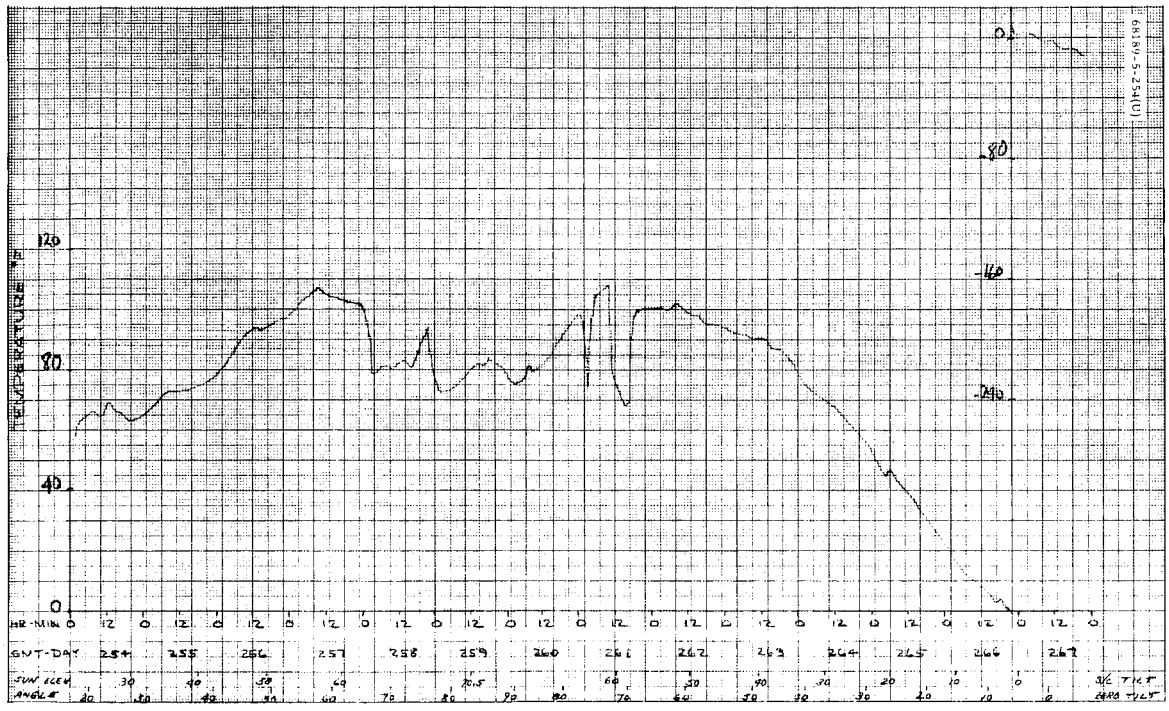

Figure 5.1-147. Sensor V-49: Compartment A Temperature Switch 3 in Face Radiator

5.2 ELECTRICAL POWER SUBSYSTEM

5.2.1 INTRODUCTION

The electrical power (EP) subsystem generates, stores, converts, and controls electrical energy for distribution to other spacecraft subsystems. There are two sources for this energy: storage batteries and radiant energy converted directly to electrical energy used for system loads or battery charging. During transit, the primary source of power is radiant energy via the solar panels. Figure 5.2-1 shows associated equipment groupings.

Performance of the EP subsystem during the Surveyor V flight, and first lunar day operation was nominal as compared to test data and simulation analysis predictions. Additional energy was extracted from the battery during the five additional burn periods that occurred after the initial midcourse. Nevertheless, the battery performed excellently through terminal descent and during the first lunar day. Solar panel energy output for the transit phase was slightly greater than expected. During the lunar phase, solar panel output was as predicted. All other units performed as anticipated.

Flight data were used to calculate solar panel input power and regulator efficiencies. Analysis of specific loads, comparison to prediction, and explanation of discrepancies will be made.

In Table 5.2-1, major events are presented in GMT. In general, the divisions of Table 5.2-1 correspond to flight phases of importance to the EP subsystem and may not correspond to flight phases in other subsections. Basically, the flight is divided into times corresponding to significant changes in electrical loads. Load changes corresponding to these flight phases are partially illustrated by the regulated current (EP-14) and more completely by the battery discharge current (EP-9).

5.2.2 ANOMALY DESCRIPTION

No anomalies were detected in the electrical power subsystem during the transit or the first lunar day.

PRECEDING PAGE BLANK NOT FILMED.

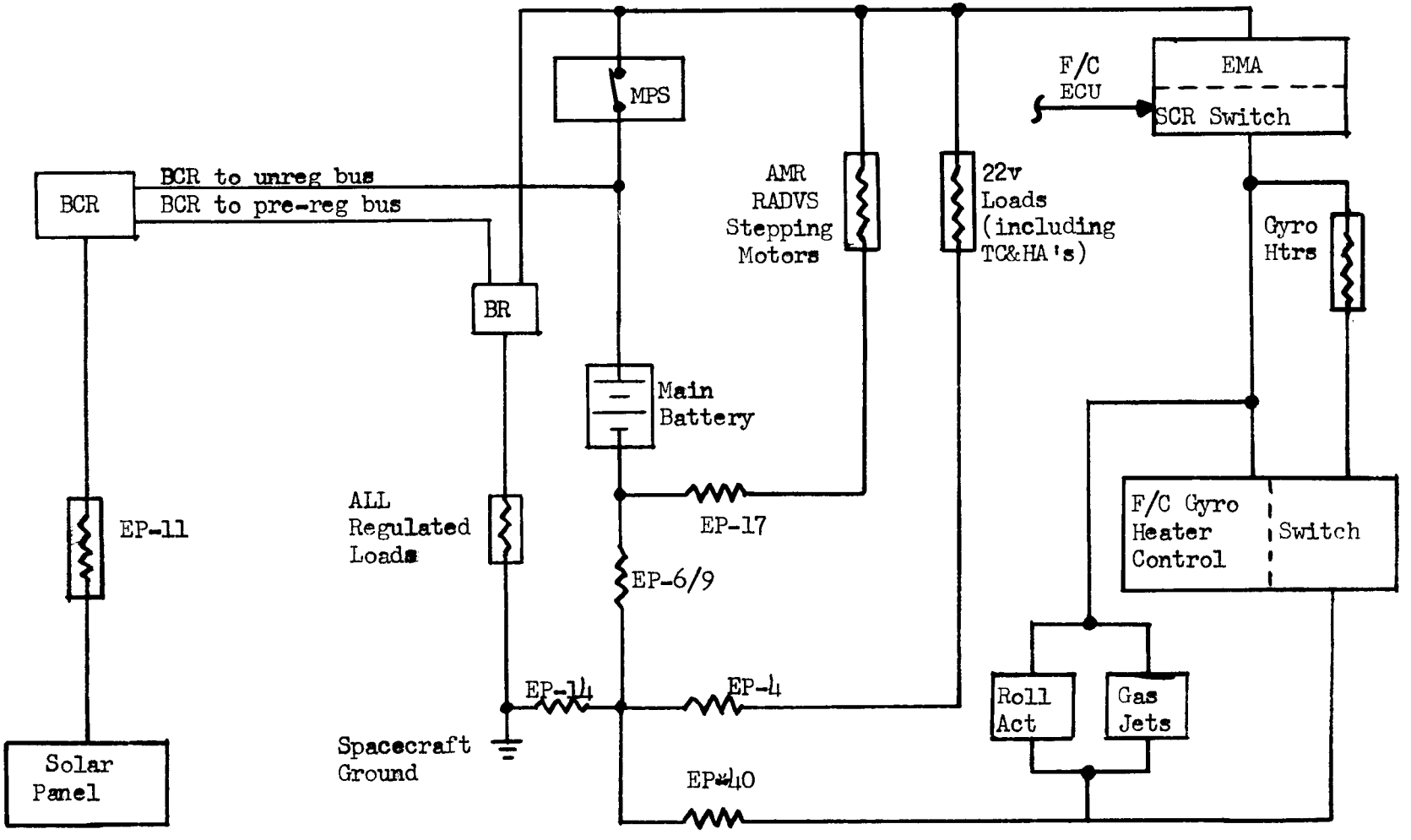

Figure 5.2-1 Power Subsystem Block Diagram, Flight Configuration

TABLE 5.2-1. ELECTRICAL POWER EVENTS AND TIMES

GMT, day:hr:min:sec		Comments
From	To	
251:07:57:01	251:08:16:26	Launch and separation
251:08:16:41	251:08:37:25	Transmitter high power
251:08:37:25	251:14:03:27	Coast
251:14:03:27	251:14:33:40	Coast, transmitter high power
251:14:33:40	252:01:15:32	Coast
252:01:15:32	252:01:43:15	Transmitter high power
252:01:43:15	252:01:45:35	Midcourse maneuver, transmitter high power, and flight control thrust phase power on
252:01:45:35	252:02:55:45	Vernier engine burn period, transmitter in high power
252:02:55:45	252:04:16:13	Coast
252:04:16:13	252:05:01:51	Vernier engine burn period, transmitter in high power
252:05:01:51	252:08:21:09	Coast
252:08:21:09	252:08:47:10	Vernier engine burn period, transmitter in high power
252:08:47:10	252:10:31:26	Coast
252:10:31:26	252:11:30:46	Transmitter high power
252:11:30:46	252:23:06:28	Coast
252:23:06:28	252:23:51:32	Vernier engine burn period, transmitter in high power
252:23:51:32	253:18:12:14	Coast
253:18:12:14	254:00:20:24	Transmitter high power, preretro maneuvers
254:00:20:24	254:00:44:48	Transmitter high power, AMR on, RADVS on, terminal descent and touchdown

5.2.3 SUMMARY AND CONCLUSIONS

5.2.3.1 Summary

Table 5.2-2 presents a summary of flight data for Surveyor V compared to test data for the electrical power subsystem.

5.2.3.2 Conclusion

Operation of the electrical power subsystem was nominal throughout the spacecraft's flight.

5.2.4 ANALYSIS

The analysis considers four areas: mission telemetry plots, power loads and sources budget, comparison of flight loads and flight acceptance test loads, and cyclic loads.

5.2.4.1 Mission Telemetry Plots

Figures 5.2-2 through 5.2-5 are selected mission plots which are pertinent to the EP subsystem. They represent line plots of the analog signals at 100-point averaging. Consequently, due to the scale of these plots and data averaging, they give excellent information for consideration of trends in data flow. The plots extend only to the first midcourse. Figure 5.2-6 gives actual RADVS load, and Figure 5.2-7 gives a plot on unregulated current (EP-4) prior to terminal descent.

5.2.4.2 Power Loads and Sources Budget

Energy Used

Table 5.2-2 contains a summary of energy expended as calculated from flight telemetry and predictions derived from solar thermal vacuum tests on specifications. Since solar panel output power was approximately 2.5 percent greater than expected, energy taken from the battery was less than predicted.

Power Data

Incorporation of the new power subsystem into Surveyor V required a revision for efficiency calculations. Efficiencies for the transit portion of the mission were calculated as follows:

1) BCR Efficiency

$$\mathrm{Eff}_{BCR} = \frac{(EP\text{-}30)\,(EP\text{-}11 - 0.125)}{(EP\text{-}10)\,(EP\text{-}11)} \times 100$$

TABLE 5.2-2. ELECTRICAL POWER SUMMARY

Item	Flight Data	Predicted or Specification
Boost regulator efficiency, transmitter low power, percent	80	77 (minimum)
Boost regulator efficiency, transmitter high power, percent	86	82 (minimum)
Battery charge regulator efficiency	94.5	93.3 (minimum)
Battery charge regulator output energy, w-hr	5226	5070*
Solar panel output power, watts	85.5	81 (minimum)
Battery energy used, w-hr	1782	2090*
Total energy used, w-hr	7008	7160
Selected loads		
Transmitter B high power, watts	56.09	58.0
Transmitter B filament power, watts	3.13	2.9
Flight control thrust phase power on		
Regulated, watts	29.61	31.32
Unregulated, watts	12.51	11.66
AMR on, watts	40.96	41.53
AMR enable, watts	31.55	31.60
RADVS power on, watts	530.21	551
Vernier ignition		
Midcourse, watts (first midcourse)	37.1	39.6
Terminal descent, watts	33.86	39.6
Vernier line 2 heater, watts (29 percent duty cycle)	1.91	6.6 (maximum)
Altitude marking radar heater, watts (64.3 percent duty cycle)	3.23	5.04 (maximum)
Gyro heater, watts (28.7 percent duty cycle)	9.48	33.0 (maximum)

*Predictions derived from solar thermal vacuum tests.

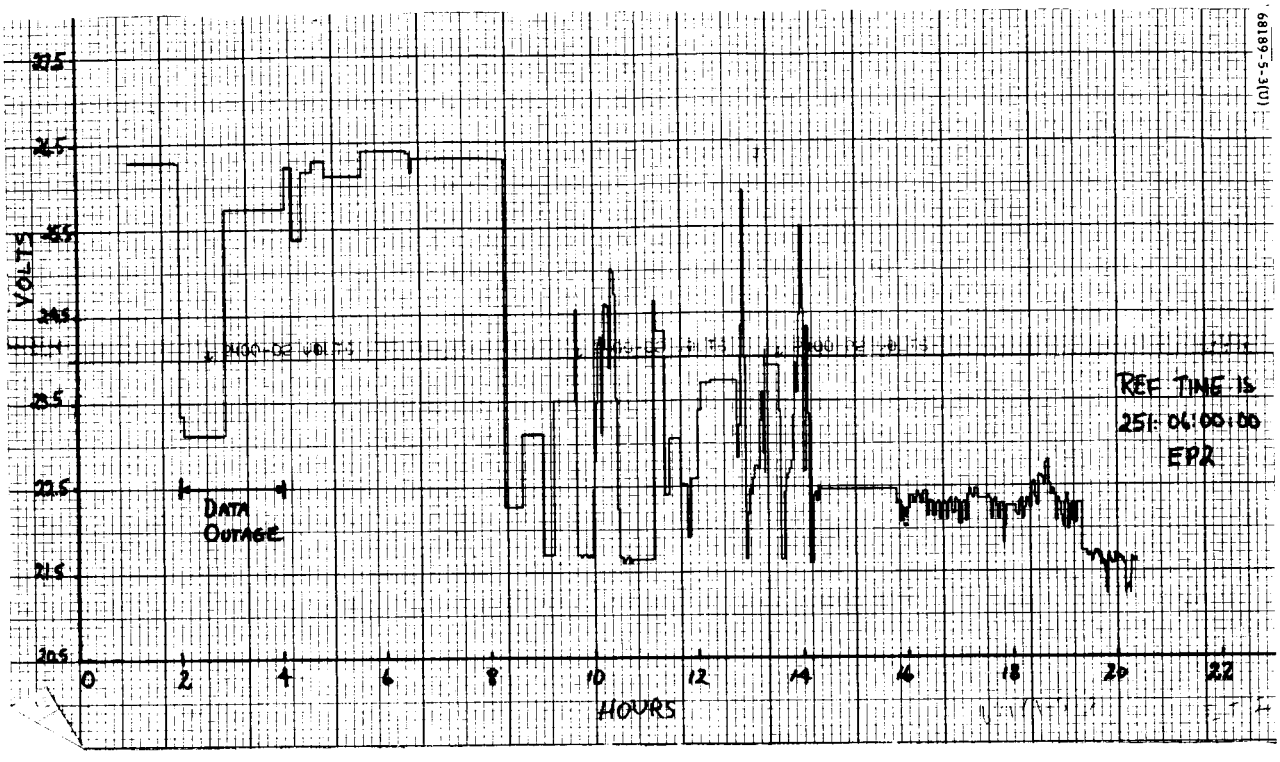

Figure 5.2-2. Unregulated Bus Voltage — Averaged Data

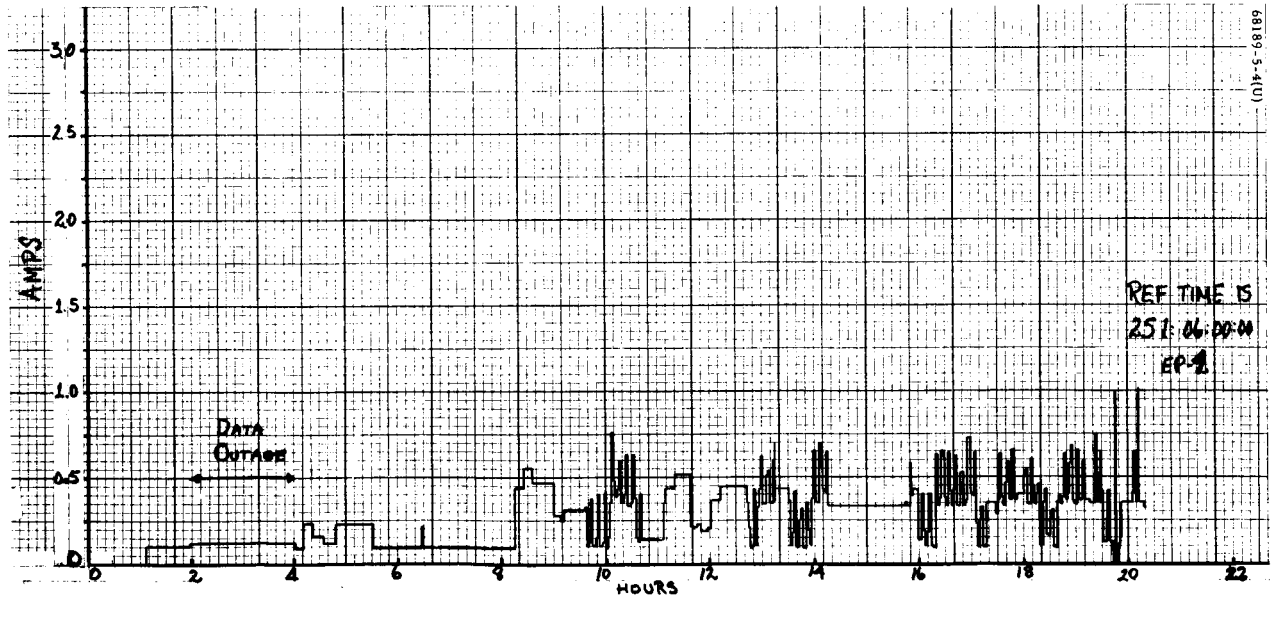

Figure 5.2-3. Unregulated Output Current (EP-4) — Averaged Data

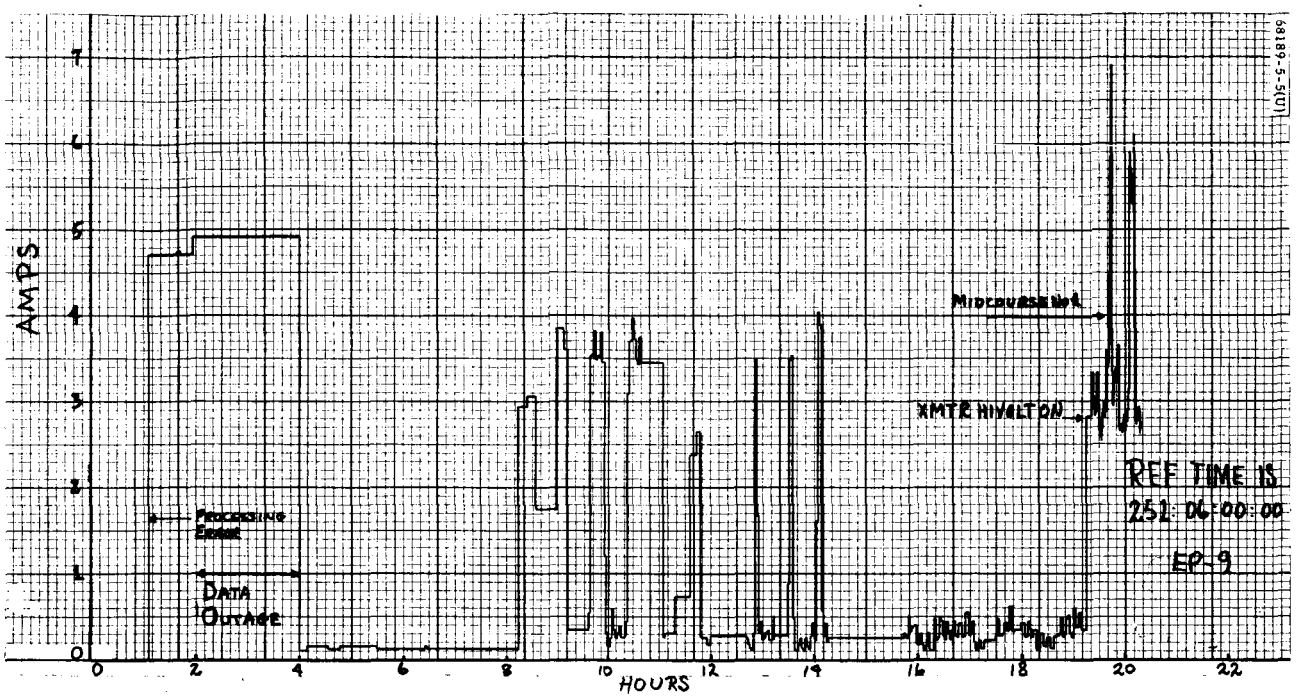

Figure 5.2-4. Battery Discharge Current — Averaged Data

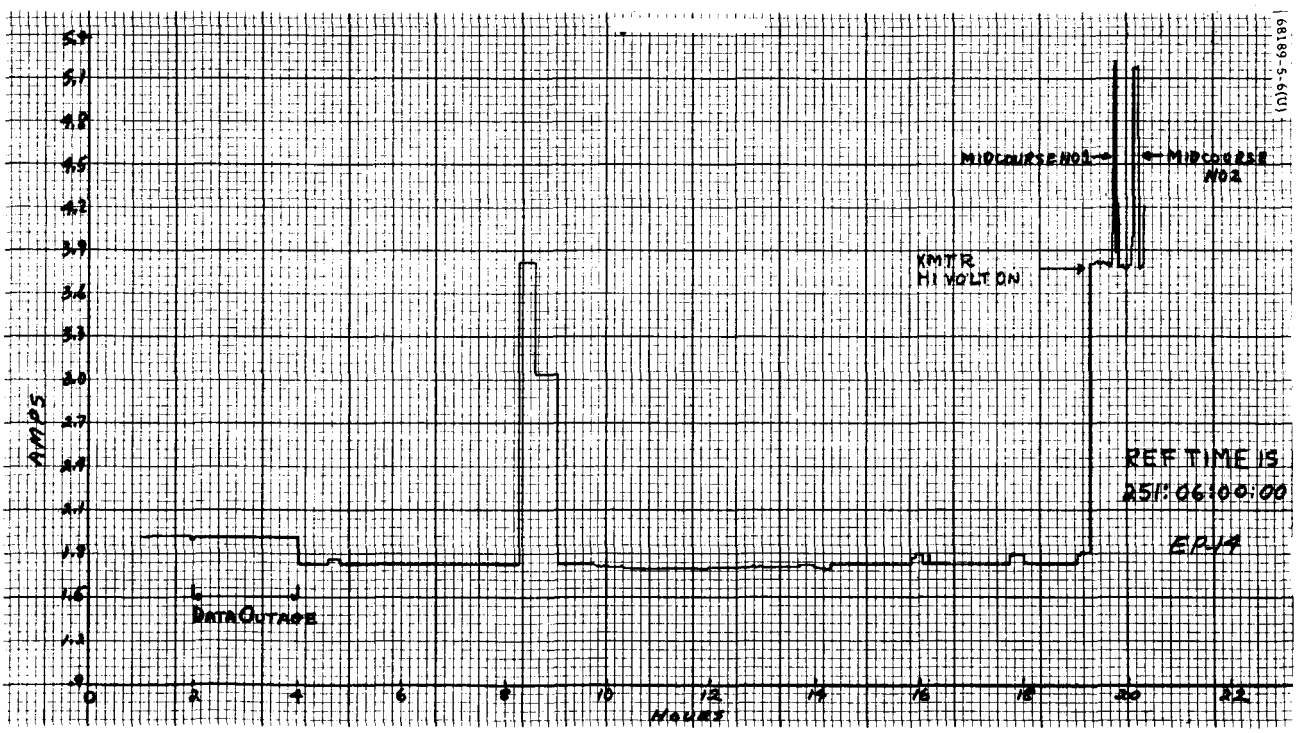

Figure 5.2-5. Regulated Output Current — Averaged Data

where (EP-11 - 0.125) is the output of the BCR. EP-11 represents solar panel output and 0.125A the loss in the BCR. No shunt is provided to measure output current.

2) BR Efficiency

a) For EP-14 < BCR output.

$$Eff_{BR} = \frac{(EP\text{-}1)\,(EP\text{-}14) + (EP\text{-}2)\,(EP\text{-}11 - 0.125 - EP\text{-}14/0.92)}{(EP\text{-}30)\,(EP\text{-}11 - 0.125) + (EP\text{-}2)\,(EP\text{-}7)} \times 100$$

where EP-14/0.92 represents input to the postregulator (postregulator efficiency is estimated at 92 percent).

b) For EP-14 > BCR output.

$$Eff_{BR} = \frac{(EP\text{-}1)\,(EP\text{-}14)}{(EP\text{-}30)\,(EP\text{-}11 - 0.125) + (EP\text{-}2)\,\left[EP\text{-}7 + EP\text{-}14/0.92 - (EP\text{-}11 - 0.125)\right]}$$

Efficiency data provided in Table 5.2-2 represent an average of values derived from the CDS computer which was programmed to make the above efficiency calculations.

5.2.4.3 Comparison of Flight Loads and Flight Acceptance Test Loads

Comparison of telemetry-measured and flight acceptance test-measured loads (Reference 1) will be made for selected units, various heaters, and large current drains.

Selected Equipment Loads

Results of comparing flight and test specification selected equipment loads are presented in Table 5.2-3. The loads and equipments considered are as follows:

1) Transmitter High Voltage On. Command 0106 turns on the high voltage power supply. Flight data compares favorably with data taken during flight acceptance tests.

2) RADVS Power On. Command 0637 applies power to the RADVS. The power consumed is close to that expected. Figure 5.2-6 (EP-17, radar and squib current) shows the current profile.

3) Flight Control Thrust Phase Power On. Command 0727 turns on the thrust phase dc power supply in the flight control unit. Load current for the thrust phase command was consistent with flight acceptance test data.

TABLE 5.2-3. SELECTED EQUIPMENT LOADS

Command(s)*	Command Time, GMT, day:hr:min:sec	Current, milliamperes		Power, watts	
		Flight	Specification (Reference 1)	Flight	Specification (Reference 1)
Flight control thrust phase power on (0727)	Midcourse 252:01:43:16				
R		1204	1210	34.916	35.09
U		410	480	9.02	10.56
R	Terminal 254:00:41:00	1178	1210	34.16	35.09
U		395	480	8.69	10.56
Transmitter B (0106)	252:01:15:19				
R		1934	2000	56.09	58.0
Filament B power on	252:01:13:26				
R		108	100	3.13	2.9
Vernier ignition (0721)	Midcourse 252:01:45:01				
U		1749	1800	37.1	39.6
U	Terminal 254:00:44:46	1678	1800	33.86	39.6
AMR on (0626)	254:00:40:00				
U		1845	1886	40.96	41.53
AMR enable (0625)	254:00:43:00				
U		1524	1439	31.55	31.60
RADVS power on (0637)	254:00:44:55				
U		28910	29000	530.21	551

*R = regulated; U = unregulated.

Gyro Heater

The periodic loading that occurs in EP-40 contains gyro heater effects. The gyro heaters have a short on-off cycle when compared to the altitude marking radar (AMR) and vernier line heaters (EP-4). Each gyro heater load is approximately 0.48 ampere, which compares favorably to the flight acceptance test data.

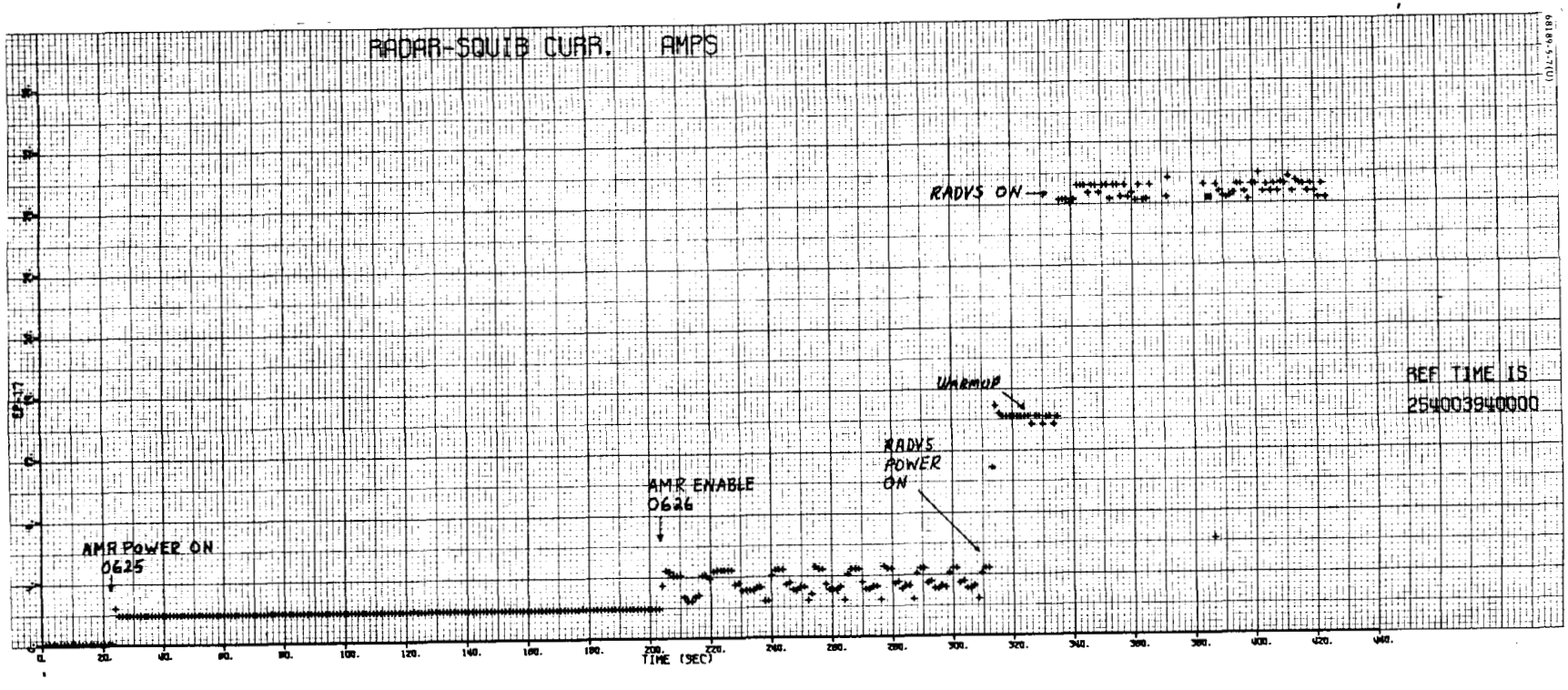

Figure 5.2-6. Radar and Squib Current (RADVS) Power On

AMR and Vernier Line Heaters

Figure 5.2-7 is a plot of EP-4 at 20 sec/in. Gyro heater effects are noted on a separate shunt. The cyclic load effects of the vernier line 2 heater are apparent. Only the AMR and vernier line 2 heaters are cyclic at this time. The vernier line 2 heater uses approximately 283 milliamperes, and the AMR heater draws about 230 milliamperes. This agrees favorably with test data, indicating that vernier line 2 heater should draw about 300 milliamperes and that the AMR heater should draw about 230 milliamperes.

5.2.5 REFERENCE

1) J. Mundy, "System Specification Power Management Data Summary SC-5 Spacecraft," Hughes Aircraft Company, No. 302393, Revision A, 25 August 1967.

5.2.6 ACKNOWLEDGMENTS

N. J. Kaman, technical coordinator and writer.

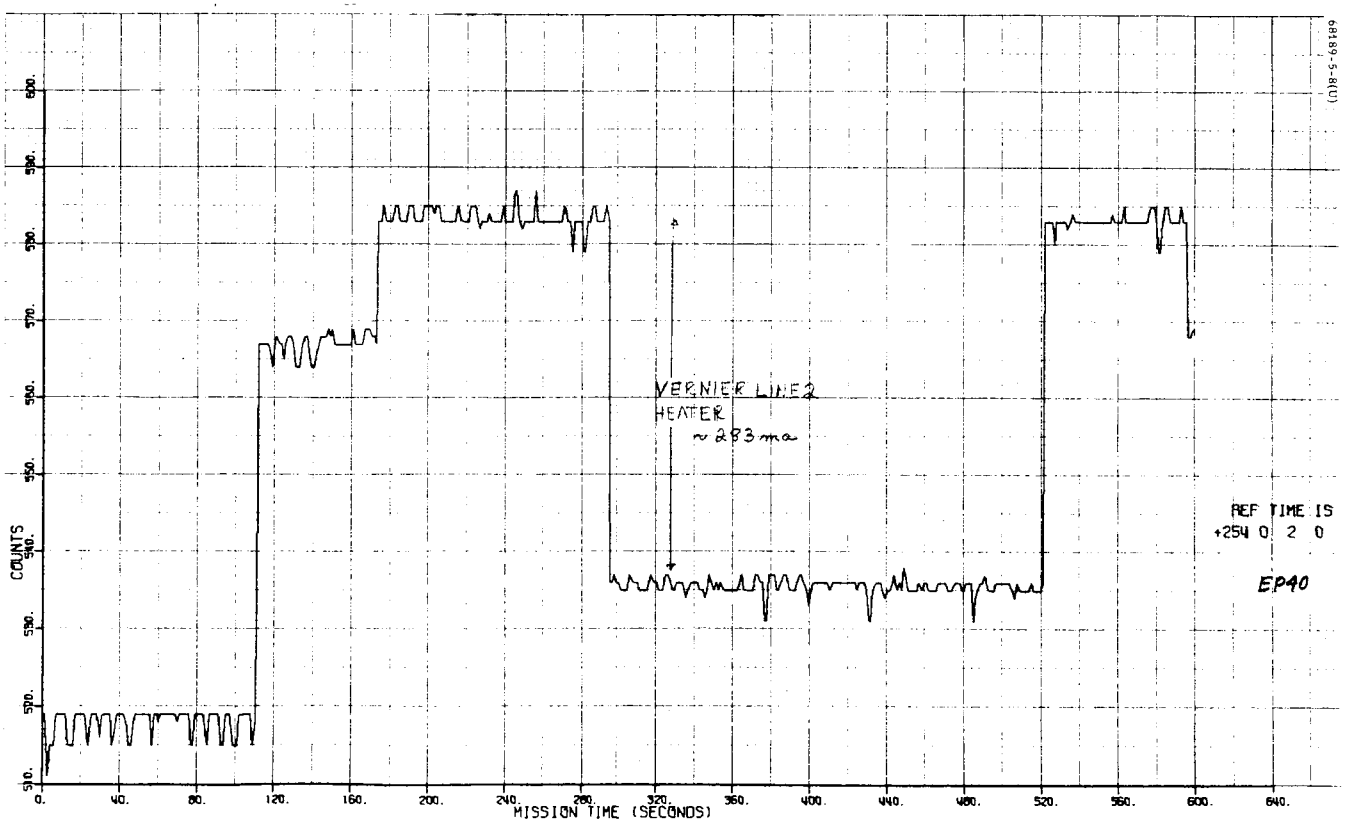

Figure 5.2-7. Unregulated Output Current — Coast II

5.3 RF DATA LINK SUBSYSTEM

5.3.1 INTRODUCTION

This section contains a summary and analysis of the performance of the data link subsystem during Surveyor Mission E.

The data link subsystem consists of the transmitters, transponders, receivers, command decoders, and antennas. It is the function of this subsystem to: 1) provide engineering data transmission from the spacecraft at bit rates compatible with specific mission phases, 2) provide analog data, such as that from television and strain gauges, at signal levels high enough for proper discrimination, 3) provide phase coherent two-way doppler for tracking and orbit determination, and 4) provide command reception capability throughout the mission to allow for complete control of the spacecraft from the ground. A simplified block diagram of the communications subsystem is shown in Figure 5.3-1.

The pertinent subsystem units on the spacecraft during the mission are as follows:

Unit	Part Number	Serial Number
Receiver A	231900-3	19
Receiver B	231900-3	20
Transmitter A	3024400-1	12
Transmitter B	3024400-1	14
Command decoder unit	232000-5	6

Unlike most subsystems, individual data link subsystem parameters, such as losses, threshold sensitivity, modulation index, etc., are not measured or individually determined from mission data. The composite effect of these parameters on the performance is measured as received signal power at the spacecraft and the tracking station (DSS) and as telemetry and command error rates. Consequently, it is impossible to compare individual link parameters to specified performance criteria. The best that can be done is to compare measured signal levels to predicted levels, and telemetry quality and command capability to predicted capabilities. To further cloud the analysis, omnidirectional antenna gain is a major contributor to the uncertainty in received signal levels. Accurate omnidirectional antenna gain

PRECEDING PAGE BLANK NOT FILMED.

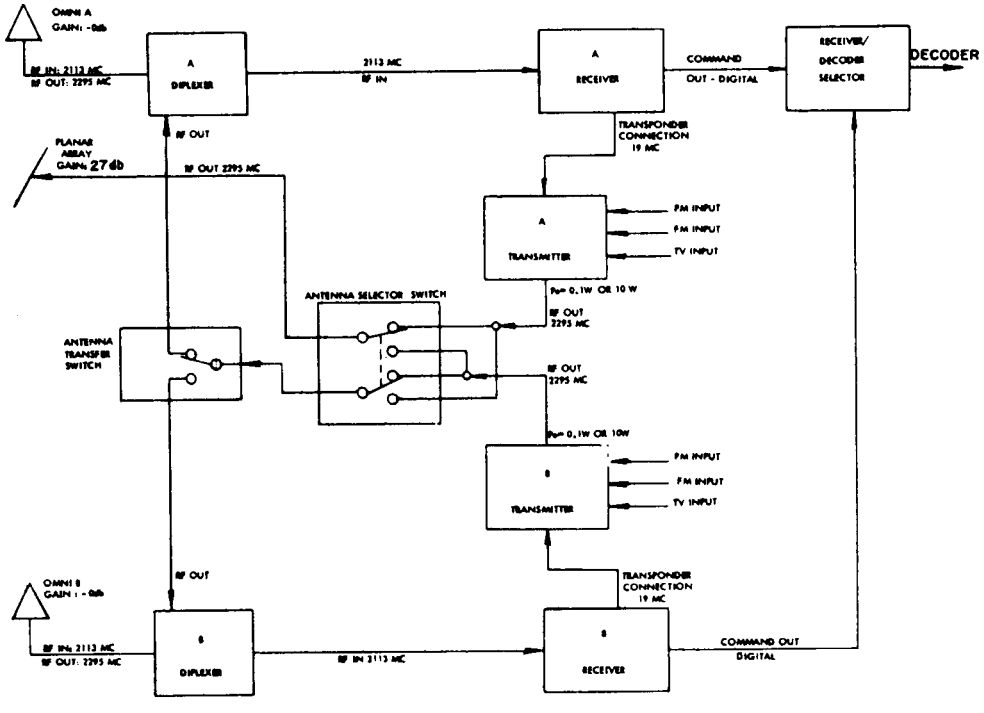

68189-2-134

Figure 5.3-1. Communications Subsystem Block Diagram

measurements are difficult to achieve and, in most cases, deviations from predictions can most likely be attributed to antenna gain uncertainty. Because of the problems outlined above, analysis of the data link subsystem performance will, in general, be a qualitative analysis of the performance of the entire subsystem rather than a quantitative assessment of the performance of the individual subsystem parameters. Equally as important as subsystem performance evaluation in this analysis is the qualitative assessment of the premission and real-time prediction techniques used during the mission, since future missions must rely on these techniques as guidelines during the real-time operation.

In general, the RF data link subsystem performed as expected. The single exception was the performance of receiver B, which, while still within the expected tolerance region, indicated approximately a -2 db offset from predicted nominal receiver signal level values. All other subsystem units performed very close to the nominal predictions.

The data contained in this report consist of spacecraft telemetered, DSS, and mission event time data. Where meaningful, the data are correlated to and compared with equipment specifications, previous test data, preflight predictions, and in-flight analysis predictions. Specifically, this section contains the following discussions which are shown with the appropriate subsection notation:

Anomaly Discussion (subsection 5.3.2) – This subsection contains a discussion of the -2 db deviation in the performance of receiver B from the predicted performance.

Summary and Conclusions (subsection 5.3.3) – This subsection contains a summary of subsystem performance with conclusions relative to performance and postflight analysis.

Subsystem Performance Analysis (subsection 5.3.4) – This subsection contains the following items:

1) General discussion of data, equations used, and path of the earth vector relative to omnidirectional antenna gain contours.

2) Discussion of subsystem performance during specific mission phases.

3) Discussion of pertinent subsystem telemetry signals plotted as a function of time from launch.

The major mission event times relative to the RF data link subsystem are tabulated in Tables 5.3-1 and 5.3-2. Table 5.3-1 contains telemetry mode and bit rate, primary tracking station number, and station automatic gain control values as a function of time. Table 5.3-2 contains a tabulation of the subsystem configuration as a function of time. Both tables cover the mission from launch to touchdown. Also, in some cases, the times in these tables are accurate only to the nearest minute.

TABLE 5.3-1. TELEMETRY MODE SUMMARY

GMT, hr:min:sec	Mode	Bit Rate	DSIF Station	DSIF, AGC-dbm	Telemetry Margin, db	Comments
DAY 251						
07:57:01.257	5	550				Lift off. Az = 79.517 degrees. Low mod index
08:20:00			72			One-way acquisition
08:24:15			72	-128.0		Aided track
08:24:25			51	-116.0		Rcvr 2 in lock one-way (SAA)
08:24:31			51			Rcvr 1 in lock
08:24:28			51			Decom in lock
08:25:43				-113.0		Auto track SAA/paramp
08:26:40						Ant to SCM maser
08:27:45						Xmtr on
08:28:43						Rcvr out of lock
08:28:44				- 95.0		Ant to aided track
08:28:53						Rcvr in lock SAA/paramp
08:29:00						Two-way lock confirmed
08:29:50						Ant to SCM maser
08:30:10				>- 95.0		Xmtr locked to synthesizer
08:31:20						Cmd mod on
08:36:40				- 95.0		
08:37:12				-124.0	Low power	(51 reports locked to sidelobe)
08:37:24						Ant to auto track SAA
08:37:53						Ant to SCM
08:38:40				-123.0		(Apparently locked to sidelobe)
08:39:34						Ant to aided track
						Lock on sidelobe suspected
08:40:20						Ant to SCM
08:41:00				-110.0		Confirmed sidelobe lock
08:45:00				-113.0		
08:45:38	1					
08:46:10				-113.8		
08:46:51		1100				
08:47:45				-116.0		
08:48:19	4					
08:51:01	2					
08:52:56	6					
09:00:00	5			-115.0	+23.6	
09:04:10				-117.5	+21.1	
09:05:50				-118.5	+20.1	
09:09:00				-121.0	+17.6	
09:41:10				-124.0	+14.6	
10:00:00				-127.8	+10.8	
10:18:00				-130.5	+ 8.1	
10:30:02			51			Xmtr off – xfer to DSS-42
11:04:00			42	-131.0	+ 7.6	
11:30:02			42			Xmtr off – xfer to DSS-51
11:30:20			51			Two-way confirmed
11:32:07						Cmd mod on
12:04:00				-139.0	- 0.4	
12:07:00				-141.0	- 2.4	BER = 9×10^{-3}; Sig level = 140.2
12:16:00				-142.0	- 3.4	
12:19:02						Omni A selected
12:19:20				-125.0	+13.6	
13:00:00				-125.3	+13.3	
13:30:02						Xmtr off – xfer to DSS-61
13:31:56			61			Confirms two-way
13:47:46	4					
13:51:16	2					
13:54:12	1					
14:00:00			51	-126.6	+12.0	
14:01:40			61	-126.7	+11.9	
14:03:29						Xmtr B to high power
14:04:20				-108.0		Δ = 18.7 db

Table 5.3-1 (continued)

GMT, hr:min:sec	Mode	Bit Rate	DSIF Station	DSIF, AGC-dbm	Telemetry Margin, db	Comments
14:04:31						Omni B selected
14:05:41		4400				
14:10:02				-132.7		Start roll for star map
14:28:00				-113.2		
14:31:03	5					
14:32:18				-116.4		
14:32:40		1100				
14:33:00				-111.1		
14:33:50						Xmtr B low power
14:34:25				-129.2	+ 9.4	Δ = 18.1 db
15:01:30				-129.5	+ 9.1	
15:30:02						Xmtr off – transfer to DSS-51
15:30:05			51			Two-way confirmed
15:32:28						Cmd mod on
15:45:52						Start gyro drift check
15:49:00				-130.0	+ 8.6	
16:00:00				-130.1	+ 8.5	
16:01:00			61	-129.3	+ 9.3	
16:13:00			51	-130.1	+ 8.5	
16:30:00				-130.7	+ 7.9	
17:00:00				-130.8	+ 7.8	
17:00:00			61	-130.2	+ 8.4	
17:00:00			72	-143.0		
17:22:16	4					
17:26:50	5					
17:30:00			51	-131.3	+ 7.3	
17:30:00			61	-131.2		
17:30:00			72	-143.5		
18:00:00			51	-132.2	+ 6.4	
18:00:00			61	-130.7		
18:00:00			72	-144.0		
18:16:28						Cruise mode on
18:30:00			51	-131.9	+ 6.7	
18:30:00			61	-131.7		
18:30:00			72	-145.0		
18:34:28						Start gyro drift check
19:00:00			51	-132.1	+ 6.5	
19:00:00			61	-132.2		
19:00:00			72	-145.0		
19:30:00			51	-133.0	+ 5.6	
19:30:00			61	-132.1		
19:30:00			72	-145.0		
20:00:00			51	-133.8	+ 4.8	
20:00:00			61	-134.5		
20:00:00			72	-145.5		
20:16:02						Cruise mode on (sun and Canopus lock)
20:18:36		137.5				
20:27:00			72	-149.0		
20:30:07			51			Xmtr off – xfer to DSS-72
20:43:26		17.2				
21:13:58			11	-139.0		
21:30:20			11			Two-way
21:41:06		1100				
21:47:56	4					
21:53:24	2					
21:56:43	1					
21:57:50			11	-133.9	+ 4.7	
22:01:06	5					
22:05:50			14	-123.6		
22:28:16			11	-134.6		
23:14:40			11	-134.8		
23:40:31						Cruise mode on – end gyro drift

Table 5.3-1 (continued)

GMT, hr:min:sec	Mode	Bit Rate	DSIF Station	DSIF, AGC-dbm	Telemetry Margin, db	Comments
23:41:45	4					
23:45:46	2					
23:48:46	1					
23:53:55	5					
23:55:14		None				Gyro speed sig processing on
23:56:26			11	-139.7		
23:58:57		1100				
			DAY 252			
00:24:43	5	1100	11	-134.8	+ 3.8	
00:50:40			14	-126.9		
00:59:45	4					
01:02:42	2					
01:05:56	1					
01:08:00			11	-134.9	+ 3.7	
01:15:20				-116.6		Xmtr B high power; Δ = 18.3 db
01:15:57		4400				
01:23:00			11	-121.0		
01:27:00			42	-122.8		
01:32:57						Start roll — midcourse 143.8 seconds + 71.0 degrees
01:36:30				-121.9		After end of roll
01:38:06						Start yaw 71.4 seconds -35.7 degrees
01:40:00			11	-119.9		After end yaw
01:39:45	2					
01:40:46	1					
01:45:02						Start thrust (14.25 seconds)
01:45:19						Approx time end of thrust
01:46:34	5					
01:49:55	1					
01:55:52			11	-122.0		
01:53:51						Start post midcourse yaw 71.4 seconds +35.7 degrees
02:00:09						Sun acquire mode on
02:12:02						Start second vernier burn
02:17:49	5					
02:20:23	1					
02:24:33						Start yaw maneuver 360.2 seconds -180.1 degrees
02:30:35			11	-130.0		
02:39:51						Start third vernier burn
02:45:22						Start yaw maneuver 360.2 seconds -180.1 degrees
02:53:24						Sun acquire mode on
02:54:05			11	-122.2		
02:55:12		1100				
02:55:51						Xmtr B low power
02:56:54	5					
02:58:00				-136.2		
04:00:47						Start roll maneuver 143.8 seconds - 71.9 degrees
04:04:19						Cruise mode on
04:05:55				-136.9		Start roll maneuver 137.0 seconds + 68.5 degrees
04:09:33						Start yaw maneuver 213.4 seconds +106.7 degrees
04:13:44	1					
04:18:00						
04:18:48				-133.5		Start thrust (125 seconds)
04:19:01.5						Start thrust 0.5 second
04:19:03						Start thrust 0.5 second
04:30:00			42			Two-way
04:53:30				-134.0		
04:56:15				-133.9		

Table 5.3-1 (continued)

GMT, hr:min:sec	Mode	Bit Rate	DSIF Station	DSIF, AGC-dbm	Telemetry Margin, db	Comments
04:58:13						Start yaw maneuver 213.4 seconds -106.7 degrees
05:03:00						Sun acquire mode on
05:04:10						Start sun and roll 137.0 seconds - 68.5 degrees
05:07:51						Cruise mode on
05:08:00				-136.4		Locked on sun and Canopus
05:26:44	2					
05:32:52	4					
05:39:00						Two-way lock confirmed Up link not locked from 04:31:15 to 05:39:00 GMT
05:44:02	5					
05:51:00				-136.6		
06:05:53	4					
06:15:27	2					
06:29:12	4					
06:38:24	5					
06:40:00				-136.8		
07:24:00				-137.1		
07:48:00				-137.2		
07:49:35				-119.1		Xmtr B high power
07:51:25		4400				
07:52:11	1					
07:52:20				-124.2		
07:54:30						Start sun and roll 129.0 seconds + 64.5 degrees
07:57:00				-124.0		End of roll
07:58:31						Start yaw 286.6 seconds +143.3 degrees
08:24:04						Start thrust 33.05 seconds
08:26:10	5					
08:30:04	1					
08:33:51						Start yaw 286.6 seconds -143.3 degrees
08:39:27						Sun acquire mode on
08:40:35						Start sun and roll 129.0 seconds - 64.5 degrees
08:43:00				-124.0		After end of roll
08:45:43		1100		-119.3		
08:47:01						Xmtr B low power
09:05:00				-138.0		
09:08:32						Start gyro drift check
09:21:03	4					
09:22:31		550	42			
09:25:00				-138.9		
09:55:12	1					
09:56:50						End gyro drift check
10:02:04	2					
10:05:48	5					
10:11:17	4					
10:30:00				-138.9		
10:33:27				-120.7		Xmtr B high power
10:35:03				-117.9		Low mod index SCO on
10:36:48				-123.5		Alpha scat on
11:27:43						Alpha scat off
11:28:30				-118.5		
11:29:31						3.9 kHz A/D SCO on
11:30:34				-139.8		Xmtr B low power
11:32:51	1					
11:39:31						Start gyro drift check
11:44:25	5					
11:47:17	1					
11:48:00				-139.8		
12:00:00			51			Xmtr on
12:03:58			51			Cmd mod on

Table 5.3-1 (continued)

GMT, hr:min:sec	Mode	Bit Rate	DSIF Station	DSIF, AGC-dbm	Telemetry Margin, db	Comments
12:03:35				-138.8		
12:21:00			42	-139.4		
12:30:00			51	-138.8		
12:54:54	5					
12:59:54	1					
13:00:00			51	-138.8		
13:00:00			42	-139.4		
13:15:29						Terminate gyro drift check
13:17:57						Start gyro drift check – roll
13:30:00			51	-139.2		
13:30:00			42	-139.7		
13:53:28	4					
13:56:54	5					
14:00:00			51	-138.5		
14:00:00			42	-140.1		
14:02:17	2					
14:04:18	1					
14:24:00			61	-138.8		
14:30:00			51	-138.7		
14:30:00			61	-139.1		
15:00:00			51	-138.7		
15:02:34	5					
15:08:09						Terminate gyro drift check
15:10:41						Start gyro drift check
15:11:37	1					
15:30:00			51	-138.7		
15:30:00			61	-138.7		
16:00:00			51	-139.0		
16:04:27	4					
16:17:08	5					
16:24:32	1					
16:30:00			51	-139.3		
16:50:02			51			Xmtr off for xfer to DSS-61
16:54:00			61	-139.0		
17:00:00			51	-139.3		
17:04:00			61	-139.1		
17:12:26	5					
17:15:29	1					
17:18:08						End gyro drift check
17:30:00			51	-138.8		
17:33:00			61	-139.0		
18:00:00			51	-139.3		Start gyro drift check
18:00:36	5					
18:11:17	4		61	-138.9		
18:16:03	1					
18:30:00			61	-138.9		
18:30:00			51	-139.0		
19:00:00			61	-138.9		
19:00:00			51	-139.3		
19:09:56						
19:12:51	5					
19:16:22	1					
19:30:00			61	-139.1		
19:30:00			51	-139.5		
20:00:00			51	-139.5		
20:00:59	4					
20:05:30	5					
20:09:54	1					
20:10:23			61	-139.1		End gyro drift check
20:20:00			51			Xmtr on
20:21:50			51			Cmd mod on
20:30:00			51	-139.5		
20:59:05						Start gyro drift check
20:59:50	5		51	-139.5		

Table 5.3-1 (continued)

GMT, hr:min:sec	Mode	Bit Rate	DSIF Station	DSIF, AGC-dbm	Telemetry Margin, db	Comments
21:30:00			51	-140.0		
21:35:02			51			Xmtr off for xfer to DSS-11
21:48:52						Terminate gyro drift check
21:52:44			11	-140.0		
22:04:24			11	-139.9		
22:34:17	4					
22:34:56			11	-139.9		
22:35:58	2					
22:38:04	1					
23:06:17			11	-140.0		
23:06:30			11	-122.0		Xmtr B high power
23:07:17		4400				
23:12:18						Cruise mode on
23:13:51						Start roll maneuver -76 degrees
23:17:30				-131.2		After end of roll
23:19:36						Start yaw maneuver -100.6 degrees
23:23:30	2			-124.0		
23:24:49	1					
23:30:58						Start of thrust 5.45 seconds
23:32:24	5					
23:36:07						Start of yaw +100.6 degrees
23:40:17				-133.4		
23:44:05						Start of roll +76.0 degrees
23:49:53	2					
23:50:49		550				
23:51:42						Xmtr B low power
23:52:37				-140.4		
23:54:06	4					
23:56:54	5					
			DAY 253			
00:07:55	1					
00:17:00				-140.5		
01:16:07	5			-140.5		
01:22:05	4					
01:27:36	2					
01:34:17	1					
01:35:19						Start gyro drift check
01:58:33	5					
02:02:36	4					
02:06:52	1					
02:23:00				-140.6		
02:46:34	5					
03:00:02			11			Xmtr off for xfer to DSS-42
03:03:00			42	-140.1		
03:16:20	4					
03:23:36	2					
03:30:15	1					
03:59:00			42	-139.8		
03:59:00			11	-141.0		
04:33:03						End gyro drift check
04:34:20	5					
04:42:49	4					
04:50:00			42	-140.9		
04:51:52	2					
04:58:36	1					
06:05:46	5					
06:13:22	4					
06:20:58	2					
06:24:37	1					
06:26:00				-141.0		
07:00:00				-141.1		
07:08:24	5					
07:14:33	4					

Table 5.3-1 (continued)

GMT, hr:min:sec	Mode	Bit Rate	DSIF Station	DSIF, AGC-dbm	Telemetry Margin, db	Comments
07:17:41	2					
07:20:30	1			-141.1		
07:22:00				-141.2		
08:05:00						
08:16:18	5					
08:22:45	4					
08:28:26	2			-141.2		
08:30:17	1			-141.4		
09:02:00						
09:17:44	5					
09:23:12	4					No SCO change
09:25:12		137.5				
09:27:56		550				
09:30:29	2					
09:32:46	1			-141.4		
09:40:00			42	-141.4		
10:00:00			51	-141.0		
10:00:00						
10:16:51	5					
10:28:47	4					
10:30:34	2					
10:32:17	1					
11:00:00			42	-141.5		
11:00:00			51	-141.0		
11:30:00			42	-141.7		
11:30:00			51	-140.9		
11:38:22	5		42			
11:41:17	4					
11:42:52	2					
11:44:25	1					
11:50:45			42	-141.7		Rcvrs out of lock
11:57:50			42			Xmtr on
12:00:00			51	-140.9		Confirms two-way lock
12:00:10			51			Cmd mod on
12:02:10			51			
12:05:00			51	-140.9		
12:05:00			42	-141.7		
12:30:00			51	-140.9		
12:52:36	5					
12:57:02	4					
12:59:37	2					
13:00:00			51	-141.0		
13:00:00			42	-141.5		
13:04:23	1		51			Sun mode on – gyro drift check
13:05:03						Roll only
13:30:00			51	-141.0		
14:00:00			51	-140.6		
14:00:00			42	-140.5		
14:05:52	5		51			
14:11:33	4					
14:15:06	2					
14:18:53	1					
14:23:00			61	-146.3		
14:30:00			51	-140.6		
14:50:00			51	-140.6		
15:00:00			51	-140.8		
15:09:55	5					
15:14:34	4					
15:20:17	2					
15:22:34	1					
15:23:00				-140.5		End roll gyro drift check
15:24:13						Start gyro drift check
15:27:08						

Table 5.3-1 (continued)

GMT, hr:min:sec	Mode	Bit Rate	DSIF Station	DSIF, AGC-dbm	Telemetry Margin, db	Comments
15:30:00			51	-141.2		
15:30:00			61	-142.1		
16:00:00			51	-141.0		
16:00:00			61	-141.7		
16:17:33	5		51			
16:23:33	4					
16:26:26	2					
16:30:00			51	-140.9		
16:30:00			61	-141.7		
16:30:14	1		51			
17:00:00			51	-140.6		
17:25:05	5					
17:29:28	4					
17:30:00				-140.6		
17:34:33	2					
17:37:33	1					
17:55:00			51	-140.6		
17:55:00			61	-141.6		
17:59:42						End gyro drift check
18:12:16						Start + yaw (359.8 seconds, 179.9 degrees)
18:22:52						Start + yaw (360.2 seconds, 180.1 degrees)
18:30:14						Cruise mode on
18:32:09	5					
18:34:00				-141.4		
18:37:07	4					
18:56:26	2					
19:00:00			51	-141.4		
19:01:01	1					
19:06:00			61	-142.1		
19:30:00			51	-141.7		
19:31:37	5					
19:35:11	4					
19:38:50			51	-141.6		
19:41:51	2					
19:49:01	1					
20:00:00			51	-141.6		
20:00:00			61	-142.7		
20:12:34	4					
20:30:00			51	-141.8		
20:30:00			61	-142.4		
20:39:58	1					
21:00:00			51	-141.8		
21:00:00			61	-142.5		
21:15:59	5					
21:37:00			11	-150.0		
21:40:02			51			Xmtr off for xfer to DSS-11
21:48:32			51	-142.1		
21:48:06			11	-144.6		
21:50:00			14	-135.5		
21:51:14	4					
21:56:06	2					
21:59:08	1					
22:01:39	5					
22:11:00			11	-144.6		
22:13:00			14	-135.9		
22:32:56	4					
22:34:21	2					

Table 5.3-12 (continued)

GMT, hr:min:sec	Mode	Bit Rate	DSIF Station	DSIF, AGC-dbm	Telemetry Margin, db	Comments
22:36:21	1					
22:38:40	5		11	-144.5		9×10^{-3} BER
22:45:20	None	None				Gyro speed check
22:50:55	5	550				
22:53:47			11	-144.5		Xpndr power off
22:55:33						Xpndr B power on
23:10:00			11	-144.5		
23:10:00			14	-136.0		
23:42:22	6					
23:44:40	4					
23:51:00			11	-144.7		
23:51:41						Xmtr B high power
23:52:00			11	-125.4		Δ = 19.3 db
23:52:19		1100	11	-124.5		
23:55:24	2					
23:57:05	1					
23:59:13	5					
			DAY 254			
00:04:21						Xpndr power off
00:07:00			11	-124.6		
00:08:00			14	-117.1		
00:12:15						Start preterminal roll (+ roll; 147.8 seconds; 73.9 degrees)
00:15:10			11	-125.2		
00:16:21						Start + yaw (239 seconds, 119.5 degrees)
00:20:45			11	-124.7		
00:21:38			11	-127.7		TD strain gage SCOs on
00:30:08	6					
00:46:45						Touchdown
00:48:40			11	-131.4		
00:48:57	5					
00:50:53	2					
00:51:50						TD strain gage SCOs off
00:52:25			11	-128.1		
00:53:09	5					
01:07:52		137.5				
01:07:58			11	-133.0		
01:09:38						Xmtr B low power
01:10:00			11	-157.0		
01:10:59						DSS-11 rec out of lock
01:12:41						DSS-11 rec in lock
01:13:10			11	-151.6		
01:16:50			14	-144.0		
01:19:17						Xmtr A high power
01:19:50			11	-132.8		
01:19:50			14	-124.9		
01:20:58		1100				
01:21:10			11	-128.2		
01:24:20				-127.4		
01:26:22						Select omni A
01:26:30			11	-122.6		
02:37:20			11	-122.1		

TABLE 5.3-2. SPACECRAFT CONFIGURATION SHEET

Time, hr:min:sec	Major Sequence Title	Transmitters		Omni A/B	A/D Conv 1/2	Receiver A		Receiver B		Cmd Dec A/B	Comments
		A/B	Pwr H/L			ØL/AFC	Transponder A	ØL/AFC	Transponder B		
						DAY 251					
07:57:01	Launch	B	Low	B	1		Off		On	B	
			High								
08:29:07	Initial acquisition					AFC		ØL			DSS-51
08:31:22											DSS-51-cmd mod on
08:37:07			Low								
10:24:08	Station transfer										DSS-51-cmd mod off
10:33:20											DSS-42-cmd mod on
11:24:11	Station transfer									A	DSS-42-cmd mod off
11:32:10											DSS-51-cmd mod on
12:19:02				A							
13:24:03	Station transfer										DSS-51-cmd mod off
13:32:01											DSS-61-cmd mod on
14:03:28	Star verification and acquisition		High								
14:04:31				B							
14:16:10										B	During star mapping roll
14:33:49			Low								
15:24:04	Station transfer										DSS-61-cmd mod off
15:32:31											DSS-51-cmd mod on
16:37:10										A	Cmd mod off
16:40:07											Cmd mod on
20:24:16	Station transfer										DSS-51-cmd mod off
20:39:28											DSS-72-cmd mod on
20:40:45										B	
21:24:47										A	
21:26:04	Station transfer										DSS-72-cmd mod off
21:35:01											DSS-11-cmd mod on
						DAY 252					
01:15:20	Midcourse		High								
02:55:51			Low								
04:23:24	Station transfer										DSS-11-cmd mod off
04:31:22								Out of lock			
04:31:48											DSS-42-cmd mod on
04:46:41										B	
04:47:07										A	
04:47:24										B	
04:47:38										A	
04:47:50										B	
04:48:02										A	
04:48:26										B	
04:48:52										A	
04:49:31										B	
04:50:23										A	
05:13:49										B	
05:15:43										A	
05:16:14										B	

Table 5.3-2 (continued)

Time hr:min:sec	Major Sequence Title	Transmitters		Omni A/B	A/D Conv 1/2	Receiver A		Receiver B		Cmd Dec A/B	Comments
		A/B	Pwr H/L			ØL/AFC	Transponder A	ØL/AFC	Transponder B		
05:17:33										A	
05:36:56											DSS-42-cmd mod off to reacquire up link
05:40:05								ØL			
05:42:45											DSS-42-cmd mod on
07:49:35			High								Nonstandard midcourse thrusting
08:47:01			Low								
10:33:27			High								Alpha scattering check
11:30:34			Low								
11:54:34	Station transfer									B	DSS-42-cmd mod off
12:03:12											DSS-51-cmd mod on
16:44:45	Station transfer										DSS-51-cmd mod off
16:51:45											DSS-61-cmd mod on
20:13:42	Station transfer									A	DSS-61-cmd mod off
20:21:58											DSS-51-cmd mod on
21:35:00	Station transfer										DSS-51 to DSS-11 no data during transfer
23:06:30		B	High								Nonstandard midcourse correction
23:51:42			Low								
						DAY 253					
02:54:05	Station transfer									B	DSS-11-cmd mod off
03:06:24											DSS-42-cmd mod on
07:43:08											DSS-42-cmd mod off
08:15:50											DSS-42-cmd mod on
11:54:18	Station transfer									A	DSS-42-cmd mod off
12:02:16											DSS-51-cmd mod on
14:22:44											DSS-51-cmd mod off
14:28:47											DSS-51-cmd mod on
21:25:10	Station transfer									B	DSS-51-cmd mod off
21:40:46								Not Ø/L			Loss of up link lock during transfer
21:43:34								Ø/L			
21:46:03											DSS-11-cmd mod on
22:53:59								AFC	Off		
22:55:33									On		
22:56:39											Cmd mod off to reacquire up link
22:57:39								Ø/L			
22:59:32											Cmd mod on
23:28:13										A	Cmd mod off
23:30:56											Cmd mod on
23:51:48		B	High								
						DAY 254					
00:04:23								AFC	Off		
00:57:23				2							
01:09:30		B	Low								
01:17:40		A	Low								
01:19:17		A	High								
01:26:22				A							

5.3.2 ANOMALY DISCUSSION

The only RF subsystem anomaly observed during the mission was an apparent bias of approximately -2 db in receiver B performance. Other events occurred during the mission which caused the spacecraft RF subsystem and/or the tracking station performance to be questioned. Discussions of these events can be found in Reference 1 and will not be repeated here. No spacecraft RF subsystem anomaly existed in any of these cases.

5.3.2.1 Bias in Receiver B Performance

During Mission E coast periods, deviations from the predicted received signal level curves were noted in both the up and down links. Gyro drift checks performed during these periods account for omnidirectional antenna gain variations that are not taken into consideration when generating predictions. However, deviations in receiver B received signal levels, above those expected due to the gyro drifts, as well as deviations from predictions during maneuvering periods, indicated that an approximate -2 db bias existed in either the performance or calibration of the receiver.

Omnidirectional antenna B up link gain variations during the transit phase of the mission are illustrated in Figure 5.5-2. This figure shows the earth vector variation superimposed on the omnidirectional antenna B up link antenna gain contour map. For the most part, the mission was flown with the relative spacecraft/ground station attitude so that the antenna operated in a high-gain region ($G \geq -3$ db). However, during the Canopus acquisition sequence, the required 360-degree spacecraft roll resulted in gains as low as -33 db. Figure 5.3-6c illustrates measured versus actual gain values for this maneuver and indicates an offset of approximately 2 db between the two sets of data. Also, a third midcourse type maneuver, anti-sunline maneuver, was performed during the mission which involved a 360-degree yaw that resulted in omnidirectional antenna B gain variations of approximately 11 db. Figure 5.3-7 illustrates measured versus actual gain values for this maneuver and also indicates a 2-db offset. Figure 5.3-5 is a similar presentation for the coast phases and indicates the same general bias.

A deviation from the expected performance of receiver B is not unique to Surveyor V. A -2 db bias was observed during Mission C (Reference 2) and -5 db in Mission D (Reference 3). During all three missions, this degraded behavior could not be considered an anomaly since the combined effect of gyro drift checks and receiver bias caused the signal level to remain at the predicted negative tolerance level which, due to the nature of the negative tolerances on system parameters, is accepted as an expected signal level.

It was pointed out in References 2 and 3 that the bias was attributed to some unexplained calibration error or to some unaccountable insertion loss peculiar to receiver B. It was also stated that it was unlikely that the bias seen in the data could be attributed to any uncertainty in the antenna pattern data due to the consistency of the measured data throughout the wide range of sampled antenna gain values. However, this conclusion did not consider the

case where the whole antenna pattern could contain some fixed bias as a result of not considering some loss factor when reducing the measured data used to generate the existing antenna B up link pattern. This appears to be the most likely explanation. Positive gain values over wide areas are not characteristic of omnidirectional antennas. However, Figure 5.3-6c shows that 125 degrees out of 360 degrees of the antenna B up link pattern values for θ = 74 degrees have positive gains, with the maximum gain being almost +4 db. Both Surveyor C and D missions had a value for θ of approximately 110 degrees at Canopus acquisition, and large regions of positive gains were not as apparent in those data as it is for Mission E. Examination of previous mission analysis data, however, does indicate that the antenna patterns themselves contain the bias and not receiver B performance. Predictions and analysis on future missions will contain a 2-db adjustment in the up link antenna B gain values.

5.3.3 SUMMARY AND CONCLUSIONS

Table 5.3-3 contains a summary of the measurable performance parameters compared with applicable requirements and premission predictions. Most subsystem parameters are not directly measurable and those that are measurable are difficult to summarize due to time variability.

Received signal level, for example, is a function of time and spacecraft attitude. The summary for these parameters reflects wide tolerances, with corresponding wide variations in actual performance in cases when the earth vector was in the omnidirectional antenna null. Performance and predictions outside the null are much more closely bounded. More detailed information is found in the subsections dealing with each mission phase.

The following conclusions can be drawn as a result of the foregoing analysis:

1) Close to nominal predicted RF subsystem performance was experienced in both up and down links with the exception of receiver B.

2) Receiver B indicated performance was biased by approximately -2 db from predicted. Analysis of mission data shows that this bias and similar biases on previous spacecraft are a result of an apparent offset in the measured antenna pattern data.

3) RF subsystem premission predictions and real-time analysis techniques used during Mission E were relatively accurate with the exception of those associated with the descent and touchdown phases. The actual performance during descent was worst-case predicted and, at touchdown, exceeded worst case.

TABLE 5.3-3. RF PERFORMANCE PARAMETER SUMMARY

Parameter	Predicted Value	Requirement	Actual Performance
Transmitter frequency at acquisition	2294.993699 MHz	2295 MHz ± 23 kHz	2294.993024 MHz
Receiver B frequency at acquisition	2113.304384 MHz	2113.31 MHz ± 21 kHz	2113.306464 MHz
Receiver A signal levels during coast phases*	Time variable predictions. Predicts are some nominal value ±10 db.	> -114 dbm**	Level between +10 and -4 db of nominal and ≥ -108 dbm
Receiver B signal levels during coast phases*	Time variable predictions. Predicts are some nominal value ±5 db.	> -114 dbm**	Level between +0.5 and -4 db of nominal and ≥ -97.0 dbm
Receiver A signal levels during star maneuver	Time variable predictions. Predicts are some nominal value ±10 db.	> -114 dbm**	Level between +8 and -6 db of expected and ≥ -108.5 dbm
Receiver B signal levels during star maneuver	Time variable predictions. Predicts are some nominal value ±8 db.	> -114 dbm**	Level between +6 and -6 db of expected and ≥ -114.0 dbm
Receiver A signal levels during mid-course maneuvers	Time variable predictions. See Table 5.3-9.	> -114 dbm**	See Table 5.3-9. Signal level ≥ -102.2 dbm.
Receiver B signal levels during mid-course maneuvers	Time variable predictions. See Table 5.3-9.	> -114 dbm**	See Table 5.3-9. Signal level ≥ -116.4 dbm.
Receiver A signal levels during terminal maneuver	Time variable predictions. Predicts are some nominal value ±10 db.	> -114 dbm**	Level variations of 22.9 db and > -119.7 dbm (predicted variations of 14.4 db)

Table 5.3-3 (continued)

Parameter	Predicted Value	Requirement	Actual Performance
Receiver B signal levels during terminal maneuver	Time variable predictions. Predicts are some nominal value ± 4.8 db.	>-114 dbm**	Level variations of 10.8 db and >-92.6 dbm (predicted variations of 10.5 db)
DSS signal levels during coast phases*	Time variable predictions. Predicts are some nominal value ±5 db.	>-157.4 dbm (carrier power) (17.2 bits/sec threshold)	Level between +3 and -1 db of nominal and >-145 dbm at 550 bits/sec
DSS signal levels during star maneuver	Time variable predictions. Predicts are some nominal value ±10 db.	None	Level between +16 and -5 db of expected and ≥-143.7 dbm (carrier power at 4400 bits/sec)
DSS signal levels during midcourse maneuvers	Time variable predictions. See Table 5.3-9.	>-136.1 dbm (carrier power at 4400 bits/sec/ high power)	See Table 5.3-9. Signal level ≥-133.6 dbm (carrier power at 4400 bits/sec)
DSS signal levels during terminal maneuver	Time variable predictions. Predicts are some nominal value ±3.0 db.	>-130.4 dbm (carrier power at 1100 bits/sec/ high power)	Level variations of 3.8 db and ≥-125.1 dbm carrier power at 1100 bits/sec (predicted variations of 3.7 db)
DSS signal levels during descent and touchdown	Time variable predictions. Predicts are some nominal value ±3.0 db.	>-129.8 dbm (carrier power at 1100 bits/sec and strain gages)	Level variations of 7.4 db and ≥-133.7 dbm carrier power at 1100 bits/sec and strain gages on 85-foot antenna (predicted variations of 6.5 db)

Table 5.3-3 (continued)

Parameter	Predicted Value	Requirement	Actual Performance
Transmitter A high power output	40.8 dbm $^{+0.0}_{-0.4}$ db	>39.6 dbm	Output between 40.4 and 40.7 dbm
Transmitter A low power output	24.8 dbm $^{+1.2}_{-0.8}$ db	>20.0 dbm	Output between 20.7 and 22.3 dbm (after touchdown)
Transmitter B high power output	40.8 dbm $^{+0.2}_{-0.9}$ db	>39.6 dbm	Output between 40.7 and 41.6 dbm
Transmitter B low power output	23.3 dbm $^{+1.2}_{-0.9}$ db	>20.0 dbm	Output between 21.4 and 23.3 dbm
Phase jitter 152 Hz bandwidth (thrust phase)	<22 degrees	<22 degrees (3σ)	<15 degrees during retro engine burn
Command reject rate	<1/2000	≤1/2000 at signal level >-114 dbm	No known rejected commands sent at signal levels greater than -108 dbm
Telemetry bit error rate	<3/1000	≤3/1000 at input SNR ≥10 db	Minimum BER $= 3 \times 10^{-3}$ at input SNR $\simeq 9.8 \pm 1.7$ db

*Gyro drift checks during coast phases caused antenna gain variations not taken into account in the predicted signal levels.

**Threshold value applies to command threshold and, as such, only requires one of the two receivers to be above -114 dbm at any one time.

TABLE 5.3-4. UP LINK PARAMETERS FROM FAT, STV, AND CDC TESTS

Description	Value
Transmitting system (DDS)	
RF power	$70.0\ ^{+0.5}_{-0.0}$ dbm
Antenna gain	
SAA	20.0 ± 2.0 db
SCM	51.0 (+1.0, -0.5) db
Circuit loss	
SAA	-0.5 ± 0.0 db
SCM	-0.4 ± 0.1 db
Receiving system (Surveyor V)	
Circuit loss	
Receiver A	-3.85 ± 0.5 db
Receiver B	-3.00 ± 0.5 db
Up-link carrier tracking loop	
Equivalent noise	
Bandwidth	240 ± 24 Hz
Threshold SNR	12 db
Up-link channel	
Threshold SNR	9 db
System noise	
Temperature	2700° K
Equivalent noise	
Bandwidth (predetection)	13430 Hz
Data/subcarrier modulation index	7.2
Subcarrier/carrier modulation index	1.6 ± 0.16

5.3.4 SUBSYSTEM PERFORMANCE ANALYSIS

5.3.4.1 General Discussion

Before specific phases are discussed, a general treatment of the mission will be undertaken. Information applicable to all mission phases is included in this subsection.

Subsystem Parameters

Most quantitative estimates of performance are based on received signal levels which, in turn, are determined from individual link parameters. Those parameters used in the performance predictions and the subsystem analyses are tabulated in Tables 5.3-4 and 5.3-5. Equations using these data are derived here; parameters discussed in later portions can be evaluated from these data. Tables 5.3-4 and 5.3-5 consist of measured data taken from flight acceptance (FAT), solar thermal vacuum (STV), and command and data handling console (CDC) tests or specification values where measurements were not available.

Computations Used

In this subsection, reference is made to received signal levels and quantities computed from these levels. The equations used are listed below and will not be derived again:

1) Spacecraft transmitter high power output is

$$P_{xmtr}(\text{dbm}) = 10 \log (P_{tm} \times 10^3) + L$$

where

P_{xmtr} = transmitter power (dbm) = P_{high}

P_{tm} = telemetered power output (watts)

L = loss from transmitter to power monitor. (Value for transmitter B/omnidirectional antenna B ≃ as determined from STV calibration data.)

2) Spacecraft transmitter low power output is

$$P_{low} = P_{high} - P_{DDS_H} + P_{DSS_L} \text{ (dbm)}$$

TABLE 5. 3-5. DOWN LINK PARAMETERS FROM FAT, STV, AND CDC TESTS

Description	Value
Transmitting system (Surveyor V)	
RF power	
Transmitter A (low power)	24. 8 (+1. 2, -0. 8) dbm
Transmitter B (low power)	23. 3 (+1. 2, -0. 9) dbm
Transmitter A (high power)	40. 8 (+0. 0, -0. 4) dbm
Transmitter B (high power)	40. 8 (+0. 2, -0. 3) dbm
Planar array gain	27. 0 ± 0. 5 db
Circuit loss	
Transmitter A Omnidirectional antenna A	-2. 45 (±0. 5) db
Transmitter B Omnidirectional antenna A	-2.54(±0. 5) db
Transmitter A Omnidirectional antenna B	-2.75(±0. 5) db
Transmitter B Omnidirectional antenna B	-3.19(±0. 5) db
Planar array	-2. 3 (+0. 0, -0. 22) db
Carrier frequency	2295 MHz
Receiving system (DSS)	
Antenna gain	
SAA (acquisition aid antenna)	21. 0 ± 1. 0 db
SCM (85-foot antenna)	53. 0 (+1. 0, -0. 5) db

Table 5.3-5 (continued)

Description	Value
Circuit loss	
SAA	-0.5 ± 0.0 db
SCM	-0.18 ± 0.05 db
Effective noise temperature	
Maser	55 ± 10° K
Parametric amplifier (SAA antenna)	
All DSS except Johannesburg	270 ± 50°K
Johannesburg	320 ± 50°K
Lunar temperature	110 ± 25° K
Carrier channel	
Equivalent noise bandwidth for maneuvers (at threshold)	152 Hz
Equivalent noise bandwidth for coast mode (at threshold)	12 Hz
Threshold SNR	
Acquisition	9.0 db
Maneuvers	14.0 ± 1.0 db
Coast mode	11.4 db
Subcarrier oscillator	
Equivalent predetection noise bandwidth, Hz ± 10 percent	
4400 bits/sec	5160
1100 bits/sec	1290
550 bits/sec	685
137.5 bits/sec	169
17.2 bits/sec	26.7
Strain gauge 1	169
Strain gauge 2	169
Strain gauge 3	169
Reject/enable	405
Gyro speed	948
Alpha counts	11400
Proton counts	948

Table 5.3-5 (continued)

Description	Value
Subcarrier oscillator center frequencies, kHz	
4400 bits/sec	33.0
1100 bits/sec	7.35
550 bits/sec	3.90
137.5 bits/sec	0.96
17.2 bits/sec	0.56
Strain gauge 1	0.96
Strain gauge 2	1.30
Strain gauge 3	1.70
Reject/enable	2.3
Gyro speed	5.4
Alpha counts	70.0
Proton counts	5.4
Threshold signal-to-noise ratio for telemetry data, ±1.0 db	
4400 bits/sec	9.0
1100 bits/sec	9.0
550 bits/sec	9.0
137.5 bits/sec	9.0
17.2 bits/sec	9.0
Strain gauge 1	7.0
Strain gauge 2	7.0
Strain gauge 3	7.0
Reject/enable	10.0
Gyro speed	10.0
Alpha counts	11.0
Proton counts	10.0
Subcarrier oscillator modulation indices, ±10 percent	
4400 bits/sec	1.6
1100 bits/sec	0.935
550 bits/sec (acquisition)	0.3
550 bits/sec	1.15
137.5 bits/sec	1.45
17.2 bits/sec	1.45
Strain gauge 1	0.65
Strain gauge 2	0.65
Strain gauge 3	0.65
Reject/enable	0.655
Gyro speed	1.600
Alpha counts	1.40
Proton counts	0.60

where

P_{low} = transmitter low power output

P_{high} = telemetered transmitter high power output

P_{DSS_H} = DSS received signal level at high power

P_{DSS_L} = DSS received signal level at low power

3) Spacecraft omnidirectional antenna gain (up-link) is

$$G_R = \frac{P_R}{P_T G_T \left(\frac{\lambda}{4\pi R}\right)^2 L}$$

where

G_R = received omnidirectional antenna gain (up-link gain)

P_R = received signal level (determined from spacecraft AGC)

P_T = DSS nominal transmitter power

G_T = DSS nominal antenna gain

λ = wavelength of up-link signal

R = slant range at time of computation

L = nominal spacecraft and DSS losses

(Note: For down-link gain, appropriate down-link parameters are inserted in a similar equation.)

4) Signal-to-noise ratio (SNR) for any subcarrier is

$$SNR = \frac{P_S}{P_N} = \frac{MP_R}{KT_{eff}BW_{sc}}$$

where

P_S = signal power in predetection noise bandwidth

P_N = total noise power in predetection noise bandwidth

M = carrier to subcarrier modulation loss adjustment constant based on subcarrier oscillator modulation index on the carrier

P_R = received carrier power reported by the DSS

K = Boltzmann's constant

T_{eff} = DSS system temperature reported by the DSS

BW_{sc} = subcarrier equivalent predetection noise bandwidth

When using these equations, attention must be given to the desired accuracy of the answer. Since several parameters not measurable in flight, spacecraft telemetry, and DSS station reports are used, computed parameters have potentially large errors. Their validity is thus weighed against similar test data and/or is judged quite subjectively based on past experience. These equations are not used so much for their numerical results as for the total picture of subsystem performance generated. Any gross subsystem problems or computation errors will tend to be uncovered in this analysis, but subtle errors will not.

Bit Error Rate Calculations

One subsystem parameter of interest is the telemetry bit error rate (BER). This parameter serves as an example of the problems encountered when attempting to evaluate postmission data. BER is required to be less than 3×10^{-3} at input signal-to-noise ratios (SNR) of 9 ± 1 db. BER cannot be measured in flight, but word error rate can. On day 253 at approximately 22-1/2 hours GMT, DSS-11 began counting parity errors. Based on the assumption that a bad parity word represented a single bit error, a BER of 9×10^{-3} was observed at a reported -144.5 dbm ground station received carrier power.

The SNR at the time of the observed 9×10^{-3} BER was computed as shown below:

DSS AGC/550 bits/sec = -144.5 dbm

System noise temperature = 52.0°K = 17.2 db
(DSS-11 post-track)

Boltzmann's constant = -198.6 dbm/deg/Hz

Bandwidth = 685 Hz ± 10 percent = 28.4 (+0.41, -0.46) db

Noise power = -153.0 (+0.41, -0.46) dbm

Modulation loss

Carrier	-3.15 (+0.65, -0.75) db
Subcarrier	-3.27 (+0.51, -0.63) db

Δ modulation loss = -0.12 (+1.26, -1.28) db

Subcarrier power = -144.38 (+1.26, -1.28) dbm

SNR = subcarrier power — noise power = 8.62 (+1.72, -1.69) db

The tolerance in this computation is only approximate and may be greater. Also, the computation is based on a measured BER of 9×10^{-3} and the parameter to be compared is specified at a BER of 3×10^{-3}. The theoretical BER versus SNR expression indicates that a deviation of -1.15 db from the predetection SNR at a BER of 3×10^{-3} will produce a BER of 9×10^{-3}. Applying this to the results computed above predicts that a BER of 3×10^{-3} occurred at a SNR = 9.77 (+1.72, -1.69) db and therefore meets the minimum specification of the required SNR of 9 ± 1.0 db.

Omnidirectional Antenna Gain Maps

In order to better visualize and interpret the significance of the signal level data, traces of the earth vector on the omnidirectional antenna gain contour maps are presented. Figures 5.3-2 and 5.3-3 show the antenna up and down links. Since signal level variations are, for the most part, the result of increasing range (i.e., more space loss) and changing omnidirectional gain, these plots allow visualization of the expected signal level changes for comparison with plots of up link and down link signal levels versus time.

5.3.4.2 Mission Phase One: Prelaunch to Spacecraft Acquisition

Subsystem performance is assessed during the launch pad systems readiness test and prelaunch countdown test. Next to assuring normal system performance prior to launch, the most important subsystem data taken during this phase are transmitter and receiver frequency data. Frequency data are used to predict the frequencies at initial acquisition and are transmitted from the Cape prior to launch. The DSS, in turn, uses these data to tune the DSS receiver for one-way lock and the DSS transmitter for eventual two-way lock.

The measured transmitter and receiver frequency data are tabulated in Table 5.3-6. Compartment temperature during the countdown period was increasing, thus causing the measured frequencies to decrease, as expected. The temperature directly affecting the frequency is not actually measured since the telemetered sensor is in the thermal tray and not at the voltage

TABLE 5.3-6. PRELAUNCH FREQUENCY SUMMARY*

Frequency Message, time in minutes	Measured Frequencies, MHz		Predicted Acquisition Frequencies, MHz		Lower Tray Temperature, °F
	One-Way NBVCXO	Best Lock	One-Way NBVCXO	Best Lock	
T-554 (Transmitter A)	2295.002187	2113.321336	2295.000187	2113.319336	73
T-490 (Transmitter B)	2295.002443	2113.308736	2295.001443	2113.306736	74
T-320 (Transmitter A)	2294.997051	2113.316128	2294.995051	2113.314128	79
T-83 (Transmitter B)	2295.003515	2113.311232	2295.002515	2113.310232	76
T-51 (Transmitter B)	2294.996571	2113.307376	2294.995571	2113.306376	76
T-30 (Transmitter B)	2294.994699	2113.305384	2294.993699	2113.304384	80

*Final frequencies used by FPAC for initial DSS-51 acquisition were those contained in the T-30 Report.

controlled crystal oscillator. Relative temperature versus frequency information is thus considered to be most reliable. Based on this judgment, the measured frequency data were consistent with previous Surveyor V test data.

Acquisition frequencies are determined by extrapolating the measured values by essentially predicting the compartment temperature increase due to the high power operation from just prior to Centaur/Surveyor separation to the time of initial spacecraft acquisition. The measured frequencies were biased by -1 kHz as determined from data obtained from Reference 4 and assuming 10 minutes of high power operation from injection to initial DSS-51 acquisition.

The actual frequencies at initial DSS-51 acquisition were:

Transmitter (one-way) = 2294.993024 MHz

Receiver (two-way) = 2113.306464 MHz

The difference between predicted and actual was:

Transmitter = 675 Hz

Receiver = 2080 Hz

Table 5.3-7 is a summary of the significant events during initial RF acquisition at DSS-51 (Johannesburg). One-way acquisition was accomplished 45 seconds before the predicted first visibility, and good two-way lock was accomplished 5 minutes and 46 seconds later. Telemetry data indicated a signal in the passband of receiver B at DSS transmitter turn-on. However, two-way lock was delayed due to a pointing problem associated with the ground station antenna system (Reference 1). The spacecraft received signal levels for both receivers A and B were greater than -80 dbm during the initial acquisition phase.

With the exception of the ground station antenna pointing problem, the initial spacecraft acquisition was nominal. The spacecraft high power transmitter was turned off 20 minutes and 44 seconds after being commanded to high power by the Centaur. The maximum allowable time to accomplish turnoff is 1 hour.

5.3.4.3 Mission Phase Two: Coast

The coast phases consist of the following:

1) Pre-Canopus acquisition — Period from initial spacecraft acquisition until Canopus acquisition. During this time, the spacecraft attitude is uncertain in roll, and the spacecraft -Z axis is pointed toward the sun.

2) Premidcourse — Period from Canopus acquisition until midcourse maneuvers.

TABLE 5.3-7. ACQUISITION EVENTS

Events	GMT (Day 251), hr:min:sec	Comments
Transmitter B high power on	08:16:16	Spacecraft commanded to high power by Centaur.
DSS-72 reports one-way acquisition	08:20:00	Not the initial acquisition station. Pass ended at 08:32:00 GMT.
DSS-51 acquires spacecraft one-way on SAA (acquisition aid antenna)	08:24:25	
DSS-51 auto tracking on SAA/paramp	08:25:43	
DSS-51 switch from SAA to SCM/Maser (85-foot antenna)	08:26:40	
DSS-51 transmitter turn-on	08:27:45	
Signal in passband of spacecraft receiver B	08:28:03	(From telemetry – first good line of TTY data since 08:25:19 GMT.) Receiver B not phase locked.
Signal in passband of spacecraft receiver A	08:28:34	(From telemetry) in AFC capture.
Phase lock receiver B	08:28:43	DSS receiver dropped phase lock, indicating phase lock on receiver B.

Table 5.3-7 (continued)

Events	GMT (Day 251), hr:min:sec	Comments
DSS-51 antenna to aided track	08:28:44	
DSS-51 receiver in lock on SAA/paramp	08:28:53	
Receiver B phase lock verified by telemetry	08:29:07	First good line of TTY data since 08:28:36 GMT.
DSS-51 antenna to SCM maser	08:29:50	
DSS-51 reports good two-way data	08:30:11	Good two-way acquisition 33 minutes and 10 seconds after launch.
DSS-51 command modulation on	08:31:20	
Transmitter B high power off	08:37:00	Spacecraft was in high power for 20 minutes and 44 seconds for initial acquisition phase (a maximum time of 1 hour is allowed).
DSS-51 suspects lock to antenna sidelobe	08:39:34	Signal level low (-122 dbm) and demodulator glitching.
DSS-51 confirms sidelobe lock. Good data restored.	08:41:00	Signal level restored (-110 dbm) DSS-51 back on main lobe.

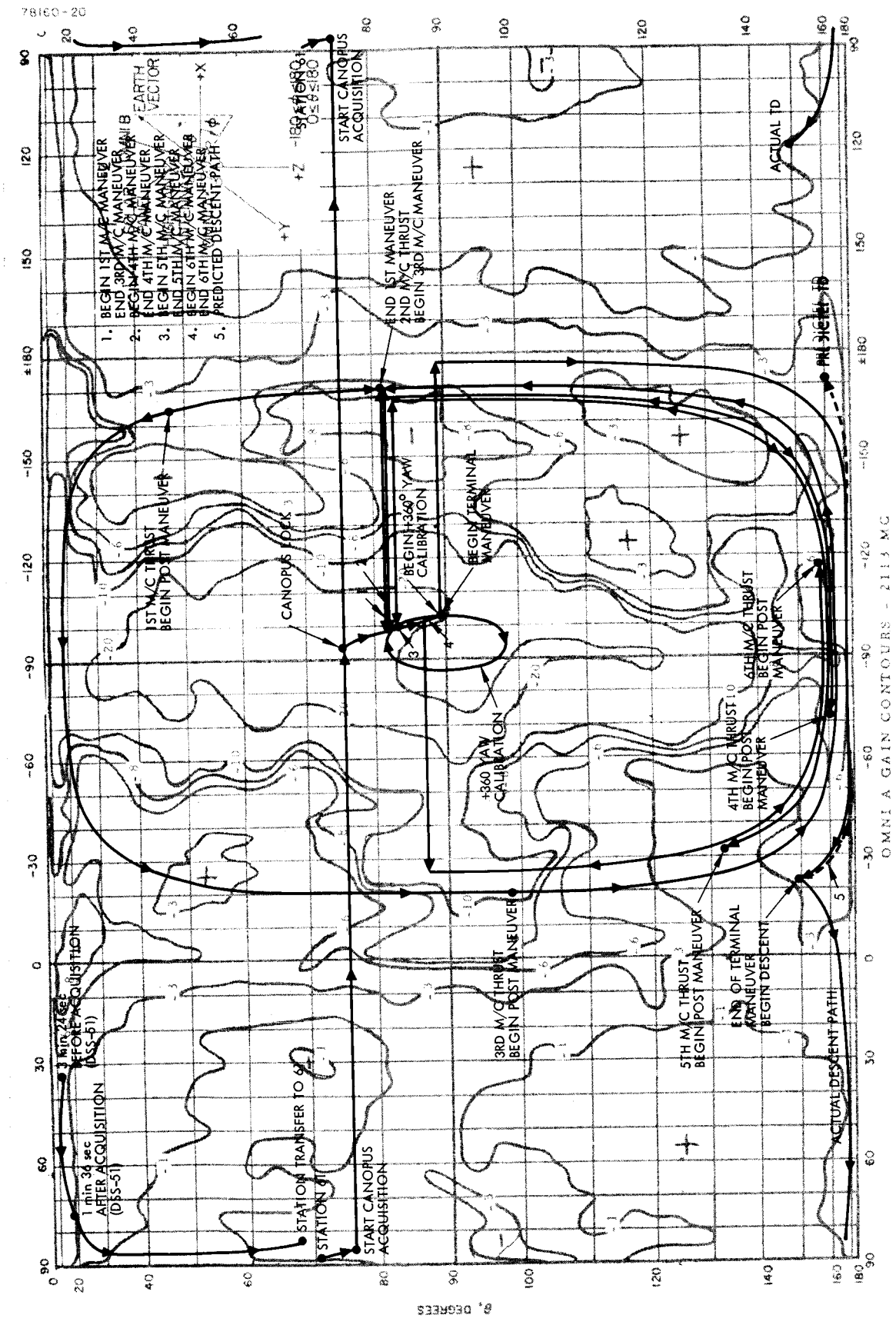

a) Omnidirectional Antenna A

Figure 5.3-2. Up Link (2113 MHz) Omnidirectional Antenna Gain Map

3) Postmidcourse – Period from completion of midcourse maneuvers until terminal maneuvers.

Figures 5.3-4 and 5.3-5 are plots of DSS, receiver A, and receiver B signal levels from launch to touchdown. The premission predicted signal level after Canopus acquisition is shown in each figure. Since the spacecraft attitude in roll is uncertain to ±60 degrees about an estimated reference point prior to Canopus acquisition, no premission predictions are made for this period.

Both up and down link signal level readings prior to Canopus acquisition indicated that omnidirectional antenna A was operating in a more favorable position relative to the ground tracking station than omnidirectional antenna B. Approximately 4 hours after launch, the ground received signal level with the spacecraft transmitting on omnidirectional antenna B had reached the nominal 1100 bits/sec threshold value (3×10^{-3} BER). Omnidirectional antenna A was selected for spacecraft data transmission in order to improve the quality of the PCM data. A 17-db increase in the signal level was noted with the resulting -125.0 dbm received carrier power providing a 13.6-db nominal telemetry margin for the 1100 bits/sec data. The spacecraft transmitted on omnidirectional antenna A for the remainder of the pre-Canopus mission phase.

Referring to Figures 5.3-3 and 5.3-4, which show traces of the earth vector relative to omnidirectional antenna B down link and omnidirectional antennas A and B up link gain contours, it can be noted that changes in signal levels during the pre-Canopus acquisition phase and right at Canopus acquisition are in complete agreement with the antenna gain contour maps. The approximate antenna gains during the pre-Canopus phase are noted in Table 5.3-8.

Figures 5.3-5 and 5.3-6 indicate that, during the premidcourse and postmidcourse coast periods, received signal levels deviated from the predicted values in both the up and down links. Gyro drift checks performed during these two periods account for earth vector variations not taken into consideration when generating the predictions. As pointed out in Reference 2, these minor look angle variations can cause the observed signal level variations. However, the data indicate that the tolerances on the nominal predicted signal level, which also includes antenna gain variations, bound those values seen in the mission data.

On GMT day 252, after execution of the fifth midcourse-type maneuver, an alpha scattering background count experiment was performed. The spacecraft configuration was transmitter B, high power, omnidirectional antenna B, and 550 bits/sec low modulation index data multiplex mode. Good quality data were obtained during the experiment with the DSS-42 received carrier power of -123.5 dbm, indicating nominal SNRs of 16.0 db for the PCM data, and 19.8 and 20.9 db for the two alpha scattering channels.

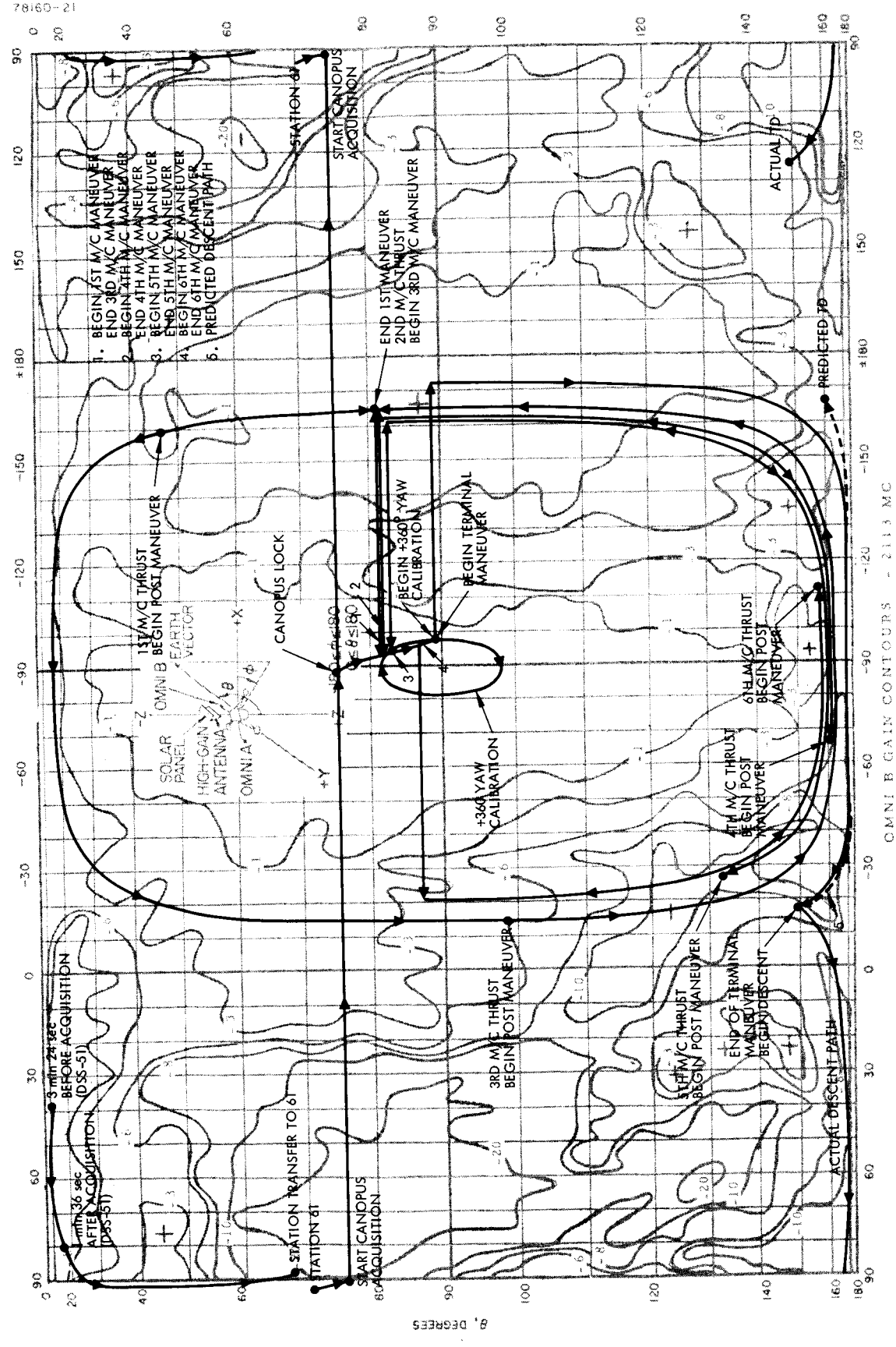

b) Omnidirectional Antenna B

Figure 5.3-2 (continued). Up Link (2113 MHz) Omnidirectional Antenna Gain Map

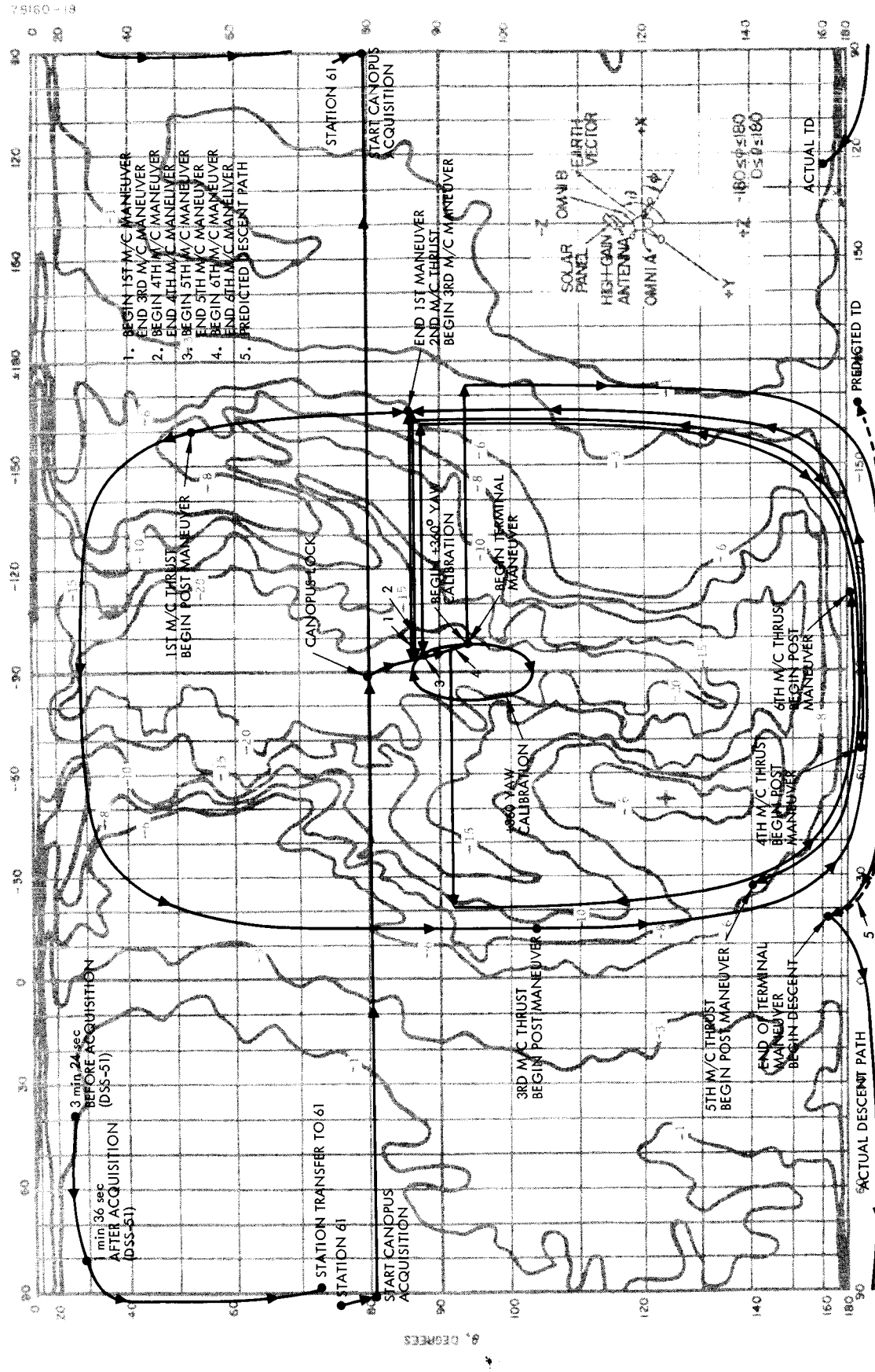

a) Omnidirectional Antenna A

Figure 5.3-3. Down Link (2295 MHz) Omnidirectional Antenna Gain Map

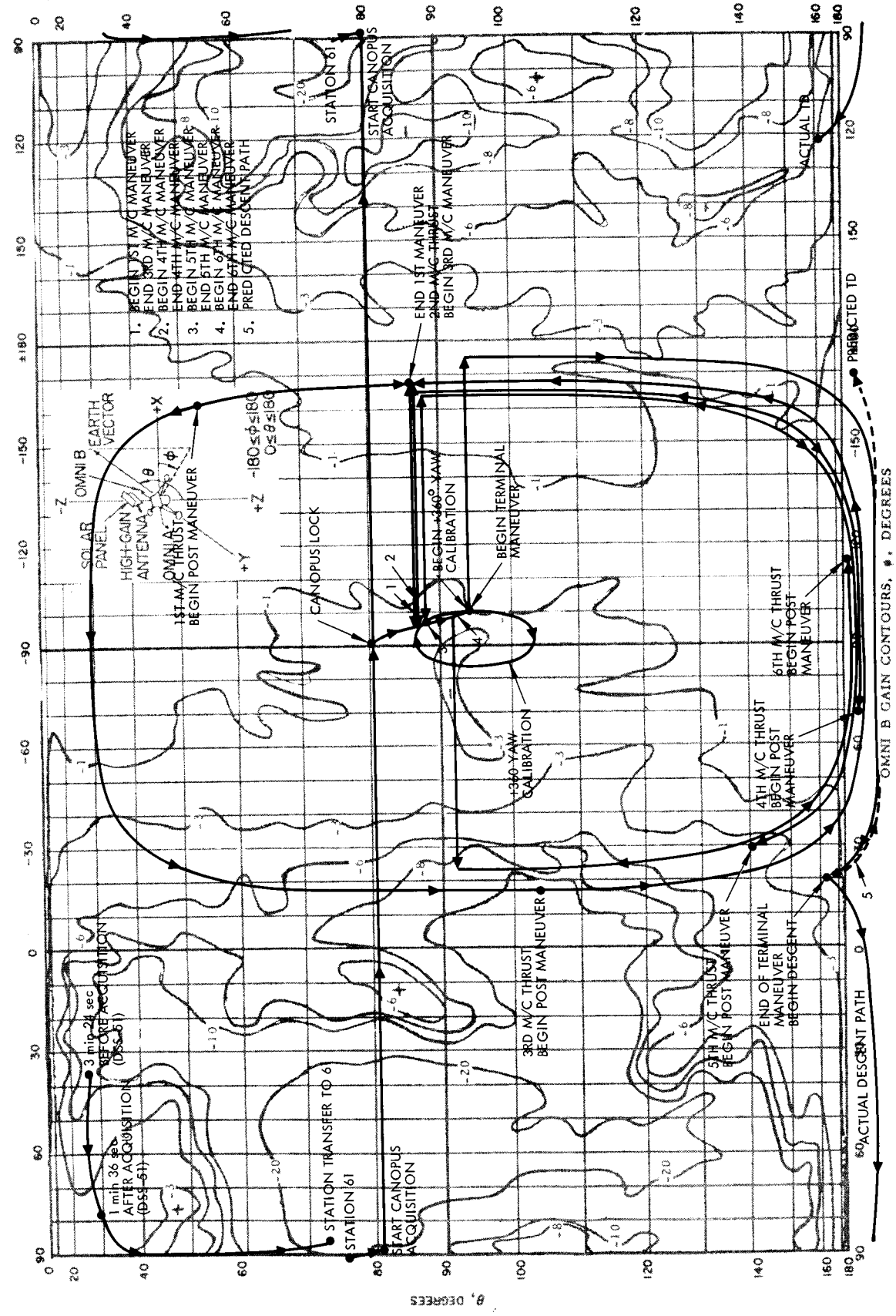

b) Omnidirectional Antenna B

Figure 5.3-3 (continued). Down Link (2295 MHz) Omnidirectional Antenna Gain Map

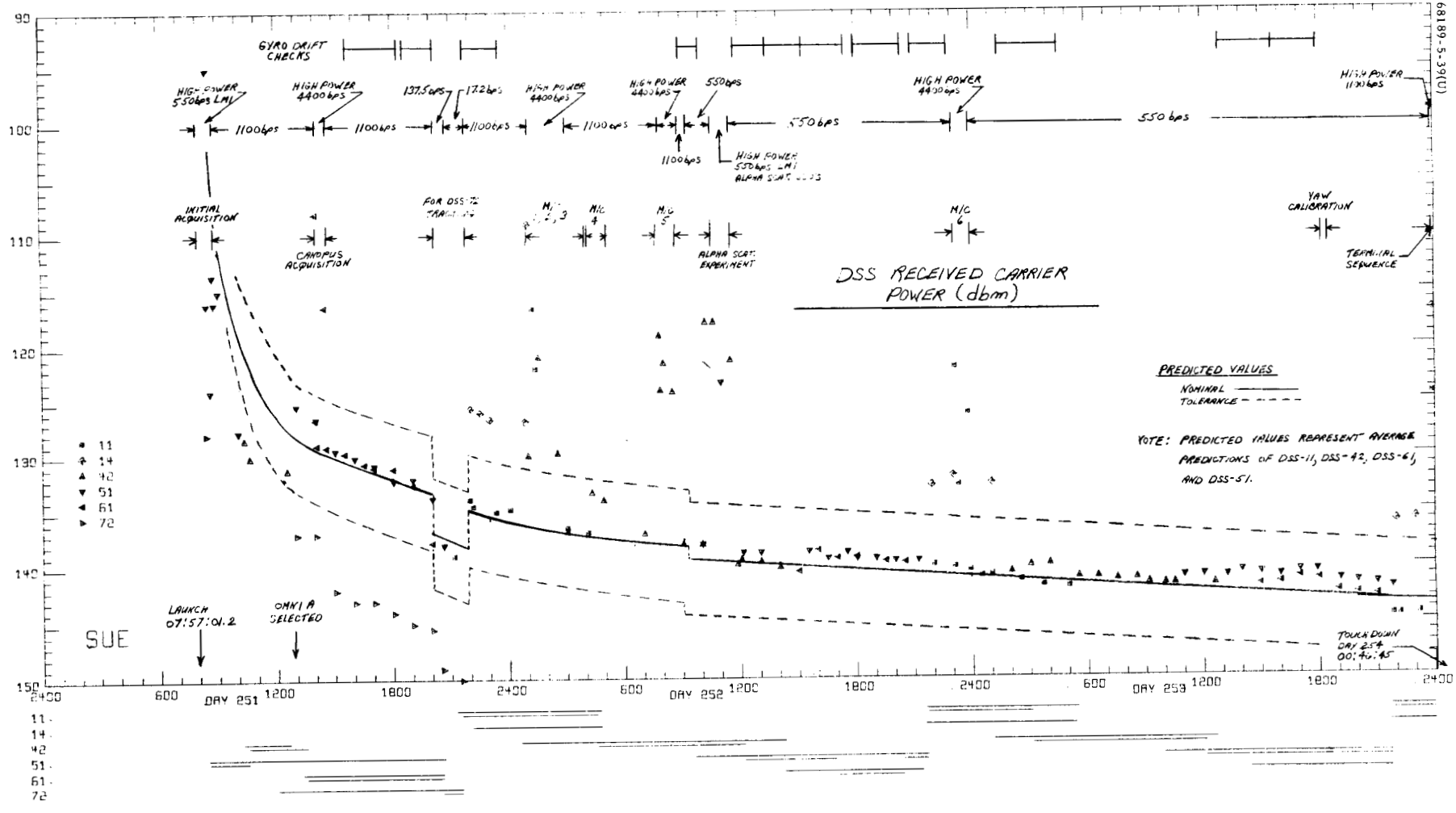

Figure 5.3-4. DSS-Received Carrier Power (dbm)

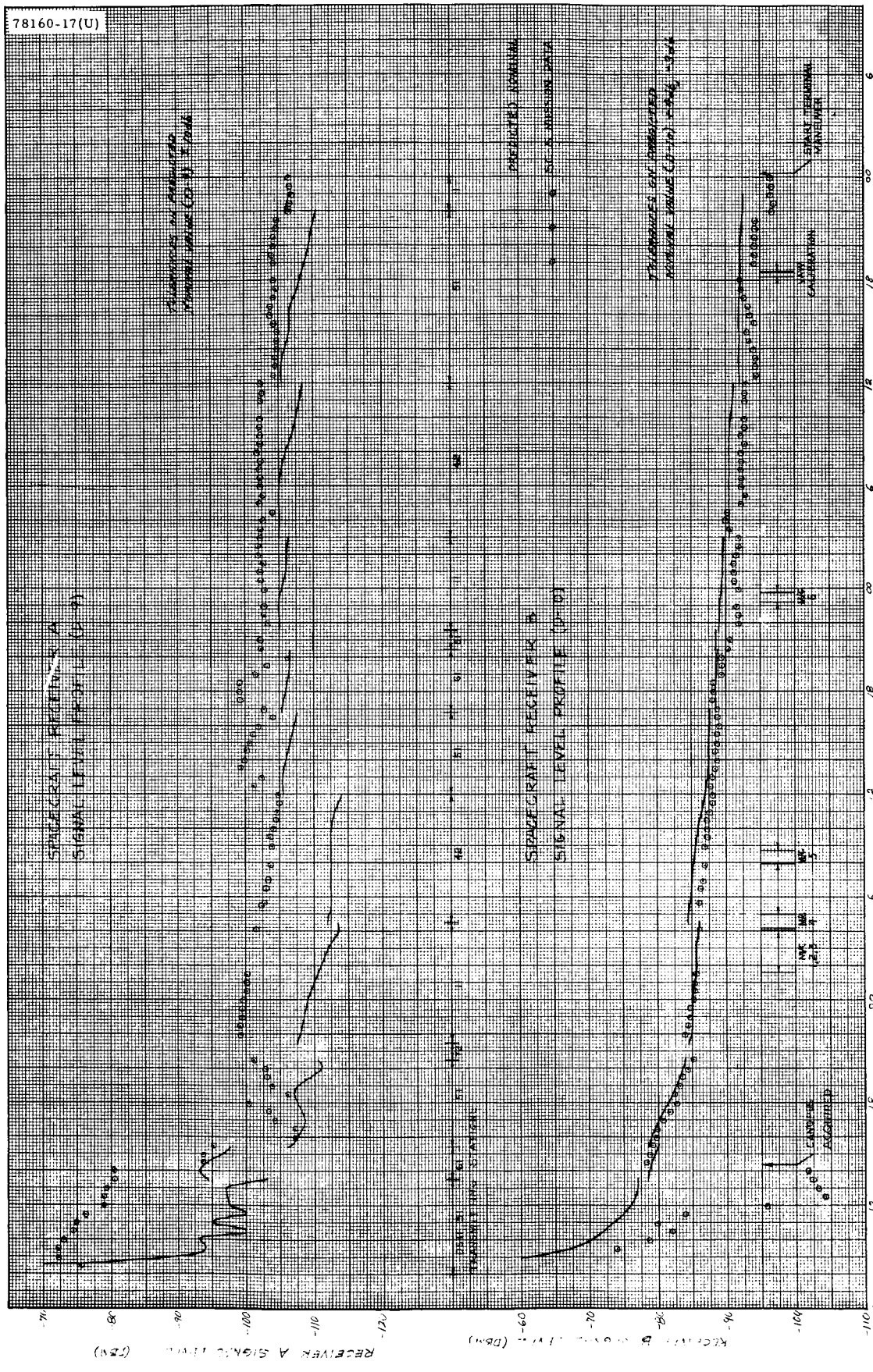

Figure 5.3-5. Spacecraft Receiver Signal Level Profile

TABLE 5.3-8. PRE-CANOPUS ANTENNA GAIN VARIATIONS

	Gain Variations (Coast), db		Pre-Canopus Gain, db		Gain at Canopus, db	
	Predicted	Actual	Predicted	Actual	Predicted	Actual
Omnidirectional antenna A down link	0.0 steady	-0.6 steady	—	—	—	—
Omnidirectional antenna B down link	-1.0 to -20.0	-9.8 to -17.3	-19.2	-19.4	-1.4	+0.4
Omnidirectional antenna A up link	-1.0 to -4.0	+0.2 to -15.3	-0.2	-1.2	-13.6	-13.0
Omnidirectional antenna B up link	-2.0 to -20.0	0.0 to -29.0	-13.7	-17.0	+2.0	+0.9

A special in-flight plus yaw maneuver calibration test was performed at approximately 18:00 GMT of day 253. Analysis of the required 360-degree maneuver indicated that it would not be necessary to alter the spacecraft from its normal cruise configuration. Two-way lock was maintained at DSS-51 for the duration of the maneuver, with the spacecraft transmitting in low power at 550 bits/sec data. Spacecraft received signal level variations were 7.8 db for receiver A and 4.9 db for receiver B.

At approximately L+25-1/2 hours, the spacecraft data rate was reduced to 550 bits/sec. At 1100 bits/sec data, the received carrier power at DSS-42 had been running approximately -138.9 dbm with a nominal telemetry margin of -0.3 db. Excessive errors in the data were not noted; however, the ground system was experiencing some data processing difficulties. The 550 bits/sec data rate continued to be the normal data mode for the remainder of the coast phase. A maximum bit error rate of 9×10^{-3} was reported from DSS-11 just prior to initiation of the terminal sequence. The signal level at this time was -144.5 dbm, which results in a -0.8 db nominal margin at 550 bits/sec data based on a 3×10^{-3} bit error rate.

5.3.4.4 Mission Phase Three: Canopus Acquisition Maneuver

At approximately L+6 hours, the star acquisition maneuver was initiated. One roll about the Z-axis was required to make a star map and adequately identify Canopus. An additional 179 degrees of roll were required to finally acquire the star.

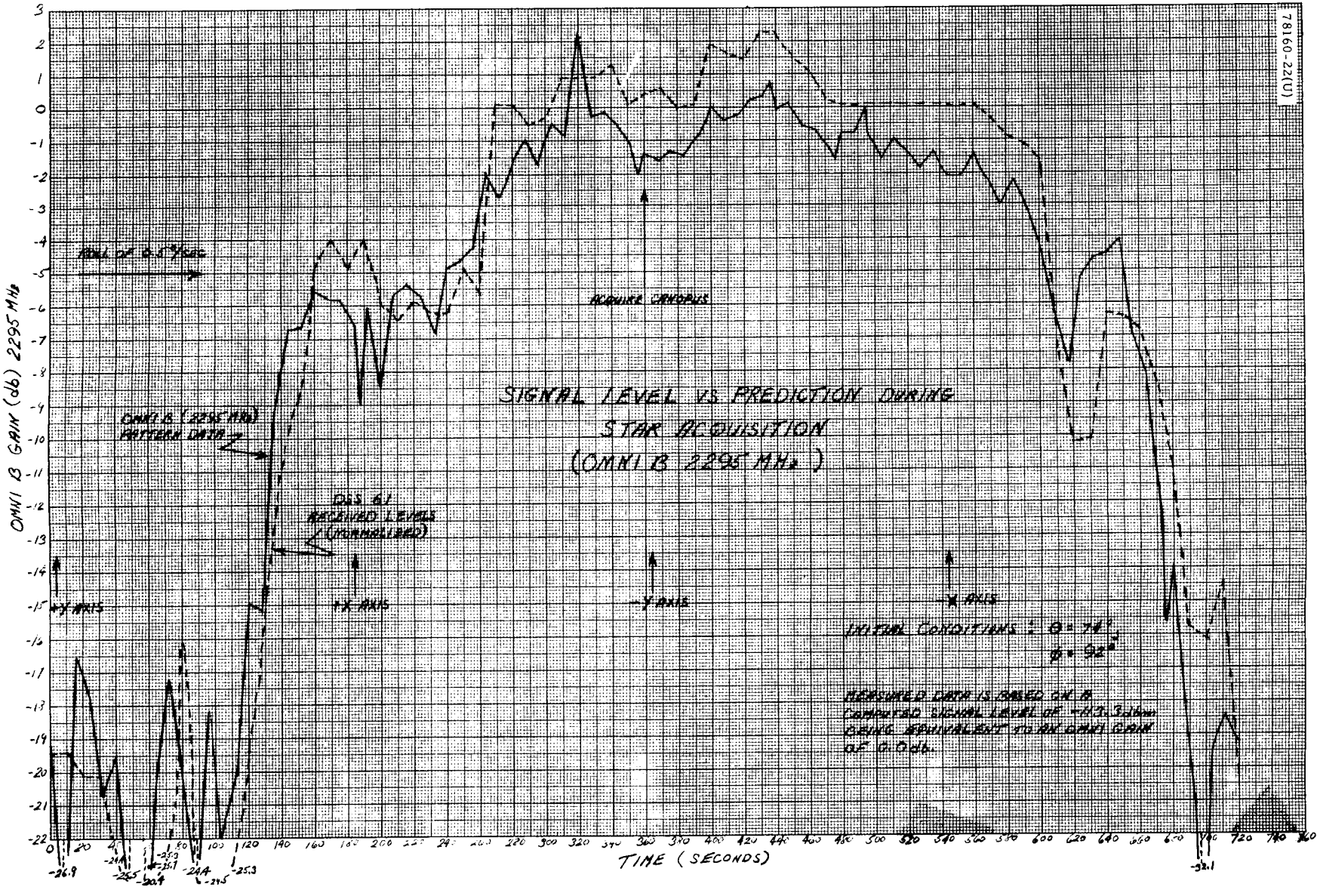

a) Omnidirectional Antenna B Down Link (2295 MHz)

Figure 5.3-6. Signal Level Versus Predictions During Star Acquisition

Real-time analysis indicated that the roll maneuver would take the earth vector through deep antenna nulls on both the up and down links of both omnidirectional antennas A and B. However, predicted signal level values during the maneuver, even considering worst-case tolerances, would not exceed the two-way tracking threshold. The transponder mode was therefore recommended for the acquisition sequence. Also, the analysis indicated that no significant stars existed in the vicinity of possible data outages with the spacecraft transmitting via omnidirectional antenna B at a data rate of 4400 bits/sec.

At 14:03:28 GMT, transmitter B was commanded to high power with the ground received signal indicating an increase of 18.7 db. Omnidirectional antenna B was selected at 14:04:31 GMT, and star mapping was initiated at 14:10:02 GMT from DSS-61 with the spacecraft operating in the transponder B mode and transmitting data at 4400 bits/sec in mode 1. The 360-degree roll produced down link signal variations of approximately 33 db, which agreed with the premaneuver predictions. Data outages occurred within the predicted region; however, down link carrier lock was maintained throughout the mapping maneuver. Spacecraft received signal levels during the roll maneuver indicated deviations of approximately 30 db on receiver A and 33 db on receiver B. This again agreed with premaneuver predictions. Phase lock on receiver B was maintained throughout the maneuver, and Canopus lock-on was accomplished at 14:27:52 GMT.

Transmitter B high power was commanded off at 14:33:41 GMT, which resulted in 30 minutes and 13 seconds of high power operation for star acquisition. DSS-61 received signal level for low power operation was -129.2 db, with a resulting +9.4 db nominal telemetry margin for 1100 bits/sec data.

The spacecraft was 179 degrees in a positive roll sense from Canopus prior to the initiation of the Canopus acquisition/verification sequence. With this information and the antenna contour patterns, the variations in antenna gain seen in the data are compared to predicted variations and are illustrated in Figure 5.3-6 which compares omnidirectional antenna B down link, omnidirectional antenna A up link, and omnidirectional antenna B up link, respectively. Both omnidirectional antenna B up and down link signal level variations agree well with antenna gain variations. However, again as has been the case in previous missions, it was during this maneuver that the first evidence of a possible bias in receiver B performance was noted.

Relatively good agreement exists between omnidirectional antenna A up link gain values and the actual signal level variations, except for those values in the region between the +X axis and the -Y axis. The observed gain values within this region lie below those values obtained from antenna pattern data. Similar unexplained deviations such as this have been noted on previous missions (References 2 and 3).

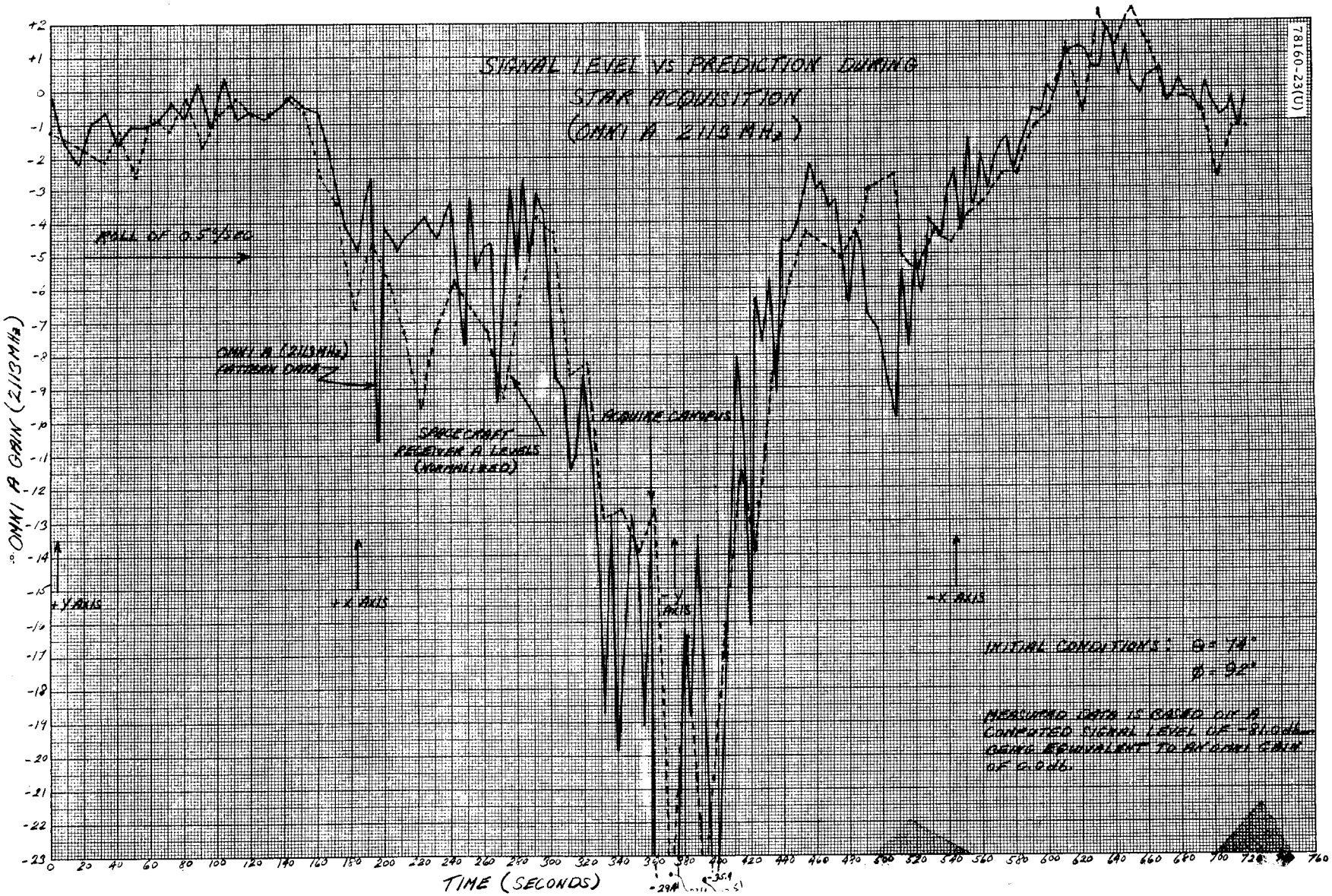

b) Omnidirectional Antenna A Up Link (2113 MHz)

Figure 5.3-6 (continued). Signal Level Versus Predictions During Star Acquisition

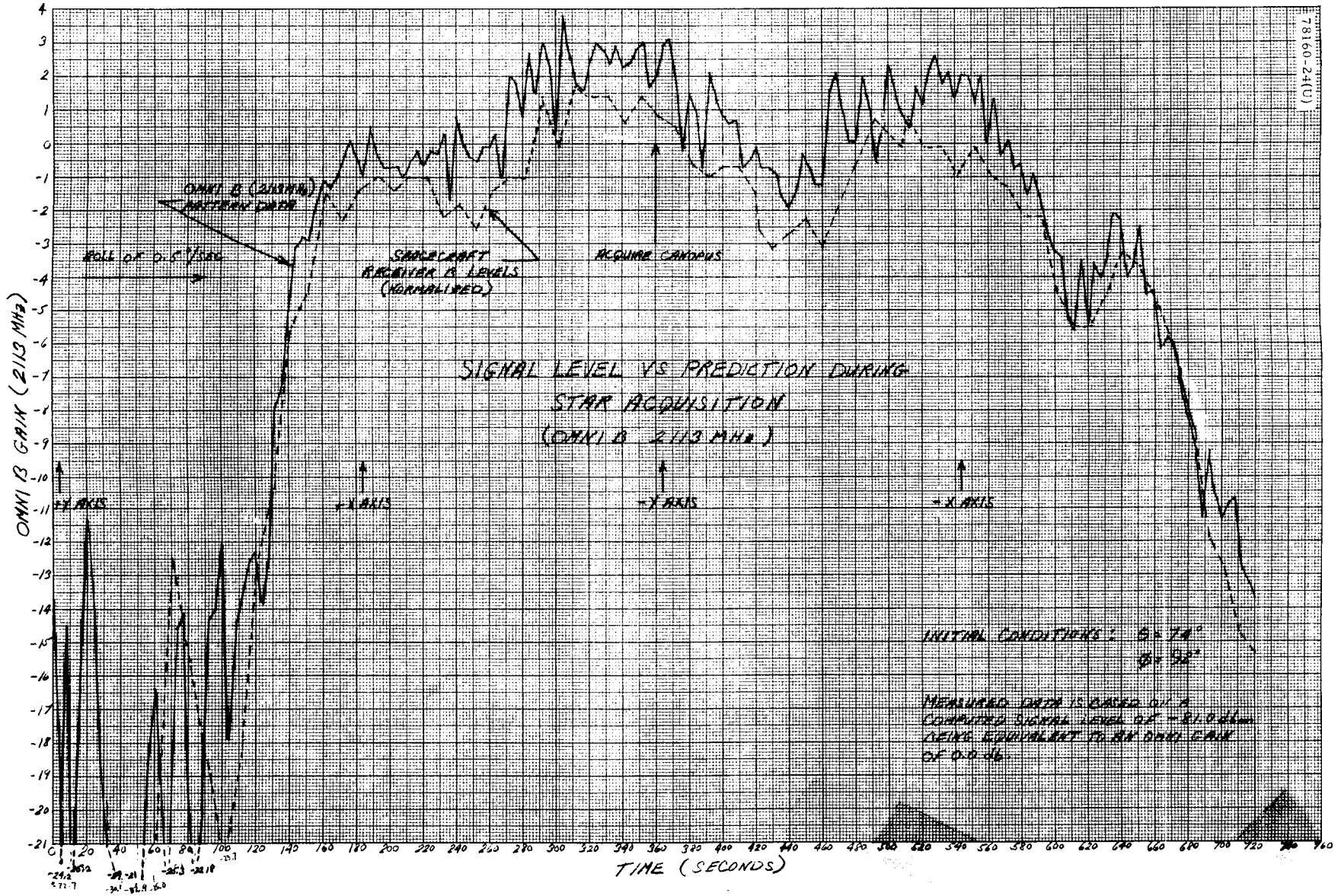

c) Omnidirectional Antenna B Up Link (2113 MHz)

Figure 5.3-6 (continued). Signal Level Versus Predictions During Star Acquisition

TABLE 5.3-9. SURVEYOR V MIDCOURSE MANEUVER SUMMARY

Maneuver	Start Time (GMT), day 252 hr:min:sec	Attitude Rotations and Thrusting	Signal Level Variations, db: Spacecraft to Earth (Omni B) Predicted	Spacecraft to Earth (Omni B) Observed	Earth to Spacecraft: Receiver A Predicted	Receiver A Observed	Receiver B Predicted	Receiver B Observed	Spacecraft to Earth PCM Data Rate, bps	Spacecraft to Earth (PCM Data) Predicted	Spacecraft to Earth (PCM Data) Observed	Minimum Margins, db: Earth to Spacecraft (Command) Receiver A Predicted	Receiver A Observed	Receiver B Predicted	Receiver B Observed	Comments
Midcourse 1 (nominal midcourse)	01:32:57	Prethrust Roll +71.8 degrees	2.8	3.3	18.2	17.5	5.4	7.1	4400	15.2	17.0	8.4	4.7	23.1	21.8	High power on at 01:15:20
	01:38:06	Prethrust yaw -35.6 degrees	1.7	2.4	3.9	3.5	2.4	3.2	4400	15.8	17.4	18.8	21.9	25.9	25.7	High power not commanded off until after midcourse 3
	01:45:02	Thrust 14.25 seconds	--	0.2	--	0.3	--	0.0	4400	--	19.3	--	25.1	--	25.7	
	01:53:51	Post-thrust yaw +35.6	1.7	2.3	3.9	2.7	2.4	3.8	4400	15.8	17.0	18.8	22.7	25.9	24.7	
Midcourse 2 (sunline maneuver)	02:12:02	Thrust 10.05 seconds	--	0.4	--	1.2	--	0.4	4400	--	17.2	--	20.2	--	28.5	High power on before midcourse 1 and not turned off until after midcourse 3
Midcourse 3 (anti-sunline maneuver)	02:24:33	Prethrust yaw -180 degrees	10.0	10.9	13.0	11.8	8.0	9.3	4400	5.8	9.4	11.0	12.7	20.0	19.2	High power off at 02:55:41
	02:39:51	Thrust 23.05 seconds	--	0.7	--	0.2	--	0.0	4400	--	8.7	--	19.2	--	22.9	High power operation for 1 hour 40 minutes and 21 seconds
	02:45:22	Post-thrust yaw -180 degrees	11.0	11.5	7.0	10.2	17.0	9.7	4400	4.8	8.8	17.0	15.8	11.2	19.2	
	04:00:47	Post-thrust roll -71.8 degrees	2.8		18.2	13.2	5.4	7.0	1100	18.3		8.4	7.5	22.9	21.2	Roll executed in low power
Midcourse 4	04:05:55	Prethrust roll +68.5 degrees	2.8		18.2	14.0	5.4	7.0	1100	17.9		8.4	7.9	22.5	21.5	Maneuver executed in low power
	04:09:33	Prethrust yaw +106.8 degrees	1.0		6.0	6.4	8.0	7.4	1100	17.7		17.6	13.7	19.6	21.5	Post-thrust maneuvers executed over DSS 42
	04:18:48	Thrust 13.1 seconds	--		--	0.7	--	0.4	1100	--		--	18.4	-	22.4	
	04:58:13	Post-thrust yaw -106.8 degrees	1.0		6.0	8.1	8.0	7.0	1100	17.7		17.6	14.6	19.6	17.7	
	05:04:11	Post-thrust roll -68.5 degrees	2.8		18.2	10.9	5.4	6.7	1100	17.9		8.4	12.0	22.5	17.7	
Midcourse 5	07:54:30	Prethrust roll +64.6 degrees	2.8		18.2	9.8	5.2	5.9	4400	13.8		7.0	11.8	21.7	21.5	High power on at 07:49:35
	07:58:31	Prethrust yaw +143.2 degrees	4.3		6.7	9.9	9.3	10.1	4400	12.6		17.0	14.2	13.2	19.2	High power off at 08:46:51
	08:24:04	Thrust 33.05 seconds	--		-	0.0	--	0.0	4400	--		--	24.1	--	20.6	High power operation for this maneuver 57 minutes and 16 seconds
	08:33:51	Post-thrust yaw -143.2 degrees	4.3		6.7	9.3	9.3	8.8	4400	12.6		17.0	14.8	13.2	19.7	
	08:40:35	Post-thrust roll -64.6 degrees	2.8		18.2	11.6	5.2	5.3	4400	13.8		7.0	8.5	21.7	21.8	
Midcourse 6	23:13:51	Prethrust roll -76.0 degrees	8.0	7.0	15.0	19.3	3.0	7.5	4400	5.4	6.5	-3.1	-2.4	17.9	17.5	High power on at 34:06:30
	23:19:36	Prethrust yaw -100.6 degrees	10.0	10.0	10.0	10.9	13.0	5.9	4400	3.7	5.9	9.9	10.0	6.9	12.8	High power off at 23:51:35
	23:30:58	Thrust 5.45 seconds	--	1.4	--	0.0	--	0.3	4400	--	15.9	--	11.4	--	15.0	High power operation for this maneuver 45 minutes and 5 seconds
	23:36:07	Post-thrust yaw +100.6 degrees	10.0	10.8	10.0	11.2	13.0	17.9	4400	3.7	5.8	9.9	9.5	6.9	11.8	
	23:44:05	Post-thrust roll -76.0 degrees	8.0	6.9	15.0	11.0	3.0	5.1	4400	5.4	6.1	-3.1	5.7	17.9	18.9	

5.3.4.5 Mission Phase Four: Midcourse Maneuvers

The L+17-1/2 hours standard roll-yaw negative $\dot{U}_3$ maneuver was selected from 16 possibilities as the midcourse maneuver. Real-time analysis predicted the following variations in nominal omnidirectional antenna gain during the maneuver:

1) Omnidirectional antenna B down link: $-1.8 < G < +1.0$ db

2) Omnidirectional antenna A up link: $-17.8 < G < +0.4$ db

3) Omnidirectional antenna B up link: $-3.1 < G < +2.3$ db

Predicted maneuver margins were 15.8 db for 4400 bits/sec telemetry, 9.0 db on receiver A, and 26.5 db on receiver B command links. Two-way (transponder) mode was recommended.

At 1:15:20 GMT, the spacecraft was commanded to high power, and, at 1:15:57 GMT, the 4400 bits/sec data rate was selected. The ground received signal increased by 18.3 db when the spacecraft was commanded from low power to high power, with DSS-11 reporting a received carrier power of -121.8 dbm prior to maneuvering. Maneuver initiation times were 1:32:57 GMT for the roll and 1:38:16 GMT for the yaw. The DSS-11 received carrier power at the end of the premidcourse maneuver was reaching -119.8 dbm and had indicated approximately a 3.3-db variation during the maneuvers, as predicted. Spacecraft receiver signal level variations were approximately 17.5 db for receiver A and 7.1 db for receiver B as opposed to predicted variations of 18.2 and 5.4 db for receiver A and B, respectively.

At 1:45:02 GMT, midcourse thrust was executed. DSS-11 received carrier power was steady with reported 0.2-db variations during the thrusting period.

After termination of thrusting, a leak in the helium pressurization system was detected. The normal postmidcourse yaw maneuver was performed, followed by nonstandard operational attempts to correct the observed anomaly. A series of five subsequent midcourse-type maneuvers was performed during the nonstandard sequence, with the last of the maneuvers being completed at approximately L+40 hours. Each maneuver was evaluated prior to initiation, and all were determined to not violate any constraint of the telecommunication subsystem in the proposed maneuvering configuration. Table 5.3-9 contains a summary of the observed performance and predicted performance for all the maneuvers.

No telecommunication problems were encountered during any of the maneuvering. All maneuvers were executed in high power and 4400 bits/sec data with the exceptions of midcourse 4 and the post-thrust roll of midcourse 3 which were executed in low power at 1100 bits/sec. Two-way transponder B operation was supported during all maneuvers, with the exception of the post-thrust yaw and roll of midcourse 4. Adequate two-way tracking margin was available for this case; however, the ground tracking station, DSS-42,

did not phase lock the spacecraft receiver during the station transfer which took place after the midcourse 4 thrust and prior to the post-thrust yaw (Reference 1). Maneuvers 1, 2, 3, and 6 were initiated over DSS-11, and maneuver 5 over DSS-42. The prethrust roll, prethrust yaw, and thrusting of midcourse 4 were executed over DSS-11, with the post-thrust yaw and roll maneuvers being handled by DSS-42.

The third midcourse-type maneuver, anti-sunline, involved a 360-degree yaw that caused the look angle to move through a rather wide range of antenna gain values. This had never been the case for any maneuver, other than Canopus roll maneuvers, on any previous spacecraft. The variations in antenna gain seen in the data are compared to predicted variations and are illustrated in Figure 5.3-7 which compares data for omnidirectional antenna B down link, omnidirectional antenna A up link, and omnidirectional antenna B up link. The data contained in this figure produce the same general conclusions as those resulting from a similar comparison using the data obtained during the Canopus roll maneuver.

5.3.4.6 Mission Phase Five: Terminal Maneuver

The influencing factor in the determination of the terminal maneuver was the anomaly in the helium pressurization system. The roll-yaw standard maneuver was selected in preference to the other computed maneuvers from considerations other than optimization of the telecommunication subsystem and was therefore the only maneuver evaluated in regard to RF performance. The real-time analysis predicted the following variations in nominal omni-directional antenna gains during the maneuver:

1) Omnidirectional antenna B down link: $-2.6 < G < +1.1$ db

2) Omnidirectional antenna A up link: $-16.5 < G < -2.1$ db

3) Omnidirectional antenna B up link: $-7.6 < G < +2.9$ db

Predicted minimum margins were 5.6 db for 1100 bits/sec telemetry, and 2.9 db on receiver A and 11.8 db on receiver B command links. One-way mode was recommended even though adequate margins were available for transponder operation. This recommendation was made since the one-way configuration was desired for the terminal descent sequence and, operationally, it was safer to establish this mode before the terminal maneuver.

The spacecraft was commanded to high power at 23:51:41 GMT of day 253. The resulting -124.5 dbm signal level indicated an increase of 19.3 db over low power operation. Transponder B was turned off at 00:04:21 GMT of day 254, establishing the spacecraft for the terminal sequence. Maneuver initiation times were 00:12:15 GMT and 00:16:21 GMT for the roll and yaw, respectively. The terminal maneuvers ended at approximately 00:20:20 GMT with the DSS-11 received carrier power reading -124.7 dbm and having indicated approximately a 3.8-db variation during the maneuver, as compared to a predicted variation of 3.7 db.

Up link signal level variations observed in the telemetry data, as compared to predicted variations, are summarized as follows:

	Gain Variations, db	
	Actual	Predicted
Omnidirectional antenna A	22.9	14.4
Omnidirectional antenna B	10.8	10.5

5.3.4.7 Mission Phase Six: Descent and Touchdown

A preterminal maneuver analysis was performed to evaluate the anticipated data link performance during the descent phase with the strain gauges on prior to retro ignition. This deviation from previous procedure was desired due to the nature of the operational sequence for the special descent which was necessary as a result of the existing spacecraft anomaly. Also, as a result of the Surveyor 4 postmission failure analysis, it was felt that touchdown strain gauge data could provide a better understanding of the failure if it recurred on subsequent spacecraft (Reference 3).

The preterminal analysis indicated that 1100 bits/sec data with strain gauges could be obtained at DSS-14 (210-foot antenna) with a BER less than 3×10^{-3} under worst-case descent conditions. A worst-case BER of 1.3×10^{-2} could be expected at DSS-11 for the same conditions. Also, it was determined that minimum margins would be encountered during retro burn and the initial part of the steering phase. The performance at touchdown was predicted not to be marginal even at DSS-11.

The touchdown strain gauges were turned on at 00:21:38 GMT. The DSS-11 received carrier power was -127.7 dbm prior to retro ignition, which was in agreement with the predicted nominal value used for the preterminal strain gauge feasibility analysis.

Retro burn was initiated at approximately 00:44:53 GMT, and the signal level at DSS-11 remained steady with approximately a 0.9-db variation during the burn period. Burnout occurred at approximately 00:45:33 GMT, and the spacecraft began the steering phase of descent. Signal level variations during descent followed the worst-case predicted values, indicating that the earth vector did not follow the expected nominal path during this phase. Signal level variations were 7.7 db for receiver A, 3.9 db for receiver B, and 7.4 db at the ground station receiver. The minimum down link signal level at DSS-11 was -133.7 dbm, which resulted in a -1.5 db nominal margin for 1100 bits/sec data based on a 3×10^{-3} BER.

Figure 5.3-8 illustrates the received carrier power profile at DSS-11 during the descent phase. Also included on this plot are the number of parity errors in the 1100 bits/sec data observed in each frame of data obtained during this period. If one assumes that the number of parity errors is representative of the number of bit errors, then the ratio of the parity

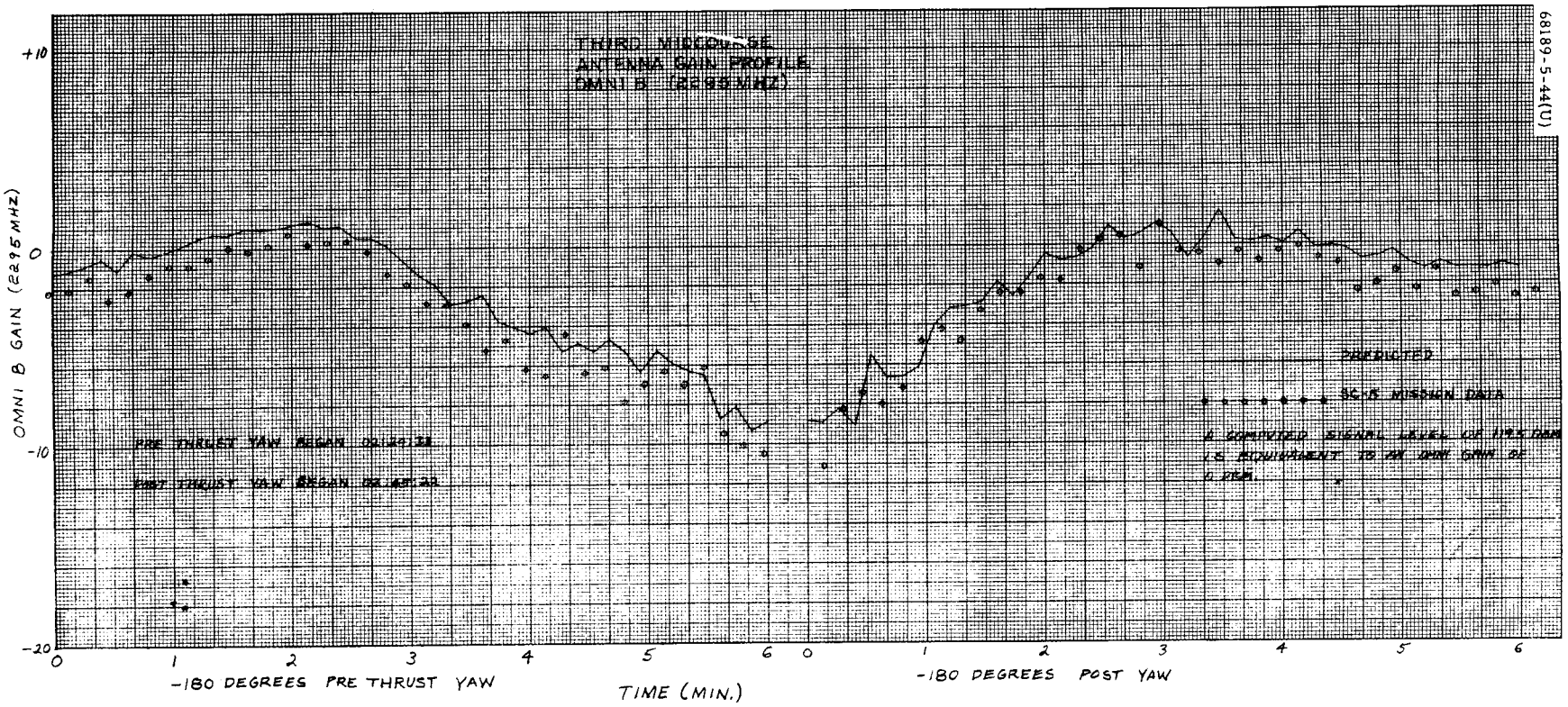

a) Omnidirectional Antenna B (2295 MHz)

Figure 5.3-7. Third Midcourse Antenna Gain Profile

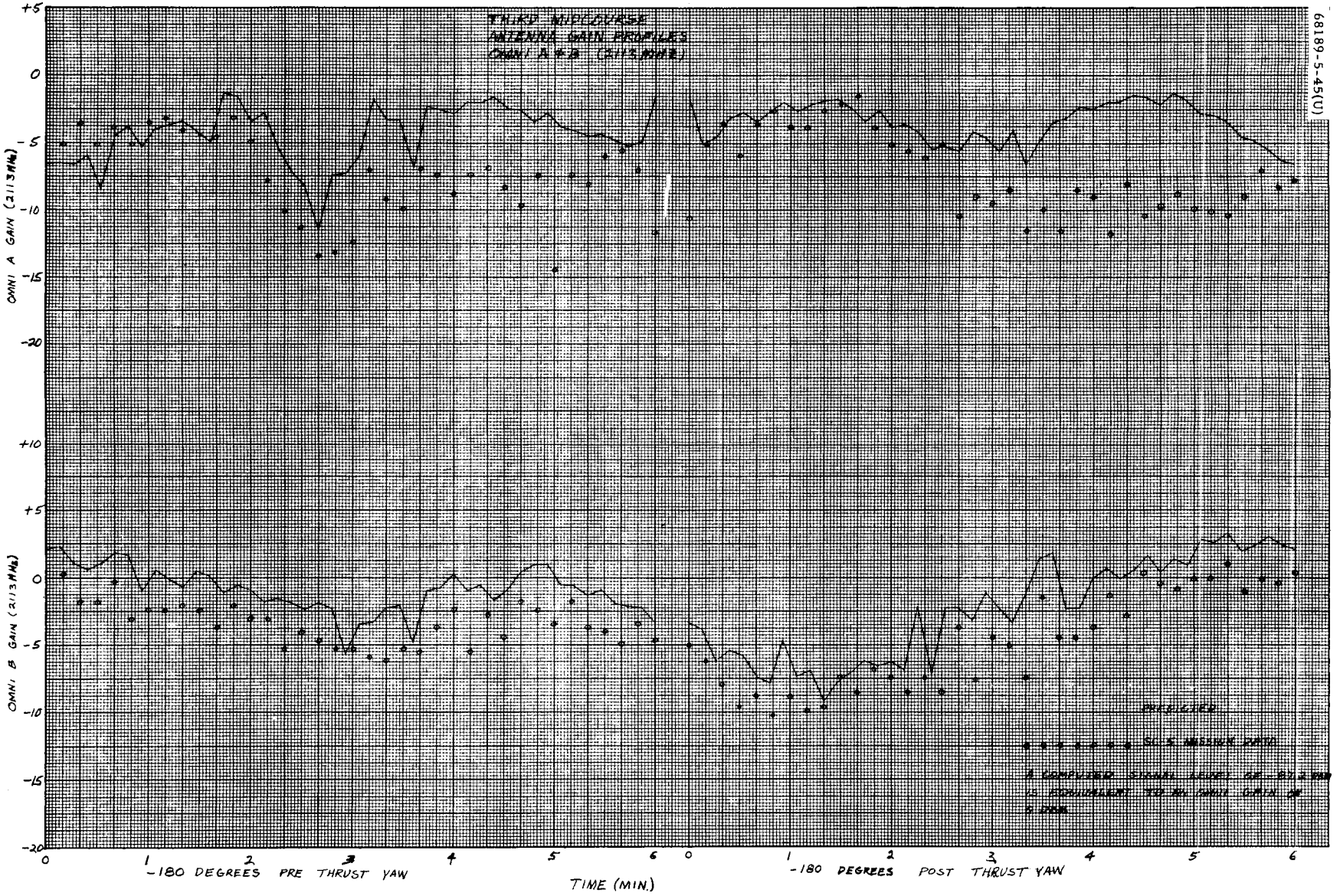

b) Omnidirectional Antennas A and B (2113 MHz)

Figure 5.3-7 (continued) Third Midcourse Antenna Gain Profile

68189-5-46(U)

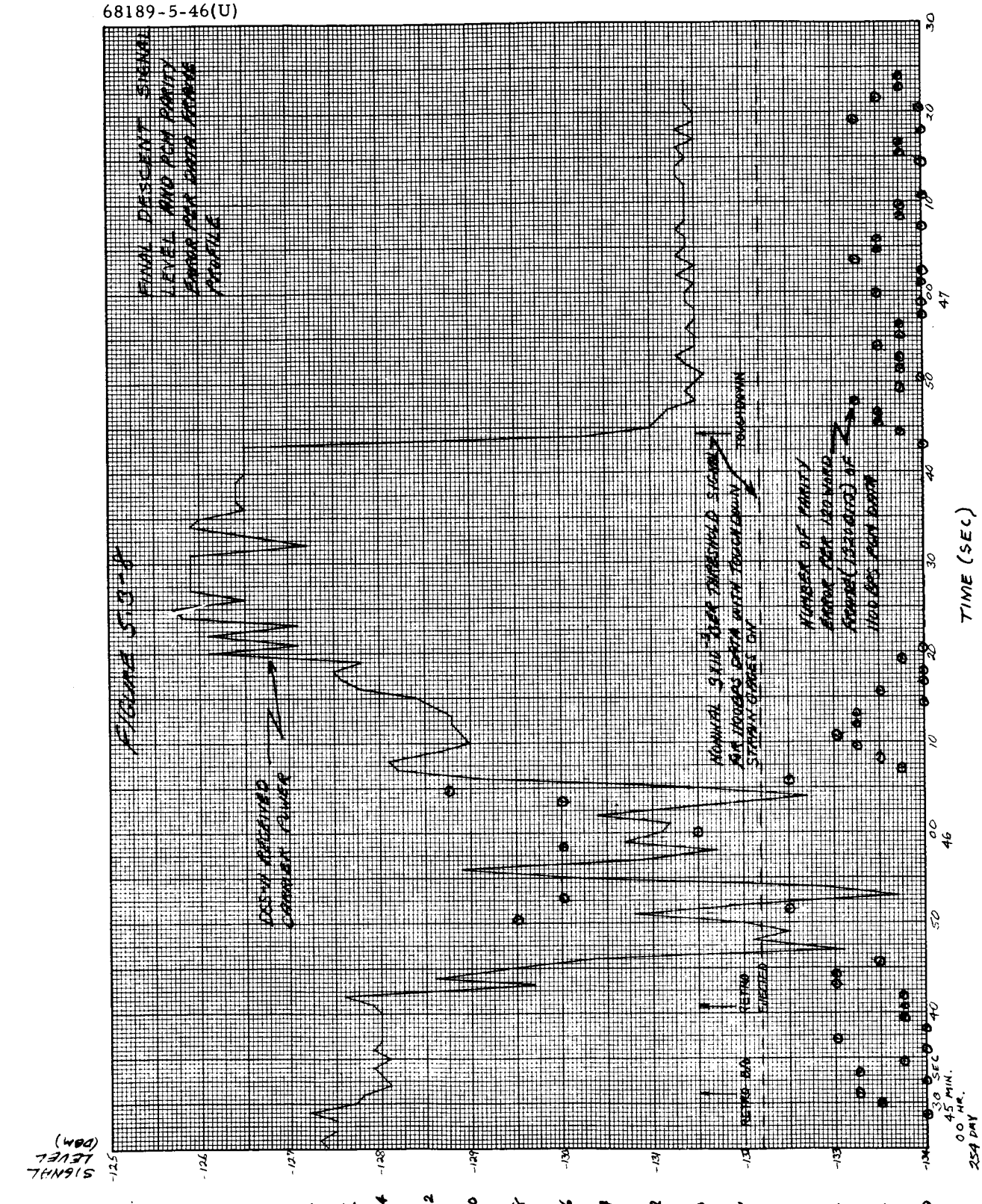

Figure 5.3-8. Parity Errors Per Frame

errors per frame to the number of bits per frame is a measure of the BER in the data to some level of confidence. Since the number of measured samples considered is quite small, a high level of confidence cannot be assigned to such a statistically-derived parameter. However, if a large number of samples were available under the dynamic conditions that existed during the descent, it is not obvious that a comparison of that data to the theoretically-derived data, which assumes a static signal level condition, would be any more directly comparable than a comparison using the data contained on the included figure. Figure 5.3-8 shows that, in general, when the signal level is above -132.2 dbm (nominal threshold received carrier power for a 3×10^{-3} BER assuming a 10.5-db SNR), the number of observed parity errors is less than four. Four errors is a BER of 3×10^{-3} under the assumed conditions. Also, for signal levels less than -132.2 dbm, the parity errors exceed four. The largest number of errors observed was 21, which corresponds to an error rate of approximately 1.6×10^{-2}, with the minimum signal level encountered being -133.7 dbm. The theoretically-derived BER curve indicates that a -1.5 db deviation from the 3×10^{-3} BER signal value would produce a BER of 1.25×10^{-2}, which is in agreement with the observed 1.6×10^{-2} maximum value.

Preterminal analysis predicted that under worst-case descent conditions, a BER of 1.3×10^{-2} could be expected. It can be concluded that the performance during descent was predictable and therefore expected, but certainly was worst case. Figure 5.3-8 shows that after touchdown the number of parity errors, on the average, is the same as the number observed during the initial part of the descent phase. It is also noted that the signal level at touchdown is approximately 3.5 db lower than that where the number of parity errors corresponds. No explanation is available for this; however, it certainly can be speculated that noise could be generated at the spacecraft as a result of dynamic conditions that existed during the descent, thus resulting in a higher threshold signal level for a given BER condition.

Touchdown occurred at 00:46:45 GMT. At this time, the signals in spacecraft receivers A and B decreased 5.5 and 1.5 db, respectively, and the signal level at DSS-11 decreased 4.6 db (Figure 5.3-8). These decreases, which exceeded worst-case predictions, indicated that the spacecraft orientation changed abruptly, which could have resulted from a spin or tilt at touchdown. It was subsequently determined that the spacecraft had indeed landed on a 20-degree slope. Signal level dispersions at touchdown, assuming a 5-degree slope, were used for predicting the worst-case condition in the preterminal analysis. The ground station signal level at touchdown was -131.5 dbm at DSS-11, with a corresponding +0.7 db nominal margin for 1100 bits/sec data (3×10^{-3} BER). Good PCM data and touchdown strain gauge data were obtained, and ground receiver lock was retained through touchdown.

5.3.4.8 Mission Phase Seven: Lunar

The data relative to the lunar phase consist of several disjointed topics. Topics applying to the RF subsystem are summarized in the following text. Reference is made, where applicable, to the source of detailed discussions and analysis.

Post-Touchdown Spacecraft Assessment (Day 254)

Transmitter B high voltage was commanded off at 01:09:30 GMT after having been in high power for 1 hour, 17 minutes, and 49 seconds during the terminal phase of the mission. An 18.6-db decrease from high to low power was observed. Transmitter A was turned on for the first time since the pre-launch countdown approximately 1/2 hour after touchdown. DSS-11 receiver carrier power was reported to be -127.4 dbm with the spacecraft at 1100 bits/sec data with transmitter A in high power on omnidirectional antenna B. Omnidirectional antenna A was selected with a resulting 4.8-db increase in the ground received signal, which again indicated a spacecraft touchdown orientation other than that planned prior to retro ignition.

TV Performance

The first 200-line television picture was transmitted approximately 1 hour after touchdown. Based on reported DSS-11 signal levels, the computed SNR for the first picture was 15.3 ± 1.0 db.

The first 600-line television picture was transmitted approximately 5 hours after touchdown, shortly after the planar array was roughly aligned with the earth. Based on reported DSS signal levels, the computed SNR for the first picture was 15.1 ± 1.0 db.

In both cases, the SNR was high enough to provide good quality detected video data which is apparent in the quality and resolution of the pictures.

Alpha Scattering Performance

The alpha scattering experiment was performed during much of the first lunar day. The total power at the ground station, with the planar array pointed toward the earth, was reported to be, in general, -115.0 dbm (spacecraft transmitter A). This signal level for the 1100 bits/sec alpha scattering multiplex mode resulted in SNRs of 20.0 db for the 1100 bits/sec data, and 15.8 and 16.9 db for the two alpha scattering channels. Good quality data, therefore, were expected and received for this experiment.

RF Assessment

A spacecraft RF performance assessment was made on day 264 with DSS-42 providing the ground station support. This assessment essentially exercises the subsystem in all possible transmitting and command receiving configurations. It was clearly evident from this assessment that all aspects of the subsystem were performing in a nominal manner.

Static Firing Experiment

A static firing on Surveyor V was performed on 12 September 1967. The gain of the omnidirectional antenna A (up link) was -7.4 db before A/SPP positioning for firing, and -8.4 db after positioning. Degradation from the

expected antenna gain (-1 to -6 db) was attributed to antenna gain pattern perturbations caused by the position of the solar panel and planar array. During the A/SPP stepping, 3 to 4 db peak-to-peak variations in spacecraft received AGC were noted. The spacecraft earth vector was such that there was no line-of-sight interference from the solar panel and planar array.

Spacecraft movement during firing was indicated by a shift in signal level of approximately 1 db for both the spacecraft receiver AGC and DSIF AGC. The firing time was so short that plume effects were neither expected nor observed.

Television Gain Margin Experiment

The television gain margin experiment conducted 20 September 1967 from DSIF 42 had the following objectives:

1) To establish the relationship between 600-line mode television picture quality and SNR.

2) To permit a comparison between the quality of 600-line mode television at less than maximum planar array gain and the quality of 200-line mode television using an omnidirectional antenna

3) To evaluate present SNR functional requirements

4) To establish the feasibility of earth tracking with sidelobes or a position on the mainlobe which produces less than maximum gain

5) To provide data from which contingency plans could be developed for failure of one or more of the A/SPP drive mechanisms

6) To establish a basis for realistic A/SPP repositioning schedules

Although results for the experiment are not available at this time, it was noted during the experiment, by word of mouth from station 42, that satisfactory 600-line pictures were being received when the signal was 3 db less than the predicted threshold SNR of 10.5 db.

Special Telecommunications Frequency Test

The purpose of the frequency test is to investigate the temperature versus frequency characteristics of a transmitter and receiver under actual space environmental conditions. The tests took place on six different occasions during the interval of day 261 to 267 GMT. Station 61 assisted in the test on days 261, 262, 263, 265, and 267, and station 42 assisted on day 265.

The resultant data seems to be consistent with Surveyor 4 data taken during reacquisition and the transit phase. However, the analysis of the data is not complete at this time.

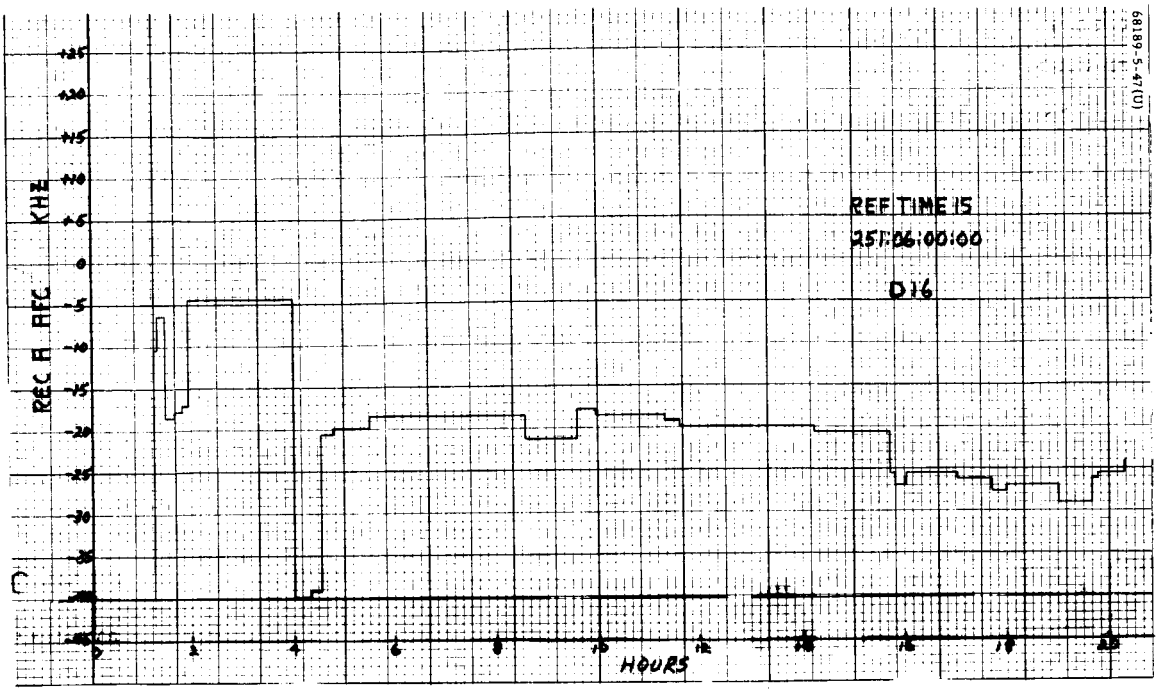

Figure 5.3-9. Receiver A AFC

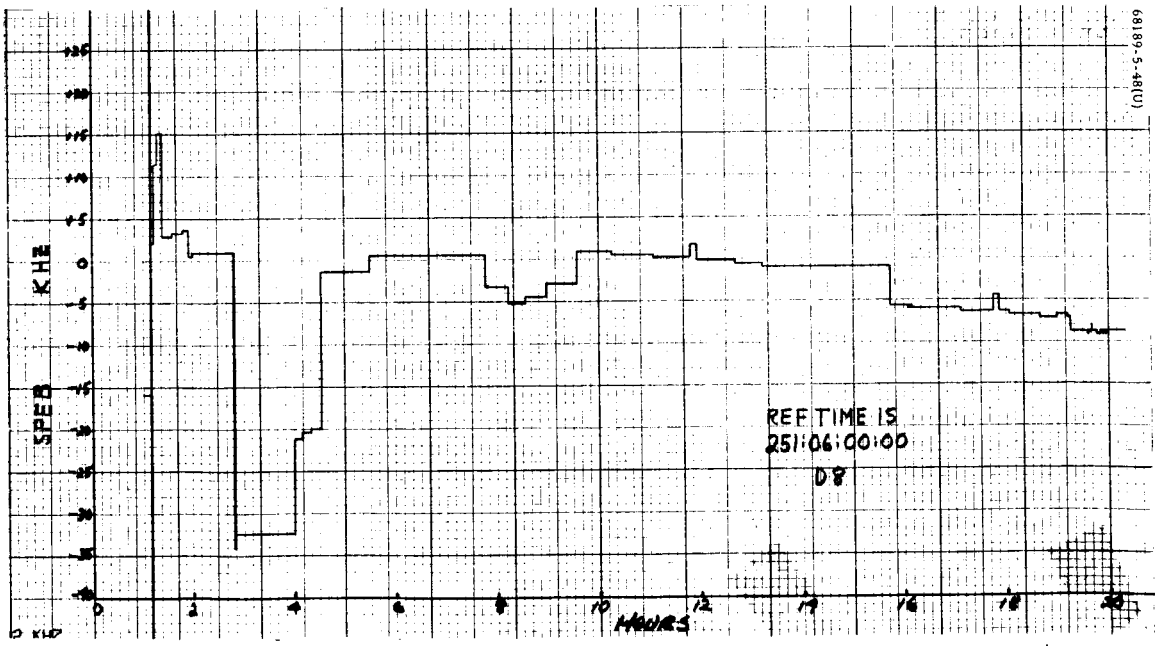

Figure 5.3-10. Receiver B SPE

Telemetry Bit Error Rate Experiment

During Surveyor V lunar operations, an experiment was performed in which data were taken to establish the BER as a function of subcarrier SNR. The purpose of the experiment was 1) to gather data to be used for comparison of the different stations relative to telemetry BER performance, 2) to evaluate actual BER performance relative to specified requirements, and 3) to evaluate present prediction and analysis techniques. This experiment also provided data on the effect of intermodulation distortion relative to PCM performance for the 1100 bits/sec/touchdown strain gauge multiplex and the 550 bits/sec/touchdown strain gauge multiplex.

Data were taken at DSS-11, -42, and -61 at bit rates of 1100 bits/sec, 550 bits/sec, and with the touchdown strain gauges multiplexed with the 550 PCM channel. In addition, data were taken at DSS-42 and -61 with the touchdown strain gauges multiplexed with the 1100 PCM channel. From the data, the following was determined:

1) Performance of the stations appears to be equivalent or within measurement tolerances if estimated biases are included. (It was concluded that the DSS-61 bandwidths and the DSS-11 noise temperature are in error, and therefore biases of $\approx$ -1.0 db (DSS-61) and $\approx$ -1.5 db (DSS-11) were used to interpret data.)

2) The telemetry performance, based on nominal measured data with the estimated biases, is within the specified required performance relative to BER at threshold.

3) The only discrepancy between theory and the actual results is in the DSS-42 data. These data indicate that the intermodulation distortion degradation is greater for the 1100 bits/sec PCM/touchdown strain gauge multiplex than for the 550 bits/sec PCM/touchdown strain gauge multiplex.

4) The DSS-61 data indicate the following degradation in performance for the PCM channels at a BER of 3×10^{-3}:

550 bits/sec PCM $\approx$ 1.2 db

1100 bits/sec PCM $\approx$ 0.8 db

5.3.4.9 Mission Data Plots

Subsystem telemetry signals are shown in Figures 5.3-9 and 5.3-10. (Also see Figure 5.3-5 in the coast phase discussion for automatic gain control signals.) All data indicated normal subsystem performance, and no unexplainable variations were noted. Plots of receiver B automatic frequency control and receiver A static phase error are omitted since, for the most part, the spacecraft configuration was such that these data points were essentially meaningless. A brief summary of each figure and the more significant events follows:

Receiver A Automatic Frequency Control (Figure 5.3-9) – Receiver A was in the automatic frequency control mode throughout transit. These data represent the DSS transmitter frequency offset from the automatic frequency control center frequency during the transit phase. A large error due to doppler shift rate is noted at acquisition. Steps in the data occurred at station transfer because the stations retuned their transmitters. Because of the high impedance of this signal, several predicted signal processing effects are apparent. Steps occurred in the data at high power turnon due to return line drop caused by the additional current in the ground return lines during high power operation. Spikes occurred during engineering interrogations of mode 4 due to step change in commutator unbalance current.

Receiver B Static Phase Error (Figure 5.3-10) – Receiver B was used for transponding through most of the mission. These data thus represent the DSS transmitter frequency offset from the receiver phase lock center frequency. Since these data are analogous to the automatic frequency control data discussed above, the comments apply equally well to these data. It should be noted, however, that this signal is not as sensitive to signal processing effects.

Transmitter B Traveling-Wave Tube Temperature (Figure 5.1-9) – These data represent the temperature of the traveling-wave tube used for high-power transmitter operation during transit.

5.3.5 REFERENCES

1) "Surveyor Mission E Space Flight Operations Report," Hughes Aircraft Company, SSD 78160, October 1967.

2) "Surveyor III Flight Performance Final Report," Hughes Aircraft Company, SSD 68189-3, July 1967.

3) "Surveyor IV Flight Performance Final Report," Hughes Aircraft Company, SSD 68189-4, September 1967.

4) "Final Report, Surveyor Spacecraft 5 Mission Operations System Compatibility Test (Conducted at AFETR)," Jet Propulsion Laboratory, July 1967.

5) H. Mitchell, "Telemetry Calibration Data for SC-5," Hughes IDC 2255.1/1997.

6) W. C. Collier, "Command Receivers 231900-3 S/N 19 and S/N 20 Calibration (Signal Input Versus AGC in BCD's) Space Environment," Hughes IDC 2294.2/122.

7) "Surveyor Mission E Telecommunication Subsystem Prediction and Performance Summary Document," Hughes Aircraft Company, SSD 74097, 21 July 1967.

5.3.6 ACKNOWLEDGMENTS

1) J.O. Votaw was the coordinator and author of this section.

2) Q.D. Howard and W. Mitchell for their assistance in reducing, formatting, and analyzing much of the data contained in this section.

3) The DSS tracking advisors at JPL for supplying ground station data.

4) The Spacecraft Performance/Analysis/Command Telecommunications Team, consisting of V.S. Amstadter, W. Mitchell, W.G. Moore, Q.D. Howard, and M.R. Weiner, for maintaining accurate mission records and logs.

5) F.K. Rickman who, although not officially a member of the Spacecraft Performance/Analysis/Command Telecommunications Team, significantly contributed to the real-time operational support of the subsystem.

5.4 SIGNAL PROCESSING

5.4.1 INTRODUCTION

The signal processing subsystem is composed of the following units:

1) Engineering signal processor (ESP)

2) Auxiliary engineering signal processor (AESP)

3) Central signal processor (CSP)

4) Signal processing auxiliary (SPA)

5) Low data rate auxiliary (LDRA)

These units contain two electronic commutators with a total of 6 operational modes, 2 analog-to-digital converters that have available 5 digital bit rates, 17 subcarrier oscillators for transmission of pulse coded modulation data and continuous real-time data, 9 summing amplifiers, and signal conditioning subsystem performed normally throughout the mission.

A summary of test and flight values for signal processing telemetry can be found in Table 5.4-1. Values for the Surveyor I, 2, III, and 4 flights have been included for comparison.

5.4.2 ANOMALIES

There were no anomalies in the signal processing subsystem throughout the transit flight.

5.4.3 SUMMARY

The signal processing subsystem performed properly throughout the transit flight.

A thorough analysis of the touchdown strain gages was performed in which computerized signal processing techniques were used, such as diversity combining and digital filtering.

PRECEDING PAGE BLANK NOT FILMED.

TABLE 5.4-1. COMPARISON OF SIGNAL PROCESSING VALUES FROM TEST AND FLIGHT

Telemetry Signal	Surveyor V Flight Values, Day 251	Surveyor 4 Retest Values, STV	Surveyor 4 Flight Values, Day 197	Surveyor III Retest Values, STV-C4	Surveyor III Flight Values, Day 107	Surveyor 2 Flight Values	Surveyor I Flight Values
S-1 reference voltage, volts*	4.90	4.88	4.875	4.86 to -4.9	4.86	4.9	4.88
S-2 reference return, volts*	0.0024	0	0	0	0	0.003	0.0024 to 0.0072
S-5 ESP commutator unbalance current, microamperes*	-0.7649	-1.7	-1.714	-2.2 to -2.6	-2.1	-1.4	-3.1
S-7 AESP commutator unbalance current, microamperes**	-2.062	-3.0	-2.813	-1.0 to -1.2	-1.3	-1.7	-2.8
S-8 AESP reference voltage***	4.95		4.938		4.94		

*Mode 4.
**Mode 5.
***Mode 5, not telemetered before Surveyor V.

5.4.4 SIGNAL PROCESSING ANALYSIS

5.4.4.1 Unbalance Current Corrections

In each telemetry commutator, transistor switches connect each analog output voltage (representing a spacecraft voltage, current, or temperature) with a common commutator line connected to the input of one of two analog-to-digital converters. A bootstrap unloader circuit is connected to this common line to reduce the stray capacitance, equalize the load impedance, and provide bias currents for the commutator and master switches. Since these bias currents are not exactly equal, a difference or unbalance current exists. The telemetry circuit being sampled must supply this current, causing an error in the measured voltage proportional to the output impedance of the circuit.

The unbalance current for a specific telemetry channel in each commutator (S-5 for ESP and S-7 for AESP) is measured in telemetry modes 2, 4, and 5. Figure 5.4-1 shows S-7 up to midcourse. Although no plot of S-5 has been included, typical values have already been given in Table 5.4-1.

5.4.4.2 Potentiometer Reference Voltage Corrections

The nominally 4.85 reference voltage is supplied by either the ESP or AESP units to the landing gear and solar panel position potentiometers, to the propulsion pressure transducers, and to the secondary sun sensors. This reference voltage, derived from the 29-volt nonessential bus, varies due to load

and input supply voltage changes. The ESP voltage is telemetered in modes 2 and 4, and can be used to correct the affected signals whose calibrations are based on a reference voltage of exactly 4.85 volts. The AESP voltage was not telemetered before Surveyor V; therefore, the values given in Table 5.4-1 for earlier spacecraft were obtained by computation.

5.4.4.3 Current Calibration Signals

Current measurements are accomplished by measuring the voltage drop across a low resistance shunt which is in series with the power line being monitored. This measurement is in the range of 0 to 100 millivolts. Since this voltage is not referenced to ground and is not scaled to the 0- to 5-volt telemetry input level range, it is necessary to amplify it with a differential amplifier. The nominal gain of this amplifier is 50, but its actual gain linearity and stability are not specified to a tight tolerance. To determine the current amplifier parameters and thereby increase the accuracy of current measurements, three calibration signals (with 0.2-percent stability) are amplified and telemetered in each commutator. These signals can thus be used by postmission processing for a continual in-flight calibration of the current amplifier.

The majority of the Surveyor V data was obtained in modes 5 and 6, and therefore only the AESP current calibration signals were investigated. Table 5.4-2 shows that these signals have changed by no more than 0.5 percent since being initially set at the unit flight acceptance test. It is also seen that the gain of the AESP current amplifier was reasonably constant over the mission.

TABLE 5.4-2. SUMMARY OF CURRENT CALIBRATION SIGNAL DATA IN AESP

Signal	Function, percent	Flight Data, percent	Remarks
EP-27	90	-0..072	Before midcourse
		0.12	After midcourse
EP-28	50	-0.14	Before midcourse
		-0.042	After midcourse
EP-29	10	0.036	Before midcourse
		0.43	After midcourse

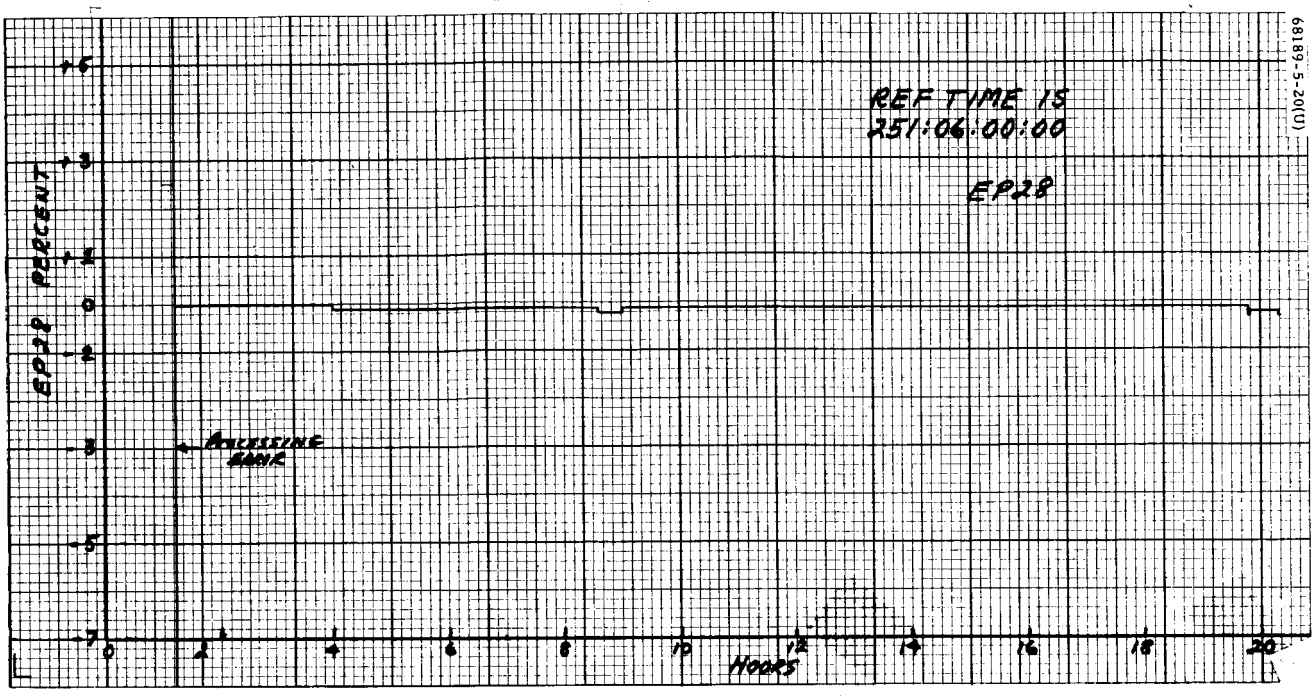

Figure 5.4-1. Commutator Unbalance Current (AESP)

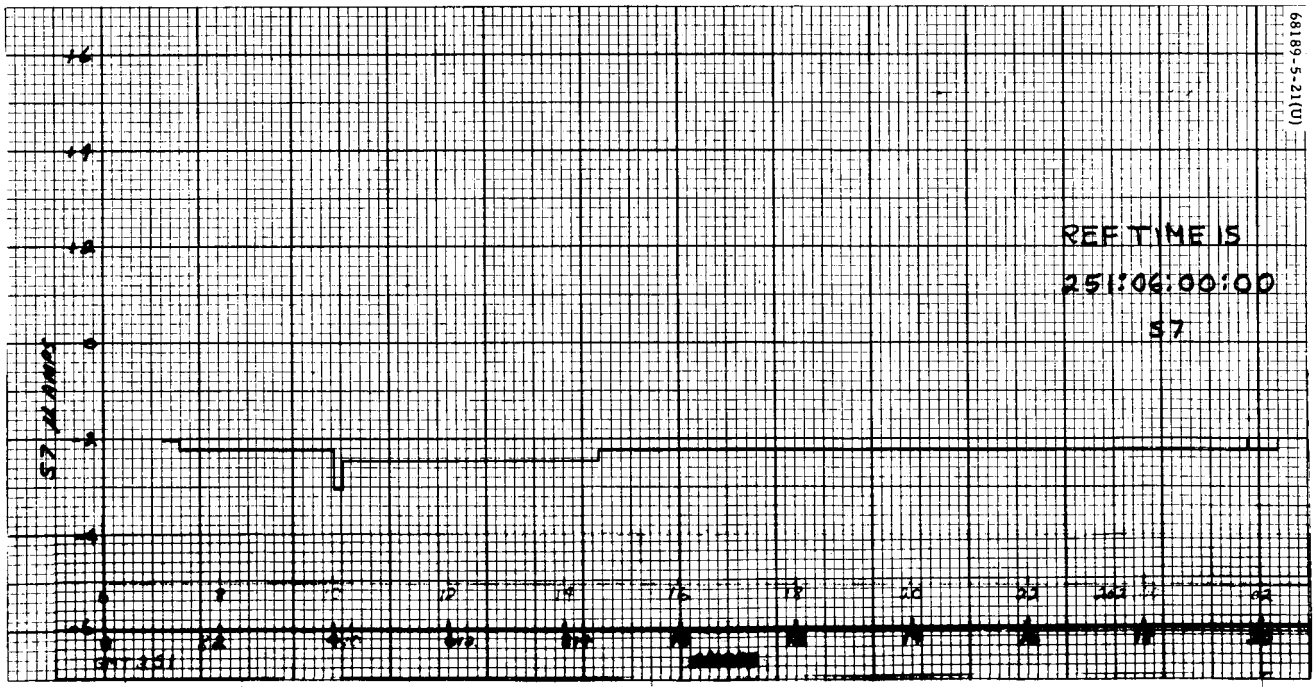

Figure 5.4-2. Midscale Current Calibration (AESP)

The AESP midscale current calibration sensor, EP-28, is shown in Figure 5.4-2 as a typical representative of the AESP calibration telemetry. It can be seen that the signal value is a function of bit rate. This effect was noted previously as occurring on Surveyors 2, III, and 4.

5.4.4.4 Touchdown Strain Gage Data

Magnetic tape data were obtained from two DSIF stations via the 85-foot diameter antenna at the Pioneer site and the 210-foot diameter antenna at the Mars site. These two independent signal paths allow the technique of space diversity combining (References 1 and 2) to be used on the two sets of touchdown strain gage (TSG) data, resulting in a signal trace with improved signal-to-noise ratio.

In addition to diversity combining, low-pass filtering (by means of digital filtering on a computer) of 50, 30, and 15 Hz (-3 db) bandwidth was employed. The data were originally recorded with a cutoff frequency of 100 Hz.

The TSG multiplex exhibits intermodulation distortion (IMD), resulting in coherent noise in the channel outputs. It can be observed that the IMD-induced "noise" contaminating the output signal is composed mainly of an approximately 45.5-Hz component. The significance of this noise is that diversity combining techniques will not be very effective since the noise is coherent. Band stop or low-pass filtering will remove the noise and would be most effective if used before diversity combining.

Figure 5.4-3 shows the diversity combined strain gage waveforms for TSG channels 1, 2, and 3, respectively. The postdetection bandwidth for these signals is about 100 Hz.

The signal-to-noise ratio listed on each plot is a mean power ratio of the signal from an assumed initial zero deflection point to an assumed final zero deflection point with respect to the noise defined over some interval prior to touchdown. This analysis assumes that the noise variance is unchanged prior to and during the signal duration.

Figure 5.4-4 shows the TSG channel outputs diversity combined, then filtered by a 50 Hz (3 db) sixth order butterworth low-pass filter. Similarly, Figure 5.4-5 shows the TSG outputs filtered at 30 Hz, and Figure 5.4-6 shows them filtered at 15 Hz.

5.4.5 DOCUMENTATION

1) A.W. Dittmer, "The Use of Diversity Receiving Techniques to Enhance Surveyor SC-1 Strain Gage Signals," Hughes IDC 2292/188, 10 January 1967.

2) A.W. Dittmer, "Computer Analysis and Prediction of Surveyor Spacecraft (SC-1) Strain Gage Signals," Hughes IDC 2292/85, 1966.

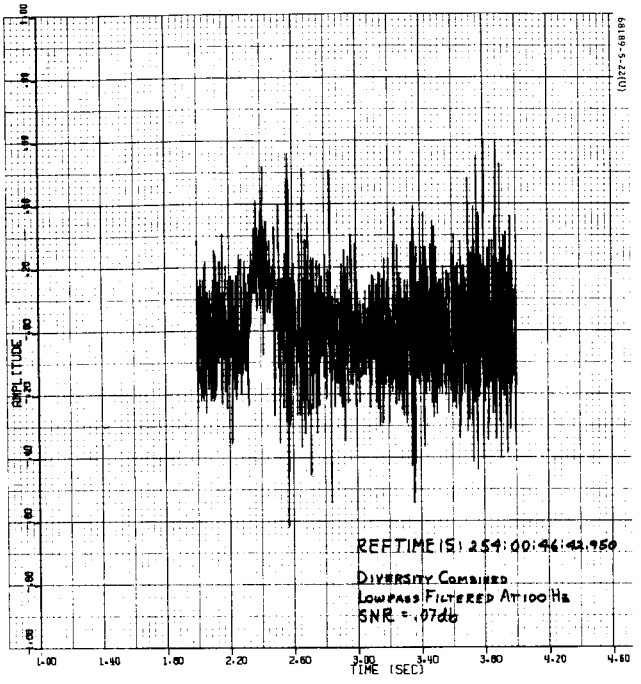

a) Strain Gage 1

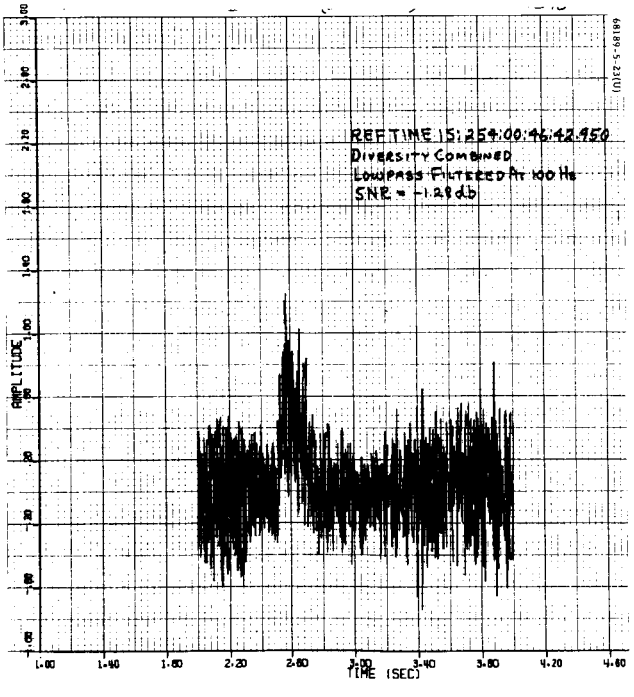

b) Strain Gage 2

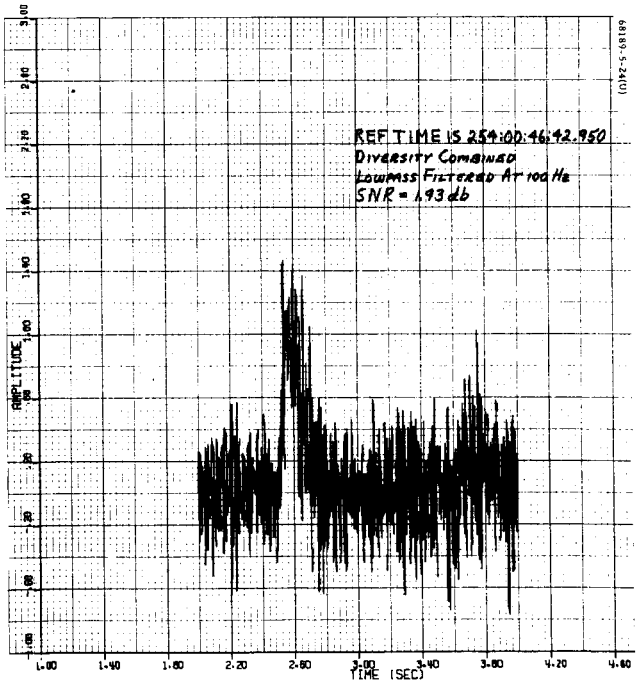

c) Strain Gage 3

Figure 5.4-3. Diversity Combined Low Pass Filtered at 100 Hz

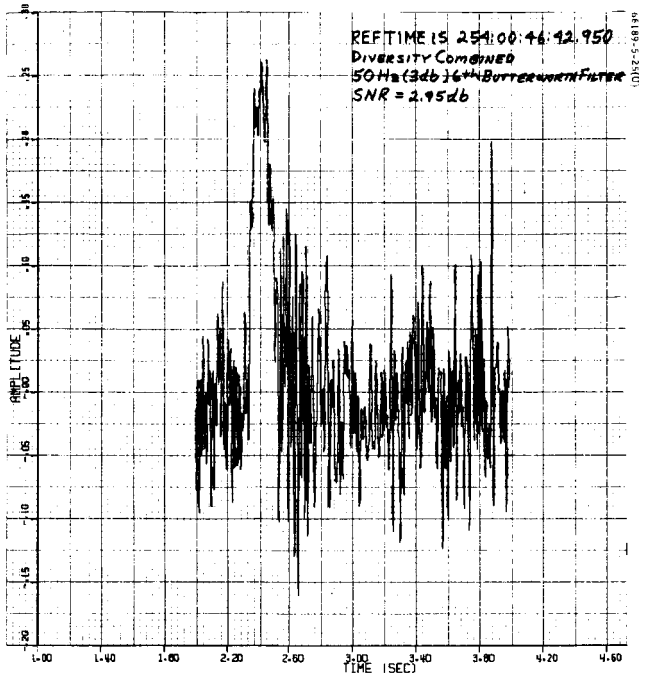

a) Strain Gage 1

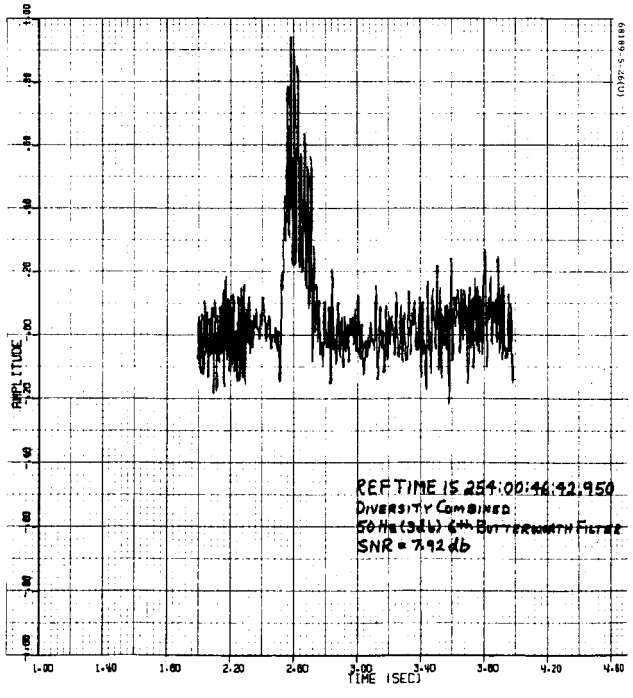

b) Strain Gage 2

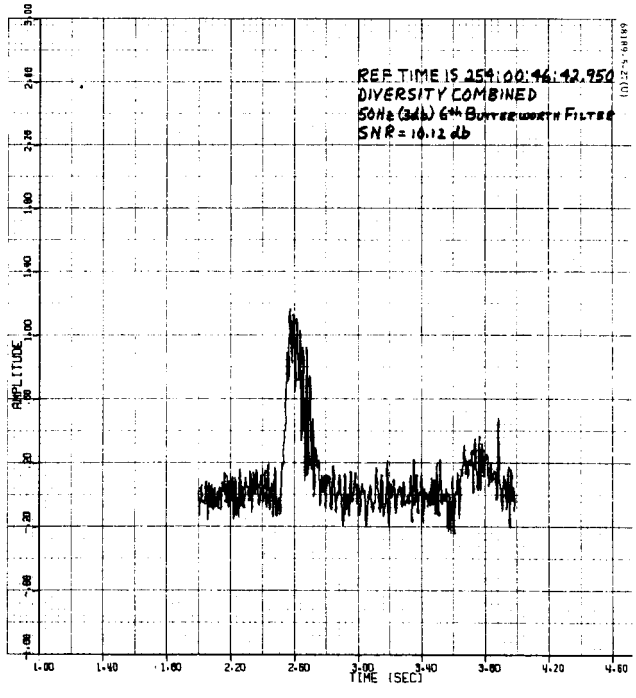

c) Strain Gage 3

Figure 5.4-4. Diversity Combined 50 Hz (3 db) Sixth Butterworth Filter

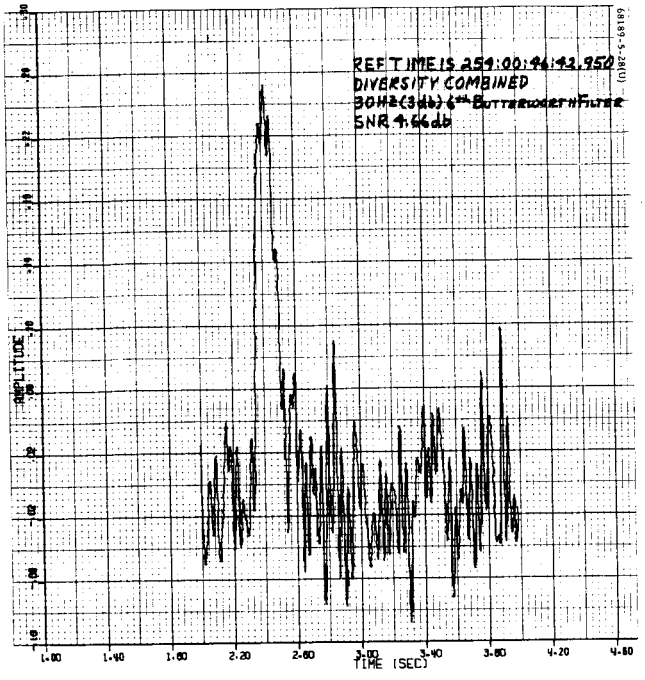

a) Strain Gage 1

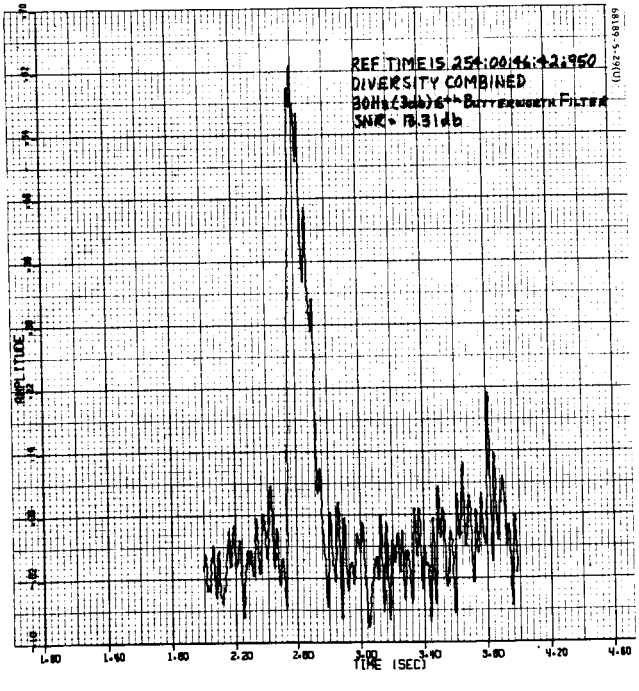

b) Strain Gage 2

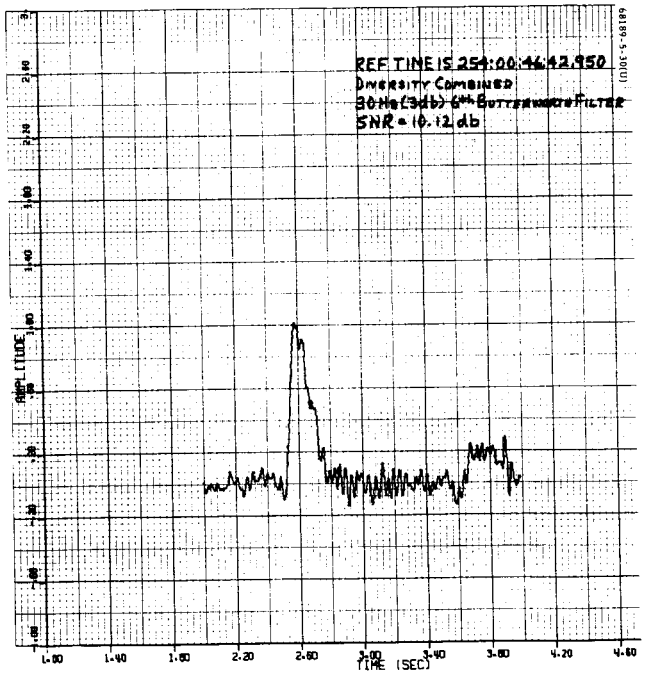

c) Strain Gage 3

Figure 5.4-5. Diversity Combined 30 Hz (3 db) Sixth Butterworth Filter

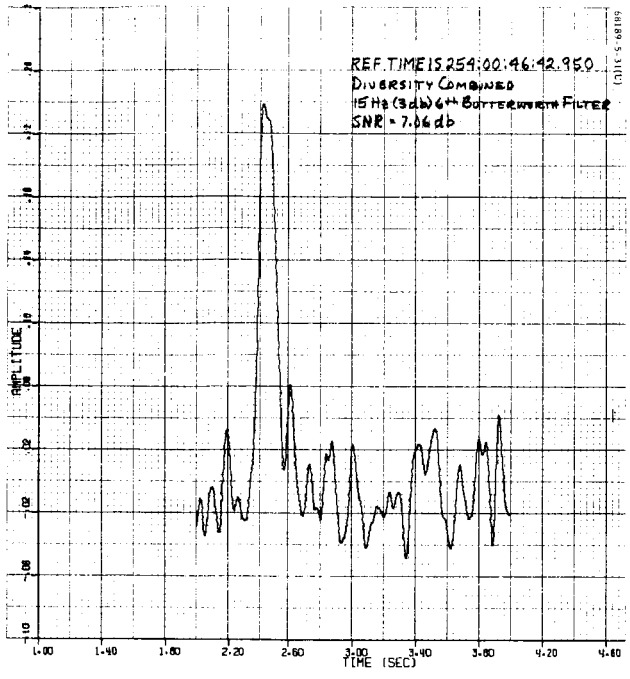

a) Strain Gage 1

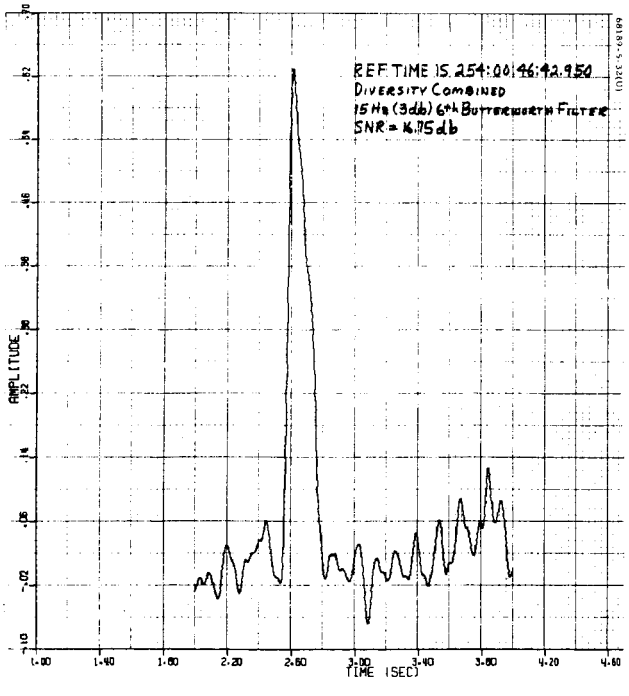

b) Strain Gage 2

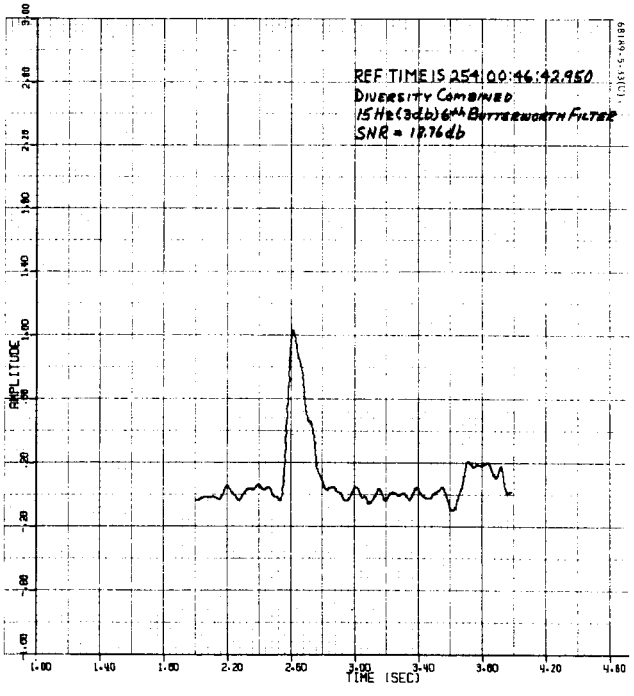

c) Strain Gage 3

Figure 5.4-6. Diversity Combined 15 Hz (3 db) Sixth Butterworth Filter

3) R. J. Rechter, "Computer Analysis of SC-3 through SC-7 TSG Multiplex Intermodulation Distortion and Other Factors," Hughes IDC 2292/223, Revision 1, March 1967.

4) M. Fashano and R. J. Rechter, "DTRB-21 Test Procedures, Results and Summary (TSG Multiplex)," Hughes IDC 2292/267, 5 May 1967.

5.4.6 ACKNOWLEDGMENTS

This section was coordinated by W. W. Mayfield.

5.5 FLIGHT CONTROL

5.5.1 INTRODUCTION

The principal requirements of the Surveyor flight control system are attitude control, accurate angular maneuvers, precision velocity corrections, and a soft lunar landing. In order to accomplish these functions, the control system utilizes such hardware as gyros, gas jets, a solid fuel engine, liquid fuel engines, optical sensors, timing devices, radars, and acceleration sensing mechanisms.

5.5.1.1 Attitude Control

Attitude control is accomplished by two basic types of active control systems. During coast phase, a bang-bang type of attitude gas jet system is employed which utilizes artifical rate feedback for loop stabilization. During periods of potentially large moment disturbances, such as the main retro phase, the throttle-controlled vernier engine system is used. The error signals required for controlling the propulsion systems are derived from optical sensors or rate integrating gyros which are mounted on the spacecraft in such a way as to provide a three-axis control system. During coast phase, when the gas jet system is used, two modes of operation are available. One is the celestial referenced mode using the sun and Canopus, and the second is self-contained inertial referencing (gyros). The first mode is used to establish accurate spatial attitude, and the second mode is generally used when momentary inertial reference is desired; such an instance occurs during an attitude maneuver.

5.5.1.2 Angular Maneuvers

The rate integrating gyros are also used for accurate angular maneuvers, accomplished by precessing the gyros at precise rates for given time intervals and slaving the spacecraft to the gyros through the gas jet system.

5.5.1.3 Velocity Correction

A midcourse velocity correction capability is provided by a system consisting of three vernier engines, a precision timer, and an accurate acceleration sensing device. The difference between the commanded acceleration level and the output from an accelerometer provides the error signal that commands the vernier engines to the required thrust levels. The constant

acceleration and variable time concept used by the Surveyor flight control system provides the flexibility of choosing velocity corrections from 0 to 50 m/sec.

5.5.1.4 Soft Landing

Surveyor's soft landing capability is provided by a sophisticated technique utilizing radars to compute velocities and range. The range information is then used by an on-board computer to provide vertical velocity commands to the vernier engine system according to an approximate, constant acceleration, V^2/R function. The velocity information is used by the vernier engine attitude control loop to produce a near-gravity turn descent by aligning the spacecraft thrust axis to the true velocity vector. The velocity information is also used, along with velocity commands, to generate error signals for the velocity control loop.

To provide the required condition of low velocity for the soft landing phase, a large amount of approach velocity is removed by a solid fuel rocket engine during the initial portion of the terminal descent phase. Spacecraft attitude during this phase is inertially stabilized by the gyro vernier engine control system.

5.5.1.5 Mission Performance

Surveyor V flight control system performance was satisfactory throughout the mission. Twenty-two minutes following completion of the initial midcourse velocity correction and reorientation of the spacecraft roll axis for the sun-line, a nonstandard vernier engine burn of 10.05 seconds was made in an attempt to reseat the helium pressure regulator valve. A third engine burn of 23.05 seconds was made approximately 27 minutes after the second with the spacecraft roll axis oriented 180 degrees from the sun-line. The fourth engine burn (12 seconds on, 1 second off, 0.5 second on, 1 second off, and 0.5 second on) was made approximately 1 hour and 39 minutes later. A fifth engine burn of 33.05 seconds was made approximately 4 hours and 6 minutes after the fourth. The sixth engine burn of 5.45 seconds was made approximately 15 hours and 7 minutes after launch. Only the first and sixth burns were based upon tracking data.

A special sequence of taped emergency commands was transmitted during the main retro burn phase of the terminal descent in order to provide early retro case separation as well as early high thrust and start of the RADVS-controlled descent. This was done to minimize the total burn time of the vernier engines in view of the limited helium gas available.

5.5.1.6 Analysis

Subsection 5.5.4 contains the analysis effort. The analysis items are categorized under major mission phases for easier identification and performance evaluation. A log of time and events is presented in Table 5.5-1, and a table of results (Table 5.5-2) is given in subsection 5.5.3.

TABLE 5.5-1. SURVEYOR V TIME AND EVENTS LOG

Event	Date, GMT	Mission Time	
		GMT, hr:min:sec	From Launch
Launch	8 September 1967	07:57:01	0
Injection		08:06:53	9M51S
Separation			
Electrical		08:16:22	19M20S
Mechanical		08:16:27	19M25S
Automatic sun acquisition			
Start		08:17:11	20M9S
Completed		08:29:12	32M10S
Canopus verification, started		14:10:01	6H13M00S
Canopus acquisition, completed (Canopus lockon)		14:27:52	6H20M51S
Gyro drift check No. 1			
Start		15:45:51	7H48M50S
Stop		18:16:27	10H19M26S
Gyro drift check No. 2			
Start		18:24:27	10H27M26S
Stop		20:16:01	12H19M00S
Gyro drift check No. 3 (roll only)			
Start		21:43:56	13H46M55S
Stop		23:40:31	15H43M30S

Table 5.5-1 (continued)

Event	Date, GMT	Mission Time	
		GMT, hr:min:sec	From Launch
Premidcourse roll +72 degrees	9 September 1967		
Start		01:32:58	17H35M57S
Stop		01:35:22	17H38M21S
Premidcourse yaw -35.8 degrees			
Start		01:38:08	17H41M07S
Stop		01:39:19	17H42M18S
Engine burn No. 1 14.3 seconds			
Start		01:45:03	17H48M02S
Stop		01:45:17	17H48M16S
Postmidcourse yaw +35.8 degrees			
Start		01:53:51	17H56M50S
Stop		01:55:02	17H58M01S
Engine burn No. 2 10.05 seconds			
Start		02:12:03	18H15M02S
Stop		02:12:13	18H15M12S
Pre-engine burn No. 3 yaw -180.2 degrees			
Start		02:24:34	18H27M33S
Stop		02:30:34	18H33M33S

Table 5.5-1 (continued)

Event	Date, GMT	Mission Time	
		GMT, hr:min:sec	From Launch
Engine burn No. 3 23.05 seconds	9 September 1967 (continued)		
Start		02:39:52	18H42M51S
Stop		02:40:15	18H43M14S
Postmidcourse roll -72 degrees			
Start		04:00:46	20H03M45S
Stop		04:03:10	20H06M09S
Pre-engine burn No. 4 roll +68.6 degrees			
Start		04:05:55	20H08M54S
Stop		04:08:12	20H11M11S
Pre-engine burn No. 4 yaw +106.8 degrees			
Start		04:09:34	20H12M33S
Stop		04:13:08	20H16M07S
Engine burn No. 4 12.1 seconds			
Start 0.5 second		04:18:48	20H21M47S
Stop 0.5 second		04:19:03	20H22M02S
Pre-engine burn No. 5 roll +64.6 degrees			
Start		07:54:30	23H57M29S
Stop		07:56:39	23H59M38S

Table 5.5-1 (continued)

Event	Date, GMT	Mission Time	
		GMT, hr:min:sec	From Launch
Pre-engine burn No. 5 yaw +143.4 degrees	9 September 1967 (continued)		
Start		07:58:31	24H01M30S
Stop		08:03:16	24H06M15S
Engine burn No. 5 33.1 seconds			
Start		08:24:04	24H27M03S
Stop		08:24:37	24H27M36S
Gyro drift check No. 4			
Start		09:08:32	25H11M31S
Stop		09:56:51	25H59M50S
Gyro drift check No. 5			
Start		11:39:31	27H12M30S
Stop		13:15:29	29H18M28S
Gyro drift check No. 6 (roll only)			
Start		13:17:57	29H20M56S
Stop		15:08:09	31H11M08S
Gyro drift check No. 7			
Start		15:10:41	31H13M41S
Stop		17:18:08	33H21M07S
Gyro drift check No. 8			
Start		17:59:59	34H02M58S
Stop		20:10:23	36H13M22S

Table 5.5-1 (continued)

Event	Date, GMT	Mission Time	
		GMT, hr:min:sec	From Launch
Gyro drift check No. 9	9 September 1967 (continued)		
Start		20:59:05	37H02M04S
Stop		21:48:52	37H51M51S
Pre-engine burn No. 6 roll of -76 degrees			
Start		23:13:51	39H16M50S
Stop		23:16:23	39H19M22S
Pre-engine burn No. 6 yaw of -100.6 degrees			
Start		23:19:36	39H22M35S
Stop		23:22:57	39H25M56S
Engine burn No. 6 5.45 seconds			
Start		23:30:58	39H33M57S
Stop		23:31:03	39H34M02S
Sun reacquired		23:39:28	39H42M27S
Canopus reacquired		23:46:37	39H49M36S
Gyro drift check No. 10			
Start		01:35:19	41H38M18S
Stop		04:33:03	44H36M02S
Gyro drift check No. 11 (roll only)			
Start		13:05:03	53H08M02S
Stop		15:24:13	55H27M12S

Table 5.5-1 (continued)

Event	Date, GMT	Mission Time	
		GMT, hr:min:sec	From Launch
Gyro drift check No. 12	9 September 1967 (continued)		
Start		15:27:08	55H30M07S
Stop		17:59:42	58H02M41S
Yaw precession rate calibration check +179.9 degrees			
Start		18:12:19	
Stop		18:18:20	
+180.1 degrees			
Start		18:22:55	
Stop		18:28:55	
Preretro roll, +74.0 degrees	10 September 1967		
Start		00:12:18	64H15M17S
Stop		00:14:46	64H17M04S
Preretro yaw, +119.6 degrees			
Start		00:16:23	64H19M22S
Stop		00:20:22	64H23M21S
AMR mark		00:44:39.119	64H47M38S
Vernier ignition		00:44:51.443	64H47M50S
Retro ignition		00:44:52.533	64H47M51S

Table 5.5-1 (continued)

Event	Date, GMT	Mission Time	
		GMT, hr:min:sec	From Launch
RADVS ON	10 September 1967 (continued)	00:44:53.456	64H47M52S
Inertia switch open		00:44:54.753	64H47M53S
Reliable operation of doppler velocity sensor		00:45:24.155	64H48M23S
Reliable operation of radar altimeter		00:45:20.555	64H48M19S
Burnout (inertia switch closed)		00:45:31.355	64H48M30S
Retro eject		00:45:40.395	64H48M39S
High thrust		00:45:40.955	64H48M38S
Start RADVS-controlled descent		00:45:42.395	64H48M41S
1000 feet		00:46:19.697	64H49M18S
10 fps		00:46:37.097	64H49M36S
14 feet		00:46:42.697	64H49M41S

5.5.2 ANOMALY DESCRIPTION

There were no flight control anomalies during the mission.

5.5.3 SUMMARY

A summary of flight control system performance is presented in Table 5.5-2.

Performance was completely normal from Centaur separation to touchdown, including automatic sun acquisition and Canopus lock-on.

5.5.4 SUBSYSTEM PERFORMANCE ANALYSIS

5.5.4.1 Prelaunch

Gyro Temperatures

The gyro temperatures just prior to launch at 05:50 GMT are shown in Table 5.5-3.

Nitrogen Weight

The estimated on-board nitrogen weight at launch was 4.57 pounds based on a telemetered tank pressure of 4708 psi at a tank temperature of 81.8°F. This agreed with the best estimate of 4.57 pounds of nitrogen loaded.

5.5.4.2 Launch Through Separation From Centaur

After extending its landing legs, Surveyor is separated from the Centaur booster. When the three legs-down signals and the separation signal have been generated, the programmer removes the logic signal which has been inhibiting operation of the gas jet amplifiers. At this same instant, the magnitude register begins to count down 1024 counts for a 51-second interval; the start of sun acquisition is inhibited for this interval to give the cold gas attitude control system opportunity to rate stabilize the spacecraft. Table 5.5-1 presents these events in time reference.

Rate stabilization is accomplished by using the three-axis attitude control system to torque the spacecraft and drive the caged integrating rate gyro error signals to within the deadband of each gas jet amplifier. Thus, at the end of a nominal rate stabilization maneuver, the spacecraft has achieved a low angular velocity at a random orientation in inertial space. The system response is dependent upon the magnitude and direction of the initial velocity vector and the gas jet thrust levels, and is essentially deadband in nature.

TABLE 5.5-2. FLIGHT CONTROL RESULTS

	Controlling Specification	Specification Value	Results	Comments
Prelaunch				
Proper gyro temperature control			Roll 169.2 °F Pitch 162.1 °F Yaw 159.7 °F	Time was 251:05:42 GMT
Verification of N_2 loading	224832A	4.57 pounds	4.57 pounds	(FC-4) = 4708 psi (FC-48) = 81.8°F
Centaur separation	(3.5.2.1)			
Time required to null rates to less than 0.1 deg/sec		<0.1 deg/sec within 50 seconds	<20 seconds	
Magnitude of angular rate at separation		≤3.0 deg/sec	<1.0 deg/sec	
Sun acquisition				
Proper sun acquisition	(7.3.3.3.4)	Minus roll maneuver until activation of acquisition sun sensor and then a plus yaw maneuver until primary sun sensor illumination		
Roll			-342.5 degrees of roll	
Yaw			+18.0 degrees of yaw	
Total time			12M2S	
N_2 gas used	Design	0.054 pound (average)	<0.1 pound	Tank temperature may not have been at steady state
Star acquisition	(7.3.3.3.5)	Positive roll maneuver sufficient to produce an adequate star map for Canopus verification. Provide a lockon signal when Canopus appears in the sensor field of view		
Proper acquisition and verification of Canopus			Automatic lockon	
Roll angle from beginning of maneuver to Canopus			179 degrees	
Objects identified			(Antares and Tau Scorpii)* (Alnitak, Alnilam, Mintaka)* Bellatrix, El Nath, Capella, Polaris, Zeta Ophiuchi, earth	
Mean roll rate during star map phase		0.5 deg/sec	0.5007 deg/sec ± 0.00008	
Effective gain (relative to nominal Canopus) of Canopus sensor			1.32 x Canopus	
N_2 gas used	Design	0.048 pound (average)	0.04 pound	
Coast mode	(7.3.3.3.6)	Roll axis shall be held to within 0.20 degree of sun-spacecraft line, plus a ±0.30 degree limit cycle		Sun and star error signal noise level were low enough to have no effect on the limit cycle performance
		Same magnitude as above for Canopus-spacecraft line		
Limit cycle (gas jet system)	(7.3.3.3.3)			
Optical mode/inertial mode	(7.3.3.3.5)	±0.30 degree		Values are that of the total deadband. Predicted values were:
Average amplitude—roll			0.46/0.3 degree	0.44/0.44 degree
Average amplitude—pitch			0.37/0.31 degree	0.44/0.44 degree
Average amplitude—yaw			0.5/0.36 degree	0.44/0.44 degree
Gyro drift	(7.3.3.3.3C)	<1 deg/hr		
Roll			Roll +0.85 deg/hr	
Pitch			Pitch +0.6 deg/hr	
Yaw			Yaw -0.6 deg/hr	
Gas jet thrust level		>0.052 pound	0.061 pound (roll)	Design value is 0.057 pound

Table 5.5-2 (continued)

	Controlling Specification	Specification Value	Results	Comments
Premidcourse maneuvers				
Maneuver angles (No. 1 burn)	(7.3.3.3.7)	Rates shall be controlled to be 0.5 ± 0.0011 deg/sec		Assuming a precession level of 0.5000 deg/sec
Roll +72 degrees			+71.9 degrees	
Yaw -35.8 degrees			-35.6 degrees	
Precession command times (No. 1 burn)		0.2 second plus 0.02 percent of command interval magnitude		These times were obtained from the gyro error signal response profile
Roll 144 seconds			143.8 seconds	
Yaw 71.6 seconds			71.2 seconds	
Attitude maneuver accuracy (includes drift, initial attitude errors, and limit cycle)			0.22 degree with 0.13 degree 3σ uncertainty	Calculated using actual data of drift, attitude errors, and execution errors
Manuever angles (No. 3 burn)				
Yaw -180.1 degrees			-179.547 degrees	
Precession command time				
Yaw 360.2 seconds			359.09 seconds	
Maneuver angles (No. 4 burn)				
Roll +68.5 degrees			+68.661 degrees	
Yaw +106.7 degrees			106.748 degrees	
Precession command times				
Roll 137.0 seconds			137.322 seconds	
Yaw 213.4 seconds			213.496 seconds	
Maneuver angles (No. 5 burn)				
Roll +64.5 degrees			+64.547 degrees	
Yaw +143.3 degrees			+143.213 degrees	
Precession command times				
Roll 129.0 seconds			129.094 seconds	
Yaw 286.6 seconds			286.416 seconds	
Maneuver angles (No. 6 burn)				
Roll -75.9 degrees			-75.891 degrees	
Yaw -100.5 degrees			-100.408 degrees	
Precession command times				
Roll 151.8 seconds			151.782 seconds	
Yaw 201.0 seconds			200.816 seconds	
Maximum midcourse acceleration error	224832A	ΔV error < ±1.3 ft/sec		
Expected ΔV/tracking ΔV			17.8 fps	
			17.4 fps	
Shutdown impulse (No.1 burn)	(8.3.1.3.2.4.1)	< 5 lb-sec/engine Δ impulse < 0.66 lb/sec		
Engine 1			-0.06 lb-sec	
Engine 2			+0.05 lb-sec	
Engine 3			+0.01 lb-sec	
Shutdown impulse (No. 2 burn)				
Engine 1			-0.1 lb-sec	
Engine 2			+0.18 lb-sec	
Engine 3			-0.08 lb-sec	

Table 5.5-2 (continued)

	Controlling Specification	Specification Value	Results	Comments
Shutdown impulse (No. 3 burn)				
Engine 1			-0.13 lb-sec	
Engine 2			+0.11 lb-sec	
Engine 3			+0.02 lb-sec	
Shutdown impulse (No. 4 burn)				
Engine 1			-0.07 lb-sec	
Engine 2			+0.10 lb-sec	
Engine 3			-0.03 lb-sec	
Shutdown impulse (No. 5 burn)				
Engine 1			-0.53 lb-sec	
Engine 2			+0.65 lb-sec	
Engine 3			-0.12 lb-sec	
Shutdown impulse (No. 6 burn)				
Engine 1			-0.29 lb-sec	
Engine 2			+0.15 lb-sec	
Engine 3			-0.14 lb-sec	
Preretro maneuvers				
Maneuver angles	(7.3.3.3.7)	Rates shall be controlled to be 0.5 ± 0.0011 deg/sec		Values only include execution error. The desired values were:
Roll			+73.9 degrees	Roll (+) 74 degrees
Yaw			+119.5 degrees	Yaw (+) 119.6 degrees
Precession command times		0.2 second plus 0.02 percent of the command interval magnitude		The command values were:
Roll			147.8 seconds	148 seconds
Yaw			139 seconds	139.2 seconds
Pointing accuracy (includes drift, initial attitude errors, and limit cycle)		Within ±1 degree	0.43 with 0.22 3σ uncertainty	
Gyro drift compensation values				
Roll			+0.85 deg/hr	
Pitch			+0.6 deg/hr	
Yaw			-0.6 deg/hr	
Terminal descent				
AMR marking altitude	(7.6.1)	Nominal slant range of 60 miles		
Main retro				
Burn time (from ignition to 3.5 g switch)	(7.3.3.3.9)	Approximately 39 seconds	39 seconds	
Maximum retro thrust		< 10,000 pounds	9740 pounds	Computed using retro accelerometer data
Peak attitude transient at vernier ignite – retro ignite	(7.3.3.3.10)			
Roll			-0.16 degree	
Pitch			+0.5 degree	
Yaw			-0.5 degree	
Main retro thrust vector to spacecraft center of gravity offset	(8.3.5.3.2.8)	<0.18 inch	-0.048 inch	

Table 5.5-2 (continued)

	Controlling Specification	Specification Value	Results	Comments
Thrust vector pointing accuracy during retro burn	(8.3.5.3.2.9)	Within ±1 degree	0.30 degree	Based on estimated versus actual burnout conditions
Mean attitude error during burn				
Roll			+0.36 degree	
Pitch			≈0 degree	
Yaw			-0.27 degree	
Roll actuator position				
Peak at retro ignition			+0.32 degree	
Mean value during burn			-0.3 degree	
Time between major events	(7.3.3.3.9)			
AMR mark and vernier ignition		0 to 20 seconds	12.324 seconds	Expected 12.3 seconds
Vernier and retro ignition		1.1 ± 0.1 seconds	1.09 seconds	
Retro ignition and RADVS power on		0.55 ± 0.1 second	$1.52\ ^{+0}_{-1.2}$ seconds	
Retro ignition and retro burnout (inertia switch closes)		39.2 seconds expected	38.9 seconds	
Retro burnout and retro eject		8.5 seconds expected	9.0 seconds	
Retro eject and high thrust		0.5 second expected	1.1 seconds	
High thrust and start of RADVS-controlled descent		1.5 seconds expected	0.9 second	
Retro burnout conditions				
Slant range		6600 feet	5950 feet	
Total velocity		94 fps	79 fps	
Angle between thrust vector and velocity vector		46 degrees	45 degrees	V_x = -41 fps V_y = +50 fps
Time to align Z-axis to velocity vector	224510E (3.10.2.1)	9 seconds maximum	< 5 seconds	
Descent segment intercept conditions		1500 feet 117 fps	806 feet 97 fps	
Touchdown conditions				
Vertical velocity		13 fps	≈13.5 fps	
Lateral velocity		0 fps	< 1.0 fps	
Additional information				
Total nitrogen gas used	Design	0.95 ± 0.52 pound	1.0	See coast mode gas consumption
Gyro speeds	235159	Telemetry value = 50 cps for all three gyros		
Roll gyro			Roll = 50 Hz (average)	
Pitch gyro			Pitch = 50 Hz (average)	
Yaw gyro			Yaw = 50 Hz (average)	
Gyro heater duty cycle				
Roll			Roll = 16 percent (on)	
Pitch			Pitch = 41 percent (on)	
Yaw			Yaw = 29 percent (on)	

*Seen as composite signal.

TABLE 5.5-3. PRELAUNCH GYRO TEMPERATURES (° F)

Gyros	Prelaunch, 05:52 GMT
Roll	169.2
Pitch	162.1
Yaw	159.7

Flight control system performance just after Centaur separation was evaluated for proper nulling of the separation rates, the time required to null rates to less than 0.1 deg/sec, the total angular excursion, and magnitude of angular rates due to separation.

Separation transients based on data received via Coastal Crusader are plotted in Figure 5.5-1. The roll transient appears normal and indicates that any separation-induced rate was essentially zero. While the pitch and yaw transients also indicate small separation-induced rates, it appears that an impulse disturbance caused a transient motion away from null at mechanical separation. In order to better understand the nature of this disturbance, the initial conditions at separation were used as inputs to a three degree-of-freedom analog simulation. The results of the simulation for the case where no external forces are present at mechanical separation is shown in Figure 5.5-2a. A good match for the pitch and yaw transients was obtained by introducing a positive 9.50 and 0.66 ft-lb-sec disturbance about the pitch and yaw axes, respectively, at mechanical separation (Figure 5.5-2b). It is assumed that the separation springs apparently were the source of the disturbance even though Centaur data indicated that extension of the three separation springs was essentially simultaneous.

All three body rates were reduced to ≤ 0.1 deg/sec in less than 20 seconds. The total attitude change of the spacecraft from the time of mechanical separation until each body rate was less than 0.1 deg/sec is the time integral of the plots in Figure 5.5-1 over the applicable time range. Graphical integration provided the following results:

Roll: 0 degree

Pitch: +2.0 degrees

Yaw: +1.1 degrees

The expected nitrogen usage for rate dissipation is small. A typical rate dissipation transient will require the use of 0.040 pound of nitrogen. Because the measurement uncertainties are large compared to the usage, no quantitative measurement of nitrogen gas consumption during rate dissipation was attempted.

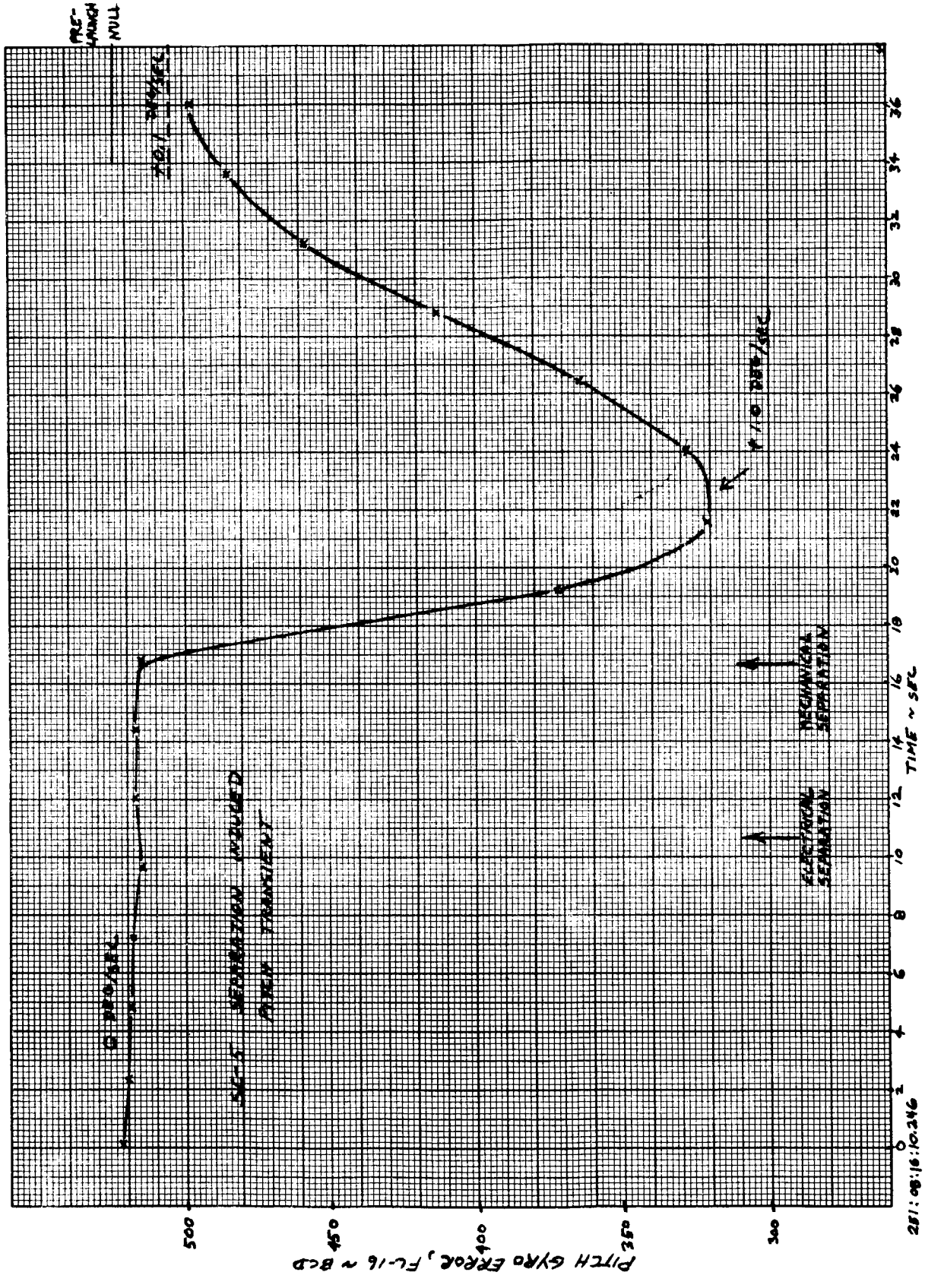

a) Pitch

Figure 5.5-1. Separation-Induced Transients

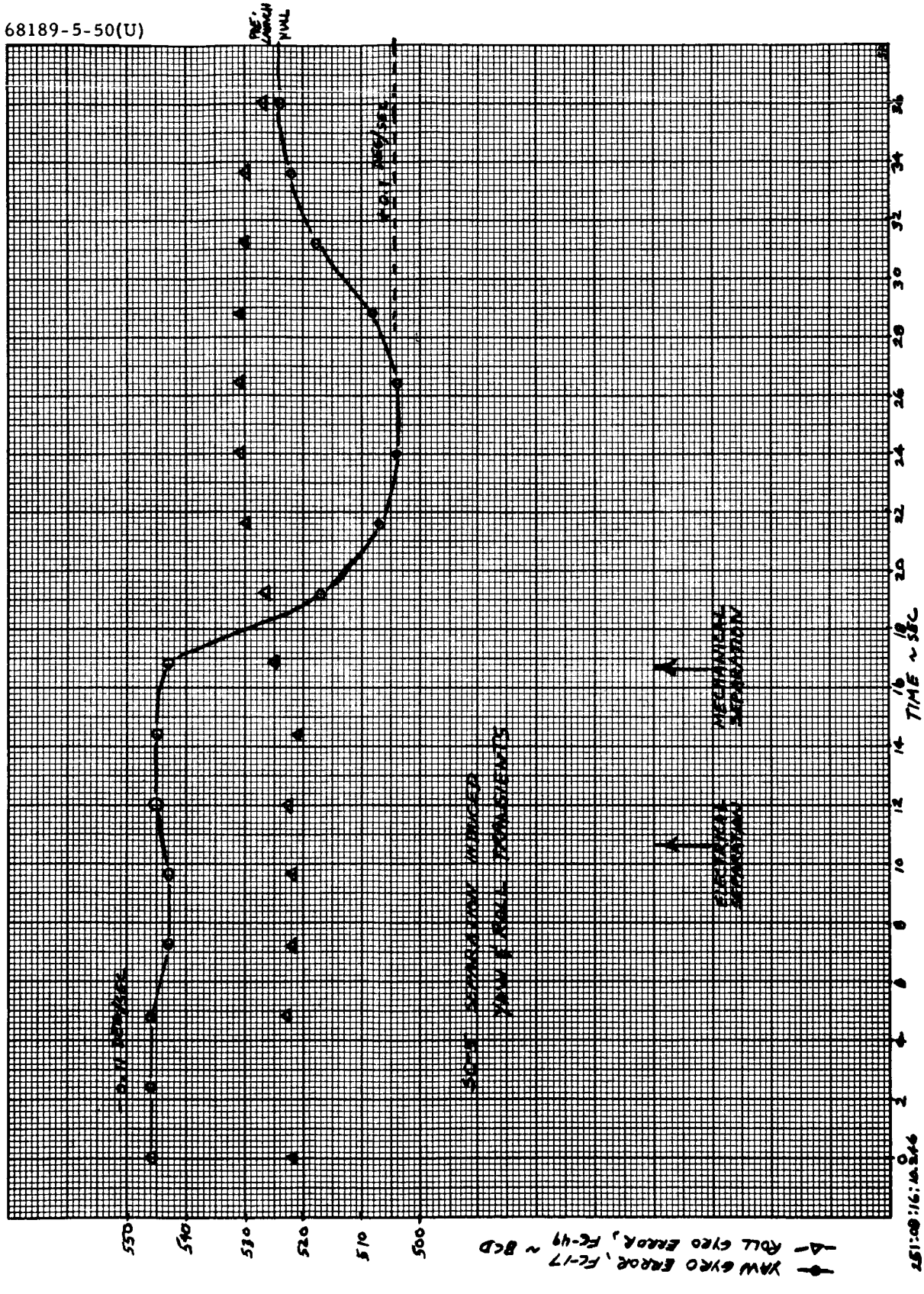

b) Yaw and Pitch

Figure 5.5-1 (continued). Separation – Induced Transients

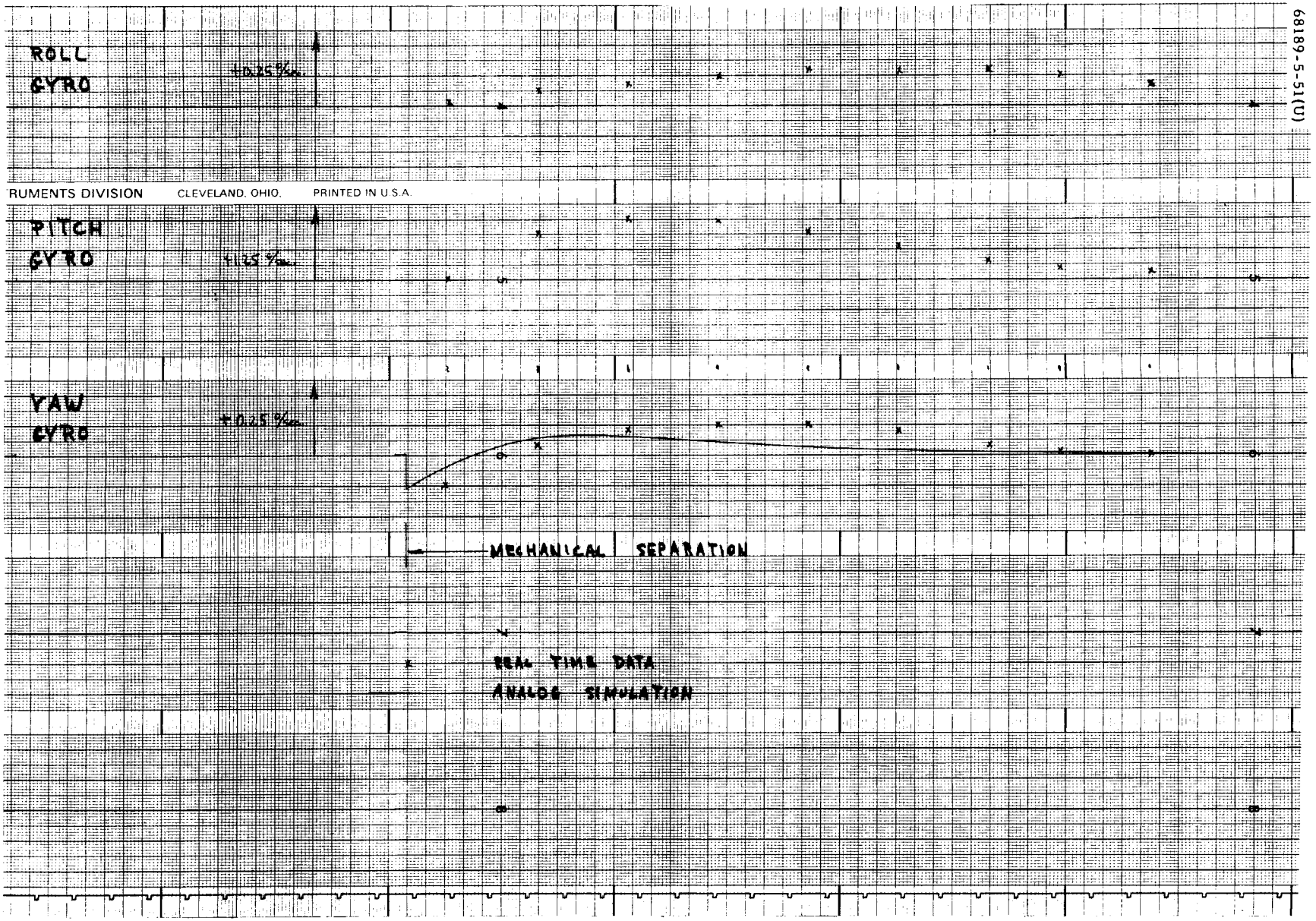

a) Without Induced Disturbance

Figure 5.5-2. Rate Dissipation Transient Simulation

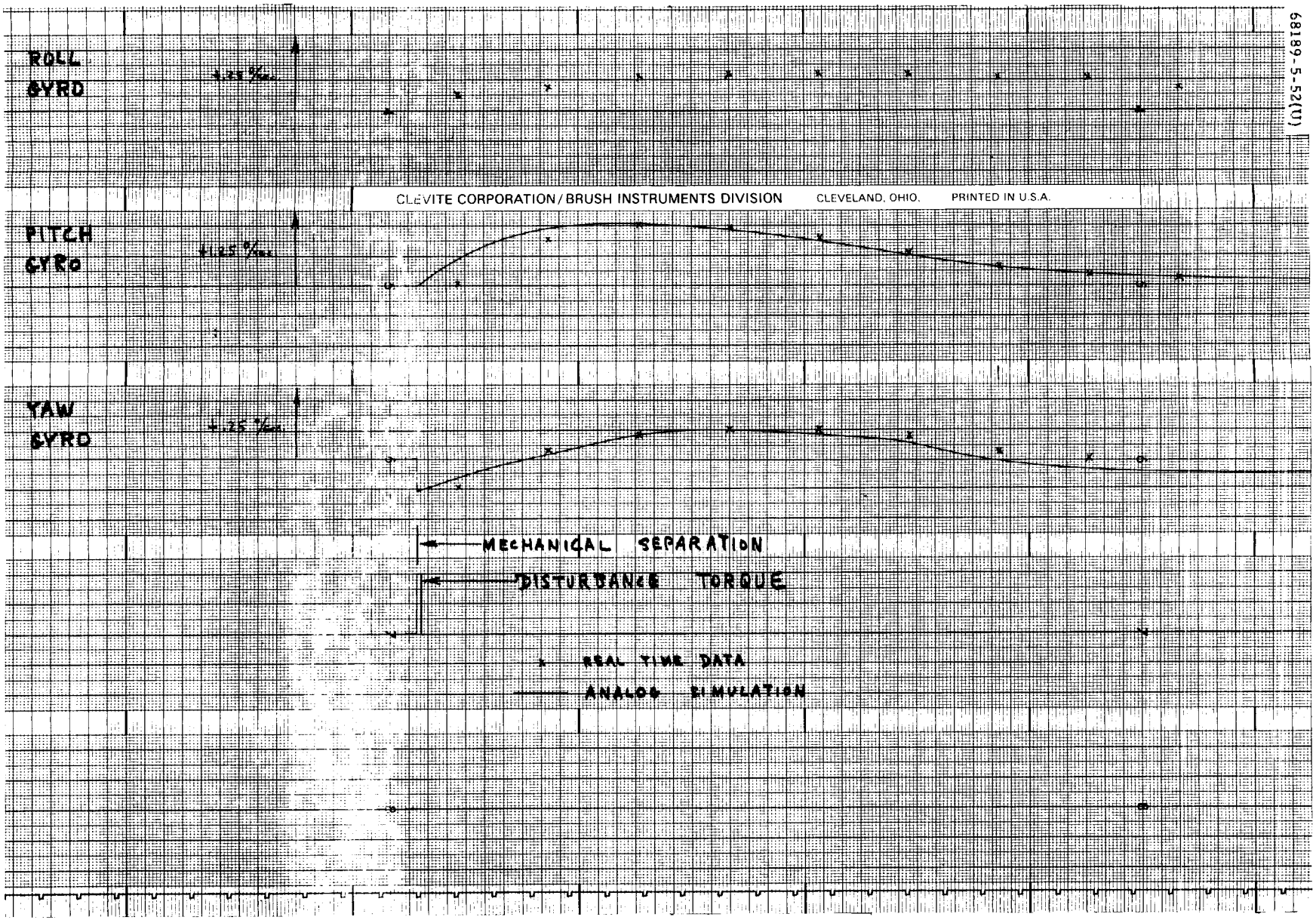

b) With Induced Disturbance

Figure 3.5-2 (continued). Rate Dissipation Transient Simulation

5.5.4.3 Sun Acquisition

Fifty-one seconds after electrical separation, sun acquisition is initiated by a command from the flight control programmer which causes a vehicle roll maneuver of -0.5 deg/sec and continues until the sun comes into the acquisition sun sensor field of view which is aligned approximately to the spacecraft roll-pitch plane. When this occurs, the roll command is removed and a plus yaw maneuver is initiated to point the primary sun sensor line of sight toward the sun. When the sun falls into the primary sun sensor field of view, a lockon signal is generated. This signal switches vehicle attitude control to the primary sun sensor and also serves to indicate (via telemetry) the completion of sun acquisition.

The automatic sun acquisition mode was initiated at 09:17:11 GMT as indicated by setting of the sun mode "on" latch. The estimated magnitude of the roll maneuver based on a constant gyro precession rate of 0.5 deg/sec was 342.5 degrees, while the yaw maneuver was estimated to be 18 degrees.

Nitrogen Utilization

Following sun acquisition, the remaining nitrogen was estimated at 4.60 pounds. This is actually 0.03 pound greater than the amount of gas estimated on board at launch, indicating that the nitrogen tank temperatures had not yet stabilized when the initial estimate was made.

5.5.4.4 Canopus (Star) Acquisition

As defined in Reference 1 (Specification 224510, Revision E) paragraph 3.4.2:

> "... the spacecraft is commanded to roll up to 720 degrees in one continuous roll. During this roll, the star intensity signal and star error signal are monitored. From these signals, a star map is made and Canopus identified. The capability for performing at least four of these verifications shall be provided. This verification shall be performed before the normal star acquisition mode is initiated. The star acquisition command starts a vehicle positive roll of 0.5 deg/sec until a star of the correct brightness falls into the sensor field of view. When this occurs, a lockon signal is generated which stops the 0.5 deg/sec roll rate and switches the vehicle roll control to the star sensor error signal."

During Mission E, the spacecraft was commanded on day 251 to roll at +0.5 deg/sec at 14:10:01 GMT. Telemetered confirmation occurred at the received time of 14:10:02.4, corresponding to L+6 hours 13 minutes 01.1 seconds. During the ensuing roll, a star map was generated by recording the analog signals star intensity (FC-14) (i.e., unthresholded star intensity) and star angle or roll error (FC-12) (i.e., thresholded star intensity) on a strip chart recorder. From this map, Canopus was positively identified (based on identifying the angular spacing of Canopus plus six other objects)

during the first 360 degrees of roll. While the spacecraft was still rolling, it was decided to continue the roll and acquire Canopus when the star entered the field of view during the second revolution, i.e., beyond 360 degrees. It had been observed during the first roll revolution that the Canopus lockon signal was present when Canopus was in the field of view. Therefore, it was possible to effect the acquisition of Canopus by employing the single sun and star command. The spacecraft was commanded to the sun and star modes at 14:25:35, and telemetered confirmation occurred at the received time of 14:25:36.3. Canopus lockon (FC-13) telemetry was received at 14:27:51.2, after which it required approximately 65 seconds for both the star intensity and roll error signals to stabilize to their deadband limits.

Star Map

At this point in time, the spacecraft, moon, sun, and earth relationships in the ecliptic plane are as shown in Figure 5.5-3a. The center of the moon would pass approximately 30 degrees outside the field of view in a plus yaw direction, and the center of the earth would pass approximately 26 degrees outside the field of view in a plus yaw direction. As shown in Figure 5.5-3a, the spacecraft is behind the moon and would therefore "see" less than a half-moon. Likewise, the spacecraft is in front of the earth and would "see" more than a half-earth. Figure 5.5-3b depicts the relationship of the sensor field of view and the earth as the spacecraft's -X axis points toward the earth during spacecraft roll.

Since large area bright objects within approximately 35 degrees of the sensor's line of sight will reflect light into the sensor from baffles in the sensor's light shield, it was expected that some star intensity signal would result when the sensor was rolling past both the moon and the earth. In addition, 36 stars, with intensities greater than 0.37×10^{-14} w/cm^2, come within the Canopus sensor's field of view during a complete roll revolution. However, based on laboratory measurements of star intensity signals versus star intensity on this particular sensor (S/N 8), it was predicted that 11 stars might be observed, although two stars were so close to earth that they might not be distinguishable, two others were close together, and three others were close together.

Figure 5.5-3c depicts the preflight calculated angular (roll angle) spacing of the moon, earth, Canopus, and the other stars actually observed.

The telecommunications subsystem was in mode 1 at 4400 bits/sec, resulting in transmission of a 100 word commutator word frame each 0.25 second. Star angle (FC-12) and star intensity (FC-14) signals, plus digital word 3, are read out each 0.05 second during each frame (equivalent to each 0.025 degree of spacecraft roll at the commanded roll rate of 0.5 deg/sec) and digital words 1 and 9 are read out once per frame (equivalent to each 0.125 degree of spacecraft roll).

During the mission, spacecraft telemetry was transmitted to the SFOF from Madrid (DSS-61) at 1100 bits/sec, resulting in the transmission of a 100 word commutator word frame each second. Thus, during the star mapping

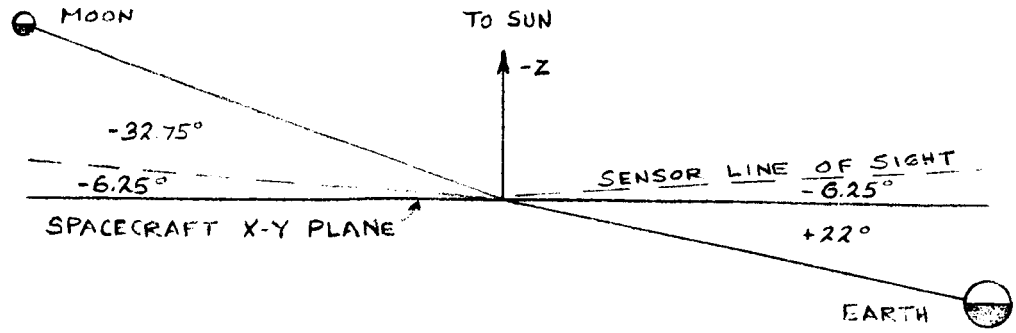

a) Ecliptic Plane Relationships

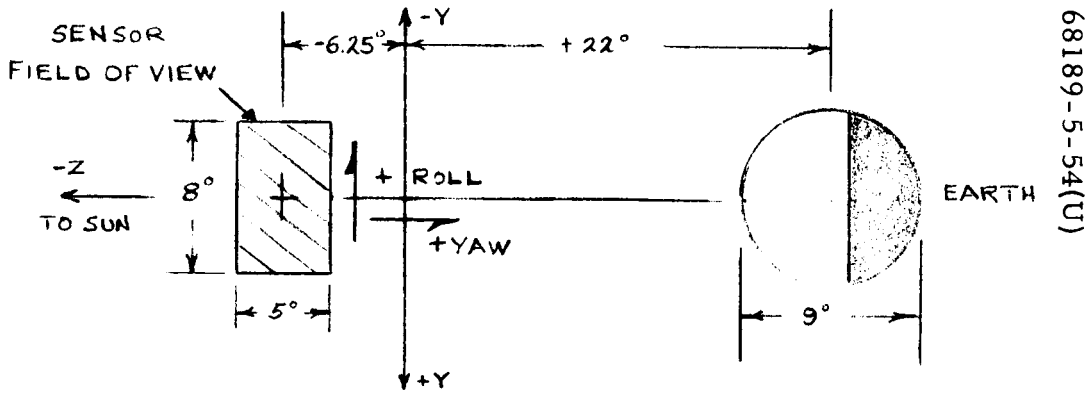

b) Sensor Field of View With Respect to Earth

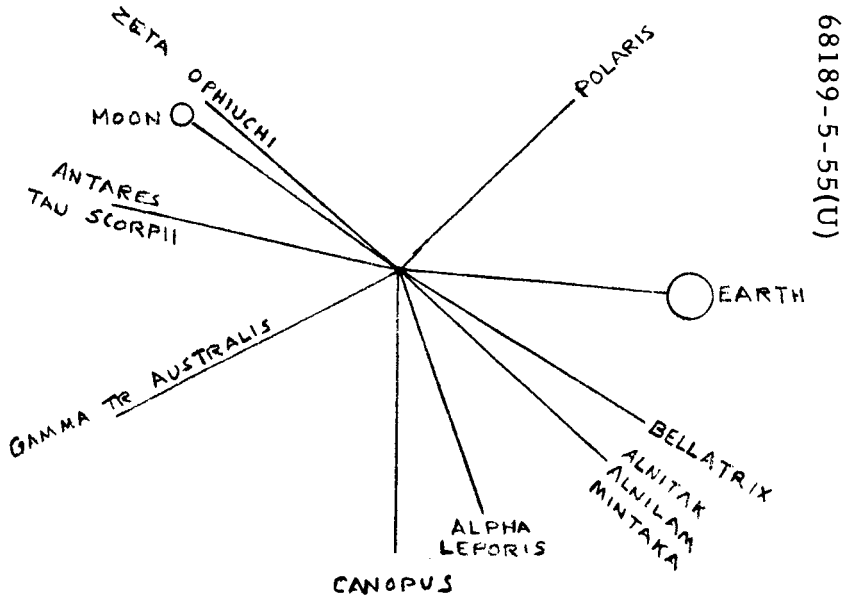

c) Angular Spacing (in Roll) of Observed Objects

Figure 5.5-3. Canopus Sensor Relationships to Observed Objects

portion of the mission in real time at the SFOF, only one-fourth of the total data was available for star identification. From the real-time SFOF analog recorder traces of star angle and star intensity, it was possible to distinguish four stars plus two groups of small stars and a 45-degree-wide high intensity signal. The angular spacing of these signals was compared with the preflight calculated star and earth angles, thus permitting positive identification of Canopus, Zeta Ophiuchi, Bellatrix, Polaris, the star group of Antares and Tau Scorpii, the star group of Alnitak, Alnilam, and Mintaka, plus the earth.

From postmission analog recorder traces utilizing all commutator frames versus every fourth frame obtained in real time, it was possible to identify two additional stars, Gamma Tr. Australis and Alpha Leporis, plus one of the two transits of the Milky Way.

Figure 5.5-4 depicts analog traces of primary sun sensor pitch angular error (FC-5), primary sun sensor yaw angular error (FC-6), roll gyro error (FC-49), star angle, star intensity, digital word 1, and digital word 9 from the start of roll through Canopus acquisition.

Table 5.5-4 indicates the responses received versus predicted responses. Roll angle is measured to the nearest 0.025 degree based on the times at which peak star intensity amplitudes are digitally recorded at the Madrid site.

Two objects appeared in the field of view during the first revolution (at 88.9 and 91.9 degrees) and one object during the second revolution (at 448.5 degrees) which did not exhibit the same type of star angle and star intensity responses as a celestial body. Since the angle between the first object and the object seen during the second revolution is (448.5 - 88.9) or 359.6 degrees, it appears that these signals emanate from the same object. The signal shapes of all three of these responses could be caused by an object traversing only one-half of the field of view at a relative angular rate in the vicinity of 1.0 deg/sec. Thus an object moving diagonally (i.e., with yaw and roll rates) across the field of view would yield the observed response, but such a yaw rate would place the object outside the field of view during the next revolution. However, since the response shape essentially repeats during the next revolution, it seems logical to conclude that these responses are due to a reflected bright spot or spots from the spacecraft.

The mean roll rate, as determined from the incremental time between the first and second crossing of the sensor's line of sight by Zeta Ophiuchi, is 360/(14:24:12.840 - 14:12:13.600) = 360/11.59.240 = 0.5007 deg/sec. The error due to sampling is ±0.25 second or ±0.00003 deg/sec, and the error due to roll gyro limiting cycling is ±0.2 degree or ±0.0003 deg/sec.

As noted in Table 5.5-4, the correlation between post- and preflight calculated angles from Canopus of all single stars varies from -0.2 to -0.5 degree, which is considered well within the capabilities of the analyst to determine the exact center of the weaker star's signals. The correlation on the earth angle is -0.7 degree, which is within the accuracy of determining the center of a widely varying amplitude signal.

GMT, hr:min:sec	Postflight Calculated Roll Angle, degrees ± Δt × 0.5007 deg/sec	Object	Postflight Calculated Angle From Canopus, degrees	Preflight Calculated Angle From Canopus, degrees	Measured Peak Intensity During Roll, telemetry volts	Predicted Peak Intensity During Roll, telemetry volts	Measured Peak Intensity at 0 Roll Rate, telemetry volts	Predicted Peak Intensity at 0 Roll Rate, telemetry volts	Occurrence of Canopus Lockon, Digital Word 1
14:10:02.4	0	(Start of roll)	-179.8						
14:12:13.6	65.7	Zeta Ophiuchi	-114.1	-113.9	0.51	0.40			No
14:12:46.6	82.2	Antares/ Tau Scorpii	- 97.6	- 97.8/ - 96.3	0.81	0.39/ 0.40			No
14:12:59.8	88.9	Object 1	- 91.0	–	0.81	–			No
14:13:06.0	91.9	Object 2	- 87.9	–	0.99	–			No
14:14:13.2	125.6	Gamma Tr. Australis	- 54.3	- 54.1	0.51	0.36			No
14:16:01.6	179.8	Canopus			4.32	4.08			Yes
14:17:13.4	215.8	Alpha Leporis	35.9	36.4	0.49	0.37			No
14:17:49.3	233.8	Alnitak/ Alnilam/ Mintaka	53.9	52.0/ 52.9/ 53.9	0.75	0.62/ 0.62/ 0.47			No
14:18:02.5	240.4	Bellatrix	60.5	60.7	0.86	0.68			No
14:18:55.9	267.1	Earth	87.3	88	4.40	4.00			Yes
14:20:49.1	323.8	Polaris	144.0	144.2	0.53	0.38			No
14:24:12.8	425.8	Zeta Ophiuchi	246.0	246.1	0.51	0.40			No
14:24:45.7	442.2	Antares/ Tau Scorpii	262.4	262.2/ 263.7	0.81	0.39/ 0.40			No
14:24:58.2	448.5	Object 1	268.7	–	0.62	–			No
14:26:11.6	485.2	Gamma Tr. Australis	305.4	305.9	0.49	0.36			No
		Canopus			4.32	4.08	4.74	4.38	Yes
		No star			0.41	0.36	0.41	0.36	No

TABLE 5.5-4. SURVEYOR V STAR MAP – RECEIVED VERSUS PREDICTED RESPONSES

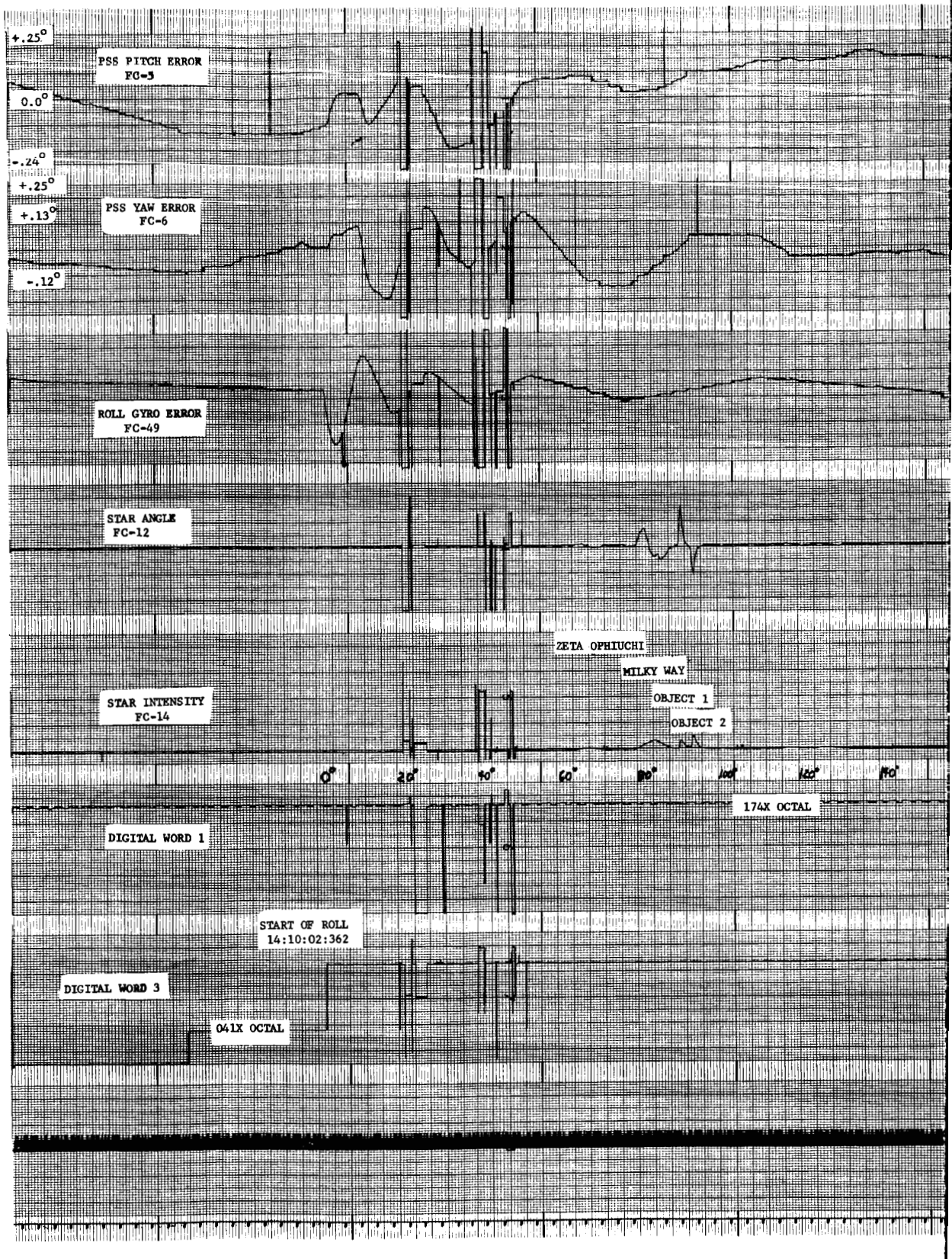

Figure 5.5-4. Analog Plot of Canpus Acquisition

FOLDOUT FRAME

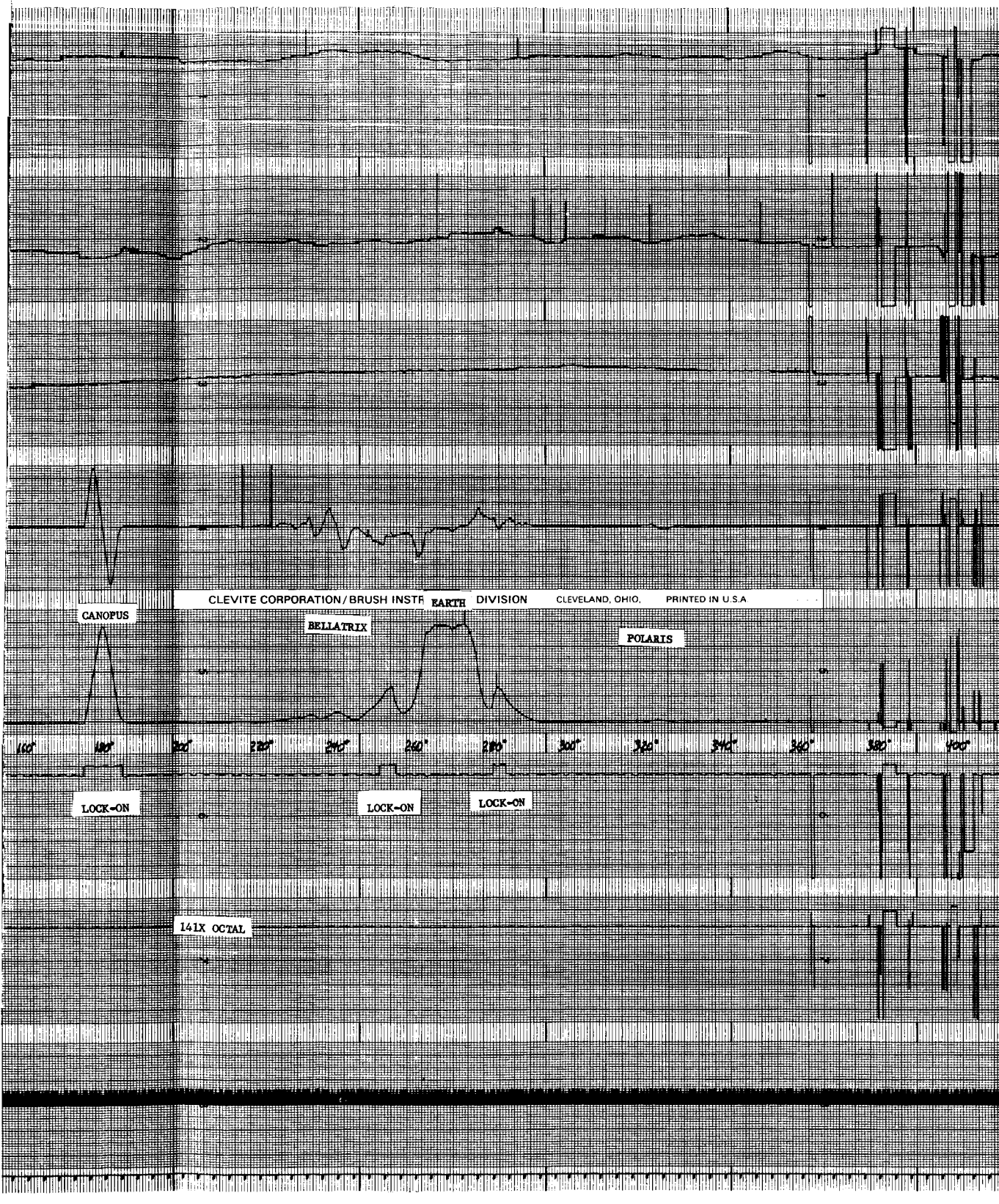

FOLDOUT FRAME

5.5-26

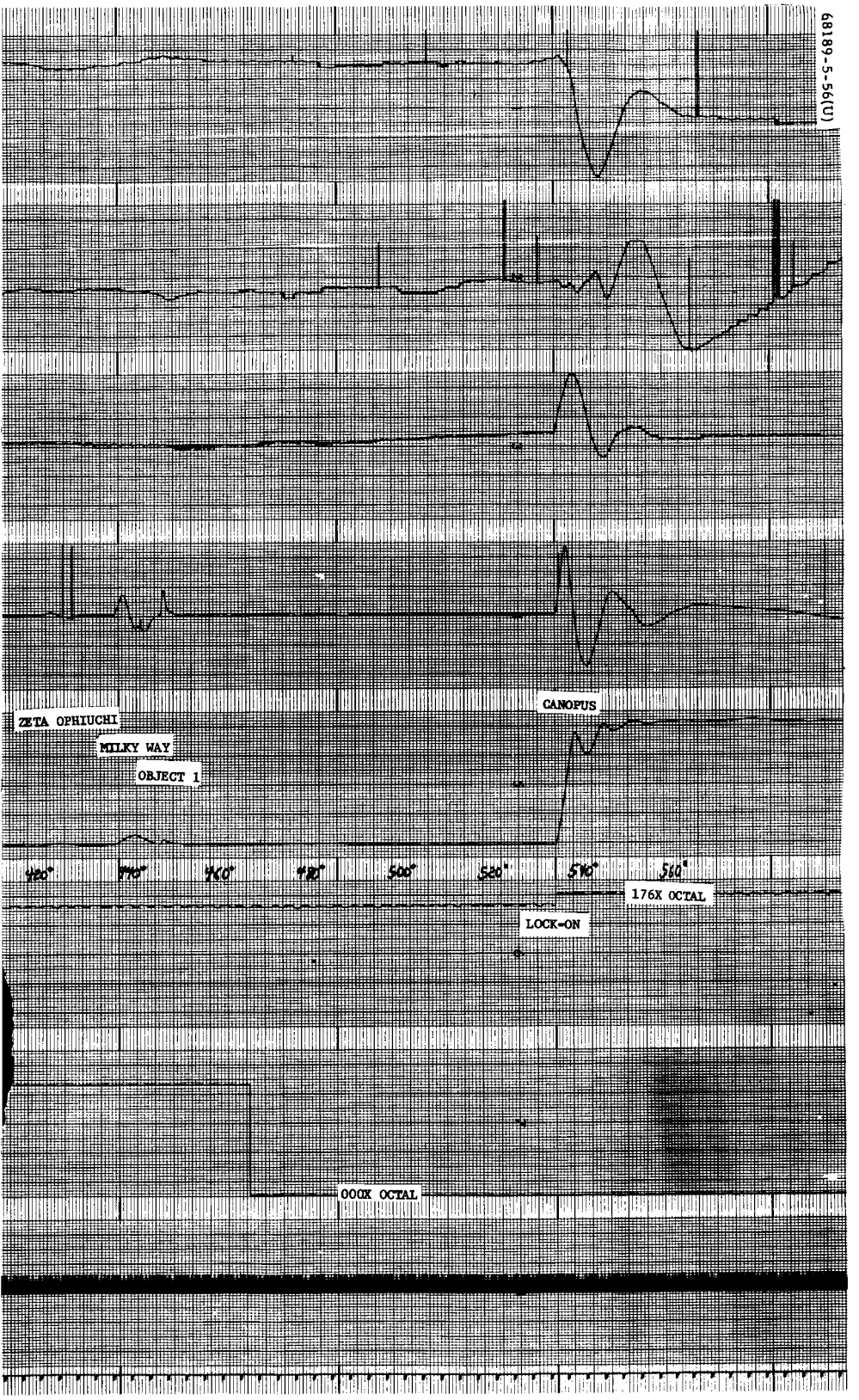

FOLDOUT FRAME
5.5-26A

Star Sensor Performance

The star sensor provides three outputs: star angle or roll error, Canopus lockon, and star intensity. A comparison of inflight and preflight measurements is used to determine how well the sensor performed in flight.

The star angle signal is designed to increase from a quiescent level, close to 512 BCD when no star is in the field of view, to a maximum, close to 1023 BCD, when Canopus is approximately +2 degrees from the X-Z plane. It returns to its quiescent level when Canopus is in the X-Z plane, then to a minimum, close to 0 BCD when Canopus is approximately -2 degrees from the X-Z plane, and finally increases to its quiescent level as Canopus leaves the field of view.

The star intensity signal is designed to increase from a quiescent level when no star is in the field of view to a maximum when Canopus is in the X-Z plane. It then decreases to its quiescent level as Canopus leaves the field of view. No star and maximum intensity values are listed in Table 5.5-4.

Figure 5.5-4 depicts the star angle and star intensity signals for all stars observed during the star map. Figure 5.5-5 depicts an enlarged view of the star intensity signal during most of the time Canopus was in the field of view in the first revolution. From these figures, it can be seen that the star angle and star intensity signals perform as designed.

Since the star intensity signal is a measure of the effective gain of the star sensor, the measurements, as recorded in Table 5.5-4, are analyzed to determine effective gain. Star sensor gain is a function of the photomultiplier tube scale factor which is controlled by the intensity of the sunlight actually reaching the tube through a sun filter in the sun channel optics. All preflight star sensor measurements are made with a unit sun intensity illuminating the sun channel. For flight, a flight filter is installed with a transmission factor that will admit more, equal, or less than a unit sun into the sensor. Mission A was flown with a sun filter calculated to increase the sensor gain so that Canopus would respond as 1.5 x Canopus. Analysis of inflight measurements indicated the effective gain was even greater than 1.5 x Canopus. Mission B was flown with a 1.17 x Canopus sun filter, and analysis of inflight measurements indicated the effective gain was still greater than 1.5 x Canopus, or 28 percent larger than expected. Mission C was flown with a 0.80 x Canopus sun filter, and analysis of in-flight measurements indicated the effective gain was in the vicinity of 1.17 x Canopus versus a prediction of 1.02 x Canopus. Mission D was flown with a 0.80 x Canopus sun filter, and analysis of in-flight measurements indicated the effective gain was in the vicinity of 1.24 x Canopus versus a prediction of 1.17 x Canopus.

Based on the prior missions, it was decided to install a 0.8 x Canopus sun filter for Mission E which should result in an effective gain close to the 1.17 x Canopus and 1.24 x Canopus values determined in Missions C and D. The actual observed peak intensity of Canopus, in an almost zero roll rate

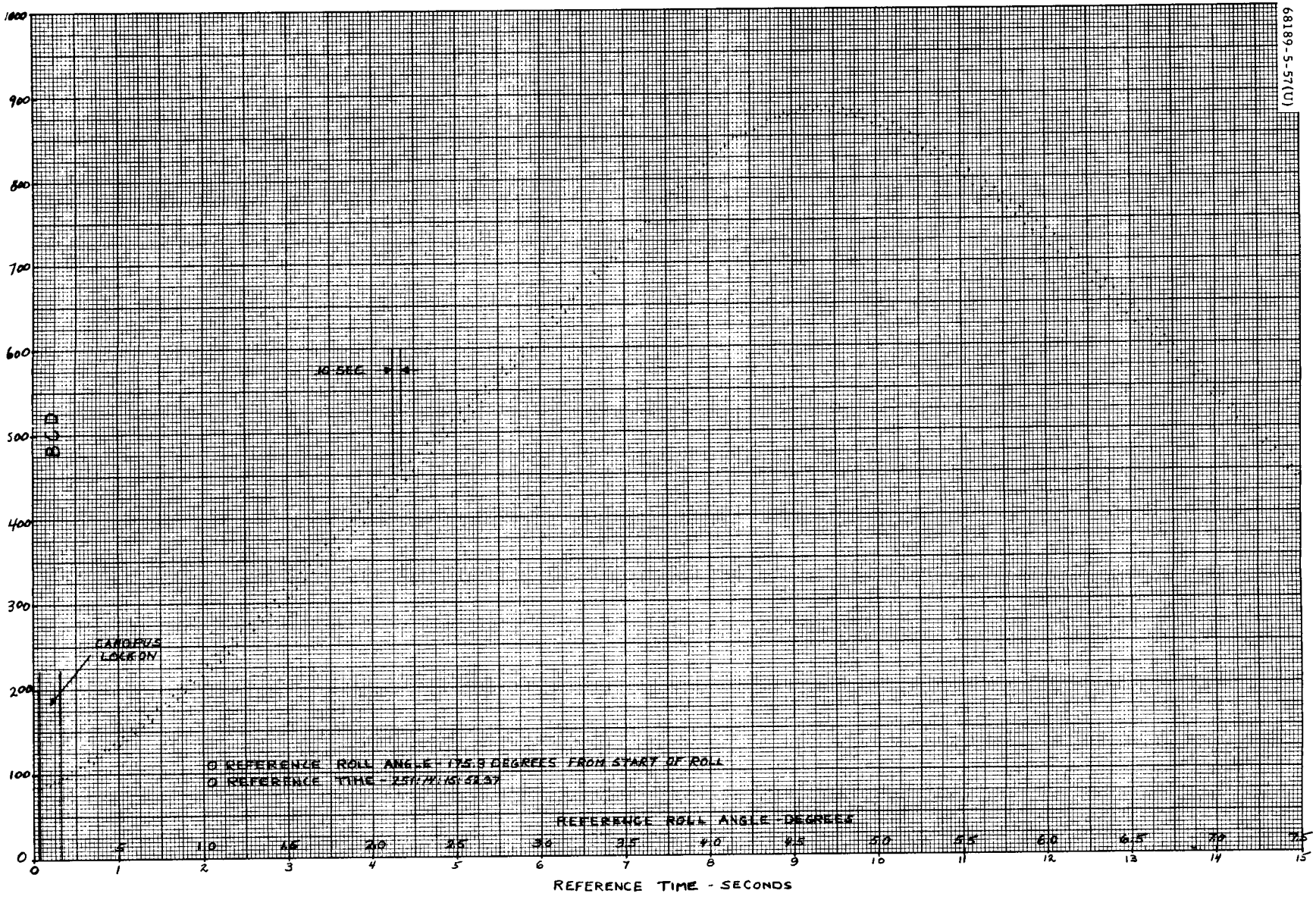

Figure 5.5-5. Star Intensity Signal During First Roll Past Canopus

condition after acquisition, is 4.74 volts compared to the Mission D value of 4.68 volts and the average preflight 1.0 × Canopus measurement of 3.54 (i.e., this is the mean of 29 intensity measurements using several different star simulators ranging from 3.24 to 3.88). The correction between Missions D and E is excellent, which probably indicates that the overall gains are nearly the same. However, the effective gain of a particular star sensor is defined as the ratio of in-flight Canopus intensity measurements to preflight 1.0 × Canopus intensity measurements and will vary from sensor to sensor since different photomultiplier tubes will exhibit different gains, as will different electronic circuitry and different sun channel optical paths. Thus, the effective gain of sensor S/N 8 flown on Mission E is calculated to be 4.74/3.54 or 1.32 × Canopus, whereas the effective gain of sensor S/N 4 flown on Mission E was calculated to be 4.68/3.77 or 1.24 × Canopus. Therefore, it is concluded that the Mission E sensor had less photomultiplier sensitivity than the Mission D sensor, but the 0.8 × Canopus sun filters were sufficiently different such that the intensity measurement of Canopus was actually higher in Mission E than in Mission D.

Missions C, D, and E have all been flown with nominally the same 0.8 × Canopus sun channel filter and have exhibited calculated effective gains of 1.17, 1.24, and 1.32 × Canopus. These differences are attributed to the inaccuracies inherent in preflight sensor intensity measurements and in sun channel filter transmission measurements.

As noted in Figure 5.5-5, the star intensity signal exhibits a high frequency oscillation superimposed on the basic ramp-shaped signal. The period of this oscillation is 0.1 second, and its amplitude is greatest at angles midway between the edges and center of the field of view. This 0.1-second period corresponds to a frequency of 10 Hz which is the frequency of oscillation of the nodding mirror in the sensor which sweeps the star image through an angle of 4 degrees each half cycle, or 0.05 second. When a star image is midway between an edge and the center of the field of view, the nodding mirror is sweeping that image ±2.0 degrees across the edge of the optical gate or slot in the star signals optical path. Thus, light falls on the photomultiplier tube for half the nodding mirror's period (i.e., 0.05 second) and no light falls on the tube during the other half period. The resultant signal is chopped, rectified, and filtered to become the star intensity signal which has a 10-Hz oscillation superimposed on a dc level and which is sampled every 0.05 second in mode 1 at 4400 bits/sec by the telemetry system. Therefore, the combination of a sampling period of 0.05 second and a nodding mirror period of 0.10 second results in an alternating telemetry signal. The peak magnitude of the telemetered oscillation is dependent upon the synchronization between the telemetry clock providing its 0.05-second sample timing and the flight control sensor group's frequency source powering the nodding mirror assembly drive motor. Since these are independent timing sources, it is expected that the phasing between them will vary with time and thus be different at various times during the mission.

The third sensor output, Canopus lockon, is shown in Figure 5.5-4 as part of digital word 1 and is listed in Table 5.5-4. Since the earth's intensity signal is between the lockon triggering levels, the lockon signal is

present for an extended period. Based on these observations, it can be seen that the Canopus lockon signal performed as desired.

Canopus Acquisition Sequence

Since Canopus was identified during the first revolution and Canopus lock was present when Canopus was in the field of view, it was decided to send the sun and star command after the earth had sufficiently cleared the field of view. The automatic acquisition sequence could then occur.

Figure 5.5-6 depicts the response of the star intensity signal after receipt of the Canopus lockon signal has put the spacecraft in a closed-loop roll error controlled mode. When lockon occurs, the spacecraft is rolling at +0.5 deg/sec, and the roll error signal is increasing to a maximum which commands the spacecraft to roll positive to obtain a nulled roll error signal. Thus, the positive command causes the plus roll rate to increase, which results in a steeper slope of the star intensity signal and a lower amplitude peak due to the effect of filtering on the faster changing signal. As the star intensity signal crosses its peak, the roll error signal is going negative, causing the plus roll rate to decrease to zero and become negative to swing the -X axis back negative to alignment with Canopus. As the star intensity signal crosses its valley, the roll rate is zero and, as the star intensity signal crosses the next peak, the roll error signal is going positive, causing the negative roll rate to increase to zero and become positive to swing the -X axis back positive to alignment with Canopus. After several such cycles, the spacecraft settles down to a slow roll oscillation which causes the star intensity signal to oscillate on either side of its peak amplitude while the roll error signal oscillates above and below its null position. This oscillation is bounded, and the bounds are referred to as the roll optical limit cycle.

As noted in Figure 5.5-6, the star intensity peak amplitudes increase as the limit cycle is approched since there is less attenuation due to filtering as roll rate decreases to almost zero.

Conclusions

The Canopus sensor performed as designed without malfunction. The star intensity signal, with Canopus in the field of view, was higher than the nominal predicted, but within the accuracy of the preflight measurements. The automatic star acquisition capability was successfully utilized.

5.5.4.5 Coast Phase

Gas Jet Thrust Level

Reference 2 developed the following expression for the gas jet thrust level, T:

$$T = \frac{I_z \dot{\Phi}_c}{R t_p}$$

68189-5-58(U)

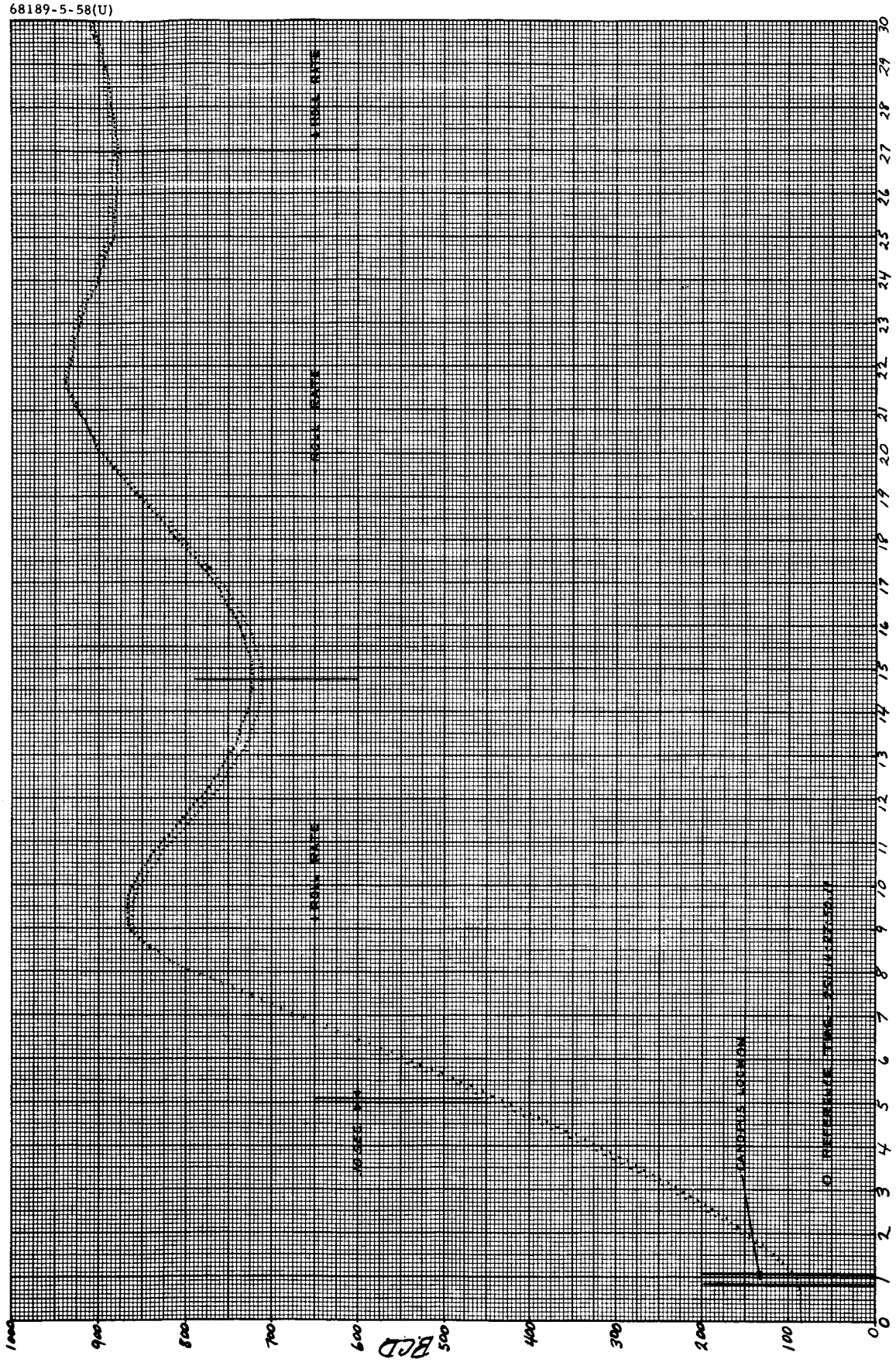

Figure 5.5-6. Star Intensity Signal During Canopus Acquisition

where

I_z = roll inertia = 211 slug-ft^2

$\dot{\Phi}_c$ = commanded precession rate = 0.5 deg/sec

R = gas jet moment arm = 6.47 feet

t_p = thrusting time of the gas jet from initiation of precession command to point at which $\dot{\Phi}_{gyro} = 0$

Using the premidcourse roll maneuver data (Figure 5.5-7), the time from command initiation until $\dot{\Phi}_{gyro} = 0$ was 6.0 seconds. Since the No. 1 gas jet amplifier is off 1.3 seconds of this time (Reference 3), t_p = 6.0 seconds - 1.3 seconds = 4.7 seconds.

$$T = \frac{(211 \text{ slug-ft}^2)\ (0.5 \text{ deg/sec})}{(6.47 \text{ feet})\ (4.7 \text{ seconds})} = 0.061 \text{ pound}$$

Section 13 of Reference 4 shows that the thrust levels for all six jets during test were within 3.5 percent of each other. On this basis, it can be assumed that the nominal thrust level for the six gas jets was 0.061 pound.

Nitrogen Consumption

Nitrogen consumption for the period from launch to preretro maneuvers was 1.0 pound. This number compares favorably with predicted usage when measurement uncertainties and postgyro drift lockon transients are taken into account. Mission nitrogen usage was obtained from pressure and temperature information telemetered on flight control signals FC-4 and FC-48.

The predicted nitrogen usage for each maneuver was determined from the simulation defined in Reference 5; a detailed breakdown of the predicted impulse and weight expenditures is documented in Reference 6.

For the number and sequence of Mission E maneuvers, Attachment 1 of Reference 6 yields the following nominal impulse consumption budget:

	lb-sec
Leakage	3.40
Vernier phase of midcourse maneuvers	12.00
Limit cycle operation	4.50
Sun acquisition	3.25

68189-5-59(U)

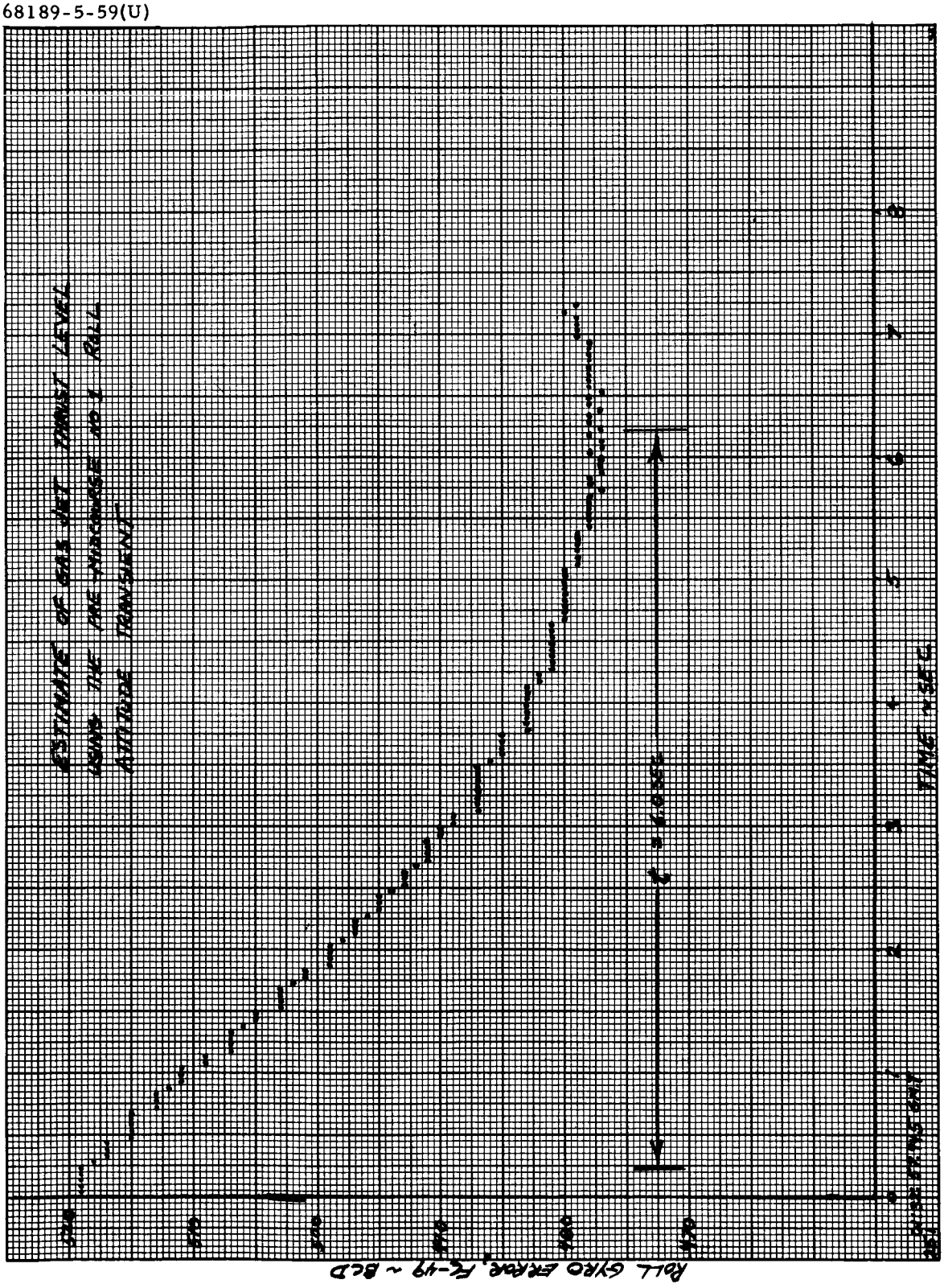

Figure 5.5-7. Gas Jet Thrust Level Determination of Firing

	lb-sec
Inertial roll maneuvers (4)	6.0
Star verification	1.50
Star acquisition	1.40
Inertial yaw maneuvers (6)	7.50
Rate dissipation	2.75
Postmidcourse rate dissipations (6)	6.00
Total	47.30

Assuming an average I_{sp} of 60 seconds yields a nominal nitrogen usage prior to the preretro maneuvers of approximately 0.79 pound. Reference 6 also predicts a 3σ usage uncertainty of 0.52 pound for this particular mission profile. The uncertainty associated with the gas usage during the post-engine firing shutdown transients accounts for 0.48 pound of this total.

The fuel consumption due to the post-gyro drift check lockon transients was determined by using the final angular attitude positions of each drift check as initial conditions to the simulation documented in Reference 7 with the following results:

1) The average impulse expenditure for a post-three-axis drift transient was 0.90 lb-sec.

2) The average impulse expenditure for a post-roll-axis-only drift transient was 0.55 lb-sec.

So there is an increase in the nitrogen consumption prediction of

$$\frac{3\,(0.55)\ \text{lb-sec} + 9\,(0.90)\ \text{lb-sec}}{60\ \text{seconds}} = 0.163\ \text{pound}$$

The net prediction would be

$$(0.79 + 0.16) \pm 0.52 = 0.95\ \text{pound} \pm 0.52\ \text{pound}$$

5.5.4.6 Premidcourse Attitude Maneuvers

Prior to five of the six vernier engine burns, the spacecraft thrust axis was oriented away from the sunline. The remaining engine burn (No. 2) was accomplished with the thrust axis (roll axis) aligned to the sunline. The roll attitude control system was in the inertial mode from the time of the initial premidcourse roll maneuver until just prior to the fourth engine burn, a total of approximately 2.5 hours. A summary of the attitude maneuvers is presented in Table 5.5-5. The telemetered roll and yaw gyro error signals

TABLE 5.5-5. SUMMARY OF ATTITUDE ORIENTATION MANEUVER ACCURACY

Maneuver	Magnitude (Bits), 0.4 sec/bit	Expected Value, degrees	Actual Results, degrees	Mode and Bit Rate, bits/sec	Comments
Roll	360	+ 72	+ 71.914	1/4400	Orientation maneuvers for burn No. 1
Yaw	179	- 35.8	- 35.622		
Yaw	901	-180.1	-179.547	1/4400	Orientation maneuvers for burn No. 3
Roll	343	+ 68.5	+ 68.661	5/1100	Orientation maneuvers for burn No. 4
Yaw	534	+106.7	+106.748		
Roll	323	+ 64.5	+ 64.547	1/4400	Orientation maneuvers for burn No. 5
Yaw	717	+143.3	+143.213		
Roll	380	- 75.9	- 75.891	1/4400	Orientation maneuvers for burn No. 6
Yaw	503	-100.5	-100.408		

and 467 BCD at the finish for a total rotation of approximately 360.1 degrees. No correction was made for gyro drift. The start and stop times for the two maneuvers are as follows:

Start +179.9 degrees yaw	18:12:19.311 GMT	360.727 seconds
Stop	18:18:20.038 GMT	
Start +180.1 degrees yaw	18:22:55.667 GMT	360.284 seconds
Stop	18:28:55.951 GMT	
	Total	721.011 seconds

The average positive yaw precession rate was then computed to be 360.1/721 or +0.4994 deg/sec.

Attitude Maneuver Error

Reference 8 develops two orthogonal equations that specify the spacecraft thrust axis pointing error during midcourse thrusting. The equations were derived for the roll-yaw rotation sequence which applies to the Surveyor V mission.

Neglecting error sources that are present only after engine ignition:

$$\text{Error about yaw axis} = -\psi_{R_E} + -\psi_{A_E} \cos\varphi - \theta_{A_E} \sin\varphi$$

$$\text{Error about pitch axis} = \left(\varphi_{A_E} + \varphi_{R_E}\right) \sin\varphi + \theta_{A_E} \cos\psi \cos\varphi - \psi_{A_E} \sin\varphi \cos\psi$$

where

$(\varphi, \theta, \psi)_{A_E}$ = spacecraft inertial reference alignment errors

$(\psi, \varphi)_{R_E}$ = rotation errors

Use of the appropriate maneuver magnitudes for φ and ψ, and the errors listed in the summary chart resulted in the total attitude errors indicated in Table 5.5-6.

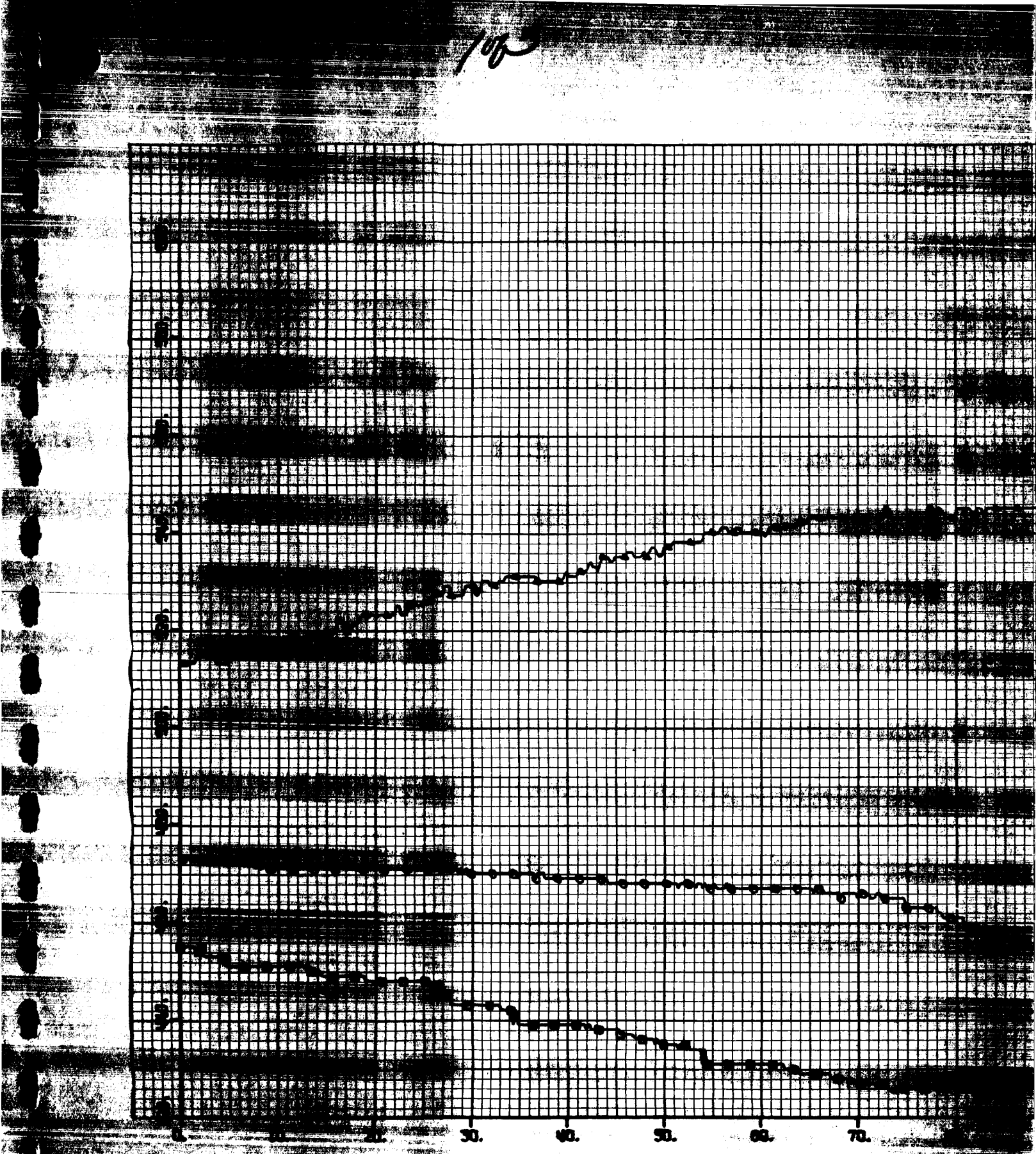

Figure 5.5-9. Premidcourse Maneuver Errors
FC-5, FC-6, and FC-12

FOLDOUT FRAME

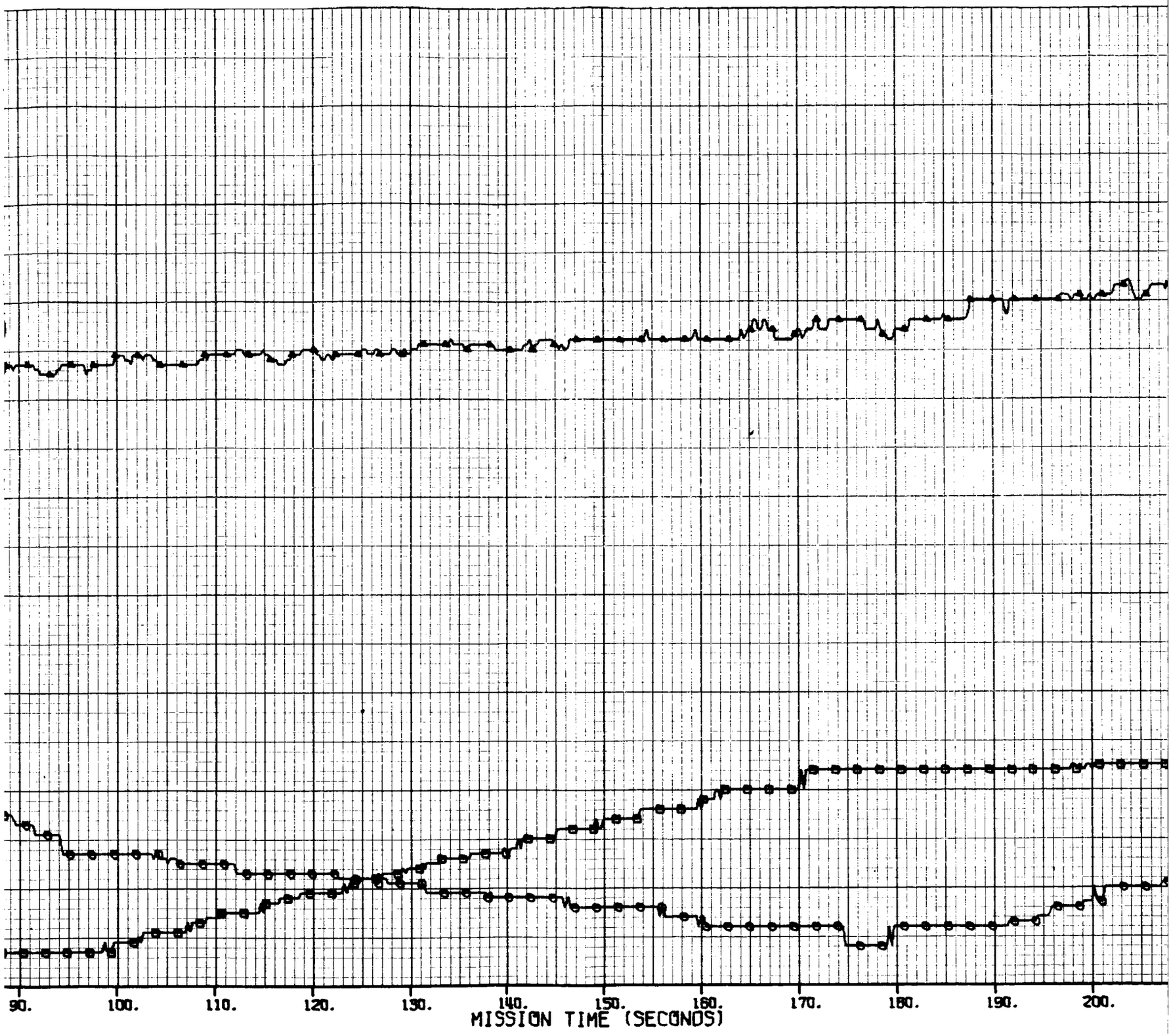

FOLDOUT FRAME

5.5-42

FOLDOUT FRAME

5.5-42A

3 of 3

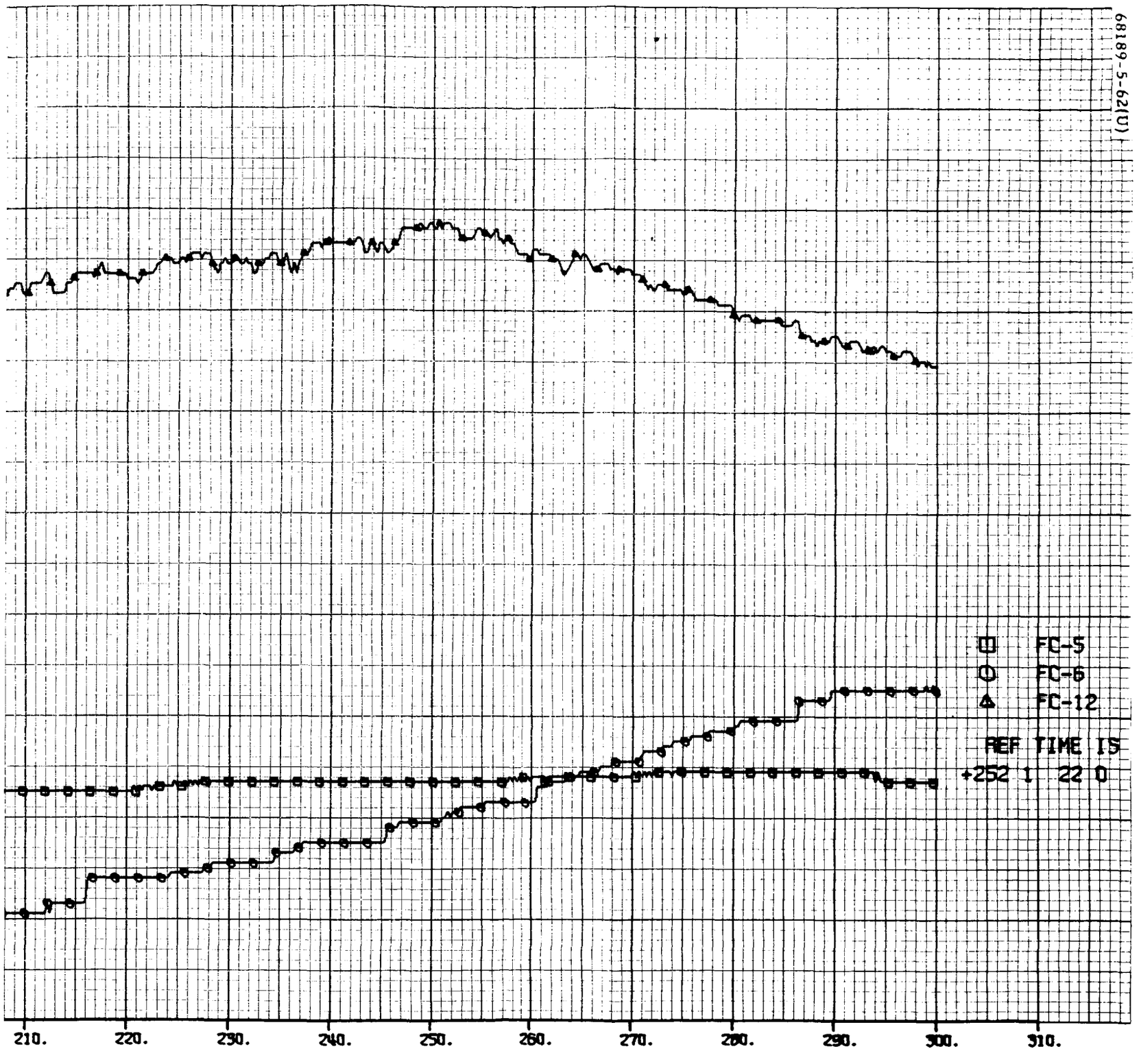

FOLDOUT FRAME

5.5-42B

FOLDOUT FRAME

5.5-42C

5.5.4.7 Postmidcourse Attitude Maneuvers

The postmidcourse attitude maneuvers are used to realign the spacecraft to the celestial reference after performing a midcourse velocity correction. To accomplish this, two reacquisition schemes are available. One method is to perform the premidcourse attitude maneuvers in reverse, and the other is to perform another automatic sun acquisition sequence. The first method is more desirable since real-time monitoring of optical sensor signals provides a good indication of premidcourse maneuver accuracy and attitude control during the thrust period. If reacquisition of the sun and Canopus is not achieved to within a fair degree of accuracy, one or more of the following conditions must have existed:

1) Nonsymmetrical precession commands

2) Spacecraft attitude change occurred between maneuver periods

3) Premidcourse maneuvers were not accurate

4) Postmidcourse maneuvers were not accurate

5) Vernier engine shutoff transients excessive

The first method was chosen for the Surveyor V mission, and the celestial reference was successfully reacquired after each engine burn. However, the spacecraft was not aligned to Canopus during burns 2 and 3.

5.5.4.8 Midcourse Velocity Correction

Of the six vernier engine burns, only the first and sixth were based on tracking data. Burns 2 and 3 were performed in an attempt to reseat the helium pressure regulator valve, while burn 4 was carried out to reduce fuel weight, reseat the helium valve, and return to the original landing site. The fifth burn was performed to reduce fuel weight and to increase the amount of gas in the propellant tanks.

From orbit determination, the actual magnitude of the velocity change due to vernier engine burn 6 was estimated to be 5.3192 m/sec compared to the commanded value of 5.4336 m/sec for a ΔV execution error of -0.1144 m/sec.

Plots of flight control variables during the six engine burns are shown in Figures 5.5-10 and 5.5-11.

Engine Ignition Characteristics

For each of the six burns, vernier ignition was smooth and followed by a nominal, uneventful thrusting phase. A summary of the pitch, yaw, and roll gyro errors is included in Table 5.5-7.

TABLE 5.5-7. VERNIER PERFORMANCE SUMMARY

Vernier Engine Burn Number	Maximum Change in Attitude, degrees			Steady-State Vernier Engine Thrust Level, pounds			Total Thrust, pounds	Burn Time, seconds	
	Pitch	Yaw	Roll	1	2	3		Expected	Observed
1	-0.24	+0.08	-0.88	77	74	69.4	220.4	14.3	14.22
2	0	+0.25	-0.88	76.45	73.36	68.95	218.76	10.05	10.04
3	-0.13	+0.19	-0.84	76.45	73.1	69.2	218.75	23.05	23.04
4	-0.05	+0.20	-0.90	76	72.8	68.4	217.2	12.0 0.5 0.5	12.32 — —
5	+0.05	+0.22	-1.0	73	72.2	67.7	212.9	33.0	33.073
6	+0.1	-0.18	-0.82	76.26	73.04	68.0	217.3	5.45	5.405

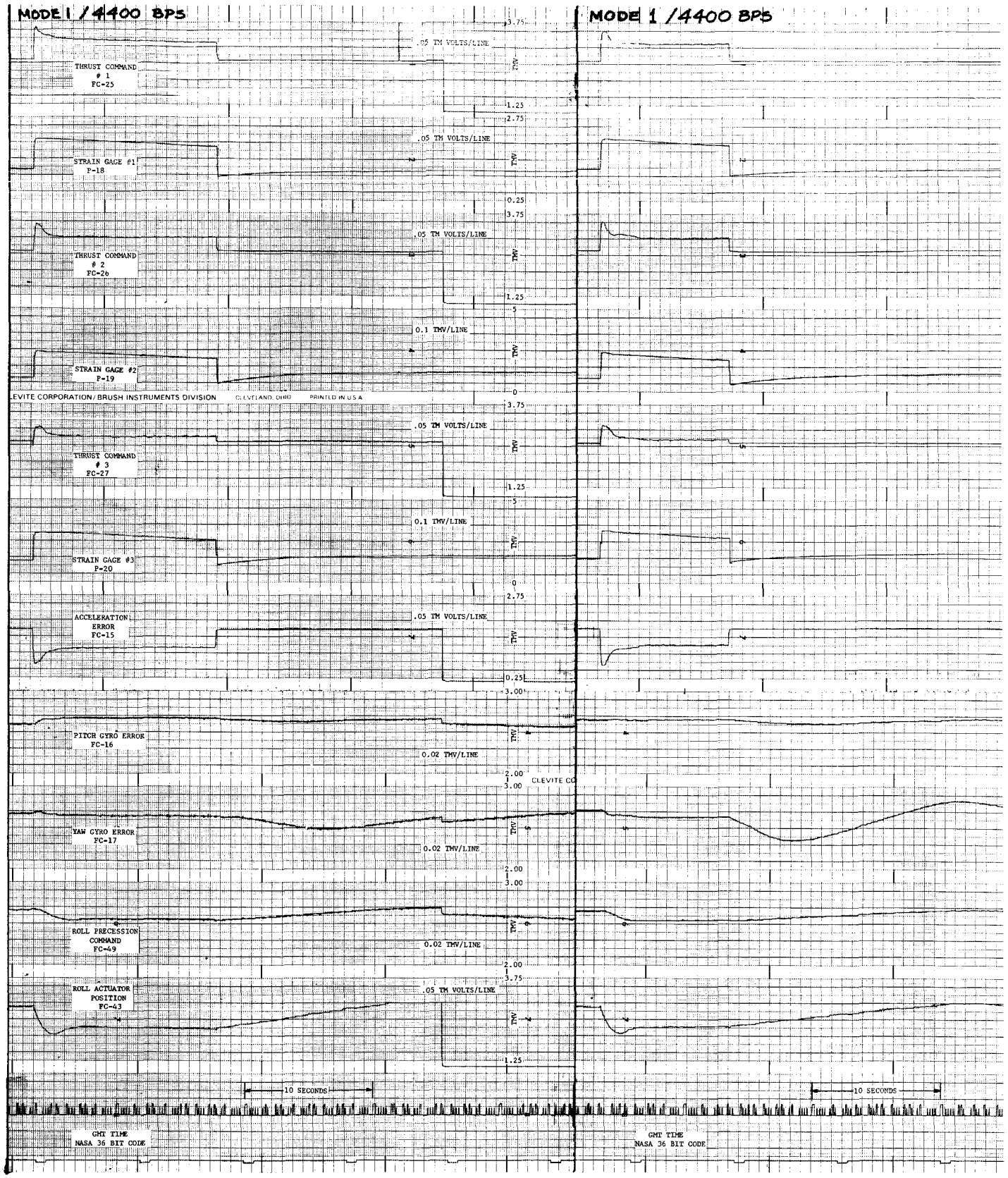

Figure 5.5-10. Flight Control Variables—Burns 1, 2, and 3

FOLDOUT FRAME

2

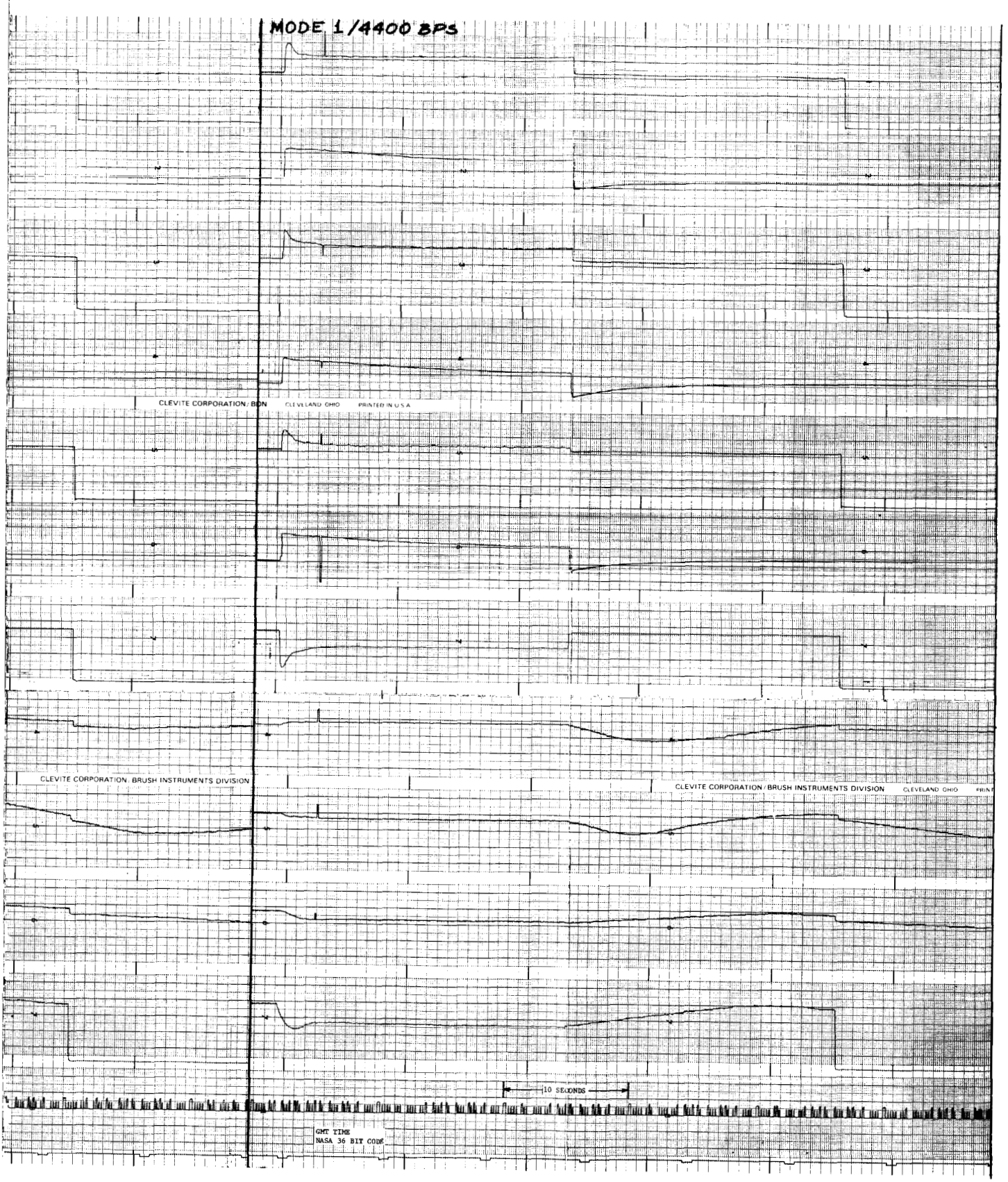

FOLDOUT FRAME

5.5-46

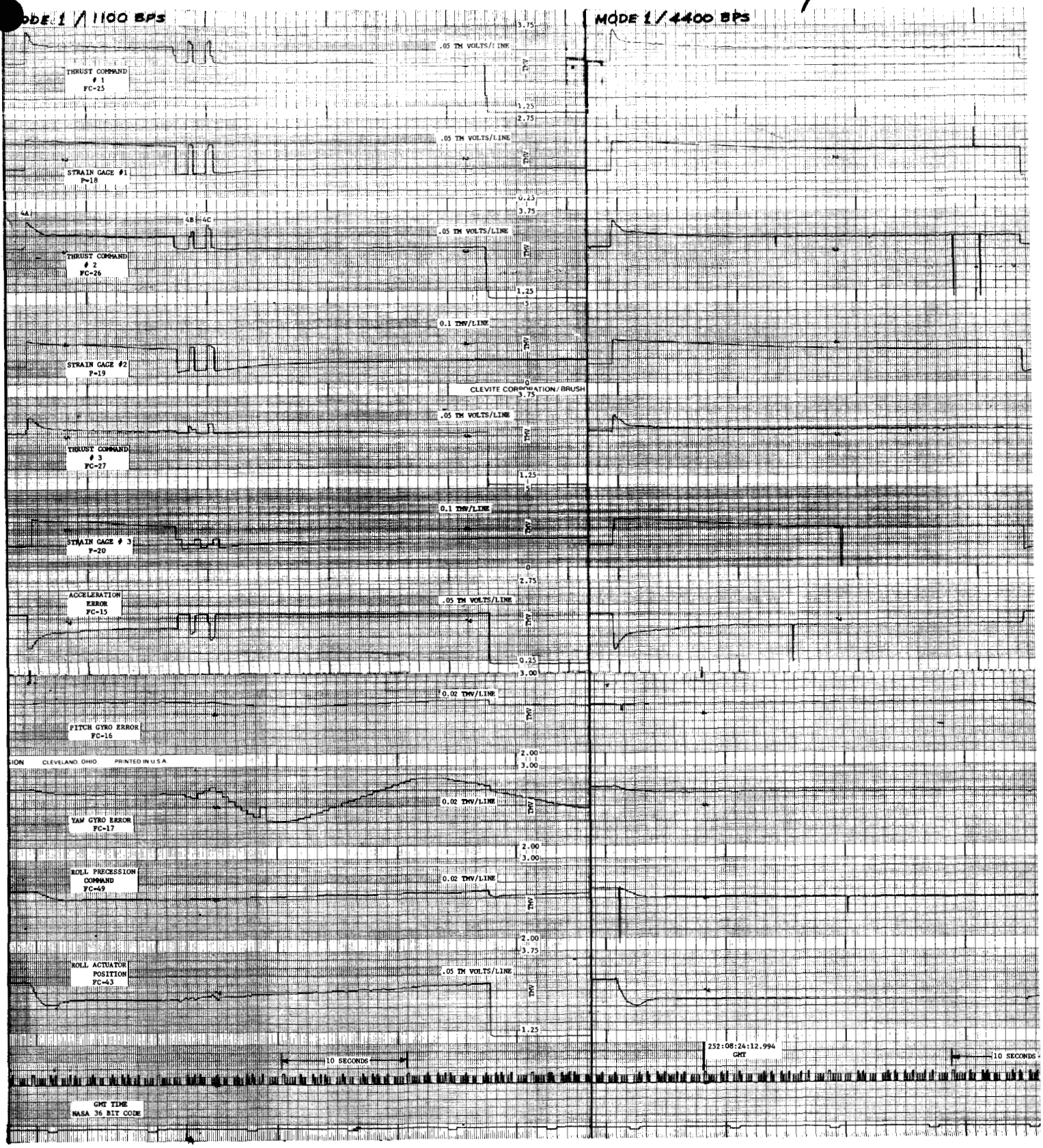

Figure 5.5-11. Flight Control Variables—Burns 4, 5, and 6

FOLDOUT FRAME

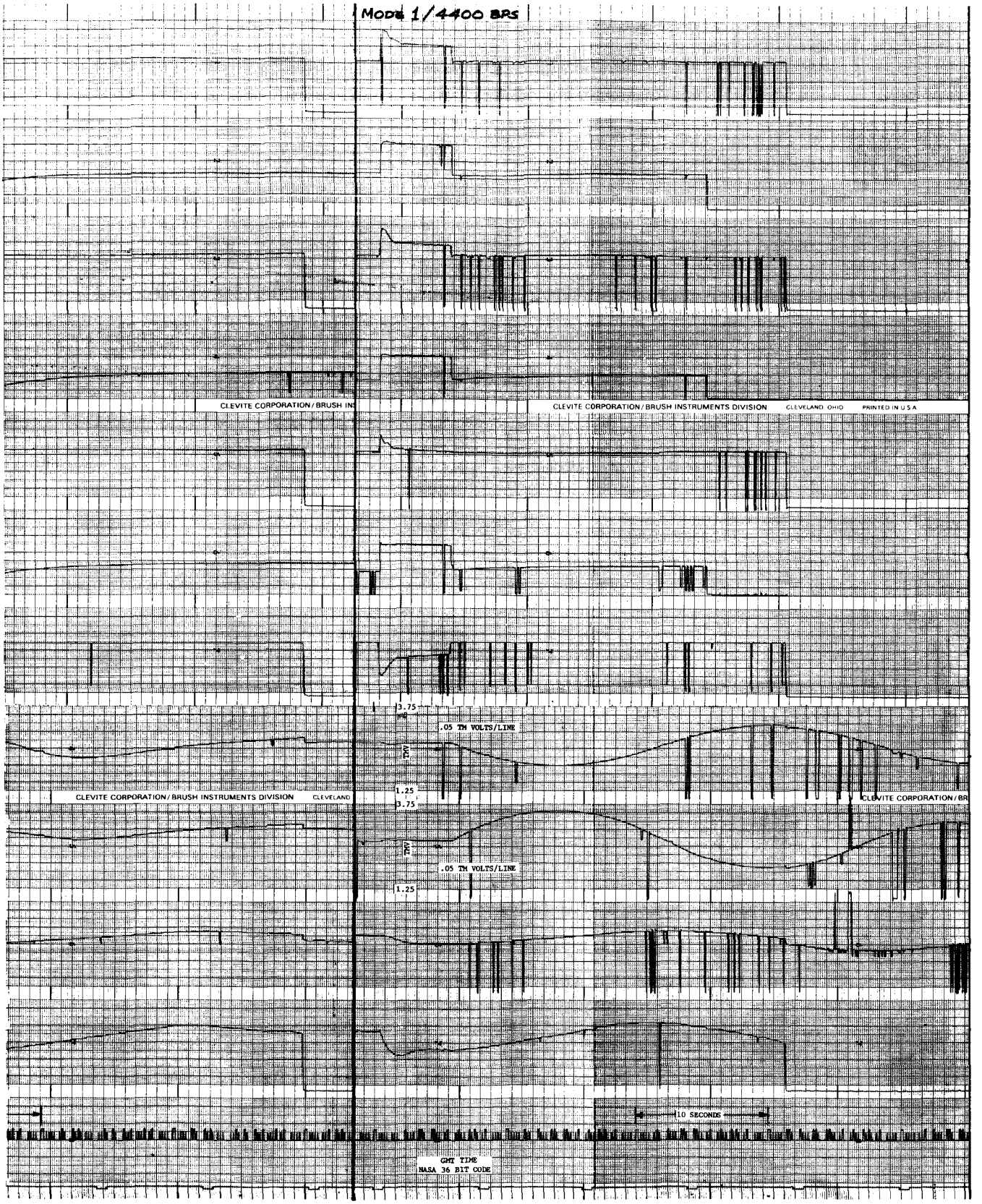

FOLDOUT FRAME

5.5-48

Based on the acceleration error telemetry signal (FC-15) (Figures 5.5-10 and 5.5-11), it was concluded that all three engines were producing controlled thrust within about 0.150 second of the ignition command signal for all six burns. Therefore, acceleration signal amplifier saturation, which requires a startup delay of 0.26 second, did not occur, and no ΔV error information was lost.

Vernier Engine Shutdown Dispersions

A summary of the peak spacecraft angles and angular rates and computed vernier engine shutdown impulse dispersions for each of the burns is given in Table 5.5-8.

It should be noted that peak gyro angles were less than 3 degrees and well within the required travel range of ±10 degrees. Inertial reference was therefore retained, and reacquisition of the sun and Canopus was accomplished via the reverse maneuver sequence.

Vernier engine shutdown impulse dispersions (relative to mean impulse of the three engines), calculated from pitch and yaw angular rate data as per the procedure outlined in the "Midcourse Engine Startup Characteristics," were well within the specification limit of ±0.63 lb-sec (Reference 10) except for burn 5 which apparently produced a shutdown impulse dispersion of +0.65 lb-sec.

Midcourse Velocity Determination

The general concept of midcourse correction capability employed by Surveyor is to apply a constant acceleration for a finite period of time. Thus, in theory, once the magnitude of the velocity correction is known, the exact duration of the constant acceleration phase can be determined. In practice, this approach is slightly altered to account for such error sources as engine ignition transients, shutdown impulse, and hysteresis. Thus, the actual command time ΔT is slightly higher.

Duration of Burn Times

The acceleration error signal data were used in an attempt to determine the actual burn times for all the firings. The results are presented in Table 5.5-7. The graphical technique used to determine engine ignition and shutdown times for burn 1 is shown in Figure 5.5-12.

Estimate of ΔV

The output of the acceleration amplifier (FC-15) remained essentially constant during each of the six burn periods at values indicated in Table 5.5-9, along with the estimated values of ΔV.

A list of parameters affecting the accuracy of the velocity correction is presented in Table 5.5-10 along with the values of maximum allowable errors. Actual performance values were used wherever possible.

TABLE 5. 5-8. VERNIER ENGINE SHUTDOWN SUMMARY

Burn Number	Maximum Change in Attitude, degrees			Peak Angular Rates, deg/sec		Impulse Dispersions, lb-sec		
	Pitch	Yaw	Roll	Pitch	Yaw	Engine 1	Engine 2	Engine 3
1	+0. 13	+0. 50	+1. 2	+0. 06	+0. 06	-0. 06	+0. 05	+0. 01
2	+0. 16	+0. 90	+1. 0	+0. 06	+0. 23	-0. 10	+0. 18	+0. 08
3	+0. 58	+0. 48	+1. 1	+0. 13	+0. 12	-0. 13	+0. 11	+0. 02
4	+0. 14	+1. 3	-0. 44	+0. 06	+0. 17	-0. 07	+0. 100	-0. 03
5	+0. 71	+0. 5	+0. 2	+0. 46	-0. 76	-0. 53	+0. 65	-0. 12
6	+1. 2	-2. 2	+0. 36	+0. 13	≈0	-0. 29	+0. 15	+0. 14

68189-5-65(U)

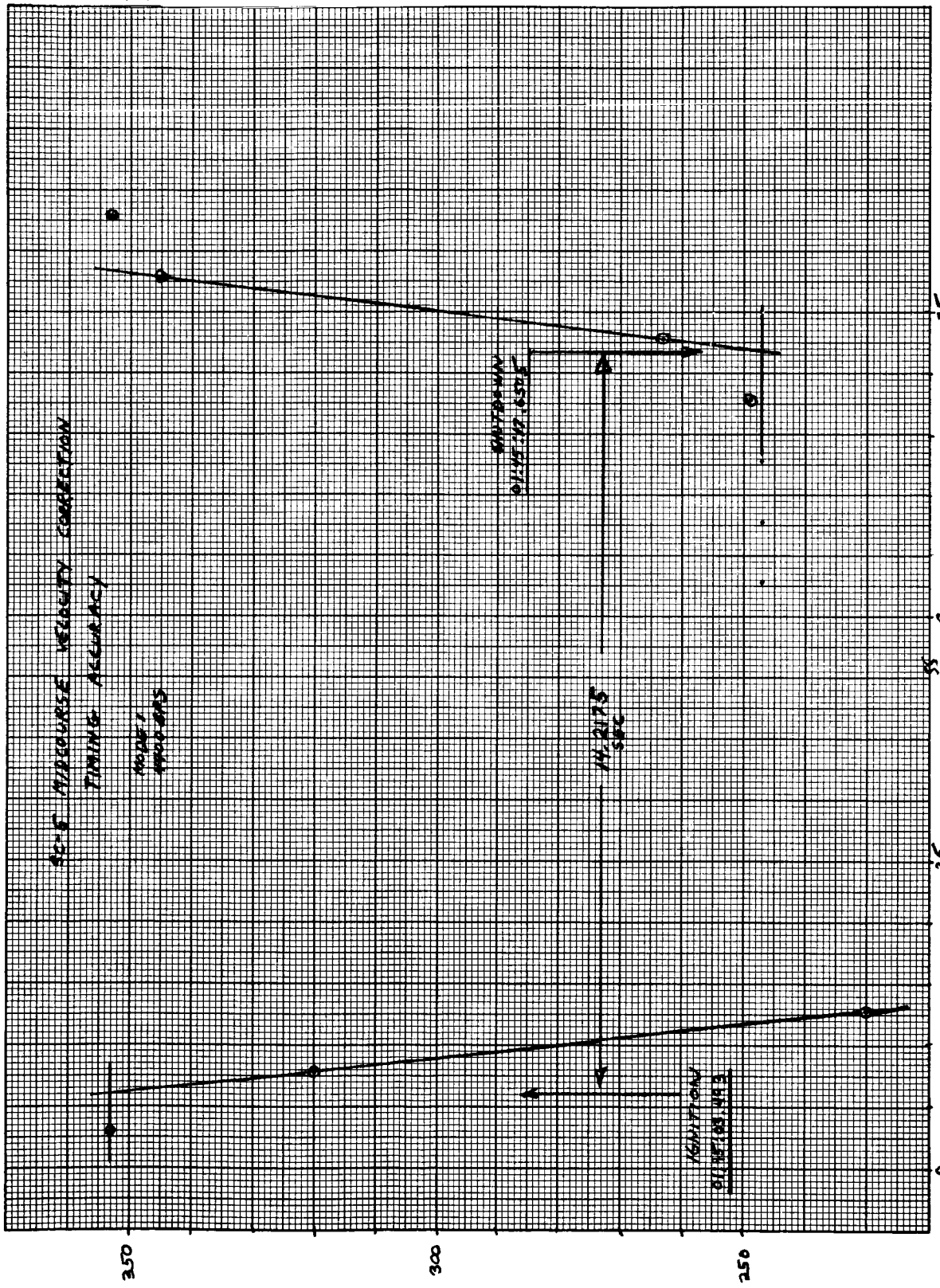

Figure 5.5-12. Midcourse Velocity Correction Timing Accuracy

TABLE 5.5-9. SUMMARY OF ACHIEVED VELOCITY CORRECTION MAGNITUDES

Burn Number	Acceleration Amplifier Output, FC-15, ft/sec^2	ΔT, seconds	$\Delta V = FC\text{-}15 \times \Delta T$, fps
1	3.207	14.22	45.60
2	3.209	10.04	32.09
3	3.210	23.04	73.96
4	3.209	12.32 0.5 0.5	42.74 1.6 1.6
5	3.207	33.073	106.06
6	3.209	5.405	17.34 (17.45 desired)

Telemetered Thrust Levels

The vernier engine thrust levels were determined from vernier engine thrust command calibration data which were obtained using the improved calibration techniques.

The approximate steady-state vernier engine thrust levels are indicated in Table 5.5-7.

5.5.4.9 Preretro Maneuvers

Before retro ignition, it is required that the spacecraft thrust axis (roll axis) be aligned to the translational velocity vector of the spacecraft as part of the gravity turn terminal descent phase guidance. The alignment is performed by means of two sequential rotations about the spacecraft body (gyro) axes. A third roll rotation may be required to align the high-gain planar array with the spacecraft-earth line to secure a favorable omni-directional antenna pattern or to satisfy a RADVS sidelobe constraint (Reference 12).

These maneuvers are accomplished by using the cold gas attitude control system, with the body-fixed integrating rate gyros as inertial references. To accomplish a rotation, the appropriate gyro torquer winding is driven by a constant current source for a precise length of time; the spacecraft is slaved to this changing reference at a constant rate of 0.5 deg/sec.

The major events and times associated with the positive roll and positive yaw preretro maneuver combination selected for Surveyor V are given in Table 5.5-11.

TABLE 5.5-10. VERNIER BURN VELOCITY CORRECTION ACCURACY

Parameter	Requirement		Performance Values, fps					
	3σ or Limit	Equivalent Error, fps	Burn 1	Burn 2	Burn 3	Burn 4	Burn 5	Burn 6
Errors proportional to velocity correction magnitude, percent								
Accelerometer accuracy	1.1	0.15	0.17	0.17	0.17	0.17	0.17	0.17
Reference signal	0.5	0.068						
Electrical null	0.15	0.02						
Thrust bias variation	0.09	0.01						
Control loop gain variation	0.07	0.009						
Accelerometer misalignment	0.06	0.008						
Total proportional errors (rss)	1.22	0.17						
Errors independent of velocity correction magnitude								
Shutdown impulse dispersions, lb-sec	±0.63	±0.016	+0.001	+0.004	-0.003	+0.0026	+0.016	-0.007
Hysteresis limit cycle, ma	3	0.035	0	0	0	0	0	0
Ignition transient	—	0.47	0	0	0	0	0	0
Timing accuracy, second	±0.1	±0.32	-0.25	-0.03	-0.03	Data granularity too large	+0.23	-0.145
Total independent errors		0.568	-0.25	-0.03	-0.03	—	+0.25	-0.15
Total velocity correction error (rss)		0.782	0.30	0.17	0.17	—	0.30	0.23

TABLE 5.5-11. MAJOR EVENTS AND TIMES (DAY 254) FOR PRERETRO MANEUVERS

Event	Command	GMT, hr:min:sec
Begin (+) roll	0714	00:12: 17.810
End roll		00:14:45.617
Begin (+) yaw	0713	00:16:23.005
End yaw		00:20:22.050
Retro ignition		00:44:52.533

The preretro maneuvers were analyzed in terms of the following:

1) The gyro precession times were determined from gyro error signals and precession logic signals and compared to commanded times.

2) Using these attitude errors and the initial sun and Canopus error signals, the preignition terminal pointing accuracy was determined.

The first attitude maneuver (roll) was initiated 32 minutes and 34.7 seconds before retro ignition. The "earliest" time constraint on break of optical lock is 33 minutes based on an allowable 1 deg/hr gyro drift contribution to the pointing error. There is also a 23-minute constraint based on Canopus sensor noise due to possible lunar reflections (Reference 1).

As in the case of the premidcourse attitude maneuvers, an attempt was made to initiate the maneuvers at the limit cycle null points. The roll maneuver was initiated within approximately +0.13 degree of null while the pitch and yaw optical errors at the start of yaw were +0.15 and +0.07 degree, respectively (Figure 5.5-13).

Gyro Precession Times

The attitude maneuvers entered into the flight control programmer magnitude register were as follows:

Maneuvers	Degrees	Bits
+Roll	73.9	370
+Yaw	119.5	598

Table 5.5-12 presents the estimated gyro precession times.

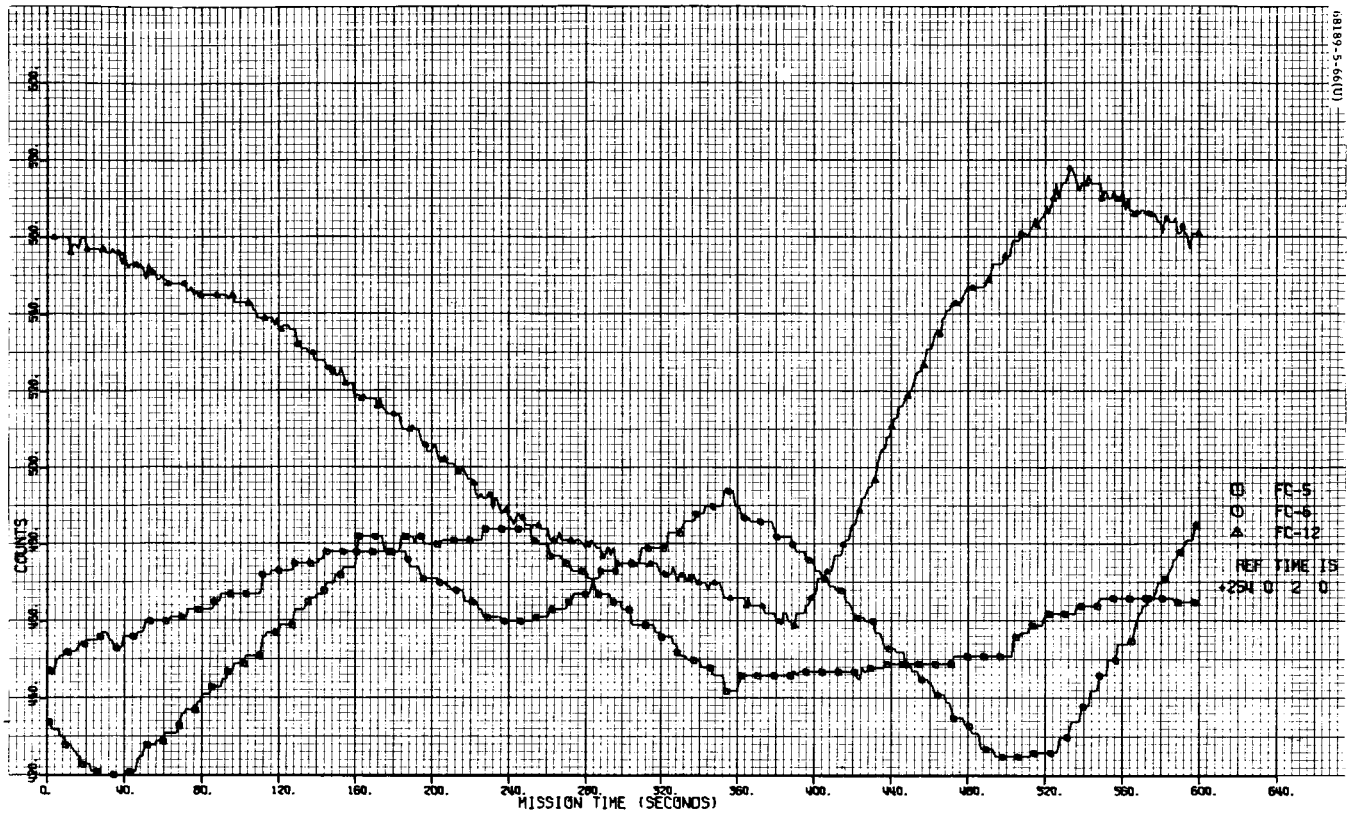

Figure 5.5-13. Preretro Maneuver Errors
FC-5, FC-6, and FC-12

TABLE 5.5-12. ESTIMATED GYRO PRECESSION TIMES

Attitude Maneuver	Commanded Time, seconds	Observed Time, seconds	ΔT, seconds	Rotation Error, degrees
Roll	147.8	147.807	+0.007	$\Delta\varphi$ = +0.0035
Yaw	239.0	239.045	+0.045	$\Delta\psi$ = +0.0225

Since the gyro error signals are only sampled once every 1.2 seconds (coast mode at 1100 bits/sec) during the preretro maneuvers, it was assumed that the shapes of roll and yaw gyro transients were the same as those observed during the premidcourse attitude maneuvers when the gyro error signals were sampled once every 0.05 second. The precession times were then estimated graphically based upon the intersection points of the start and stop transients with the steady-state gyro error values (Figure 5.5-14).

Gyro Drift Measurements

Nine three-axis gyro drift checks were made during the mission, two of them prior to the midcourse velocity correction. Three roll-axis-only drift checks were also made, one of them prior to the midcourse velocity correction. A summary of gyro drift measurement is presented in Table 5.5-13. Two techniques were used to measure the drift rates. The first was based on average slopes of the optical error signals obtained from analog Brush recorder plots. In the second technique, iterated calculations were made using the process described in Reference 13.

The preterminal attitude maneuvers were compensated for the following gyro drift rates:

Roll = +0.85 deg/hr

Pitch = +0.60 deg/hr

Yaw = -0.60 deg/hr

The gyro drift values selected for preterminal maneuver compensation were based essentially upon an average of all measurements made during the mission. The fixed drift history of each gyro is shown in Figure 5.5-15. No predictable trend is apparent.

Preretro Pointing Error

The technique described in paragraph 5.5.4.6 was used to determine the preretro pointing error of 0.43 degree with a 0.22 degree 3σ uncertainty.

68189-5-67(U)

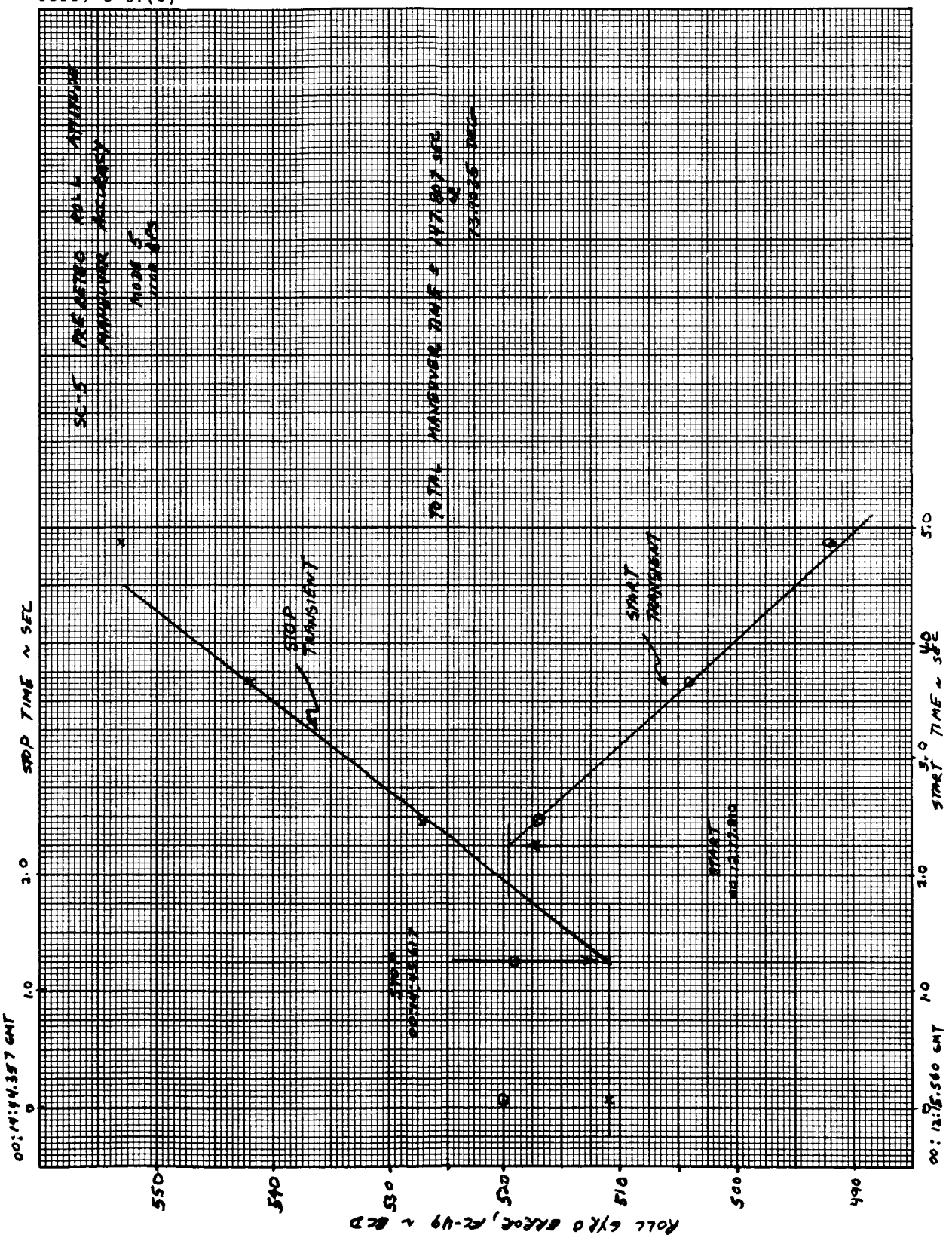

a) Preretro Roll Attitude

Figure 5.5-14. Gyro Error Signals

68189-5-68(U)

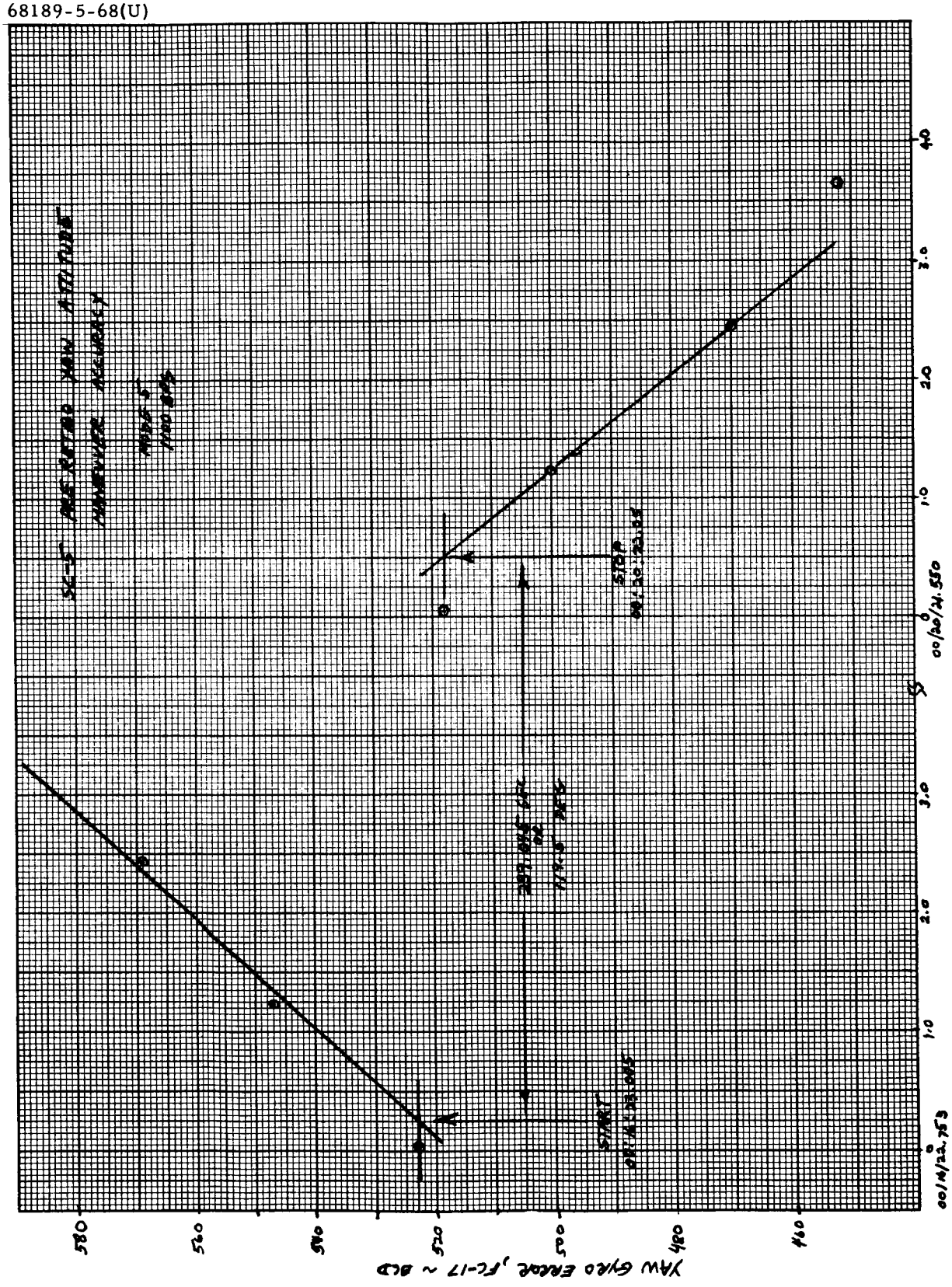

b) Preretro Yaw Attitude

Figure 5.5-14 (continued). Gyro Error Signals

TABLE 5.5-13. SURVEYOR V GYRO DRIFT SUMMARY

Day	Time, hr:min	Roll, deg/hr	Pitch, deg/hr	Yaw, deg/hr
251	#1 15:46 18:16 Three-axis	+0.97 1.25*	+0.74 0.88*	-0.63 -0.72*
	#2 18:34 20:16 Three-axis	+1.085	+0.694	-0.65
	#3 21:43 23:40 Roll only	+0.94		
	#4 09:08 09:57	Terminated early for alpha scattering exp. (data not reduced)		
252	#5 11:39 13:15 Three-axis	0.91 0.90 0.82 263 +0.88	0.66 0.52 0.84 202 0.67	0.65 0.61 0.46 172 - 0.567
	#6 13:17 15:08 Roll only	0.87		
	#7 15:10 17:18 Three-axis	0.8	0.9	-0.5
	#8 17:60 20:10 Three-axis	0.91 +0.91*	0.99 +0.85*	-0.58 -0.76*
	#9 20:59 21:48 Three-axis	+0.94 +0.99*	0.89 +0.78*	-0.58 -0.735*
253	#10 01:35 04:33 Three-axis	0.83	0.6	0.63
	#11 13:05 15:24 Roll only	0.80		
	#12 15:27 17:59 Three-axis	0.9	0.5	-0.62

*Bulk printer data

68189-5-69(U)

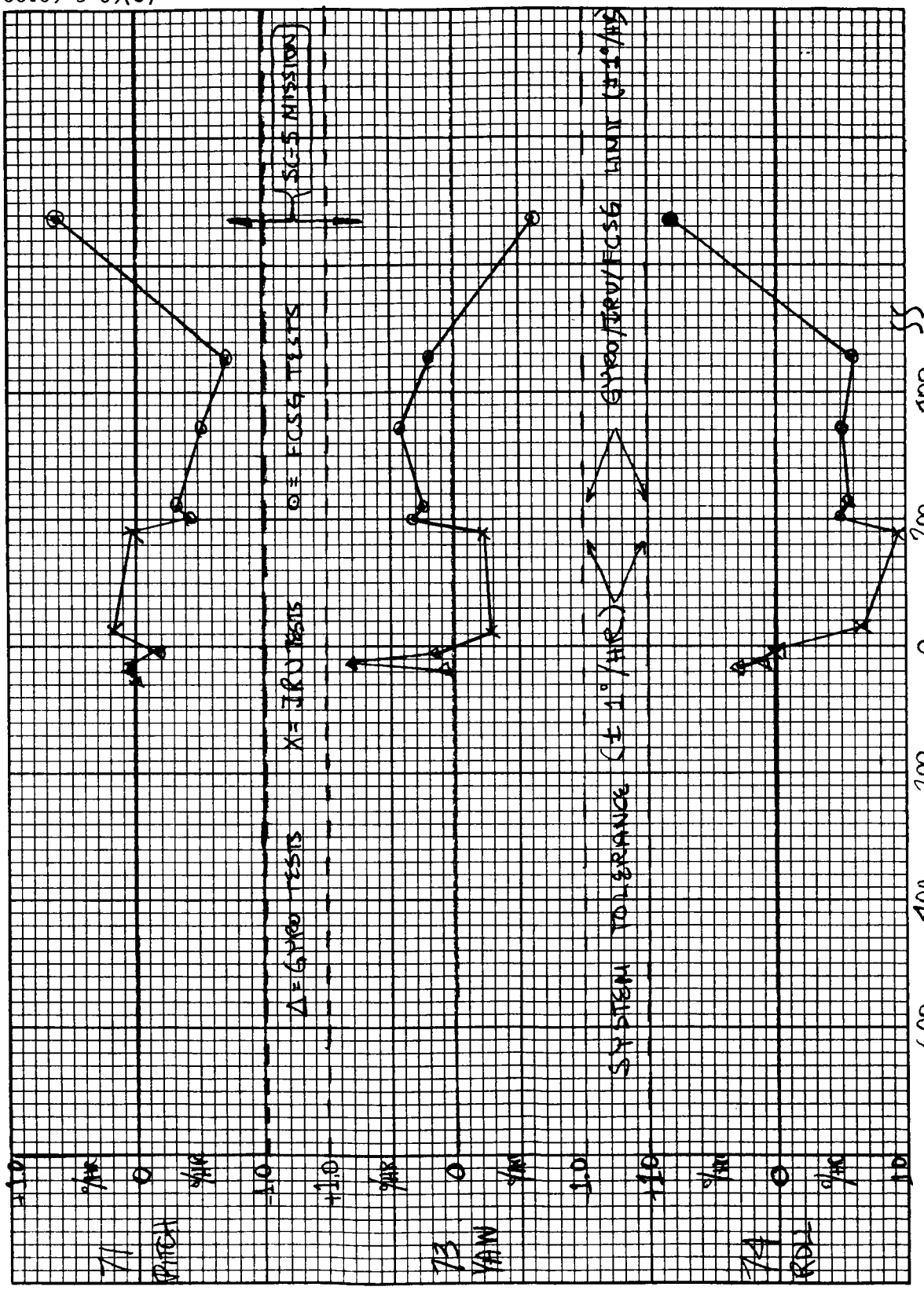

Figure 5.5-15. History of Gyro Fixed Drift

5.5.4.10 Main Retro Phase

Main retro phase began at day 254, 00:44:39.119 GMT with the indication of altitude marking radar mark and ended at 00:45:40.000 GMT with verification of retro eject. At the start of the RADVS-controlled descent phase (00:45:42.442 GMT), the longitudinal velocity had been reduced to approximately 66.5 fps at a slant range of 5750 feet.

During this phase, the function of the flight control system is to maintain the attitude of the spacecraft inertially fixed and to provide and execute a fixed sequence of commands to establish the necessary initial conditions for the vernier descent phase. The following analysis reveals that these functions were performed satisfactorily.

A list of retro phase events and their corresponding time of occurrence is given in Table 5.5-14 along with expected time intervals. These results confirm the performance of the magnitude register and programmer.

A special sequence of taped emergency commands was transmitted during the main retro burn phase in order to provide early initiation of retro case separation, high thrust, and the start of RADVS-controlled descent. A comparison of the normal timing of these events and the timing which resulted from the emergency commands is shown in Table 5.5-15.

Observation of telemetry signal FC-64 confirmed that the altitude marking radar mark occurred prior to emergency altitude marking radar since FC-64 can only be set high by the true mark signal.

Ignition of the vernier engines during the main retro phase was executed smoothly, with impulse dispersions between engines well within the specification values. As discussed previously, the change in gyro angles due to a shift in reference null at engine ignition limits the accuracy of the startup impulse dispersion calculations.

Retro Phase Attitude Control

During the main retro phase, from vernier ignition until case separation, spacecraft attitude motion was small in all three axes (Figure 5.5-16). Peak pitch and yaw inertial attitude motion, as read directly from gyro error telemetry data (FC-16 and FC-17), occurred at vernier ignition and amounted to -0.5 degree in yaw and 0 degree in pitch. Following ignition, static attitude error was virtually zero about the pitch axis and approximately -0.27 degree about the yaw axis. Roll inertial attitude error varied between -0.16 and +0.84 degree during the main retro phase (less than 1.0 degree is required).

Since all gyro error signals were maintained to within ±1.0 degree (during retro burn), each gyro was exercised less than 10 percent of the available travel range of more than ±10 degrees. A summary of pitch and yaw inertial attitude angles produced at various points in the retro phase is given in Table 5.5-16.

TABLE 5.5-14. TIME AND EVENTS LOG, RETRO PHASE

Main Retro Phase Event	Day 254, GMT, hr:min:sec	Time Between Events, seconds	Expected Time, seconds
AMR mark (FC-64)	00:44:39.119		
		12.324	12.3
Vernier ignition (FC-28)	00:44:51.443		
		1.09	1.1
Retro ignition (FC-29)	00:44:52.533		
		$1:52^{+0.}_{-1.2}$	0.55
RADVS power on	00:44:54.053		
		38.919	39.06
Retro burnout (FC-30)	00:45:31.452		
		8.992	8.54
Retro eject (FC-31)*	00:45:40.444		
		1.108	0.50
High thrust (FC-78)*	00:45:41.552		
		0.890	1.5
Start RADVS-controlled descent (FC-42)*	00:45:42.442		

*Achieved by emergency command tape.

TABLE 5.5-15. NOMINAL VERSUS EMERGENCY DESCENT TIMING

Event	Time After AMR Mark, seconds	
	Normal	Emergency Commands
Retro eject	64.4	61.3
High thrust	62.4	62.4
Start RADVS-controlled descent	64.9	63.3

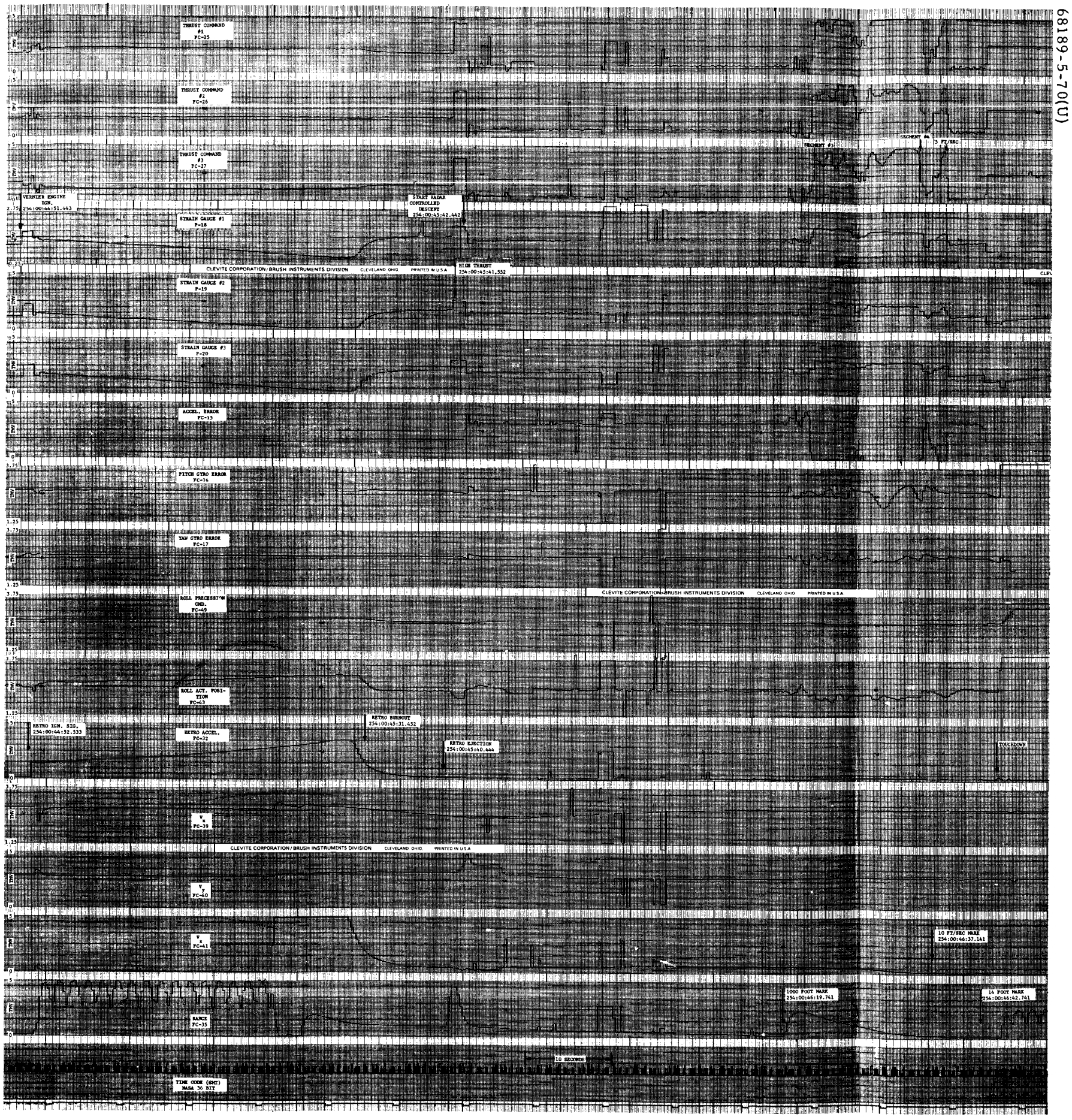

Figure 5.5-16. Surveyor V Terminal Descent

FOLDOUT FRAME

FOLDOUT FRAME

TABLE 5.5-16. RETRO PHASE ATTITUDE CONTROL SUMMARY

Event	Pitch	Yaw
Vernier ignition	0	-0.5
Retro ignition	+0.5	-0.4
Steady state	0	-0.27
Burnout	-0.16	-0.27
Retro eject	0	-0.27

Pitch and yaw control moments generated by the vernier engines were estimated by means of the following equations:

$$L_x = 2.969\ T_1 + 0.5723\ T_2 + 2.397\ T_3$$

$$L_y = -1.053\ T_1 + 3.098\ T_2 - 2.045\ T_3$$

where L_x and L_y are pitch and yaw control torques (ft-lb), respectively, and T_1, T_2, and T_3 are thrusts (pounds) generated by engines 1, 2, and 3, respectively. Values for the average value of T_1 = 58.5 pounds, T_2 = 51.25 pounds, and T_3 = 40.7 pounds were estimated from the thrust command telemetry signals (FC-25, FC-26, and FC-27). Shortly after retro ignition, differential throttling equivalent to approximately 47.0 ft-lb of control torque was produced.

The maximum thrust vector to center of gravity offset can be estimated using this maximum control torque magnitude of 47 ft-lb. Assuming a 9740-pound retro thrust, the offset was estimated as

$$\text{Maximum center of gravity offset} = \frac{47.0 \text{ ft-lb}}{9740 \text{ pounds}} \times \frac{12 \text{ inches}}{\text{feet}}$$

$$= 0.048 \text{ inch}$$

This compares to the required value of 0.18 inch (Reference 1).

The maximum attitude error produced by the retro disturbance torques was also determined from the maximum torque magnitude of 47.0 ft-lb. Since the nominal static gain (stiffness) of the pitch and yaw attitude control loops is

$$\text{static gain} = 1200 \text{ ft-lb/deg}$$

the maximum static attitude error is estimated to be

$$\text{maximum static error} = \frac{47}{1200} = 0.039 \text{ degree}$$

which is less than the allowable value of 0.12 degree.

5.5.4.11 Terminal Descent Phase

The RADVS-controlled portion of the terminal descent began at approximately 00:45:42.442 GMT with initiation of the minimum acceleration (0.9 g) phase along with spacecraft pitch and yaw attitude maneuvers to null existing lateral velocities. These attitude maneuvers are necessary to align the thrust vector (roll axis) with the total velocity vector. At this time, the vertical velocity was 46.0 fps at a slant range of 5950 feet. The lateral velocities (V_x = -41 fps, V_y = 50 fps) were nulled and remained essentially at zero to touchdown. The spacecraft roll axis was maneuvered through an estimated total angle of 45 degrees.

Intercept of the descent line segment occurred at approximately 97 fps vertical velocity at a slant range of 806 feet. Tracking of the descent segments was satisfactory as shown in Figure 5.5-17. The altitude and vertical velocity at the time the 10-fps mark was generated were estimated to be 50 feet and 10 fps, respectively. Touchdown occurred at approximately 00:46:46 GMT. A list of pertinent terminal descent events and times of occurrence is presented in Table 5.5-17.

TABLE 5.5-17. TERMINAL EVENTS

Terminal Descent Phase Event	Day 254, GMT, hr:min:sec
Start of RADVS-controlled descent	00:45:42.422
1000-foot mark	00:46:19.697
Segment intercept	00:46:22.33
10-fps mark	00:46:37.097
14-foot mark	00:46:42.697
Touchdown	00:46:44.397

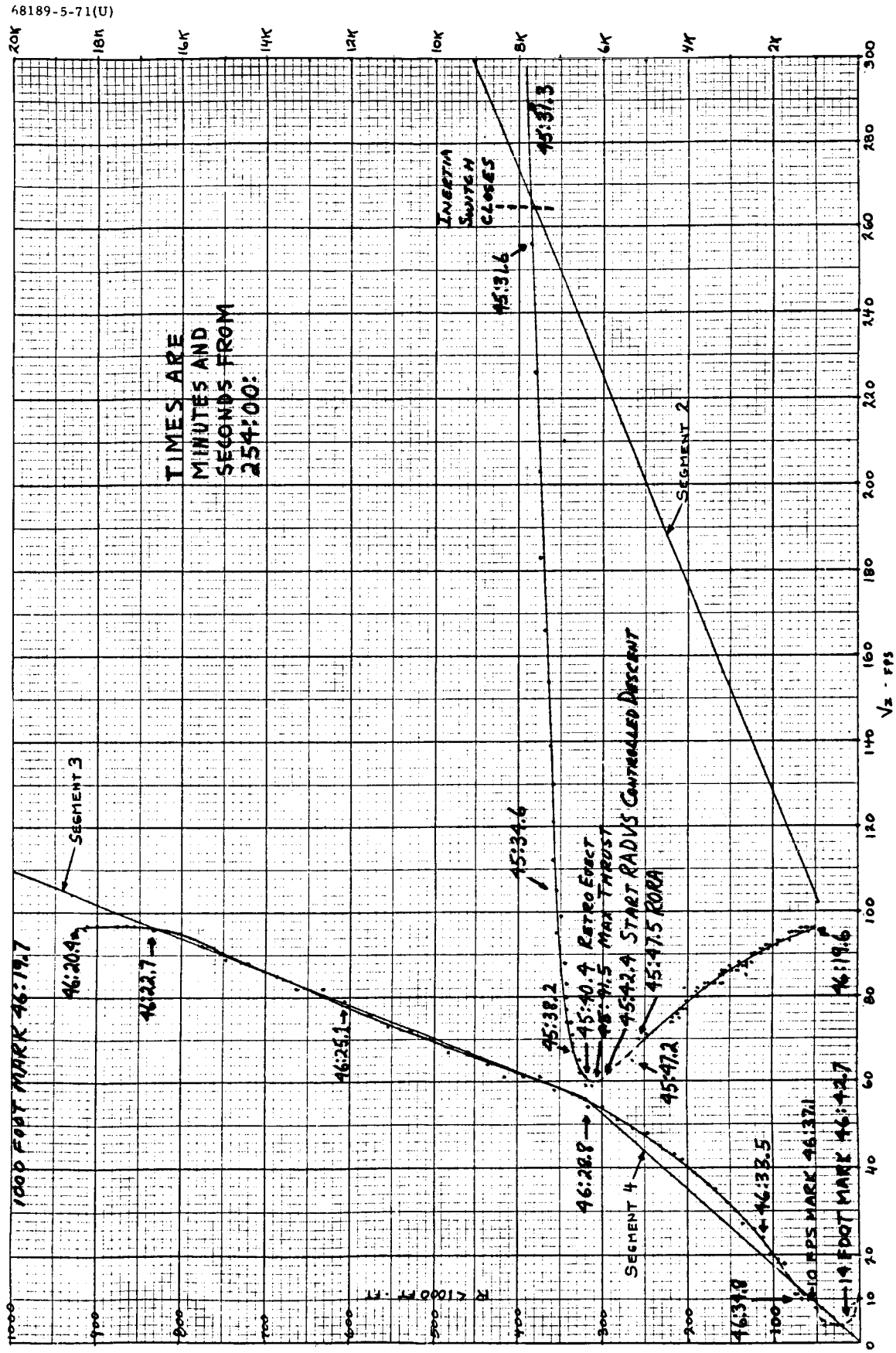

Figure 5.5-17. Terminal Descent Segments

Vernier Descent Attitude Control

Pitch and yaw attitude motions determined from pitch and yaw gyro error telemetry signals (FC-16 and FC-17) were maintained less than ±3.0 degrees in each axis during the vernier descent phase. Required gimbal freedom of each gyro is ±10 degrees. (See Figure 5.5-16.)

Measurable gyro gimbal errors (equivalent to spacecraft attitude error relative to the reference established by RADVS signals) occurred during certain portions of the vernier descent phase, according to the following summary:

Peak Gyro Gimbal Errors, degrees

Phase of Descent	Pitch	Yaw
SRCD and RODVS (start of alignment to velocity vector)	- 0.7	-0.6
R < 1000 feet	+ 2.6	-1.3
Following engine cutoff	+ 0.6	+0.6
Following touchdown	>-12.0	+1.3

At the start of the RADVS-controlled descent phase, the spacecraft initiated an attitude maneuver to align the thrust axis with the total velocity vector. Initial velocity conditions preceding the maneuver were as follows (taken from RADVS telemetry data, FC-39, FC-40, and FC-41). (See Figure 5.5-16.)

Premaneuver velocity conditions were as follows:

V_x = -41.0 fps

V_y = +50.0 fps

V_z = 46 fps

After the alignment maneuver was completed V_x and V_y were held near zero and V_z became equal to the total velocity of 88 fps. The attitude maneuver magnitudes were computed as follows:

$$\text{Pitch maneuver: } \Delta\theta_x = + \tan^{-1} \frac{V_y}{V_z} = 41 \text{ degrees}$$

$$\text{Yaw maneuver: } \Delta\theta_y = - \tan^{-1} \frac{V_x}{V_z} = -32 \text{ degrees}$$

The spacecraft Z axis was therefore maneuvered through a total of approximately 45.0 degrees.

Gyro gimbal angle errors were maintained virtually at null during the descent above the 1000-foot range. Following generation of the RADVS 1000-foot mark, which increased the lateral velocity control channel gains by a factor of approximately six and thereby increased system sensitivity to the V_x and V_y radar indications, increased gyro gimbal errors were developed but did not exceed 3.0 degrees in either axis.

Following vernier engine cutoff, gyro gimbal errors increased to approximately +0.6 degree in pitch and yaw during free-fall to the lunar surface. Following touchdown, these gimbal angles were ≥12.0 degrees in pitch and +1.3 degrees in yaw.

Effect of VPS on Attitude Control

A comparison of the Surveyor I, III, and V attitude control system performance during terminal descent indicated that attitude control was considerably more sluggish during the Surveyor V descent below 1000 feet. Figures 5.5-16 and 5.5-18 provide a comparison of flight control variables during the Surveyor III and V terminal phase. It should be noted that ranging of the thrust commands was greater during the Surveyor V descent, with actual command saturation below 1000 feet. The engine 1 thrust command was saturated more frequently than either of the other two and, at various times, the maximum commands were as large as 116 pounds on engines 1 and 2 and 123 pounds on engine 3. Saturation of the acceleration error signal (total thrust command) was also more frequent for Surveyor V, although the telemetry signal limits are well within the actual acceleration command limits and enough thrust was always available for attitude control. Attitude changes were correspondingly greater during the Surveyor V descent below 1000 feet during periods of high thrust command but did not exceed 3 degrees. Changes in pitch attitude were, in general, greater than yaw attitude changes.

Oxidizer leg 3 pressure decayed from ~605 psia to ~565 psia during the high thrust phase. Although there are no pressure measurements on the other propellant tanks, the post-touchdown correspondence between the helium tank pressure and oxidizer leg 3 pressure allows the reasonable inference that all of the propellant tank pressures were similar.

The strain gauge data (P-18, -19, and -20) were erratic, rendering quantitative results speculative. However, it seems reasonable to assume that the thrust response (at high thrust) was considerably smaller than the command based on a comparison of the strain gauge data with the thrust commands.

The flight control system performance indicated by the above observations is characterized by sluggish operation at high thrust and nominal operation at low thrust. A decrease in the effective loop gain would account for the high thrust performance observed. The saturation of a control loop element could account for the apparent gain change.

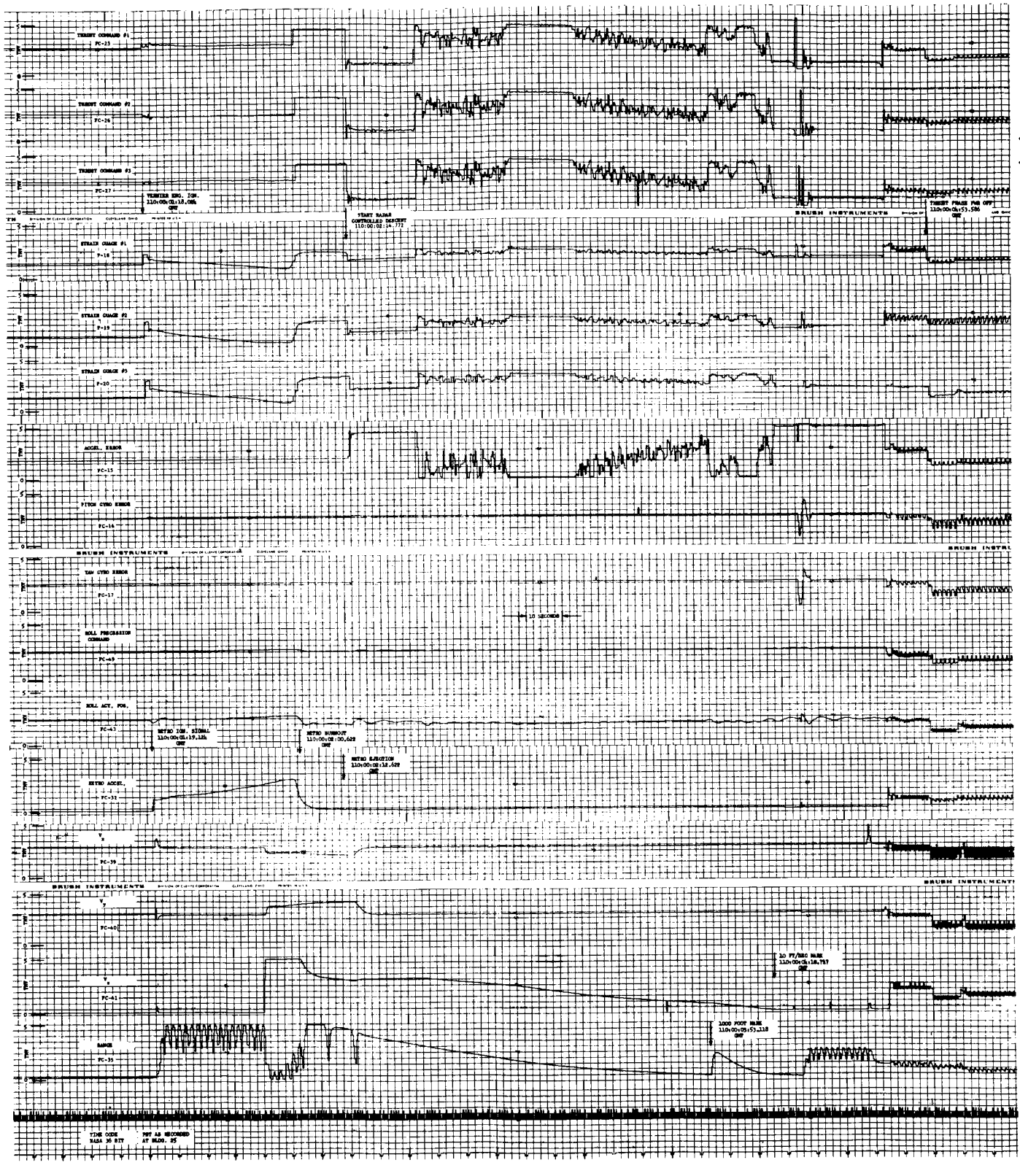

Figure 5.5-18. Surveyor III Terminal Descent

The vernier propulsion subsystem (VPS) is suggested as the saturating element since:

1) The VPS was not tracking the thrust commands at high thrust.

2) Lowered VPS supply pressure (as observed on oxidizer leg 3) will typically cause throttle valve saturation and hence engine saturation at high thrust, but will not have a gross effect on low thrust operation.

Although precise calculations are not possible since the throttle valve characteristic ("plate") curves for flight spacecraft are not available, it was concluded by examining typical "plate" curves that a decrease in supply pressure of the magnitude noted (~720 to 565 psia) will cause marked throttle valve saturation and hence the flight control performance observed.

The gyro errors which occurred during segment acquisition below 1000 feet were larger than those recorded in previous missions. This was due primarily to a lowering of the maximum thrust capability of the engines. An analog simulation of this engine saturation effect is shown in Figure 5.5-19. The limit on engine 1 was below 87 pounds (thrust required for maximum acceleration). When engine 1 is throttled into its limit, a transient is introduced into the attitude loop which then slowly responds with lower damping since its gain has effectively been halved. The acceleration loop incremental thrust command to the engines then increases from 60 to 138 pounds as a result, and the pitch attitude loop compensates the other two engine commands with a resulting gyro error. A yaw gyro error is also required but not shown because its magnitude is relatively small. Though the magnitude of the gyro errors for this simulation is less than those observed during the Surveyor V flight, the character of the data is the same. It is believed that two engines were in saturation during the Surveyor V descent which tended to produce a divergence in attitude until a large signal stable limit cycle was achieved. This divergence was prevented by the system returning to a lower acceleration command and small signal stability.

5.5.5 REFERENCES

1. "Functional Requirements," Hughes Specification 224510, Revision E.

2. K. Kobayashi, "A Method for Determining Gas Jet Thrust Level – Post Mission Analysis," Hughes Aircraft Company IDC 2253.4/25, 1 March 1966.

3. "Surveyor III Flight Performance Final Report," Hughes Aircraft Company, SSD 68189-3, July 1967.

4. G. L. Puckett, "SC-5 Flight Control Data Package," Volume I, 1 September 1967.

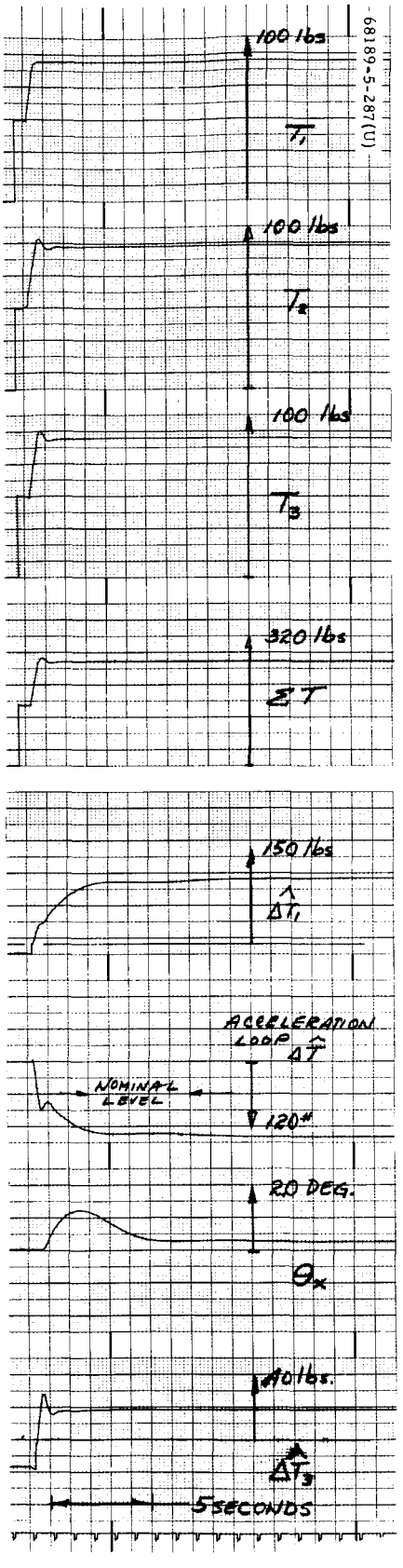

Figure 5.5-19. Simulation of Engine Saturation

5. R.H. Bernard, "Restoration and Updating of Surveyor Coast Phase Analog Computer Mechanization," Hughes Aircraft Company IDC 2223/77, 29 July 1964.

6. R.H. Bernard, "Revised Gas Jet Fuel Consumption for 66-hour Mission," Hughes Aircraft Company IDC 2223/843, 19 February 1965.

7. R.H. Bernard, "Surveyor Sun Acquisition With the Sun Sensor Oriented to Include the Roll and Pitch Uses," Hughes Aircraft Company IDC 2223/540, 14 December 1964.

8. E.I. Axelband, "Analysis of Inertial Pointing Accuracy of Surveyor Midcourse Thrust Vector," Hughes Aircraft Company IDC 2242/2706, 17 June 1963.

9. H.D. Marbach, "Angular Rates at Midcourse Shutdown," Hughes Aircraft Company IDC 2223/731, 3 February 1963.

10. "Interface Document, Surveyor Vernier Propulsion Thrust Chamber Assembly," Hughes Specification 287015.

11. "Spacecraft Flight Control Subsystem," Revision E, Hughes Specification 234600.

12. "Standard Transit Sequence of Spacecraft Operations," Hughes Specification 224550.

13. "Flight Control SPAC Handbook," Hughes Aircraft Company.

14. O.N. Hertzmann, "SC-4 Thrust Command Modulation Study," Hughes Aircraft Company IDC 2223/3055, 25 August 1967.

15. "SC-4 Preliminary Post Flight Data Analyses Report," Hughes Aircraft Company, 1 August 1967.

5.5.6 ACKNOWLEDGMENTS

J. Angerman, Technical Coordinator

B.N. Smith

L.R. Stumpf

R.H. Bernard

P.L. Welton

M.R. Buehner

5.6 VERNIER PROPULSION

5.6.1 INTRODUCTION

5.6.1.1 Description

The Surveyor vernier propulsion system (VPS) (Figure 5.6-1) is a bipropellant, variable thrust, liquid rocket system utilizing an oxidizer composed of 90 percent nitrogen tetroxide and 10 percent nitric oxide (Mon 10) and a fuel composed of 72 percent monomethyl hydrazine and 28 percent water. The VPS consists of three regeneratively-cooled thrust chambers (TCAs) with radiation-cooled expansion cones. Each TCA has a variable thrust range from 30 to 104 pounds vacuum thrust.

Propellant is supplied to the TCAs from six tanks employing positive expulsion bladders. One fuel tank and one oxidizer tank supply each TCA and are located adjacent to the TCA near each of the three spacecraft landing legs.

Propellant expulsion is accomplished by pressurizing the propellant tanks on the gas side of the bladders with helium gas. The helium is stored under high pressure in a spherical pressure vessel. The helium tank, together with the pressure regulator and servicing connections, is mounted outboard of the spaceframe between landing legs 2 and 3. The dual check and relief valves are mounted on the spaceframe between landing legs 2 and 3.

Thermal control of the VPS is both active and passive. Electric heaters are installed on two oxidizer tanks, one fuel tank, and all propellant feedlines to the TCAs. Passive thermal control consists of the application of black and white paint and vapor-deposited aluminum to selected portions of the VPS, together with super insulation applied to the propellant tanks.

The feedlines are wrapped with aluminum foil to deter heat loss.

5.6.1.2 Purpose

The VPS has three main functions during the mission:

1) Midcourse velocity correction and attitude control

2) Attitude control during retro phase

3) Attitude control and velocity correction during the final descent maneuver

PRECEDING PAGE BLANK NOT FILMED.

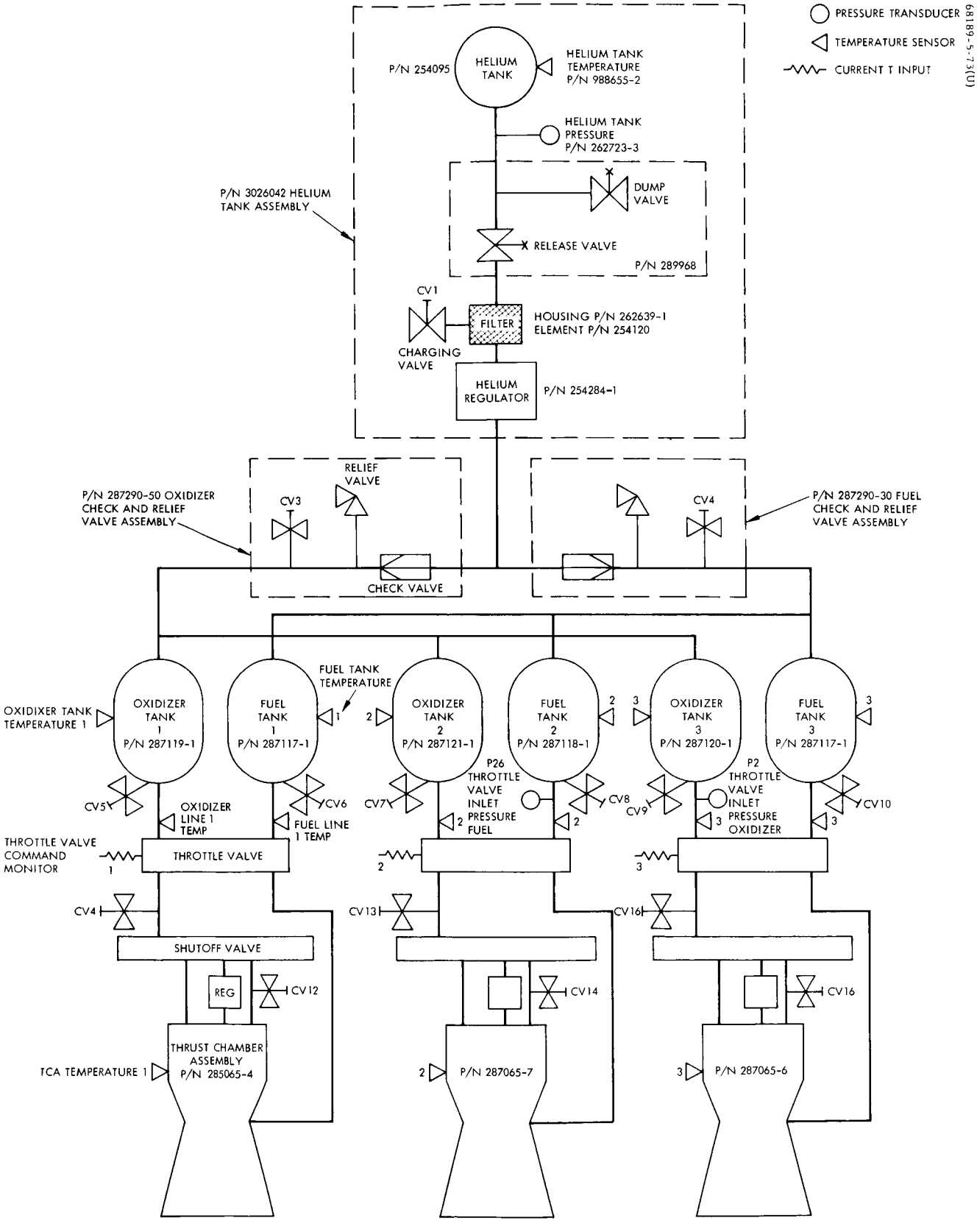

Figure 5.6-1. Vernier Propulsion System Schematic

The midcourse velocity correction may be required to correct initial launching and injection errors. The VPS provides velocity corrections up to 50 m/sec with sufficient propellant remaining to successfully land the spacecraft on the moon. The required correction is transmitted to the spacecraft in the form of a desired burn time at a constant acceleration of 0.1 g, which results in a thrust level of approximately 75 pounds for each TCA. In addition to providing the required velocity change, the VPS also provides spacecraft attitude control during the maneuver.

Attitude control during firing of the spacecraft retro motor is provided by the VPS. The VPS is ignited approximately 1.1 seconds prior to retro ignition. Attitude control by the VPS is biased around a total vernier thrust level of either 150 or 200 pounds, depending on predictions of spacecraft attitude and velocity at retro burnout. The desired vernier thrust level is transmitted to the spacecraft several minutes prior to initiation of the retro maneuver sequence. Following retro burnout, the vernier thrust level is increased to 280 pounds total thrust to further slow the spacecraft to allow the ejected retro motor case to fall clear.

Following retro motor ejection, the VPS is throttled to approximately 110 pounds total thrust under radar control. When the spacecraft intersects the first descent segment, the VPS, operating in the closed-loop mode with the radar system, acquires the predetermined altitude-velocity profile and keeps the spacecraft on the profile. Each succeeding segment of the profile is acquired in a similar manner. At an altitude of 14 feet, the VPS is shut down, and the spacecraft free falls to the lunar surface.

5.6.2 ANOMALIES

Three anomalies were observed during the earth/lunar transit:

1) A helium pressure regulator failure which allowed gas leakage from the helium storage tank into the propellant tanks (TFR 18263). (Refer to Appendix A to Section 5.6.) Reference 1 gives a complete accounting of the regulator failure.

2) Pressure saturation on engine 1 and frequently the other engines was observed during terminal descent, i.e., the high thrust command to that engine indicates it was not producing the desired thrust level.

3) Oxidizer tank pressurization rate was slower than seen on previous spacecraft.

Anomaly 2 was an expected consequence of anomaly 1; however, no direct link can be established between anomaly 3 and the others.

At the end of the first lunar day, oxidizer leg 3 pressure decreased (TFR 18265). This reduction in pressure probably is due to excessive temperatures of the lunar environment

5.6.3 SUMMARY AND RECOMMENDATIONS

5.6.3.1 Regulator Failure

An extensive discussion of the regulator failure is contained in Appendix A to Section 5.6. The contents of Appendix A follow the presentation given in Reference 2. The most likely cause of the Surveyor V regulator malfunction was contamination which damaged the helium regulator valve seat seal. This could result in an internal leak through the regulator, causing the outlet pressure to increase to a level which will cause the fuel or oxidizer relief valve to vent into space

Recommendations for corrective action (Reference 4) were as follows:

1) Design Actions

   a) Perform in parallel engineering redesign of relief valve to increase crack pressure

   b) Evaluate effects of increased relief valve crack pressure on helium pressurization subsystem

   c) Perform tradeoff study to determine suitability of redesign for SC-7.

2) Manufacturing Actions for Future Procurement or Rework

   a) Incorporate additional inspection points at subassembly and assembly levels

   b) Improve Quality Control instructions for handling and manufacturing processes on contaminate critical items

   c) Polish regulator detail parts

   d) Perform gas contaminate tests on helium tank and valve assembly during regulator flow test portion of flight acceptance test vibration

   e) Standardize regulator lockup tests at component, unit, and systems level

   f) Provide rework criteria to manufacturing for parts that fail contamination tests

3) Handling Actions

   a) Improve hardware changeout plans to avoid compromising cleanliness of VPS subsystem

b) Evaluate feasibility of application of liquid flush techniques to VPS subsystem for SC-7

c) Install millipore filters from AGE to all gas inlets of helium pressurization system

d) Standardize contamination checks on VPS units and subsystem

4) Test Actions

a) Change procedures to avoid backflow through regulator seat

b) Change order of test to perform regulator lockup check after check valve tests

c) Perform 6-hour regulator lockup test to detect leakage

d) Study feasibility of performing surge valve verification after installation into helium tank and valve assembly for SC-7

e) Perform gas contamination test on SP-2 helium tank and valve assembly and verify cleanliness.

5.6.3.2 Pressure Saturation Anomaly

A comparison of thrust commands in Figure 5.6-2 indicates that engine 1 may not have been producing its maximum rated thrust due to the low propellant tank pressure resulting from the regulator failure. Evidence of this failure and effect on spacecraft dynamics are discussed in Sections 5.5 and 5.12. No design changes are recommended since the proper operation of the regulator will prevent this from occurring.

5.6.3.3 Pressurization Rate Anomaly

Behavior of the helium tank, fuel, and oxidizer pressures during squib firing, and the six vernier burns prior to terminal descent are shown in Figures 5.6-3 through 5.6-9. It is apparent from a review of Figure 5.6-3 that a significant lag in pressurization of the oxidizer system was observed over the time to pressurize the fuel system at squib firing. Review of Figures 5.6-3 through 5.6-8 shows that during the vernier burns, however, the pressure in the oxidizer line and the fuel line behaved similarly. Since Surveyor V was the first spacecraft to employ a fuel line transducer, a comparison of spacecraft 1 through 4 cannot be directly made. However, on previous spacecraft, oxidizer line pressure reached postsquib firing lockup within 1 to 2 seconds, while on Surveyor V, the oxidizer system required 8 seconds to become pressurized. Review of spacecraft testing during Surveyor V flight acceptance testing failed to reveal any clue as to the cause of the difference in initial pressurization rates. While no significance is

attached to the phenomenon, it is cited as unexpected. One rationale available to explain the behavior is that the oxidizer check valve was sticking, which throttled the helium flow to the oxidizer side of the system. At no time did the throttling rate approach a value sufficient to influence oxidizer regulated pressure.

Table 5.6-1 lists the time of occurrence of the major events concerning or influencing the vernier engine system.

TABLE 5.6-1. SURVEYOR V PROPULSION EVENTS

Event	GMT, day:hr:min:sec	Mission Time, hr:min:sec	Engine Burn Time, seconds
Pressurize propellant tanks	252:01:42:28	17:45:27	–
Engine burn 1	252:01:45:02	17:48:01	14.3
Engine burn 2	252:02:12:02	18:15:01	10.1
Engine burn 3	252:02:39:51	18:42:50	23.1
Engine burns			
4A	252:04:18:48	20:21:47	12.1
4B	252:04:19:02	20:22:01	0.5
4C	252:04:19:03	20:22:02	0.5
Engine burn 5	252:08:24:04	24:27:03	33.1
Engine burn 6	252:23:30:58	39:33:57	5.5
Engine burn terminal descent	254:00:44:51	64:47:50	
14-foot mark (engines off)	254:00:46:42	64:49:41	111
Touchdown	254:00:46:44	64:49:43	–

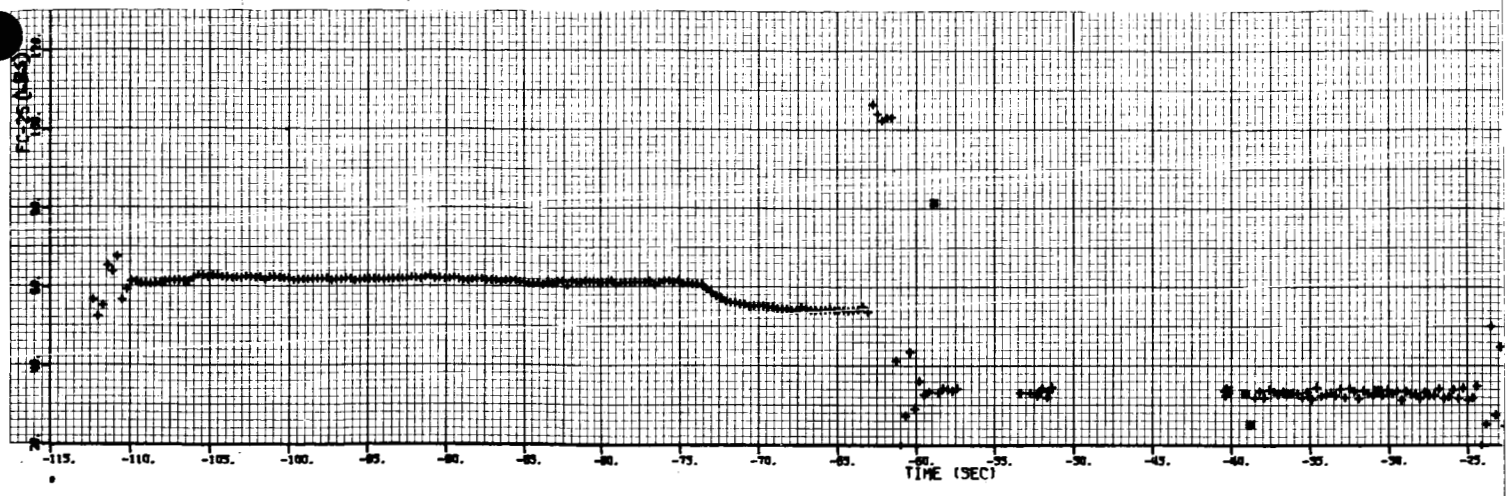

a) Engine 1

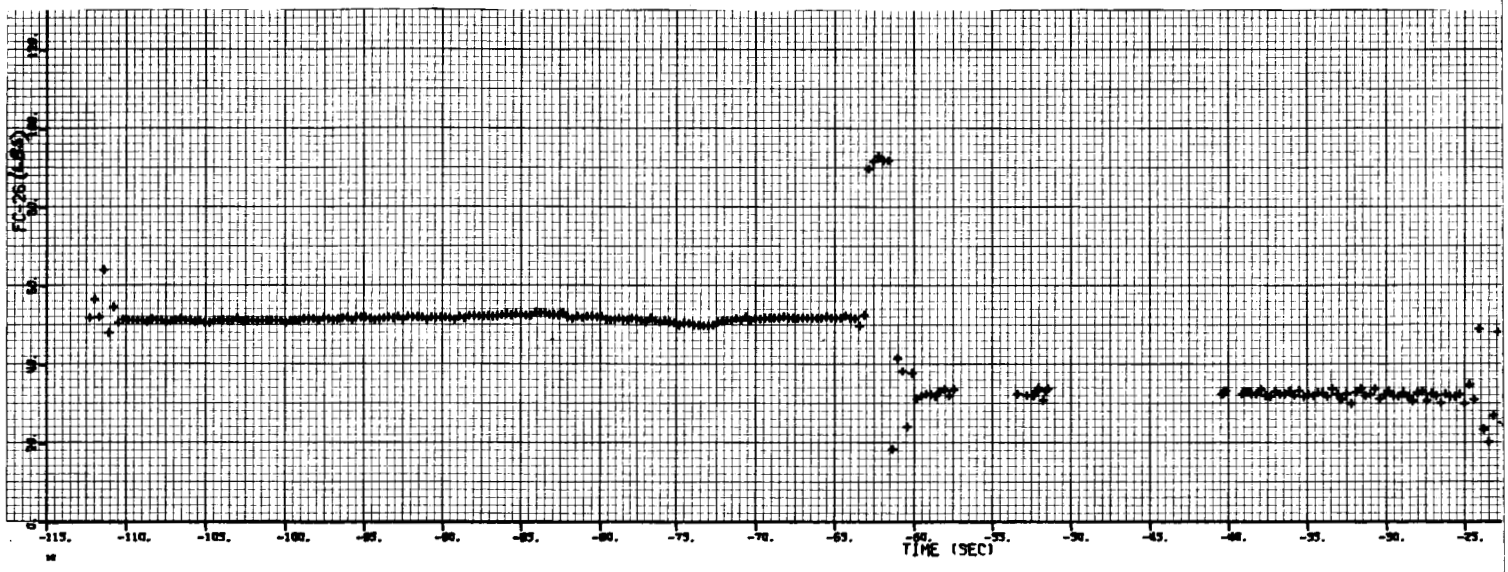

b) Engine 2

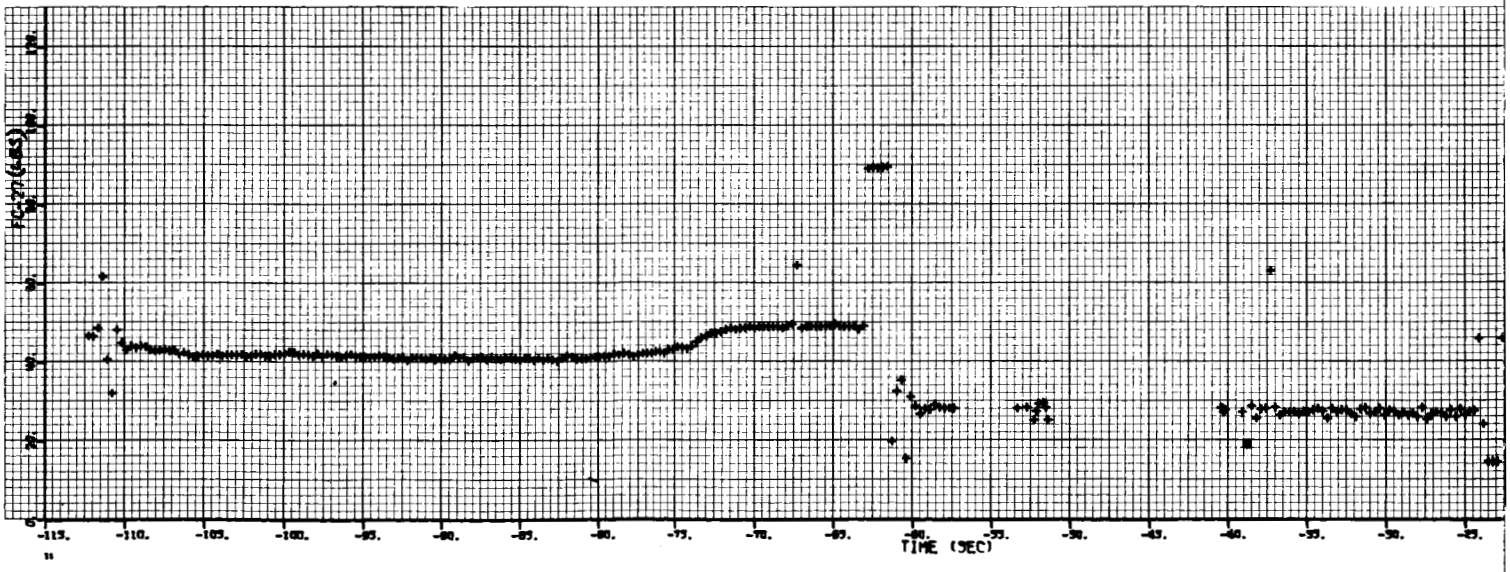

c) Engine 3

Figure 5.6-2. Thrust Command – Terminal Descent

FOLDOUT FRAME

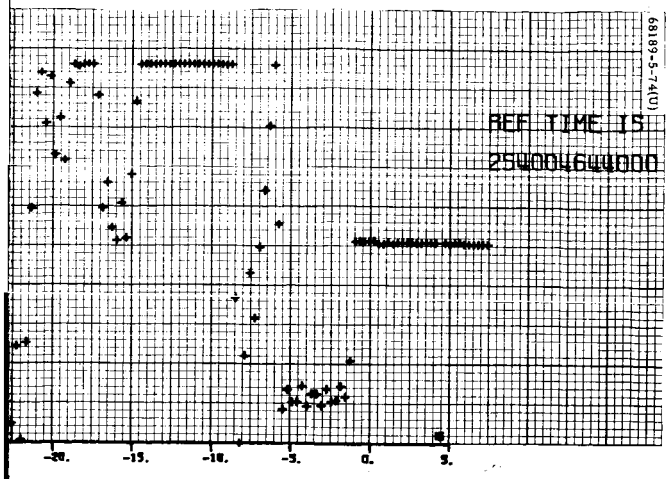

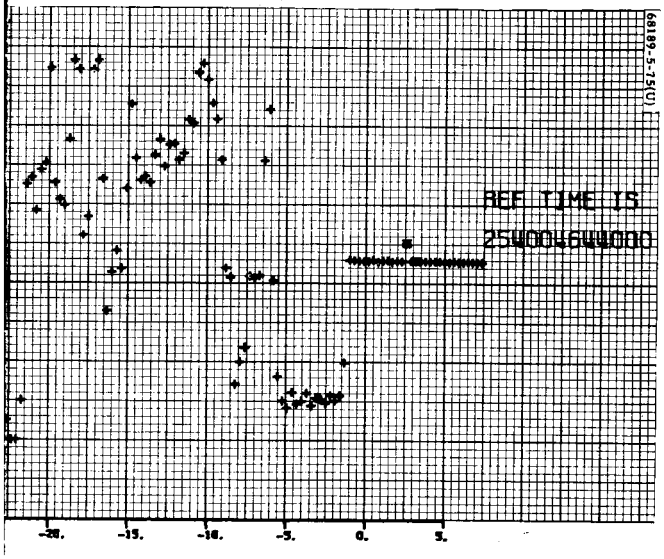

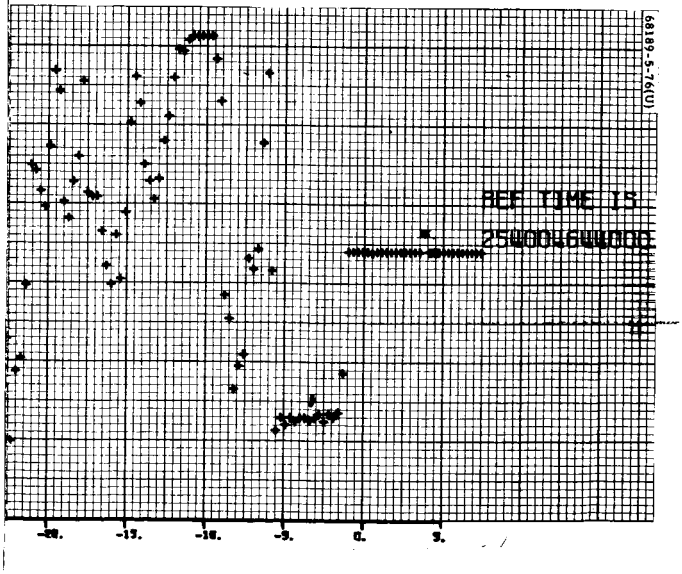

FOLDOUT FRAME

5.6-8

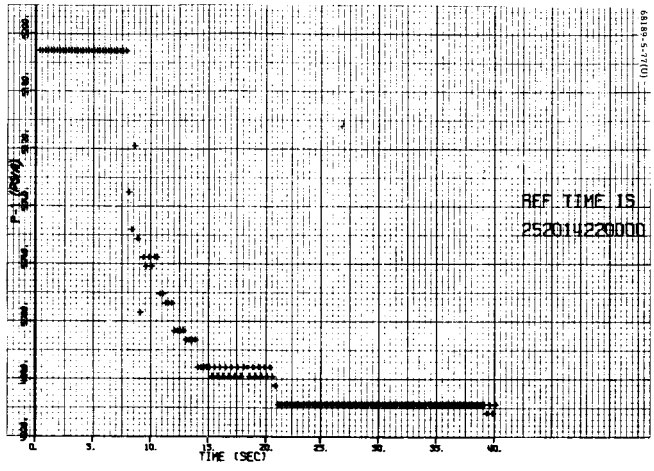

a) Helium Pressure (P1)

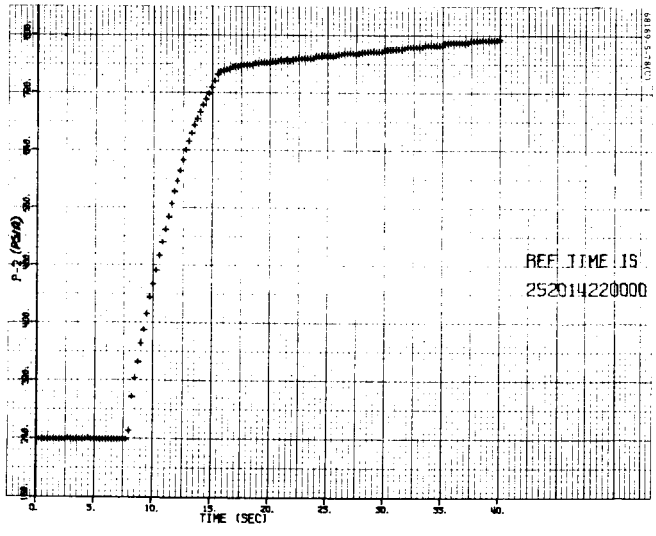

b) Oxidizer Pressure (P2)

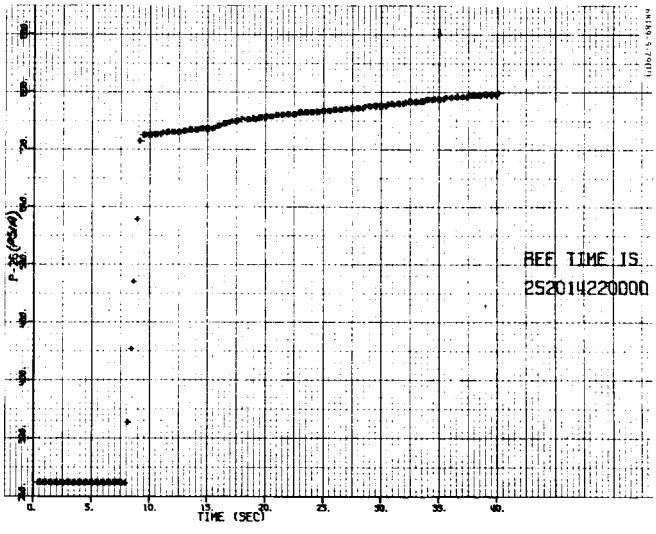

c) Vernier Line Fuel Pressure (P26)

Figure 5.6-3. Vernier Propulsion System Pressures at Squib Release

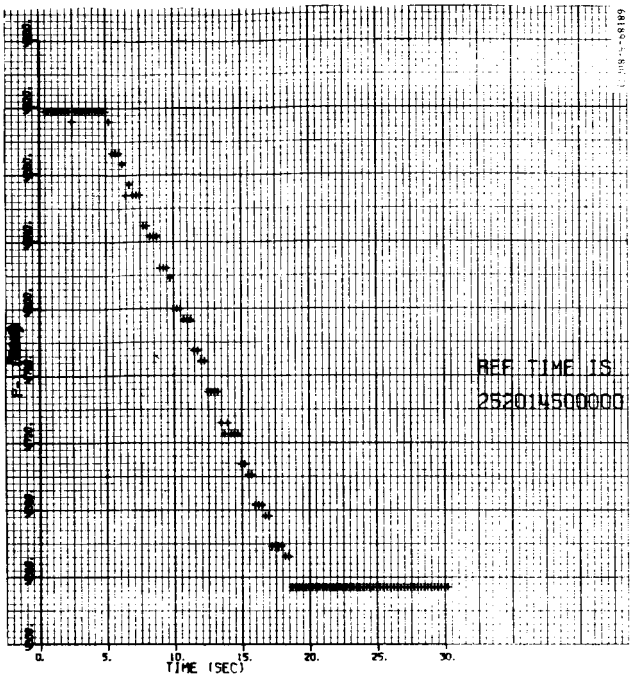

a) Helium Pressure (P1)

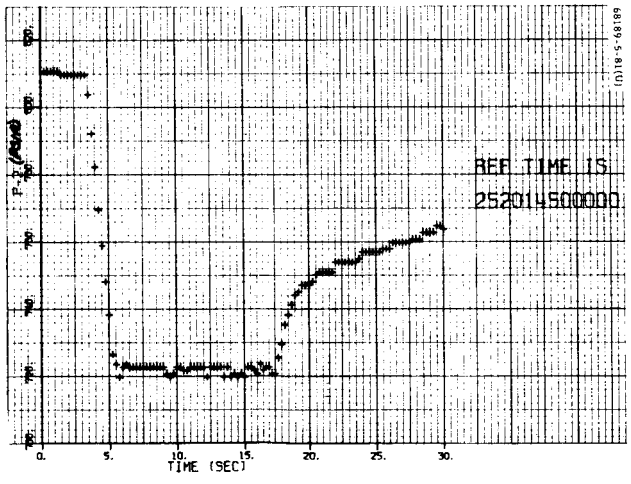

b) Oxidizer Pressure (P2)

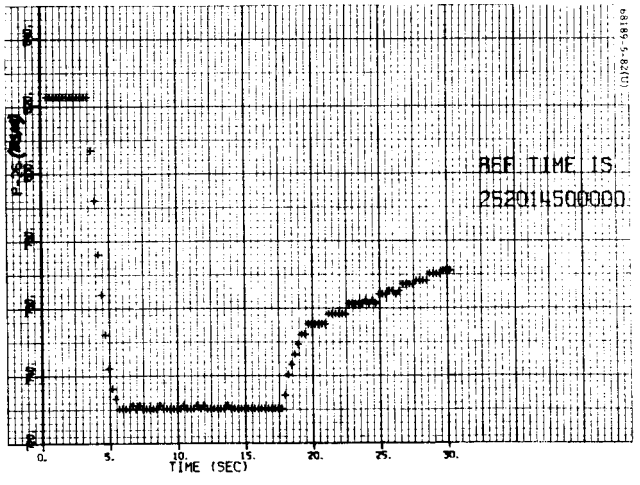

c) Vernier Line Fuel Pressure (P26)

Figure 5.6-4. Vernier Burn 1; Vernier Propulsion System Pressures

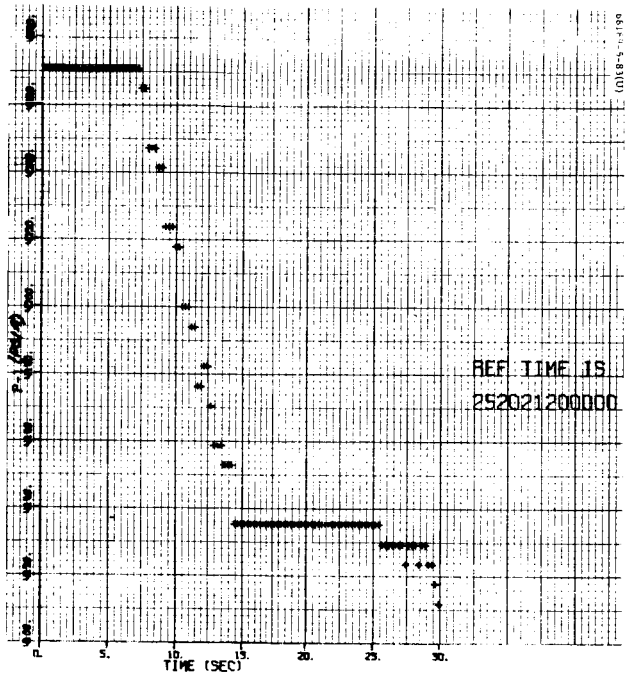

a) Helium Pressure (P1)

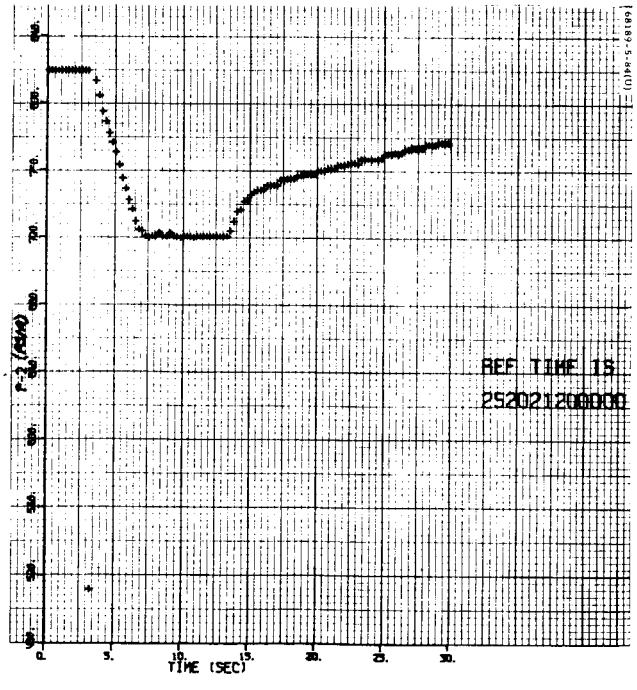

b) Oxidizer Pressure (P2)

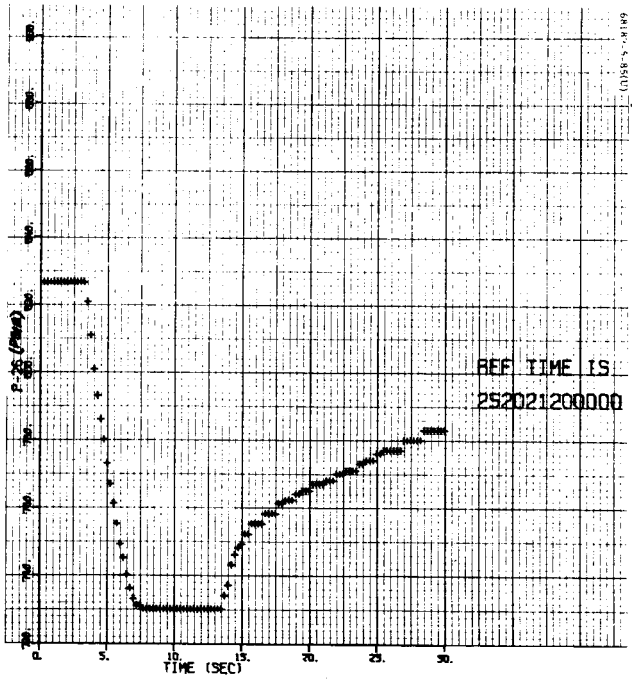

c) Vernier Line Fuel Pressure (P26)

Figure 5.6-5. Vernier Burn 2; Vernier Propulsion System Pressures

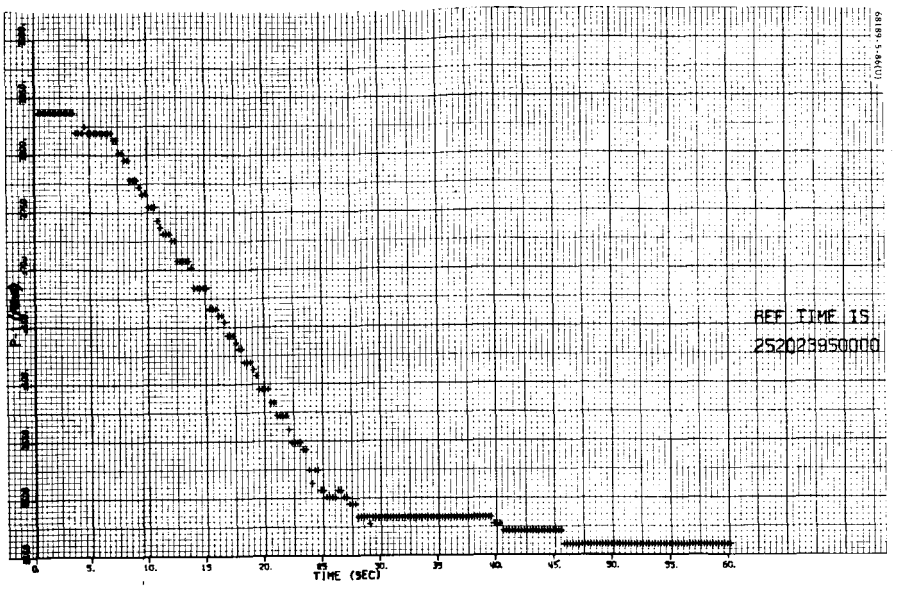

a) Helium Pressure (P1)

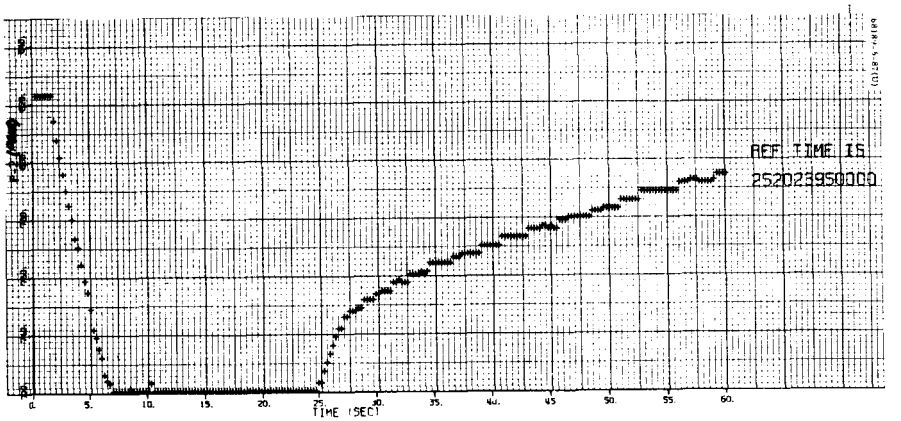

b) Oxidizer Pressure (P2)

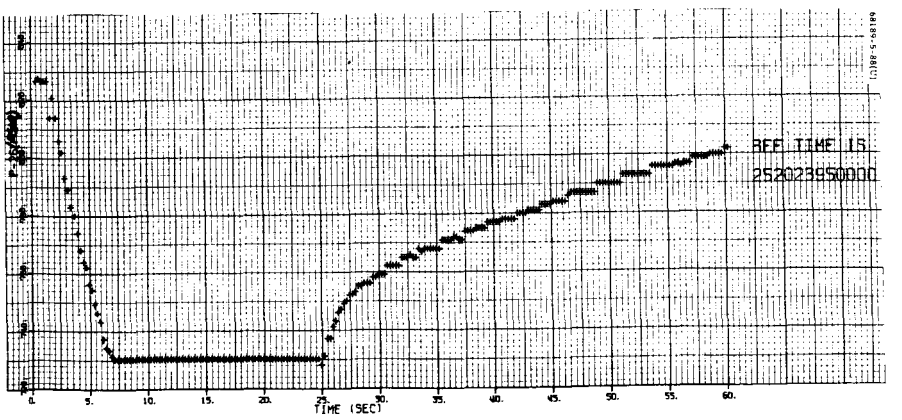

c) Vernier Line Fuel Pressure (P26)

Figure 5.6-6. Vernier Burn 3; Vernier Propulsion System Pressures

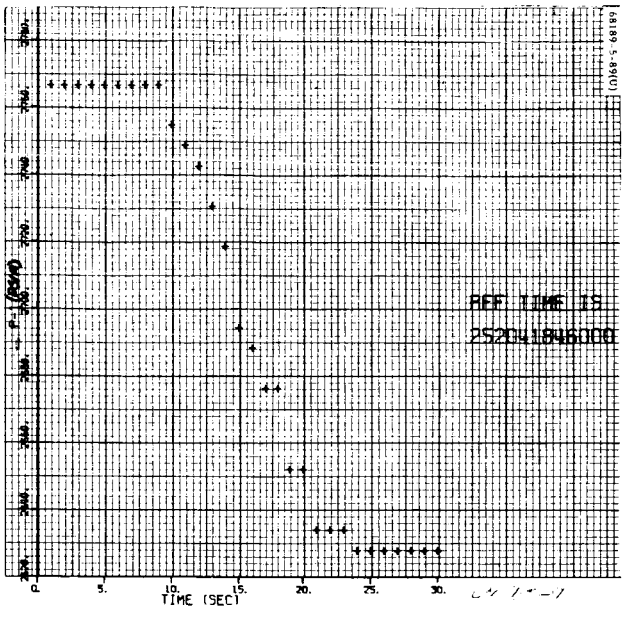

a) Helium Pressure (P1)

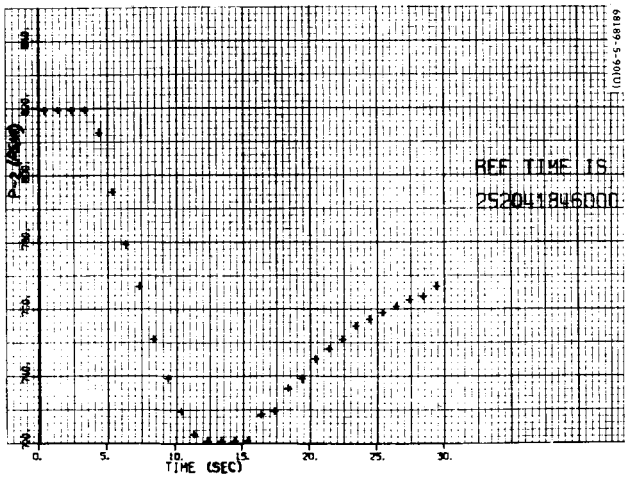

b) Oxidizer Pressure (P2)

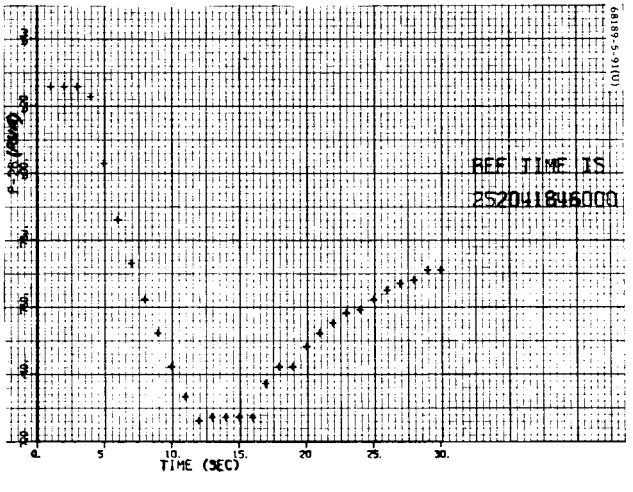

c) Vernier Line Fuel Pressure (P26)

Figure 5.6-7. Vernier Burn 4; Vernier Propulsion System Pressures

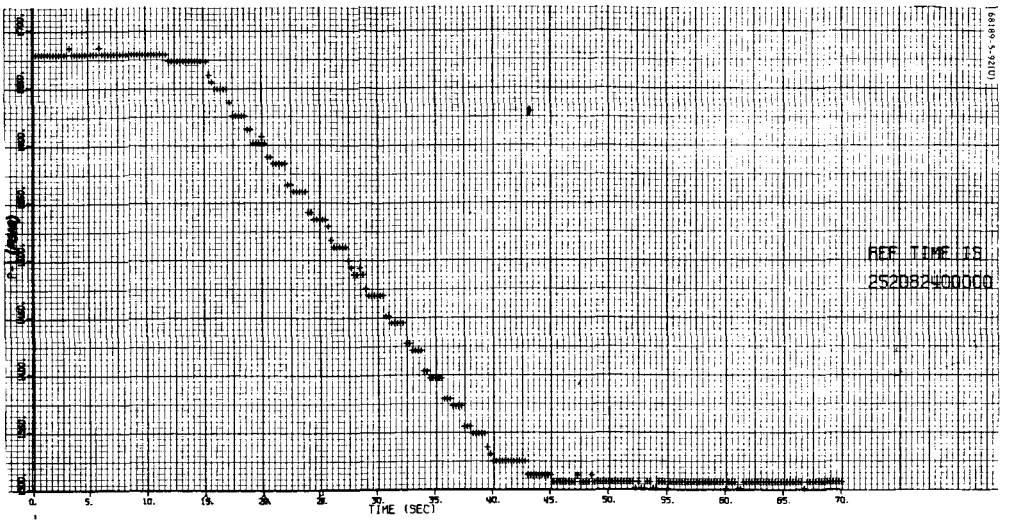

a) Helium Pressure (P1)

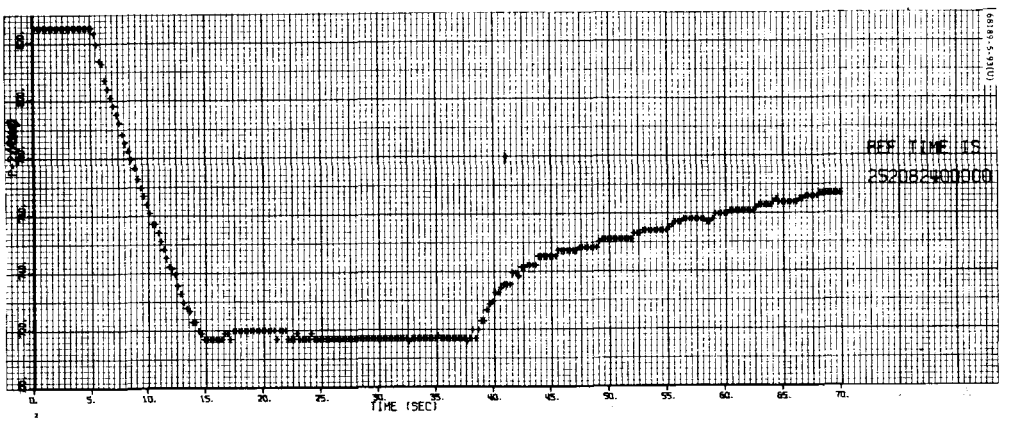

b) Oxidizer Pressure (P2)

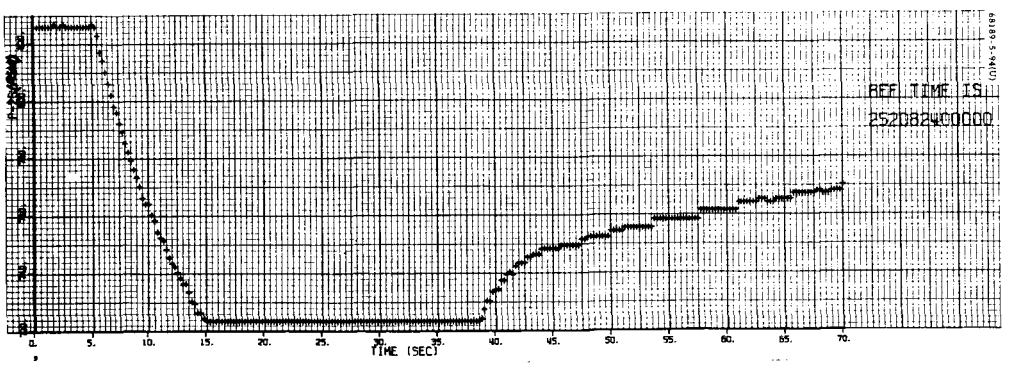

c) Vernier Fuel Line Pressure (P26)

Figure 5.6-8. Vernier Burn 5; Vernier Propulsion System Pressures

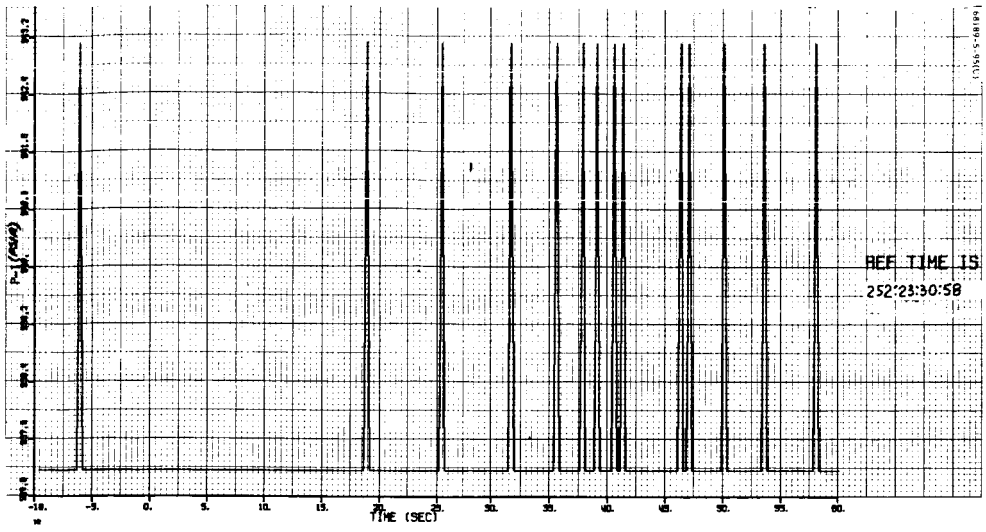

a) Helium Pressure (P1)

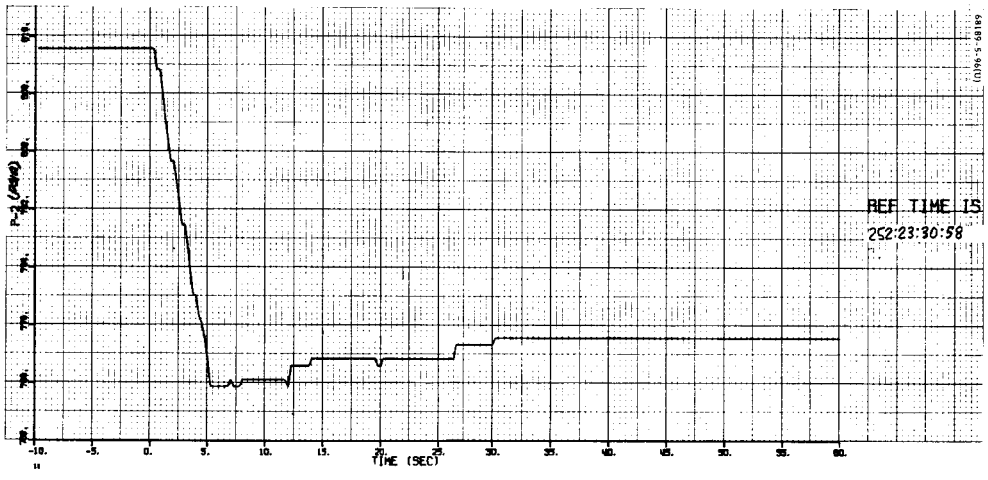

b) Oxidizer Pressure (P2)

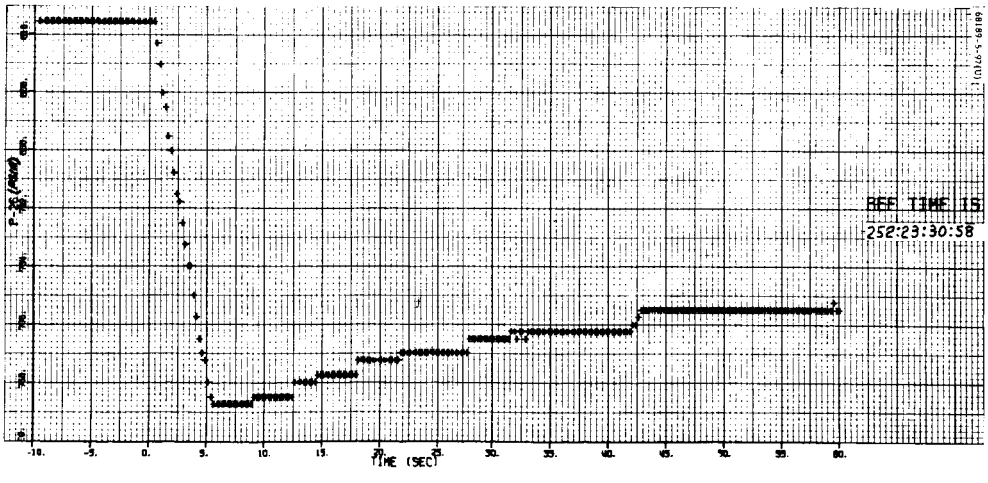

c) Vernier Fuel Line Pressure (P26)

Figure 5.6-9. Vernier Burn 6; Vernier Propulsion System Pressures

5.6.4 SUBSYSTEM PERFORMANCE ANALYSIS

5.6.4.1 Prelaunch

Final propulsion preparations for the Surveyor V launch were begun on 21 August when propellant loading of the vernier system was initiated. (Mission descriptive material is from Reference 3.) The desired and actual loadings are given in Table 5.6-2 and show that the spacecraft was loaded within the specified tolerance in Reference 4.

TABLE 5.6-2. SURVEYOR V PROPELLANT LOADING

	Predicted at 105°F, pounds		Predicted at 70°F, pounds		Actual at 70°F, pounds	
	Oxidizer	Fuel	Oxidizer	Fuel	Oxidizer	Fuel
Total loaded gross	109.79	75.08	113.39	76.57	118.84	75.81
3σ loading tolerance	0.75	0.75	0.75	0.75	0.75	0.75
Offload	0	0	3.60	1.49	9.04	0.68
Total loaded net	109.04	74.33	109.04	74.33	109.05	74.38
Unusable at 0°F	1.29	0.86	1.29	0.86	1.29	0.86
Total usable	107.75	73.47	107.75	73.47	107.76	73.52

The helium tank was charged on 29 August with 2.41 pounds of helium. Prelaunch telemetry readings of the tank temperature and pressure were taken over a 6-day period. These data indicate a helium leakage rate of 123 std cc/hour, well within the limit of 237 std cc/hour called out in Reference 2.

5.6.4.2 Launch (L-2 Hours to L+34 Minutes)

Prelaunch monitoring of the propulsion system was initiated at 22:42 PDT on 7 September 1967. At that time, the helium tank pressure and temperature were 5194 psia and 69°F, respectively. At launch, the pressure had increased to 5342 psia, and the temperature was approximately 83°F. All other propulsion parameters were also within the range specified for launch conditions. The prelaunch conditions of the propulsion system are shown in Table 5.6-3.

TABLE 5.6-3. CRITICAL TIME VPS PARAMETERS

Parameter	Sensor	Launch	Pre First Midcourse			Preterminal Descent		
Bit Rate:		550	1100	1100	1100	550	550	550
Mode:		5	5	2	1	5	1	2
GMT:		07:55	00:50	1:03	1:06	2230	2237	2235
Launch Time:		0.02	16:53	17:06	17:09	62:33	62:40	62:38
Helium tank pressure, psia	P-1	5342	5261		5187	847	836	
Oxidizer line 3 pressure, psia	P-2	264	243		240	823	815	
Upper retro temperature, °F	P-3	74	71	71		643		
Oxidizer line 2 temperature, °F	P-4	82	71		19	19	19	
Fuel tank 2 temperature, °F	P-5	74	42	41		26		26
Oxidizer tank 3 temperature, °F	P-6	75	43	43		35		35
TCA 1 temperature, °F	P-7	83	56		56	60	60	
Oxidizer line 1 temperature, °F	P-8	83	29		29	29	28	
Oxidizer line 3 temperature, °F	P-9	83	22		23	21	23	
TCA 2 temperature, °F	P-10	84	66		66	67	70	
TCA 3 temperature, °F	P-11	84	69		68	68	67	
Lower retro temperature, °F	P-12	76	56	56		43		42
Fuel tank 1 temperature, °F	P-13	75	57	58		57		
Fuel tank 3 temperature, °F	P-14	75	57	57		52		52
Oxidizer tank 1 temperature, °F	P-15	75	46	46		40		40
Oxidizer tank 2 temperature, °F	P-16	74	34	33		15		15
Helium tank temperature, °F	P-17	83	77			80		
Retro nozzle temperature, °F	P-22	80	-121			-122		
Fuel line 1 temperature, °F	P-23			60				59
Fuel line 2 temperature, °F	P-24	82	31			25		
Fuel line 3 temperature, °F	P-25			70				
Fuel line 2 pressure, psia	P-26				262			

5.6.4.3 Coast Phase 1 (L+34 Minutes to L+17 Hours)

Following launch, an assessment of the propulsion functions was made and all conditions were normal. All temperatures decreased approximately as predicted. The leg 2 oxidizer line temperature decreased to 19°F at L+1 hour and 50 minutes (251:09:52 GMT) and the heater started cycling between 19° and 22°F at that time. At L+6 hours and 14 minutes (251:14:11 GMT), the leg 3 oxidizer line temperature had decreased to 21°F. The heater started cycling between that temperature and 25°F.

Ten hours after launch, the helium tank pressure had stabilized at 5161 psia, and the tank temperature was 78°F. The leg 3 oxidizer pressure decreased normally from 264 psia at launch to 243 psia at 252:00:50 GMT. The leg 2 fuel pressure decreased normally from 265 psia at launch to 262 psia at 252:01:06 GMT.

During this period, two three-axis gyro drift checks were performed. The shadow pattern changes resulting from these checks varied the leg 2 thrust chamber assembly temperature from 45° to 75°F, well within normal transit limits. The stabilized leg 1 and leg 3 thrust chamber assemblies temperatures were 56° and 69°F, respectively.

The premidcourse conditions of the propulsion system are shown in Table 5.6-3.

5.6.4.4 Midcourse (L+17 Hours to L+19 Hours)

Midcourse preparation of the vernier system was initiated at 252:01:42:28 GMT, when the helium release squib was actuated. The noted helium pressure drop at squib actuation was 182 psi as compared with a predicted value of 155 psi. (See Figure 5.6-10.) The midcourse correction of 14.25 seconds was initiated 2 minutes and 34 seconds later. Subsequent to the apparently normal shutdown, it was noted that the helium tank pressure was dropping at a rate of approximately 10 psi/min, and it also appeared that the oxidizer or fuel relief valves were venting. This condition was indicative of a failure of the regulator to lock up the propellant tank pressure. The suspected cause of the problem was that foreign material had lodged on the helium regulator seat, thus preventing regulator lockup with the result that helium was leaking through the regulator, into the propellant tanks, and increasing the propellant tank pressure to the relief valve cracking level.

The helium pressure history during earth-lunar transit is shown in Figure 5.6-11.

Ignition of all three engines was smooth and well controlled. The average corrected commanded thrust levels for thrust chamber assemblies 1, 2, and 3, determined from telemetry, are shown in Table 5.6-4. These values agree with the predicted levels for each thrust chamber assembly within 4 pounds and within 1.4 pounds for the thrust total.

TABLE 5.6-4. VERNIER ENGINE THRUST LEVELS (POUNDS)

	First Midcourse		Terminal Descent	
Engine Number	Predicted*	Actual**	Actual**	Predicted*
1	76.4	79.2	59.5	59.9
2	73.4	73.1	52.0	51.3
3	71.1	67.2	40.0	41.0
Total	220.9	219.5	151.5	152.2

*Per Reference 5.

**Corrected for thrust command offset before maneuver.

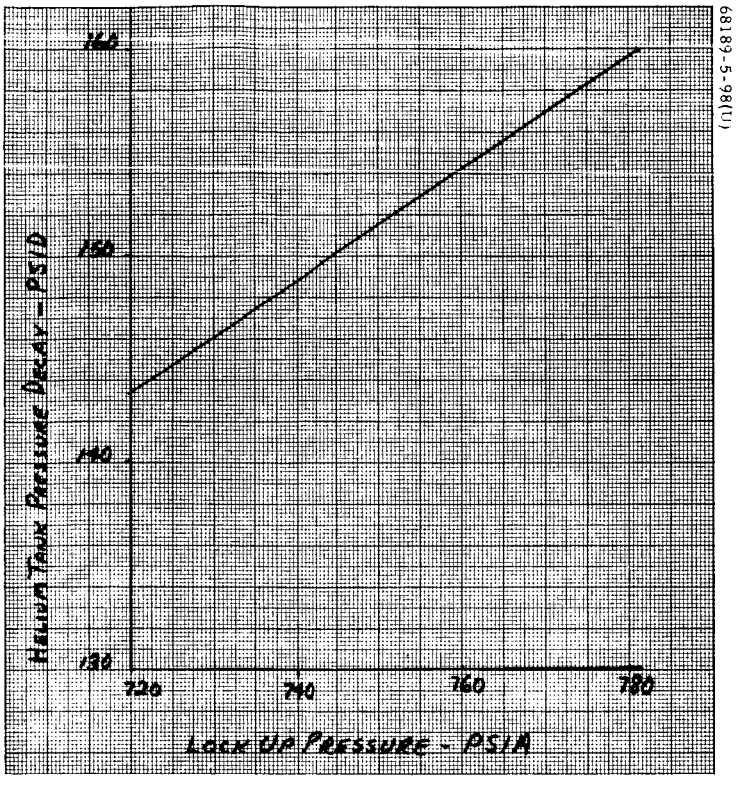

Figure 5.6-10. Predicted Helium Tank Pressure Decay at Squib Pressure

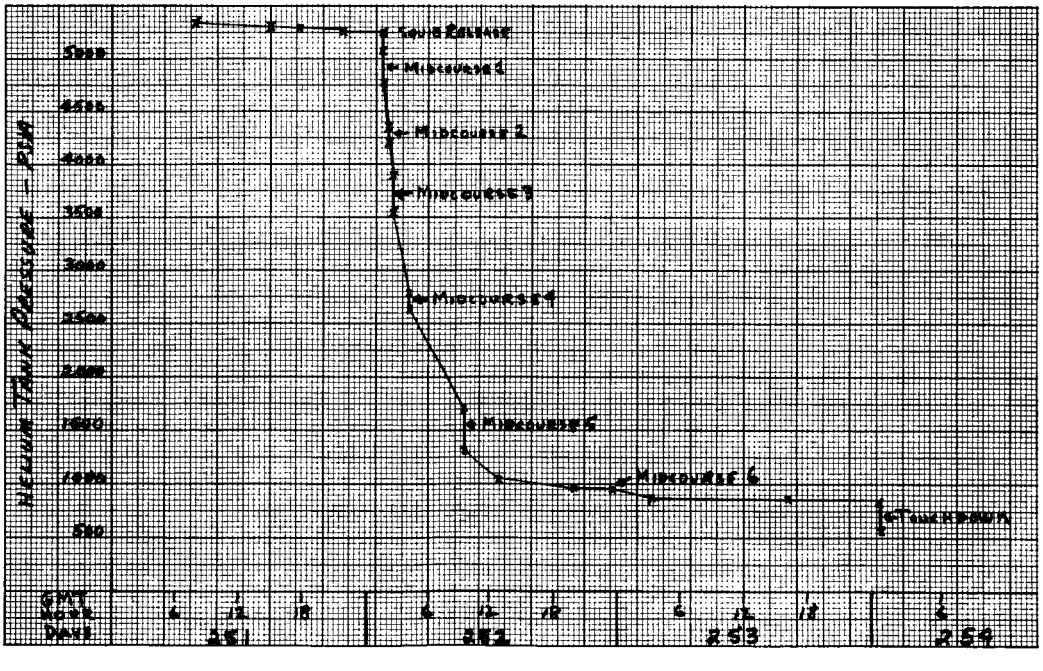

Figure 5.6-11. Helium Tank Pressure Versus Time

On the assumption that foreign material on the regulator seat was the cause of the leakage, it was recommended that the vernier system be fired again as soon as possible to unseat the regulator and attempt to dislodge any material preventing the regulator from seating properly.

The vernier system was fired again at 252:02:12 GMT for 10.05 seconds. The firing was conducted along the sunline to save time. Subsequent to termination of the burn, the helium regulator again failed to lock up and the propellant tank pressures increased to the relief valve cracking pressure and began to vent, as noted before.

It was decided to fire the vernier system again in a second attempt to reseat the helium regulator. To partially correct for the landing site variation, the firing was conducted 180 degrees from the sunline. This third firing was conducted at 252:02:40 GMT. The firing was of 23.05-seconds duration and was normal in all aspects. Again, however, the helium regulator failed to reseat and leakage was noted overboard through one of the relief valves.

5.6.4.5 Coast II (L+19 Hours to L+63 Hours 30 Minutes)

Following the third firing, it was decided by Mission Control to prepare the spacecraft for possible injection into earth orbit. Additionally, a fourth firing of the vernier system was ordered in another attempt to reseat the helium regulator and to adjust the lunar landing site in the event that the regulator did reseat the helium regulator.

The fourth firing of the vernier system was executed at 252:04:19 GMT. Originally planned for a duration of 14.1 seconds, the actual duration was 12.0 seconds followed by two 0.5-second burns at 1-second intervals. The modification was a further unsuccessful attempt to reseat the helium regulator.

At approximately this same time, it was hypothesized that, if enough propellant was burned to lighten the spacecraft and reduce the retro burnout velocity, and if retro ignition was delayed to a lower than nominal altitude, a soft landing might still be possible. Calculations at the SFOF and special testing conducted at JPL Edwards and Hughes Placerita Test Facility tended to confirm this.

It was decided to conduct another vernier firing to reduce the amount of propellant on board the spacecraft. This firing, of 33-seconds duration, was successfully conducted at 252:08:24 GMT.

Approximately 15 hours later, another firing was decided upon to further reduce the spacecraft burnout weight and velocity and to slightly change the lunar aiming point. This firing, of 5.5-seconds duration, was successfully conducted at 252:23:31 GMT.

With the exception of the helium regulator anomaly, all other propulsion parameters were normal throughout coast phase II. Subsequent to the sixth firing, the helium pressure indicated 890 psi. It decayed slowly to the relief valve reseat pressure (approximately 810 to 820 psia). At 253:20:06 GMT, a final retro burntime (T3500) of 39.06 seconds was given to FPAC. This time was based on a predicted retro bulk temperature at ignition of 52.5°F.

5.6.4.6 Terminal Descent (L+63 Hours 30 Minutes to L+65 Hours)

Terminal operations were initiated at 253:23:50 GMT when transmitter filaments were turned on.

The preignition maneuvers were uneventful. AMR mark was indicated at 254:00:44:39, vernier ignition at 00:44:51.4, and retro ignition at 00:44:52.4 GMT as programmed. Thrust levels during retro burn are shown in Table 5.6-4. Helium tank pressure at vernier ignition was 836 psia. At touchdown the helium, oxidizer, and fuel tank pressures were approximately 560 psia.

During segment acquisition, the leg 1 thrust chamber assemblies may have gone into pressure saturation as evidenced by the full-scale thrust command on that thrust chamber assembly (Figure 5.6-2).

All other propulsion parameters were normal and touchdown occurred at 00:44:48 GMT. The preignition conditions of the propulsion system are shown in Table 5.6-3.

The retro burn total thrust level of 151.5 pounds agrees well with the 152.2-pound thrust predicted (Table 5.6-4).

Helium and oxidizer pressure histories up to touchdown are shown in Figure 5.6-12. Fuel pressure is not recorded in the descent mode.

Propellant usage is shown in Table 5.6-5. A comparison of predicted and actual vernier system temperatures is given in Table 5.6-6. All temperature predictions were satisfactory except for the leg 3 fuel line. The temperature prediction was 15 to 30 degrees too low, but well within the propulsion system limits of 0° to 100°F. This parameter was measured for the first time on this spacecraft.

5.6.4.7 First Lunar Day

At lunar touchdown, the helium tank pressure and temperature were 560 psia and 58°F. Since the gas system was in a blowdown mode at touchdown, the oxidizer and fuel system were also at approximately the same pressure. Following touchdown, it was recommended that helium not be dumped as static fire operations were under consideration. A successful static firing was accomplished approximately 55 hours after touchdown at 256:05:38 GMT. All engines fired for 0.5 second, the commanded burn duration. Thrust levels indicated were: leg 1 = 22 pounds, leg 2 = 17 pounds, and leg 3 = 26 pounds.

TABLE 5.6-5. PROPELLANT USAGE

Event	Propellant Used, pounds
First engine burn	11.3
Second engine burn	8.0
Third engine burn	18.2
Fourth engine burn	10.3
Fifth engine burn	26.2
Sixth engine burn	4.3
Terminal descent*	60.1
Total propellant used	138.4
Propellant remaining at touchdown	45.0

*Assuming that all engines were operating at the correct mixture ratio.

Helium, oxidizer, and fuel pressure all gradually increased due to lunar heating. The oxidizer pressure reached a maximum of 856 psia about 130 hours after touchdown. Figure 5.6-13 is a plot of all three pressures during the lunar day.

At 261:13 GMT, a decrease in oxidizer system pressure was noted. Oxidizer pressure decayed from 812 to 328 psia over a period of about 55 hours. As the oxidizer pressure decreased, the helium pressure began to track the oxidizer tanks. The oxidizer pressure decrease ceased at 263:21 and thereafter the pressure corresponded to the vapor pressure in the leg 3 tank as expected. Concurrent with the pressure decrease, a 100°F drop in the leg 1 oxidizer temperature and a 30°F drop in leg 1 oxidizer line temperature occurred. The pressure and thermal data are consistent with an oxidizer leak from the leg 1 oxidizer tank.

Helium pressure remained approximately constant until 254:13 GMT when a pressure decrease was noted in the fuel system. At this time, fuel system pressure was 740 psia. This pressure dropped to zero over a period of 20 hours. As the fuel system pressure decreased, it vented the helium tank such that both reached 0 psia at the same time. The fuel pressure loss

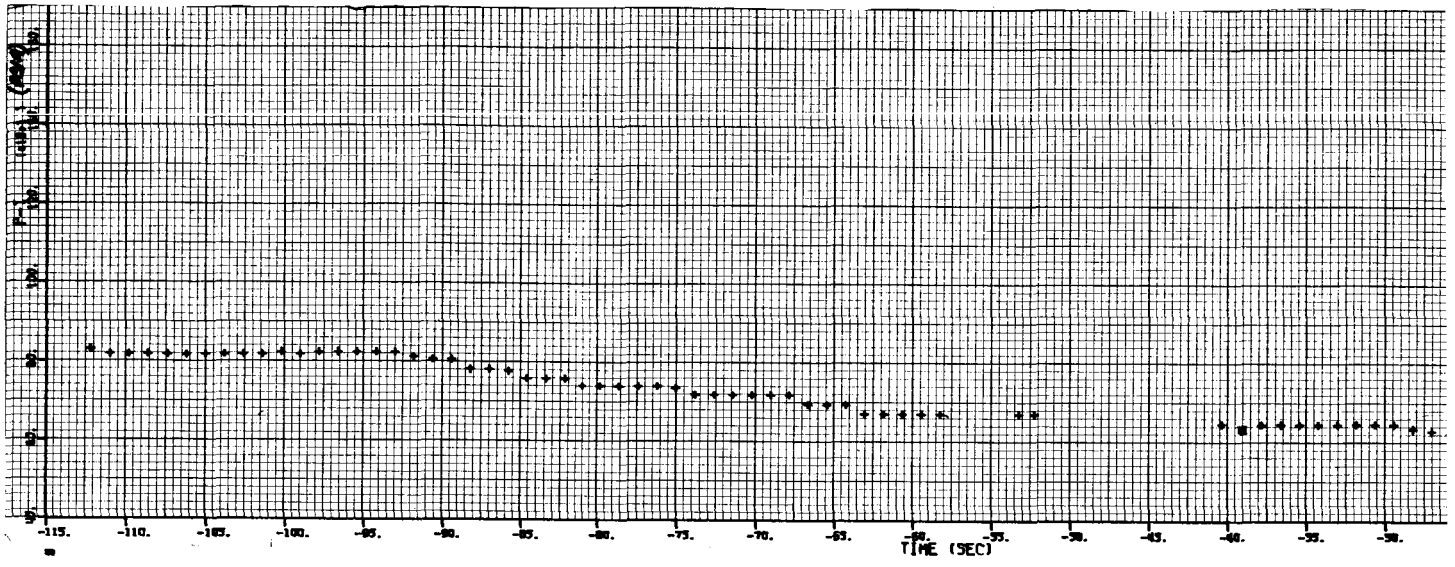

a) Helium Pressure (P1)

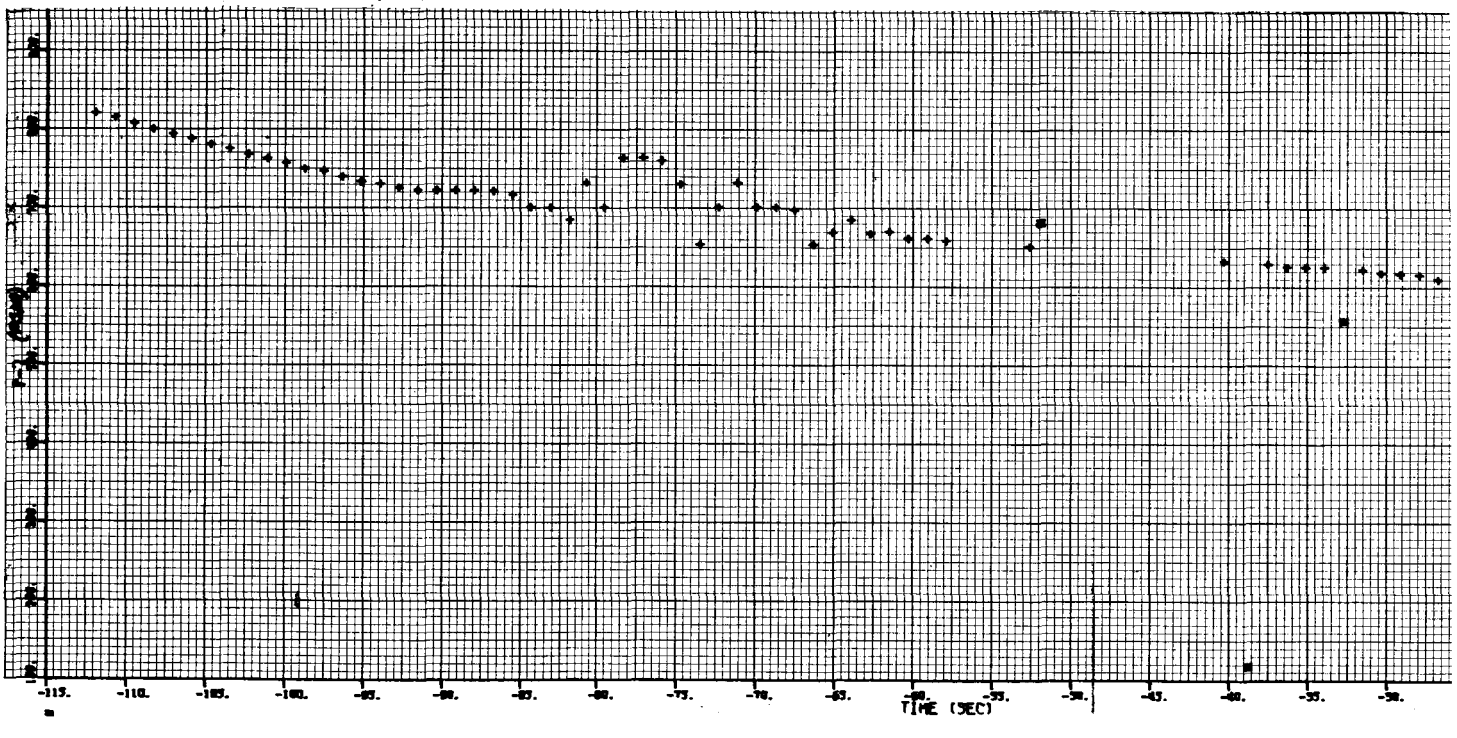

b) Oxidizer Pressure (P2)

Figure 5.6-12. Terminal Descent Vernier Propulsion System Pressures

FOLDOUT FRAME

2

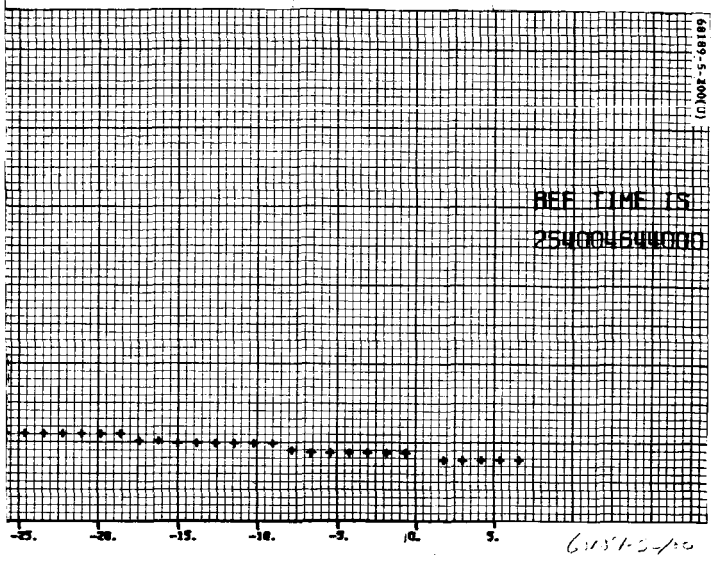

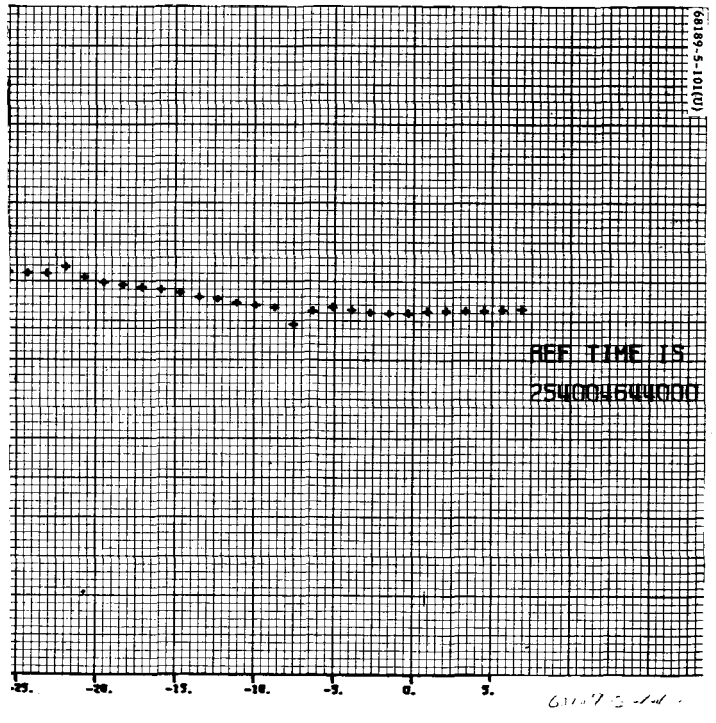

FOLDOUT FRAME

5.6-24

TABLE 5.6-6. ACTUAL VERSUS PREDICTED TEMPERATURES (°F)

Temperature Sensor	Launch		First Engine Burn		Terminal Descent	
	Actual	Predicted	Actual	Predicted	Actual	Predicted
P4, leg 2 oxidizer line	83	85	19	18-28	19	18-28
P5, leg 2 fuel tank	74	74	42	47	25	33
P6, leg 3 oxidizer tank	74	77	42	49	34	39
P7, leg 1 thrust chamber assembly	88	85	56	60	61	60
P8, leg 1 oxidizer line	83	85	29	18-28	28	18-28
P9, leg 3 oxidizer line	83	85	23	18-28	24	18-28
P10, leg 2 thrust chamber assembly	84	85	66	70	71	70
P11, leg 3 thrust chamber assembly	77	85	68	60	67	60
P13, leg 1 fuel tank	75	76	59	60	57	55
P14, leg 3 fuel tank	75	76	57	57	52	53
P15, leg 1 oxidizer tank	75	76	46	57	39	42
P16, leg 2 oxidizer tank	74	74	33	37	14	20.5
P17, helium tank	83	85	77	80	80	80
P23, leg 1 fuel line	84	84	60	53-63	59	38-48
P24, leg 2 fuel line	81	85	29	26-36	23	14-24
P25, leg 3 fuel line	85	85	69	42-52	73	36-46

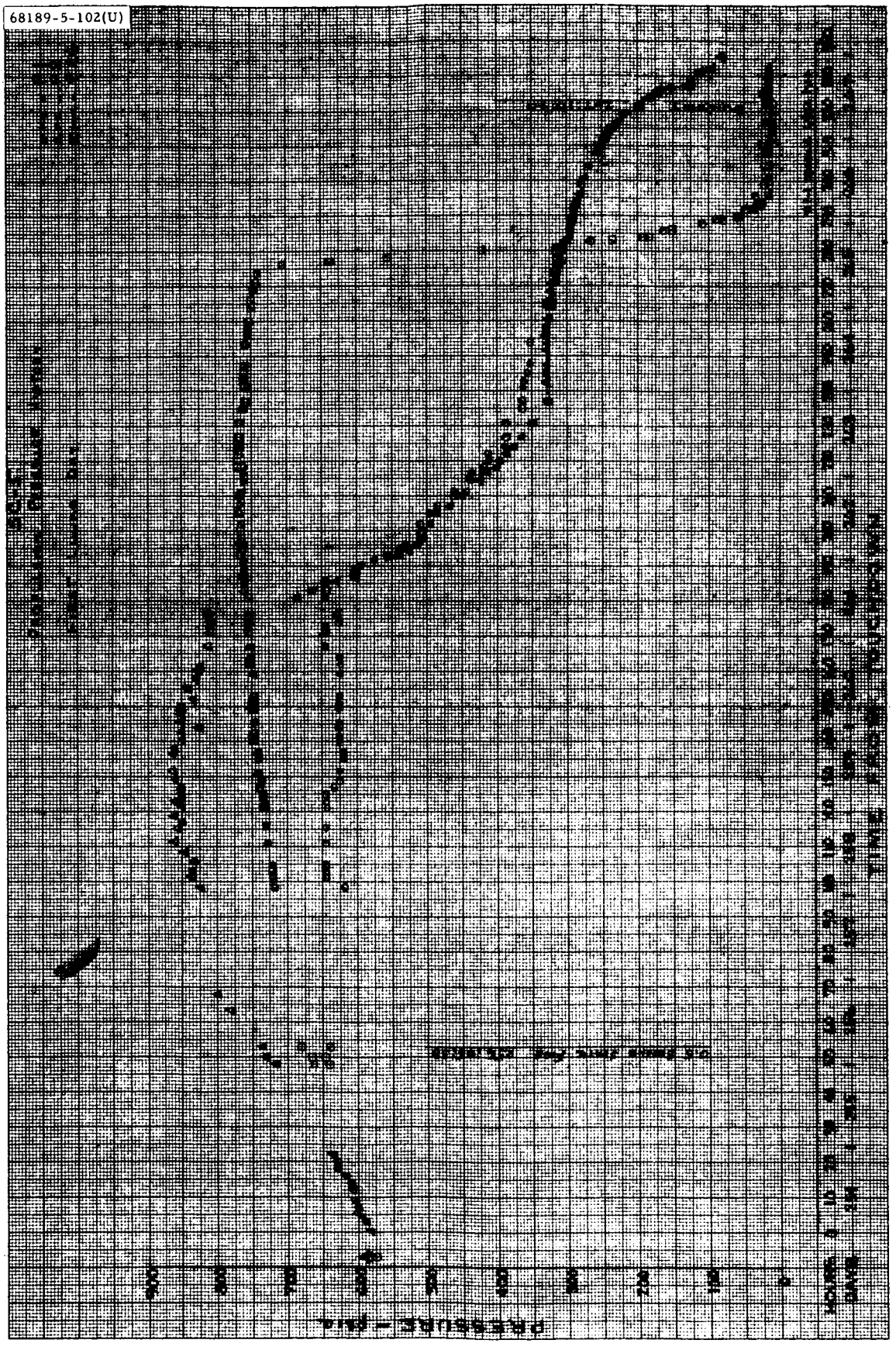

Figure 5.6-13. Propulsion Pressure History – First Lunar Day

is thought to be due to a gas side seal leakage. These leakages are attributed to seal degradation with subsequent failure due to the high temperatures seen during the lunar day.

Shortly after sundown at 268:04:20 GMT, the helium dump command was transmitted in an attempt to jar the spacecraft and open a closed thermo-switch in one of the electronic compartments.

5.6.5 REFERENCES

1) "Surveyor V Helium Regulator Failure," Surveyor Project Action Status Report, SSD 74133, 16 October 1967.

2) G. F. Pasley to Distribution, "Revised Helium Leakage Rates for the Surveyor Vernier System," Hughes Aircraft Company, IDC 2227.1/1331, 31 March 1966.

3) T. B. Shoebotham to L. Gee, "Transmittal of Propulsion SPAC Mission E Report," Hughes Aircraft Company, IDC 2227.2/1238, 21 September 1967.

4) R. Laird to Distribution, "A21 and A21A/114 Vernier Propulsion Systems Propellant Inventory," Hughes Aircraft Company, IDC 2227.1/1110, 29 September 1966.

5) J. H. Green to P. E. Sterba, "Prediction of the Vernier Engine Thrust Levels for SC-5," Hughes Aircraft Company, IDC 2292/405, 3 October 1967.

5.6.6 ACKNOWLEDGMENTS

The following people aided in the preparation of this report:

G. F. Pasley, Coordinator

T. B. Shoebotham

APPENDIX A
TO SECTION 5. 6
HELIUM REGULATOR FAILURE

INTRODUCTION

Surveyor V experienced a malfunction in the helium pressurization subsystem during the flight of the spacecraft to the moon. This malfunction occurred at the time of helium pressurization of the vernier propulsion subsystem just prior to the midcourse correction. It was noted after the midcourse correction that the helium pressure was decreasing, which is an abnormal condition, and a review of the data suggested the helium regulator had an internal leak, increasing the downstream pressure and causing the relief valves to vent to space. Subsequent vernier engine firing failed to correct the regulator internal leakage condition.

Analysis of the spacecraft system performance capabilities was made, and the terminal descent phase of the mission was redesigned during the remainder of the transit phase. The spacecraft performed the terminal descent and landed successfully.

Following touchdown, a review committee was established to determine the cause of the malfunction, as documented on TFR 18263, and make recommendations for action which would prevent recurrence in the SC-6 and SC-7 flights. Management review assessment and direction was continuously applied to the activities of the review committee. This committee was comprised of Hughes and JPL personnel. The contents of this appendix are extracted from Reference A1.

FAILURE CAUSE

Analysis of the data obtained during the Surveyor V flight indicates that the loss of helium high pressure was due to an internal helium leak in the helium regulator, allowing the downstream pressure to rise beyond the crack pressure of the oxidizer or fuel system relief valves, venting the helium into space.

The Surveyor Project has reviewed the data and results of special failure mode tests in order to determine the cause of the failure of the helium high pressure regulator. The conclusion reached by the Surveyor Project is that the most likely cause of the Surveyor V regulator malfunction was contamination which damaged the helium regulator valve seat seal. This could result

PRECEDING PAGE BLANK NOT FILMED.

in an internal leak through the regulator, causing the outlet pressure to increase to a level which will cause the fuel or oxidizer relief valve to vent into space.

The source of the contamination is indeterminate since no absolute method exists for evaluating whether any system is free of contamination particles. However, Surveyor V experienced four changeouts of check and relief valves where such acts of rework were sources for significant additional contamination. During solar thermal vacuum (STV) tests, the oxidizer check and relief valve assembly was replaced because of a bent stem on the fill and vent valve. Normal gas purge through the system was maintained while the VPS connections were open. At a later time, both oxidizer and fuel check and relief valve assemblies were replaced, due to overheating during STV. While the normal gas purge was effected during changeout, inaccessibility of the assemblies because of the dummy retro being in place prevented following the normal changeout procedures.

Following delivery of the spacecraft to AFETR, the helium regulator was checked for proper operation, and the regulated lockup pressure was within specification. At the end of this check, however, the pressure was relieved on the high pressure side of the regulator before the downstream side; this allowed the gas to backflow through the regulator seat. The check valve flow crack pressure test was made next, and again the pressure was relieved before the downstream side, and backflow of gas through the regulator seat took place.

Following these checks, the check valve leak test was performed and it was discovered that the oxidizer check valve leaked. Particulate contamination was believed to be the failure cause, probably introduced during the previous changeout made under difficult circumstances during STV at El Segundo.

In summary, the events believed to have contributed to the regulator failure are as follows:

1) Oxidizer check and relief valve changeout due to bent stem in STV

2) Oxidizer and fuel check and relief valves changed out due to overheating in STV

3) Changeout made in difficult circumstances with dummy retro installed

4) Gas backflowed through regulator seat twice during AFETR checkout

5) Changeout of contaminated oxidizer check valve without confirmation of lockup pressure following contaminated check valve replacement

DISCUSSION

Failure Mode Analysis

Failure Modes Possible

1) Contamination on, or contamination scoring of, the regulator seat can produce the type of failure experienced on Surveyor V, i.e., an internal leak through the regulator. Although no failure of this type has occurred on a regulator assembly during any Surveyor spacecraft testing, similar failures have been noted on other components such as relief valves, check valves, and solenoid valves. Contaminant protection for the relief valve has previously been incorporated into Surveyor V through SC-7 VPS subsystems by adding integral filter assemblies. No check and relief valve assembly contaminant failures had been experienced since this incorporation.

2) Surge valve malfunction could cause erosion of the regulator seat, resulting in leakage past the seat. However, subsequent testing of the regulator in which the surge valve failure was induced produced leak rates that were not sufficient to cause the type of failure experienced on Surveyor V. Additionally, the eroded seat on the T-2N regulator did not cause sufficient leakage to compromise the mission and was not detected until the regulator was disassembled. Therefore, this failure mode, though possible, is considered much less probable than contamination.

Failure Modes Examined and Discounted

1) Excessive external leakage of fluids from low pressure system – If liquid were leaking, abnormal temperatures in area of leak would result. If helium gas were leaking from the low pressure system, both high and low helium pressure would decay asymptotically toward zero after the high pressure reached the propellant tank pressure. Neither of these modes was noted.

2) Excessive external leakage of helium from the high pressure system – This failure mode would result in stabilization of propellant pressures at regulator lockup pressure while helium tank pressure would decay to zero. The above symptoms were not present on Surveyor V.

3) Regulator mechanism binds or is loose – Symptoms of a failure of this type are: 1) erratic regulations; 2) lockup shift; 3) if binding is severe, no regulation; and 4) leakage. All data indicate the regulator was mechanically functioning and not binding or loose.

4) Filter damage from shock wave when system is pressurized – Contamination would be introduced into the system from a failure of this type. The filter design has been proven through extensive testing not to be susceptible to damage of this type.

5) Shift of relief valve crack or regulator lockup pressure could cause loss of helium if the shift were to be large enough for relief valve operating pressure to overlap the regulator lockup pressure.

Surveyor V flight data indicate a generous margin between the relief valve reseat pressure and the regulator lockup pressure; therefore, shift in relief valve or regulator settings could not have caused the loss of helium in the Surveyor V flight.

Results of Design Studies and Special Testing

Design Differences

A detailed design review of the configuration differences between the A-21A regulator flown on Surveyors I through 4, and the A21-E regulator flown on Surveyor V and installed on the SC-6 and SC-7 vehicles was completed. Both regulators are identical in functional requirements and in detailed design except for minor changes in the mounting provisions and the outlet port.

Qualification Review

An investigation into the qualification of the design of the helium tank and valve assembly and its critical components, with particular attention to the qualification testing of the helium regulator, was completed. This investigation included a complete review of all engineering test data and manufacturing history of all the detailed components used in these assemblies. There was no evidence of component failures or out-of-specification conditions during the type approval testing (TAT) on both regulator configurations or during any of the flight acceptance tests of the helium tank assembly. Contamination (cleanliness) requirements were reviewed and found to be adequate for proper value performance.

Test Review

A review of all spacecraft testing for Surveyors I through V was completed and there were no out-of-specification performance conditions reported.

Special Tests

Additional tests to confirm the design changes made between the Surveyor I regulator and the Surveyor V configuration were completed at the vendor's test facility on the same test equipment used for all regulators during acceptance testing. These tests also verified that the minor changes made in mounting and port configuration had little or no effect on the regulator's performance. Both regulators used in these tests performed well within the procurement specification requirements.

In addition to the functional tests performed at the vendors, detailed contamination checks were made at the Hughes El Segundo plant to verify that regulators of this configuration were not generating contamination which could cause changes in regulator performance. In these tests, a simulated flight tank system was used and subjected to five squib firings. After each firing, regulator performance was determined and found to be well within the specification requirements, although the sample contaminants level taken after each squib firing had a gradual increase in the population in each of the particulate size ranges.

Design Changes Considered

During the review and subsequent to the completion of the review committee report, several variations in the design of the helium supply system were investigated.

Additional Valves

One basic consideration was the installation of a squib-actuated or solenoid-actuated normally open valve assemblies on the regulator outlet side. If the leakage experienced on Surveyor V were to occur, the valve could be closed and the helium preserved until final terminal descent sequence was activated, at which time the valve could be opened and the helium allowed to flow to the fuel tank assemblies. This design concept was rejected when it was determined that the regulator could not withstand pressures of 5000 psi on the regulated outlet side, and that permanent distortion of the housing would occur with resulting external helium leakage.

A second design concept considered was the installation of solenoid valves on the outlet ports of both the fuel and oxidizer relief valves. In functional concept, these would provide a command means of venting helium pressure in the fuel tank system in case of leakage of the regulator similar to that experienced on Surveyor V. In flight, the propellant tanks could be pressurized to 1000 psi under certain temperature conditions. Incorporation of these valves would require STV verification as well as signal processing and harness modifications. Because of the serious impact that this would have on the SC-6 and SC-7 schedule, the design change was rejected.

Link Helium and Nitrogen Systems

The third design change consideration was the installation of a line between the N_2 system and the helium system so that N_2 could be supplied to the high pressure side of the helium system on command through charging valve 2 (CV-2). This system was discarded when it was found that it would require complete redesign of the filter housing and/or of the CV-2 control valve which is normally a closed double seal high pressure valve. For use with this system, the valve would have to be left open with only an O-ring as a primary seal for both the N_2 and the helium system.

Increase Relief Valve Settings

The fourth design currently under investigation is the redesign of the spring used in the relief valves so that the current relief valve configuration could be modified to have a higher operating pressure. Current valves crack at approximately 825 psi and reseat at 810 psi. If this pressure is raised to 900 psi for the cracking pressure, it is postulated that a failure similar to that experienced by the Surveyor V regulator would tend to heal itself because the higher back pressure, as a result of the change in the relief valve cracking pressure, would react on the regulator sensing area, thus causing higher seat loadings and providing a greater distortion of the Kynar material until effective sealing was obtained.

Currently, this design change is being reviewed with regard to the time schedules, the availability of the new springs, and the time required for additional type approval tests to verify that the changes in spring materials will not degrade the current qualification relief valves.

Manufacturing Changes Considered

Changes were considered to improve manufacturing processes and procedures. These changes will be implemented into any new procurement or rework of regulators. The changes include polishing of regulator detail parts and incorporation of additional inspection points at subassembly and assembly levels. None were of sufficient benefit to require rework of presently assembled flight equipment.

Handling and Preparation Possible Improvement and Disposition Changeout Plans and Rework Criteria

1) Improve hardware changeout plans and techniques to avoid compromising the integrity of the cleanliness of the VPS system.

2) Define rework criteria for parts that fail contamination tests. Procedures and planning for reworking contaminated assemblies are now approved by Propulsion Engineering before they are considered acceptable. All procedures and planning involving contaminate critical items must now be approved by the Propulsion Task Manager. This section is required by SQAD 129.

Cleaning Techniques, Checks, and Filtering

1) Improve contaminate cleaning techniques and verify compatibility with control items.

A liquid flush of the regulator assembly would clean the unit better than purging with gas (either helium or nitrogen). Since liquid flushes have not been performed on these assemblies, it is not known if a flush of this type would have any deleterious effects, i.e., O-ring seal compatibility, ability to completely dry the unit after flushing, effects on operation of unit, degradation of lubricants on seals, etc. Since these effects are not known, it is recommended that flushing of any of these units be withheld until completion of a test program currently in progress in which these effects are being determined. Included in the test program are the following items: functional test, leakage test (internal and external), freon flush, vacuum dry, gas purge, ambient storage test, propellant compatibility test, vibration test, combined vacuum-high temperature test, and squib firing test.

2) Install a millipore filter at inlet to CV-1, -2, -3, and -4 of the VPS after assembly to remain with system until final loading of helium and propellants. In lieu of semipermanent millipore filter installation, procedures have been revised to install hard lines between millipor filters and inlets to the gas valves. Flex line connections will be made at the filter inlet port.

Filters on SC-7 at El Segundo have been incorporated per PCR 1679 to HAC Procedure 225869-2.

Filters have been incorporated on SC-6 by planning additions to procedures. For SC-7, the following PCRs incorporate filters in the listed procedures:

PCR	Hughes Procedure
1943	229134D
1944	229155E
2546	288107G
1945	288109G
1946	288117G
1947	288118G
1948	288119E
1949	288127F
1950	288362D
1951	288415E
1952	288441F
1953	288443D
1954	288492E
2539	288496C

3) Standardize contamination checks on the VPS components, units, and system level tests. The cleaning specification is being revised to provide consistent checks for component acceptance, control item FAT, and vehicle checks. Revision includes standardization of pressures, gages used, and time and flow rates so that cleanliness of the components can be assessed. ECR 359996 requests revisions of the cleaning specification, HAC 262613C.

Improved Test Procedures and Criteria Considered and Disposition System Tests

The following tests should be added or revised into the VPS system test program:

1) Perform regulator functional and lockup test after relief and check valve tests

2) Perform lockup test for sufficient time to determine internal leak rate of regulator

3) Perform a gas contamination test of helium supply system

4) Change pressure bleed down procedures to prevent possible back flushing of contaminants into regulator

The preflight checkout test sequence for SC-6 has been modified to give confidence that the helium regulator will function properly in flight. The regulator was tested as the final step in the vernier propulsion (gas) system tests. The regulator was subjected to a forward gas flow test at high and low flow levels and then a gas sample was taken to verify the system cleanliness. This check was followed by a 6-hour lockup test and the system, then blown down with helium flowing forward through the regulator. This test was performed on 10 October 1967 per step 47.14 of 227541F, Post J-FACT Procedure. This lockup pressure variation was only 1 psi over the 6-hour period, which is well within the required limits. The contamination check verified a clean system. PCR 2546 revised HAC 228107G for use with SC-7 at AFETR. El Segundo testing of SC-7 will be accomplished per HAC 225869-2 as modified by STR 309.

Unit Tests

1) Perform a gas contamination test on the SP-2 helium tank and valves assembly in order to verify cleanliness of assembly. In addition, a functional test will be performed to verify proper regulator operation.

   This test, specially requested by TWX 001 on 13 October 1967, will be performed per the applicable portions of HAC 288107G. The required completion date is on or before 3 November 1967.

2) Perform a gas contamination test on the helium tank and valve assembly during the regulator flow test portion of flight acceptance test vibration. ECR 359995 requests revision to the helium tank and valve assembly flight acceptance test specification to include the gas sampling.

3) Verify surge valve performance after assembly of the regulator into the helium tank and valves assembly. Performance of the test requires removal of CV-2 and may introduce contamination into the system. Additional flushing, cleaning, and drying operations would have to be performed to ensure that the system is contaminate free. A repeat of the high pressure leak check is required if CV-2 is removed from the assembly. Schedule limitations do not permit incorporation of the test on SC-6. Studies are currently under way to evaluate the effect the additional required operations on the helium tank and valve assembly on SC-7.

Launch Procedure Changes Considered

1) Actuate the helium release squib on the pad and verify proper helium regulator lockup characteristics prior to launch. This recommendation has been rejected for the following reasons:

   a) Propellant tankage is not man-rated at flight operating pressure, and an abort would require manual venting of the propellant system.

   b) The propellant tanks are not type approved test qualified for boost vibration at flight operating pressure.

   c) This procedure would also require a design change including the spacecraft harness.

CORRECTIVE ACTION SUMMARY

The actions which have been directed by Surveyor Project Management as a result of the Surveyor V helium regulation failure are as follows.

Design Actions

1) Perform, in parallel, engineering redesign of the relief valve to increase crack pressure

2) Evaluate effects of increased relief valve crack pressure on the helium pressurization subsystem

3) Perform tradeoff study to determine the suitability of redesign for SC-7

Manufacturing Actions for Future Procurement or Rework

1) Incorporate additional inspection points at subassembly and assembly levels
2) Improve quality control instructions for handling and manufacturing processes on contaminate critical items
3) Polish regulator detail parts
4) Perform gas contaminate tests on helium tank and valve assembly during regulator flow test portion of flight acceptance test vibration
5) Standardize regulator lockup tests at component, unit, and systems level
6) Provide rework criteria to manufacturing for parts that fail contamination tests

Handling Actions

1) Improve hardware changeout plans to avoid compromising cleanliness of VPS subsystem
2) Evaluate feasibility of application of liquid flush techniques to VPS subsystem for SC-7
3) Install millipore filters from AGE to all gas inlets of helium pressurization system
4) Standardize contamination checks on VPS units and subsystem

Test Actions

1) Change procedures to avoid backflow through regulator seat
2) Change order of test to perform regulator lockup check after check valve tests
3) Perform 6-hour regulator lockup test to detect leakage
4) Study feasibility of performing surge valve verification after installation into helium tank and valve assembly for SC-7
5) Perform gas contamination test on SP-2 helium tank and valve assembly and verify cleanliness

REFERENCE

A1) "Surveyor V Helium Regulator Failure," Surveyor Project Action Status Report, SSD 74133, 16 October 1967.

5.7 PROPULSION – MAIN RETRO

5.7.1 INTRODUCTION

The main retro-rocket, which performs the major portion of the deceleration of the spacecraft during terminal descent, is a spherical solid propellant unit with a partially submerged nozzle.

The unit is attached at three points to the spacecraft near the landing leg hinges, with explosive nut disconnects for postfiring ejection. Friction clips around the main retro-rocket engine nozzle flange provide attachment points for the altitude marking radar. The igniter gas pressure ejects the altitude marking radar when the retro firing sequence is initiated. The main retro-rocket engine ignition squibs and retro release explosive nuts operate from a pulsed, 19-ampere, constant-current source. Commands are initiated by the flight control system.

The nozzle is partially submerged to minimize overall length. The nozzle has a graphite throat insert backed up by laminates of carbon cloth phenolic with a fiberglass exit cone lined with bulk carbon phenolic. The case is of high strength steel and insulated with asbestos and inorganic fiber filled buna-N rubber to maintain the case at a low temperature level during burning.

The main retro-rocket engine with propellant weighs approximately 1394 pounds. The engine utilizes an aluminum, ammonium perchlorate, polyhydrocarbon, case-bonded, composite-type propellant, and conventional grain geometry. The engine thrust may vary between 8000 to 10,000 pounds over the temperature range of 50° to 70°F.

Two thermal sensors are installed on the main retro-rocket engine case for telemetering engine temperature during transit. One thermal sensor is installed for monitoring nozzle temperature during transit.

The main retro-rocket engine employs a safe and arm device that has dual firing and single bridgewire squibs for the engine igniter. In addition, provisions for local and remote safe and actuation and remote indication of inadvertent firing of the squibs are included. Both mechanical and electrical isolation exists between squib initiator and pyrogen igniter in the safe condition.

5.7.2 ANOMALY DESCRIPTION

No anomalies were noted in the main retro subsystem.

5.7.3 SUMMARY AND RECOMMENDATIONS

The Surveyor V main retro-rocket engine operated within all required tolerances. No changes to the SC-6 retro-rocket engine or to the engine performance prediction models are recommended. Table 5.7-1 presents a summary of main retro performance parameters.

TABLE 5.7-1. SUMMARY OF MAIN RETRO PERFORMANCE PARAMETERS

Parameter	Predicted Main Retro Value	Required Main Retro Value and Tolerance	Actual Value	Uncertainty
Bulk temperature, °F	55	±15	52.5	±5
T3500, seconds	38.96	±0.4	38.56	±0.1
Maximum thrust, pounds	9850	<10,000	9950	±100
Total impulse, lb-sec	362,272		362,146	±1800
Specific impulse, seconds	298.5	±0.3	289.4	±1.5
Center of gravity excursion, inch	—	<0.030		
Thrust vector excursion			0.024*	±0.005
Displacement, inch	—	<0.040		
Angular, degree	—	<0.2		
Roll torque, in-lb	—	<80	12*	±6

*Total value from all sources.

5.7.4 SUBSYSTEM PERFORMANCE ANALYSIS

Table 5.7-2 gives the major events and times associated with the firing of the retro engine.

TABLE 5.7-2. MAJOR EVENTS AND TIMES FOR RETRO OPERATION

Event	GMT minutes:seconds	Maximum Error, second
Vernier ignition	44:51.426	+0.02 to -0.02
Retro ignition	44:52.496	+0.05 to -0.05
3500-pound thrust level	45:31.056	+0.05 to -0.05
3.5 g switch	45:31.355	+0.6 to - 0.6
"Actual" 3.5 g	45:31.430	+0.05 to -0.05
Retro ejection signal	45:40.395	+0.05 to -0.05

Items constituting the analysis effort are as follows:

1) Reconstruction of thrust versus time curve from accelerometer and doppler data (Figure 5.7-1)

2) Calculation of engine specific impulse

3) Determination of thrust vector excursions and roll moments generated by the retro engine

4) Determination of T3500

5.7.4.1 Thrust Versus Time

The technique used in reconstruction of the thrust versus time trace from both accelerometer and doppler data is discussed in subsection 5.15.6.2 of Reference 1. This reconstructed trace varies from the predicted trace as shown in Figure 5.7-1. The maximum difference is 3 percent, and it occurs 8 seconds after ignition. This, however, is in an area of higher error for the accelerometer data since the spacecraft passes through a period of rapid change in acceleration to a fairly steady acceleration.

68189-5-1(U)

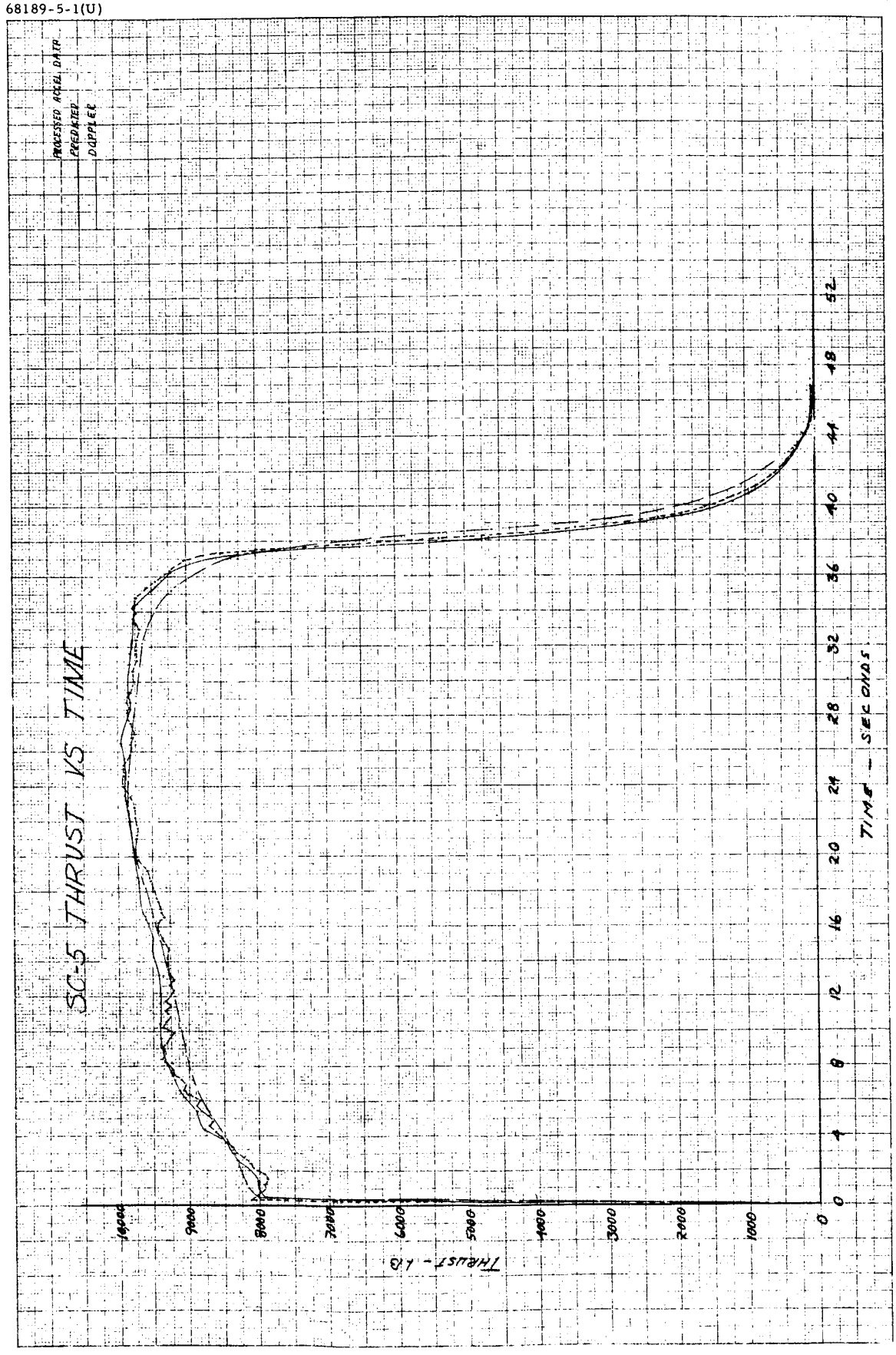

Figure 5.7-1. Surveyor V Thrust Versus Time

5.7.4.2 Specific Impulse

The main retro-rocket engine specific impulse was obtained by correcting the predicted nominal specific impulse used in the preflight descent trajectory computer program by the change in velocity measured during retro burning on Surveyor V. The difference between the actual and predicted change in velocities, 8411 and 8414 fps, respectively, amounts to 0.03 percent low versus the 1 percent allowed. This approach is conservative from the retro-rocket engine point of view since the velocity difference is actually due to a number of sources in addition to the main retro-rocket engine. Some of these other sources are as follows:

1) Uncertainty in vernier engine specific impulse

2) Uncertainty in vernier engine thrust level

3) Uncertainty in vernier engine weight versus time

4) Uncertainty in retro-rocket engine specific impulse versus time

5) Uncertainty in retro-rocket engine weight versus time

6) Uncertainty in doppler data

5.7.4.3 Retro Disturbance Torques

The following retro disturbance torques were noted:

1) Retro ignition produced a short duration disturbance torque of approximately 20 ft-lb.

2) Following retro ignition, all three vernier engines settled near their midthrust condition and remained very steady throughout retro burning. This indicates that the retro engine did not experience any measurable thrust vector excursion or lateral cg shift during operation.

3) The maximum required corrective roll torque produced by the vernier engine after accounting for bracket bending was 1 ft-lb. Assuming all this torque was produced by the main retro engine, the engine roll torque is still well below the 7 ft-lb maximum moment allocated to the retro engine.

4) Retro engine ejection from the spacecraft was very smooth and required no apparent corrective torque.

5.7.4.4 T3500

The T3500 (time from ignition to the time when thrust decays to 3500 pounds) prediction was marginal. The total error of 1 percent equals the

1 percent tolerance for the prediction. This total error is the result of the actual engine temperature gradient uncertainty, the error in calculating the bulk temperature corresponding to that gradient, telemetry error, and prediction error.

5.7.5 REFERENCES

1) "Surveyor I Flight Performance Final Report," Volume III, Hughes Aircraft Company, SSD 68189R, October 1966.

2) "Surveyor Spacecraft A21 Model Description," Hughes Aircraft Company, Document No. 224847B, 1 March 1965.

3) "Surveyor Main Retro Engine A21-28 Support Documentation," Thiokol Chemical Corporation.

4) "SC-5 Event Times from Teltab," Hughes Aircraft Company.

5.7.6 ACKNOWLEDGMENTS

The following people contributed to the main retro analysis:

L. M. Spicer, Coordinator

E. W. White, systems analysis

L. H. Davids, systems analysis

J. H. Green, systems analysis

5.8 ALTITUDE MARKING RADAR

5.8.1 INTRODUCTION

The Surveyor altitude marking radar (AMR) is a small, conventional, pulsed, X-band, fixed dual-range gate, marking radar designed and supplied by Hughes Division 27. The purpose of the AMR is to provide, with high accuracy and reliability, a positive indication that slant range from the Surveyor spacecraft to the lunar surface has decreased through a preset value, nominally 60 statute miles for the A-21 series of engineering models. This signal starts an on-board timer, whose run-out time is set by ground command earlier in flight to initiate vernier and main retro engine ignition. Since the AMR is installed in the exhaust cone of the main retro engine and has served its purpose in providing ignition timing, it is forcibly jettisoned from the spacecraft when that engine is ignited.

The AMR is a conventional noncoherent radar, employing a pulsed magnetron, single antenna, duplexed mixer, crystal-controlled, solid-state local oscillator, wideband IF amplifier, noncoherent detector, and video processing circuitry. Dynamic range is extended by automatic gain control (AGC) of the IF amplifier; AGC voltage is telemetered and provides an indication of received signal power. The video circuitry is of special design to mark at a preset range with high accuracy and reliability. Two fixed, adjacent range gates continuously examine the video signal. Their outputs are continuously summed and differenced. When the sum exceeds a fixed threshold and the difference simultaneously crosses zero with positive slope, the mark signal is generated. Sum threshold is set for an extremely low probability of marking on noise (false mark) throughout the operating time, while video integration plus a very substantial radar gain margin ensure a high probability of marking successfully.

Two separate ground commands, whose timing is controlled, are required to fully activate the AMR. The first signal, called simply AMR on, commands on the primary power to the AMR, which includes all internal power except high voltage to the transmitter. The video signal is inhibited from reaching the marking circuits until the second command, thus eliminating any residual probability of false marking on noise during this warmup interval. The second signal, called AMR enable, commands on the transmitter high voltage and also removes the video inhibit. This enabling function is timed not only for favorable thermal conditions at the expected marking time but also to preclude premature marking on second-round echoes at

much longer ranges. In a lunar mission, FPAC supplies a marking time prediction based upon trajectory data. The prescribed times for SPAC transmission of these two commands are "on" at 280 ± 10 seconds, and "enable" at 100 ± 10 seconds before predicted marks.

For proper analysis, complete trajectory information is required. While either known or assumed for preflight predictions, it must be known or derived for postflight evaluation. Spacecraft attitude and velocity data are supplied by FPAC from tracking and trajectory computations. Residual range uncertainty, however, exceeds that of the AMR itself, which is assumed to have marked with mean value and dispersion predicted by radar analysis prior to each mission. In conjunction with approach velocity and attitude conditions from FPAC, the trajectory can then be extrapolated backward with high accuracy by a special two-body program. This program derives all the significant AMR parameters throughout the nominally 100-second interval from enable to mark, and calculates correction factors to be applied to observed telemetry data before comparison with predicted received signal power.

AMR telemetry includes three digital and three analog signals, plus analog temperature data. The digital signals confirm on-board discrete events: prime power application (R-1, AMR on), high voltage and video enabling (R-11, AMR enable), and slant range trigger (FC-64, AMR mark). It should be noted that FC-64 is telemetered only when the on-board mark is generated, and not in response to the backup command from earth. The three analog signals (besides temperature) are magnetron current (R-12), AGC voltage level (R-14), and late gate detected video voltage level (R-29). The AGC not only confirms receiver response to RF return, but is also useful in evaluating terrain reflectivity. The magnetron current confirms pulsing of the magnetron after enable, and is useful primarily as a transmitter failure mode indication. The late gate signal, primarily a receiver failure mode indication, normally confirms presence of gated video signal rising quickly to a peak at the time of mark and decaying quickly thereafter. All but a few of its values are normally at the quiescent noise level, and in no way constitute repeated events.

5.8.2 ANOMALIES

There were no anomalies in the operation of the AMR during the Surveyor V mission.

The entire terminal descent, however, was so nonstandard that a background discussion is presented in Appendix A of the RADVS section (5.9). Since AMR operation was not affected, but was an influence in the revised descent, AMR comments are included in that discussion (Appendix A and 5.9.2) for continuity and convenience.

5.8.3 SUMMARY AND RECOMMENDATIONS

5.8.3.1 Summary

The Surveyor V AMR functioned normally. The true altitude mark was generated at the expected time and initiated the automatic terminal descent sequence as planned. The significantly increased time delay for engine ignition is discussed in subsection 5.9.2. The routine emergency mark backup command was received by the spacecraft after the on-board mark had been generated.

The AMR was turned on 276.6 ± 0.65 seconds before the mark, acceptably within the 280 ± 10 seconds specified. It was enabled 95.4 ± 0.65 seconds before the mark, acceptably within the 100 ± 10 seconds specified. EP-17 showed normal current drain characteristics throughout AMR operation and jettison, and AMR magnetron current (R-12) was normal before, during, and after enabled operation. The late gate signal (R-29) was normal, confirming the presence of RF return signal and detected video within the gate at the time of the mark.

AGC-indicated signal strength, after proper evaluation, showed excellent correlation with the nominal predicted value throughout the enabled interval; only one data point prior to mark was more than 1.0 db off the nominal. Quiescent level properly prevailed for the first 60 seconds until received signal reached the onset of AGC action, after which the AGC level rose essentially as predicted. The expanded AGC calibration and the appreciably expanded evaluation effort initiated with Surveyor III has reached full fruition with Surveyor V. The unexpectedly high quiescent level observed for the first time in Surveyor 4 did not occur in Surveyor V.

5.8.3.2 Recommendations

There are no recommendations arising directly from the Surveyor V mission.

The successful Surveyor V terminal descent does help to illustrate, however, certain recommendations previously made and repeated again herewith (see also paragraph 5.9.3.2).

The nominal expected marking range predicted for the AMR before each mission should be used in the real-time guidance and trajectory programs. This nominal uses analytically predicted range bias relative to measured gate setting. Marking accuracy test data, necessarily measured by a far more complicated setup and procedure than that for the gate alone, should be viewed only as a preflight confidence check on functional operation.

Continued use of the AMR on future spacecraft is required for reliable terminal descent initiation. The backup command may be retained for residual reliability as long as its timing continues to be tightly controlled.

5.8.4 SUBSYSTEM PERFORMANCE ANALYSIS

5.8.4.1 Event Times

From the table of Surveyor V events associated with radar operation (subsection 5.9.4), the following AMR events are repeated below. The times listed are GMT when recorded at DSIF-11.

Channel	Name	GMT at DSIF-11, day:hr:min:sec
R-1	AMR on	254:00:40:02.458 ± 0.6
R-11	AMR enable	254:00:43:03.656 ± 0.6
FC-64	AMR mark	254:00:44:39.088 ± 0.05
FC-28	Vernier ignition	254:00:44:51.389 ± 0.05
FC-29	Retro ignition	254:00:44:52.490 ± 0.05
FC-64	AMR mark off	254:00:44:52.588 ± 0.05

The warmup time (on to enable) was 181.2 ± 1.2 seconds, well within the nominal 180 ± 20 seconds. The time from on to mark was 276.63 ± 0.65 seconds, acceptably within the 280 ± 10 seconds specified. The enabled time (enable to mark) was 95.43 ± 0.65, acceptably within the 100 ± 10 seconds specified.

From readings of the magnitude register (FC-18), actual mark time can be refined to 254:00:44:39.097 ± 0.041, and actual vernier ignition time can be refined further to 254:00:44:51.431 ± 0.025, still referred to GMT at DSIF-11.

In Surveyor V, the unusual coincidence occurred of FC-64 still being on (last appearance) only 2 milliseconds before the first appearance of FC-29 (both on in same word). If AMR jettison were physically instantaneous, retro ignition time would be 254:00:44:52.539 ± 0.001.

5.8.4.2 Load Current Signals

Radar and squib current (EP-17) was normal. It was zero until AMR on, when it rose to normal AMR warmup load, which continued until AMR enable. During the enabled interval, it properly cycled in the manner characteristic of magnetron pulsing, which is not synchronized with the telemetry data sampling. This continued until engine ignition, when the AMR load was removed (by jettison of the AMR) and replaced by the RADVS warmup load.

Magnetron current (R-12) (Figure 5.8-1) also was normal. It was zero until AMR enable, when it rose to normal high voltage load during magnetron pulsing. This continued until engine ignition, when AMR signals normally go full-scale as the AMR itself is forcibly jettisoned by the retro engine.

5.8.4.3 Late Gate Signal

The late gate video detected analog voltage signal (R-29) (Figure 5.8-2) was normal, confirming the presence of RF signal and detected video at the time of the mark.

From the trajectory reconstruction for AGC evaluation, the total stretched pulse length as received was about 34 microseconds and the effective closing rate was 8440.9 fps, both at the time of the mark. The corresponding video pulse closing rate was therefore about 17.13 microseconds per second. The video late gate has a nominal duration of 20 microseconds (20.0 ± 1.0 required). It should therefore have produced output within 3 db of peak for (34 + 20)/17.13 = 3.15 seconds.

With R-29 sampled at 1.2-second intervals, high level samples should be at least two in number, perhaps three if the sampling time phase were right. In Surveyor V, it happened that there were two high level samples that occurred at the proper times relative to the time of the mark. There was also one partial amplitude sample on each side, as is typical and normal.

5.8.4.4 DB Budget

The Surveyor V AMR db budget, revised for the postflight parameters in the trajectory reconstruction for AGC evaluation, shows a 26.1-db margin above that required for a 0.999 cumulative probability of successful marking, as follows:

P_t (average)	+ 34.39 dbm
G^2	+ 69.0 db
β_1	- 13.57 db
σ (0 degrees) = 0.065	- 1.17 db
R^{-3}	- 53.34 db
f^{-2}	-199.37 db
f_r^{-1}	- 25.44 db
$\left(\frac{1}{2}\right)\left(\frac{c}{4\pi}\right)^3$	+122.12 db

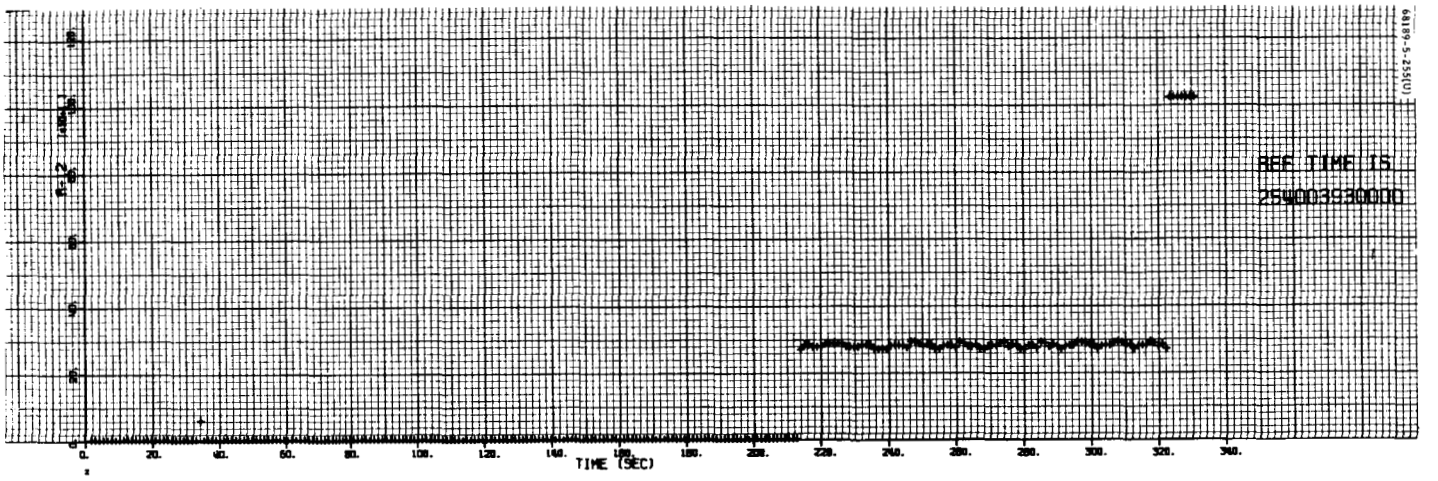

Figure 5.8-1. Magnetron Current (AMR)

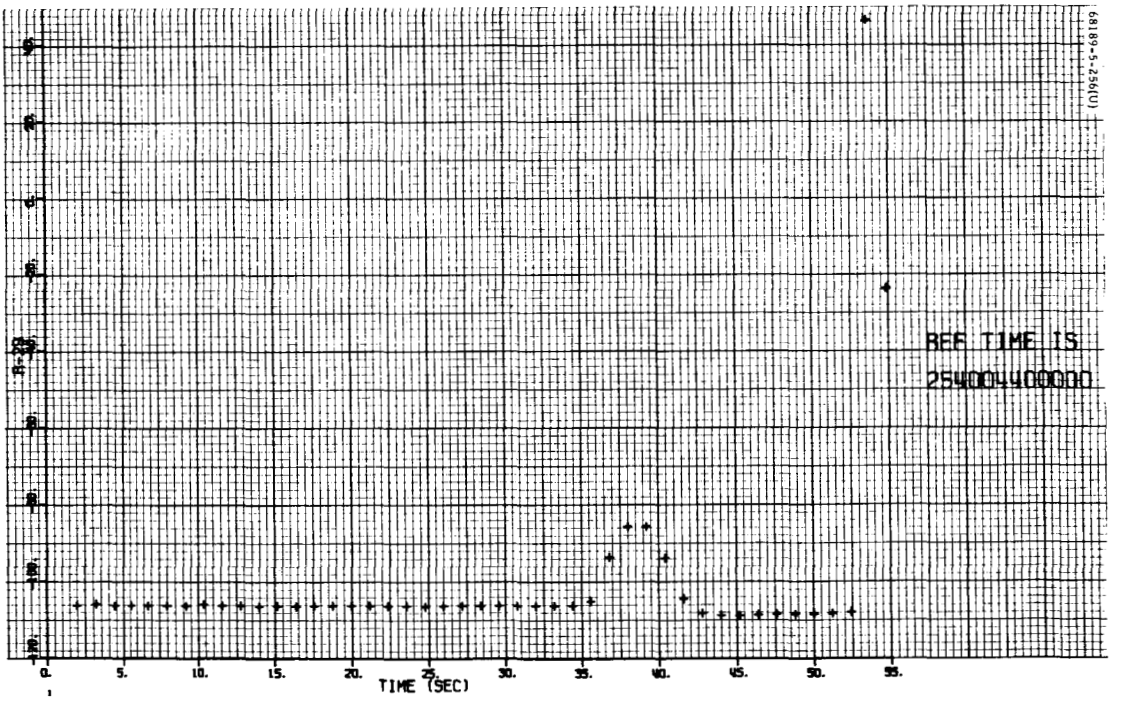

Figure 5.8-2. Late Gate Signal (AMR)

cotan 47.44 degrees	- 0.37 db
F (47.44 degrees)	- 12.24 db
	+225.51 dbm
	-305.50 db
P_r	- 79.99 dbm
P_{min} (30 microseconds)	-101.5 dbm (nominal)
P_{min} (30 microseconds)	-105.8 dbm (measured)
Receiver margin	+ 4.3 db
P_{min} (34 microseconds)	-101.8 dbm (nominal)
P_{min} (34 microseconds)	-106.1 dbm (predicted)
Total margin above threshold for 0.999 cumulative probability:	- 79.99 dbm
	-106.1 dbm
	+ 26.1 db

5.8.4.5 Expected Marking Range

The expected value of the slant range along the AMR antenna electrical axis when the mark is produced will vary slightly from the nominal value of 60 statute miles. This expected value is supplied before each mission to FPAC, which inserts this value and both mechanical alignment and electrical boresight data into its trajectory programs. These determine the time delay value to be commanded into the on-board magnitude register so that automatic engine ignition will occur at the altitude desired for that mission.

Previous study and experience, confirmed by Surveyor V itself, have demonstrated that the expected marking range is affected significantly by only two parameters, according to the well-documented equation:

$$R_m = R_o + (2.02 \times 10^{-4})\,\varphi - (1.01 \times 10^{-4})\,\varphi^2$$

The operational parameter is the angle φ, the incidence angle in degrees off the local lunar vertical of the AMR beam at its intersection with the lunar surface. The equipment parameter is the value R_o, which is the expected

marking range at vertical incidence characteristic of the specific AMR hardware aboard each spacecraft. The result R_m is the expected marking range in statute miles.

The value R_o is determined for each AMR as the measured gate setting (leading edge of late gate) minus the nominal analytical value of range bias at vertical incidence; the latter is equal to 12.20 microseconds. The former is measured in test.

The Surveyor V AMR (283827-1, S/N 14) gate setting was 657.2 microseconds. The R_o value was therefore:

Gate (measured)	657.2	microseconds
Bias (analytical)	- 12.2	microseconds
R_o	= 645.0	microseconds
	= 60.07	statute miles

(at 10.737 microseconds per round-trip statute mile)

The trajectory reconstruction for AGC evaluation (Figure 5.8-3) showed an incidence angle of 47.44 degrees at the time of the mark. The expected marking range for Surveyor V was therefore 59.85 statute miles.

5.8.4.6 Marking Range Dispersion

The standard budget of allowances for in-flight drifts of AMR parameters that affect marking range at any incidence angle has been documented as a rss total of ±893 feet, 3σ.

From a model of AMR cumulative probability (Reference 1) of successful marking, the spread from 0.001 to 0.999 probability is ±1250 feet at 45 degrees. The allowable pointing error (3σ) contribution is ±3220 feet at 45 degrees.

The total (rss) marking range dispersion at 45 degrees is therefore ±3570 feet (3σ), well within the specified maximum of ±1.0 mile (3σ) at 45 degrees. (For perfect pointing error compensation in the guidance and trajectory programs, the actual dispersion would be only ±1540 feet (3σ) at 45 degrees.)

At the Surveyor V velocity of 8440.9 fps at the time of the mark, the total dispersion of ±3570 feet (3σ) would be a time error of ±0.424 second (3σ). By coast phase orbit determination from earth tracking, the a priori mark time uncertainty has been reported as 0.8 second (1σ), or almost six

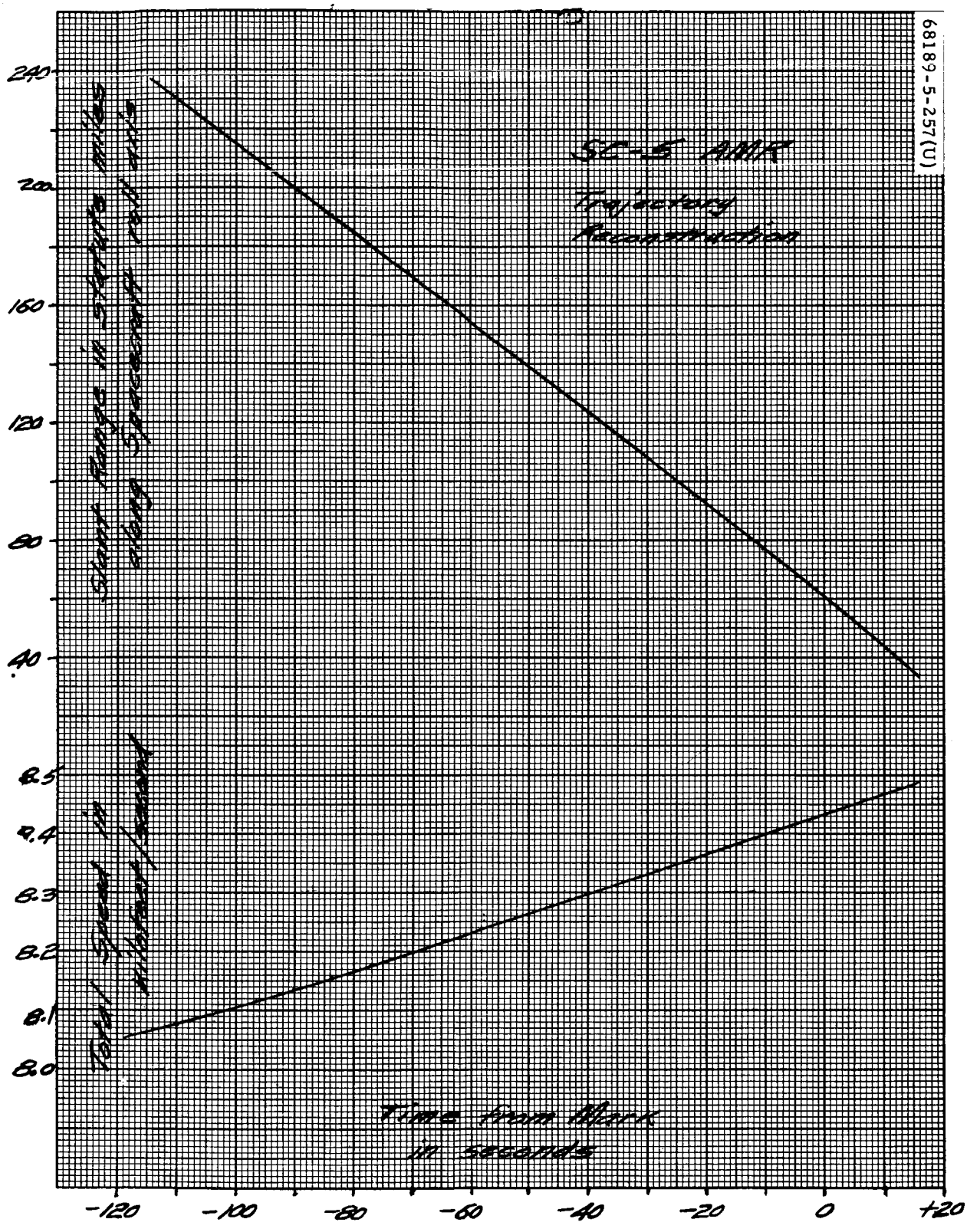

Figure 5.8-3. Trajectory Reconstruction (AMR)

times larger. Hence, while orbit determination provides excellent velocity data, integration into position is less accurate, and the predicted value of expected marking range remains the best available estimate of actual conditions.

5.8.4.7 AMR Parameter Reconstruction

Because of the significant distance traveled during the nominal 100 seconds of enabled operation, the AMR parameters during this interval are evaluated accurately as functions of time and of the mission variables. This is done by a separate computer program developed for this purpose.

Trajectory constants are found from conditions at mark and/or at engine ignition. Velocity, velocity angle, and attitude angle are supplied by FPAC; slant range at mark is the predicted expected marking range. All quantities are then evaluated analytically without approximation at each of a number of two-body trajectory points determined by stepping speed in arbitrary increments. Negative increments of speed produce a backward extrapolation from mark, or from ignition to enable. The only approximation used is for the time interval between trajectory points, which assumes linearized distance and velocity between points. Adequate time accuracy results with the -20 fps increments normally used.

Of particular interest are the AMR slant range, the beam incidence angle at the surface, and the accompanying received pulse stretching effect (Figure 5.8-4). The latter is seen to vary quite significantly because of slant range variation over a dynamic range of about two octaves. Despite variation of both flight path and attitude angles relative to instantaneous local lunar vertical, however, the beam incidence angle remains remarkably constant as a result of the constant inertial attitude of the spacecraft in this phase.

The Surveyor V trajectory conditions supplied by FPAC were as follows:

	At Mark	At Vernier Ignition
Velocity angle, degrees	44.63	45.05
Attitude angle, degrees	43.70	44.27
Speed, fps	8440.9	8477.1

From these, it was determined that the AMR beam incidence angle was 47.44 degrees at mark, and varied less than 0.02 degree throughout the enabled time. Because of the unusually long 12.33-second delay time, Surveyor V AMR evaluation has been extended beyond the mark to ignition.

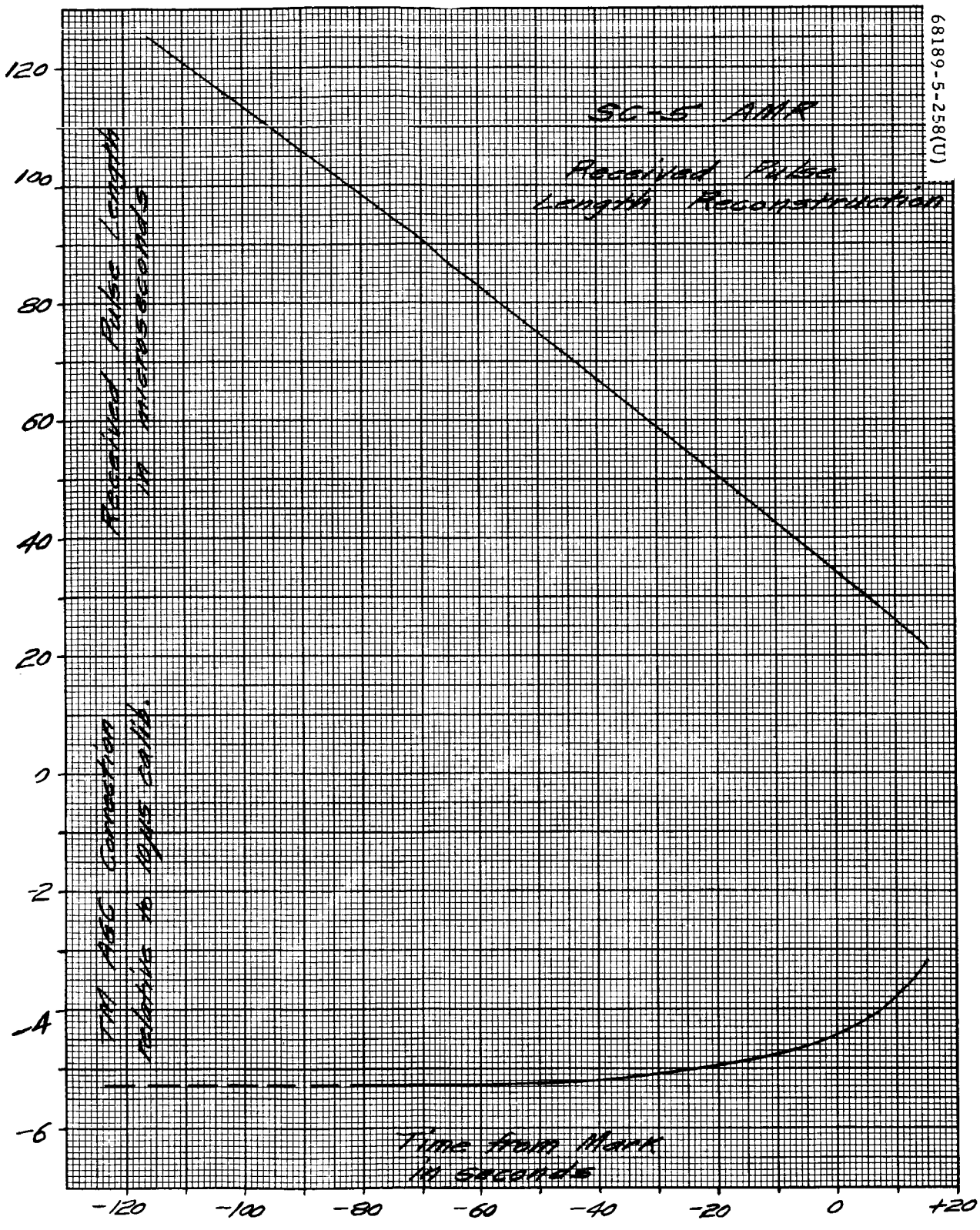

Figure 5.8-4. Received Pulse Length Reconstruction (AMR)

5.8.4.8 AMR AGC Evaluation

The original standard test conditions of 3, 10, and 30 microseconds for preflight AGC calibration (Figure 5.8-5) encompass approximately the region of stretched pulse lengths as received over the required range of A-21 approach angle (0 to 45 degrees) at the nominal marking range. The AGC response curves are nonlinear, however, and intermediate values are helpful for proper interpolation of a given approach angle even at the marking range. In addition, because of the appreciable variation in received pulse length during enabled operation prior to the mark, particularly at angles of more than several degrees, proper AGC interpretation at times other than the mark requires extended AGC calibration. The analysis was fully documented for Surveyor III (Reference 2).

Extended AGC calibration for Surveyor V is shown herein (Figure 5.8-6). The stretched pulse length as received is also shown (Figure 5.8-7), and has been applied in the interpretation of AGC telemetry data (Figure 5.8-8). It should be noted that for the first approximately 60 seconds the AMR receiver was in its linear range, below the onset of AGC action, and that the AGC voltage was therefore at its quiescent level. (This behavior is distinctly different from that of the RADVS reflectivity signals, which detect the IF signal itself, with no AGC involved.) It is seen that Surveyor V showed excellent correlation of the interpreted AGC response with the proper nominal model.

5.8.5 REFERENCES AND DOCUMENTATION

1) S. Thaler, "The AMR – Predicted Performance," Hughes IDC 2729.1/11, 29 March 1965.

2) "Surveyor III Flight Performance," Hughes Aircraft Company, SSD 68189-3, July 1967.

3) I. Holtzman, "AMR Marking Range Bias as Function of Angle of Incidence," Hughes IDC 2253.3/294, 13 May 1965.

4) R.A. Dibos, "Post-Mission Analyses Involving Radar Data," (unpublished), 25 March 1966.

5) Lincoln Laboratory, "Radar Studies of the Moon," Quarterly Report No. 2, 15 May 1966, p. 11.

6) R.A. Dibos, "Radar Performance Evaluation," SC-1 Symposium (NASA at JPL), September 1966.

7) "Surveyor I Flight Performance," Hughes Aircraft Company, SSD 68223R, Vol. III, October 1966.

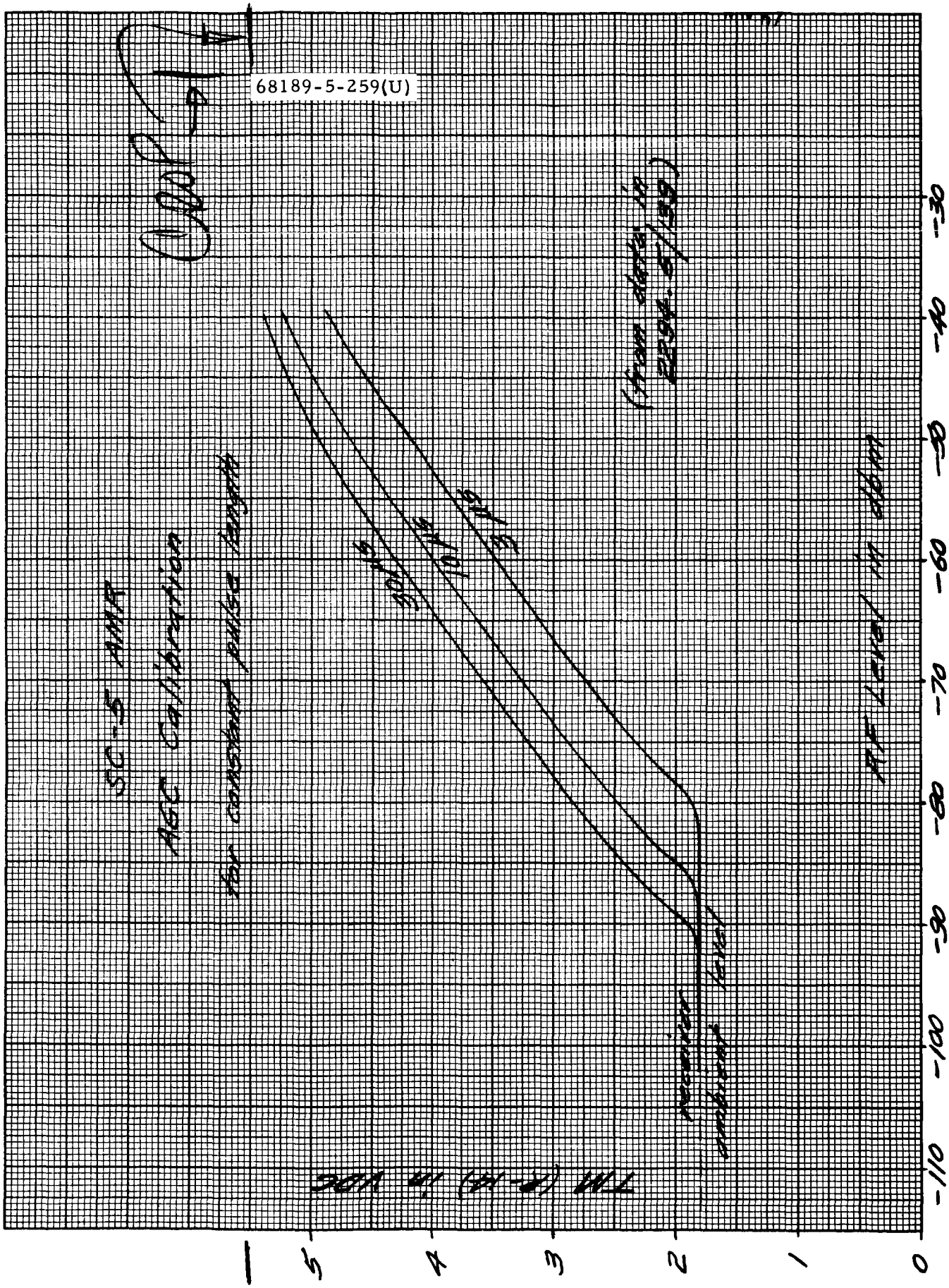

Figure 5.8-5. AGC Calibration for Constant Pulse Length (AMR)

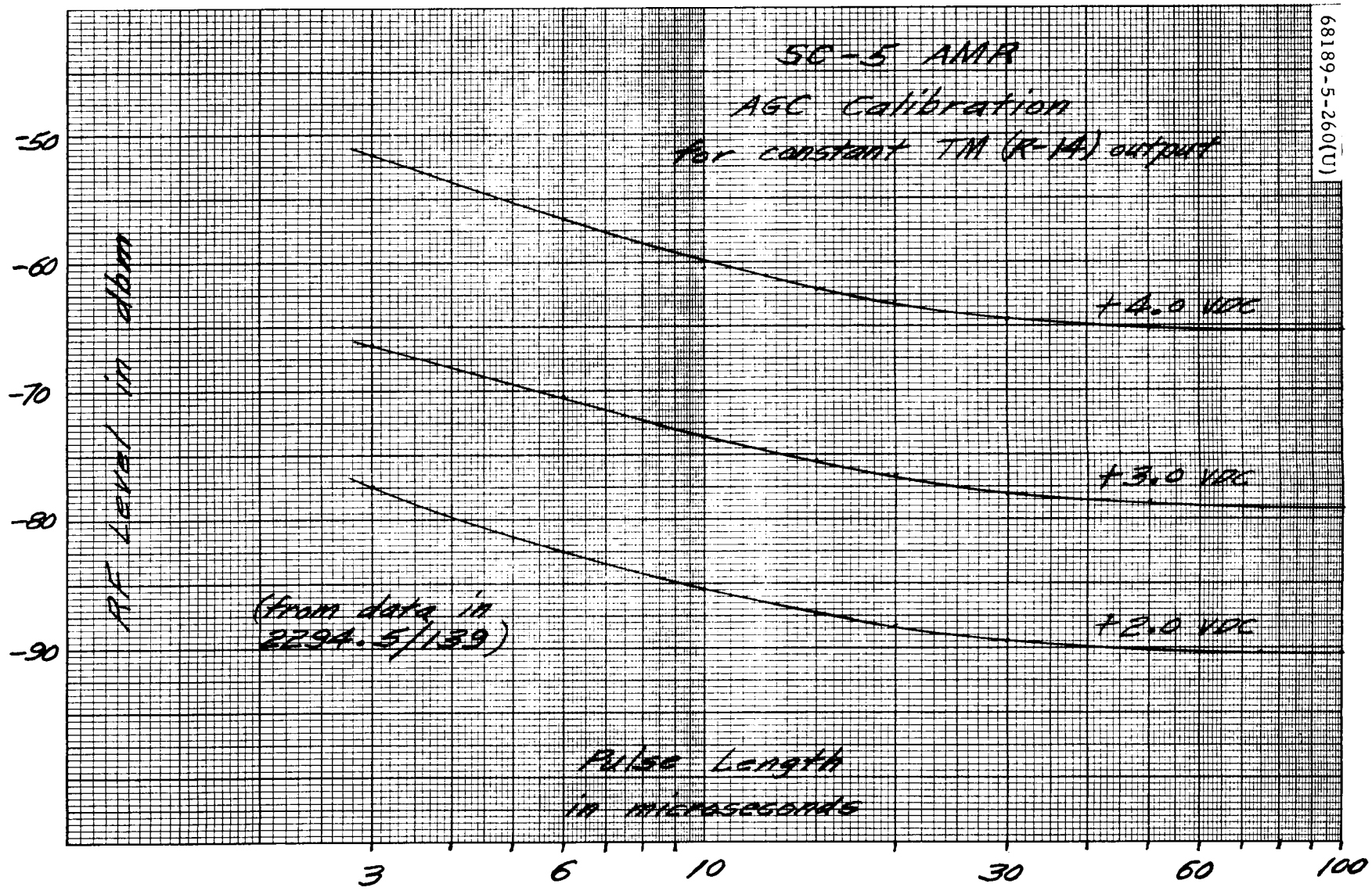

Figure 5.8-6. AGC Calibration for Constant Telemetry (R-14) Outputs

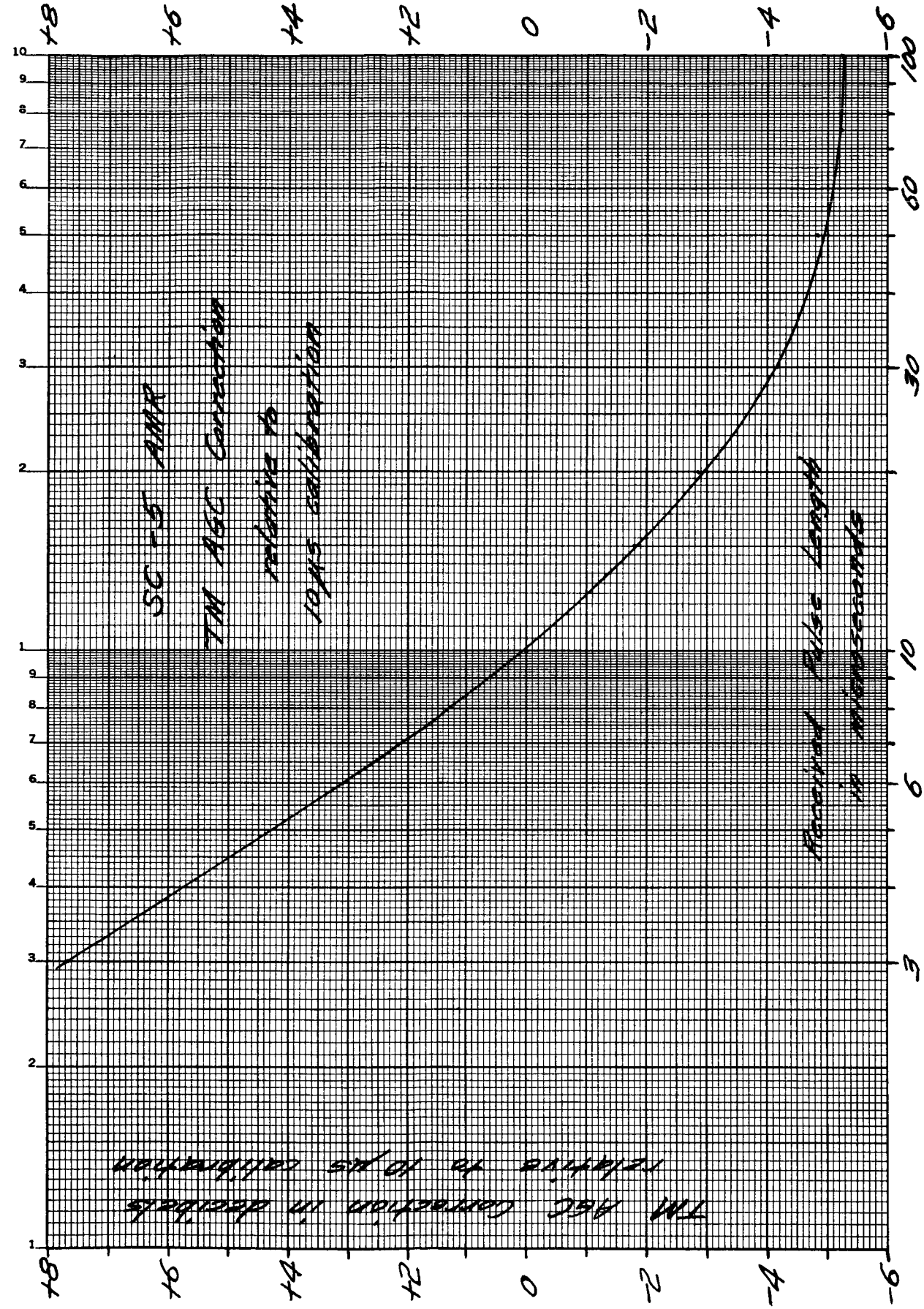

Figure 5.8-7. Telemetry AGC Correction Relative to 10-Microsecond Calibration

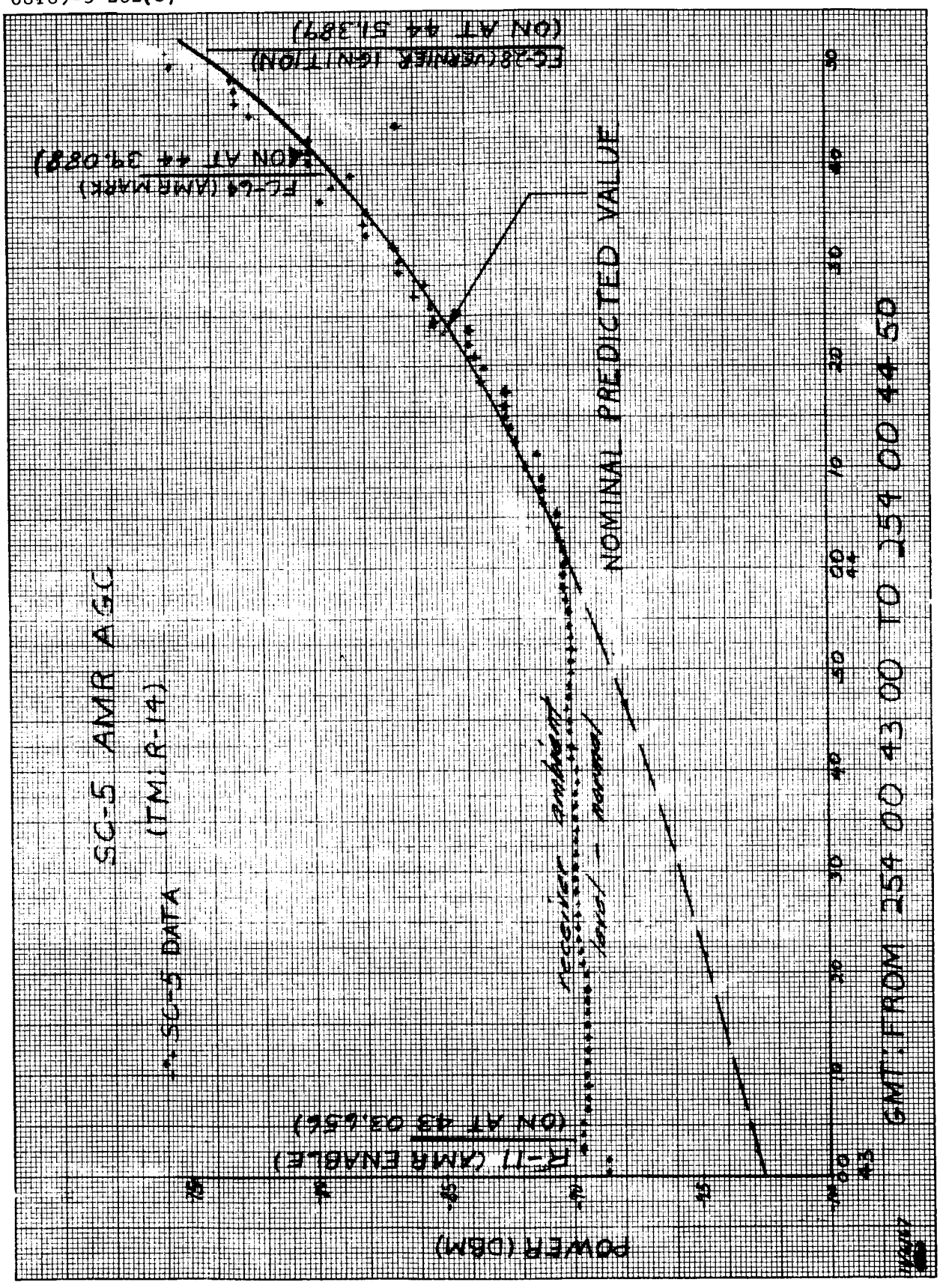

Figure 5.8-8. AMR AGC (TM:R-14)

8) R. A. Dibos, "Preliminary Study of AMR at Large Angles," (unpublished IDC), 4 November 1966.

9) "Decibel Allocation and Margin Summary," Hughes Aircraft Company, SSD 4021R-2, 28 November 1966.

10) R. A. Dibos, "AMR Test Data Required for Analyses," Hughes IDC 2253. 4/71, 20 March 1967.

11) R. A. Dibos, "SC-3 AMR (S/N-15) Predictions," Hughes IDC 2253. 4/79, 10 April 1967.

12) R. A. Dibos, "TM Mode 6 Data Relating to Radar Performance," Hughes IDC 2253. 4/84, 15 June 1967.

13) R. A. Dibos, "AMR AGC Post-Mission Evaluation," Hughes IDC 2253. 4/88, 27 June 1967.

14) "Surveyor IV Flight Performance," Hughes Aircraft Company, SSD 68189-4, September 1967.

15) W. T. Black, "SC-5 AMR Marking Accuracy," Hughes IDC 2294. 5/133, 1 September 1967.

16) F. K. Rickman, "SC-5 AMR Marking Range Data," Hughes IDC 2292/383, 6 September 1967.

17) J. Sikola, "SC-5 Radar Calibration Data," Hughes IDC 2294. 5/139, 26 September 1967.

5.8 6 ACKNOWLEDGMENTS

Calibration data were supplied by W. T. Black and J. Sikola. Telemetry data in raw counts were supplied by R. H. Leuschner and W. McIntyre.

Guidance and trajectory data were supplied by L. H. Davids and T. L. Parker of FPAC.

Trajectory reconstruction and AGC evaluation were performed by M. R. Weiner.

This section was technically coordinated and written by R. A. Dibos.

5.9 RADVS PERFORMANCE

5.9.1 INTRODUCTION

The radar altimeter and doppler velocity sensor (RADVS) is a coherent CW microwave radar designed and supplied by Ryan Electronics, San Diego. Its primary function is to measure velocity and slant range relative to the lunar surface during the terminal descent of the Surveyor spacecraft. These quantities are measured directly in spacecraft coordinates, allowing direct utilization by the spacecraft flight control system for both attitude steering and deceleration thrust control.

The doppler velocity sensor (DVS) portion of the system is essentially a three-beam coherent CW autodyne doppler radar. A single klystron (two-cavity type) provides undeviated output at a nominal frequency of 13,300 MHz. Its output is divided equally among the transmitting horns for beams 1, 2, and 3. Each beam has a separate receiving horn, with adequate RF isolation against direct leakage, and a separate and independent receiver utilizing a small sample of the transmitted signal as a local oscillator (bias). Associated with each receiver is a separate and independent frequency tracker capable of acquiring and tracking the doppler signal corresponding to that component of velocity associated with the spacecraft orientation of that particular beam. The spacecraft beam orientations are such that the nominal velocity components V_i ($i = 1, 2, 3$) along the axes of these three beams are determined by the spacecraft coordinate components of velocity according to the matrix multiplication:

$$\begin{pmatrix} V_1 \\ V_2 \\ V_3 \end{pmatrix} = \begin{pmatrix} +A & +A & +B \\ -A & +A & +B \\ -A & -A & +B \end{pmatrix} \begin{pmatrix} V_x \\ V_y \\ V_z \end{pmatrix}$$

where

$$A = \sin 45 \text{ degrees} \sin 25 \text{ degrees} = 0.29884$$

$$B = \cos 25 \text{ degrees} = 0.90631$$

PRECEDING PAGE BLANK NOT FILMED.

and the spacecraft coordinates are a Cartesian right-handed triad with +z along the roll axis in the normally descending direction.

The frequency outputs of these three frequency trackers are properly scaled and summed in three converters whose outputs are analog voltages representing the spacecraft velocity components:

$$V_x = \frac{V_1 - V_2}{2A} \; ; \quad V_y = \frac{V_2 - V_3}{2A} \; ; \quad V_z = \frac{V_1 + V_3}{2B}$$

The radar altimeter (RA) portion of the system is basically a single-beam coherent FM-CW microwave radar altimeter. Beam 4, fixed along the spacecraft +Z axis, also contains separate transmit and receive horns, a fourth receiver, and a fourth frequency tracker. The same kind of transmitter-derived local oscillator (bias) signal configuration is used, but the RA uses a reflex klystron whose frequency is sawtooth deviated in standard FM-altimeter fashion. The operating portion of the sawtooth has negative slope (with time) to avoid any range-velocity ambiguities. The beam 4 receiver and frequency tracker therefore operate at a frequency which is the sum of scaled slant range and scaled doppler velocity inevitably appearing along that beam. The RA converter corrects the frequency output of the beam 4 tracker by a properly scaled term (V_Z compensation), obtained from the DVS V_Z converter, to provide an analog output voltage proportional to R_Z, the slant range along the spacecraft +Z axis. (The nominal RA operating frequency is 12, 900 MHz. Deviation is nominally 40 MHz at 8000 MHz/sec below 1000 feet, and 4 MHz at 800 MHz/sec above 1000 feet.)

Each receiver is actually two parallel receiving channels, each with separate microwave mixers and audio preamplifiers. Microwave mixer signal and bias inputs are phased so that the parallel audio channels are essentially in phase quadrature, and with equal amplitudes, for all normal doppler signals. Each frequency tracker uses these quadrature audio signals to single-sideband modulate an internal reference signal held at 600 kHz, thus reproducing doppler frequencies unambiguously. In Surveyor, this serves primarily to reject negative velocity at tracker IF, thereby preserving the sense of the velocities. (In a more general application, this would permit measuring negative and positive beam velocities including the unwanted radar return from the main retro engine after separation from the spacecraft.) Each frequency tracking loop is closed by a voltage controlled oscillator whose frequency is controlled by a discriminator-integrator combination, whose output is a direct measure of the frequency being tracked.

To preserve the high degree of both amplitude and phase balance between the parallel quadrature channels of each receiver over the full dynamic range of signals and over the region of operating temperatures, the preamplifier gains are switched in discrete steps by wideband (at audio) gain-switching threshold circuits. Automatic gain control is <u>not</u> used. A set of discrete outputs is provided and telemetered to indicate the gain state of each receiver, as follows:

	Gain Switch 1	Gain Switch 2
High gain (DVS, 90 db; RA, 80 db)	Off	Off
Mid gain (DVS, 65 db; RA, 60 db)	Off	On
Low gain (DVS and RA, 40 db)	On	On

Other discrete outputs are also provided and telemetered. One is a confirmation of application of prime power. This initiates a warmup interval ended by an internal timer which applies high voltage to both klystrons. A set of tracker-lock signals indicates the search or track status of each of the four frequency trackers. A reliable operate doppler velocity sensor (RODVS) discrete indicates, both prior to 3.5 g + 3.7 seconds and subsequent to the 1000-foot mark, that all three DVS beams are locked; between these two times (in Surveyor IV and subsequent spacecraft), it indicates that any one or more of the DVS beams is locked. RODVS causes the flight control to switch attitude steering inputs from gyros to lateral velocities. A RORA (reliable operate radar altimeter) discrete is on when and only when beams 1, 3, and 4 are locked, thus providing reliable V_Z and R_Z for the flight control acceleration control loop. From the analog range output, the RADVS itself derives and supplies two discrete range mark signals, one at 1000 feet (used to change flight control loop parameters), and the other at 12 feet (used to cut off vernier engines).

The latter is termed the 14-foot mark for RADVS purposes, since it is measured from the RADVS antenna boresight reference, which is 24 inches above the legs-extended position of the landing pads on the spacecraft structure (whose position at vernier engine cut off, in turn, has been used in landing stability analyses).

The RADVS hardware is packaged in five units, each of which is a control item in Hughes Spacecraft Configuration Control. Since temperature is measured separately for most of these units, their basic composition is indicated below:

A/VS antenna	— beams 1 and 4 antenna, mixer, and pre-amplifier components
DVS antenna	— beams 2 and 3 antenna, mixer, and pre-amplifier components
Klystron power supply modulator (KPSM)	— includes all components for both DVS and RA
Signal data converter	— all frequency trackers and data converters
Waveguide assembly	

5.9.2 ANOMALIES

There were no radar anomalies in the Surveyor V mission. Possibly as a result of the PCM data margin situation described later, the data contain one anomaly in that the RADVS on digital signal (R-28, bit 6 of digital word 3) went off at vernier engine cutoff at the 14-foot mark. Radar current (EP-17) properly remained high until after touchdown, indicating that the R-28 indication was fallacious.

The entire Surveyor V terminal descent was so nonstandard that a general discussion is included in Appendix A to this section. It should be recognized that the real-time redirection was to a "revised nominal" vastly different from a standard mission, and that performance is therefore evaluated relative to this revised nominal.

The unlock of beam 4 following retro separation is attributed to brief interruption by the separating retro case, as was experienced by both beam 4 of Surveyor III and beam 3 of Surveyor I.

The unlock of beam 3, virtually concurrently with the relock of beam 4 and just after the start of steering, is attributed to steering action causing beam 3 in turn to sweep across the receding but still close retro case. The duration of the beam 3 unlock and the apparently strange data at its inception posed a particularly interesting problem whose analysis, presented later in this section, explains how multiple radar actions were perfectly normal, given only a retro case interruption. CRO steering worked as intended and actually helped to reduce steering time, which was critical.

5.9.3 SUMMARY AND RECOMMENDATIONS

5.9.3.1 Summary

1) All DVS beams locked during retro at their upper sweep limits, as is normal and as has been experienced in all prior missions (except Surveyor 2).

2) Since the only DVS unlock (after initial acquisition) was after delayed burnout (3.5 g to 3.7 seconds) and before the 1000-feet mark, the RODVS signal was properly on from initial lock to touchdown, in accordance with the logic modification accompanying engineering charge proposal (ECP-23) in Surveyor 4 and up. (RODVS = D1 · D2 · D3 before delayed burnout and after 1000 feet. RODVS = D1 + D2 + D3 after delayed burnout and before 1000 feet.)

3) Beam 4 (RA) acquired at about 16,000 feet slant range, because this was its upper sweep limit at the still very high velocity during retro. This appears quite normal, occurring about 3.5 seconds after DVS acquisition (normally at about 3300 fps) and still more than 7 seconds before 3.5 g, hence near maximum retro deceleration. Since beams 1 and 3 were already locked, RORA also properly appeared. (RORA = D1 · D3 · R at all times.)

4) Spacecraft trajectory conditions at retro separation were approximately the following:

From FPAC

ϕ = 45.7 degrees ρ = +4.9 degrees

From TM data

R_z = 6400 feet h = 4500 feet

V_x = -35.8 fps V_1 = +60.8 fps

V_y = +49.8 fps V_2 = +82.2 fps

V_z = +62.5 fps V_3 = +52.4 fps

V_t = 87.5 fps

5) At retro separation, beam 4 gain-switched from GS 3 (80 db) to GS 2 (60 db) and dropped lock, RORA also going off. Relock occurred in one sweep with the return to GS 3. (RORA stayed off, however, because beam 3 unlocked as described later.) This action is normal for a brief interruption by the receding retro case, as in beam 4 of Surveyor III and in beam 3 of Surveyor I.

6) There was also a gain-switch of beam 4 about 2 seconds prior to retro separation. Unlike the one about 6 seconds before separation in beam 4 of Surveyor III, however, this one (in Surveyor V) did not cause a dropout, but appears to have been normal on the lunar signal at Surveyor V's lower altitude.

7) While beam 4 was out, FC-42 occurred and initiated steering, confirmed by thrust commands and the indicated V_y. At FC-42, thrust control switched to the minimum-acceleration phase; with the modified time sequence tape-commanded in Surveyor V, this terminated the 1.5-second interval of maximum thrust (for separation) which had started 0.5 second after retro eject. The direction of initial steering was a significant negative pitch in response to the + V_y, plus some negative yaw in response to the $-V_x$ of smaller magnitude. At Surveyor V's initial attitude, the former was primarily to the right, out of the original trajectory plane, while the latter was primarily downward toward the vertical.

8) Essentially concurrent with the beam 4 relock, beam 3 dropped out and RORA stayed off. The direction of steering suggests, and RADVS analysis presented later strongly indicates, that the receding but still close retro case also interrupted beam 3 as

the latter swept across it in a compound dynamic geometry almost impossible to reconstruct precisely. All available data support this hypothesis, however, and none has been found to refute it. Further, it is not only physically reasonable, but is also adequate, to explain fully certain RADVS data otherwise physically impossible without a most unlikely multiple anomaly situation at just the right time and with just the right duration, a combination too improbable to be seriously considered.

9) DVS beams 1 and 2 maintained lock from initial acquisition to touchdown. This in not only indicated by all once-per-frame lock signals, but is also confirmed by every available four-times-per-frame value of V_x, which was continuous and regular throughout the descent.

10) The beam 3 dropout was neither a mainlobe rejection by ECP-23 nor a momentary crosslobe acquisition followed by rejection; the Surveyor V geometry precluded both possibilities.

11) During all but the leading edge of the beam 3 unlock, indicated values were normal for the CRO mode. The "plateau" of artificially high indicated V_y for nine successive data samples was normal for D3 = 0 and really denotes a V_2 of around 80 fps. During this interval, V_z was artificially low at essentially half its true value, also normal for D3 = 0, and indicated R_z was slightly high because of the velocity compensation effect. The virtually constant indicated V_y implies a nearly constant V_2, hence an angle of beam 2 with the total velocity vector whose consine is changing little.

12) At the leading edge of the beam 3 unlock interval, however, three successive data samples of both indicated V_y and indicated V_z, too systematic to have constituted six related double-parity errors (no single parity indicated), comprised a special situation described in the next section. Given only the retro case interruption hypothesized, RADVS action is explainable in terms of its actual design.

13) There was no possibility of flight control attitude loop instability at the very low velocities involved, even with saturated lateral velocities during CRO (as occurred in V_y). This was essentially the only favorable factor in the Surveyor V real-time analysis of descent conditions.

14) CRO steering operated as intended and probably aided the successful descent. The increased steering rate during CRO reduced the steering time to a significantly out-of-plane velocity angle at burnout (still a relatively small dispersion at the revised nominal conditions), thus saving critical steering time.

15) The 1000-foot mark occurred at about 1040 feet (1090 feet indicated, with TM lag), within normal tolerances.

16) Segment acquisition was at about 800 feet (850 feet indicated, with TM lag), and at about 98 fps.

17) The 14-foot mark and vernier engine cutoff occurred within normal tolerances (1.7 seconds free-fall versus 1.4 seconds nominal).

5.9.3.2 Recommendations

There are no recommendations arising directly from the Surveyor V mission.

5.9.4 SUBSYSTEM PERFORMANCE ANALYSIS

5.9.4.1 RADVS Turnon

RADVS power on occurred properly, within a second of retro ignition, as confirmed by EP-33, R-28, EP-17, and the altimeter search sweep pattern in FC-35. Subsequent time-in of the high voltage occurred approximately 21 seconds later, as indicated by EP-17 (Figure 5.2-6), a normal internal delay.

5.9.4.2 Velocity Acquisition Conditions

All three beams of the doppler velocity sensor (DVS) acquired and commenced tracking lunar reflected signals as soon as they came within each tracker's acquisition sweep frequency limits. From the 6DOF computer program reconstruction, conditions at initial acquisition for each beam are shown in Table 5.9-1. Assuming conditions at the most probable tracker lock times, whose telemetry time accuracies are ±0.6 second, or about ±140 fps in beam velocities.

Spacecraft conditions at the time of RODVS (all DVS beams locked, and converters reporting reliable V_x, V_y, and V_z), again from the 6DOF program reconstruction, were as follows:

V_x = +30.7 fps

V_y = +27.0 fps

V_z = +3332 fps

Range = 26,200 feet

Attitude = 45.58 degrees

Altitude = 18,310 feet

TABLE 5.9-1. CONDITIONS AT INITIAL ACQUISITION

Beam	Slant Range Along Beam, 1000 feet	Velocity Component Along Beam, fps	Beam Incidence Angle, degrees	Doppler Frequency, kHz	Upper Search Limit, kHz
1	41.2	2992	63.91	81.06	≈85
2	24.1	3251	30.07	88.14	≈85
3	22.6	3026	34.02	82.18	≈85

again assuming conditions at the most probable time of RODVS, whose telemetry time accuracy is also ±0.6 second.

5.9.4.3 Range Acquisition Conditions

From telemetry and terminal descent 6DOF program reconstruction, conditions at the time of range tracker lockon and RORA were:

V_x = +20.9 fps

V_y = +33.3 fps

V_z = +2349 fps

Range = 16,220 feet

Attitude = 45.65 degrees

Altitude = 11,330 feet

Altimeter frequency = 88.4 kHz

Upper sweep limit ≈ 91 kHz

again assuming conditions at the most probable time, whose telemetry accuracy is also ±0.6 second.

5.9.4.4 Beam Drop-outs

The unlock of beam 4, followed by relock within one sweep interval, occurred virtually at retro separation and is attributed to interruption by the receding retro case. This and related gain switching events have already been described in (subsection 5.9.3.1).

Also referred to and discussed in general terms in both subsections 5. 9. 2 and 5. 9. 3. 1 is the unlock of beam 3 at virtually the same time as the relock of beam 4, also described as caused by retro case interruption induced by the activation of steering. It is the purpose of this section to review and eliminate alternative interpretations of the data.

The duration of the beam 3 unlock appears to be two sweep intervals, suggesting two events, since case interruptions (especially during steering) normally last for only one sweep. Apparent candidates are a case interrupt and/or one or two mainlobe rejections by ECP-23. Tracker starvation by excessive rolloff at low velocity is precluded by the beam 3 velocity component at separation and by the direction of steering which increased its component rather than reducing it.

Just before the beam 3 unlock, the reflectivity signals indicate levels near -90 dbm on beam 1, -80 dbm on beam 2, and -85 dbm on beam 3, all of which correlate well relative to their nominal relationships. The beam 2 and 3 difference of about -5 db is still some 11 db from K_{23} = -16 db in equal states, in ECP-23. (K_{23} = -25 db in unequal states, but both of beams 2 and 3 were in GS 2 (65 db state) at this time.) The beam 1 and 3 difference of about +5 db is some 30 db from K_{13} = -25 db in all gain state combinations. It is apparent, therefore, that beam 3 was not rejected even once by ECP-23, and that there were no mainlobe rejections of any beam by ECP-23 in Surveyor V.

Actually, the smallest margin in Surveyor V was the beam 2 and 1 difference of about -10 db against K_{21} = -18 db in equal gain states. This was recognized as discussed in subsection 5. 9. 2, and proved to be adequate in the descent.

Since the beam 3 dropout followed the start of steering, and since the direction of steering was largely out-of-plane to the right, it is physically logical that beam 3 actually was swept across the receding retro case. Certain radar data remain to be explained.

The "plateau" of nine successive words of V_y during the beam 3 out interval is a normal CRO condition, since then

$$\tilde{V}_y = \frac{V_2 - 1.48}{0.59768}$$

instead of the usual

$$V_y = \frac{V_2 - V_3}{0.59768}$$

Associated with this is:

$$\tilde{V}_z = \frac{V_1 + 1.48}{1.81262}$$

instead of the usual

$$V_z = \frac{V_1 + V_3}{1.81262}$$

and also an increase in indicated slant range because of the inadequate V_z compensation.

At the start of this interval, however, a leading edge spike shows values larger than those associated with the above CRO values. This had no effect on the flight control system since even the $\tilde{V}_y$ plateau was into the flight control signal limiting action, and the spike was levelled off also for steering action purposes.

The explanation of RADVS behavior during this interval is as follows. As beam 3 swept across the receding retro case, the lunar signal (at 1300 Hz) was shadowed and/or the case reflection in the noise sampling filter (then centered at -100 Hz) conspired to starve the threshold detector, which went low. The dual time constant (0.2 second before drop lock) maintained the lock signal (R-17) and the search inhibit; in this interval, the tracking loop is still closed, has a natural negative drift, and can and should have very quickly acquired the negative doppler retro case signal.

This is not at all the same thing as retro case acquisition in the search mode. In search, the tracking loop is open, a search function sawtooth sweep voltage is applied to the VCO, and this resets (flyback) at 800 Hz. Even at this lower sweep limit, there is significant negative doppler discrimination inherent in the signal filter bandpass characteristics, the basic single-sideband design of the system, and the noise sampling filter in the acquisition control.

With search still inhibited, however, there is no sweep voltage and hence no reset (flyback). The VCO is still driven in closed-loop tracking by the discriminator-integrator combination. The zero signal closed loop is not static, however. It has an inherent negative drift at an initial rate of almost 60 kHz/second. This arises from the integrator time constant of 18.45 seconds, and from the VCO tune-line design characteristics of 100 kHz/volt about a reference of 11 volts. (The 400 kHz/volt at 2.4 MHz is also effectively counted down to 100 kHz/volt at 600 kHz.)

During the 0.2-second dropout time, the inherent zero-signal integrator drift in the zero doppler region is:

$$(11.0 \text{ volts})(e^{-\frac{0.2}{18.45}} - 1)(100 \text{ kHz/volt})$$

$$= (1000 \text{ kHz})(0.98922 - 1) = -11.86 \text{ kHz}$$

Therefore, to drift from 1300 Hz to 0 requires only 0.1096 of the 0.2 second provided by the dual time constant circuit.

It is postulated that the beam 3 tracker therefore jumped to the negative doppler retro case signal and essentially maintained its lock status, on that signal, at least briefly. Three successive telemetry samples of both V_y and V_z are associated with this action at the leading edge of the unlock interval, or more correctly just prior to it. These three words represent two data intervals of 0.3 second each. In 0.6 second, at the CRO saturated steering rate, the beam 3 beamwidth would have effectively crossed the retro case.

This interval is more than adequate for the threshold detector, quickly returned to high by the case signal, to reset the dual time constant circuit before it timed out after loss of lunar signal. Hence, the effective dropout of the tracking loop did not start until the retro case signal lost lock as a result of spacecraft steering (continuous in this region) and inverse fourth power range decay of the case signal. (Range decay is only partially effective because increased velocity causes reduced rolloff in the preamplifiers, which individually are insensitive to algebraic sign of the doppler frequency.)

When the case signal is lost, the threshold detector again went low and started another 0.2-second dropout time constant. In this situation, the lunar signal (now returning) would appear in the upper image of the noise sampling filter and may have aided the loss of the case signal. The zero signal closed-loop drift would now drive the tracker away from the lunar signal in frequency, preventing its immediate reacquisition. Thus, the zero-signal closed loop can snap quickly downward (as from the moon to the case) but is virtually incapable of snapping quickly upward (from the case back to the moon) to a signal already within its noise sampling filter.

During this second dual-time constant interval, there is no new signal (subject to the above) to prevent time-out of the full 0.2 second. Starting from a low but already negative doppler, the zero signal closed-loop natural drift would carry the tracker algebraically below -12 kHz before the search inhibit and the tracker lock signal are removed. Two additional factors are significant to the timing of these events.

During the closed-loop mode, the tracker special logic uses the tracker lock signal as the command to supply VCO frequency to the arithmetic converters, thus producing the leading edge spike V_y and V_z values actually observed. Not until time-out of the 0.2 second is the lock signal off, after which the special logic sends zero-doppler (600 kHz) reference to the converters, producing the CRO plateau values previously noted. Simultaneously, the reset function is inactive during the search inhibit (closed-loop) mode, and becomes active with the removal of the search inhibit. The reset detector uses a low-pass filtered output of a mixer, fed by 600 kHz and by VCO frequency, without regard to phase; hence, the reset should occur for any tracker frequency between -800 Hz and +800 Hz. With the tracker already below -800 Hz when search function is applied, normal reset would not occur.

Having bypassed the usual reset detector, application of sweep voltage drives the tracker still more negative in (doppler) frequency. Before beam velocities were constrained by specification to positive values, negative doppler acquisition had been a system requirement. The basic sweep was, designed to carry to -25 kHz before flyback by a -0.25 volt dc (relative to 11 volt dc) tune-line voltage detector. This was not removed when the 800 Hz reset detector was added to the system. Hence, flyback would have occurred from -25 kHz. After flyback, all sweep functions would again be normal, with reacquisition on the downsweep from +23 kHz.

This explains the duration of the beam 3 unlock interval. It was essentially a single sweep of double the normal width, hence constituting a single event – the retro case interruption – rather than multiple events.

One item more in the data needed explaining, and this was the rise in V_z along with the V_y spike. The explanation of this lies in the design of the arithmetic converters. The V_x and V_y converters are true algebraic devices because of the bipolar nature of these quantities. The V_z converter was made simpler, however, since V_z itself is never negative operationally. Study of the design of this converter shows that it actually produces:

$$\tilde{V}_z = \frac{/V_i /+ / V_3 /}{1.81262}$$

rather than the algebraic quantity

$$V_z = \frac{V_1 + V_3}{1.81262}$$

With D_3 more negative than D1 is positive, there is an effective "foldover" in the V_z output. It therefore appears to rise at the same time as the indicated V_y is driven above the CRO level by the algebraic nature of the V_y converter.

The picture appears complete. A single event, retro case interruption is adequate to explain all data points in this interval in terms of RADVS operation as designed. The event itself is not only plausible but almost necessary as a consequence of steering. Any other explanation poses either physically impossible velocity values by conventional data interpretation (including CRO), or a complex highly correlated set of multiple anomalies at just the right times and disappearing again.

5.9.4.5 Revised Nominal db Budget

The db budget for the revised Surveyor V conditions is shown in Table 5.9-2.

TABLE 5.9-2. RADVS INDIVIDUAL BEAM db BUDGETS BEFORE STEERING

Using measured Pt and G values and nominal reflectivity model

For Φ = 45.7 degrees; ρ = + 4.9 degrees; and R_z = 6419 feet

Values	Beam 1	Beam 2	Beam 3	Beam 4
Pt, dbm	+ 33.79	+ 34.35	+ 33.87	+ 24.64
G, db	+ 28.55	+ 28.45	+ 28.50	+ 28.05
(1/2), db	- 3.01	- 3.01	- 3.01	- 3.01
λ^2, db	- 22.64	- 22.64	- 22.64	- 22.36
$(4\pi)^{-2}$, db	- 21.98	- 21.98	- 21.98	- 21.98
(4.48 kilofeet)$^{-2}$, db	- 73.03	- 73.03	- 73.03	- 73.03
$\cos^2 \theta i$, db	- 7.18	- 1.27	- 1.64	- 3.12
$F(\theta i)$, db	- 13.16	- 10.01	- 10.67	- 12.12
$\eta(K/\alpha^3)$, db	- 1.72	- 1.72	- 1.72	- 1.72
Sum of + values	+ 62.34	+ 62.80	+ 62.37	+ 52.69
Sum of - values	-142.72	-133.66	-134.69	-137.34
P_r, dbm	- 80.38	- 70.86	- 72.32	- 84.65
θi, degrees	64.0	30.2	34.1	45.7
$\sigma(\theta)$, db	- 14.88	- 11.73	- 12.39	- 13.84
R, kilofeet	10.21	5.19	5.41	6.42

5.9.4.6 TM Mode 6 Data Word Summary

Tables 5.9-3, 5.9-4, and 5.9-5 are PCM telemetry data related to radar performance.

Additions to GMT at start of frame are shown for digital data; these are used to correct for word and bit location at 1100 bps. Events will normally be interpolated as occurring midway between last off (or on) and first on (or off), plus or minus half the sampling interval. Because of their short time constants and frequent reversals (only some of which are observed), gain states normally will be indicated only as at the actual times of sampling.

Additions to GMT at start of frame are not shown for analog data, but are being treated as 0.010 second times the commutator word number for analog values at 1100 bps.

TABLE 5.9-3. SELECTED DIGITAL DATA, SAMPLED ONCE PER FRAME

	TM Mode 6	At 1100 bps, Add Seconds to Start of Frame
Digital word 2	Commutator word 53	Computer ID 12
(bcd) FC-18	Magnitude register	(+0.530)
Digital word 3	Commutator word 13	Computer ID 13
Bit 4 FC-66	Thrust phase power on	(+0.124)
Bit 6 R-28	RADVS on	(+0.126)
Bit 10 FC-28	Vernier ignition	(+0.130)
Digital word 9	Commutator word 83	Computer ID 19
Bit 5 FC-63	Inertia switch	(+0.825)
Bit 9 FC-33	RORA	(+0.829)
Bit 10 FC-34	RODVS	(+0.830)
Digital word 11	Commutator word 113	Computer ID 184
Bit 8 EP-33	RADVS pyro switches	(+1.128)
Digital word 12	Commutator word 73	Computer ID 21
Bit 3 R-17	D3 lock	(+0.723)
Bit 5 V-4	Retro not ejected	(+0.725)
Bit 6 R-18	R lock	(+0.726)
Bit 7 R-1	AMR on	(+0.727)
Bit 8 R-11	AMR enabled	(+0.728)
Digital word 13	Commutator word 103	Computer ID 185
Bit 1 R-15	D1 lock	(+1.021)
Bit 2 R-19	D1 GS1	(+1.022)
Bit 3 R-20	D1 GS2 or 1	(+1.023)
Bit 4 R-21	D2 GS1	(+1.024)
Bit 5 R-22	D2 GS2 or 1	(+1.025)
Bit 6 R-23	D3 GS1	(+1.026)

Table 5.9-3 (continued)

		TM Mode 6	At 1100 bps, Add Seconds to Start of Frame
Bit 7	R-24	D3 GS2 or 1	(+1.027)
Bit 8	R-25	R GS1	(+1.028)
Bit 9	R-26	R GS2 or 1	(+1.029)
Bit 10	R-16	D2 lock	(+1.030)

TABLE 5.9-4. DIGITAL DATA SAMPLED 12 TIMES PER FRAME

		TM Mode 6	At 1100 bps, Add Seconds to Start of Frame
Digital word 4 Computer ID No. 14 Commutator words 2, 12, 22, 32, . . . , 102, 112 (Let N = 1, 2, 3, 4, . . . , 11, 12)			
Bit 1	FC-62	Retro sequence mode on	+0.011 +0.1 (N-1)
Bit 2	FC-64	AMR mark	+0.012 +0.1 (N-1)
Bit 3	FC-28	Vernier ignition	+0.013 +0.1 (N-1)
Bit 4	FC-29	Retro ignition	+0.014 +0.1 (N-1)
Bit 5	FC-30	Retro burnout	+0.015 +0.1 (N-1)
Bit 6	FC-31	Retro eject	+0.016 +0.1 (N-1)
Bit 7	FC-42	Start RADVS descent	+0.017 +0.1 (N-1)
Bit 8	FC-37	1000-foot mark	+0.018 +0.1 (N-1)
Bit 9	FC-36	10-fps mark	+0.019 +0.1 (N-1)
Bit 10	FC-38	14-foot mark	+0.020 +0.1 (N-1)

TABLE 5.9-5. SELECTED ANALOG DATA, TM MODE 6

		Computer ID No.	Commutator Word(s)
EP-2	Unregulated bus voltage	23	69
EP-17	Radar and squib current	37	49
FC-35	R_z	66	18, 48, 78, 108
FC-39	V_x	67	24, 54, 84, 114
FC-40	V_y	68	25, 55, 85, 115
FC-41	V_z	69	26, 56, 86, 116
FC-77	Reference return	122	99
P-18	Vernier engine 1 strain gauge	108	7, 37, 67, 97
P-19	Vernier engine 2 strain gauge	109	11, 41, 71, 101
P-20	Vernier engine 3 strain gauge	110	28, 88
R-2	Beam 4 reflectivity	113	4, 64
R-3	Beam 1 reflectivity	114	44, 104
R-4	Beam 2 reflectivity	115	14, 74
R-5	Beam 3 reflectivity	116	34, 94
R-8	KPSM temperature	119	10
R-12	AMR magnetron current	132	59
R-14	AMR AGC	124	43
R-29	AMR late gate signal	183	89

5.9.4.7 Surveyor V Event Times

The GMT at DSIF-11 at time of data recording is shown. Table 5.9-6 gives a number of significant spacecraft and related radar events defining the major items in the terminal descent sequence. Table 5.9-7 shows the use of the magnitude register (FC-18) to refine the times of vernier ignition and AMR mark. Table 5.9-8 shows RADVS tracker lock signals and repeated associated spacecraft events. In all of these tables, a signal is shown as going on at a time interpolated between its last absence and its first presence, plus or minus one-half the data sampling interval.

Table 5.9-9 shows every gain state indication at the time of data sampling, except that repeated gain states are deleted. Their presence was confirmed in the data, however, except for data outages as noted.

TABLE 5.9-6. SURVEYOR V EVENTS (EXCEPT TRACKER LOCKS AND GAIN STATES

		GMT: minutes: seconds
R-1	AMR on	40:02.458±0.6
R-11	AMR enable	43:03.656±0.6
FC-64	AMR mark	44:39.088±0.05
FC-28	Vernier ignition	44:51.389±0.05
FC-29	Retro ignition	44:52.490±0.05
FC-64	AMR mark off	44:52.588±0.05
EP-33	RADVS pyro switch	44:53.254±0.6
R-28	RADVS on	44:53.452±0.6
FC-63	Inertia switch off	44:54.151±0.6
FC-34	RODVS	45:20.555±0.6
FC-33	RORA	45:24.154±0.6
FC-63	Inertia switch	45:31.350±0.6
FC-30	Retro burnout	45:31.490±0.05
FC-31	Retro eject	45:40.391±0.05
V-4	Retro ejected	45:40.850±0.6
FC-78	High thrust	45:40.951±0.6
FC-33	RORA off	45:40.954±0.6
FC-78	High thrust off	(parity error)
FC-42	Start RADVS descent	45:42.392±0.05
FC-33	RORA (from EDPLOT)	45:47.000±0.7
FC-37	1000-foot mark	46:19.692±0.05
FC-36	10 fps	46:37.092±0.05
FC-38	14-foot mark	46:42.691±0.05
FC-52	Nominal thrust off	46:42.151±0.6
R-28	RADVS off	46:42.649±0.6
(from P-18)	Touchdown	46:44.397+0, -0.07
FC-33	RORA off	46:44.552±0.6
FC-34	RODVS off	46:46.953±0.6

TABLE 5.9-7. TIMING REFINEMENT

Digital Word 2 — Magnitude Register (FC-18)

GMT	bcd
254:00:44:38.856	247 (stored)
40.056	228
41.256	204
49.656	36
50.856	12
52.056	1012

Vernier ignition at:

44:50.856
0.575 ± 0.025
44:51.431 ± 0.025

Actual delay = 247 bcd
= 12.325 ± 0.025

Clock start at 44:39.106 ± 0.050

FC-64 at 44:39.088 ± 0.050

Actual mark at 44:39.138 maximum
44:39.056 minimum
= 44:39.097 ± 0.041

TABLE 5.9-8. SURVEYOR V RADVS TRACKER LOCK AND RELATED SIGNALS

		GMT minutes:seconds
R-16	D2 lock	45:19.555±0.6
FC-34	RODVS	45:20.555±0.6
R-17	D3 lock	45:20.448±0.6
R-15	D1 lock	45:20.746±0.6
R-18	R lock	45:24.051±0.6
FC-33	RORA	45:24.154±0.6
$\overline{\text{V-4}}$	Retro ejected	45:40.850±0.6
$\overline{\text{R-18}}$	R lock off	45:40.851±0.6
FC-78	High thrust	45:40.951±0.6
$\overline{\text{FC-33}}$	RORA off	45:40.954±0.6
FC-42	Start RADVS descent (at minimum acceleration)	45:42.392±0.05
$\overline{\text{R-17}}$	D3 lock off	45:43.248±0.6
R-18	R lock	45:43.251±0.6
R-17	D3 lock	45:46.846±0.6
FC-33	RORA (from EDPLOT)	45:47.000±0.7
FC-38	14-foot mark	46:42.691±0.05
$\overline{\text{R-28}}$	RADVS off	46:42.649±0.6
(from P-18)	Touchdown	46:44.397±0, -0.07
$\overline{\text{R-18}}$	R lock off	46:44.449±0.6
$\overline{\text{FC-33}}$	RORA off	46:44.552±0.6
$\overline{\text{R-15}}$	D1 lock off	46:45.944±0.6
$\overline{\text{FC-34}}$	RODVS off	46:46.953±0.6
$\overline{\text{R-17}}$	D3 lock off	46:46.846±0.6
$\overline{\text{R-16}}$	D2 lock off	46:47.153±0.6

Table 5.9-9 shows every gain state indication at the time of data sampling, except that repeated gain states are deleted. Their presence was confirmed in the data, however, except for data outages as noted.

TABLE 5.9-9. SURVEYOR V RADVS GAIN STATES AT SAMPLING TIMES

(Omitting intervals with no charge indicated)

GMT: minutes:seconds	Beam 1	Beam 2	Beam 3	Beam 4
45:15.35	3	3	3	3
45:16.55		2		
45:20.15	3		3	
45:21.35	2		2	
45:30.95	2	2	2	3
45:32.15		(parity error)		
45:33.35	3	2	2	3
45:34.55	2			
45:35.75	3			3
45:36.95	2			2
45:38.15	3			2
45:39.35				3
45:40.55				2
45:41.75	3			2
45:42.95	2			3
45:44.15	2			
45:45.35	3			
45:46.55	3	2	2	3
45:47.75		(data outage)		
45:48.1 (EDPLOT)	3	2	2	3
45:48.95		(data outage)		
45:50.15		(data outage)		
45:51.35		(parity error)		
45:52.55	2	2	2	3
45:53.7 (EDPLOT)	2	2	2	3
45:54.9 (EDPLOT)	2	2	1	3
45:56.1 (EDPLOT)	2	2	2	3
45:57.3 (EDPLOT)	2	2	2	3
45:58.5 (EDPLOT)	2	2	2	3

Table 5.9-9. (continued)

GMT: minutes:seconds	Beam 1	Beam 2	Beam 3	Beam 4
45:59.7 (EDPLOT)	2	2	2	3
46:00.9 (EDPLOT)	2	2	2	2
46:02.1 (EDPLOT)	2	2	2	3
46:03.3 (EDPLOT)	2	2	2	3
46:04.55	2	2	2	3
46:15.35			2	3
46:16.55			1	2
46:17.75	2	2	2	
46:18.95	1	1		
46:20.15	2			
46:21.35	1		2	2
46:22.55			1	1
46:23.75				2
46:24.95				2
46:26.15				1
46:28.55				1
46:29.75				2
46:30.95				1
46:32.15				2
46:34.55	1			
46:35.75	2	1	1	2
46:36.95		2	2	3
46:38.15			2	
46:39.35	2	2	3	
46:40.55	3	3	2	3
46:41.75	2	2		2
46:42.95	3	2	2	3
46:44.15	1	1	1	
46:45.35	3	3	3	3

5. 9. 4. 8 Descent Reconstruction

The first set of graphs of R, V_x, V_y, and V_z (Figures 5. 9-1 and 5. 9-2) compare PREPRO processed telemetry data with the 6DOF program values for the revised nominal conditions.

The second set of R, V_x, V_y, and V_z graphs (Figures 5. 9-3 and 5. 9-4) are direct Cal-Comp plots from data tapes, through telemetry conversion coefficients, in engineering units. Missing data have been filled in by hand from other tape dumps where available. Revised nominal 6DOF values have been overlaid by hand.

5. 9. 4. 9 Radar Reflectivity Analysis

RADVS gain-switching events and reflectivity signal amplitudes for the Muhleman reflectivity model were derived, described, and presented in a succession of radar description and Surveyor I prediction packages, and were presented again in the Surveyor I postmission report. The unusual difference in frequency responses seen by the signal circuits and by the gain-switching threshold circuits was treated in detail, with predictions of higher than necessary gain states at very low altitude, starting about 10 seconds before touchdown. This response was confirmed in the Surveyor I mission performance and again in Surveyor V.

Not just for radar purposes, but for the larger analyses of the entire terminal descent of each mission, an appreciable effort is devoted to a complete and accurate nine-dimensional trajectory versus real-time reconstruction. While this process is hampered by lack of direct data on spacecraft attitude once steering has started, it is possible to converge on an accurate and unique solution in which attitude is implicit by iteration of a precise spacecraft simulation against every significant telemetry channel, as described in the terminal descent discussion. Radar data aid in this reconstruction, and in return, the simulation provides expected or predicted reflectivity signal strengths throughout the descent. This process was almost trivial in the almost exactly nominal Surveyor I, but has proved its utility in matching Surveyors III and V.

The results were presented in subsection 5. 9. 4. 8, and the received signal strength versus time plots are represented here along with the actual telemetered received signal strength data for comparison. Also shown on these plots are the gain states for each receiver throughout the descent phase. Figure 5. 9-5 shows beam incidence angles and reflectivity factors from 6DOF versus time.

It should be noted that the reflectivity signal voltage is not always a true indicator of received signal strength when the preamplifier is switching between two gain states. This is quite evident on all beams in the regions where the transition from gain state 2 to 1, for example, occurs over an interval in which switching is temporarily frequent and even rapid-sometimes more rapid than the gain state signal sampling. For this reason, not all gain

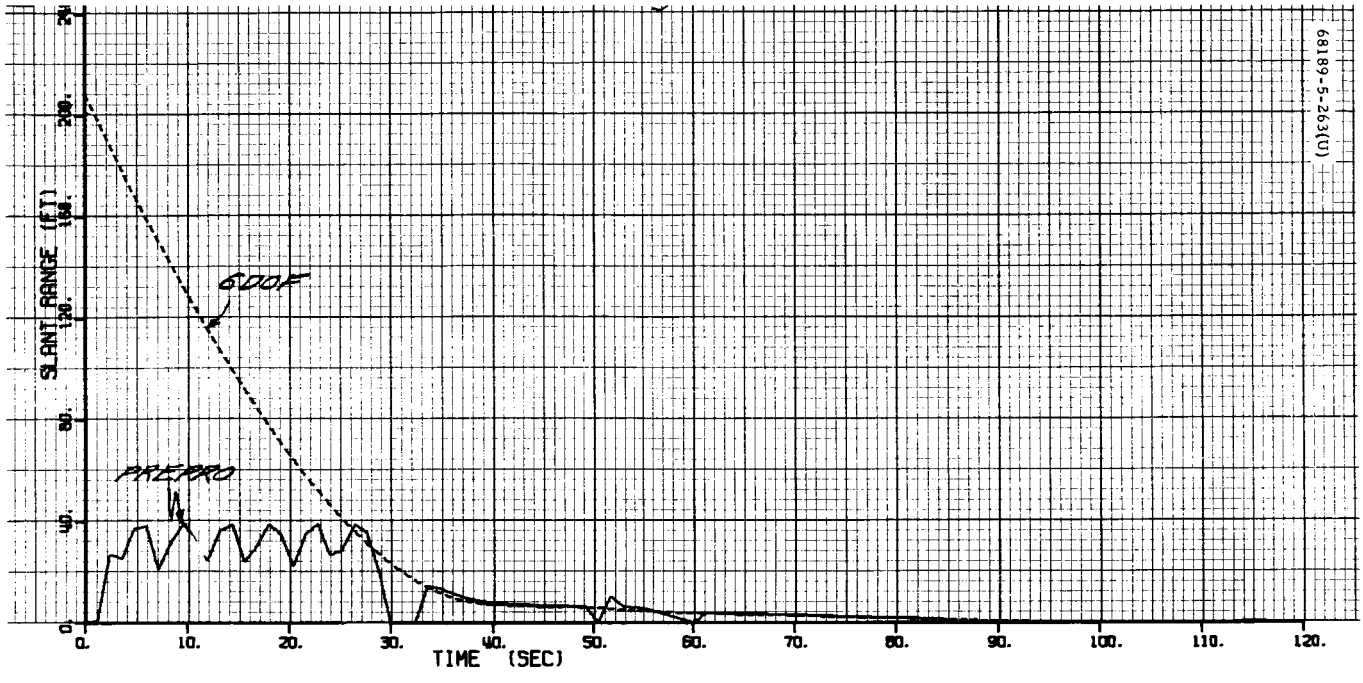

Figure 5.9-1. Slant Range — Reconstructed

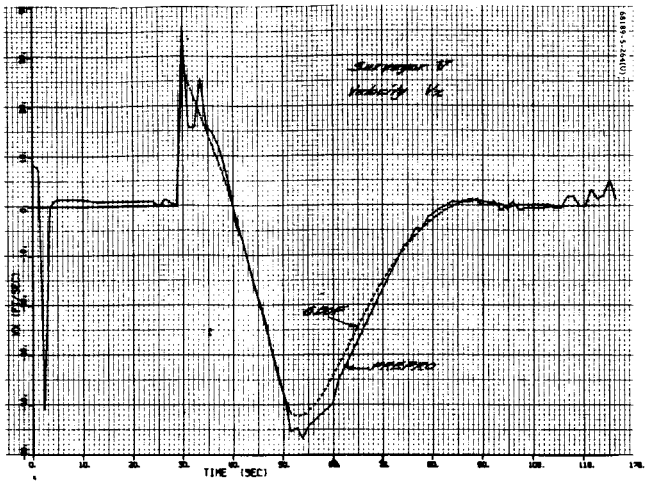

a) V_x

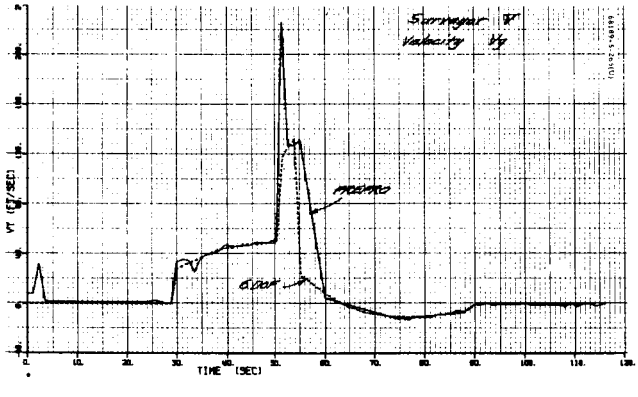

b) V_y

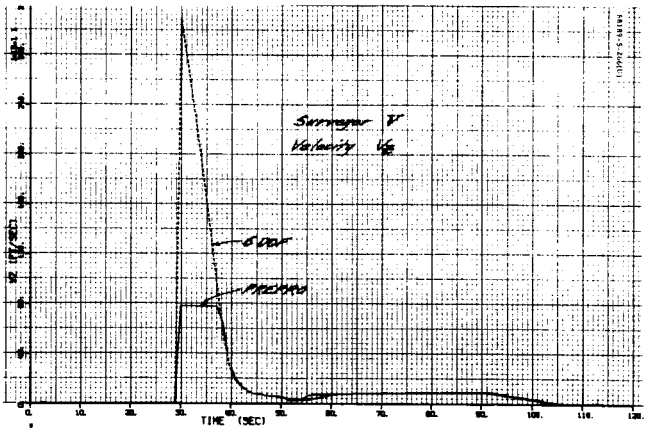

c) V_z

Figure 5.9-2. Spacecraft Velocities – Reconstructed

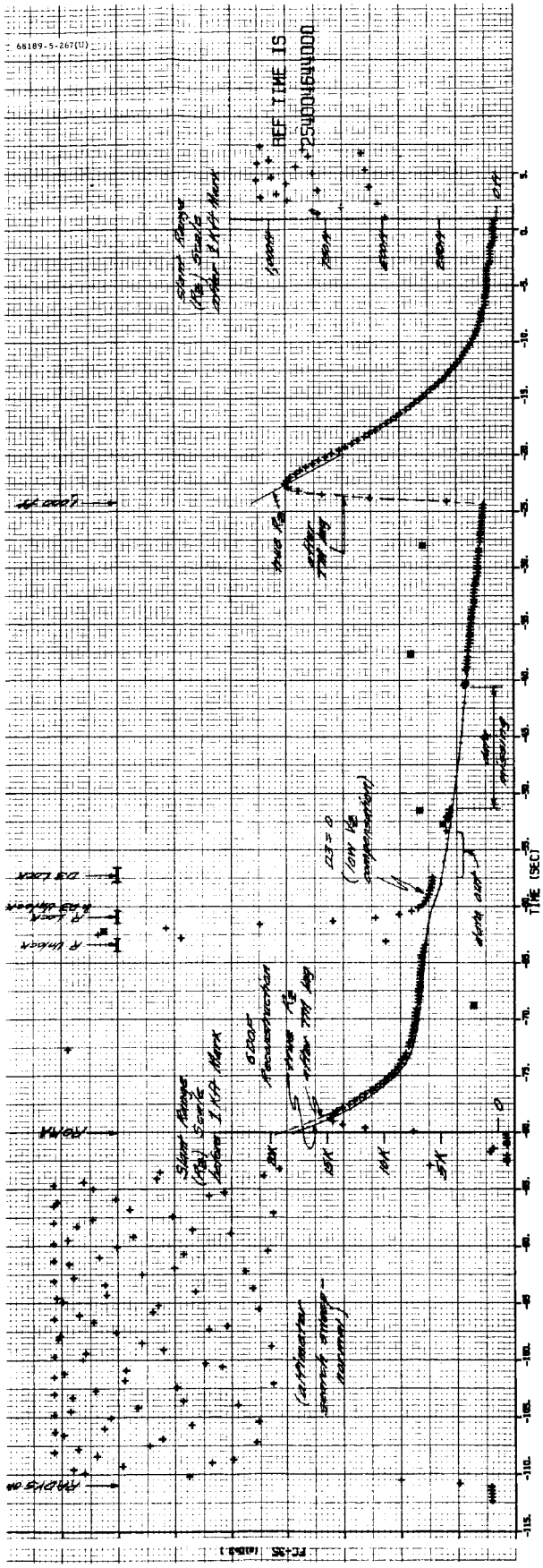

Figure 5.9-3. Slant Range – Telemetry (FC-35)

state signal indications can be taken at face value, particularly since the switching time constant can be appreciably less than the state signal sampling interval.

Reflectivity signal voltage is an unambiguous value, but its dbm interpretation may be either ambiguous or completely obscure. For this reason, special symbols are employed in Figure 5.9-6. Where there is no apparent ambiguity or inconsistency with state indications, three symbols are used, namely

△	0	X
GS3	GS2	GS1

Where the indicated state is probably correct but an alternative interpretation is possible, the probable value is shown by one of the above, and the alternative value by a box (□). The converse of this, one of the above and a box-stroke (▯ or ◺) implies that the state has probably changed since last sampling, and a literal reading of data appears wrong. Two boxes imply uncertainty as to true value, which is probably somewhere in between.

5.9.4.10 Reflectivity Model

The lunar radar reflectivity model used by Hughes and approved by JPL for design and evaluation of both Surveyor radars was developed by D.O. Muhleman. Dr. Muhleman is still active on the Surveyor scientific evaluation team's Electrical Working Group. This model has been completely described in previous documentation. (See, for example, the Surveyor III Final Post-Mission Report.)

5.9.5 RADVS DOCUMENTATION

R.A. Dibos, RADVS Design Review Material, 22 July 1965.

R.A. Dibos, "Behavior of Telemetered Range Near 1000-ft Scale Factor Charge," Hughes IDC 2253.1/523, 27 December 1965.

R.A. Dibos, "Post-Mission Analyses Involving Radar Data," 25 March 1966.

Lincoln Laboratory, "Radar Studies of the Moon," Quarterly Report No. 2, 15 May 1966.

R.A. Dibos, "Nominal Descent RADVS Signals and Gain-Switching," 20 May 1966.

R.A. Dibos, "A-21 RADVS-Predicted Minimum Margin Performance," 30 May 1966.

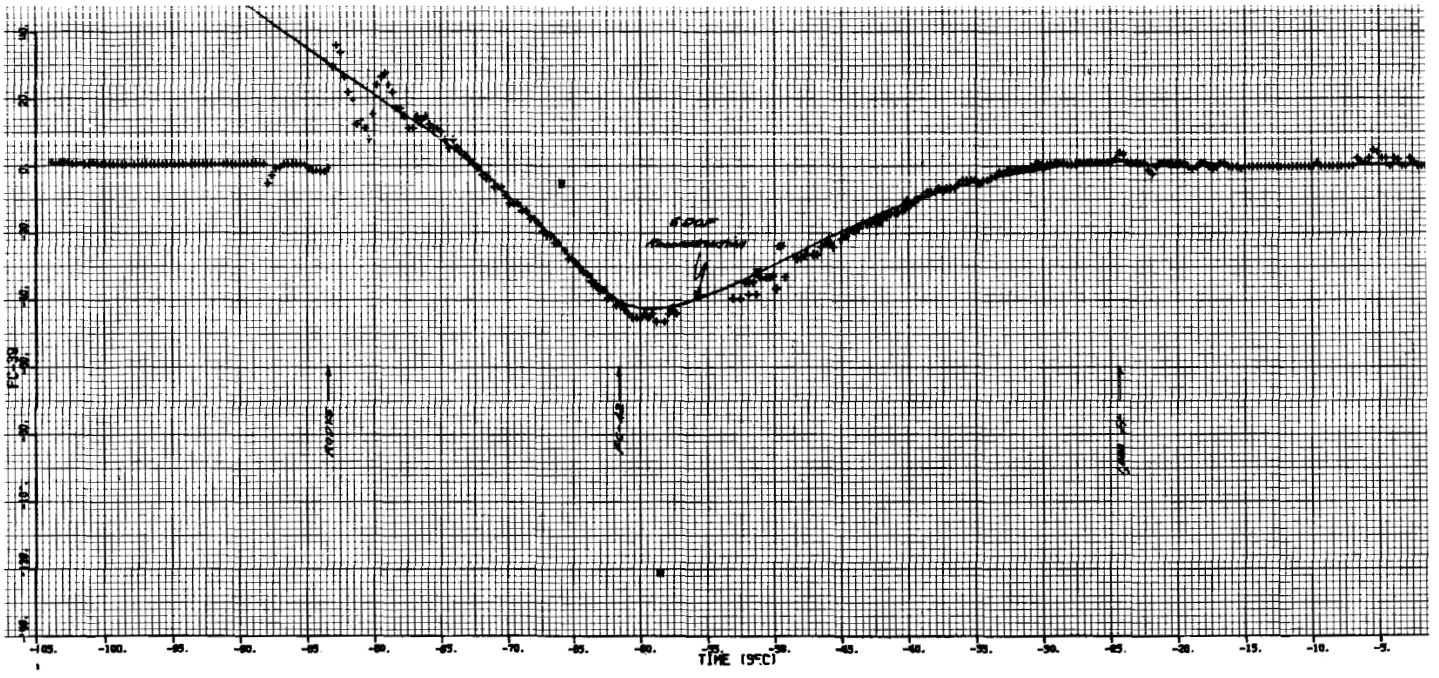

a) V_x (FC-39)

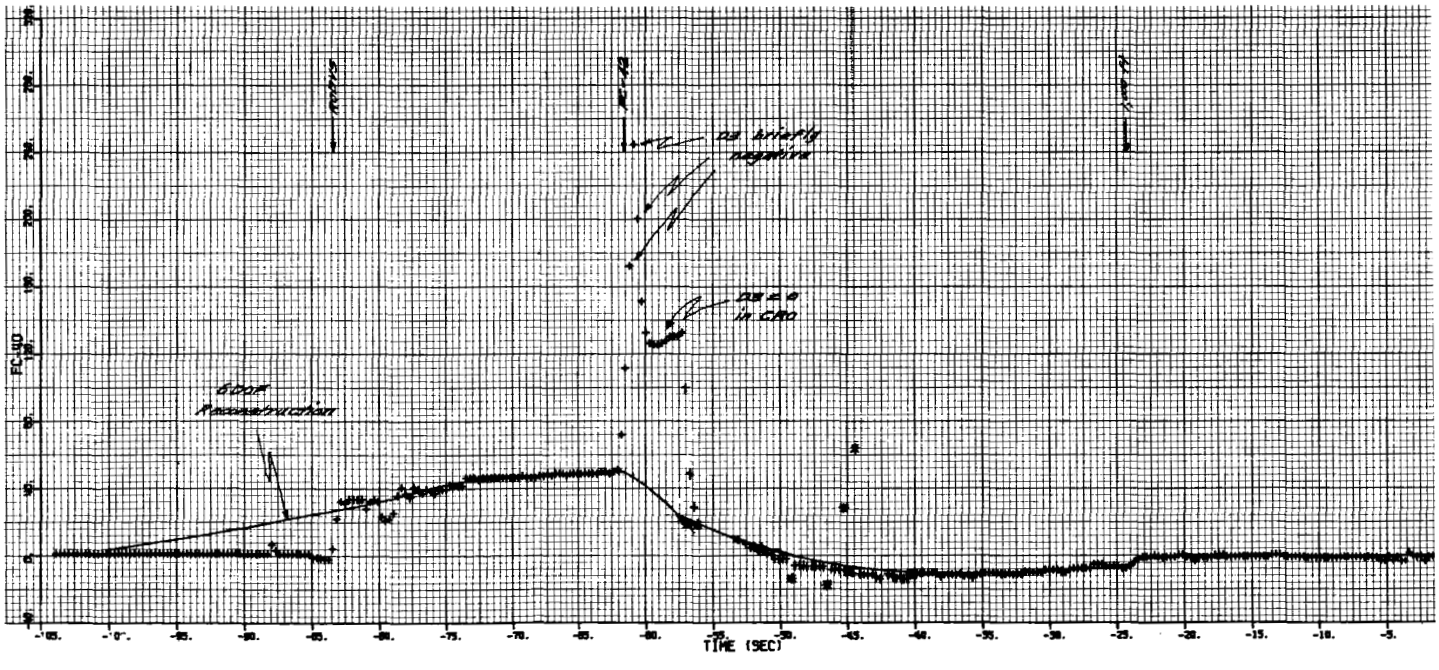

b) V_y (FC-40)

Figure 5.9-4. Spacecraft Velocities — Telemetry

FOLDOUT FRAME

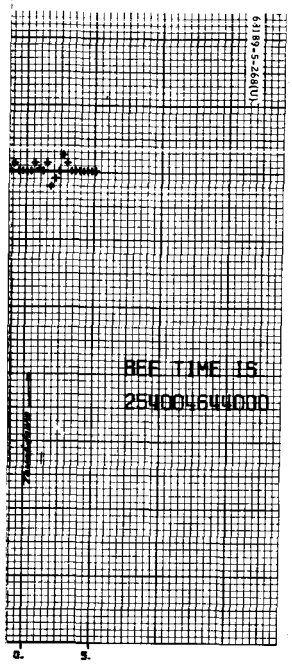

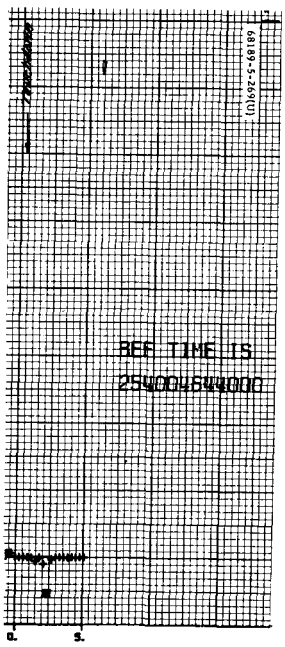

FOLDOUT FRAME

5.9-28

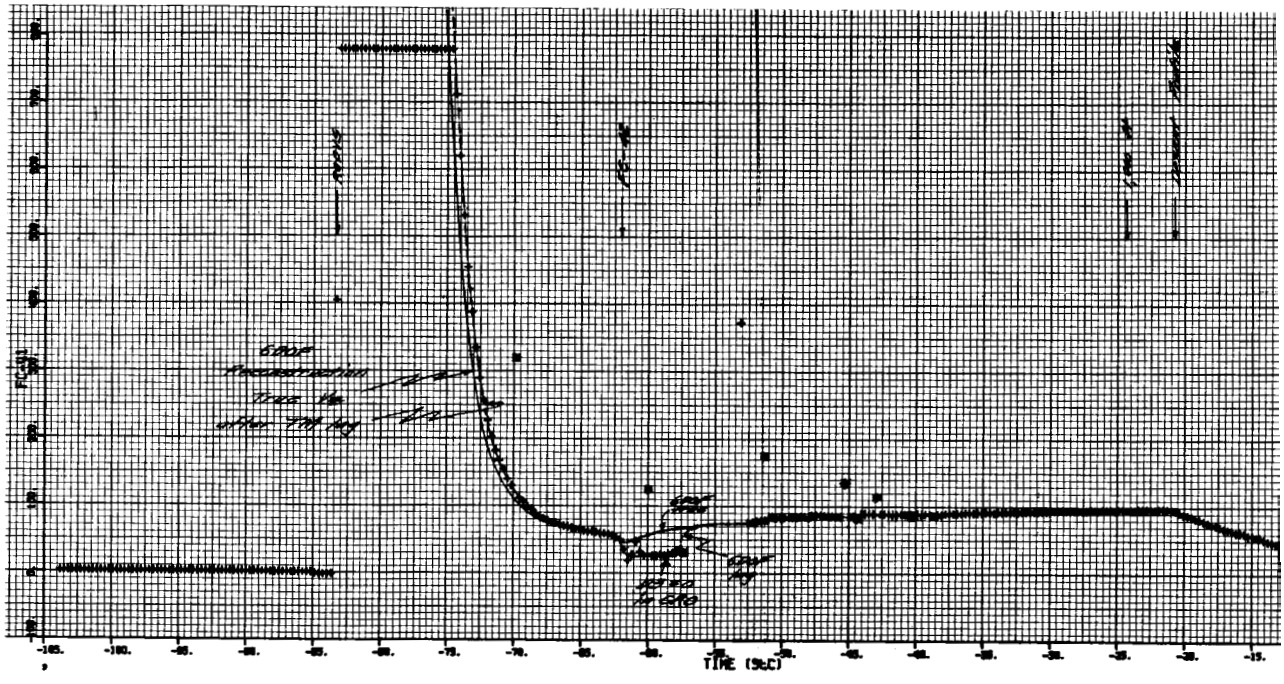

c) V_z (FC-41)

Figure 5.9-4(continued). Spacecraft Velocities – Telemetry

FOLDOUT FRAME

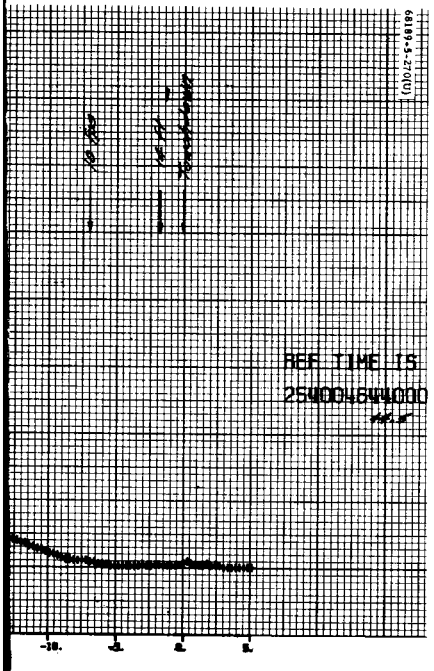

FOLDOUT FRAME

5.9-30

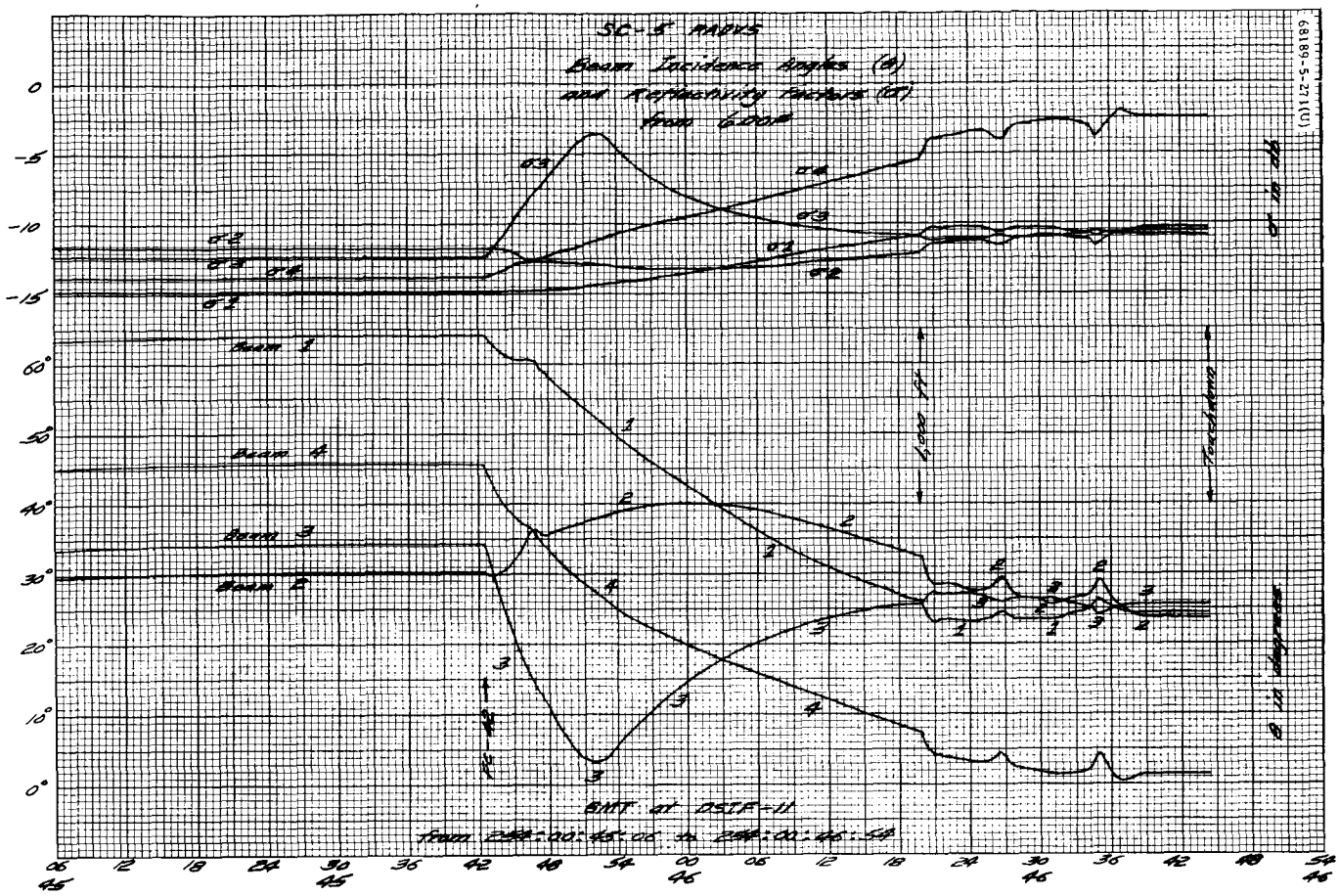

Figure 5.9-5. Beam Incidence Angles (θ) and Reflectivity Factors (σ) From 6DOF Program

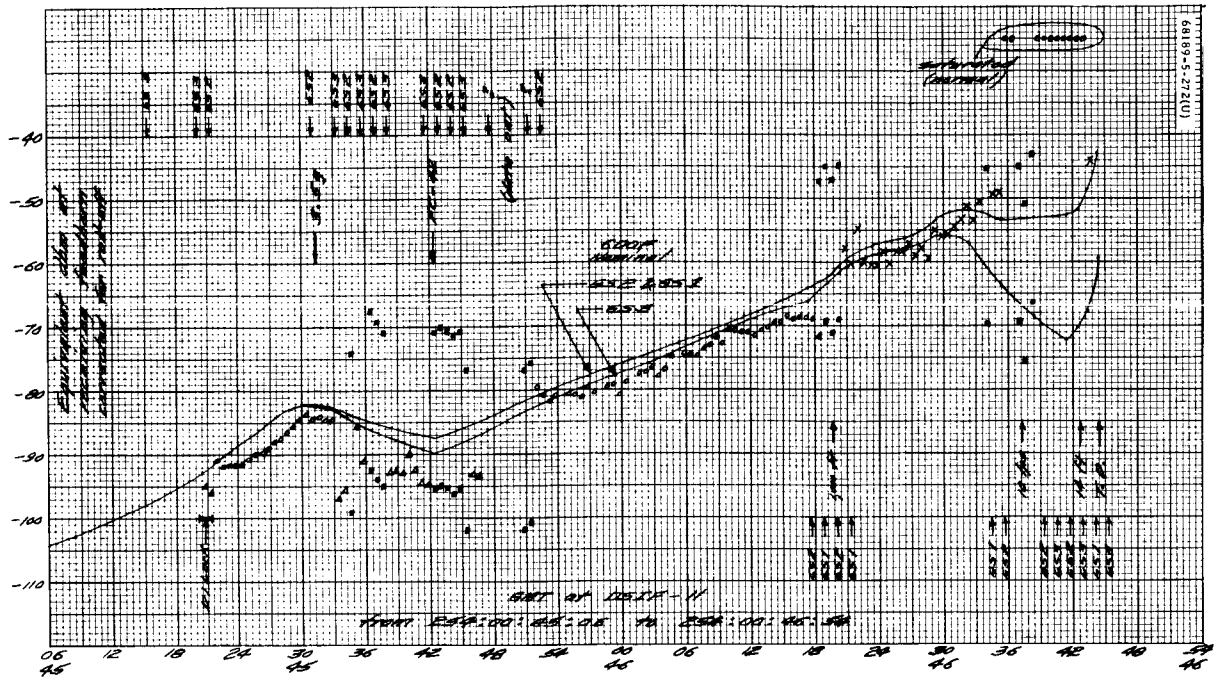

a) Beam One

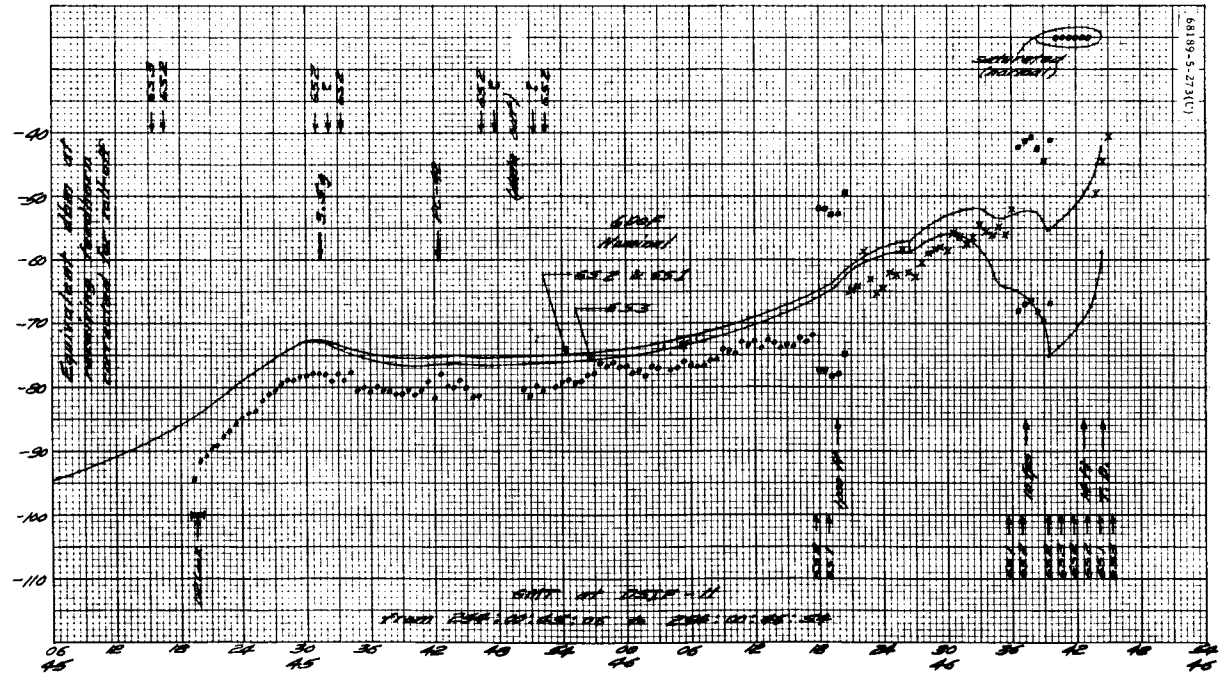

b) Beam Two

Figure 5.9-6. RADVS Reflectivity

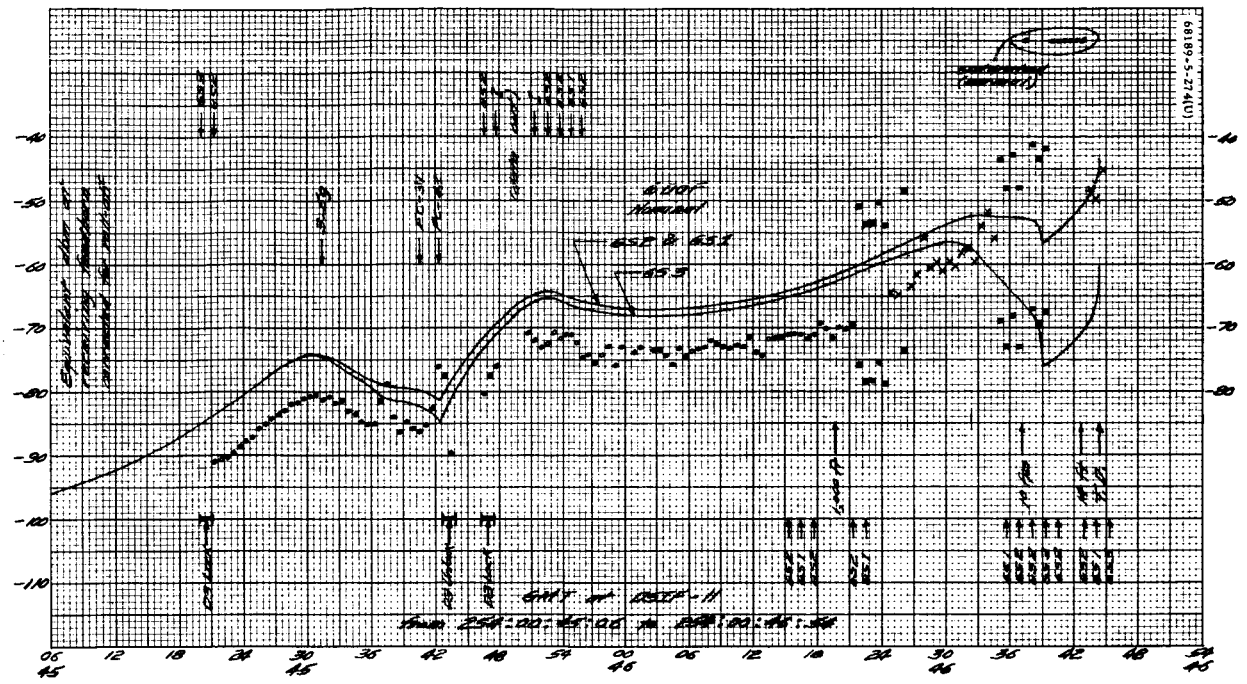

c) Beam Three

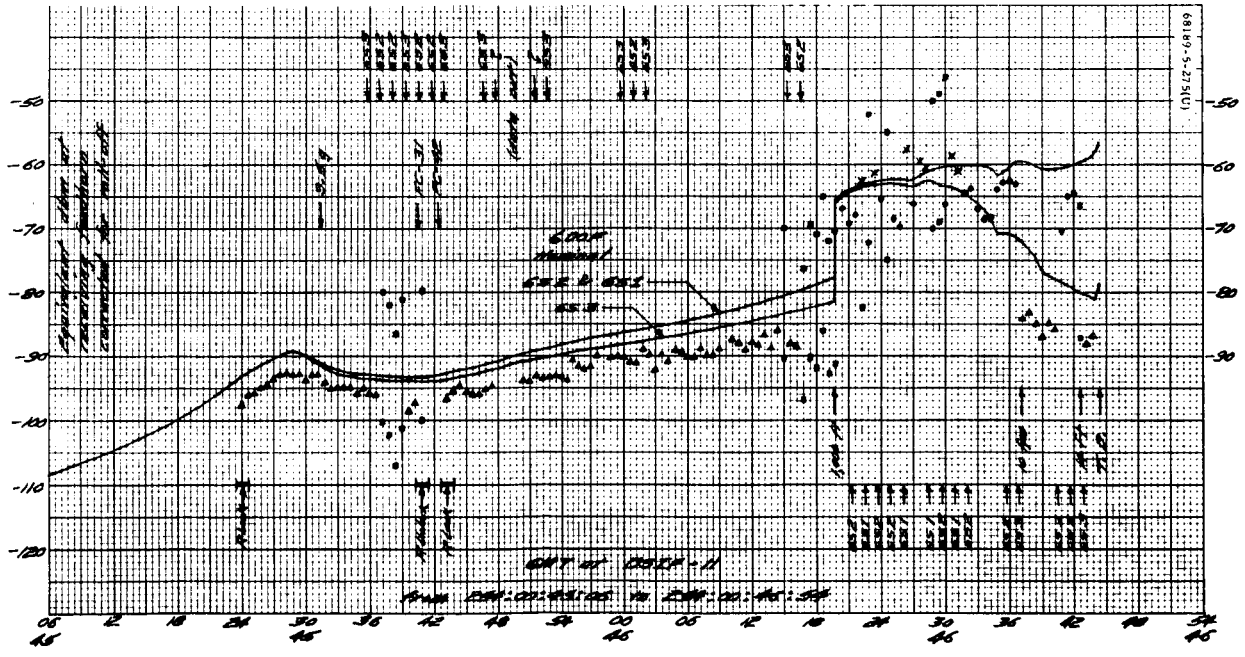

d) Beam Four

Figure 5.9-6(continued). RADVS Reflectivity

R.A. Dibos, "SC-1 RADVS-Real Time Predictions," 31 May 1966.

R.A. Dibos, "RADVS Cross-Coupled Sidelobe Study," 9 September 1966.

R.A. Dibos, "Radar Performance Evaluation," SC-1 Symposium (NASA at JPL), September 1966.

R.A. Dibos, "Graph of A-21 Cut-Off/Touchdown Conditions," Hughes IDC 2292/119, 4 November 1966.

R.A. Dibos, "RADVS Preamplifier Roll-Off Characteristics," 15 November 1966.

"Decibel Allocation and Margin Summary," SSD 4021 R-2, 28 November 1966.

R.A. Dibos and F.K. Rickman, "Recommended SC-3 Attitude at Retro Burnout," Hughes IDC 2292/193, 15 February 1967.

R.A. Dibos, "RADVS Lateral Velocity Saturation," Hughes IDC 2253.4/67, 9 March 1967.

R.A. Dibos, "Extended RADVS Equations for Six-Degree Digital Program," Hughes IDC 2253.4/69, 15 March 1967.

E. White, "Timetic Method for Determining Surveyor System Errors," Hughes IDC 2293/105, 14 April 1967.

N.C. Smith, "Use of Lower Order Polynomial Equations in Telemetry Handbook," (SC-4 and up), Hughes IDC 2294.8/104, 22 May 1967.

K.L. Arends, "RADVS Dropout Sensitivity at Low Altitudes and Velocities," Hughes IDC 2294.5/89, 22 May 1967.

B.O. Steenson, "RADVS Range Sweep Search Function After TM Smoothing," Hughes IDC 2253.4/89, 7 July 1967.

R.A. Dibos, "TM Mode 6 Data Relating to Radar Performance," Hughes IDC 2253.4/84, 15 June 1967.

M.R. Weiner, "Least Square Polynomial Fit of the DVS Tracker Non-Linearity for SC-5," Hughes IDC 2292/349, 2 August 1967.

S.G. Oxley, "SC-5 Telemetry Calibration Handbook 291035 Final Post-Flight Update," Hughes IDC (22-94), 18 September 1967.

J. Sikola, "SC-5 Radar Calibration Data," Hughes IDC 2294.5/139, 26 September 1967.

5.9.6 ACKNOWLEDGMENTS

All DSN station data were supplied by R. H. Leuschner and W. McIntyre.

Nominal beam powers and differences versus roll angle were prepared by Q. D. Howard.

PREPRO processing was performed by Nancy Krupa. 6DOF processing was performed by E. R. Kopitzke.

Terminal descent trajectory reconstruction was performed by V. Marelia, E. White, E. R. Kopitzke, T. L. Parker, and D. C. Passey, under the direction of L. H. Davids.

Preparation of remaining material and technical coordination and writing of this section were by R. A. Dibos.

APPENDIX A TO SECTION 5.9
REVISED TERMINAL DESCENT

The Surveyor V vernier propulsion problem (see Section 5.6) necessitated a complete revision of original planning for the terminal descent. The prime consideration was a minimal thrust-time demand upon vernier engines, dictating a short descent time from very low altitude-velocity conditions at main retro burnout. The revised nominal conditions had to be selected far below the normally predicted 3σ variation about even the lowest nominal set normally considered. Revised dispersion estimates about the revised nominal conditions showed a 40 percent probability of even having enough time to complete steering properly in conjunction with capturing the descent profile, and this was only one of the conditions to be satisfied. Nevertheless, performance was notably close to the revised nominal conditions.

In contrast with typical burnout conditions of around 35,000 feet slant range and 470 fps total velocity, the revised nominal Surveyor V conditions were 6000 feet and 80 fps; post-flight data showed 6400 feet and 85 fps. Instead of a typical descent profile capture at about 22,000 feet with 100 seconds to touchdown, Surveyor V acquired the third descent segment at about 800 feet, essentially the revised nominal, with 22 seconds to touchdown. The total decent time under RADVS control of 62 seconds was well under half the typical value. That actual performance was so close to the revised nominal values is a remarkable tribute to spacecraft system and guidance and trajectory analyses which re-evaluated in real time every significant factor in the system under those conditions.

There was essentially no effect of the revised descent upon the Surveyor V AMR since marking range is fixed and lower terminal conditions were achieved by increasing the commanded delay between mark and engine ignition. This delay was 12.33 seconds in Surveyor V, as opposed to a more typical 2 to 3 seconds. (At unbraked velocity, every second of delay is a travel of about 8500 feet.)

While the Surveyor V approach velocity was actually reduced slightly by the prior six midcourse burns, the effect upon AMR marking was only to slightly reduce a minor contributor to marking dispersion. The significant AMR analysis problem was to refine as closely as possible the expected marking range; just the difference between nominal and test data values

PRECEDING PAGE BLANK NOT FILMED.

was over 700 feet. At high altitudes, this is normally a small fraction of total dispersion; in Surveyor V it could have upset conditions. The analysis recommendation prevailed, and the nominal value was used.

In the RADVS, the markedly reduced altitude at burnout tended to produce stronger returned signals, in itself a benefit. Capable of more than offsetting this, however, were velocity effects — especially the much larger velocity (magnitude and angle) dispersions to be expected at such low speeds. There were significant probabilities of having extremely low or even negative velocities on one, two, or even all three DVS beams. Most such situations correlated directly with failure cycles in Monte Carlo runs showing a 60 percent probability of inadequate steering time because of the dynamic geometry. Hence, the best that could be done was to favor the revised nominal case, hoping it could be achieved (as it was, essentially), with as much dispersion capability as could be accommodated without degrading revised nominal performance.

Given the approach angle of about 45.7 degrees defined by the landing site, and given the revised nominal burnout conditions required for propulsion, the only operational parameters available to favor RADVS operation were a retro pointing bias to keep the revised nominal burnout velocity close to local lunar vertical and the spacecraft roll attitude before terminal descent steering. This roll attitude parameter is normally chosen to simultaneously meet the three varying influences of RADVS operation, omniantenna coverage for telecommunications, and landed orientation for thermal, photographic, and other scientific purposes. In the Surveyor V real-time operation, all post-touchdown considerations were cancelled, and data coverage was subjugated to attempting a successful soft landing. By management decision, roll angle selection was based upon RADVS analysis recommendations.

An earlier tentative choice of $\rho = +45$ degrees was recommended as less than optimum for the following reasons. While probably the best angle for beam 2 alone while making beams 1 and 3 symmetrical, $\rho = +45$ degrees still posed several significant risks. With either or both of beams 1 and 3 locked, a retro case interrupt of beam 2 would cause CRO steering upward, a waste of steering time (twofold) that was already critical. Lacking this, the revised nominal burnoutvelocity close to vertical posed a significant probability that beam 2 would be the only beam initially acquired. Also, even the revised nominal case would sweep beam 2 right across the local vertical, making likely a mainlobe rejection by beam 2. At standard (high) altitude conditions, this would in itself be no problem, but in Surveyor V every second of steering time was critical.

It was therefore recommended that two beams be favored rather than only one. Considering the revised burnout velocity hoped for, $\rho = +90$ degrees would favor beams 1 and 2, while $\rho = 0$ degree would favor beams 2 and 3. Either of these appeared to offer more dispersion capability than would $\rho = +45$ degrees. Each also offered CRO steering in more favorable directions in the event of a retro case interruption of either of the two lower beams (as in fact did occur). Each also offered minimal chance of any DVS beam crossing vertical and thereby making mainlobe rejection(s) likely.

The angle $\rho = 0$ degree was preferred over $\rho = +90$ degrees because there was 2 db more margin (in ECP-23) against beam 2 rejecting beam 1 at $\rho = 0$ degree ($K_{21} = 18$ db) than against beam 2 rejecting beam 3 at $\rho = +90$ degrees ($K_{23} = 16$ db). A slightly positive roll angle would favor both beam 1 alone and the beam 2, 1 pair. It was found that a standard roll-yaw maneuver would produce $\rho = +5$ degrees without a third (roll) maneuver, and that angle was selected. The in-flight angle developed was $\rho = +4.88$ degrees.

The soft-landing priority was unfortunately not without some penalty in omniantenna coverage, as was predicted by telecommunications analyses. As a result, Station 11 PCM data contained a brief outage as well as relatively frequent parity errors during much of the descent, as predicted by a -1.5 db PCM margin. This was accepted during the Surveyor V real-time operation not only because of the soft-landing priority but also because Station 14 was up and supporting the mission with a predicted comfortably positive PCM margin. Unfortunately, Station 14 had unpredicted difficulties, producing data with fewer basic parity errors but severely sustained out-of-synch intervals and a long complete outage. Station 11 data are still the best available.

For this reason, post-mission analysis has been less accurate than is normally desirable in a standard mission. This is a small price for mission success in such an extremely nonstandard situation. It is also considered that sufficient analysis has been possible, and performed as reported here, to establish clearly all qualitative aspects of the descent, and to do so with sufficient quantitative accuracy to justify the conclusions. Accurate scale factor error and noise evaluation have not been possible. Reflectivity evaluation is good during the inertial attitude phase before steering. As pointed out repeatedly in previous documents, however, reflectivity interpretation after start of steering is necessarily subject to a complete nine-dimensional time-varying trajectory reconstruction, which has necessarily been only approximate for Surveyor V.

5.10 STRUCTURES PERFORMANCE

5.10.1 INTRODUCTION

Structures postmission analysis is normally confined to launch and touchdown phases of the mission and the resulting structural loads, landing gear performance, and landing dynamics. Structures support is also required if vernier engine static firing or a hopping maneuver is performed. The failure of the landing gear to lock on Surveyor V involved Structures in additional postmission analysis during lunar operations.

During the launch phase, vehicle separation and extension of the landing gear were verified. During touchdown, shock absorber strain gages indicated the landing gear load time histories and enabled a prompt, but approximate, assessment of landing conditions, such as impact velocity and vehicle incidence relative to the lunar surface. During vernier engine static firing, the strain gage outputs were again monitored. Before and after a landing, leg deflections were monitored to establish whether or not the operating characteristics of the shock absorbers had been impaired during the mission. Failure of the landing gear locking system was verified from leg deflection data.

Postmission analysis consists of analyzing 1) leg deflection potentiometer data, particularly the deflection data associated with the leg lock failure; and 2) shock absorber strain gage data during landing and static firing. A mathematical model was used to simulate Surveyor V landing conditions. The analytical results obtained from the mathematical model, combined with other data, can facilitate evaluation of lunar surface mechanical properties.

5.10.2 ANOMALY DESCRIPTION

On day 266, about 12 hours before lunar night, commands were sent to lock the landing gear. As the vehicle entered lunar night, a deflection of 4.4 degrees was observed on leg 2 and a deflection of 6.9 on leg 3. These deflections indicated that the landing gear locking system had failed to work (TFRs 18266 and 18267).

PRECEDING PAGE BLANK NOT FILMED.

5.10.3 SUMMARY

Surveyor V landing legs deployed in a normal fashion during the launch phase and operated normally during the landing and through most of the lunar day. Deflections of legs 2 and 3 were noticed as the first lunar night was entered, indicating that the landing gear lock mechanism had failed to work. The shock absorbers re-extended to their full lengths on the second lunar day, indicating that their partial collapse was not due to pressure leakage but rather to a decrease in the fluid volume at the low temperatures experienced.

Analysis indicated that the vehicle landed on a slope of approximately 17 degrees with a vertical impact velocity of approximately 12 fps and a lateral velocity not greater than 1 fps. In the analysis, these conditions resulted in penetrations into the lunar soil of 2.5 inches for footpad 1 and 4.9 inches for footpads 2 and 3. These soft surface touchdown simulations have implied a surface static bearing strength of 4 psi. This is less than the 5- to 7-psi bearing strength that was implied from the investigations of Surveyors I and III.

The structural loads experienced by Surveyor V during landing were low relative to design levels.

5.10.4 PERFORMANCE ANALYSIS

5.10.4.1 Launch Phase

Leg Extension and Vehicle Separation

Landing gear extension and vehicle separation were first confirmed at 08:16:41 GMT of day 252.

Leg Deflections

The landing gear position potentiometers were first monitored at 08:51:32 GMT of day 252 and were as follows:

Leg 1: V-5 = 0.1 degree

Leg 2: V-6 = 0.1 degree

Leg 3: V-7 = 0.3 degree

With the landing gear extended, the nominal value for these signals is 0.0 degree with an allowable variation of ±5 percent, or ±1.2 degrees.

5.10.4.2 Touchdown

The actual landing process of the spacecraft can be reconstructed quite accurately from a variety of telemetry signals in connection with available dynamic landing simulations. Pertinent telemetry data are as follows:

1) Commutated indications of spacecraft altitude

2) Continuous analog signals monitoring three strain gage bridges, one being mounted on each leg shock absorber, indicating its axial loading

3) Postlanding television coverage of footpads, crushable blocks, and areas on the lunar surface in which these spacecraft elements contacted the surface and came to rest

4) Postlanding attitude determinations based on the high gain directional antenna position, horizon sightings, etc.

These telemetry data and the dynamic landing simulations have led to the conclusion that the vertical velocity of Surveyor V at impact was 12 to 13 fps, the horizontal velocity was not greater than 1 fps, and the spacecraft was essentially horizontal.

Figure 5.10-1 shows the time histories of the axial forces in the landing gear shock absorbers from prior to initial surface contact until after the spacecraft came to rest. After leg 1 contact, a negative pitch motion with a velocity in excess of 13 deg/sec was encountered (the range of the pitch gyro was exceeded), accompanied by little angular motion in yaw and roll, until legs 2 and 3 contacted the ground almost simultaneously – leg 2 at 186 milliseconds and leg 3 at 194 milliseconds after leg 1 impact. A slide-out period of approximately 1.7 seconds followed, during which the spacecraft rolled approximately +6 degrees.

Initially, each shock absorber experienced a force for approximately 0.25 second and then zero force for approximately 0.8 second. This was followed by a rather poorly defined low amplitude oscillatory force which rapidly damped out to a low constant value consistent with forces resulting from the static lunar weight of the spacecraft. These force-trace characteristics are consistent with those expected from an initial vehicle impact, during which maximum pressures are exerted on the lunar surface. This is followed by a relief of the load as the spacecraft rebounds under the action of landing gear spring forces, then by a final low energy impact and oscillatory forces related to the elasticity of the spacecraft and the lunar surface. The frequency of the observed oscillation is approximately 4 Hz, which is considerably lower than corresponding oscillation frequencies observed during Surveyor I and III touchdowns (approximately 6.5 Hz). Hence, it is assumed that for Surveyor V a different natural mode of the spacecraft was excited (rocking mode) due to the hillside landing as compared to the bounce mode of Surveyors I and III. Table 5.10-1 gives the maximum force levels experienced by each shock absorber and also the impact times of each footpad.

68189-5-9(U)

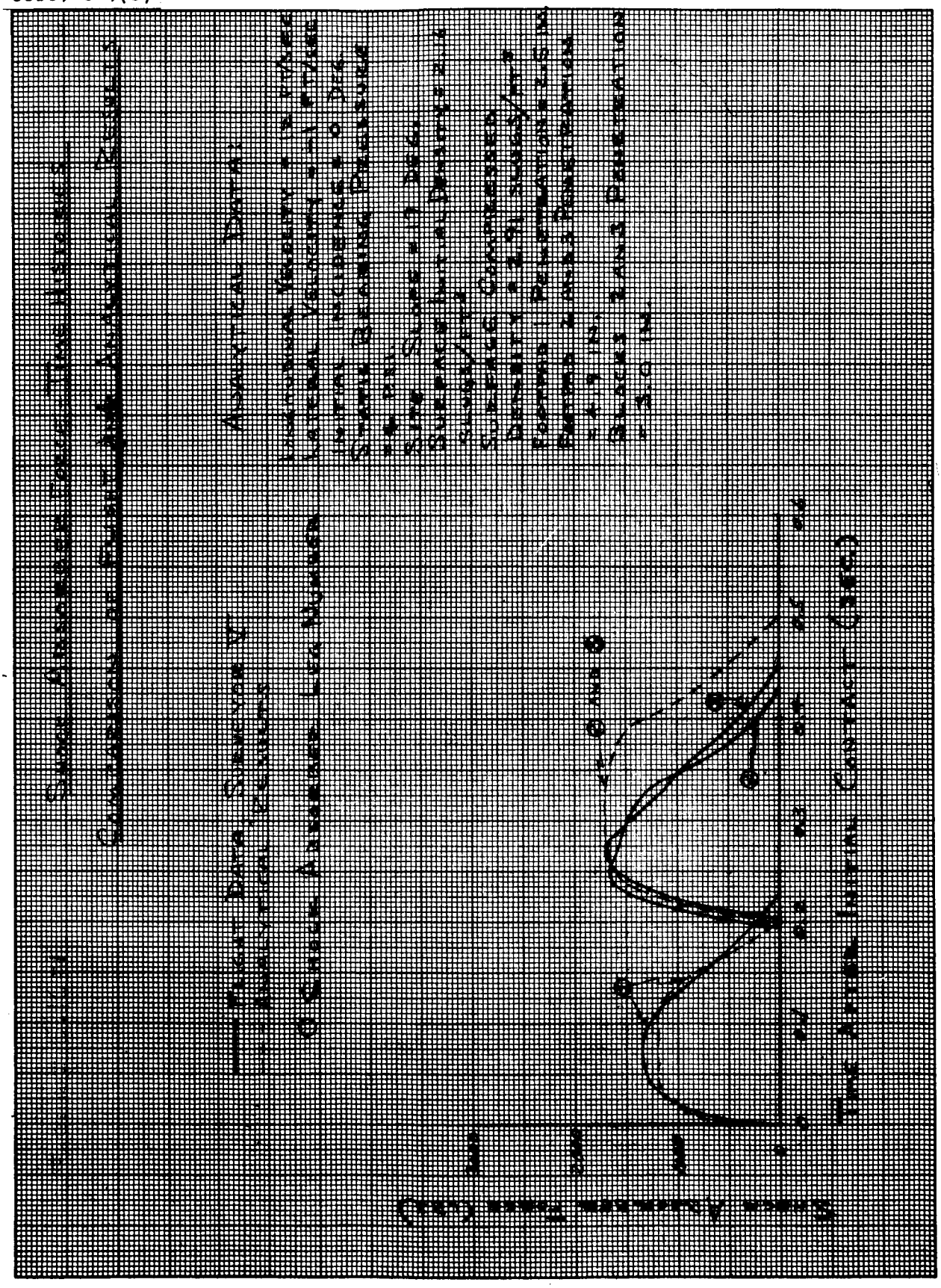

Figure 5.10-1. Shock Absorber Force-Time Histories

TABLE 5.10-1. MAXIMUM SHOCK ABSORBER FORCES AND FOOTPAD IMPACT TIMES

Leg Assembly	Maximum Shock Absorber Force, pounds	Footpad Impact Time After 254:00:46:00 GMT, seconds
1	1265 ± 80	44.284 ± 0.002
2	1635 ± 80	44.474 ± 0.002
3	1640 ± 80	44.481 ± 0.002

Television data have shown that during the slide-out period of the landing footpad 2 traveled a considerable distance (estimated to be 32 ±2 inches) along the lunar surface, leaving a clearly visible trench. Although it is not as conspicuous as for pad 2, there is evidence that footpad 3 also moved by approximately the same distance. In the trench made by footpad 2, a very clear indication of the first footpad impact is given. A footpad penetration of approximately 5 inches is estimated to have occurred here, accompanied by very little sliding motion. During the spacecraft rebound caused by landing gear spring forces, the footpad lifted out of its impression, resulting in a continuation of the trench with considerably less surface penetration (approximately 2 inches) than the original imprint showed.

Computer simulations of the landing have achieved the best correlations with flight data when the angle between spacecraft and slope at the time of impact has been taken as 17 degrees. The measured spacecraft incidence (from high gain inertia and solar panel position data) is 20 degrees. The difference between 17 and 20 degrees could be due to several factors: 1) if the slope itself is 20 degrees, then the spacecraft had an initial incidence of 3 degrees; 2) the slope is 20 degrees, and footpad 1 landed just outside the crater but slid into it during the slide-out period; 3) the slope is 17 degrees, but differential footpad penetrations give the spacecraft an incidence greater than the slope. Obviously, these effects could all exist in various proportions for the true situation.

In summary, the Surveyor V landing can be regarded as a nominal one except for encountering a slightly higher-than-expected lunar surface slope (nominal maximum of 15 degrees) in a position most unfavorable for a stable landing, i.e., one leg pointing in the uphill direction. Because of sufficient margins in the landing stability capability, no stability problem was anticipated or encountered for the spacecraft's landing conditions.

Dynamic Simulation

Computer simulation studies of landings have been performed to estimate the landing conditions and mechanical properties of a surface material that will yield surface penetrations and shock absorber axial loads

similar to those obtained during the Surveyor V landings. Representative analytical force-time histories for a landing on a 4-psi static bearing strength surface are compared with reduced Surveyor V data in Figure 5.10-2. The impact velocities used are 12 fps vertical and 1 fps horizontal with the spacecraft horizontal at the moment of impact on a 17-degree slope and with leg 1 pointing directly uphill. Footpad 1, 2, and 3 penetrations corresponding to the analytical results of Figure 5.10-2 are 2.5, 4.9, and 4.9 inches, respectively. From television data, the estimate of the initial penetration of footpad 2 is 5 inches. Initial impact areas of footpads 1 and 3 are not visible to the television camera. In the analytical simulation, body blocks 2 and 3 each penetrated 3 inches; block 1 did not touch the surface.

The soil model used in the analysis is shown in Figure 5.10-3. The surface material, initially of density ρ_1, is compressed to density ρ_2 under the penetrating action of a footpad. Forces resisting penetration are the static bearing pressure (assumed constant with depth), a friction force which increases linearly with penetration and is equal to the static bearing pressure at a penetration of 1 foot, and the soil inertia forces. For purposes of analysis, the relationships between ρ_1, ρ_2, and static bearing pressure are shown in Figure 5.10-4. For the 4-psi surface used in the analytical results of Figure 5.10-4, ρ_1 and ρ_2 were, respectively, 2.16 and 2.91 slug/ft^3.

The analytical results obtained to date for Surveyor V show significant differences from those achieved for Surveyors I and III. For the earlier vehicles, good correlation between analysis and flight data was achieved assuming surface static bearing pressure of 5 psi and, for shock absorber traces alone, the correlation was good even for a rigid surface (i.e., a surface having a static bearing strength of 10 psi or greater). However, in the Surveyor V analysis, it has been necessary to consider surfaces of static bearing pressure less than 5 psi to obtain reasonable agreement with flight data.

Structural Response Loads

From the above analysis, the longitudinal velocity of Surveyor V was approximately 12 fps. This compares with a Surveyor I impact velocity of approximately 11.5 fps. Structural loads calculated to occur during the Surveyor I landing were less than 20 percent of the design load levels. It is considered that Surveyor V structural loads would not be considerably greater than those of Surveyor I and that a detailed analysis was therefore unwarranted.

Leg Deflections

Shortly after touchdown (00:50:58 GMT of day 254), the landing gear leg deflections were monitored and found to be as follows:

Leg 1: V-5 = 0.6 degree

Leg 2: V-6 = 0.7 degree

Leg 3: V-7 = 0.6 degree

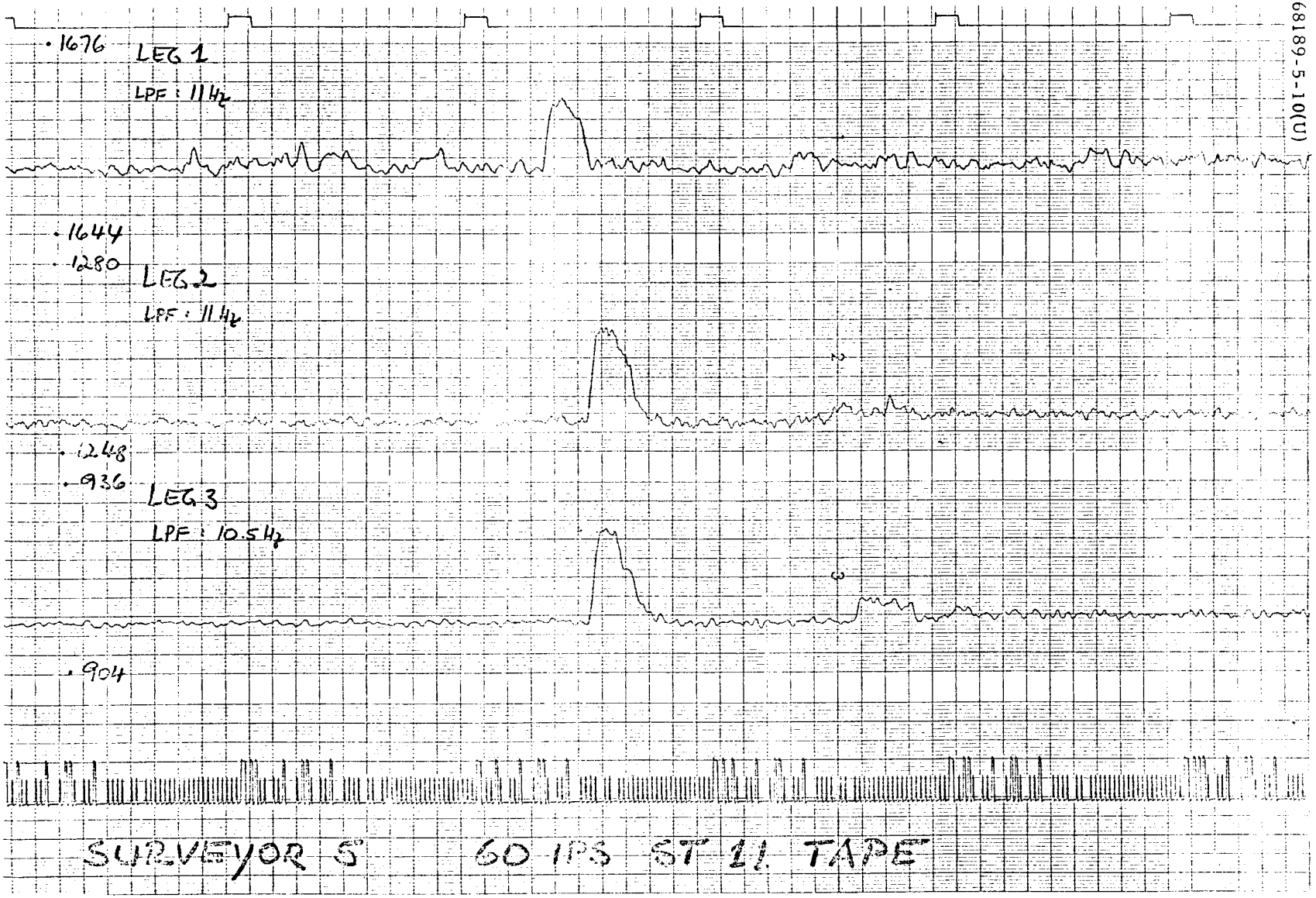

Figure 5.10-2. Touchdown Strain Gage Histories

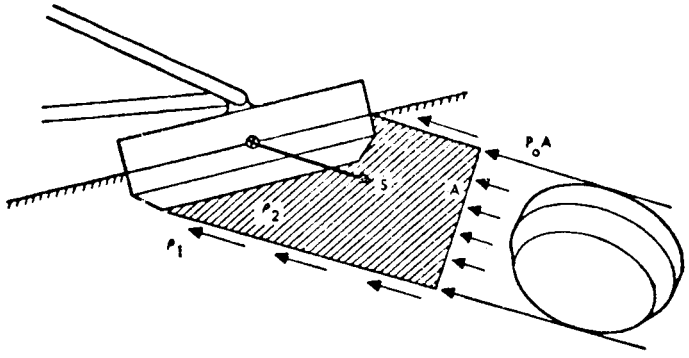

68189-5-11(U)

$$F = P_o A (1 + CS) + \frac{\rho_1 \rho_2}{\rho_2 - \rho_1} A\dot{S}^2$$

where

P_o = surface static bearing pressure

S = depth of penetration

C = frictional constant

Figure 5.10-3. Soft Surface Model for Landing Dynamics Analysis

68189-5-12(U)

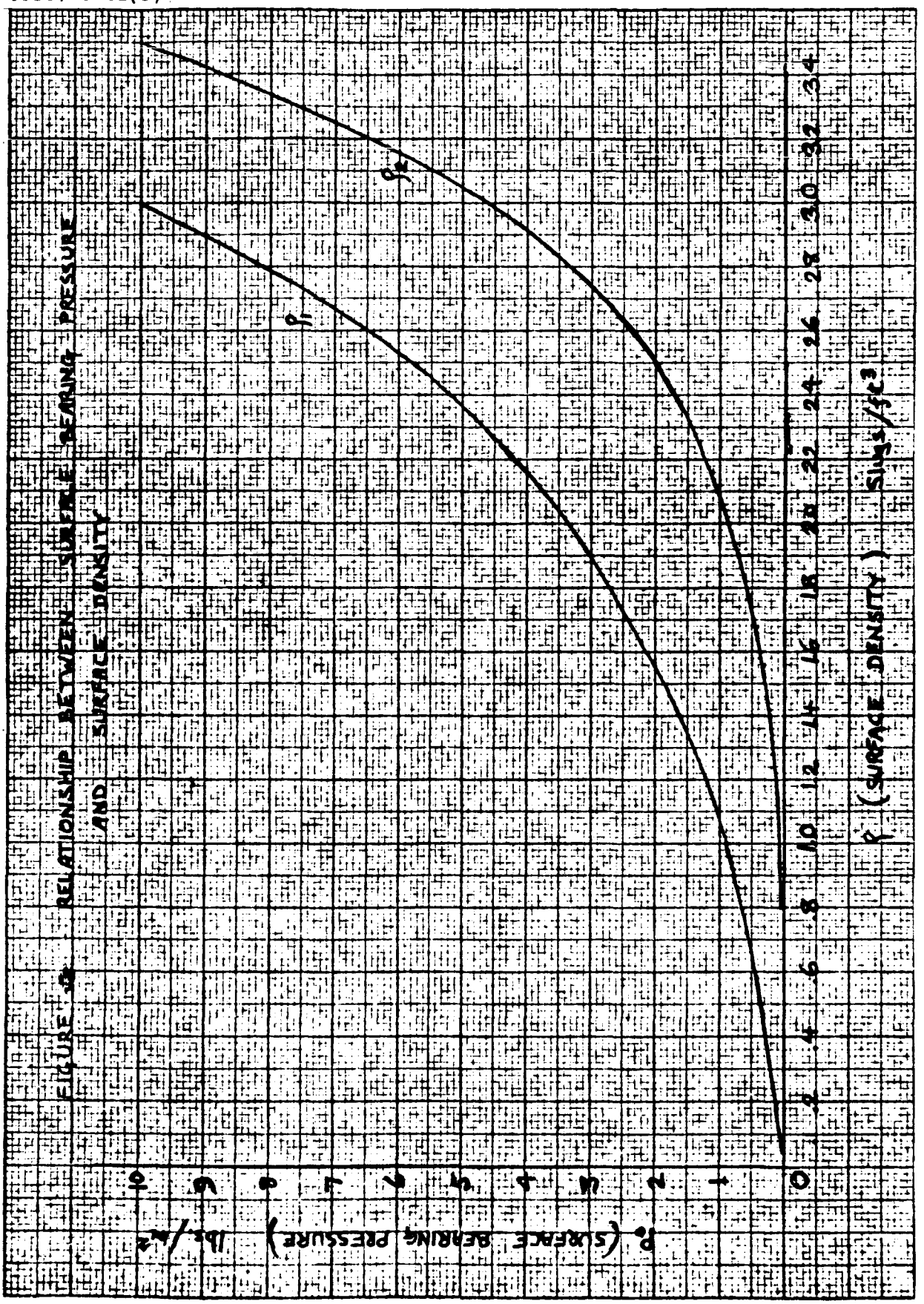

Figure 5.10-4. Relation Between Surface Bearing Pressure and Surface Density

Since these angles were not excessive, it was considered unnecessary to lock the landing gear at that time. The decision not to lock the gear is made to facilitate gear actuation during any executed lunar hopping maneuver or during inadvertent hopping which could occur during a static firing experiment.

5.10.4.3 Lunar Operations Phase

Static Fire

The command to perform the static firing experiment was transmitted at 256:07:38:08 GMT. Shock absorber strain gage signals were monitored and indicated that the firing actually took place at 256:07:38:11.58 GMT. The signal-to-noise ratio for these channels was too low to permit any meaningful interpretation of shock absorber force-time histories

Landing Gear Lock Failure

The shock absorbers remained unlocked during most of the lunar day, and the leg deflection signals, which were monitored at intervals, remained essentially constant. Events and data associated with Surveyor V are shown in Table 5.10.2. (Fluctuations of up to about half a degree were noted, but these are attributed to telemetry and thermal characteristics and not to mechanical actuation of the legs.) Late in the lunar day it was decided to lock the gear to preclude the possibility of leg deflections resulting from shock absorber pressure leakage caused by the extremely low temperatures of lunar night. At the time of the decision to lock, the temperatures of the shock absorber on legs 1, 2, and 3 were approximately 110°, -50°, and 110° F, respectively. The shock absorber locking device has been tested at temperatures between 0° and 120° F, and the squib device is operable between ±250°F. A real-time decision by the Structures specialist placed the lower temperature limit for operation of the locking device at -100° F. A single-lock gear command, 0636, was transmitted at 266:04:01 GMT when shock absorber 1, 2,and 3 temperatures were 103°, -55°, and 107° F, respectively. Four more 0636 commands were sent at 266:06:19 GMT when shock absorber temperatures were 100°, -58°, and 100° F. At the time of firing, it is not possible to positively establish if the landing gear has been successfully locked. Successful locking must therefore be assumed until evidence to the contrary arises.

At approximately 267:07:40 GMT, an anomaly in television data resulted in examination of the leg potentiometer readings which indicated that deflections of legs 2 and 3 had occurred. The deflections provided a positive indication that shock absorbers 2 and 3 failed to lock. No deflection of leg 1 was observed then or subsequently. Time histories of temperatures and deflections of each leg assembly are shown in Figure 5.10-5. From these data, it can be established that shock absorber 2 began deflecting at a temperature between -103° and -115° F, and shock absorber 3 began deflecting between -112° and -115° F. Early during the deflection of leg 3, a steady deflection rate of approximately 0.1 deg/min was observed. (Between 267:05:17.28 and 267:05:20:42 GMT, leg 3 deflected from 1.7 to 2.0 degrees.)

TABLE 5. 10-2. EVENTS AND DATA ASSOCIATED WITH SURVEYOR V SHOCK ABSORBER LOCKING FAILURE

Event	GMT, day:hr:min	Leg Deflection, degrees			Shock Absorber, °F		
		V-5	V-6	V-7	V-30	V-32	V-33
Touchdown	254:01	0. 6	0. 7	0. 6			
	265:03:10	0. 8	0. 6	0. 6	127	- 20	145
0636 lock (1 sent)	266:04:01				103	- 55	107
Gear command (4 sent)	266:06:19				100	- 58	100
Last constant V-6	266:22:01	0. 8	0. 8	0. 5		-103	- 70
V-6 change	267:00:02	0. 8	4. 0	0. 3		-115	- 86
Last constant V-7	267:04:19	0. 8	4. 0	0. 3			
	267:04:21				65	-141	-112
	267:04:45				64		-115
V-7 change	267:04:49	0. 8	4. 1	1. 1			
V-7 change	267:05:17	0. 8	4. 1	1. 7			
Rate observed	267:05:20	0. 8	4. 2	2. 0			
V-7 maximum change	267:07:13	0. 7	4. 2	6. 5	58	-160	-130
TV anomaly indicates deflection possibility	267:07:40						
	267:08:47	0. 7	4. 3	6. 6			
	270	0. 87	4. 4	6. 9	—	-265	—
Second lunar day	288:08:10	1. 3	0. 3	0. 8	177	198	154
Lunar eclipse	291:11:55	1. 5	0. 6	0. 5	- 65	- 67	- 55
Post eclipse	291:13:15	1. 0	0. 6	0. 8	100	45	102
Second lunar night	297:03:00	1. 2	0. 6	8. 2	-124	-193	-175

No further leg deflection data were received during the next 2 hours, and so the time of achieving the maximum deflection of approximately 7 degrees was not established. However, if the established rate continued, the total deflection would have been achieved in approximately 1 hour. When the leg deflections were first observed at approximately 267:07:13 GMT on V-5, -6 and -7 telemetry channels, the deflections were 0. 7, 4. 2, and 6. 5 degrees with corresponding temperatures of approximately 58°, -160°, and -130°F. The deflections thereafter remained essentially constant, and, on day 270, with each shock temperature at about -265°F, the deflections were 0. 87, 4. 4, and 6. 9 degrees.

68189-5-13(U)

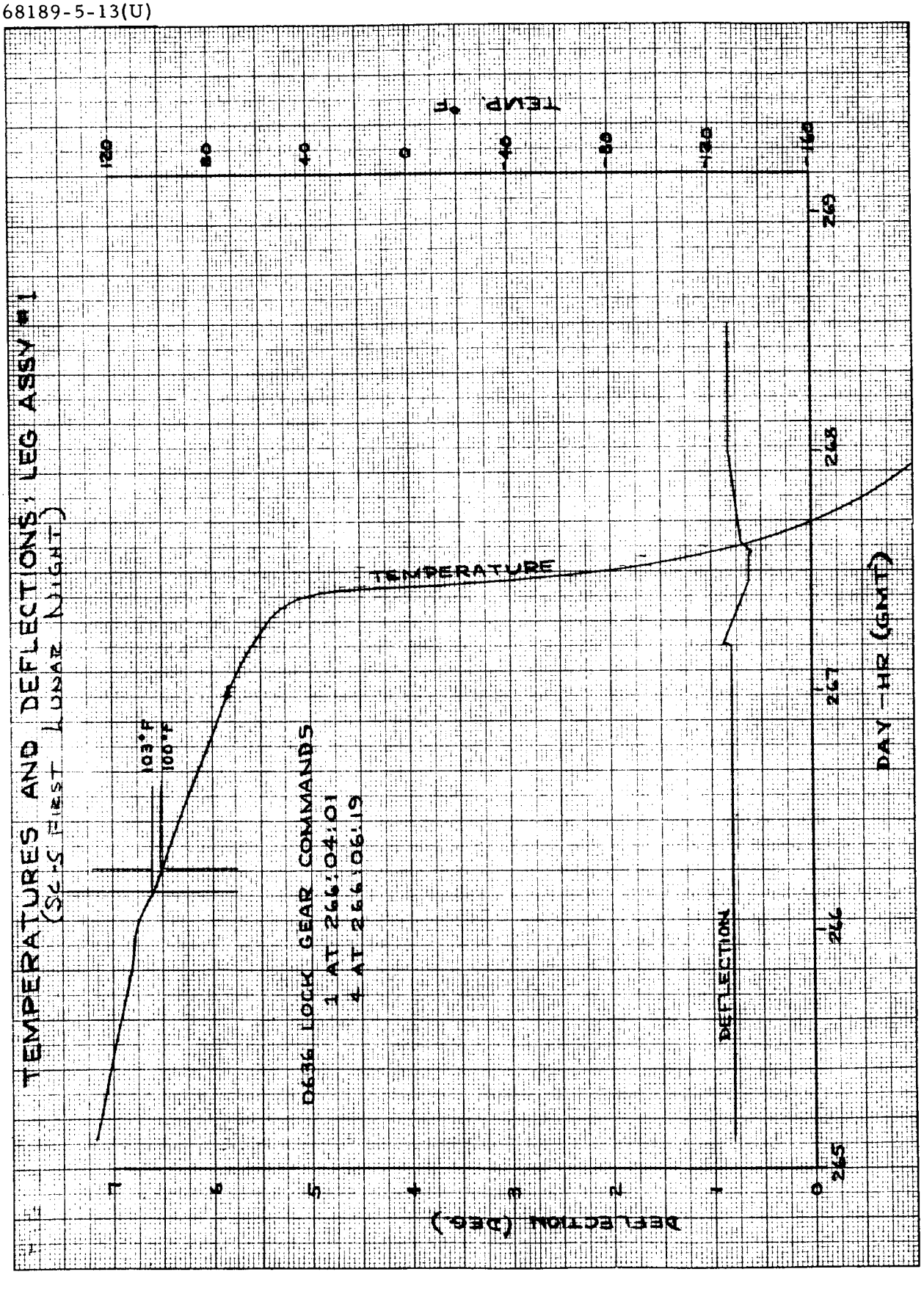

a) Leg Assembly 1

Figure 5.10-5. Temperatures and Deflections – First Lunar Night

68189-5-14(U)

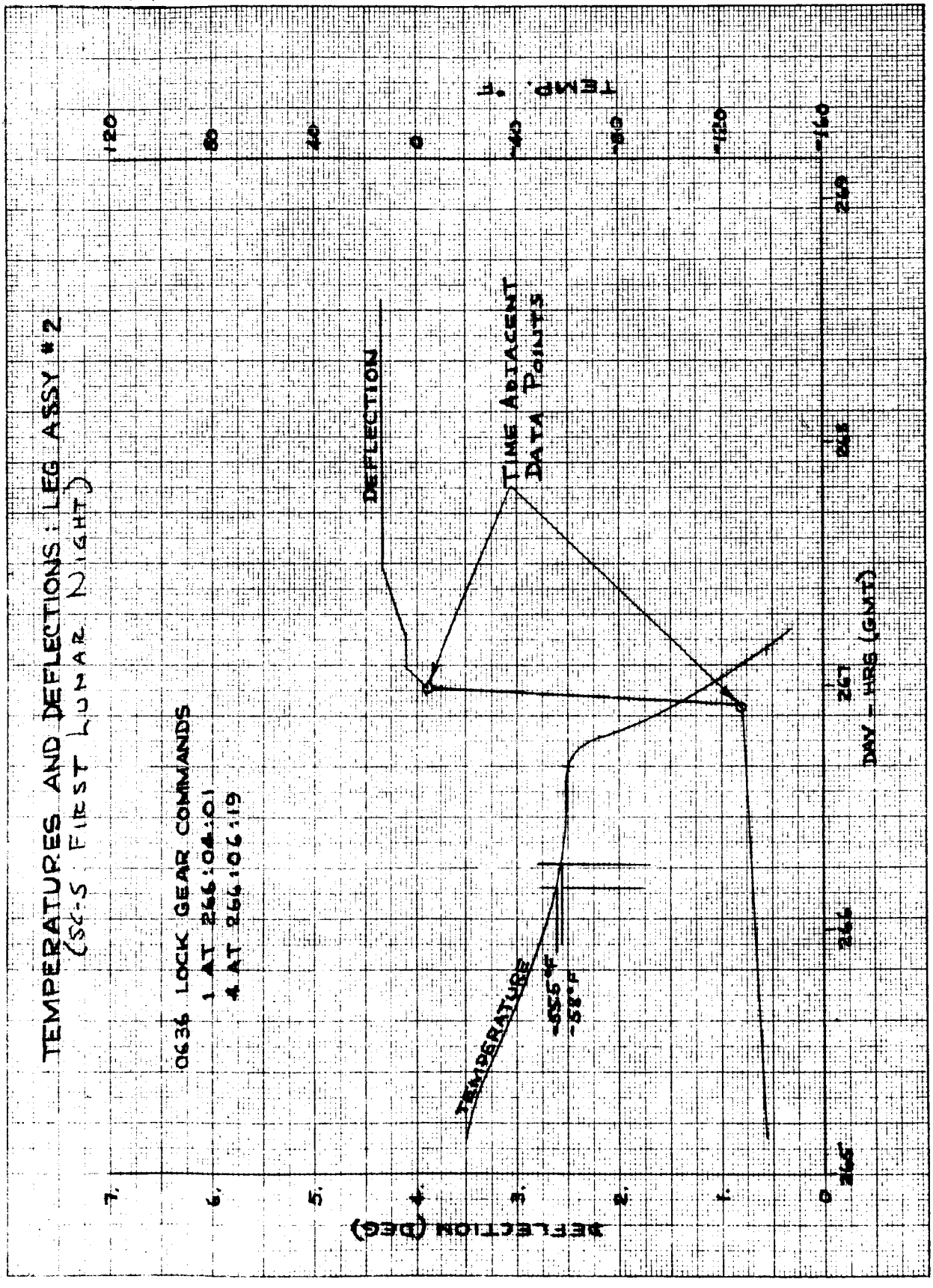

b) Leg Assembly 2

Figure 5.10-5 (continued). Temperatures and Deflections – First Lunar Night

68189-5-15(U)

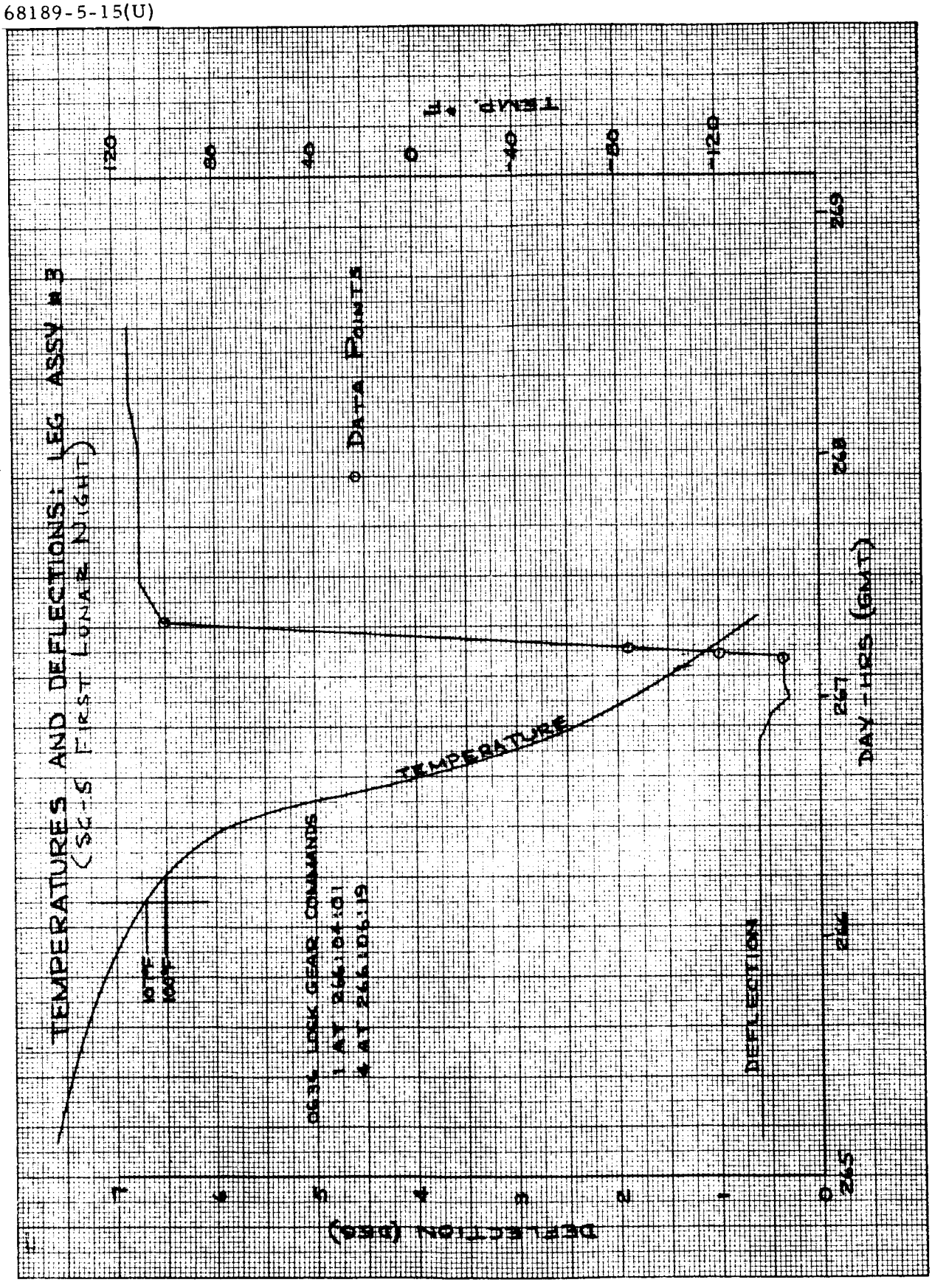

c) Leg Assembly 3

Figure 5.10-5 (continued). Temperatures and Deflections – First Lunar Night

After warming up on the second lunar day, Surveyor V was revived on day 288. Subsequent evaluations indicated that the downhill landing legs were no longer collapsed. Leg 2 had returned to a deflection of 0.3 degree, and leg 3 to 0.8 degree. This means that the shock absorbers on these legs had re-extended to the lengths existing before the low lunar night temperatures caused their partial collapse. This return to full extension indicates that the partial collapse was due to shock absorber fluid contracting at the low temperatures rather than a leakage of high pressure helium gas with resulting preload loss.

On day 190, an eclipse of the moon caused the temperatures of the shock absorbers to drop to between -55° and -67°F. The shock absorbers did not deflect, and only minor random changes in the leg deflection angles were recorded (see Table 5.10-2).

During the second lunar day, a sequence of 86 lock landing gear commands was sent. As the temperature dropped on the second lunar night, leg 3 deflected 8 degrees, while leg 1 remained undeflected as it had on the first lunar night. Leg 2, which had deflected 4.4 degrees during the first night, did not deflect. Figure 5.10-6 shows the deflection and temperatures for leg 3 as it entered the second lunar night.

Crushable Block Clearance

It is possible that the deflection rates of legs 2 and 3 ceased when crushable blocks 2 and 3 came into contact with the surface. However, analysis and observations indicate this is not necessarily so. The analysis considered a two-dimensional situation (leg 1 directly uphill) and a planar surface. The downhill legs (2 and 3) were assumed to have penetrated 5.5 inches and the uphill leg 1.5 inches. For the case of a 1-degree deflection of leg 1 and a 4.5-degree deflection of legs 2 and 3, the blocks would have a 4-inch surface clearance. For a 1-degree deflection of leg 1 and a 7-degree deflection of legs 2 and 3, the blocks would have a 3-inch surface clearance. Therefore, for the three-dimensional case that actually exists with leg 2 deflected approximately 4.5 degrees and leg 3 approximately 7 degrees, planar surface clearance of between 3 and 4 inches should exist for blocks 2 and 3. This amount of clearance could well be taken up by surface irregularities. However, analysis by JPL of television pictures obtained before the legs began to deflect indicated that the nozzle on vernier engine 3 was 16 inches above the surface. This is an inch higher relative to the surface than the nozzle would be if the craft were on a planar surface with no penetration of the footpads into the surface. Since the television pictures show no gross discontinuities in the surface beneath block 3 and vernier engine 3, this analysis implies a block surface clearance of about 12 inches prior to the leg deflections and a present clearance of 8 to 9 inches.

Shock Absorber Loads

The loads experienced by each shock absorber on the downhill leg assemblies for a vehicle sitting on a 20-degree slope are shown in

68189-5-16(U)

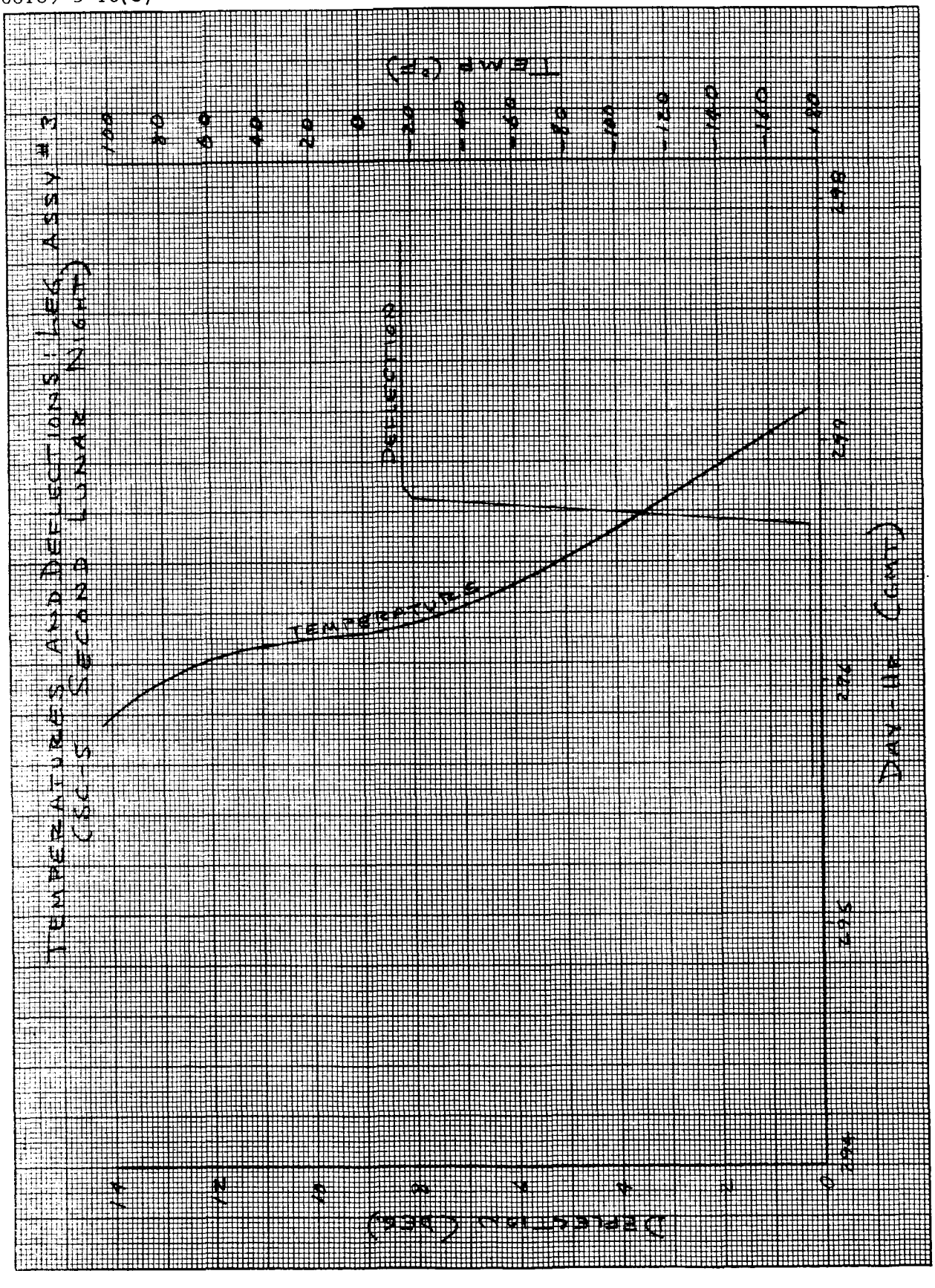

Figure 5.10-6. Temperatures and Deflections – Second Lunar Night Leg assembly 3

Figure 5. 10-7 for deflections of the downhill legs of from 0 to 18 degrees. The uphill leg is assumed to be in the undeflected position. On a 20-degree slope and with all legs undeflected, the uphill shock absorber would experience an 85-pound load. For the same situation, but with the downhill legs deflected 7 degrees, the uphill shock absorber would be loaded to 80 pounds. Hence, the shock absorber loads are calculated to be as shown in Table 5. 10-3.

TABLE 5. 10-3. SHOCK ABSORBER LOAD OF SURVEYOR V ON LUNAR SURFACE

Leg	Shock Absorber Load, pounds	
	Before Deflection	After Deflection
1	85	80
2	129	134
3	129	136

5. 10. 5 ACKNOWLEDGMENTS

The total analysis effort of the section was coordinated by C. D. Conaway. Margaret Dove and J. D. Hinchey aided in obtaining the analytical simulation of the landing.

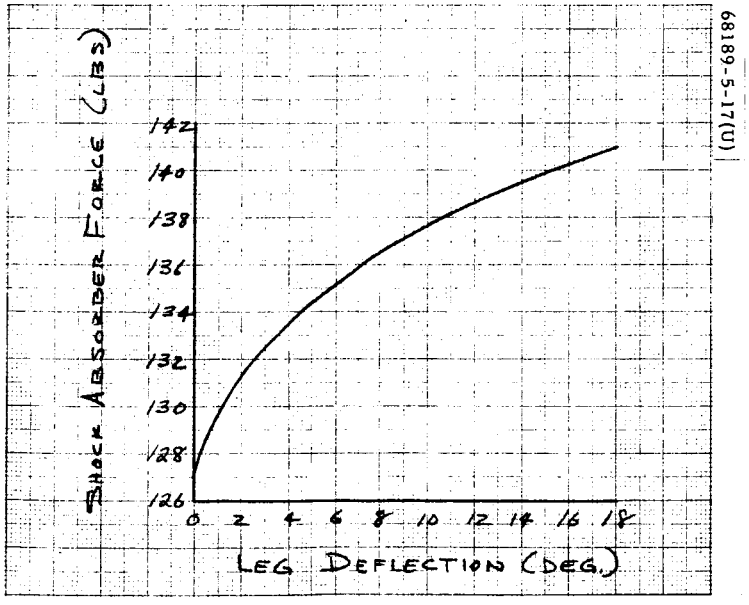

Figure 5. 10-7. Shock Abosrber Force Versus Deflection — Downhill Legs Resting on 20-Degree Slope

5. 11 MECHANISMS SUBSYSTEM

5. 11. 1 INTRODUCTION

This section deals with the mechanical performance of the spacecraft landing legs, omnidirectional antennas, and antenna/solar panel positioner (A/SPP). For purposes of this report, these mechanisms are collectively defined as the mechanisms subsystem.

1) Landing gear deployment – When each landing gear is fully deployed, it opens an electrical switch on the telescoping strut. The actuation of these switches indicates that the landing gear is deployed, and is required for initiation of automatic sun acquisition at separation from Centaur. The telemetry designations for these functions are V-1, V-2, and V-3 for each landing leg, respectively.

2) Omnidirectional antenna deployment – When each omnidirectional antenna is fully deployed, it opens an electrical switch to produce a change of state for telemetry purposes only. The telemetry designation for omnidirectional antenna A is M-1, for omnidirectional antenna B, M-2.

3) A/SPP automatic solar panel deployment – The A/SPP function after separation is to deploy the solar panel surface perpendicular to the roll axis to achieve maximum receipt of solar energy during transit.

The A/SPP has four rotation axes which are moved in steps upon command from earth. The axes are polar, solar, elevation, and roll. The polar axis rotates 1/16 degree per command; the other axes rotate 1/8 degree per command. Figure 5. 11-1 illustrates the A/SPP with the polarity of rotation for each axis. The telemetry designation for the A/SPP axis positions are as follows:

Solar panel	M-3
Polar axis	M-4
Elevation axis	M-6
Roll Axis	M-7

PRECEDING PAGE BLANK NOT FILMED.

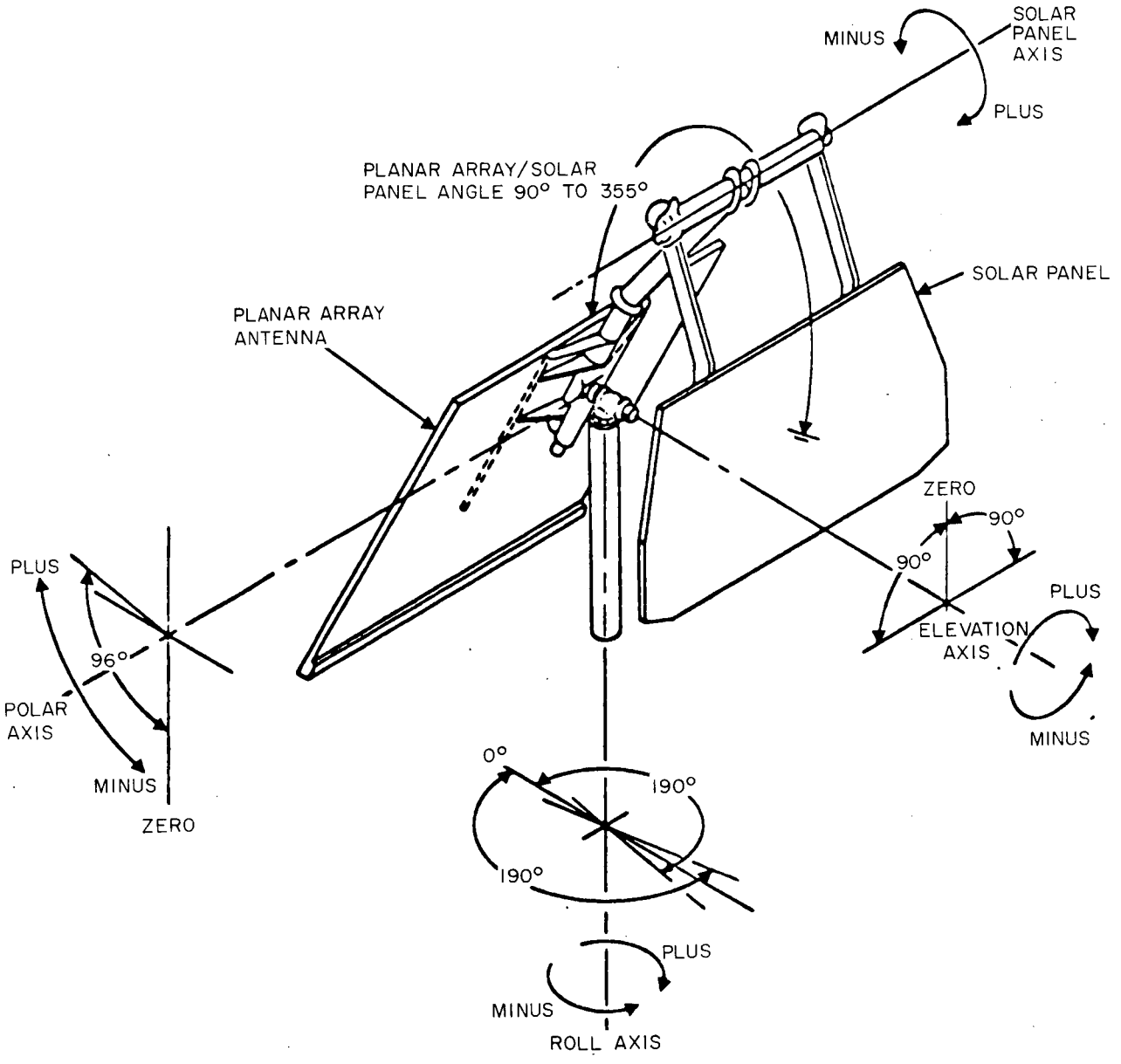

Figure 5.11-1. Antenna and Solar Panel Positioner

5.11.2 ANOMALY DESCRIPTION

No anomalies were detected in the mechanisms subsections during separation. Telemetry data during transit indicated no anomalous conditions.

5.11.3 SUMMARY AND RECOMMENDATIONS

All mechanism functions performed properly and at the correct times.

5.11.4 SUBSYSTEM PERFORMANCE ANALYSIS

Table 5.11-1 shows the occurrence of major events for the mechanisms subsystem. Table 5.11-2 presents a summary of the subsystem parameters reduced from telemetry data. The expected values were obtained from flight acceptance, type approval, and solar thermal vacuum testing, and from specified design performance values.

5.11.4.1 Landing Gear Deployment

Table 5.11-2 shows the nominal expected deployment time for the landing gear to be about 2.3 seconds. Flight data show the deployment time to be 2.265 ±1.2 seconds, which indicates nominal deployment time. The leg deflection signals (V5-7) also indicated normal and complete extension of the landing gear.

5.11.4.2 Omnidirectional Antenna Deployment

The nominal expected omnidirectional antenna deployment time is 2.4 seconds. The mission deployment time was 1.065 ±1.2 seconds, which is slightly below the expected value. Data show that both omnidirectional antennas were deployed at the same time.

5.11.4.3 A/SPP Performance

Automatic Solar Panel Deployment

Automatic solar panel deployment begins upon closure of the 22-volt switch in the separation sensing and arming device at vehicle separation. The solar panel launch lock is unlocked and the solar panel is stepped from 355 to 270 degrees where it is relocked. At this point, the roll axis is stepped from -60 to 0 degrees and relocked. Both positions are locked until after touchdown.

The Surveyor V mission solar panel deployment time was 521 seconds. Comparing this mission deployment time to that in solar thermal vacuum phase B (522 seconds), the agreement is excellent.

TABLE 5. 11-1. MECHANICAL EVENTS AT SEPARATION

Event	Mission Time, GMT, Day 251, hr:min:sec
Launch	07:57:01. 257
Extend landing gear (Centaur command)	08:15:45. 5*
Landing gears extended (V-1, V-2, V-3 on)	08:15:47. 765 ±1. 2
Extend omnidirectional antennas (Centaur command)	08:15:55. 7*
Omnidirectional antennas extended (M-1, M-2 on)	08:15:56. 765 ±1. 2
Spacecraft electrical separation (Centaur command)	08:16:22. 2*
Spacecraft electrical separation (M-9 on)	08:16:21. 365 ±1. 2
Spacecraft mechanical separation	08:16:26. 8*
A/SPP solar panel unlocked (M-14 on)	08:16:27. 965 ±1. 2
A/SPP solar panel locked in transit position (M-11 on)	08:22:29 ±1. 2
A/SPP roll axis locked in transit position (M-13 on)	08:25:36 ±1. 2

*Reported times from Centaur data (Reference 1).

TABLE 5.11-2. PERFORMANCE PARAMETERS SUMMARY

Parameter	Expected Value, Nominal	Measured Value
Time from Centaur extend landing gear command to legs extended indications (V-1, V-2, and V-3 on)	< 2.3 seconds	2.265 ±1.2
Time from Centaur extend omni-directional antenna command to omnidirectional antennas extended (M-1 and M-2 on)	< 2.4 seconds	1.065 ±1.2
Solar axis deployment time (A/SPP solar panel autodeployment)	306 seconds*	298 seconds
Roll axis deployment time (A/SPP solar panel autodeployment)	216 seconds*	223 seconds
Total A/SPP solar panel auto-deployment time	522 seconds*	521 seconds
Solar axis launch position (355 degrees) (M-3)	361.0degrees*	359.4 degrees
Polar axis launch position (0 degree) (M-4)	0.97 degree*	0.6 degree
Elevation axis launch position (0 degree) (M-6)	1.88 degrees	1.48 degrees
Roll axis launch position (-60 degrees) (M-7)	-58.4 degrees*	-58.4 degrees
Solar axis transit position (M-3)	270 degrees	273.8 degrees
Roll axis transit position (M-7)	0 degree	1.61 degrees
Leg deflection signals, prelaunch:		
Leg 1	24 degrees 0 BCD	24.5 degrees 2 BCD
Leg 2		25.5 degrees 1 BCD
Leg 3		26.2 degrees 2 BCD
Leg deflection signals, postlaunch:		
Leg 1	0 degree 958 BCD	-0.25 degree 968 BCD
Leg 2	0 degree 966 BCD	0.16 degree 960 BCD
Leg 3	0 degree 969 BCD	-0.22 degree 977 BCD

*Solar thermal vacuum test phase 2B.

Table 5.11-3 shows the positions of the A/SPP axis before and after the automatic solar panel deployment. These all fall within the required limits when corrections are applied to the telemetry data.

TABLE 5.11-3. A/SPP AXIS POSITIONS FOR PRELAUNCH AND POST-AUTODEPLOYMENT CONDITIONS

	Prelaunch*				Post-autodeployment, Transit**			
	Raw Data		Corrected Data		Raw Data		Corrected Data	
	BCD	Indicated Angle, degrees	BCD	Angle, degrees	BCD	Indicated Angle, degrees	BCD	Angle, degrees
M-03 solar axis	927	379.8	917	355.3	717	293.8	711	272.9
M-04 polar axis	248	3.7	246	0.12	247	3.49	245	0.01
M-06 elevation axis	521	16.18	515	0.01	520	15.7	516	0.28
M-07 roll axis	355	-49.8	352	-60.57	505	13.8	501	-0.80
S-01 reference voltage	1004	–	–	–	1001	–	–	–
S-02 reference return	0	–	–	–	0	–	–	–
S-05 commutator unbalance current	112	–	–	–	112	–	–	–

*Prelaunch data time 251:07:09:03.919

**Post-autodeployment data time 251:13:48:40.194

Postlanding Performance

Table 5.11-4 presents the complete record of stepping commands during lunar operations. It also includes a statement of the functions being performed during each block of stepping. Figure 5.11-2 presents this in graphical form.

Table 5.11-5 provides the number and direction of step commands sent for each A/SPP gimbal axis.

Drive Stepping Response

An evaluation of stepping count tallies for the first lunar day, as compared with telemetry readings, indicates that, as far as can be determined, the gimbal drives responded successfully to all commands. Table 5.11-6 is a comparison of telemetry versus step count angular increments for each axis. In the table, a positive difference means the telemetry indicated a larger angular motion than the actual number of steps commanded,

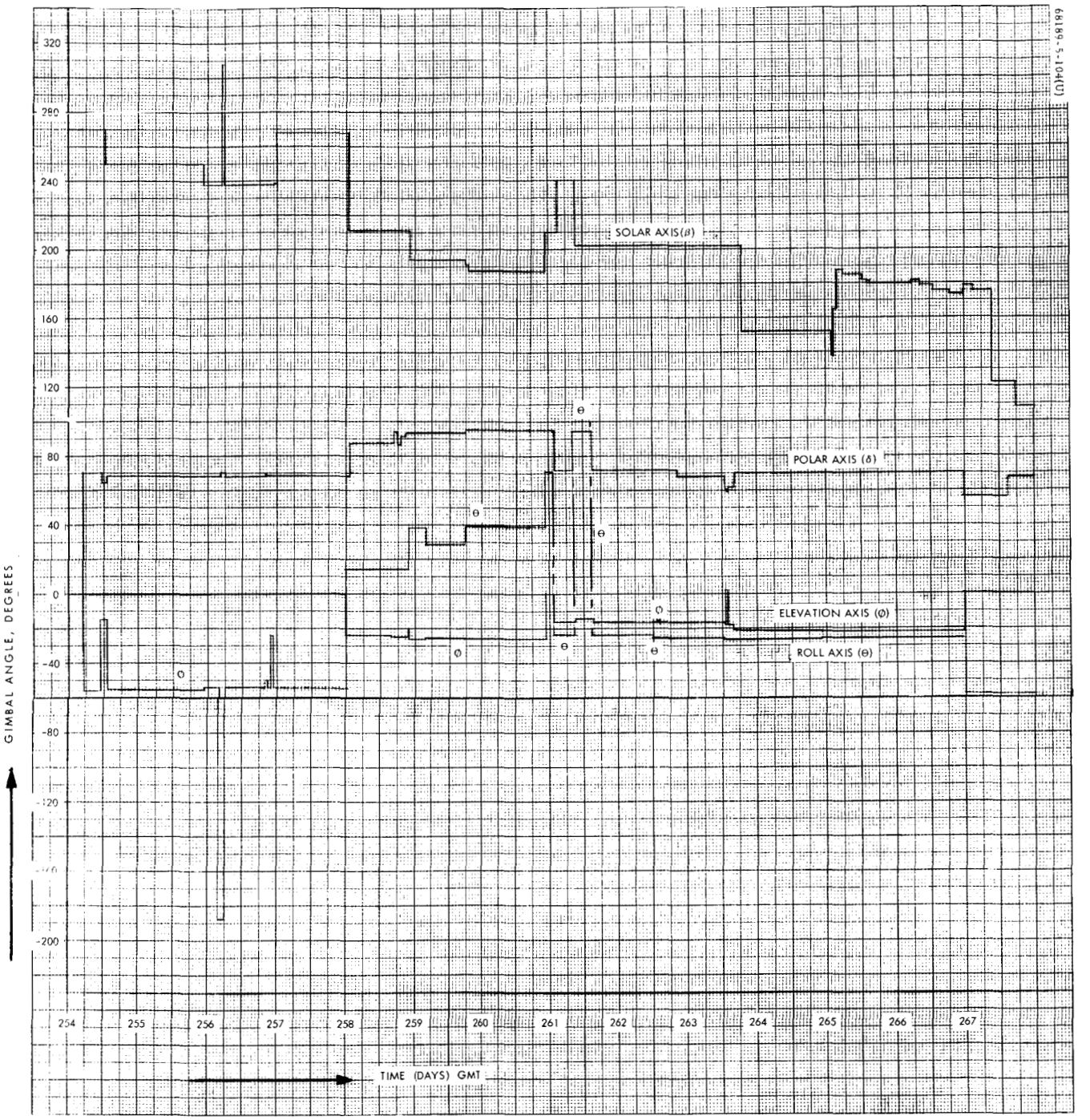

Figure 5.11-2. A/SPP Gimbal Angles Versus Time During First Lunar Day

TABLE 5.11-4. A/SPP STEPPING COMMAND LOG

Execution Time, day:hr:min	Command	Quantity	Function
254:02:58	403	584	Initiate earth search
03:08	403	570	
03:14	406	145	
03:20	405	217	
03:25	405	72	
03:28	404	44	
03:30	406	361	
03:39	404	292	
03:55	405	108	Initiate sun search
03:58	406	22	
04:02	403	219	
04:10	404	59	Complete sun acquisition
05:15	403	69	Resume earth search
05:16	406	282	Complete earth acquisition
10:43	404	106	
10:45	405	279	
11:09	405	22	
11:20	406	4	
11:23	405	2	
11:26	404	18	
11:31	403	2	
11:53	402	145	First spacecraft attitude determination
11:59	403	50	
12:01	406	290	
12:18	406	18	
12:23	405	32	
12:34	406	14	
12:35	403	28	
12:44	404	14	
255:22:41	405	15	
22:43	402	87	
256:04:30	403	33	
04:34	406	966	
04:41	401	505	Stow panels in safe position for engine static firing and return to normal position
05:50	402	505	
05:59	404	33	
05:59	405	966	

Table 5. 11-4 (continued)

Execution Time, day:hr:min	Command	Quantity	Function
256:19:51	405	19	Second spacecraft attitude determination
20:00	406	35	
20:07	405	18	
20:20	403	42	
20:27	404	42	
21:41	405	361	
21:47	401	7	
22:03	405	47	
22:13	406	10	
22:14	405	8	
22:18	402	10	
22:22	401	1	
22:29	406	406	
23:34	401	220	Lag sun with solar panel to adjust charge rate (SPAC power support)
258:00:29	410	40	Reposition to shade TV camera and compartment A
00:35	402	412	
00:39	403	277	
00:42	410	132	
00:43	405	489	
16:41	403	102	Support TELCOM in BER test, then return to shading configuration
16:43	410	11	
16:44	404	32	
16:54	403	5	
16:55	404	1	
16:58	403	2	
17:07	403	4	
17:14	403	4	
17:19	403	4	
17:20	404	1	
17:28	404	7	
17:37	403	5	
17:48	403	4	
17:58	403	4	
18:04	404	93	
19:08	403	72	
19:33	403	5	
19:34	404	1	
19:46	403	4	
19:59	403	4	
20:00	404	2	

Table 5.11-4 (continued)

Execution Time, day:hr:min	Command	Quantity	Function
258:20:09	403	3	Support TELCOM in BER test, then return to shading configuration
20:21	404	8	
20:23	403	2	
20:46	403	4	
20:47	404	2	
21:01	403	3	
21:18	403	18	
21:23	407	40	
21:33	404	1	
21:34	410	40	
21:36	405	181	
21:38	402	116	
21:39	410	4	
259:04:17	406	87	Reposition to shade TV camera
04:19	407	7	
17:36	405	87	Reposition to shade compartment A and alpha scattering device
17:39	410	7	
17:41	402	29	
17:42	403	16	
20:14	402	29	Improve shading of compartment A
260:23:10	405	238	Reposition to maximize compartment A shading by removing planar array from earth
23:19	407	188	
23:20	401	166	
261:01:57	406	686	Return planar array to earth
02:03	404	336	
02:07	410	121	
03:27	401	217	
08:55	402	275	Resume maximum compartment A shading by again breaking planar array earth lock
08:58	403	336	
09:05	407	20	
09:06	405	889	
14:37	404	336	Return planar array toward earth
14:41	410	20	
14:42	406	889	
262:21:16	404	58	
21:17	406	42	
21:35	405	32	
21:37	406	16	
21:39	403	20	
21:47	404	39	
21:48	403	16	

Table 5.11-4 (continued)

Execution Time, day:hr:min	Command	Quantity	Function
263:12:25	405	10	Support second part of TELCOM BER test over DSIF 11
12:27	410	13	
12:28	404	111	
13:02	404	5	
13:07	404	10	
13:14	404	6	
13:24	403	10	
13:29	404	10	
13:41	407	75	
13:57	407	60	
14:01	404	28	
14:14	410	135	
14:15	403	32	
14:26	403	122	
15:55	407	12	Support TV gain margin experiment (No. 22)
15:57	410	36	
16:01	407	8	
16:08	403	16	
16:09	404	98	
16:22	403	82	
17:08	404	32	
17:10	404	12	
17:11	404	9	
17:12	404	7	
17:13	404	6	
17:13	404	5	
17:14	404	4	
17:15	404	4	
17:16	404	3	
17:17	404	3	
17:18	404	3	
17:19	404	2	
17:21	404	2	
17:22	404	2	
17:23	404	2	
17:28	403	96	
17:51	404	32	
17:52	404	12	
17:53	404	9	
17:54	404	7	
17:57	404	6	
17:58	404	5	
17:59	404	4	

Table 5. 11-4 (continued)

Execution Time, day:hr:min	Command	Quantity	Function
263:17:59	404	4	Support TV gain margin experiment (No. 22)
18:00	404	3	
18:00	404	3	
18:01	404	3	
18:01	404	2	
18:02	404	2	
18:03	404	2	
18:03	404	2	
18:05	404	2	
18:12	403	97	
19:23	402	363	The solar panel was stepped numerous times to adjust the battery charge rate
264:21:34	404	26	
21:35	410	11	
21:37	405	16	
21:38	404	8	
21:41	403	44	
21:50	404	16	
21:51	405	14	
22:04	406	24	
22:10	405	16	
265:01:56	402	100	
02:42	401	200	
03:47	401	200	
03:53	402	35	
06:46	402	35	
06:48	401	15	
12:48	402	15	
12:57	402	15	
14:14	402	10	
266:05:09	401	10	
08:05	402	10	
08:08	402	10	
12:51	402	17	
13:08	402	5	
19:19	402	15	
23:14	404	101	
23:17	406	66	
23:19	407	43	
23:21	406	51	
23:23	407	36	
23:24	404	58	

Table 5. 11-4 (continued)

Exeuction Time, day:hr:min	Command	Quantity	Function
266:23:26	406	58	The solar panel was stepped numerous times to adjust the battery charge rate
23:45	407	36	
23:46	406	51	
23:48	407	46	
23:49	406	26	
23:51	404	26	
23:57	401	37	
267:03:19	402	36	
03:33	401	10	
09:45	402	30	
10:24	402	352	
15:32	403	147	
17:32	402	98	Reposition solar panel to second lunar day optimum position

TABLE 5. 11-5. POSTLANDING A/SPP STEPPING COMMANDS SUMMARY

Axis	Solar		Polar		Elevation		Roll	
Direction	Plus	Minus	Plus	Minus	Plus	Minus	Plus	Minus
Command	0401	0402	0403	0404	0407	0410	0405	0406
Total	1588	2754	3158	2221	571	570	4138	4549
Total plus and minus	4342		5379		1141		8687	
Grand total	19, 549							

TABLE 5. 11-6. STEP COUNT AND TELEMETRY INCREMENT COMPARISONS

GMT, day:hr:min	Angle	Angular Value		Increment Value		Difference, degrees
		Step Count, degrees	Telemetry, degrees	Step Count, degrees	Telemetry, degrees	
256:03:48	Solar (M3)	237.89	239.74	69.89 degrees plus stepping was followed by 69.89 degrees of negative stepping. Telemetry returned to initial value within 1 BCD.		–
05:42	Solar (M3)	307.78	Mode 4 unavailable			
05:42	Solar (M3)	307.78	Mode 4 unavailable			
07:12	Solar (M3)	237.89	239.48			
03:48	Roll (M7)	- 53.84	- 54.64	-133.69 degrees of stepping was followed by +133.69 degrees of stepping. Telemetry returned to within 1 BCD of initial value.		–
05:42	Roll (M7)	-187.53	Mode 4 unavailable			
05:42	Roll (M7)	-187.53	Mode 4 unavailable			
07:12	Roll (M7)	- 53.84	- 54.39			
257:15:35	Solar (M3)	268.06	270.74	-57.02	-59.15	2.13
258:06:59	Solar (M3)	211.04	211.59			
257:15:35	Polar (M4)	67.74	67.91	+18.95	+18.43	-0.52
258:06:59	Polar (M4)	86.69	86.34			
257:15:35	Elevation (M6)	0.00	0.44	-25.33	-24.53	-1.20
258:06:59	Elevation (M6)	- 25.33	- 24.09			
260:23:02	Solar (M3)	186.96	187.57	+22.97	+23.53	0.56
260:23:40	Solar (M3)	209.93	211.10			
260:23:02	Elevation (M6)	- 25.88	- 26.23	+26.02	+26.83	0.81
260:23:40	Elevation (M6)	0.14	0.60			
260:23:02	Roll (M7)	39.17	38.66	+32.94	+33.48	0.56
260:23:40	Roll (M7)	72.11	72.14			
261:01:53	Polar (M4)	94.72	94.26	-23.01	-22.45	-0.56
261:02:24	Polar (M4)	71.71	71.81			
266:23:09	Polar (M4)	66.65	66.86	-12.67	-12.62	-0.05
266:23:57	Polar (M4)	53.98	54.24			
266:23:09	Elevation (M6)	- 22.00	- 22.85	+22.13	+23.20	1.07
266:23:57	Elevation (M6)	0.13	0.35			
266:23:09	Roll (M7)	- 22.00	- 22.87	-34.88	-34.42	-0.46
266:23:57	Roll (M7)	- 56.88	- 57.29			

and vice versa for a negative difference. All telemetry values of the angles in Table 5. 11-6 have had all correctable errors removed. These corrections are described in Reference 2. The difference magnitudes are seen to be as large as 2. 13 degrees. These magnitudes exceed the tolerances that would have been expected for the Surveyor I through 4 drive series, but are within the increased tolerances of the Surveyor V through SC-7 redesign ($\leq$ 4 degrees). Therefore, all stepping efficiencies are completely within drive error tolerances.

5.11.5 REFERENCES

1) "Surveyor V Flight Path Analysis and Command Operations Report," Hughes Aircraft Company, SSD74131, 17 October 1967.

2) R. L. Lackman and W. R. Heathcote, "Error Analysis of the SC-3 Spacecraft Attitude on the Lunar Surface," Hughes Aircraft Company, IDC 2292/246, 4 April 1967.

5.11.6 ACKNOWLEDGMENTS

J. M. Berger, Technical Coordinator

R. L. Lackman

L. L. Gamer

5.12 TERMINAL DESCENT TRAJECTORY PERFORMANCE

5.12.1 INTRODUCTION

After the primary midcourse correction was initiated, a helium leakage was detected and the cause determined to be the direct result of improper reseating of the helium regulator. In an attempt to correct this malfunction, four additional midcourse maneuvers were performed. Although the problem persisted, extensive analysis during this period, including vernier propulsion system testing, indicated that a soft landing could possibly be achieved. The reduction in the helium supply governed a highly nonstandard, low retro burnout terminal descent sequence. Therefore, the sixth and final midcourse maneuver was performed to provide the necessary adjustments in order to attempt the soft landing. These adjustments were 1) to lighten spacecraft weight to reduce retro burnout velocity to the desired value, 2) to increase helium volume within the vernier engine propellant tank subsystem to provide sufficient vernier engine descent capability, and 3) to correct the trajectory back to the original aiming point.

The modified terminal descent, as determined from the extensive analysis, resulted in the generation of an emergency backup command tape that would override the on-board flight programmer governing the retro phase sequence of events. Based on a calculated retro burn time (from retro ignition to the 3.5 g point) of 39.28 seconds, the command tape was generated so that the retro case would be ejected 8 seconds after the 3.5 g point, followed 0.5 second later by the vernier engine command to high thrust, followed by 1.5 seconds delay until the start of the RADVS-controlled descent. In addition to the tape generation, the vernier ignition delay time from the AMR mark was determined to be 12.325 seconds. To conserve vernier propellant, the low thrust option during retro burn of 152.2 pounds would be implemented. This redesign, if successful, would result in a retro burnout condition of approximately 4600 feet altitude and 94 fps velocity as compared to 37,743 feet and 463 fps for the nominal mission. These burnout conditions were selected so that the nominal burnout would be within the possible burnout region defined by the maximum vernier descent capability as shown in Figure 5.12-1.

In order to achieve the desired burnout velocity and a near vertical flight path angle at burnout, the retro thrust direction at ignition was calculated to be biased 0.78 degree downward in the trajectory plane.

PRECEDING PAGE BLANK NOT FILMED.

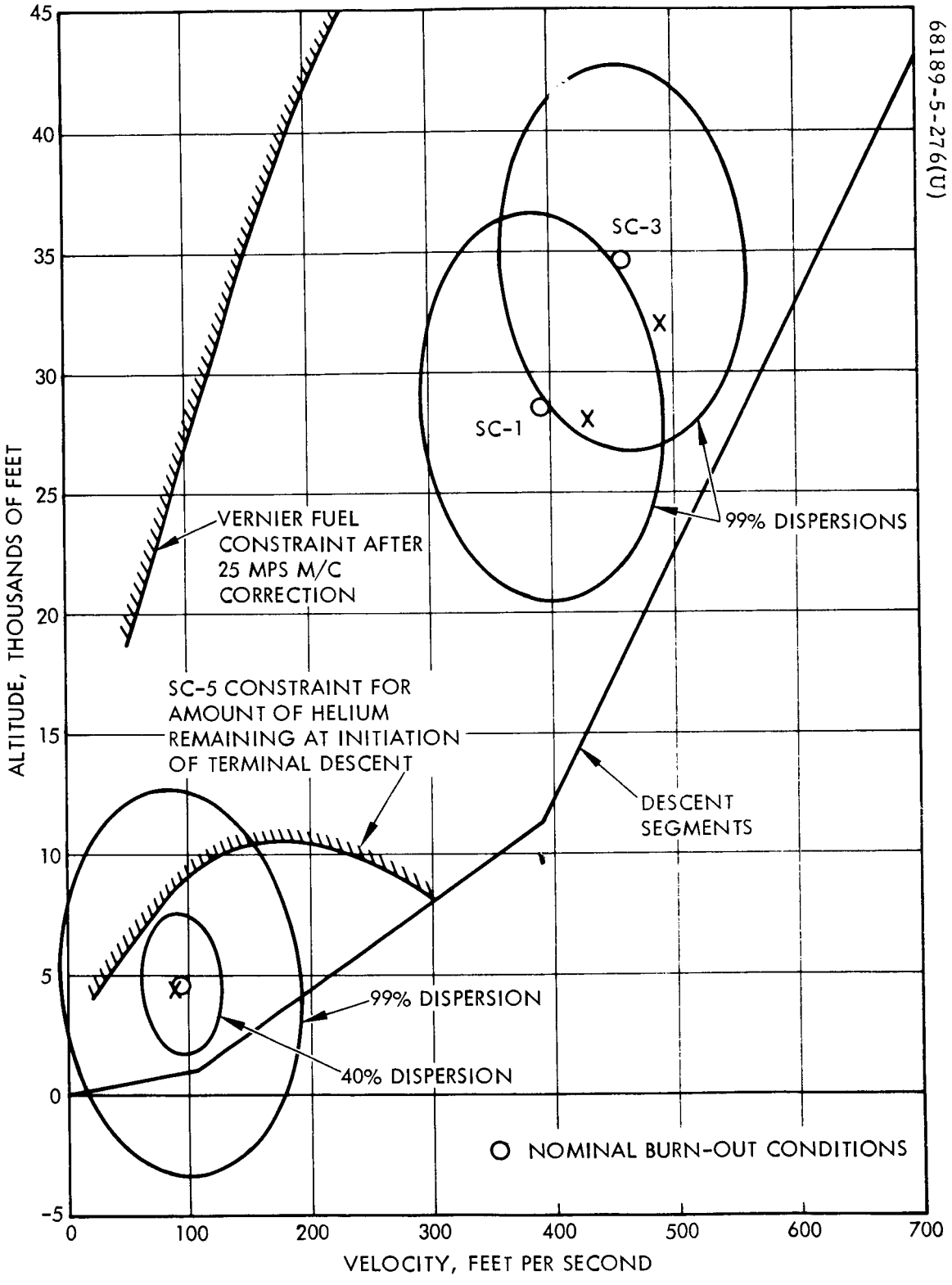

Figure 5.12-1. Retro Burnout Conditions (State of RADVS-controlled Descent)

The Surveyor V spacecraft, though subjected to extreme conditions during the terminal phase, performed miraculously well during the descent and successfully soft landed on the edge of a small lunar crater. The spacecraft landed on about a 20-degree slope with a velocity of approximately 13.5 fps.

The vernier engine performance during the vernier phase was expected to be degraded due to the helium loss. During the command descent contour phase, the postflight analysis of the telemetry data indicated a degradation in the vernier engine performance. This is further discussed in subsection 5.12.4.7.

Approximately 0.5 second after the retro case ejected, the radar altimeter beam dropped lock and then reacquired lock approximately 1.4 seconds after the start of the RADVS-controlled descent phase. Approximately 0.8 second after the start of RADVS-controlled descent, radar doppler velocity sensor beam 3 dropped lock and reacquired lock approximately 4.4 seconds after the start of RADVS control.

The loss of lock of both beams was probably caused by the retro case passing through the beam direction. The drop lock of beam 3 resulted in the loss of reliable operation of the doppler velocity sensors (RODVS), and the loss of lock of both the radar altimeter and beam 3 resulted in the loss of reliable operation of the radar altimeter (RORA). The loss of RORA at this point had no effect on the mission since the spacecraft was in the minimum acceleration control mode. However, the loss of RODVS resulted in erroneous spacecraft steering for approximately 4 seconds at which time beam 3 reacquired lock. The drop lock of beam 3 had an apparent effect on the spacecraft predicted performance in which optimal performance of all spacecraft subsystems was desired; fortunately, the erroneous steering was in a favorable direction.

The terminal descent performance and the major time events are summarized in this section, after which a discussion of the spacecraft terminal descent performance, as reconstructed by calibrated telemetry data and analytic reconstruction techniques, is presented.

5.12.2 ANOMALY DESCRIPTION

An anomaly during the terminal descent phase is defined as any deviation from the expected mission or system performance during this phase of the mission.

The radar altimeter dropped lock approximately 0.5 second after retro case eject and reacquired lock approximately 1.4 seconds after the start of the RADVS-controlled descent phase. Doppler velocity beam 3 dropped lock approximately 0.8 second after the start of the RADVS-controlled descent and reacquired lock approximately 3.5 seconds after loss of lock. This resulted in the loss of RORA and RODVS. The loss of

RORA had no effect on this phase of the descent; however, the loss of RODVS resulted in erroneous spacecraft steering. The radar beam reacquired in time for proper steering of the spacecraft.

Performance of the vernier engines was apparently degraded due to the helium loss; fortunately, the degradation was not critical to the success of the mission. Further discussions of this problem are given in section 5.6 and paragraph 5.12.4.7.

5.12.3 SUMMARY AND RECOMMENDATIONS

Table 5.12-1 lists significant terminal descent events and the most accurate determination of each event's time of occurrence. The DSS time is either plus or minus the one-way transit time delay (approximately 1.234 seconds), depending on whether the event is a command or a telemetered spacecraft action.

The significant terminal descent performance parameters are summarized in Table 5.12-2, along with the predicted values for the nonstandard descent sequence. The Surveyor V spacecraft performed extremely well during the terminal descent even with the ground command override of the retro phase sequence of events, the drop lock of beam 3, and the degradation of the vernier engine performance.

5.12.4 PERFORMANCE ANALYSIS

5.12.4.1 Introduction

The Surveyor V terminal phase performance has been investigated and analyzed by comparing processed telemetry data by the PREPRO (described in paragraph 5.12.4.2) program with a precision six-degree-of-freedom (6DOF) digital simulation reconstruction. Various nominal predicted preflight and preterminal inflight parameters within the 6DOF were adjusted so as to coincide discrete time events with discrete telemetry time events. These events provide the 6DOF program with significant data points for constructing a best-fit trajectory. Table 5.12-3 shows the discrete time events determined from telemetry data and compared with the best match reconstruction by the 6DOF program.

The one-way doppler data, as received by the tracking station, provides information for reconstructing a highly accurate retro thrust-time curve. These data, utilized by the DOPP program, also allow determination of the retro specific impulse, retro performance, and characteristic velocity (total ΔV removed) during the retro phase. From the retro accelerometer telemetry data, a thrust-time curve is also reconstructed by the TTC program, and comparison is made with the DOPP program reconstruction.

TABLE 5.12-1. BEST ESTIMATE TIMES FOR SURVEYOR V TERMINAL DESCENT

Event	GMT, Day 254, Hour 00	
	At DSS 11, min:sec	At Spacecraft, min:sec
AMR mark	44:39.081 ± 0.025	44:38.847 ± 0.025
AMR backup command sent	44:46.380 ± 0.05	44:47.614 ± 0.05
Vernier engine ignition	44:51.426 ± 0.02	44:50.192 ± 0.02
Retro engine ignition	44:52.496 ± 0.05	44:51.262 ± 0.05
RODVS on	45:20.555 ± 0.6	45:19.321 ± 0.6
RORA on	45:24.155 ± 0.6	45:22.921 ± 0.6
3.5-g switch	45:31.430 ± 0.025	45:30.196 ± 0.025
Retro eject	45:40.395 ± 0.05	45:39.161 ± 0.05
Retro ejected	45:40.855 ± 0.6	45:39.621 ± 0.6
RORA off	45:40.954 ± 0.6	45:39.720 ± 0.6
Start maximum thrust	45:40.955 ± 0.6	45:39.721 ± 0.6
Start RADVS-controlled descent	45:42.430 ± 0.025	45:41.196 ± 0.025
Beam 3 unlock	45:43.248 ± 0.6	45:42.014 ± 0.6
RORA on	45:47.000 ± 0.7	45:45.766 ± 0.7
Beam 3 lock	45:46.846 ± 0.60	45:45.612 ± 0.60
1000-foot mark	46:19.697 ± 0.05	46:18.463 ± 0.05
Segment intercept (segment three)	46:22.134 ± 0.15	46:20.900 ± 0.15
End of segment three	46:28.724 ± 0.15	46:27.490 ± 0.15
10-fps mark	46:37.097 ± 0.05	46:35.863 ± 0.05
14-foot mark	46:42.697 ± 0.05	46:41.463 ± 0.05
Touchdown	46:44.397 + 0, - 0.07	46:43.163 + 0, - 0.07

TABLE 5. 12-2. SUMMARY OF TERMINAL DESCENT PERFORMANCE PARAMETERS

Parameter	Predicted Value	Best Estimated Value
Vernier ignition initial conditions		
Time, hr:min:sec	00:44:50. 05	00:44:50. 192
Altitude, feet	150, 164	147, 604
Velocity, fps	8, 484. 84	8, 487. 68
Attitude, degrees	44. 27	44. 27
Thrust vector bias, degrees	-0. 78	-0. 78
Start RADVS controlled descent		
Altitude, feet	4, 598	4, 139. 5
Total velocity, fps	94	79. 3
V_x	—	-40. 9
V_y	—	49. 9
V_z	—	45. 7
Attitude, degrees	45. 73	45. 72
Flight path angle, degrees	-5. 05	-35. 67
Retro burn time, seconds	39. 28	38. 934
Misalignment angle during retro		
In plane, degrees	0	-0. 06
Out of plane, degrees	0	-0. 291
1000-foot mark conditions		
Slant range, feet	1, 000	1, 048
Total velocity, fps	106. 45	96. 03
V_z	—	95. 7
Attitude, degrees	-8. 3	-7. 5
Segment acquisition conditions		
Slant range	1, 500	806
Velocity (V_z), fps	117	97
10-fps mark conditions		
Slant range, feet	43. 0	46
Velocity (V_z), fps	8. 6	9. 3
Attitude, degrees	-0. 24	-0. 53
Vernier engine cutoff conditions		
Slant range, feet	13. 0	14. 5
Velocity (V_z), fps	5. 04	5. 2
Attitude, degrees	-0. 10	0. 11
Touchdown conditions		
Longitudinal velocity, fps	13. 0	13. 5
Lateral velocity, fps	0. 0	0. 5
Total vernier propellant used, pounds	136. 65	136. 62

TABLE 5.12-3. 6DOF DISCRETE TIME EVENTS VERSUS TELEMETERED

Event	6DOF Time, (Figures 5.12-8 to 14), seconds	GMT	
		Converted Figure Time to GMT, min:sec	Actual GMT at DSS-11, min:sec
Vernier engine ignition	0.0	44:51.40	44:51.426±0.025
Retro ignition	1.1	44:52.50	44:52.496±0.05
3.5-g mark	40.01	45:31.41	45:31.430±0.025
Retro eject	49.01	45:40.41	45:40.395±0.05
Start maximum thrust	49.51	45:40.91	45:40.955±0.6
Start RADVS-controlled descent	51.01	45:42.41	45:42.430±0.025
1000-foot mark	88.33	46:19.73	46:19.697±0.05
Segment intercept (segment 3)	90.70	46:22.10	46:22.134±0.15
Segment 3 — engine thrust command unsaturate	94.80	46:26.90	46:26.634±0.15
End of segment 3	97.25	46:28.65	46:28.724±0.15
Segment 4 — engine thrust command unsaturate	104.00	46:35.40	46:35.334±0.15
10-fps mark	106.55	46:37.95	46:37.097±0.05
14-foot mark	112.32	46:43.72	46:42.697±0.05
Touchdown	113.86	46:45.26	46:44.397+0,-0.7

An additional feature implemented within the 6DOF program, which provides a measure of confidence to the 6DOF reconstruction, is a simulation of the doppler data. The doppler data were converted to radial velocity, the velocity in the direction of the earth tracking station-spacecraft line of sight. The same parameter is computed within the 6DOF program. The two methods are then compared, thus providing an additional confidence measurement of the 6DOF reconstruction.

The total vernier propellant consumption (Table 5.12-4) for the individual midcourse maneuvers and retro and vernier phases was determined by utilization of the vernier engine flight acceptance data of mixture ratio and specific impulse as a function of thrust. However, the test data are also a function of helium pressure and temperature characteristics. The

TABLE 5.12-4. VERNIER PROPELLANT CONSUMPTION, POUNDS

Phase	Engine 1	Engine 2	Engine 3	Total	Preterminal Mission Predictions
Midcourse 1	3.69	3.69	3.65	11.03	
Midcourse 2	2.62	2.61	2.58	7.81	
Midcourse 3	5.97	5.97	5.90	17.84	
Midcourse 4	3.38	3.38	3.34	10.10	
Midcourse 5	8.56	8.56	8.46	25.58	
Midcourse 6	1.41	1.41	1.39	4.21	
Total midcourse	25.63	25.62	25.32	76.57	77.00
Main retro phase	10.43	9.84	8.76	29.03	28.70
Vernier phase	10.34	10.34	10.34	31.02	30.95
Total used	46.40	45.80	44.42	136.62	136.65
Total loaded	61.25	61.25	61.25	183.75	
Trapped (lines and expulsion efficiency)	0.71	0.71	0.71	2.13	
Usable loaded (total-trapped)	60.54	60.54	60.54	181.62	181.62
Remaining propellant (usable and unusable)	14.14	14.74	16.12	45.00	44.97

vernier propellant consumption determination therefore cannot be assigned to within any high degree of accuracy due to the degraded performance of the vernier engine subsystem caused by the helium regulator malfunction. However, the results are included since they will indicate the probable propellant consumption.

The best-fit terminal descent trajectory reconstruction scheme employed for Surveyor V was similar to that of previous flights. Again, the scheme depends on establishing a good reference point near retro burnout in which the spacecraft V_x, V_y, and V_z telemetry data are reliable. The point selected was at retro case eject since at this point all doppler velocity sensor beams were reliable. Based on postmission assessment of the RADVS and telemetry systems, the calibrated V_x, V_y, and V_z velocities at retro case eject were determined to be:

V_x = -33.75 fps

V_y = 49.84 fps

V_z = 60.79 fps

These values are accurate to within 1 percent.

With the DOPP program retro thrust-time curve as input into the 6DOF program, the initial conditions at vernier ignition of velocity, altitude, and retro thrust vector misalignment (as determined from orbit determination postflight data) were perturbed within the 6DOF program until the above velocities at retro case eject and the elapsed time from start of RADVS-controlled steering to the 1000-foot mark and command descent contour intercept (as indicated by telemetry) were matched. Telemetry data also indicated a degradation in the vernier engine performance during the command descent contour phase. Therefore, additional adjustments were made to the engine model within the 6DOF program in order to match the telemetry indicated conditions (see paragraph 5.12.4.7 for further discussion).

Also simulated in the 6DOF program was the drop lock of beams 3 and 4 at the time of RADVS-controlled descent. With the velocities at retro case eject and the discrete time events matched, the 6DOF reconstruction provided a fairly close comparison to the telemetry data. Therefore, the 6DOF reconstruction was considered a good estimate of the actual Surveyor V performance. The 6DOF reconstruction is discussed further in paragraph 5.12.4.7.

5.12.4.2 Postflight Analysis Computer Programs

PREPRO

The PREPRO program converts an input tape of processed telemetry data into appropriate engineering units. The input telemetry data tape is preprocessed by Hughes into raw BCD counts and appears in commutator sequence. The spacecraft preflight telemetry calibration coefficients are utilized within the program for the conversion into engineering units. Prior to the conversion, the flight control reference return (FC-77 telemetry signal) correction is made to the appropriate signals. The program interpolates engineering data significant to terminal descent reconstruction into preselected equal time intervals. PREPRO then writes two output tapes: tape No. 1 of the interpolated engineering data, and tape No. 2 of all the input signals in proper engineering units as they appear in commutator sequence.

POSTPR

POSTPR provides machines plots (CALCOMP) of any combination of variables from the following input data tapes: PREPRO tape No. 1, 6DOF data tape, and both PREPRO tape No. 1 and the 6DOF tape, thus providing a superimposed plot of the best estimated 6DOF reconstruction and the telemetered data.

6DOF

6DOF is a precision six-degree-of-freedom digital program simulating the Surveyor terminal phase from vernier ignition to touchdown. The program assumes rigid body dynamics, including spacecraft weight and moment of inertia changes. The program also models the spacecraft flight control and radar subsystems. The flexibility of the data input is such that preflight and postflight reconstructions of the terminal phase can be made. By matching significant time events with telemetry discrete times, a fairly accurate reconstruction of the terminal phase trajectory can be established by the 6DOF program in the absence of gross system errors or telemetry errors in spacecraft V_x, V_y, and V_z velocities. The program outputs are velocity, position, acceleration, attitude, moments, weight, inertia, angular velocity, control loop states, engine commands and thrusts, and radar system states. The program also writes a tape that can be used for machine plots (CALCOMP) of any combination of variables. The tape can also be set up for input into the POSTPR program.

TD1

TD1 is a two-dimensional, three-degree-of-freedom simulation of the terminal phase of the Surveyor mission. The main use of TD1 is to determine the vernier propellant consumption. The program can also be used to a limited extent for terminal descent trajectory reconstruction since it is restricted to a planar case. However, the program models the spacecraft to the extent necessary for accurate propellant consumption determination, that is, if no apparent degradation appears in the vernier engine performance.

TTC

TTC reconstructs the retro thrust-time curve from raw accelerometer telemetry data. Corrections are made to the telemetry data by removing bias, scale factor, and hysteresis errors. This reconstruction is used for comparison with the DOPP program reconstruction.

DOPP

DOPP reconstructs the main retro thrust-time curve from the spacecraft transmitter's one-way doppler data. This reconstruction technique is especially accurate since the frequency of the spacecraft transmitter is very stable. The program accounts for errors introduced by the transmitter's temperature sensitivity drift, variation in retro thrust vector direction during retro burn, and flight control sensor deflection. The program is also utilized for determining the main retro specific impulse.

5.12.4.3 Velocity Change Due to Thrusting During Retro Phase

Determination of Ignition Conditions

Ignition velocity V_o, flight path angle γ, and roll angle Φ serve as initialization parameters and are determined from tracking data. The 3σ uncertainty in free flight velocities is < 0.5 fps. Since ignition altitude has a calculated 3σ inaccuracy of 3570 feet due to marking range errors (with a V = 8500 fps and an incidence angle with respect to local vertical of 45 degrees), the equivalent ignition velocity uncertainty due to this error source is

$$\Delta V = gt = 5 \times \frac{3570}{8500} = 4.2 \text{ fps}$$

Hence, the total uncertainty in ignition velocity is 4.2 fps when these two independent error sources are combined. The direction of V_o at ignition has an uncertainty of < 0.07 degree. Therefore, the best estimate ignition conditions are

$$V_o = 8484.84 \pm 4.2 \text{ fps}$$

$$\gamma_o = -44.95 \pm 0.07 \text{ degree}$$

Gravity-Induced Component of Velocity

During the retro phase (from vernier ignition to signal loss), gravity contributes to the spacecraft velocity by an amount $\int \underline{g}\, dt$. Lunar gravity varies in magnitude from 5.07 ft/sec^2 (at vernier ignition) to 5.33 ft/sec^2 (at start of RADVS). In addition, $\underline{g}$ varies in direction since the spacecraft has horizontal motion. The change in direction of $\underline{g}$ over the retro phase (to signal loss) is about

$$\int_o^t \sin^{-1}\left[\frac{V \sin \psi \, dt}{R_\ell}\right] = 1.46 \text{ degrees}$$

where

t = retro time

ψ = velocity vector incident angle

V = spacecraft velocity

R_ℓ = moon centered radial distance

Since the vehicle spends more time at lower altitudes than at higher ones, the average value of g for the retro phase will be closer to 5.33 ft/sec^2. The time duration of the retro phase is 51.0 seconds (see Table 5.12-1). Actual numerical integration of $\int g\,dt$ gives gt = 268.7 ± 1 fps.

Thrust-Induced Velocity Change

The two methods used to calculate velocity change during the retro phase due to the thrusting of the engines are as follows:

1) $\underline{\Delta V}$ from vector addition — The vector equation (Figure 5.12-2a) $\underline{V}_{BO} = \underline{V}_o + \underline{gt} + \underline{\Delta V}$ can be solved to find $\underline{\Delta V}$. $\underline{V}_o$ and $\underline{gt}$ are available as discussed above; the spacecraft axis components of $\underline{V}_{BO}$ (the velocity at retro case eject) are available from calibrated telemetry data. The axial velocity V_z is known to an estimated accuracy of better than 1 percent at a given time, based on correlation of simulated versus actual discrete time events such as the 1000-foot mark and the 10-fps mark. V_x and V_y at retro case eject have calculated uncertainties of 1.96 and 1.42 fps, respectively, based on 3σ telemetry and RADVS sensor errors. At retro case eject, the velocity components are:

$$V_{BO_x} = -33.7 \pm 2.0 \text{ fps}$$

$$V_{BO_y} = 49.8 \pm 1.4 \text{ fps}$$

$$V_{BO_z} = 60.8 \pm 0.6 \text{ fps}$$

This method will yield ΔV to an accuracy of ±5.0 fps. δI, the in-plane thrust misalignment angle (Figure 5.12-2b) between $\underline{V}_o$ and z, defined as positive when z is "above $\underline{V}_o$" as shown, is known to be within ±0.02 degree based on uncertainties in V_{BO_x}, which is primarily in-plane. δo, the out-of-plane angle between these two directions, is known to be within ±0.02 degree based on uncertainties in V_{BO_y}. δo is positive when z has a component out of the paper. This method yields ΔV at the start of RADVS-controlled descent of

$$\Delta V = 8619 \pm 5.0 \text{ fps}$$

also,

$$\delta I = -0.06 \pm 0.02 \text{ degree}$$

$$\delta o = -0.291 \pm 0.02 \text{ degree}$$

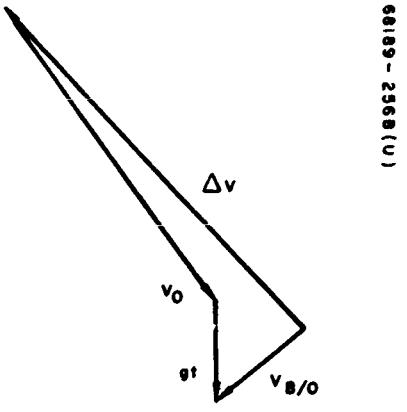

68189-256B(U)

a) Vector Diagram

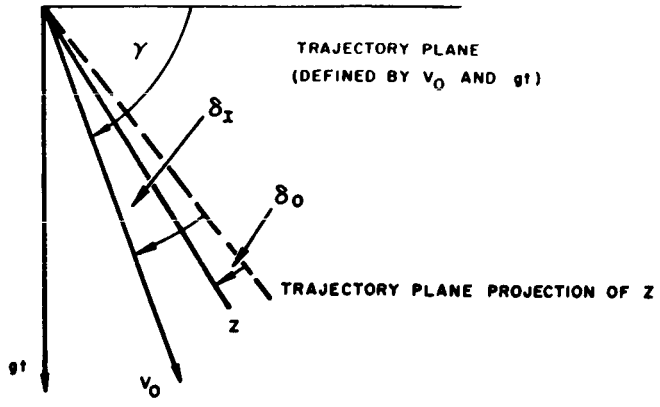

68189-256A(U)

b) Trajectory Plane

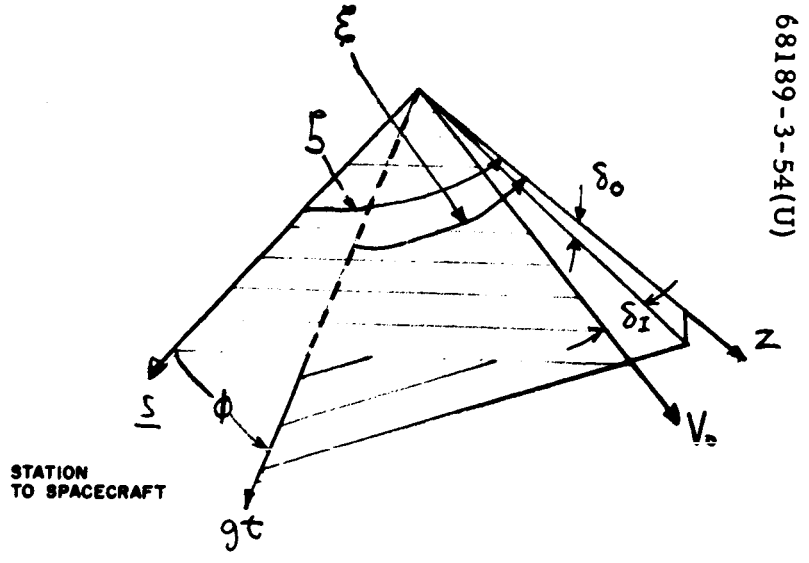

68189-3-54(U)

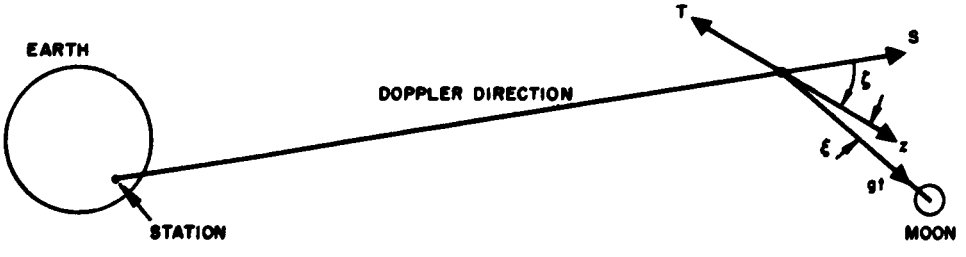

c) Doppler Geometry

Figure 5.12-2. Spacecraft Velocity During Retro Phase

Values of the other angles in degrees shown in Figure 5.12-2c are as follows:

$$\xi = 44.06$$

$$\zeta = 29.19$$

$$\varphi = 17$$

2) $\underline{\Delta V}$ from doppler data — The thrust-induced velocity change of the spacecraft is determined from the spacecraft one-way doppler data by the DOPP program. These data are input into DOPP and are corrected for the transmitter's temperature-dependent frequency drift within the program. This correction is determined by comparing postflight doppler data prior to vernier ignition with a simulated determination of the expected doppler shift since, at this period in the flight, the actual doppler shift is well defined.

The ΔV during this phase is found by dividing the sum of the radial velocity change as determined from the doppler data and the gravity-induced velocity component in the same radial direction by the cosine of the angle between the tracking station-spacecraft line and the spacecraft thrust axis. A correction is made to the doppler data to account for the radial velocity change, ΔV_{ROT}, due to the earth's rotation. The thrust-induced velocity change, ΔV, can therefore be determined as follows:

$$\Delta V = \frac{\Delta V_{DOPP} + gt \cos \varphi + \Delta V_{ROT}}{\cos \xi}$$

where

ΔV_{DOPP} = velocity change seen by tracking station

φ = angle between tracking station-spacecraft line and lunar gravity direction

ξ = angle between tracking station-spacecraft line and thrust direction

Therefore,

$$\Delta V = \frac{7270 + 257 + 4}{\cos 29.19} = 8627 \text{ fps}$$

An uncertainty exists in the angle ξ of ±0.03 degree due to uncertainties in δI and δo, the thrust misalignment angles. An uncertainty also exists in the temperature-dependent doppler frequency drift of ±5 fps. The above uncertainties result in an uncertainty of ±8 fps in ΔV.

Comparison of ΔVs and Retro Performance Implications

It is interesting to note that not only do the absolute magnitudes of ΔV check surprisingly well, but, out of necessity, so does the inertial thrusting direction as computed from burnout conditions. The doppler data are inherently one-dimensional and, to be useful in computing the retro thrust ΔV, the angular information supplied by the vector addition method of computing ΔV must be accurate. Thus, due to the geometric relation of the earth vector and trajectory plane, an uncertainty of 0.1 degree in the in-plane angle (δi) would cause an 8.0-fps variation in the total ΔV as computed by doppler. Since the two ΔVs check to ±8 fps, this would give added confidence in the thrusting direction computed from the telemetered and corrected burnout conditions.

Assuming a nominally performing main retro and vernier system, the main retro phase ΔV should have been 8611 fps as compared to 8623 fps actual (average of the two methods). Of the nominal 8611 fps total ΔV, a nominal performing vernier system would have contributed 208.7 fps. Based on a retro phase trajectory reconstruction by DOPP, the nominal vernier system would have contributed 214.6 fps due to the slight increase in actual time from vernier ignition to the beginning of RADVS control over predicted time.

The retro performance, based upon the ΔV which it took out, was very nearly nominal. The slight increase in actual total impulse over nominal ($\delta T_{imp}/T_{imp}$) is given by

$$\frac{\delta T_{imp}}{T_{imp}} = \frac{\delta \Delta V}{\Delta V retro} \times 100 \text{ percent}$$

$$= \left(\frac{8623 - 214.6}{8611 - 208.7} - 1 \right) \times 100 \text{ percent} = 0.07 \text{ percent}$$

The above percent increase in total impulse results in a retro specific impulse of 289.35 seconds as compared to the nominal predicted value of 289.56 seconds.

5.12.4.4 Main Retro Thrust Versus Time Curve

Two independent methods used to calculate the retro's thrust versus time curve are as follows:

1) Thrust/time from retro accelerometer data – Before being used to calculate a thrust curve, the raw accelerometer data are given the following three corrections:

   a) Biases are removed by comparing telemetered values with known values of acceleration which occur at times such as those prior to vernier ignition (zero g), after retro separation $\approx$ (0.9 g), etc.

   b) A scale factor error is removed. This is done by integrating the unbiased accelerometer data over time and comparing the resulting integral with the retro phase ΔVs found by the other two methods of computing ΔV described above. The scale factor is then the integral divided by the mean of the other two ΔVs. The unbiased acceleration divided by this scale factor is then assumed free of bias and scale factor errors.

   c) A hysteresis error is removed by actually determining two biases: one for the rising part of the acceleration curve, and the other for the falling part.

   The bias on each part of the curve can be removed to an accuracy of 0.1 g_{earth}, and the accuracy of the scale factor is 0.1 percent.

   The corrected acceleration is then used in the equation

$$T(t) = \frac{a(t)}{g_o}\left[W_o - \int_o^t \frac{T(t)}{I_{sp}}\,dt\right]$$

   which is integrated numerically to obtain total thrust (W_o is weight at retro ignition). Vernier thrust is then subtracted out to obtain the retro thrust.

   I_{sp} for this calculation is found from the relation below where W_L is the weight lost from retro ignition to burnout.

$$I_{sp} = \frac{\Delta V}{g_o \ln \frac{W_o}{W_o - W_L}}$$

   Figure 5.12-3 shows the Surveyor V thrust-time curve as determined from accelerometer data, with the raw accelerometer and corrected accelerometer curves also shown. Since the reconstructed thrust-time curve indicated a shorter burn time than the predicted (0.35 second less between retro ignition and the 3.5-g point), the nominal predicted curve was first modified

before being plotted on Figure 5.12-3 in order to give a better comparison between reconstructed and predicted thrust versus time shapes. The predicted curve plotted on Figure 5.12-3 was obtained by decreasing the time scale on the actual predicted curve by a scale factor to match up the 3.5-g points and by scaling up the thrust by a corresponding factor so that the total predicted impulse would not be changed.

2) Thrust/time from doppler data — Figure 5.12-4 shows the main retro thrust curve as constructed from doppler counts received at Goldstone. Since this reconstruction showed the same 0.35-second decrease to the 3.5-g point as did the accelerometer reconstructed thrust curve, the actual predicted curve was again compressed to match the 3.5-g point and raised to preserve total impulse before it was plotted on Figure 5.12-4.

   To construct the curve, a retro phase simulation trajectory program using a nominal thrust curve calculates nominal radial velocities relative to the tracking station and converts these to doppler counts that the station would receive from a stable spacecraft transmitter on a nominal trajectory.

   The nominal thrust curve is then perturbed until the doppler data from the perturbed curve are arbitrarily close to the doppler data actually received. For each point considered on the thrust curve, a difference between actual and perturbed counts over a 1-second interval of two counts (i.e., about 0.4 fps) is considered close enough. In addition, the sum of such differences is constrained to be within 20 counts (4.3 fps).

   Radial velocity divided by the cosine of the angle between the tracking station and the thrust direction (29.19 ± 0.08 degrees) gives total velocity. When gt cos $\bar{\gamma}$ is added, the remaining velocity differences are entirely due to thrusting and give the thrust acceleration. Multiplication by the mass then gives the thrust level.

Comparison of Two Methods for Retro Thrust/Time Curve

Of the two curves shown in Figures 5.12-3 and 5.12-4, the doppler reconstructed curve is much smoother. The roughness in the accelerometer reconstructed curve is due to accelerometer striction which is very difficult to remove from the data. Both reconstructions agree closely with respect to the nominal predicted curve. The maximum variation between actual and predicted is not substantial (generally less than 200 to 300 pounds). As explained previously, the actual total impulse was only 0.07 percent above the predicted.

The most significant discrepancy between the actual and predicted thrust-time curve for this flight is the 0.35-second decrease in the actual burn time since a slight variation in burn time causes a significant variation in burnout altitude.

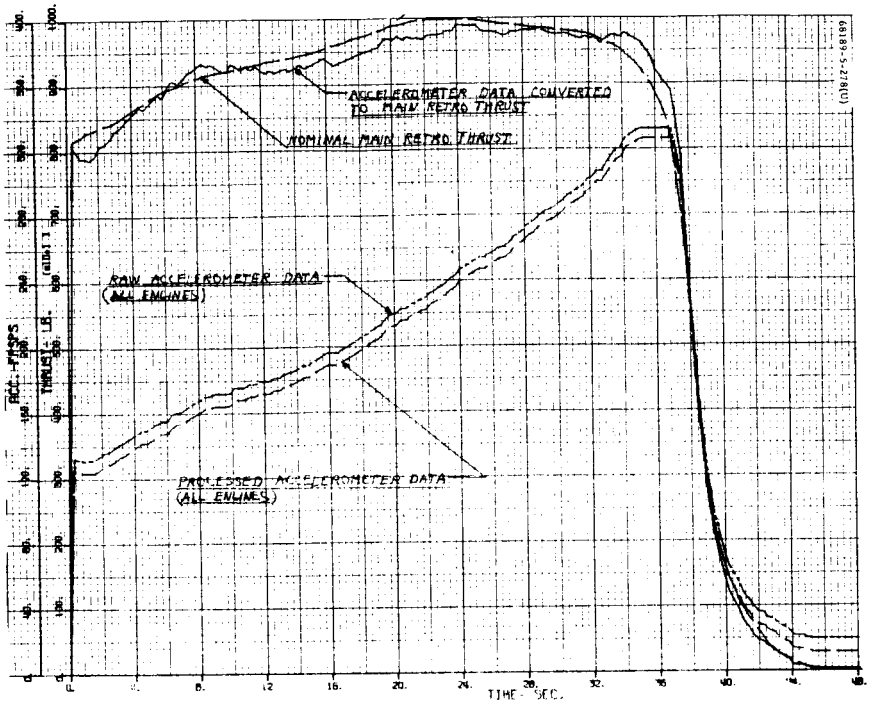

Figure 5.12-3. Retro Phase Thrust and Acceleration Versus Time (From Retro Accelerometer Data)

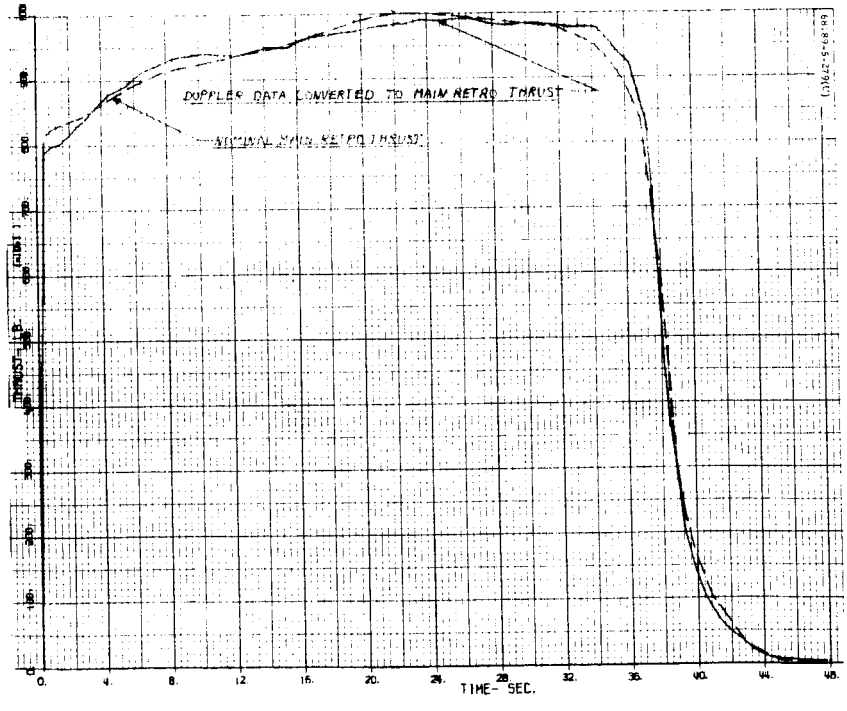

Figure 5.12-4. Main Retro Thrust Versus Time (From Doppler Data)

Since the 6DOF program trajectory reconstruction indicated that the main retro ignited at a lower altitude than predicted, it appears that the altitude dispersion caused by the 0.35-second decrease in burn time was offset by a lower than predicted ignition altitude.

Main Retro Tailoff from Doppler Data

Figure 5.12-5 shows an enlargement of the thrust tailoff region of Figure 5.12-4 (doppler reconstruction). This region was of special interest for the Surveyor V flight since the retro case was ejected sooner than normal. Had the retro thrust been too high at this time, the retro case could have made contact with the spacecraft instead of dropping away.

After removing the temperature-dependent frequency drift from the doppler data, the remaining noise level in the tailoff region is within ±3 doppler counts on each 1-second data point. This gives a possible radial acceleration error as measured by the earth tracking station of $\pm 0.65\ ft/sec^2$ or $0.75\ ft/sec^2$ along the spacecraft thrusting direction. With a spacecraft mass of about 26 slugs at this point, the possible error in doppler reconstructed thrust-time curve in this region is given by $\Delta T = (\pm 0.75)(26) = \pm 20$ pounds. This is the possible error after the retro thrust has dropped below 200 pounds. The possible error for higher thrust values is larger.

5.12.4.4 Best Estimate Reconstruction Summary

The 6DOF trajectory reconstruction and the DOPP retro thrust-time reconstruction in conjunction with the calibrated telemetry data indicated several differences from those predicted. From Table 5.12-2, the retro burn time is 0.346 second less than predicted. This would result in approximately 1400 feet higher burnout altitude than predicted; however, the best estimate of burnout altitude is approximately 458 feet lower. This can be explained from two conditions indicated by the postflight analysis. First, the large out-of-plane misalignment of the retro thrust vector would result in a lower burnout altitude. This is also the reason for the differences between best estimate and predicted values of velocity and flight-path angle at burnout. The other condition that would cause a lower burnout altitude is the vernier ignition altitude being 2560 feet lower than predicted.

Since the best estimates of velocity, flight-path angle, and spacecraft attitude at vernier ignition are the same as predicted, and the in-plane retro thrust vector misalignment is essentially zero, the differences in the ignition altitude are therefore primarily due to errors in the AMR. This difference is within the 3σ AMR uncertainty (3570 feet) in altitude (see subsection 5.12.4.3).

The postflight analysis indicated a 9-second duration from the retro 3.5-g point to the retro case eject signal. This time is approximately 1 second longer than designed for by the backup command tape override. Part of this time is attributed to the reduction of 0.346 second in the predicted retro burn time. The other remaining 0.6 second is probably attributed to the initialization of the command tape. The AMR backup command was the first

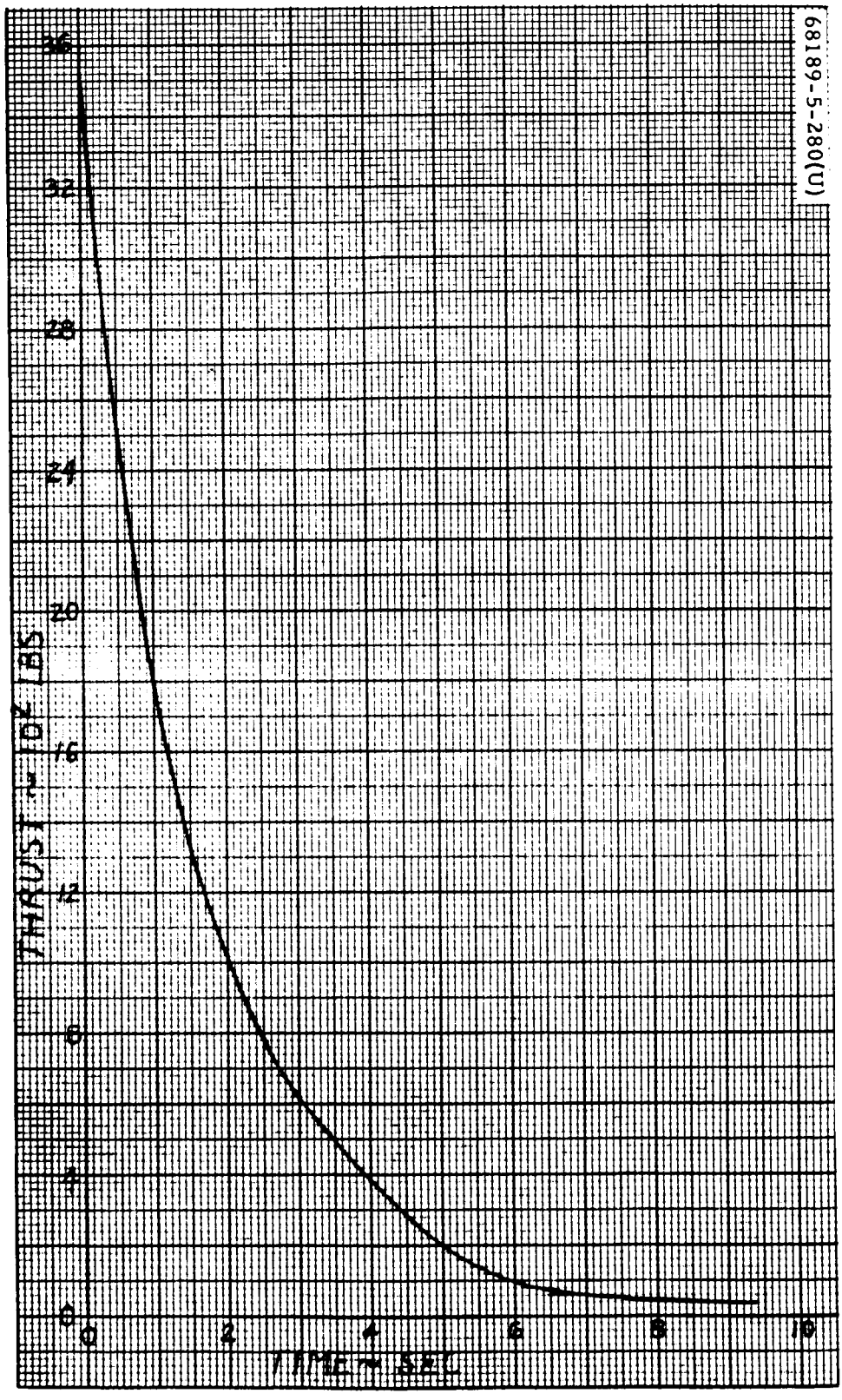

Figure 5.12-5. Main Retro Tailoff Versus Time (From Doppler Data)

command sent to the spacecraft by the command tape. The next command on the tape was the retro case eject; therefore, there was a possible 0.6-second delay in sending the backup command tape.

The 1000-foot mark was predicted to occur after segment acquisition; however, the postflight analysis indicated the reverse. This resulted from the lower burnout conditions of altitude and velocity.

6DOF Simulation of Doppler Data

The 6DOF determination of the radial velocity change (velocity change in the direction of the earth tracking station-spacecraft line), as compared to the doppler data reconstruction of the radial velocity change for the retro and vernier phases, is shown in Figures 5.12-6 and 5.12-7. Figure 5.12-6 shows an almost identical match from vernier ignition to the start of RADVS-controlled descent. Since the actual doppler data is a highly accurate measurement of the radial velocity change, this close match increases the confidence in the 6DOF reconstruction during this portion of terminal descent.

An excellent match between the 6DOF doppler simulation and the actual doppler data was also obtained during the vernier phase (Figure 5.12-7). The close match of key events, such as the start of RADVS control, segment intercept, the constant velocity phase, and touchdown, can easily be seen. The discrepancy between the 6DOF doppler simulation and the actual doppler data is generally less than 2 fps during this phase.

5.12.4.5 Vernier Propellant Consumption

As previously stated, the vernier propellant consumption determination is based on flight acceptance test data of specific impulse and mixture ratio as a function of thrust under nominal expected helium pressure and temperature characteristics. With the helium loss and the definite indication from the telemetry data of vernier engine degradation, the actual vernier performance becomes indeterminate in the sense of accurate determination of propellant consumption.

Table 5.12-4 presents a tabulation of the propellant consumption. The model used (TD1) for the six midcourse maneuvers and the retro phase assumed nominal vernier engine characteristics.

For the vernier phase portion, the propellant consumption was determined from the best-fit 6DOF program reconstruction. The 6DOF program also utilized the flight acceptance test data; however, the vernier engine model was modified in order to match the degradation as implied by the telemetry data (described in detail in subsection 5.12.4.7).

The propellant consumption of each midcourse maneuver was based on postflight determination of burn time and preflight data of engine thrust for the midcourse maneuver. The retro phase propellant consumption was based on premission computations of vernier thrust levels of 152.2 pounds during retro burn and 268 pounds during retro separation.

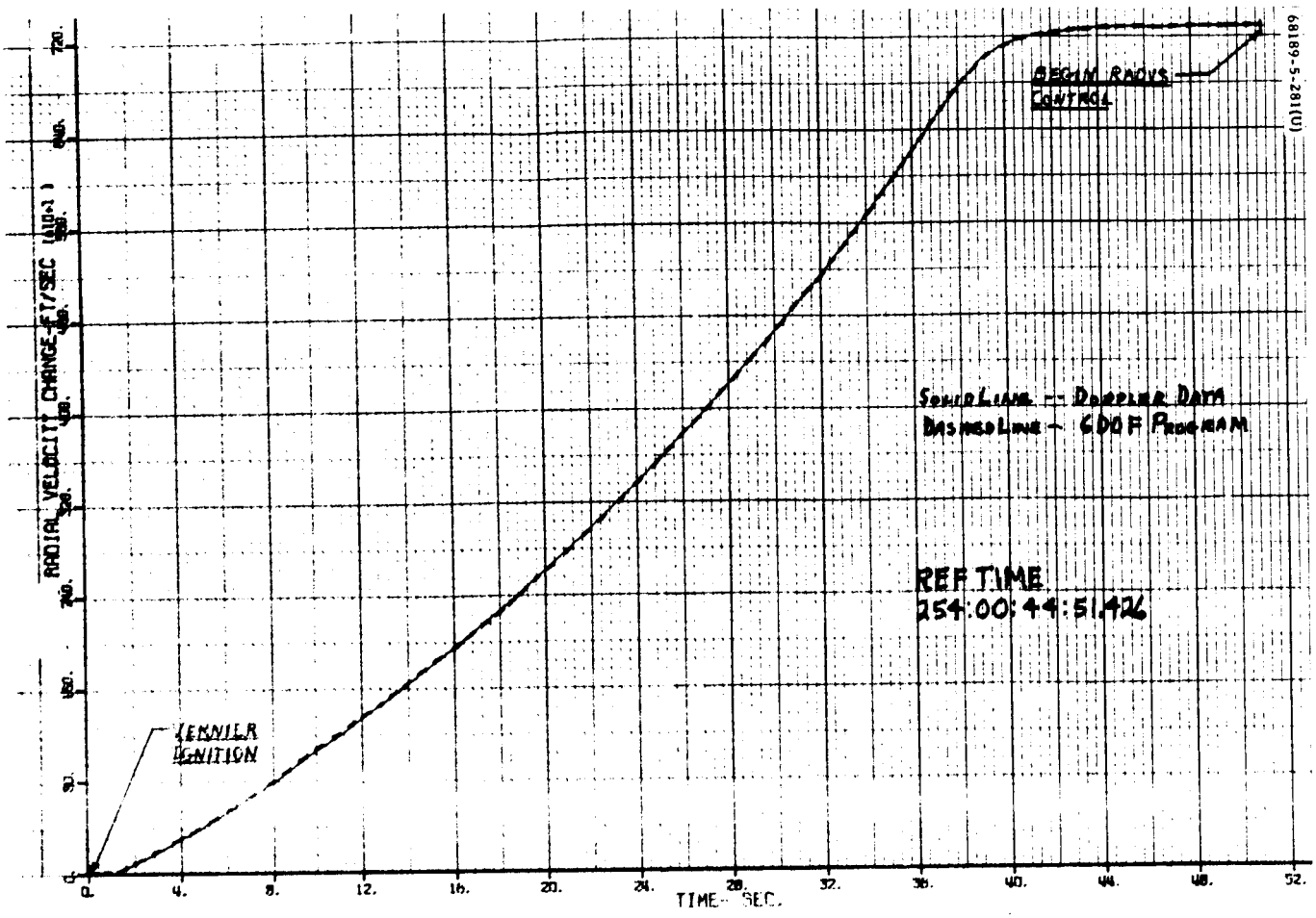

Figure 5.12-6. Radial Velocity Change – Retro Phase Doppler Data

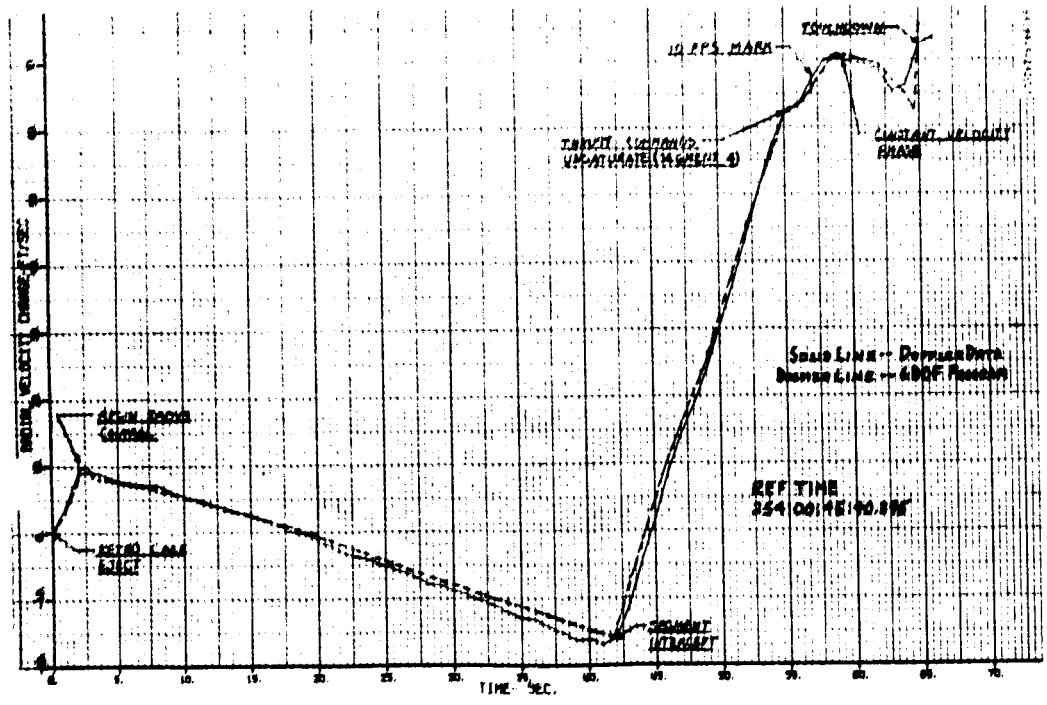

Figure 5.12-7. Radial Velocity Change – Vernier Phase

5.12.4.6 Spacecraft Landing Location

The original targeted landing site for Surveyor V was 0.916°N latitude and 24.083°E longitude. The computed midcourse to enable the spacecraft to land at the desired landing site was 14.01 m/sec. However, after the primary midcourse correction, a series of midcourse maneuvers was performed in an attempt to correct the malfunction within the helium regulator. As a result, the spacecraft trajectory was altered from the desired direction. A final midcourse correction (sixth) was performed in an attempt to correct the trajectory to the desired landing location.

The final landing site, based on the orbit determination postflight analysis data, was computed to be at 1.50°N latitude and 23.19°E longitude. The final computed landing site is approximately 30 km from the original targeted point. The 1σ error ellipse about the computed landing location is 2.3 km semi-major axis and 0.9 km semi-minor axis, with the major axis in approximately a north-south orientation.

5.12.4.7 Trajectory Reconstruction

This subsection discusses the reconstruction of the vernier phase of the terminal descent trajectory from the 6DOF program to provide a best estimate of the actual trajectory parameters. The DOPP program reconstruction of the retro thrust-time curve was input into the 6DOF program. The DOPP reconstructed retro burn time (from retro ignition to the 3.5-g point) was 38.934 which is the same time duration as indicated by telemetry data (see Table 5.12-1). The nominal Surveyor V subsystem parameters from preflight assessment were input to the 6DOF program. Initial conditions at vernier ignition of velocity, altitude, and retro thrust vector bias, as determined from orbit determination postflight data, were perturbed until the retro case eject conditions of velocity coincided with the calibrated telemetry data values indicated in paragraph 5.12.4.1. Further perturbations had to be made to the ignition altitude to arrive at the telemetry discrete time events of the 1000-foot mark and the descent segment acquisition. With these conditions matched, the 6DOF reconstruction from vernier ignition to segment acquisition agreed very well with postflight analysis of the telemetry data. However, with the assumption of nominal subsystem performance within the 6DOF program, the trajectory from segment acquisition to touchdown did not agree. From review of the telemetry data, the vernier engine subsystem performance was degraded from nominal due to the helium regulator malfunction. The vernier engine model within the 6DOF program was therefore modified in a manner so indicated by the telemetry data.

Figure 5.12-12 of the vernier engine telemetered thrust commands shows that engine 1 did not achieve its required thrust level of approximately 87 pounds along both the third and fourth descent line segment. This is indicated by the telemetered thrust command of engine 1 being saturated at 117 pounds, while engines 2 and 3 oscillated to take out the induced attitude error. Also, the telemetered strain gage data (Figure 5.12-13), although not considered accurate for indicating thrust magnitudes, implies that engine 1's maximum thrust level was diminishing along segment 4 during the saturated

command period, as indicated in Figure 5.12-13a. This figure shows a relative change in maximum thrust level of engine 1 of approximately 5 pounds. Figure 5.12-13 also shows a degradation in engines 2 and 3 along segment 4, but not as severe as in engine 1.

With these data, the vernier engine model within the 6DOF program was modified in the following manner: 1) engine 1's maximum thrust capability along segment 3 was limited to 86 pounds, while engines 2 and 3 were not limited. All engine thrust commands were limited to 117 pounds maximum. 2) Engine 1's maximum thrust was limited to 85 pounds along segment 4, and this limit was diminished 5 pounds linearly with time as indicated by the strain gage data. Engines 2 and 3 were also limited in the same fashion. 3) All three engine responses to their thrust commands were degraded from 2 to 5 percent as a function of time. Also, the telemetry discretes of the 10-fps mark and the 14-foot mark resulted in perturbing the nominal values within the 6DOF program. The final reconstruction by the 6DOF program compared favorably with telemetry data, as indicated by Table 5.12-3, and the close correlation between significant subsystem parameters is indicated by the POSTPR machine plots in Figures 5.12-8 through 5.12.14.

The above modification to the engine model does not imply that these conditions actually happened. What they do indicate is that the engines were probably degraded in a similar, but not necessarily the same, manner.

POSTPR Program Plots

Figures 5.12-8 through 5.12-14 are plots of important parameters for trajectory reconstruction. The processed data from PREPRO (solid lines) and the best-fit 6DOF trajectory (dashed lines) are superimposed on the plots. The time scale starts at 0.0 second, which corresponds to vernier ignition (254:00:44:51.4 GMT). The spacecraft touchdown at 254:00:46:44.4 GMT corresponds to 113 seconds on the time scale. After 113 seconds, the magnitude changes on the PREPRO curves are the direct result of spacecraft touchdown. The PREPRO curves are plots of interpolated telemetry data in equal time intervals of 1.2 seconds designed to coincide with the 6DOF intervals. Therefore, part of the transients within the telemetry data will not be plotted on the PREPRO curves.

The low transmission signal level received at DSS-11 during the terminal descent periods, from 254:00:45:46.7 to 254:00:45:50.3 and from 254:00:45:52.7 to 254:00:46:03.5 GMT, resulted in excessive parity error in the telemetry data during these periods along with total loss of data. Aside from the loss of data, the Hughes reformatting program (RFM) that processed the telemetry data rejected telemetry word frames which are unreliable due to excessive parity error. Therefore, the output tape from the RFM program, which is used as input to the PREPRO program, did not contain telemetry data during the above periods. Accordingly, the POSTPR plots will be erroneous during these periods and, in general, will plot in a straight line between the available data points. The above GMT periods for which data are not available corresponds to 55.3 to 58.9 and 61.3 to 72.1 seconds on the time scale of Figures 5.12-8 through 5.12-14.

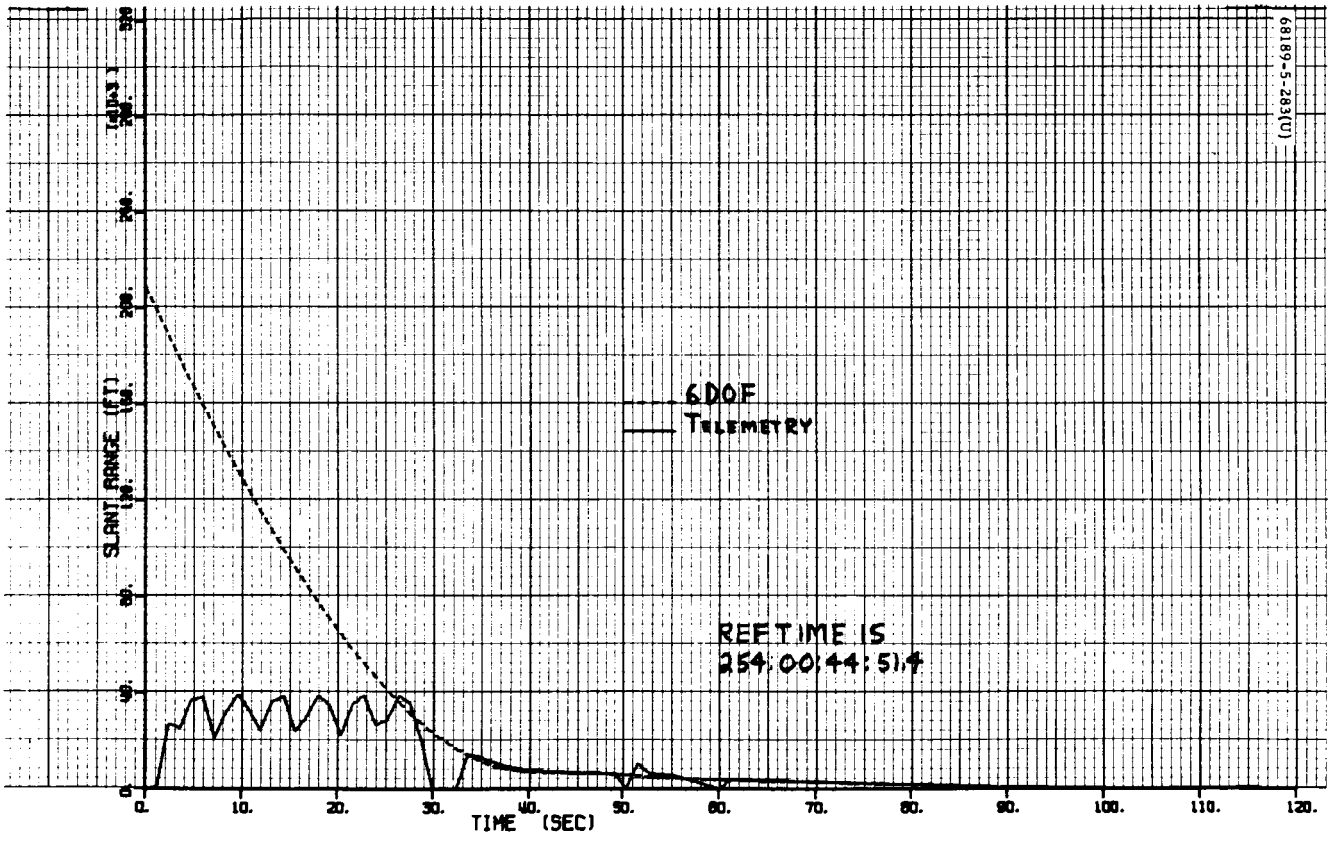

Figure 5.12-8. Slant Range

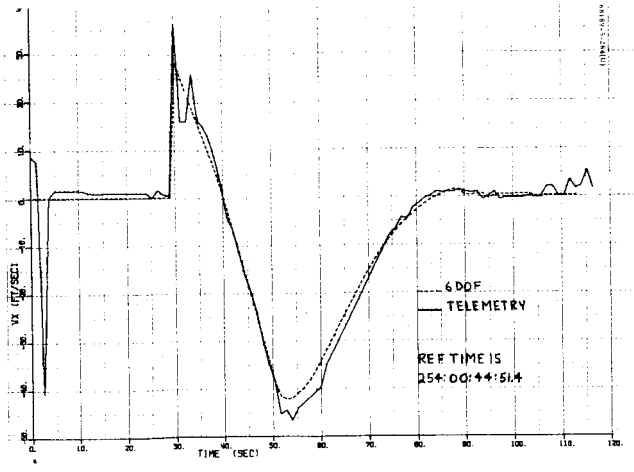

a) X-axis

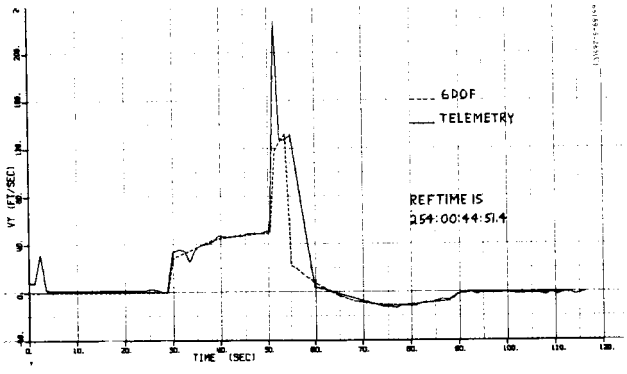

b) Y-axis

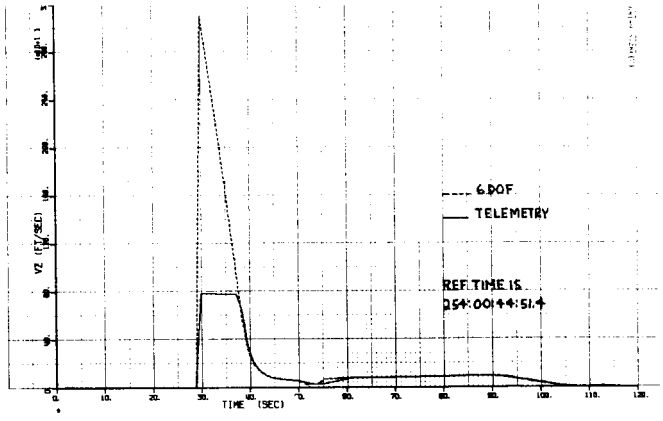

c) Z-axis

Figure 5.12-9. Spacecraft Velocity

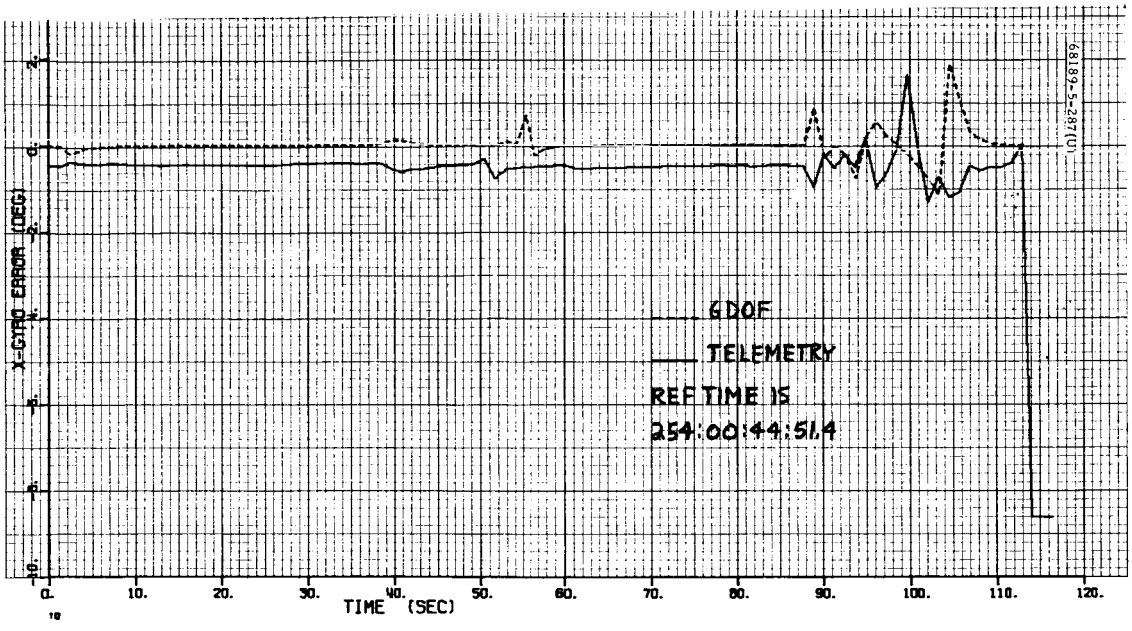

a) X-Gyro

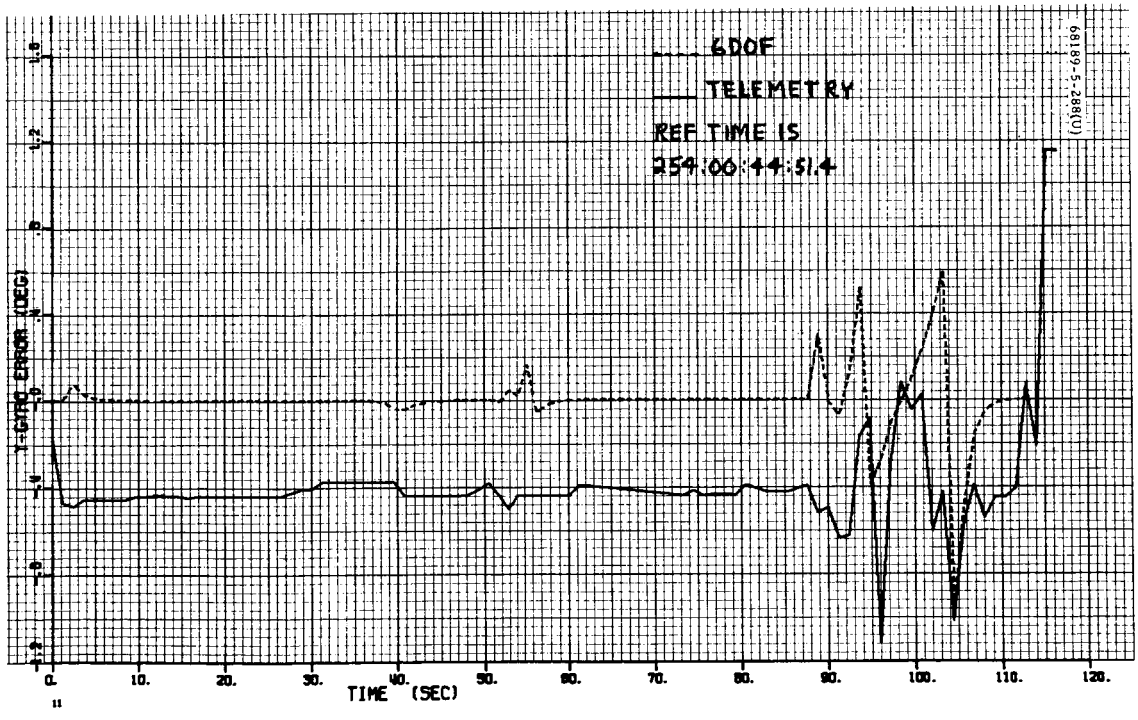

b) Y-Gyro

Figure 5.12-10. Gyro Error Signal

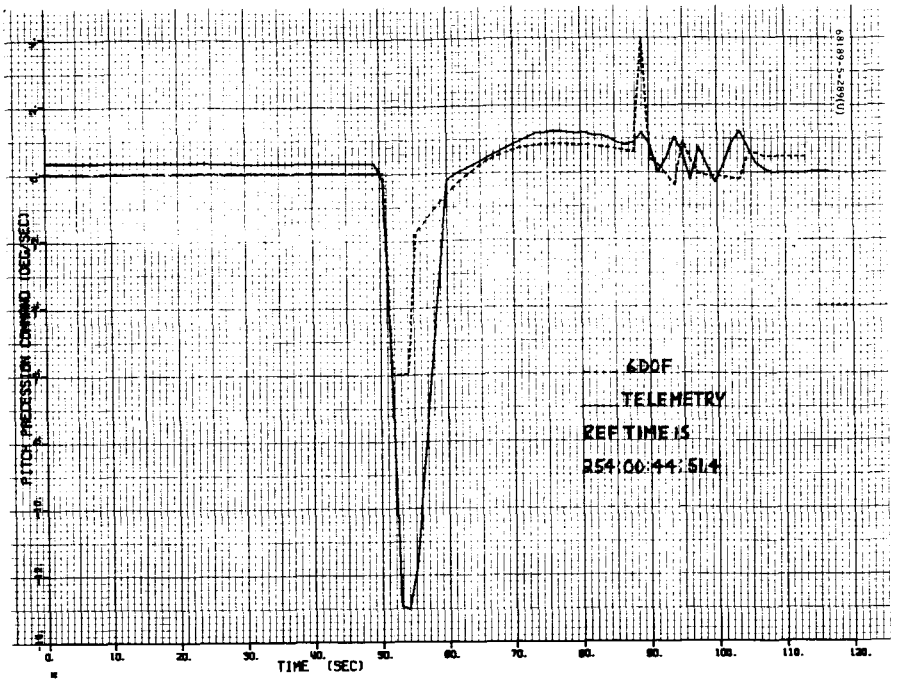

a) Pitch

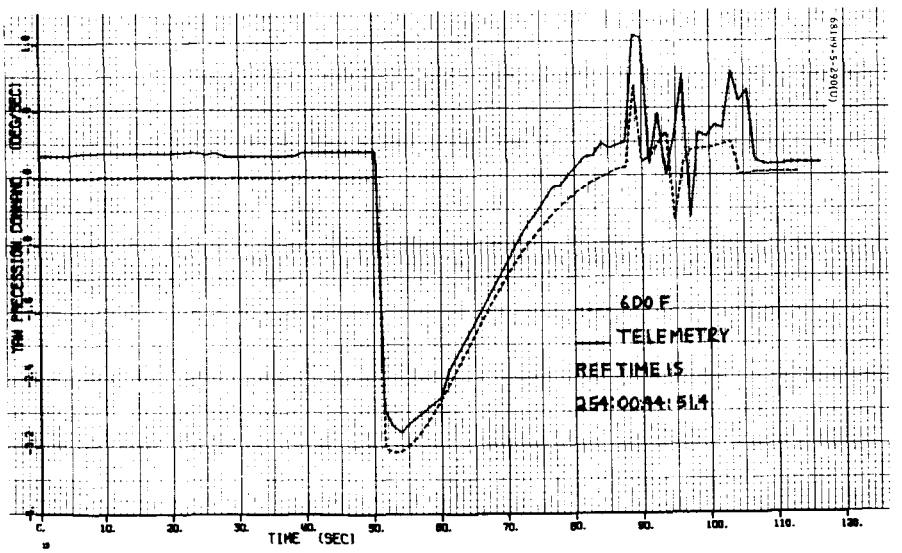

b) Yaw

Figure 5.12-11. Spacecraft Precession Commands

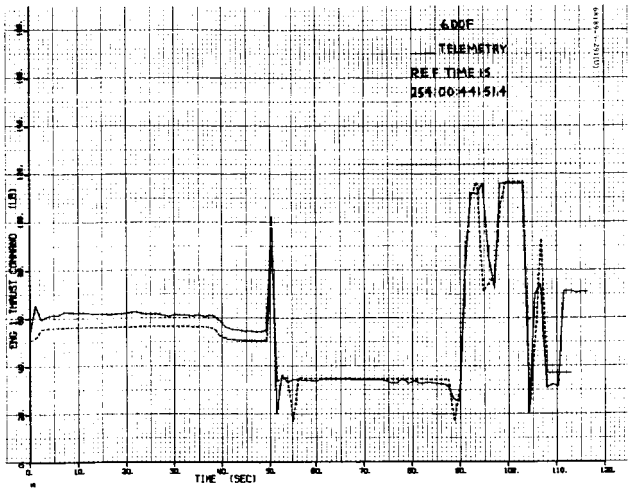

a) Engine 1

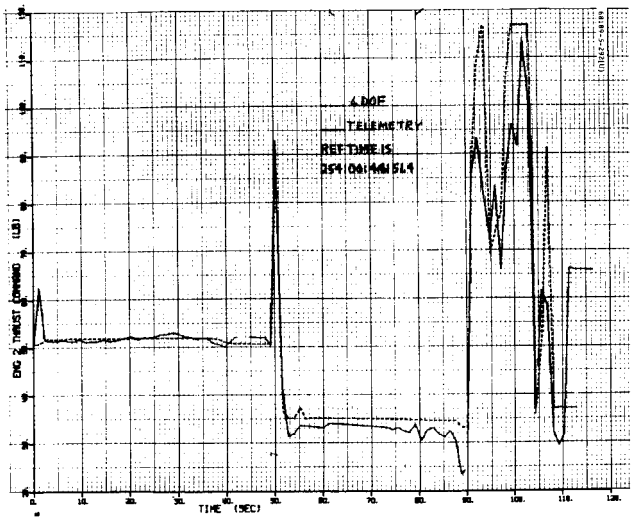

b) Engine 2

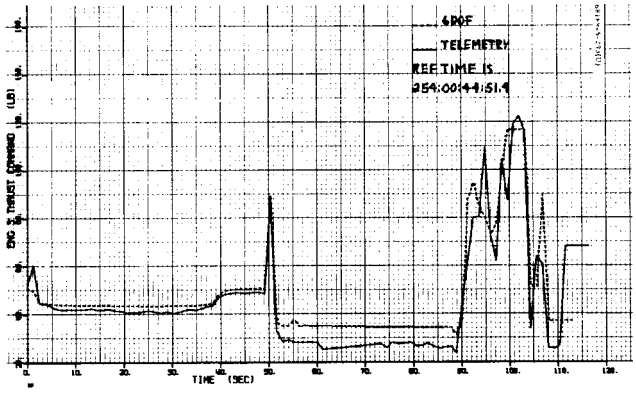

c) Engine 3

Figure 5. 12-12. Vernier Engine Thrust Commands

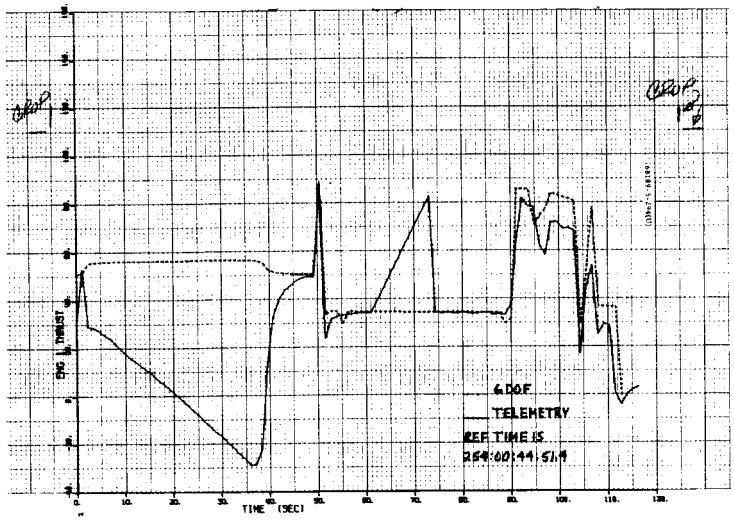

a) Engine 1

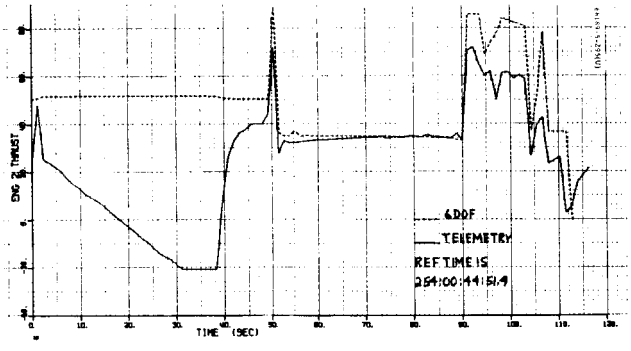

b) Engine 2

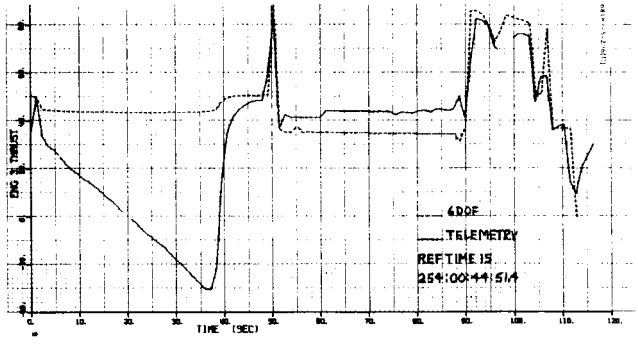

c) Engine 3

Figure 5.12-13. Telemetry Engine Strain Gage Data and 6DOF Engine Thrust Level Versus Time

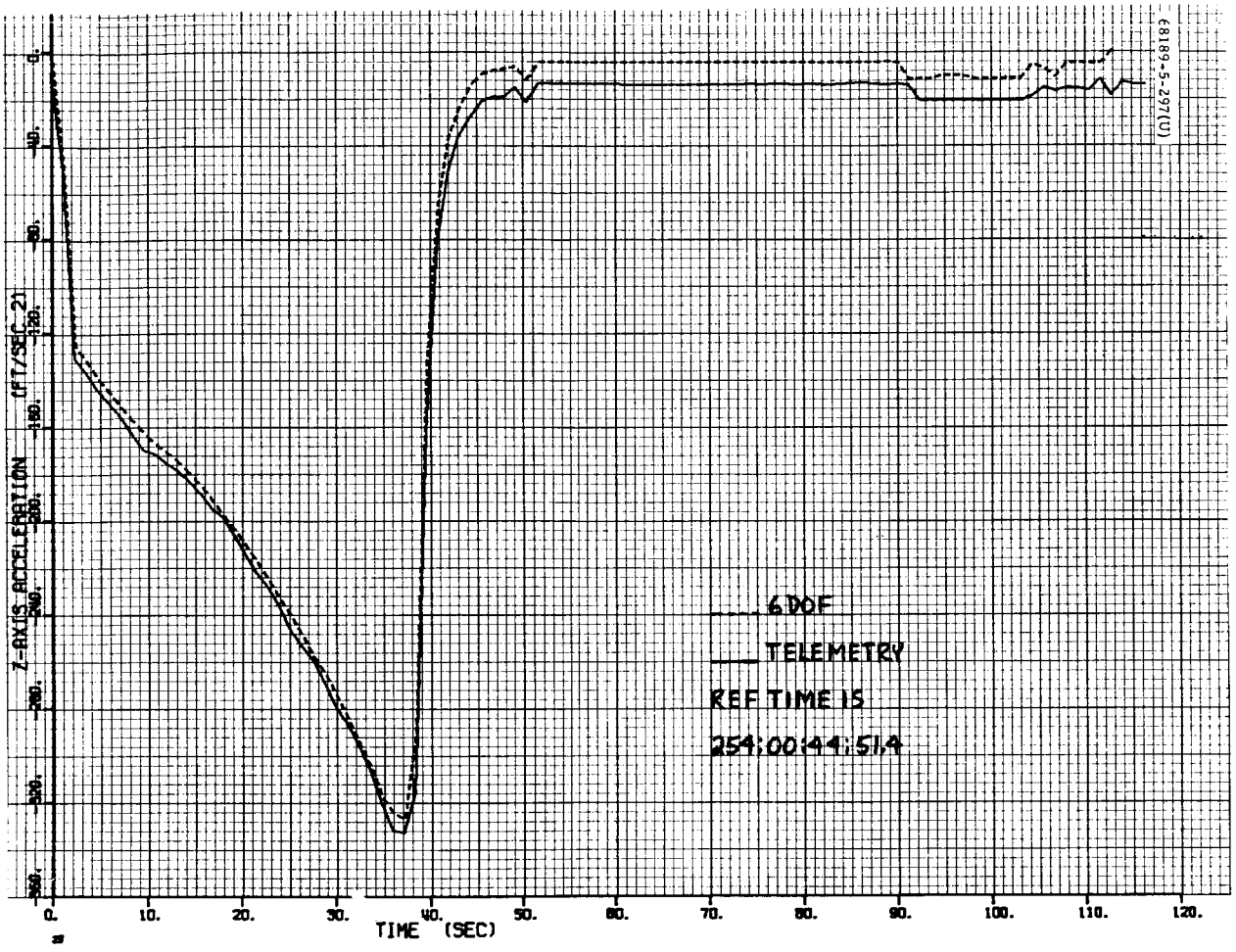

Figure 5.12-14. Telemetry Retro Accelerometer Data and 6DOF Z-Axis Acceleration Versus Time

Table 5. 12-3 gives the time occurrences of pertinent events as reconstructed by the 6DOF program. The PREPRO curves are referenced to the actual GMT as listed in the table.

Figure 5. 12-8 shows slant range as a function of time. The oscillation in the telemetry data from 2 to 30 seconds is a result of the tracker sweep limit. At approximately 33. 5 seconds, RORA occurred. The spike at 50 seconds is due to loss of RORA.

Figures 5. 12-9a and 5. 12-9b show an almost identical V_x and V_y reconstruction between the 6DOF and telemetry data. As indicated in Table 5. 12-3, start of RADVS-controlled descent occurred at 51 seconds. It took approximately 40 seconds to steer out the V_x and V_y components of velocity developed by the retro burn phase. Approximately 2 seconds after vernier ignition, the RADVS is turned on, resulting in the spikes in the V_x and V_y plots. The straight lines in the telemetry plots from 55 to 60 seconds and from 60 to 72 seconds are due to the data outage as described earlier.

Figure 5. 12-9c indicates a difference between the telemetry data and the 6DOF from 30 to 37 seconds. This is due to the telemetry saturation level of 800 fps.

Figures 5. 12-10a and 5. 12-10b show both telemetry gyro error signals to be biased about -0. 45 degree beyond that determined by pre-flight calibration. The 6DOF curve is opposite in direction to the telemetry curve due to the sign convention associated with the gyro error in the 6DOF program. The change in the error signal at 40 seconds (the 3. 5-g point) is caused by the reduction in retro moment due to the reduced retro thrust. The spikes at 54 seconds are a result of the reacquiring of radar beam three. The spikes at 88 seconds are a result of the gain change in the steering loop. The oscillations in the curves from 90 to 106 seconds are a result of the induced attitude errors introduced by the degraded vernier engine system.

Figure 5. 12-11 shows the pitch and yaw precession commands. The telemetry curve shows a bias of 0. 3 deg/sec beyond that determined by pre-flight calibration. Compensating for this bias, both curves compare favorably with the reduction of the V_x and V_y components of velocity during the minimum acceleration phase. From Figure 5. 12-11a, it can be seen that the pitch precession command saturates. This is due to the large apparent y-velocity component caused by radar beam loss of lock. After the beam reacquired lock at approximately 54 seconds, the command came out of saturation, since the true y-velocity component was of a magnitude not to result in a saturated command. The 6DOF program assumed a pitch and yaw rate limit of 6. 0 deg/sec.

Figure 5. 12-12 shows the vernier engine thrust commands. The roughness in the telemetry data is due to RADVS noise. The 6DOF curves are smooth since the RADVS noise was not simulated. The premission computations of total vernier engine thrust during retro burn is 152. 2 pounds.

The 6DOF program assumed this level and is so indicated by the sum of the three engine commands; however, the sum of the telemetered commands is approximately 156 pounds, a 4-pound difference between 6DOF and telemetry. Also, during the minimum acceleration phase, the total vernier engine thrust should be approximately 105 pounds, based on preflight determination of the minimum acceleration (4.79 ft/sec^2). The telemetry total of vernier engine thrust commands during this phase is approximately 95 pounds, 10 pounds less than expected. The differences of 4 and 10 pounds during the retro burn phase and the minimum acceleration phase implies a bias and scale factor error in the calibrated telemetry data.

The three different thrust commands of each engine during the retro burn phase are due to the moment introduced by the retro thrust to spacecraft center of gravity offset. The 6DOF program assumed preflight calculations of spacecraft center of gravity and retro thrust vector location.

The degradation in the vernier engine performance as discussed previously is shown clearly in these figures (from 90 to 106 seconds). The close similarity between the 6DOF and telemetry data during this period implies a degradation in a manner similar to that modeled within the 6DOF program.

Figure 5.12-13 shows the 6DOF engine thrust levels superimposed with the processed vernier engine strain gage data. Although the strain gage data are not an accurate source of indicating the actual engine thrust magnitude, they are suitable for indicating the engine thrust variation characteristics. The telemetry data have almost the same characteristic changes in thrust as does the 6DOF program. This close correlation further substantiates the assumed degradation within the 6DOF program. The rapid change in slope of the telemetry data between 2 and 40 seconds is caused by the retro thrust.

Figure 5.12-14 compares the retro accelerometer telemetry data with the 6DOF Z-axis acceleration. The telemetry data are apparently biased by 10 ft/sec^2. The peak acceleration of 10 earth g (excluding the 10 ft/sec^2 bias) occurs at 37 seconds, which compares with the strain gage data of Figure 5.12-13 and the retro accelerometer reconstruction on Figure 5.12-3.

5.12.5 ACKNOWLEDGMENTS

Victor Marelia, coordinator and author

Eddy White, retro thrust-time curve reconstruction, retro ΔV determination, and 6DOF doppler reconstruction

Ed Kopitzke, 6DOF reconstruction and 6DOF doppler reconstruction

Nancy Krupa, POSTPR machine plots

5.13 TELEVISION

5.13.1 INTRODUCTION

On 9 September 1967, Surveyor V successfully soft-landed on the lunar surface. Shortly thereafter, eighteen 200-line mode pictures were taken by the spacecraft's television system, which were of excellent quality. The spacecraft and ground equipment were then reconfigured for 600-line mode television to perform standard photogrammetric and photometric operations for the remainder of the first lunar day, approximately 14 earth days.

Eighteen thousand six high quality pictures were taken on the first lunar day surpassing all mission objectives, and an additional 1048 pictures were taken during the second lunar day, resulting in a grand total of 19,054 pictures. Many of the pictures were of the spacecraft and the alpha scattering device. Especially interesting were pictures before and after static firing which showed relative motion with respect to the alpha scattering device.

5.13.2 ANOMALIES

During the first lunar day several performance characteristics were reported which were not all necessarily problems but which required investigation. TFR 59592 was written against the focus, filter wheel, and focal length nonresponse to command before lunar sunset.

Calibrate Voltage Change

Shortly after touchdown, about 24 hours, the calibrate voltage increased from that measured in PVT-4 calibration.

200-Line Mode Frame Time Decrease

During the first 18 pictures in 200-line mode, the frame time was reported to be below that measured at PVT-4 calibration.

Vertical Blanking Pulse Time Decreased

After several hundred 600-line mode pictures were taken, TV-1 (JPL ground data handling system) reported the vertical blanking

PRECEDING PAGE BLANK NOT FILMED.

pulse time had decreased during operation from 210 milliseconds to 192 milliseconds. This number has also been quoted as 202 milliseconds to 196 milliseconds.

Focus, Filter Wheel, and Focal Length Did Not Respond to Command

During Station 42 (Canberra) television operations on day 266, at 19:43 GMT, 14 hours before lunar sunset, the focus, filter wheel, and focal length functions failed to respond to repeated commands (TFR 59592).

Video Gain Decreased

On 15 October 1967 (second lunar day), Surveyor V was reacquired. It was noted that the television video signal was attenuated seriously degrading performance. All other functions appeared normal. Camera operations were initially performed by Station 11 (Goldstone).

5.13.3 SUMMARY AND RECOMMENDATION

5.13.3.1 Summary

Although the television system met all mission objectives, one failure occurred just prior to lunar sunset on the first lunar day. All other reported problems have been resolved. This failure was the inability of the focus, filter wheel, and focal length functions to respond to command. A circuit analysis did not disclose a critical circuit or component failure unique to the three functions, primarily, in the ring counter or steering multivibrator circuits. The environment and operation of the camera prior to and during the failure appeared to be quite normal and no other effects could be seen. Moreover, no failure of this type had occurred before.

The second lunar day operation disclosed normal operation of the focus, filter wheel, and focal length functions, preventing further trouble-shooting and indicating most likely a temperature-related problem, in which the extreme cold and subsequent heating had corrected the problem. Consequently, the most likely failure appears to be a loose connection in either the ring counter or steering multivibrator.

The second lunar day operation disclosed a second failure in the television camera, loss of video gain. Because of the additional data available, amount of gain loss, video reversal in 200-line mode, and loss of video noise, the failure could be isolated with a high degree of confidence to an open circuit, most likely caused by the extreme low temperatures during lunar night. Total loss of video did not occur since there was a small amount of coupling within the video amplifier.

Reference 1 presents a more complete analysis of failures in the Surveyor V camera.

5. 13. 3. 2 Recommendations

Consideration has been given to what could be done to the SC-7 cameras to preclude the failures noted in the Surveyor V mission, especially the failure on the focus, filter wheel, and focal length. Because of the limited data available and undetermined cause, it is impossible to provide corrective action.

The S/N 13 camera (SC-7) and S/N 11 camera (SP-2), were physically inspected for workmanship and electrical connections in the area within the camera where the failure might have occurred. No problems were discovered. All cameras are extensively tested at ambient and in thermal vacuum environments in which these functions are specifically monitored, in addition to vibration.

One might consider the uniqueness of both failures and the obviously extensive age and rework history of this camera and conclude that in over 2 years of test history and many cycles of assembly and disassembly (the vidicon alone was changed twice), almost any failure is likely – not due to design, operation, or environments, but primarily caused by weakening of these circuits due to handling.

The remaining cameras for SC-6, SC-7,and spares are all less than a year old since first initial FAT. They are all of the new series 290512 and have been assembled and reworked by personnel with experience gained from earlier cameras.

It is therefore recommended that nothing should be done to the SC-7 or spare cameras as a result of the failures noted on the Surveyor V mission, except the now-sensitized monitoring during testing.

5. 13. 4 SUBSYSTEM PERFORMANCE ANALYSIS

5. 13. 4. 1 Historical Background

The TV survey camera P/N 284312-8 S/N 11 was installed on Surveyor V on 5 July 1967, just prior to PVT-4 at AFETR.

The history on this camera dates back to September 1965 when it was installed on Surveyor I. It had some 31 TFRs written against it and was on and off Surveyor I until January of 1966, when it was removed for the last time. None of these failures appear related to the Surveyor V mission anomaly (TFR 59592).

After removal from Surveyor I, the vidicon was replaced due to degradation of the cathode at greater than 1000 hours operation. The camera was then installed on Surveyor 2 in January 1966 and was on and off until September 1966. An additional 30 TFRs were written against this camera. Again, however, none of the problems appear to be related.

In October of 1966, the camera was installed on Surveyor III, and was returned to the unit area in November of 1966 to incorporate vidicon cleaning access, after which it was returned to the spacecraft. It remained with Surveyor III until the spacecraft was returned from AFETR in January of 1967, when the camera azimuth gear suffered damage due to prolonged vibrations on the return trip.

During the camera rework the vidicon was changed out again because of a shading problem at saturation that was not understood at the time. The damaged gear was replaced and new azimuth and elevation motors installed. The camera was then shipped to AFETR in March of 1967 as a spare. During this time an additional 12 TFRs were written against the camera that appear to have no relative importance.

In July of 1967, per direction of NASA/JPL Change Order 160, this camera was installed on Surveyor V, to provide a camera with a vidicon which could survive lunar night. During television testing at AFETR, three additional TFRs were written. In all there were a total of 76 TFRs written against this camera; not all of them were camera failures. None of them appear to be directly related to the failure during the mission. It is apparent that this camera has been disassembled a great many times and has the longest history of any flight camera, which may have indirectly contributed to the failure.

5.13.4.2 Investigation of Anomalies

The following investigations and analysis were performed on the anomalies reported on the Surveyor V television system.

Calibrate Voltage Change

The calibrate voltage increase was found to be normal and should have been expected. The increase was due to characteristic behavior of the camera circuits, due to increased ambient temperature. The unit FAT data during thermal vacuum testing correlated very well with flight data. Further monitoring of this voltage during the mission at decreasing temperatures also verified normal behavior.

200-Line Mode Frame Time Decrease

The 200-line mode frame time was measured during television operation during the first picture sequences, which was 19.6 seconds. The last measurement was made at PVT-4 and was 20.2 seconds. This was reported to determine if this was indicative of a possible failure.

The specification for 200-line mode is 20.0 seconds, ±10 percent. Most cameras, after manufacturing, hold to ±5 percent.

The change from PVT-4 data is again attributed to the higher ambient temperature on the lunar surface, as compared to the PVT-4 temperature

and verified by unit data. The decrease in time agrees with unit data and is therefore not considered to be a problem.

Vertical Blanking Pulse Time Decreased

After several hundred 600-line mode pictures were taken, it was reported that the vertical blanking pulse time had decreased. The decrease was of concern, since this would not correlate with expected drift characteristics caused by temperature.

The camera specification requires the vertical blanking pulse to be 200 milliseconds, ±10 percent. The value first quoted for the decreased time appeared to be abnormally close to the maximum tolerance. Further, it was reported that the JPL ground data handling system (GDHS) required readjustment to maintain synchronization. Further investigations and monitoring of the system indicated this was not a problem and was most likely a momentary measurement or ground equipment problem.

Focus, Filter Wheel, and Focal Length Did Not Respond to Command

On day 266 at 19:43 GMT, Station 42, then in control of the spacecraft, reported the three functions, focus, filter wheel, and focal length, failed to respond to repeated commands. It appears they failed simultaneously and without previous indication. No changes could be detected in either telemetry readout or in video data. Further attempts were made by Station 11 until final shutdown, but the functions would not respond.

At the time of initial failure, camera temperatures were decreasing rapidly but were well within operating limits. TV-16, camera electronics temperature, located on chassis 3, was +2°F. TV-17, mirror baseplate temperature, was +40°F. The lower operating limits are -20°F and -10°F respectively. All other functions on the camera worked satisfactorily during this period.

The fact that all three functions appeared to have failed simultaneously and that there was no intermittency or partial failure precludes the assumption of mechanical problems, potentiometer problems, or motor problems.

Considering the above, which appears valid, the investigation was concentrated on a probable electronic failure, common to all three functions. The three functions were in the following positions:

Focus	Step 37 (14.5 feet)
Filter wheel	Green
Focal length	100 mm (narrow angle)

With the small amount of data available and no opportunity to trouble-shoot the problem, it was difficult to indicate possible failure mechanisms; however, some problem areas are:

1) Cracked components due to excessive freezecoat

2) Component failures

3) Harness and printed circuits short or open

4) Operational errors

5) Camera temperatures

Surveyor V was reacquired on 15 October, and all three functions performed satisfactorily. The video gain was quite drastically reduced, apparently due to lunar night temperature extremes, seriously affecting picture quality.

Considering the normal operation of the three functions which failed on the first lunar day, it appears that the failure is obviously temperature related. Since further troubleshooting could not be accomplished, it was possible to determine or further isolate the failure.

Video Gain Decreased

The loss in video gain appeared to be approximately 30 db down from normal. It was also noted in the 200-line mode. The white/black voltage polarity was reversed in the 200-line mode but not in the 600-line mode. An analysis of the video amplifier circuit was conducted (Reference 2). Because of the unique effect of video reversal coupled with the gain loss it was not difficult to isolate the failure. If R9 opened or a similar effect, such as interconnection of R9 occurred, then the video gain loss and video reversal in 200-line mode only would be equivalent to that noted in flight. This appeared to be the only single circuit failure which would cause this effect.

A laboratory test was conducted on a similar circuit, chassis 5, in which R9 was opened. The effect was similar to that encountered in the mission, although there appeared to be a larger dynamic range in the lab unit. This is probably due to the simulated input, a sine wave generator, as compared to a video scene and differences in interstage coupling between the units. Although the gain was severely reduced, usable video was obtained by modification of ground equipment operations.

5.13.5 REFERENCES

1. A. M. Lauletta Jr., M. I. Smokler, "Special Report, Surveyor V Television System Mission Anomalies Investigation," Hughes Aircraft Company, SSD 74139, 25 October 1967.

2. Hughes Schematic 283656.

5. 13. 6 ACKNOWLEDGMENTS

This section was compiled by W. McIntyre primarily from data generated by A. M. Lauletta (see Reference 1).

5.14 ALPHA SCATTERING EXPERIMENT

5.14.1 INTRODUCTION

5.14.1.1 Purpose

The alpha scattering experiment was added to Surveyor V in order to perform a compositional analyses of the lunar surface. The alpha scattering technique of surface chemical analysis takes advantage of the characteristic interactions of α particles with matter to provide information on the chemical composition. The energy spectrums of the large-angle, elastically scattered α particles are characteristic of the nuclei doing the scattering. In addition, certain elements, when bombarded with α particles, produce protons, again with characteristic energy spectrums. Consequently, these energy spectrums and intensities of scattered α particles and protons can be used to determine the chemical composition of the material being exposed to the α particles.

The method has good resolution for the light elements expected to be contained in rocks (unfortunately, however, it can give only indirect information about hydrogen). The resolution under this technique decreases as the atomic weight increases (Fe, Co, and Ni cannot easily be resolved), even though the sensitivity is greater for heavy elements than for most light elements. (The sensitivity for elements heavier than lithium is approximately 1 atomic percent.)

The absence of an atmosphere on the moon made practical the use, for such chemical analyses, of the relatively low-energy α particles from a radioactive source. Cm^{242} ($t_{1/2}$ = 163 days, T_a = 6.11 mev) is a convenient nuclide for this purpose. The use of low-energy α particles, however, restricts the information obtained to that pertaining to the uppermost few microns of material, i.e., the method is one of surface chemical analysis. Moreover, using practical source intensities ($\sim$100 mc), the rate of analysis is rather slow: a relatively complete analysis requires about 1 day. In spite of these disadvantages, the simplicity of the instrumentation associated with using a radioactive source made this a feasible, attractive method.

5.14.1.2 Description

The alpha scattering subsystem consisted of five principal units: sensor head, digital electronics, electronic auxiliary, thermal compartment/heater assembly, and deployment mechanism/standard sample, having a total

PRECEDING PAGE BLANK NOT FILMED.

weight (including mechanical and electrical spacecraft interface substructure and cabling) of approximately 13.1 kg (28.8 pounds). Power dissipation of the subsystem was normally 2.1 watts (approximately) which increased to 17.1 watts, when both the thermal compartment and the sensor head heaters were active. A brief description of each of the principal units follow.

Sensor Head (GFE)

The sensor head is a box measuring 17.1 by 16.5 by 13.3 cm which contains a 30.5-cm-diameter plate on the bottom. The main purpose of this plate is to minimize the probability of the box appreciably sinking into a soft (lunar) surface. At the bottom of the head is a 10.8-cm circular opening, and recessed 7.0 cm above the opening are six α sources, which are orientated in such a way that the α particles are directed only at the opening of the head. Close to the α sources are two silicon semiconductor detectors arranged to detect α particles scattered back at an average angle of 174 degrees from the sample. Also contained in the head are four detectors ($\sim$1 cm^2 area each) designed to detect protons produced in the sample by the α particles. A gold foil of $\sim$21 mg cm^{-2} prevents scattered α particles from reaching these detectors. Because the proton rates were expected to be low, and because these detectors are particularly sensitive to solar protons, the proton detectors were backed by guard detectors. The electronics associated with the guard detectors was arranged so that an event registered in both detectors (and, therefore, due to space radiation) will not be counted as coming from the sample. The anticoincidence arrangement had the effect of significantly reducing the backgrounds of the instrument when operating in the proton mode.

In addition to the sources, detectors, and associated electronics, the head contained a temperature sensor, a 5-watt heater, and an electronic pulser. The electronic pulser was used to calibrate the electronics of the instrument by introducing electrical pulses of known magnitudes (two) into the detector stages of the system. The calibration mode is initiated by earth command.

The output of the head characterizes the energy of an event, in either the scattered α or proton mode of the instrument, by a signal in time analog (pulse) form.

Digital Electronics (GFE)

The time analog output signal of the sensor head is processed by the digital electronics unit and converted into a nine-bit digital word that has seven information bits. Stated differently, the event energy spectrum is analyzed and expressed, in terms of channels, by 128-channel pulse-height analyzers having a threshold of about 600 kev and a gain of about 54 kev per channel. The nine-bit digital words characterizing each event are transmitted in near-real time (essentially no spacecraft storage) to earth at a rate of 2200 bits/sec for the α mode and 550 bits/sec for the proton mode.

The digital electronics unit contains, in addition to the digital processing electronics, the necessary power supplies and the logical electronic interfaces between the GFE and the Hughes spacecraft equipment. The digital electronics unit contained circuits so that the output of any one individual detector, together with its associated guard detector, could be inhibited by earth command; the temperature of the sensor head, as well as other monitoring voltages, could be transmitted to earth. Finally, a crude rate-meter provided information on the number of events occurring in the guard (anticoincidence) detectors.

Electronics Auxiliary (Hughes)

The electronics auxiliary unit provided the necessary command decoding, signal processing, and power management so that the GFE equipment could interface with the basic spacecraft bus. Basic items interfacing directly with the sensor head and the digital electronics are 1) the central signal processor that provides 2200 and 550 bits/sec sync to the digital electronics clocks, and 2) the engineering signal processor that provides temperature sensor excitation current and commutation of the GFE engineering data outputs.

The electronics auxiliary also provides the two data channels employed by the alpha scattering subsystem for the alpha and proton counts. The characteristics of these two subcarrier oscillator channels are as follows:

	Alpha Counts	Proton Counts
Data input to electronic auxiliary	Digital, NRZ	Digital, NRZ
Input data rate	2200 bits/sec	550 bits/sec
Subcarrier oscillator center frequency	70,000 Hz	5400 Hz

Thermal Compartment/Heater Assembly

The digital electronics and the electronic auxiliary units were contained in a thermal compartment attached to the spacecraft. Thermal control was obtained by compartment thermal design in conjunction with a 10-watt compartment heater assembly, which was operated by the engineering signal processor.

Deployment Mechanism/Standard Sample

The deployment mechanism provides for the operation of the experiment in any of the following three positions:

1) Stowed position where the standard sample was utilized for calibration of the system

2) Background position where the solar and surface natural radiation was calibrated

3) Lunar surface position where the lunar surface compositional analysis was performed

The standard sample is a sample of known chemical composition that was attached to the deployment mechanism and was used to assess subsystem performance prior to launch and after lunar landing. The standard sample covers the sensor head viewing part when in the stowed position, and is removed when the sensor head is in either the background or the lunar surface positions. Operation in this manner minimizes the entrance of both dust and light during spacecraft launch, transit, and landing and/or until the experiment is to be operated.

5.14.2 ANOMALIES

Operation of the alpha scattering experiment was completely successful with a total accumulation time of 93-1/2 hours, including 50 hours of lunar surface analysis.

During all flight and lunar operations of the experiment, the essential telemetry data remained within predicted limits except for the sensor head temperature, which exceeded the maximum operating temperature limit for a short period of time near lunar noon. The data, however, were not affected, and the detectors remained operable at all times.

A single anomaly occurred during the initial turn-on when the calibration pulse generator became active without being commanded on. The pulse generator was commanded off and it responded with no further malfunction. Approximately 600 commands were transmitted, received, and executed without a single error.

5.14.3 RECOMMENDATIONS

It is recommended that all functions be commanded to their proper state after turn-on to ensure that the initial condition is correct.

5.14.4 SUBSYSTEM PERFORMANCE ANALYSIS

The Lunar Operations Plan called for four modes of operation: 1) standard sample, 2) background, 3) lunar surface, and 4) calibration. There were, however, six actual modes of operation provided with addition of the transit mode and the lunar surface sample II mode.

The transit mode operation was initiated during the mission when it appeared that a safe landing on the lunar surface was questionable, and the

lunar surface sample II mode of operation was initiated after the alpha scattering sensor head changed its lunar surface location as a result of the vernier engine static firing experiment. Figure 5. 14-1 shows the location of the sensor head before and after the vernier engine experiment.

Two forms of science data were recorded during operation: the uncorrected spectra, received via teletype from the stations, which were used for near-real time analysis; and the FR-1400 prime data tapes for use during the postmission analysis. The uncorrected spectra, while not reflecting all the data transmitted from the alpha scattering subsystem, did contain the vast majority of the data recorded on the FR-1400 tapes. Table 5. 14-1 presents a summary of the science data accumulation time in each of the six operational configurations.

Operation of the alpha scattering subsystem was initiated during transit, approximately 26 hours, 43 minutes after launch, while the spacecraft was in view of DSS-42 (Canberra, Australia) for some 50 minutes. At this time, telemetry data indicated that the digital electronics and the electronics auxiliary units were at approximately -15°F and that the sensor head temperature was at 30°F. The experiment was next operated on day 254, approximately 6 hours, 44 minutes after touchdown, while the spacecraft was again in view of DSS-42. Lunar operations continued during days 254 through 257 and 259 through 265. During lunar operations, the majority of the science data was accumulated while the sensor head was within its operational temperature limits of -40° to 122°F. A small amount of data was accumulated when the sensor head temperatures were as high as +130°F and as low as -70°F. With the exception of the data accumulated during transit, all data were accumulated while the thermal compartment was within its operational temperature limits of -4° to 131°F.

TABLE 5. 14-1. SCIENCE DATA ACCUMULATION SUMMARY

Operational Configuration	Accumulation Time, minutes
Transit	20
Standard sample	75
Background	170
Lunar surface sample I	1056
Lunar surface sample II	4005
Calibration	281
Total	5607 $\approx$ 93. 5 hours

a) Before Static Firing
(Photo 68189-5-19)

b) After Static Firing
(Photo 68189-5-19)

Figure 5.14-1. Alpha Scattering Sensor Head Location

In general, the communications link from the spacecraft was excellent, and the bit error rate of 10^{-6} was at least a factor of 100 better than the predicted worst-case value. Deviations from this high quality data reception generally occurred when the spacecraft was being tracked near the earth's horizon.

For ancillary information, Table 5. 14-2 is a summary of preliminary results of the chemical analysis of the moon at the Surveyor V landing site (Reference 1), and Table 5. 14-3 is a detailed account of SSAC alpha scattering operations during the first lunar day.

TABLE 5. 14-2. CHEMICAL COMPOSITION OF LUNAR SURFACE AT SURVEYOR V SITE

Element	Atomic, percent*
Carbon	< 3
Oxygen	58 ± 5
Sodium	< 2
Magnesium	3 ± 3
Aluminum	6. 5 ± 2
Silicon	18. 5 ± 3
28 < A < 65**	13 ± 3
(Fe, Co, Ni)	> 3
A > 65	< 0. 5

*Excluding hydrogen, helium, and lithium. These numbers have been normalized to approximately 100 percent.

**This group includes, for example, S, K, Ca, Fe, Co, and Ni.

TABLE 5.14-3. SSAC SURVEYOR V ALPHA SCATTERING OPERATIONS DURING FIRST LUNAR DAY

DSS	Day	Position	Record	Calibration	Accumulation	GMT, hr:min:sec Start	GMT, hr:min:sec End
42	252	Transit					
			1		10M	10:39:05	10:49:05
			2 - 8	Cal	2M	10:51:50	11:14:45
			9		10M	11:16:05	11:26:05
42	254	Stowed					
			1		10M (pulser on)	07:30:10	07:40:10
			2		5M	07:50:42	07:55:42
			3 - 9	Cal	1M	09:18:21	09:33:45
			10		20M	09:35:54	09:55:54
			11		20M	09:56:58	10:16:58
			12		20M	10:17:25	10:37:25
		Background					
			13		10M	12:14:48	12:24:48
			14		10M	12:27:06	12:37:06
			15		20M	12:37:49	12:57:49
			16		20M	12:57:49	13:17:49
			17		20M	13:17:49	13:37:49
			18		20M	13:37:49	13:57:49
			19		20M	13:57:49	14:17:49
			20	Cal	2M (A1, A2, P4 on)	14:20:15	14:22:15
			21		20M	14:25:35	14:45:35
			22		10M	14:45:35	14:55:35
61	254	Background					
			1		10M	15:10:00	15:20:00
			2		10M	15:21:40	15:31:40
				SAMPLE I			
		Lunar surface					
			3		20M	15:37:00	15:57:00
			4		20M	15:59:00	16:19:00
			5		20M	16:20:00	16:40:00
			6		20M	16:41:00	17:01:00
			7		20M	17:02:00	17:22:00
			8		20M	17:23:00	17:43:00
			9 - 13	Cal	1M	17:45:50	17:57:03
			14		20M	17:59:00	18:19:00
			15		20M	18:20:00	18:40:00
			16		20M	18:41:00	19:01:00
			17		20M	19:02:00	19:22:00
			18		20M	19:23:00	19:43:00
			19		20M	19:44:00	20:03:00
			20		20M	20:04:00	20:24:00
			21		20M	20:26:00	20:46:00
			22		20M (lost)	20:47:10	21:07:10
			23		20M	21:10:32	21:30:32
			24 - 29		1M (lost Nos. 25)	21:32:10	21:58:10
			30		20M	21:56:10	22:16:10
42	255	Lunar surface					
			2		6M 31S	06:18:31	06:25:03
			3		10M	09:11:07	09:21:07
			4		20M	09:21:45	09:41:45
			5 - 9	Cal	2M	09:45:07	09:50:10
			10		20M	10:01:00	10:21:00
			11		40M	10:21:00	11:01:00
			12		20M	11:01:00	11:21:03
			13		40M	11:40:50	12:20:50
			14		40M	12:22:10	13:02:10
			15		40M	13:02:10	13:42:10
			16		40M	13:42:10	14:22:10
			17		40M	14:22:10	15:02:10
			18		40M	15:02:10	15:42:10
			19		10M	15:42:10	15:52:10

Table 5.14-3 (continued)

DSS	Day	Position	Record	Calibration	Accumulation	GMT, hr:min:sec Start	GMT, hr:min:sec End
61	255	Lunar surface					
			1		10M	16:19:15	16:29:15
			2		40M	16:30:15	17:10:15
			3 - 7	Cal	2M	17:14:25	17:29:10
			8		40M	17:30:30	18:10:30
			9		40M	18:10:30	18:50:30
			10		40M	18:50:30	19:30:30
			11		40M	19:30:42	20:10:42
			12		40M	20:10:42	20:50:42
			13		40M	20:50:42	21:30:42
			14		40M	21:30:42	22:10:42
			15 - 19	Cal	2M	22:12:55	22:26:40
			20		40M	22:27:35	23:07:35
			SAMPLE II				
42	256	Lunar surface					
			2		10M	08:44:30	08:54:30
			3 - 7	Cal	2M	09:33:20	09:48:17
			8		10M	09:49:40	09:59:40
			9		40M	10:26:00	11:06:00
			10		40M	11:43:30	12:23:30
			11		40M	12:24:10	13:04:10
			12 - 16	Cal	2M	13:05:55	13:19:15
			17		40M	13:20:40	14:00:40
			18		40M	14:11:00	14:51:00
			19		40M	14:51:00	15:31:00
			20		40M	15:32:30	16:12:30
			21		36M 30S	16:12:30	16:49:00
61	256	Lunar surface					
			1		10M	17:03:00	17:13:00
			2 - 6	Cal	2M	17:15:10	17:28:55
			7		40M	17:30:00	18:10:00
			8		40M	18:10:00	18:50:00
			9		40M	19:17:30	19:57:30
			10		40M	19:57:30	20:37:30
			11		40M	20:37:30	21:17:30
			12		10M	22:49:15	22:59:15
			13 - 17	Cal	2M	23:00:20	23:14:10
			18		40M	23:15:20	23:55:20
	256 - 257		19		15M	23:55:20	00:10:20
42	257	Lunar surface					
			2		25M (A1, A2, P2 on)	08:58:15	09:23:15
			3		15M (A1, A2, P4 on)	09:26:15	09:41:15
61	259	Lunar surface					
			2		20M	18:44:35	19:04:35
			3	Cal	2M	19:05:50	19:07:50
			4 - 8	Cal	2M (lost)	19:08:45	19:27:40
			9		20M (lost)	19:28:40	19:48:40
			1A	Cal	2M (A1, P1 on)	20:07:00	20:09:00
			2A		20M	20:12:50	20:32:50
			3A		20M	20:38:48	20:58:48
			4A - 8A	Cal	2M	21:01:10	21:14:40
			9A		20M	21:17:44	21:37:44
			10A		15M (lost)	21:38:30	21:53:30
			11A		20M (lost)	21:53:30	22:13:30
			12A		20M	22:13:30	22:33:30
			13A		20M	22:34:30	22:54:30
			1B - 5B	Cal	2M	23:17:00	23:32:10
			6B		20M	23:33:15	23:53:15
	259 - 260		7B		20M (lost)	23:53:15	00:13:15
	260		1C		20M	00:27:20	00:47:20
			2C		10M 10S	00:47:20	00:57:30
			3C	Cal	2M (not written on MT)	00:59:10	01:01:10
			3C - 6C	Cal	2M	01:03:45	01:16:15
			7C		20M	01:22:20	01:42:20

Table 5.14-3 (continued)

DSS	Day	Position	Record	Calibration	Accumulation	GMT, hr:min:sec Start	GMT, hr:min:sec End
11	260	Lunar surface					
			2		10M	03:43:05	03:53:05
			3		10M	03:56:01	04:06:01
			4 - 8	Cal	2M	04:14:02	04:28:30
			9		20M	04:29:34	04:49:34
			10		19M30S	04:50:30	05:10:00
			11		20M	05:11:40	05:31:40
			12		40M (lost)	05:34:30	06:14:30
			12		10M	06:16:05	06:26:05
			13		40M	06:28:40	07:08:40
			14		40M	07:10:20	07:50:20
			15		40M	07:52:15	08:32:15
			16		40M	08:42:00	09:22:00
			17		46M40S	09:23:20	10:10:00
			18		18M40S	10:17:40	10:36:20
			19 - 23	Cal	2M	10:40:40	10:55:10
			24		40M	10:56:30	11:36:30
			25		5M	11:40:00	11:45:00
42	260	Lunar surface					
			1		10M	13:05:00	13:15:00
			2		30M (A1, P1 on)	13:20:55	13:50:55
			3		30M (A1, P1 on)	13:52:15	14:22:15
			4		30M (A2, P2 on)	15:21:15	15:51:15
			5		30M (A2, P2 on)	15:53:00	16:23:00
			6		30M (A2, P3 on)	16:25:15	16:55:15
			7		30M (A2, P3 on)	17:32:20	18:02:20
			8		30M (A1, P4 on)	18:05:50	18:35:50
61	260	Lunar surface					
			1		30M (A1, P4 on)	18:44:45	19:14:45
			2		30M (A2, P2 on)	19:16:40	19:46:40
			3 - 7	Cal	2M	19:48:33	20:05:15
			8		27M20S	20:07:45	20:35:05
11	261	Lunar surface					
			2		20M	08:33:45	08:53:45
42	261	Lunar surface					
			1		10M	15:59:30	16:09:30
			2 - 6	Cal	2M	16:11:00	16:26:30
			7		20M	16:28:00	16:48:00
			8		20M	16:49:20	17:09:20
			9		20M	17:10:20	17:30:20
			10		20M	17:32:20	17:52:20
			11		20M	17:53:00	18:13:00
			12		20M	18:14:30	18:34:30
			13		20M	18:35:20	18:55:20
			14		15M	19:23:00*	19:38:00
61	261	Lunar surface					
			1		15M	19:23:00**	19:38:00
			2 - 6	Cal	2M	20:35:40	20:50:08
			7		40M	20:51:30	21:31:30
			8		40M	21:31:30	22:11:30
			9		20M	22:11:30	22:31:30
			10		20M	22:31:30	22:51:30
			11		20M	22:51:30	23:11:30
			12		20M	23:11:30	23:31:30
			13 - 17	Cal	2M (lost No. 16)	23:43:45	23:58:05
	261 - 262		18		20M	23:59:30	00:19:30
	262		19		20M	00:19:30	00:39:30
			20		20M	00:39:30	00:59:30

*Data accumulated same time as record No. 1 at Station 61 on day 261.

**Data accumulated same time as record No. 14 at Station 42 on day 261.

Table 5.14-3 (continued)

DSS	Day	Position	Record	Calibration	Accumulation	GMT, hr:min:sec Start	GMT, hr:min:sec End
61 (cont)	262 (cont)	Lunar surface (cont)	21		20M	01:00:20	01:20:20
			22		20M	01:21:05	01:41:05
			23		30M	01:44:15	02:14:15
			24 - 28	Cal	2M	02:17:05	02:30:20
11	262	Lunar surface					
			2		10M	08:07:30	08:17:30
			3		10M	08:21:00	08:31:00
			4		10M	08:35:00	08:45:00
			5 - 9	Cal	2M	08:48:00	09:02:10
			10		40M	09:03:30	09:43:30
			11		40M	09:44:30	10:24:30
			12		40M	10:25:30	11:05:30
			13		40M	11:06:30	11:46:30
			14		40M (started—lost)	11:47:30	
			14		10M	12:16:15	12:26:15
			15 - 19	Cal	2M	12:29:00	12:43:10
			20		20M	12:44:30	13:04:30
42	262	Lunar surface					
			2		40M	13:05:00	13:45:00
			3		40M	13:46:00	14:26:00
			4		40M	14:29:00	15:09:00
			5		40M	15:10:30	15:50:30
			6		40M	15:51:30	16:31:30
			7		40M	16:32:00	17:12:00
			8 - 12	Cal	2M	17:14:10	17:28:00
			13		80M	17:29:30	18:49:30
			14		29M40S	18:50:20	19:20:00
61	262	Lunar surface					
			1		20M	19:20:00	19:40:00
			2		40M	19:40:00	20:20:00
			3		80M	20:22:01	21:42:01
			4		10M	21:44:10	21:54:10
			5		10M	22:01:40	22:11:40
			6		20M	22:26:05	22:46:05
			7 - 11	Cal	2M	22:47:15	23:01:30
	262 - 263		12		80M	23:02:35	00:22:35
	263		13		80M	00:25:30	01:45:30
			14		60M	01:47:00	02:47:00
			15 - 19	Cal	2M	02:49:00	03:01:30
			20		30M (lost)	03:06:00	
42	263	Lunar surface					
			2		10M	18:33:00	18:43:00
			3 - 7	Cal	2M	18:48:00	19:01:50
			8		2M (not transmitted)	19:03:25	19:05:25
			9		40M	19:07:40	19:47:40
61	263	Lunar surface					
			1		20M	19:50:00	20:01:00
			2		30M	20:10:00	20:40:00
			3		40M	20:40:00	21:20:00
			4		40M	21:21:40	22:01:40
			5		40M	22:04:00	22:44:00
			6		40M	22:45:05	23:25:05
	263 - 264		7		40M	23:26:00	00:06:00
	264		8		40M	00:09:00	00:49:00
			9		40M	00:49:40	01:29:40
			10 - 14	Cal	2M	01:31:35	01:46:05

Table 5.14-3 (continued)

DSS	Day	Position	Record	Calibration	Accumulation	GMT, hr:min:sec Start	GMT, hr:min:sec End
61 (cont)	264 (cont)	Lunar surface (cont)	15		40M	01:47:20	02:27:20
			16		40M	02:28:05	03:08:05
			17		40M	03:09:30	03:49:30
11	264	Lunar surface					
			2		10M	13:52:15	14:02:15
			3 - 6	Cal	2M (deleted item 6.1)	14:05:10	14:19:25
			7		20M	14:21:15	14:41:15
			8		20M	14:42:15	15:02:15
			9		20M	15:03:15	15:23:15
42	264	Lunar surface					
			2		40M	15:25:00	16:05:00
			3		40M	16:06:00	16:46:00
			4		40M	16:48:00	17:28:00
			5		10M	19:41:30	19:51:30
			6		30M (A1, P1 on)	19:53:30	20:23:30
61	264	Lunar surface					
			1		30M (A1, P1, on)	20:24:45	20:54:45
			2		30M (A1, P2, on)	20:56:45	21:26:45
			3		30M (A1, P2, on)	21:27:15	21:57:15
			4		30M (A2, P3, on)	22:00:15	22:30:15
			5		30M (A2, P3, on)	22:30:15	23:00:15
			6		30M (A2, P4, on)	23:01:30	23:31:30
	264 - 265		7		30M (A2, P4, on)	23:31:30	00:01:30
	265		8 - 12	Cal	2M	00:03:00	00:17:25
			13		40M	00:18:10	00:58:10
			14		40M	00:58:45	01:38:45
			15		20M	01:38:45	01:58:45
42	265	Lunar surface					
			1		10M	18:57:00	19:07:00
			2 - 6	Cal	2M (lost Nos. 4, 5, 6)	19:08:10	19:22:10
61	265	Lunar surface					
			1 - 5	Cal	2M	22:26:25	22:39:37
			6		5M	22:40:40	22:45:40
	266		7 - 11	Cal	2M	02:38:05	02:51:10
			12		10M	02:53:15	03:03:15
			13		12M15S	04:42:45	04:55:00
42	266	Lunar surface					
			2 - 6	Cal	2M	17:25:25	17:39:40
			7		10M	17:41:20	17:51:20

Alpha scattering power off 266:17:51:54

5.14.5 REFERENCE

1) A. L. Turkevich, E. J. Franzgrote, and J. H. Patterson, "Chemical Analysis of the Moon at the Surveyor V Landing Site: Preliminary Results."

5.14.6 ACKNOWLEDGMENTS

This section was compiled by E. R. Zinn with inputs from J. N. Butterbaugh of Hughes, and Maurice Clorey and Ernest Franzgrote of JPL.